UNIVERSITY OF SOUTHAMPTON

Remote sensing of grassland with contaminated soil using the spectral red-edge

by

Gary Michael Llewellyn

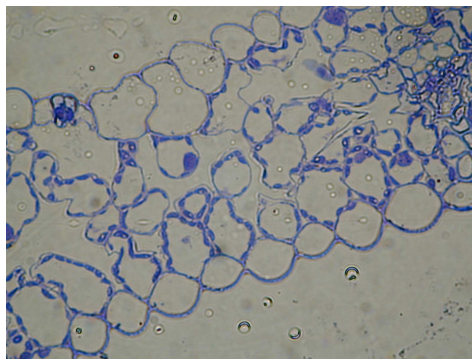Submitted for the degree of Doctor of Philosophy

School of Geography, Faculty of Engineering, Science and Mathematics

June 2009

(a) CASI-2 data (NERC ARSF - 00/04)

(b) The cellular structure of grass
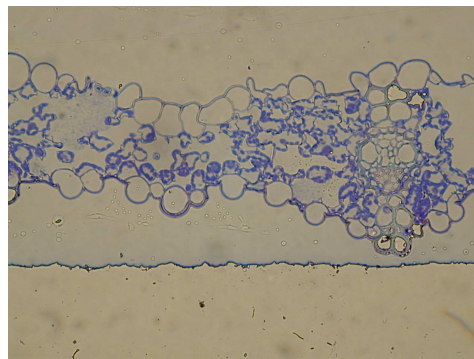
(c) The cellular structure of grass

Figure 1: Frontispiece: remote sensing at two scales

"Many of the truths that we cling to depend greatly on our point of view"

Obi-Wan Kenobi, Star Wars VI

Declaration

I declare that this thesis is the result of my own work done while I was in registered post graduate candidature, except where otherwise stated. This work has not been submitted for any other degree.

This thesis was submitted for examination in June, 2009. It does not necessarily represent the final form of the thesis as deposited in the University after examination.

Acknowledgements

This thesis has been a long time in its making. During which time a series of major events have occurred in my life. My first expressions of gratitude must go to Paul Curran and Dawn Williamson who started me on this road. In particular, Paul's breadth of knowledge and drive allowed considerable early progress and set the shape of the research to follow. The work was made possible by funding from DERA and the School of Geography, (University of Southampton) and was supported along the way by the NERC EPFS, NERC ARSF, Shell (especially Chris Lambert), RSPSoc (RSS) and NCAVEO. I am indebted to the support of Ted Milton and the collaborative enthusiasm of Lammert Kooistra without whom much of the soil analysis would have been even more logistically difficult that it was. Similarly, the supply of equipment by Trevor Tantum was invaluable. The Matlab code, transcribed by Fred Baret was supplied by Mark Danson and Clair Rowland, the initial pigment file by a LIBERTY inversion with Terry Dawson and various stages of idiot checking of Matlab code and me by Isabel Sargent. The field work assistance by Penny, Paul, Nick, Richard, Sarah, Michael and Jenny was stalwart with commendations for resilience for coping with torrential rain and burning sun while dressed in protective overalls, gloves, and hard hats. A special mention must go to Stef Webb who headed up the ranks of proof readers and (with Isabel) proved general support. Grateful thanks to Simon, Ilsa, Louise and Dom for proofreading of English and stats. Finally, eternal thanks to my father and mother who were there at the beginning but did sadly not see the end.

UNIVERSITY OF SOUTHAMPTON

ABSTRACT

Faculty of Engineering, Science and Mathematics

SCHOOL OF GEOGRAPHY

Doctor of Philosophy

Remote sensing of grassland with contaminated soil using the spectral red-edge

by Gary Michael Llewellyn

In most cases contaminants are concealed in soil and under vegetation and therefore can not be measured directly by remote sensing. However, soil contaminants were detected using the spectral red-edge to indicate vegetation stress caused by the presence of the contaminants. An improved red-edge position (REP) was developed and gave a slight improvement in the predictive capability over existing indices and an effective additional diagnostic indicator of soil contamination was found to be the spatial pattern of the REP. Where an area had high levels of hydrocarbon in the soil it also had a high level of variation. The indication was that spatial variation of spectral indices (especially the REP) may be more useful than the spectral index value for the detection and mapping of soil contamination.

Field analysis and radiative transfer modelling (using a coupled leaf and canopy model, LIBSAIL) showed the influence of vertical layering in the grassland canopy. The influence of a vegetated under-storey on the red-edge was found to be greatest when different absorption spectra were present and high within-the-leaf scattering. The former defined wavelength positions of features while the later determined if they were resolvable in a spectrum. This greater understanding of the grassland canopy identified the importance of fully surveying vegetation canopy structure, especially in complex, multi-layered canopies such as those found with contamination. With this understanding of what the red-edge can reveal, remote sensing is an effective tool for the detection of contamination.

Contents

List of Figures

List of Tables

Chapter 1

Introduction

1.1 Introduction

Contamination of soil is a problem common to most regions with a history of industrial activity. Where available land is limited and required for development or where there is a detrimental impact on flora and fauna any contamination needs to be characterised, delineated and controlled. Negative effects on health and vigour as a result of exposure to a contaminant pose the greatest concern. Therefore, UK law requires that before these areas can be used for human habitation or agriculture, the contamination must be made safe (e.g. by remediation or encapsulation). The surveying of soil contamination is expensive but constitutes a small cost compared with that of remediation. Nevertheless, a typical soil contamination survey will only sample six locations and face considerable pressure to minimise the cost of any further assessment (pers. comm. N. Rogers, 2009). Therefore, the identification of the best location from which soil samples are extracted is important. Many desk surveys (using historical reports and maps) do not capture unrecorded, mislocated or concealed areas of soil contamination and lead to costly additional sampling. When a field survey is supported by ground observations or aerial photography it can identify previously hidden areas (pers. comm. N. Rogers, 2009). One reason for the effectiveness of this technique is that many types

of contamination also affect the native vegetation; these effects may be used as a proxy to determine where contamination may be present.

Although the term contamination can cover many substances (e.g. milk, soap, radiation), this study will specifically consider the presence of hydrocarbons and heavy metals (e.g. cadmium, arsenic, lead, zinc, copper). High levels of hydrocarbons and heavy metals may be found naturally occuring in the soil; they are only termed a contaminant if not native to a location, but introduced deliberately or by chance. Typical areas with high levels of hydrocarbon or heavy metals in the soil are oil refineries, gas works and heavy industrial plants. Representative sites are positioned on floodplains because of access to cooling water and river (or sea) transportation for bulk materials.

1.2   Background

A legacy of our industrial heritage has been contamination of our environment. This has been, for example, due to leakage from pipes and storage tanks, from the dumping of waste or from other pollution incidents. Contamination may be described as 'potential pollution' (Warren 1997) and where pollution is defined as the occurrence of toxic substances in larger quantities than ecological communities or specific species can tolerate without suffering measurable damage (Freedman 1995). A common way to consider pollution is in terms of a 'pathway' or set of processes that may transfer a contaminant or potentially harmful substance from the location where it is located to a vulnerable target (Alloway and Ayres 1993). Where a contaminant accumulates in soil a change, such as from disturbance due to building, may increase the chance of harm to a nearby ecological community. The location of soil contamination is an application of this research.

The main factor that has driven public, political and legal attention towards the control and remediation of environmental contaminants is the risk of harm to humans or the ecosystem. The approach that governments have taken concerning contamina-

tion differs depending on the political, economic and social environment in which it occurs. This difference may be due to choice or circumstance. A lower priority may be attributed to health and the environment due to a lack of awareness, insufficient resources to use or install 'clean' technologies, or a conscious policy of production over environment. Over the last two decades post-industrial countries (e.g., in Western Europe & North America) have developed an increasing concern regarding health and the environment (e.g., Porritt 1990, Mannion and Bowlby 1992, Wood 1995). Advances in medical and environmental understanding about the impact of contamination have driven governments to use legislation and education as tools to address the problem (e.g., Foster 1991, Glasson *et al.* 1994, Morris and Therivel 1995). The legislation in some countries, e.g., the Netherlands and USA, directs remediation to 'uncontaminated' background levels (multifunctional approach) while UK legislation demands different target levels depending on the final use of the land (Alloway and Ayres 1993). The multifunctional strategy has proved to be expensive and many countries, e.g. the Netherlands (personal communication G. Pieters 1999), are now moving towards the more pragmatic 'fitness for use' approach adopted by the UK. For this reason and because all field research sites in this work are in the south of England, the concept and legal definition of 'contaminated land' will be taken with respect to UK legislation.

1.2.1 'Contaminated land' in the United Kingdom

In the United Kingdom 'contaminated land' is used as a general descriptor for areas where the concentrations of substances are above published Interdepartmental Committee for the Redevelopment of Contaminated Land (ICRCL) levels. ICRCL levels are calculated on the basis of a contaminant's potential to cause harm to human health and are dependent on land use (table 1.1). The lowest values are given for areas where food is grown (e.g., gardens), higher acceptable values are given for parks and open space and the highest values for land designated for industrial use. Contaminated land is a subjective term and even under UK law (Environment Act 1995) is defined as:

> *"... any land which appears to the local authority in whose area it is situated to be in such a condition, by reason of substances in, or under the land, that (a) significant harm is being caused or there is a significant possibility of such harm being caused or*
>
> *(b) pollution of controlled waters is being, or is likely to be caused."*

Environment Act 1995, Section 57, p.1312-1313

The Environment Act (1995) definition uses the terms substance and harm; these are defined as:

> *"**Substance** means any natural or artificial substance whether solid or liquid form or in the form of a gas or vapour."*

Environment Act 1995, Section 57, p.1316

[emphasis added]

> *"**Harm** means harm to the health of living organisms or other interference with ecological systems of which they form part and, in the case of man, includes harm to his property."*

Environment Act 1995, Section 57, p.1313

[emphasis added]

The second criteria (b) for land contamination is associated with the Water Resources Act 1991 (WRA 1991) and considers the potential for the pollution of controlled waters. Where the pollution of controlled waters is defined as:

"...the entry into controlled waters of any poisonous, noxious or polluting matter or any solid waste matter."

Environment Act 1995, Section 57, p.1315

The Environment Act 1995 definition also rests on the phrases 'significant possibility' and 'likely'. These terms do not provide a clear description of what is or is not contaminated. The concept of contaminated land is more concisely described by an earlier definition given by the Department of Environment when it gave evidence to the Environment Committee in 1989 (Lane and Peto 1995).

"land which represents an actual or potential hazard to health or the environment as a result of current or previous use."

Environment Committee, 1st Report, Contaminated Land, volume 1, House of Commons Papers, Session 1989-90, p.170

A significant component of land is soil. Soil conditions and the nature of the contaminant influences the contaminants residency in an environment and its risk to health and property. In moving air or a river the influence of a contaminant would tend to be reduced due to mixing and dilution but in soil a contaminant may accumulate due to absorption processes which bind inorganic and organic contaminants to soil colloids (Alloway and Ayres 1993). This research deals with the mapping of relative levels of hydrocarbon and heavy metal contaminants in soil and the problems associated with its identification in grassland. Many old industrial sites revert to grassland when neglected and require remediation of soil contamination before they may be redeveloped. This issue became particularly topical in the UK due to government declared intention for between 50 and 60% of new housing to be in brown-field sites (Clayton 2000) these are sites that have had a history of industry or housing on them.

Table 1.1: UK Department of the Environment (ICRCL) trigger concentrations.

Contaminants	Proposed use	Trigger concentration threshold level (μg.g^{-1})
Polycyclic aromatic hydrocarbons (PAHs)	Gardens & allotments	50
Polycyclic aromatic hydrocarbons (PAHs)	Landscaped areas, openspace	1000
Coal tar	Gardens & allotments	200
Coal tar	Landscaped areas, openspace	500
Acidity	Gardens & allotments	pH<5

1.3   The problems

Key questions for the control, monitoring and remediation of soil contamination are: where are the soil contaminants located and what is their potential for causing harm? The answer to the first question can be derived from the mapping of such areas and the second question may be answered from estimates of contaminant concentration related to effects established from previous research. Solving either task may be complicated because of poor record keeping and the cost (in time and money) of ground survey needed to evaluate areas where data are sparse or unavailable. Wherever ground surveys are conducted they are rarely comprehensive and are based on data from localised measurements (e.g., bore-holes, trenches, measurements of surface vapour, ground based laser induced fluorescence etc.). The interpolation of values between these points can be imprecise if the sampling scheme is insufficient to characterise the distribution or variation of the contaminant. A more comprehensive survey on the ground may not be possible due to constraints on time or resources but if a complementary survey were conducted from the air or space it could provide rapid, synoptic data to supplement the ground survey.

1.4 The solutions

"Remote sensing is the practice of deriving information about the earth's land and water surfaces using images acquired from an overhead perspective, using electromagnetic radiation in one or more regions of the electromagnetic spectrum, reflected or emitted from the Earth's surface."

Campbell 1996, p.5

Remote sensing could be a powerful tool for the location of relative levels of soil contamination. It could be used as part of a long-term monitoring strategy, to locate terrestrial pollution events or as preliminary reconnaissance for soil contamination remediation. Preliminary reconnaissance and monitoring are spatially intensive processes that are well-suited to remote sensing. Once an area has been mapped subsequent monitoring can identify movement or infer changes in concentration of soil contamination. Soil contamination can be identified directly from variations in ground reflectance (e.g., Coulson and Bridges 1984, Lomas-Clarke and Williamson 1998) or by diagnostic features in the reflectance spectra of vegetation (e.g., Jago *et al.* 1999). However, the use of vegetation relies on it being affected by the soil contaminant, i.e. vegetation stress.

1.4.1 Vegetation stress

Vegetation stress is the effect of:

"any factor that reduces the productivity of the canopy below its potential or optimal value"

Steven *et al.* 1990, p.212

It has also been defined as being caused by any environmental factor (abiotic or biotic) which is liable to cause a potentially injurious strain on plants (Levitt 1980). Technically the effect of an applied force is strain; however, the term vegetation stress is commonly used and will be hereafter used in this work to describe the action of soil contamination on vegetation. For some species stress may be beneficial in terms of relative competitive advantage or growth stimulation. Lichtenthaler (1996) distinguishes between *eu-stress* (activating or stimulating) and *dis-stress* (damage causing) and further clarifies the term 'dis-stress' by stating that:

> *"any unfavourable condition or substance that affects or blocks a plant's metabolism, growth or development, is to be regarded as a stress."*

Lichtenthaler 1996, p.4

Stress is a common response to heavy metal and hydrocarbon contamination. To understand the effect of stress on a plant and its influence on the reflectance spectrum (specifically between 650 and 750nm, the red-edge) vegetation type must be observed under controlled conditions. Ideally this should be an environment with homogeneous geology, relief and vegetation cover, known levels of soil contamination and a full account of temporal changes, with data from before the period of contamination. Such an environment can only be found in a modelled, or very controlled experimental, setting and would require physical observations to determine its accuracy.

This work concentrates on 'dis-stress' and investigates if the location of relative levels of contaminated soil can be inferred from variations in reflected radiation. Geobotanical research has not established if changes in the red-edge are due to:

1. spectral changes in vegetation due to specific stresses occurring on contaminated soil,

2. spectral changes of specific species with stress or

3. because of spectral differences between tolerant and non-tolerant species in natural vegetation (Steven *et al.* 1990).

The first two factors identify biophysical change while the third identifies a species change either by replacement by tolerent species or by evolution of tolerance by existing species. They indicate a trend with time, discussed further in chapter 3, and need to be explored in order to understand why the red-edge may change in responce to long-term stress. However, they do not provide any indication of the more immediate details concerning changes in state variables; these may be considered as:

1. physiological, cellular or biochemical changes in the plant,

2. structural or area changes in the canopy,

3. taxonomic or spatial changes in the grassland, or

4. temporal changes in terms of seasons of maturation or seed/pollen distribution.

The relative dominance of these factors will depend on five factors:

1. the toxicity of the contaminant,

2. the duration of the period of contamination,

3. the nature of the grassland and the species within,

4. the period of time with which the area has had to recover and

5. on human activity.

Most experimental activity has been directed towards the contaminant and recovery period but additional information may lie with the other components.

1.4.2   Grassland

Grassland provides a ubiquitous surface on which vegetation stress may be assessed. It is a combination of living vegetation (e.g., grass, legumes, lichens and mosses), litter, debris (e.g., timber, fragmented masonry or rubbish), the soil surface, sub-soil and lower soil horizons (described in chapter 3). All these components may collectively be considered as grassland although only those above the surface may be visible. This research seeks to locate relative levels of hydrocarbon and heavy metal contamination in soil by the measurement of its effect on overlying grassland vegetation. It builds on techniques developed at the University of Southampton (e.g., Jago and Curran 1996, Jago and Curran 1997, Jago 1998, Jago *et al.* 1999) and aims to improve our understanding of the factors that cause and confuse the relationship between soil contamination and reflected radiation. Grassland has been selected for three main reasons.

1. Previous work has been carried out on the remote sensing of grassland (e.g., Pinar and Curran 1996) and soil contaminated grassland (Jago *et al.* 1999). A description of remote sensing follows in chapter 2.1.

2. Grass is present on many areas that have a potential to be contaminated, e.g., oil storage areas and refineries and metal processing plants.

3. Grass has a relatively simple structure in terms of canopy architecture and homogeneity.

1.4.3   Aims and objectives

The aim of this study is to identify the spatial extent and relative concentration of soil contamination using remote sensing. The main soil contaminants to be investigated are hydrocarbons in grassland soil, though low levels of heavy metal are also present. The method by which different relative levels of soil contamination will be determined is by their effect on grassland vegetation. This research aims to understand, characterise and explain the relationships between soil contamination and reflected solar radiation.

Within this relationship are the effects of soil contamination on vegetation and the effect of vegetation of the reflected radiation as may be measured in the field or from the air or space. Both components need to be explained to understand how soil contamination has influenced reflected radiation. This knowledge will be used to increase the accuracy with which the soil contamination of grassland can be mapped. These aims will be achieved by the pursuit of specific objectives:

1. test the statistical relationship between soil contamination and reflected solar radiation.

2. test the statistical relationship between soil contamination and vegetation variables (state variables).

3. test the statistical relationship between vegetation variables (state variables) and reflected solar radiation.

4. model the relationship between vegetation state variables and reflected solar radiation.

The modelling will use a combined leaf and canopy radiative transfer model. The leaf model used will be Leaf Incorporating Biochemistry Exhibiting Reflectance and Transmission Yields (LIBERTY); Dawson *et al.* (1998) and the canopy model will be Scattering from Arbitrarily Inclined Leaves (SAIL); Verhoef (1984). As sub-objectives associated with the modelling aspect of this study this research will combine the code for the LIBERTY and SAIL models and include a component in the combined model that can simulate the effect of the vegetated understorey and soil reflectance.

To explore these areas a series of hypotheses have been posed. These guide the components of the investigation into the relationship between soil contamination and the red-edge. These data were used to test the hypotheses that:

1. (H_1): *differences in the relative concentration of contaminants in a grassland soil can be detected using the position and shape of the red-edge of reflected radiation,*

2. (H$_1$): *stress effects in vegetation (attributed to the effects of soil contaminants) can be measured in the vegetation that grows in that soil,*

3. (H$_1$): *stress effects in vegetation (attributed to the effects of soil contaminants) are greater than those found by natural variation,*

4. (H$_1$): *stress effects in vegetation (attributed to the effects of soil contaminants) can be detected using the position and shape of the red-edge of reflected radiation,*

The first hypothesis tests the technique while the following three hypothesis allow the relationships that form it to be investigated. By these means the potential for remote sensing soil contamination may be determined for actual and modelled conditions. The following chapter introduces the reader to some of the principles and methods that determine how passive optical remote sensing is conducted and its existing use for the measurement of soil and vegetation.

Chapter 2

The remote sensing of vegetation

2.1 Introduction

Through remote measurement and interpretation of reflected or emitted electromagnetic energy (Mather 1999) remote sensing is perhaps the most efficient technique to use for the acquisition of spatial data. As such, it has the potential to improve the efficiency of soil contamination surveys. However, the use of remote sensing for the assessment of soil contamination assumes a difference in reflected or radiated electromagnetic energy between areas with and without soil contamination. Generally, soil contamination has no direct effect on reflectance but under some circumstances it does influence vegetation in its proximity. Where vegetation differences are due to soil contamination, remote sensing may be used to indicate the presence of soil contamination.

Remote sensing is a set of methodologies for the measurement of properties relating to a target from a point of measurement distant from that target. In this chapter, the principles and techniques that allow the interpretation of measured electromagnetic energy are considered with particular emphasis on the estimation of vegetation variables, especially the vegetation red-edge. The chapter then describes and critiques vegetation indices as tools for (i) estimating variables related to vegetation and (ii) summarising

14
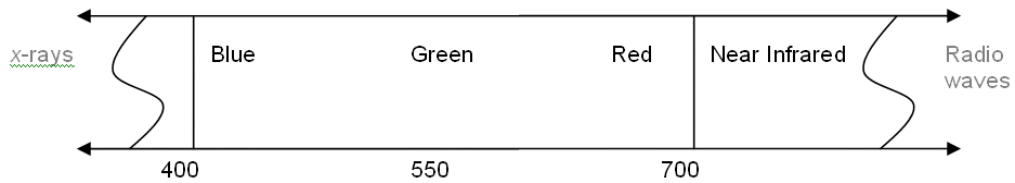
Figure 2.1: Electromagnetic spectrum (wavelength in nm)

remote sensing data.

2.2 Radiation

The most evident source of radiation is the Sun. Radiation can be regarded as an electromagnetic (em) wave and is measured in terms of its wavelength. Ultraviolet wavelengths lay between 10 nm and 400 nm and infrared wavelengths lay between 700 nm and 100 000 nm (Banwell 1983). Between these is the narrow region of the spectrum visible to the human eye (400 to 700 nm; visible wavelengths) and used by plants for photosynthesis. Solar radiation in these wavelengths is less attenuated by the atmosphere than other wavelengths (figure 2.1). Electromagnetic energy occurs in indivisible units of energy (quanta) that occur in pulses (photons) and can be described by frequency and wavelength. The energy (ϵ) in a photon varies inversely with the wavelength. This is described in equation 2.1 where c is the speed of light (3×10^8 ms^{-1}) and h is Planck's constant (6.63×10^{-34} J.s). This means that a photon of wavelength 700 nm contains only 57% of the energy of a photon at a wavelength 400 nm (Barrett and Curtis 1982).

$$\epsilon = h\frac{c}{\lambda} \qquad (2.1)$$

Radiant flux (quanta s^{-1} or W) is the rate at which photons strike a surface and, when applied to a unit area (quanta, m^{2}s^{-1} or Wm^{-2}), is termed irradiance (Campbell 1996). If radiant flux at a given solid (three-dimensional) angle (θ) and direction (θ)
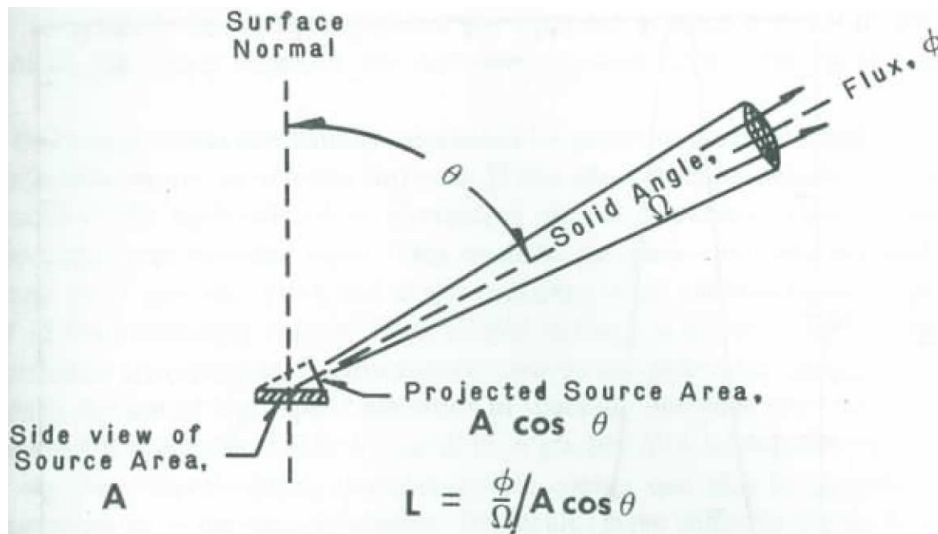
Figure 2.2: Radiance (L). Source: Elachi 1987.

is measured per unit area (corresponding to that from which it was projected) it is termed radiance (Wm^{-1} steradian^{-1}) (figure 2.2). Reflectance measurements are measurements of radiance that has been empirically corrected against a reference standard to give a 0 to 1 or 0 to 100% scale. However, the term reflectance required additional details, such as those described by (Schaepman-Strub *et al.* 2006), to describe incomming and exiting radiation. this conventon is used later in this thesis to descibe specific measurements. The advantage of transforming reflected radiation into absolute units is that remotely sensed data may be compared between different locations, time periods or sensors.

2.3 Radiation interactions

Radiation may be absorbed, emitted, transmitted, reflected or scattered. The combination of these effects determines the radiation directed towards or away from a sensor and therefore the scene presented to the sensor.

2.3.1   Absorbed radiation

The absorption of radiation can be due to a variety of reasons depending on the frequency and wavelength of the radiation. At wavelengths in the middle-infrared, radiation is absorbed due to vibrations arising from the stretching and bending of hydrogen bonds associated with carbon, oxygen and nitrogen (Workman (Jr) and Springsteen 1998, Clark 1999); these produce a series of harmonics and overtones in the shortwave-infrared (Card *et al.* 1988). The study of these harmonics and overtones measured from a sample allow an estimate of its chemical composition (Marten *et al.* 1989). Visible wavelength radiation is absorbed by the transition of electrons between energy levels within an atom (Workman (Jr) and Springsteen 1998). An example of this electron transition process is photosynthesis. During photosynthesis, visible wavelengths of radiation are absorbed to form molecules containing energy that can be distributed and stored elsewhere in the plant. Absorption analysis is based on known spectral features where the depth and width (described by the Lambert-Beer law) are used to determine the concentration of the absorptive compound.

2.3.2   Emitted radiation

All objects whose temperature is greater than absolute zero (-273 ^{o}C) emit radiation. Planck's law describes the spectral emitance per unit wavelength for perfect emitters (blackbodies) (equation 2.2). Within equation 2.2, M_λ = spectral exitance per unit wavelength, C_1 = 3.742 x 10^{-16}, C_2 = 1.4388 x 10^{-2}, λ = wavelength (metres) and T = temperature (Kelvin). The wavelength of the radiation emitted (related to the temperature of the object from which it is emitted) is described by equation 2.3 (Wein's displacement law), where λ is the wavelength at which radiance is at a maximum and T is the absolute temperature (K). In summary, the hotter the object the shorter the wavelength of maximum emittance. When solar radiation (from a very hot source) is absorbed and re-emitted from a cooler object, the re-emitted radiation will be at a longer wavelength. This is the basis of the re-emmission of visible wavelength radiation

from plants and is termed fluorescence.

$$M_\lambda = \frac{C_1}{\lambda^5[e^{C_2/(\lambda T)} - 1]}$$ (2.2)

$$\lambda = \frac{2897.8}{T}$$ (2.3)

2.3.3 Transmitted radiation

Transmission occurs when the passage of radiation is uninterrupted after crossing a boundary between two media (figure 2.3). In some cases a change in density of the medium through which the energy travels causes refraction or bending of the radiation and although no reflection occurs the direction of flux propagation is altered, the angle of refraction is described by Snell's law. Refraction from media with multiple structures may therefore result in the vector of radiation being nearly reversed as if reflection has occurred.

2.3.4 Reflected radiation

Reflection of radiation is characterised by two extremes: specular and diffuse reflection. Specular reflection occurs when the angle and distribution of radiation intercepting the target are equal to the angle and distribution of radiation reflected from the target 2.4. At the other extreme is the diffusion of energy such that reflected radiation is uniformly distributed (with equal magnitude) in every viewing direction. Such a surface is termed Lambertian. Actual surfaces usually reflect in a manner between these theoretical extremes.
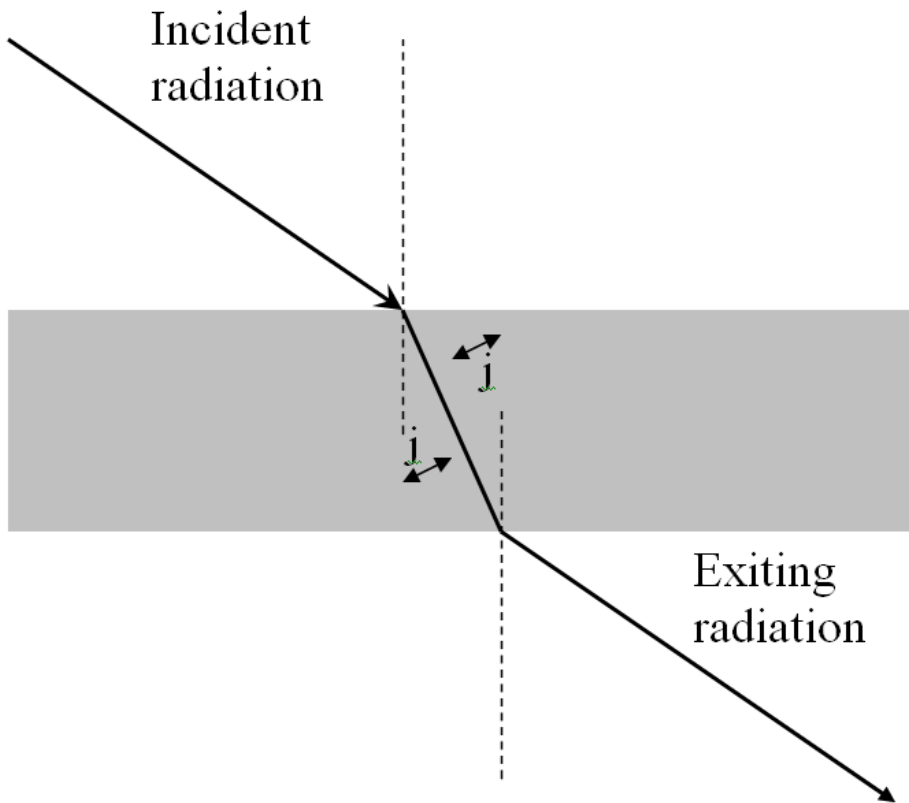
Figure 2.3: Refraction of radiation as it passes from one medium to another. The medium shown in grey has a higher refractive index that the areas either side. Angles i and j are equal.

(a) Specular reflection

(b) Diffuse scattering
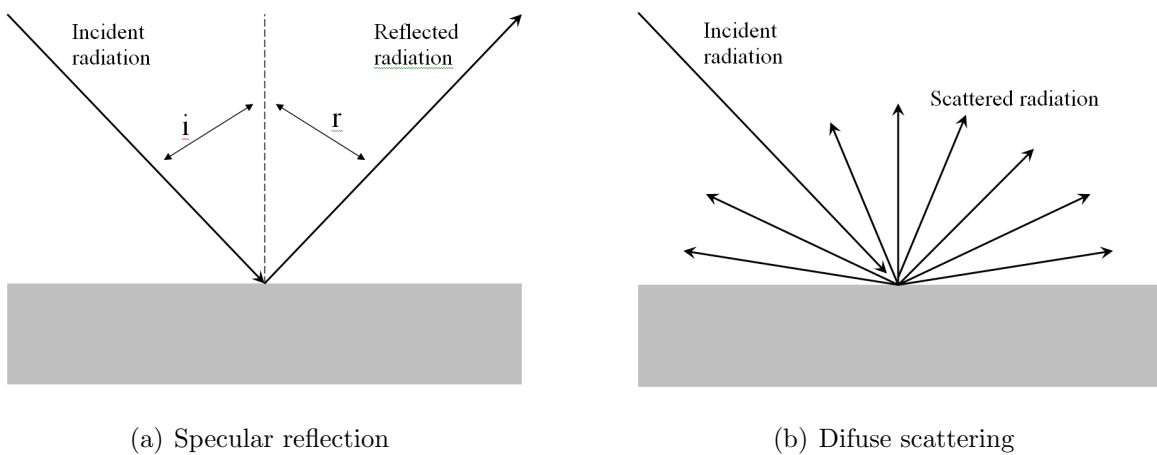
Figure 2.4: Specular and diffuse reflection, where angles i and j are equal.

2.3.5   Scattered radiation

Where radiation passes through a heterogeneous medium it may interact with different molecules and particles; when partial refraction and reflection occurs it is known as scattering. There are three types of scattering: Rayleigh scattering, Mie scattering and non-selective scattering. Rayleigh scattering is wavelength dependent, it follows Rayleigh's law which relates the degree of scattering to the inverse of the fourth power of the wavelength. Mie scattering is also wavelength dependent; in this instance scattering is caused by large particles in the medium, e.g., smoke and water droplets in air, and occurs when the diameters of these particles are approximately the same as the wavelength of the radiation. The third and least prolific form of scattering is non-selective scattering; this is caused by particles much larger than the wavelength of the radiation they scatter. Non-selective scattering is not wavelength dependent and scatters all visible wavelengths equally. The modelling of scattering in different media has been used as one approach for the estimation of the pre-scattered radiation signal. However it relies on assumptions concerning the scattering effect and homogeneity of the medium. In addition, the signal recorded by a sensor will include signals from other areas scattered towards the sensor and scattering of signal from the target to the sensor. This latter effect is known as path radiance and where obvious is called haze. Path radiance and atmospheric scattering combine to create atmospheric attenuation.

2.4   The interaction of radiation with vegetation: the red-edge

Reflected radiation from red to infra-red wavelengths is of particular interest in this research due to its specific relationship with green terrestrial vegetation. The red-edge is a distinctive characteristic of green terrestrial vegetation because of the dramatic contrast between high absorption of photosynthetically-active-radiation (PAR), in the wavelength region 400 nm to 700 nm, and the high reflectance of near-infrared (NIR)
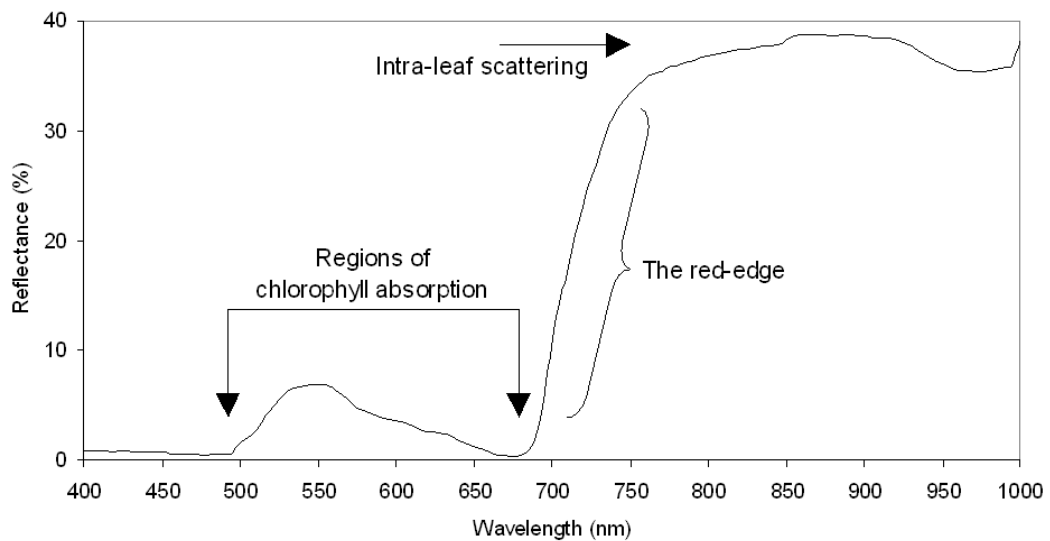
Figure 2.5: Vegetation spectrum

wavelengths (figure 2.5). The manner in which vegetation influences reflected radiation in visible and NIR wavelengths is due to chemical compounds (e.g., photosynthetic pigments) and structures (e.g., air voids between cells) within the plant, and the angle at which light impacts them (e.g., Gates 1970). Visible wavelength radiation is absorbed in a multi-stage operation in which photosynthetic pigments harvest PAR after which it may be stored as carbohydrates (Rabinowitch 1951).

2.4.1   Remote sensing in visible and NIR wavelengths.

Visible and NIR wavelengths can be exploited using either broad or fine spectral resolution sensors. All remote sensing instruments are a compromise between spectral, spatial and radiometric resolution and the position of the sensor in relation to the target. This is because the reflected energy from a target is finite and therefore can only provide data for a limited number of data dimensions; i.e., spectral, spatial, radiometric (brightness) components. For the study of grassland the relationship between visible and NIR wavelengths can serve as a general indicator of vegetation but finer spectral resolutions are required for more detailed examination.

2.5   The measurement of radiation

The object of remote sensing is to measure radiation and thereby estimate data related to a target or the media through which it has travelled (e.g., the atmosphere). Remotely sensed radiation measured by a sensor (R) can be considered as a function of location (x), time (t), wavelength (λ), and viewing geometry (θ) (Verstraete and Pinty 1996) (equation 2.4).

$$R = f(x, t, \lambda, \theta) \tag{2.4}$$

When reflected radiation (R) is measured from adjacent cells, each referenced to its spatial location (x), it can be used to produce an image. If R is recorded at different times (t) for a specific spatial position it may be used to record temporal change, and if recorded for different wavelengths (λ) produces a spectrum. Some distinctive spectra are associated with specific surface characteristics and are used as 'spectral signatures' to identify them. The fourth variable in the above equation (2.4) is the relative viewing geometry, θ (e.g., Gates 1970). Illumination and viewing angle may be considered in terms of two neighbouring fields of grass. For nadir illumination, an observer in one field will see the other field as greener. This is simply because the grass in the other field is viewed obliquely and therefore includes more biomass and less background. When the zenith angle of illumination is changed further differences in the observed scene are introduced. In a laboratory, a sample may be illuminated from a single controlled source and viewed from a known direction. However, natural targets are usually illuminated by the whole hemisphere of the sky and thus receive direct solar flux and scattered skylight (Milton 1987). The viewing and illumination geometry affect the way in which reflected radiation interacts with a target. Viewing and illumination geometry may be considered relative to one another and relative to the angular orientation of surfaces within the target. The variations incurred by these geometric effects are summarised by the term bidirectional reflectance distribution function and widely discussed in general literature (e.g., Campbell 1996).

All four of these variables come together to form a scene; where a scene has been described as:

> *"the spatial (and temporal) distribution of matter and energy fluxes from which the sensor draws measurements"*

Strahler *et al.* 1986, p.122

To consider one variable (from equation 2.4) a remote sensing study must either hold other variables constant or be able to measure any that are not constant; otherwise the cause or reason for any difference can not be identified. In addition, remotely sensed data may need to be corrected for instrument error and atmospheric attenuation; these may be empirically estimated and modelled.

2.5.1   The platform compromise

Field-based, airborne and spaceborne remote sensors, by necessity, have a more portable and robust design than laboratory instruments. In addition, airborne and spaceborne remote sensors are subject to atmospheric attenuation. While greater portability is a basic requirement for remote platforms, it also imposes restrictions on the operation of a given system, although an instrument can be optimised for the data collection required. Experimental conditions are most controllable in a laboratory setting and at their most complex when mounted on remote platforms (e.g., aircraft and satellites). This is because laboratory instruments restrict ambient illumination and typically measure a near simultaneous reference with each sample measurement. Data from more remote instruments (used in the field or mounted on aircraft or satellites) suffer from atmospheric attenuation and require a more portable and robust design. All remote sensing instruments are a compromise between the measurement of the four functional components identified in equation 2.4 and the detail at which measurements are made.

Laboratory spectrometers maintain a controlled distance and angle from which measurements are conducted. This provides a very effective environment in which to measure wavelength-dependent variation in radiation. Spectrally-dependent absorption is the basis for most laboratory spectrometry, although most field, airborne and space-borne systems have to consider the many means by which radiation may be affected. Laboratory spectrometry is typified by a high degree of control in the following ways:

1. heterogeneity is minimised by using highly prepared samples,

2. the signal from the sample is maximised by concentrating the sensor on the sample and minimising any unassociated signal,

3. an artificial constant and known (calibrated) source of illumination is used and

4. measurements are taken over a long time to maximise the volume of photons detected by the sensor.

Therefore, the ratio of sensor-signal to sensor-noise (SNR) of most laboratory spectrometers does not limit data collected. However, more mobile sensors are limited by the ambient condition in which they can operate with the expectation of collecting good data. For remote sensing instruments the energy collected by the sensor is finite; this means that a degree of specialization in terms of the measurement variables (equation 2.4) and data quantity are necessary. For example consider an imaging spectrometer and a goniometer. An imaging spectrometer records many wavelengths of reflected radiation over a wide spatial area but it will do so from a single viewing position and within a short period of time (e.g., a few seconds). In contrast, a goniometer records many wavelengths of reflected radiation over a small area from many viewing angles within a narrow period of time. The design of a remote sensor depends on the balance between portability, robustness and the collection of sufficient radiation for the sensor's detectors to record the level of detail specified while preserving an acceptable SNR.

2.5.2   Data resolution

Resolution is the level of detail that may be detected by an instrument. An instrument collects data with a spatial, spectral and radiometric resolution. Spatial resolution describes the finest detail rsolved in a scene; it approximates a FOV or pixel size and is dependent on the optical arrangement and the position of the sensor relative to the target. Spectral resolution describes the finest detail rsolved in a spectrum; it approximates the bandwidth and configuration of bands and is dependent on the optical and electronic configuration of the sensor. Radiometric resolution is the brightness grades within dynamic range for each spectral band. An additional consideration is instrument performance (indicated by gain and offset) which describes the accurate transfer of reflected radiation into a recordable variable such as a voltage change.

In the above example both instruments (imaging spectrometer & goniometer) have a high spectral resolution, the imaging spectrometer has a high spatial resolution but a low geometric capability whereas the goniometer has a high geometric capability but a low spatial resolution. Temporal resolution is determined by the frequency and the number of repeat measurements which are a function of field design or the time period of a satellite's orbit. While these capabilities describe the dependent variables that determine measured radiation, they do not account for the limitations presented by the recording of it.

2.5.3   The instrument compromise

Instruments are optimised for specific requirements because the finite reflected energy from a target must be divided between spatial, spectral and radiometric (brightness grades within the dynamic range) requirements. The amount of radiation reaching the detector can be increased by collecting reflected radiation over a larger ground area (field-of-view, FOV) and increasing the amount of time over which radiation is collected (dwell time) (table 2.1). However, a large FOV limits the spatial resolution while the dwell time is often limited by the capabilities of the platform carrying the

instrument or by changes in the atmospheric and illumination conditions. The energy requirement can be reduced by using less spectral bands, by broadening the width of the bands or by recording a reduced number of brightness grades within each band (the dynamic range). The following sections expand these principles within the headings: FOV, dwell time, spectral characteristics, radiometric brightness. It ends with a brief description of spectroradiometers.

Table 2.1: Restrictions in data resolution and the signal-to-noise ratio

	Spatial	**Temporal**	**Spectral**	**Radiometric**
Increase resolution	Decrease the field-of-view	Increase the time between repeat measurements. Frequent acquisitions	Increase the number of spectral bands. Decrease the bandwidth	Increase the brightness grades within the dynamic range
Decrease resolution	Increase the field-of-view	Increase the integration time (dwell time). Infrequent acquisitions	Decrease the number of spectral bands. Increase the bandwidth	Decrease the brightness grades within the dynamic range

2.5.3.1 Field-of-view

The area over which a sensor records data is its instantaneous field-of-view (FOV). In geostatistical terms it is the support over which the data has been collected. Reflected radiation recorded by a sensor is an integration of reflected radiation within a single instantaneous FOV (figure 2.6). The response of a sensor within its instantaneous FOV is not linear but conforms to a point spread function (PSF) which typically gives greater emphasis to some areas (usually the centre) than to others. These influences are often approximated by a simple Gaussian representation but are not easily assessed in collected field data (Rollin & Milton, pers. comm., 1999). An understanding of the processes involved within the atmosphere and the scene can be achieved by the use of
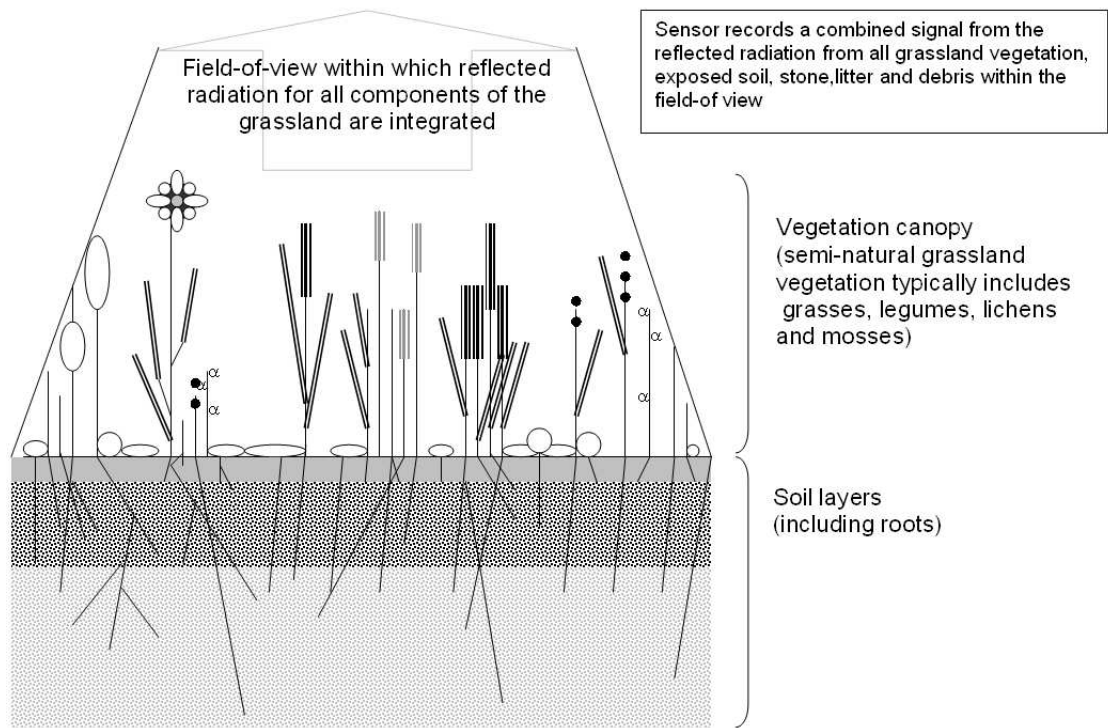
Figure 2.6: A field-of-view of a grassland environment

modelled simulations. For image data an instantaneous FOV is configured in separate picture elements or pixels.

2.5.3.2 Dwell time (integration period)

The dwell time (or integration period) directly affects the quantity of radiation (photons) measured by the sensor and therefore relies on the assumption that reflected radiation is constant within that dwell time. The longer the dwell time and more changeable the atmosphere conditions the less reliable this assumption is. An alternative method of increasing the radiation recorded is to average the measured radiation from successive integration periods.

2.5.3.3 Spectral characteristics

For many targets there is a variation in the radiation that they reflect; this is commonly dependent on the wavelength of that radiation. A spectrum is formed by plotting a series of reflected radiation responses against wavelength. The radiation interactions described in section 2.3 can depend on the wavelength of the radiation. In addition, the measurement of each reflected radiation response is dependent on the characteristics and capabilities of the sensor with which the reflected radiation is measured. The following five terms describe spectral characteristics: spectral resolution, spectral sampling interval, spectral bandwidth, number of bands and radiometric resolution. Spectral resolution is a measure of the narrowest spectral feature resolved by a spectrometer (Anon.). Sampling interval is the interval in wavelength units between data points in the measured spectrum (Anon.). Bandwidth is the wavelength extent over which the estimate of reflected radiation is made, it is characterised by full-width at half maximum (FWHM, see figure 2.7) of an instrument response to a monochromatic signal (Schaepman 1998). The number of spectral bands refers to the extent over which the spectrum is sampled. In its simplest form the number of spectral bands marks the extremes of a continuous sequence of spectral bands found in a spectrometer and a single (or few) bands present in a radiometer.

2.5.3.4 Radiometric brightness grades within the dynamic range

Radiometric resolution determines the number of different brightness grades within the dynamic range that marks the full contrast within each spectral band. It is determined in a practical sense by the time available for analogue/digital conversion. Therefore, it is typically described in terms such as 4 bits; which would provide a contrast range of between 0-15 and 8 bits; which would provide a contrast range of between 0-255.
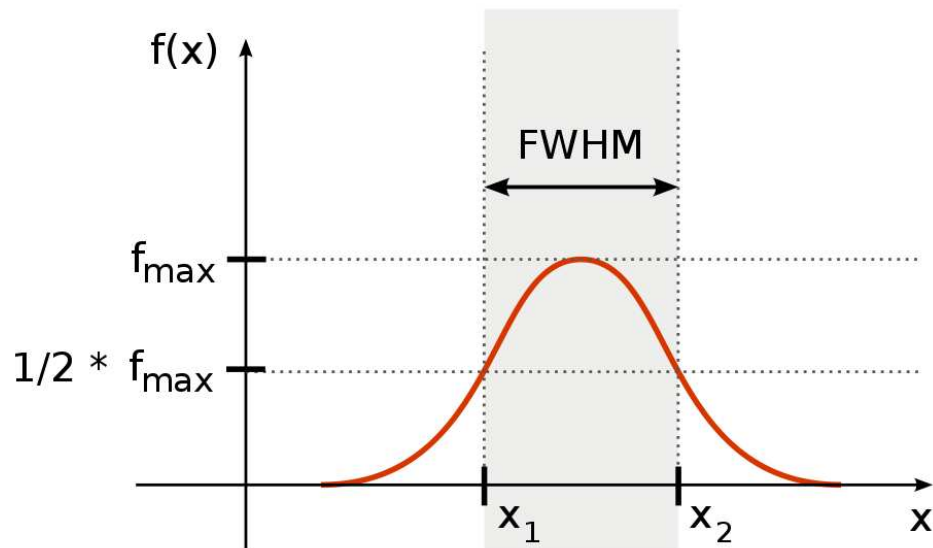
Figure 2.7: Full-width half-maximum. Source: Sharp 2010.

2.5.3.5 Spectrometers

The 'trade-off' between spatial, spectral and radiometric resolution is decided by the requirements for which the instrument was designed (figure 2.5.3.5). Although sensors have had sufficient resolution to identify vegetation by the use of broad spectral bands they have only been able to provide a series of measurements over the red-edge region since the 1960s (e.g., Gates *et al.* 1965). A discussion of the use of remote sensing for the estimation of vegetation variables is further discussed in chapter 3. In addition to spectral data to identify the vegetation a survey requires spatial data for surveying and radiometric data for any but the most rudimentary spectral analysis (figure 2.5.3.5). Therefore, specific regard has been directed to spectroradiometers, spectrometers and imaging spectrometers. Spectrometers sequentially sense a range of wavelengths in a continuous sequence while those that sense in a limited number of pre-set spectral bands are radiometers (Milton 1987). Technological improvements have caused this division to become less distinct, some systems with pre-set bands now provide such a continuous sequence of narrow-spectral bands that they simulate the output available from spectrometers and are often described as such.

Spatial
information

Imagers
Altimeters
Sounders

Imaging
spectrometers

Imaging
radiometers

Spectrometers　　　Spectrradiometers

Radiometers
Scatterometers

Spectral
information

Intensity
information
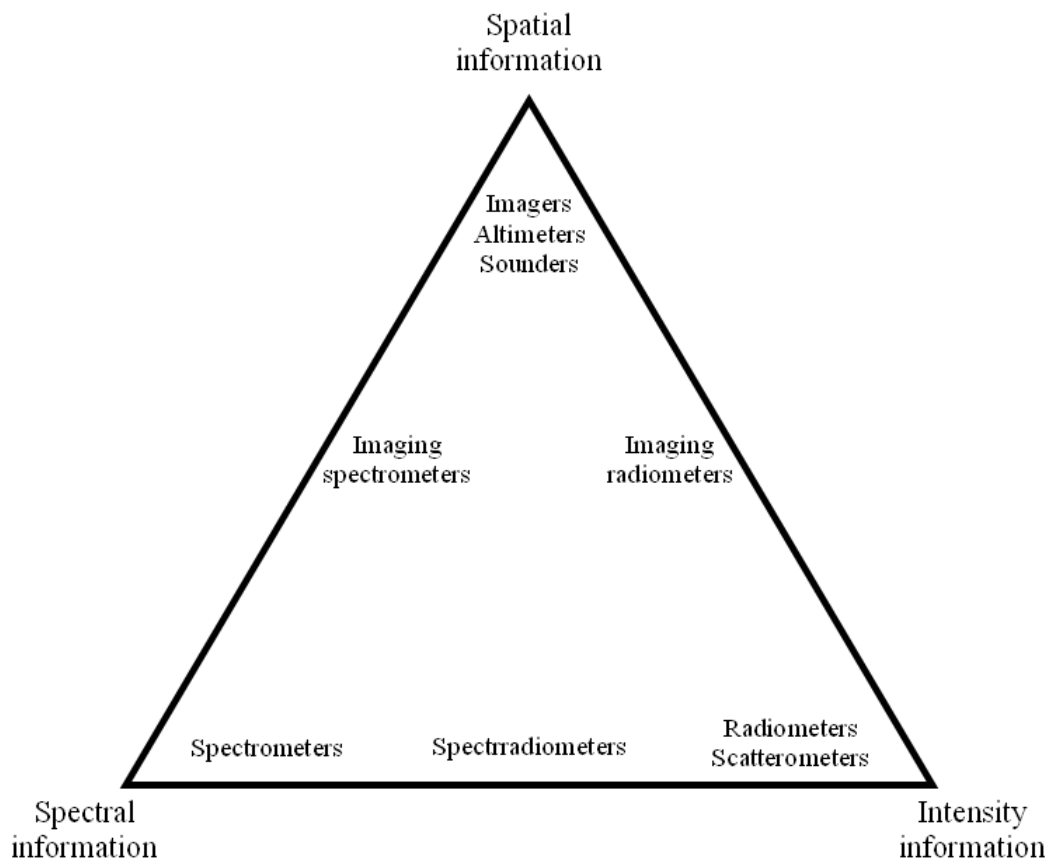
Figure 2.8: Instruments and the trade-off between different capabilities.
Source: Elachi 1987.

2.5.4 Spectrometry

There are essentially two approaches to spectrometry. Both approaches relate to a known spectrum of radiation with one recorded after interaction with a target object or sunstance. One records the spectrum after transmission through the object, while the other records the spectrum reflected from the object. In this second group imaging spectrometers collect spectral data over large areas. Spectral features in grass have been recorded using both transmission (Palta 1990, Yoder and Daley 1990) and reflectance (Milton *et al.* 1995, Pinar and Curran 1996) spectrometry. Transmission spectrometry records the difference between energy applied and energy measured after transmission through a sample.

2.5.4.1 Transmission spectrometry

Transmission spectrometry records the difference between energy applied and energy measured after transmission through a sample. Most transmission techniques use artificial sources of illumination of known output. Nevertheless unless specific biochemicals are first extracted the measurement of transmitted radiation is of limited use for the estimation of vegetation variables. This is because the optical and physical thickness of many vegetation structures (e.g., leaves) restrict the passage of sufficient radiation for accurate analysis. Although transmission spectrometry is generally a laboratory technique, a field instrument for the estimation of chlorophyll concentration is produced by the Minolta company (e.g., Markwell *et al.* 1995; de Rosny *et al.* 1995).

2.5.4.2 Diffuse reflectance spectrometry

Near-infrared reflectance spectrometry (NIRS) measures a sample's spectrum in NIR wavelengths (800 to 2500 nm; Willard *et al.* 1974) in controlled laboratory conditions. Most quantitative analysis is conducted between 1200 and 2500 nm because below 1200 nm the absorption bands are regarded as 'too weak' and above 2500 nm

'too strong' (Norris 1989). Curran (2001) highlights three areas of current NIRS research. These are the biochemical assay of leaves, formulation of theory and technique development. NIRS methods use an empirical multivariate approach to biochemically assay leaves. Many diffuse reflectance evaluations assume infinite depth or semi-infinite homogeneous medium (Lee *et al.* 2001). To obtain laboratory data, these techniques often grind and dilute samples to minimise specular effects (Lee *et al.* 2001).

Two types of instruments may be used for NIRS; the filter-type instruments and the scanning monochromator. Filter-type instruments can be used to estimate the concentrations of moisture, crude protein and oil in cereal grains and oil-bearing seeds (Clark 1989). They measure diffuse reflectance at a set of wavebands determined by a series of interference filters (Norris 1989). Scanning monochromators (SM) are modifications of prism-grating spectrometer technology (Norris 1989). They use the whole NIR spectral region (Clark 1989), chopping the light beam into an on-off sequence causing the wavelength to be recorded at intervals of either 1 or 2 nm (Norris 1989). NIRS methods use an empirical multivariate approach. This assumes that a foliar spectrum is the difference between 100% reflectance and the sum of the absorption features of each biochemical, as weighted by their concentration (Curran *et al.* 1992).

Away from a laboratory, complexities introduced from the interactions of radiation with media and objects other than the target obscure the signal such that it cannot be analysed to the same degree as laboratory spectra. The source of illumination is typically the Sun and the FOV large enough to include more than one component. Nevertheless, reflectance spectrometry in the field successfully identifies absorption features from minerals and vegetation (e.g., Milton *et al.* 1983, Filella and Peñuelas 1994). Remote sensing of green vegetation by reflectance spectrometry needs to consider all the radiation interactions to estimate the effects of the energy transfer pathway in photosynthesis.

2.5.4.3   Imaging spectrometry

With the transfer of instrumentation from laboratory to platforms such as aircraft and satellites, the complexity of the scene is increased greatly. The SNR is decreased but a synoptic capability is obtained allowing spatial patterns to be derived. Early imaging spectrometers were airborne instruments and had an unacceptably low SNR despite recording at a relatively coarse spatial resolution (Curran and Kupiec 1995). The performance of these imaging spectrometers was limited because of the absence of adequate calibration or knowledge of atmospheric attenuation effects (Vane and Goetz 1993). The development of charge-coupled-devices (CCDs) in the 1970's offered the possibilities of recording many pixels simultaneously thus increasing the dwell time, signal and SNR of any particular pixel (Curran and Dungan 1989). The initial development of imaging spectrometry was for mineral identification, but it has developed as a tool for ecological research (Goetz *et al.* 1985). The first imaging spectrometer to cover the 400 - 2500 nm wavelength region contiguously was the Airborne Visible and Infrared Imaging Spectrometer (AVIRIS) (Vane and Goetz 1993). This has led the way for space-borne systems e.g., Medium Resolution Imaging Spectrometer (MERIS) (Curran and Kupiec 1995) though for the reasons identified in table 2.1 the remote position of the instrument places natural limits on the relative quality of data obtained.

2.5.5   Remote sensing applications

NIRS has been used in forage research (e.g., Coleman 1989) for both grass (e.g., Winch and Major 1981; Counts and Radloff 1979; Barton II and Burdick 1983; Minson *et al.* 1983) and cereal (e.g., Williams 1975; Watson *et al.* 1976; Stermer *et al.* 1977; Rubenthaler and Bruinsma 1978) studies. Scanning monochromators have been used in a variety of grassland research (e.g., Shenk *et al.* 1981; Marten *et al.* 1983; Marten *et al.* 1984; Norris *et al.* 1976) including the identification of legume-grass mixtures (Shenk *et al.* 1979).

Multispectral instruments tend to use broader wavebands and / or discontinuous measurement sequences. Spectrometery instruments tend to have fine wavebands (6 nm or less) and a continuous series of spectral measurements. Data from multispectral and spectrometry systems can identify areas of grazing (Todd *et al.* 1998), estimate the area of green leaves per unit ground area (Wardley and Curran 1984; Curran and Williamson 1985; Curran and Williamson 1986; Curran and Williamson 1987; Curran and Williamson 1988; Strub *et al.* 1998) and estimate the amount of chlorophyll in a grassland canopy (Pinar and Curran 1996). Multispectral techniques have also been used for the identification of roosting areas for wildfowl (Milton *et al.* 1995) and the mapping of contaminated grassland (Jago and Curran 1996; Jago and Curran 1997; Jago *et al.* 1999).

Remote sensing research on cereal crops, spring wheat (*Triticum aertivum*) (e.g., Horler *et al.* 1983b, Schutt *et al.* 1984, Boochs *et al.* 1990, Munden *et al.* 1994, Cutler and Curran 1995, Cutler and Curran 2000, Yang *et al.* 1999, Yang *et al.* 2000) and maize (*Zea mays*) (e.g., Horler *et al.* 1983b, Mariotti *et al.* 1996, McMurtrey *et al.* 1994) may also have relevance to the study of grassland.

2.6 Conclusion

Our understanding of the action of radiation in our environment allows sensor data to be used to estimate variables related to a remote target. This has been a particular success with the observation of vegetation because of a spectral feature known as the red-edge. Most vegetation indices (VIs) use the red-edge and have provided good service to the remote sensing community for the establishment of general relationships with specific vegetation state variables, especially chlorophyll. These VIs have been conceptually and empirically derived but the specific interaction of variables is concealed in each VI as they are by definition a summary albeit focused to specific application. VIs have also been developed to process large data sets efficiently. This has been essential as the data volumes produced by instrument develement place an

ever increasing load on the capability to store and process data. However most of the VIs that are applied to narrow spectral resolution data either use simple ratios of narrow-bands (modified from existing broadband VIs) or are REPs in existence since the 1980's.

Although reflected radiation is rarely directly influenced by soil contamination it is influenced by changes in vegetation variables and in some cases these may be influenced by soil contamination. The full potential of remotely sensed data needs to be explored for the evaluation of the vegetation changes associated with soil contamination. There is a need to understand the influences of both the soil contamination $\Rightarrow$ state variable relationship and the state variable $\Rightarrow$ reflected radiation relationship. Any robust, non-site-specific technique for inferring relative levels of soil contamination requires a greater understanding of what VIs actually indicate, how changes in different vegetation variables influence them and how they relate to soil properties.

The nature of each spectrum is dependent on the target, atmosphere and the instrument used to conduct the measurements. While applications provide a focus for the collection of remotely sensed data, the discipline is technology-led. Instrument considerations determine the spectral bandwidth, number of bands, radiometric resolution, precision, size of the instantaneous FOV, the integration time/dwell time needed to collect the data and the portability and durability of the instruments. Developments in sensor technology have provided smaller, lighter instruments with increasingly narrower-spectral resolutions and finer-spatial and radiometric resolutions; 16+ bit processing and a high SNR are now common. However, improvements are spreading beyond the laboratory and field instruments to airborne and satellite systems. These provide a synoptic capability that addresses the spatial problems present in the location of contaminated soil and the technological developments should allow us to achieve this with increasing efficiency. Our responsibility is to be ready with proven techniques for when the next series of improvements arrive.

Chapter 3

Literature review

3.1 Introduction

Within this chapter, I will build on those general descriptions of remote sensing identified in the previous chapter (2.1) and focus on their application for the identification of contaminated soil. Soil can contain: heavy metals, hydrocarbons (aqueous or gas phase), salt and various substances that may induce acid, alkali, anaerobic or mineral impoverished conditions. Two key factors that determine if a substance is termed a contaminant are (i) if it is naturally occurring or (ii) if the concentrations present are sufficient to have an effect on the environment. However, for the purposes of this review, I shall regard naturally occurring substances with high concentrations as contaminants. This is because many of the techniques used to identify mineral deposits have parallels in the identification of soil contamination that has been present for a long period of time.

Soil contamination can only rarely be measured directly by remote sensing. However, in some situations this may be achieved. Hydrocarbons can be identified from spectral data (Clutis 1989). Hörig *et al.* (2001) and Kühn *et al.* (2004) studied sand contaminated with lubricating oil. They used a GER Mark V IRIS IIR field spectrometer and

identified absorption maxima at about 1730 nm and 2310 nm but found that the signal was obscured if the contamination was covered by sand (Hörig *et al.* 2001). Similarly, Choe *et al.* (2008) used a spectral response in HyMap data at about 2200 nm to identify heavy metals in soil. The remote sensing of disturbed ground has also been used to indicate potentially contaminated soil (e.g., Lomas-Clarke and Williamson 1998; White *et al.* 2008) and is typically used in conjunction with *a priori* information. More common and easier to measure (using remote sensing) are those effects that a contaminant has on the environment, specifically on vegetation. This review will specifically consider those effects of soil contamination that may affect the reflectance (or emission) of radiation from vegetation growing in conditions where soil is contaminated. The field work that follows this chapter will focus on semi-natural grassland. Therefore a brief description of grass and grassland will be followed by an account of how grassland may influence relected radiation and be affected by soil contamination.

3.2   The effect of soil contamination on vegetation

The above-ground manifestations of plant stress are differences in the leaf area, leaf pigments and on vegetation metabolism and physiology (figure 3.2). More specifically, when vegetation is under negative stress the total leaf chlorophyll content and the ratio of chlorophyll *a* to chlorophyll *b* decreases (Fang *et al.* 1998; Carter and Knapp 2001). The spectral region where change in chlorophyll is most evident is known as the red-edge (Carter 1994) because it marks an abrupt increase in reflectance at the boundary between the longest visible wavelengths and the near infra-red (NIR)(see chapter 2.1).

Studies on the red-edge have assessed a wide variety of vegetation types and stress factors, examples include senescence (Miller *et al.* 1991), disease (Malthus and Madeira 1993), water stress (Filella and Peñuelas 1994), iron deficiency (Mariotti *et al.* 1996) as well as stress imposed by heavy metal (Horler *et al.* 1980; Horler *et al.* 1983a; Horler *et al.* 1983b; Collins *et al.* 1983; Chang and Collins 1983; Darch and Barber 1983; Milton and Mouat 1989; Banninger 1991; Farrand and Harsanyi 1997; Ferrier 1999)
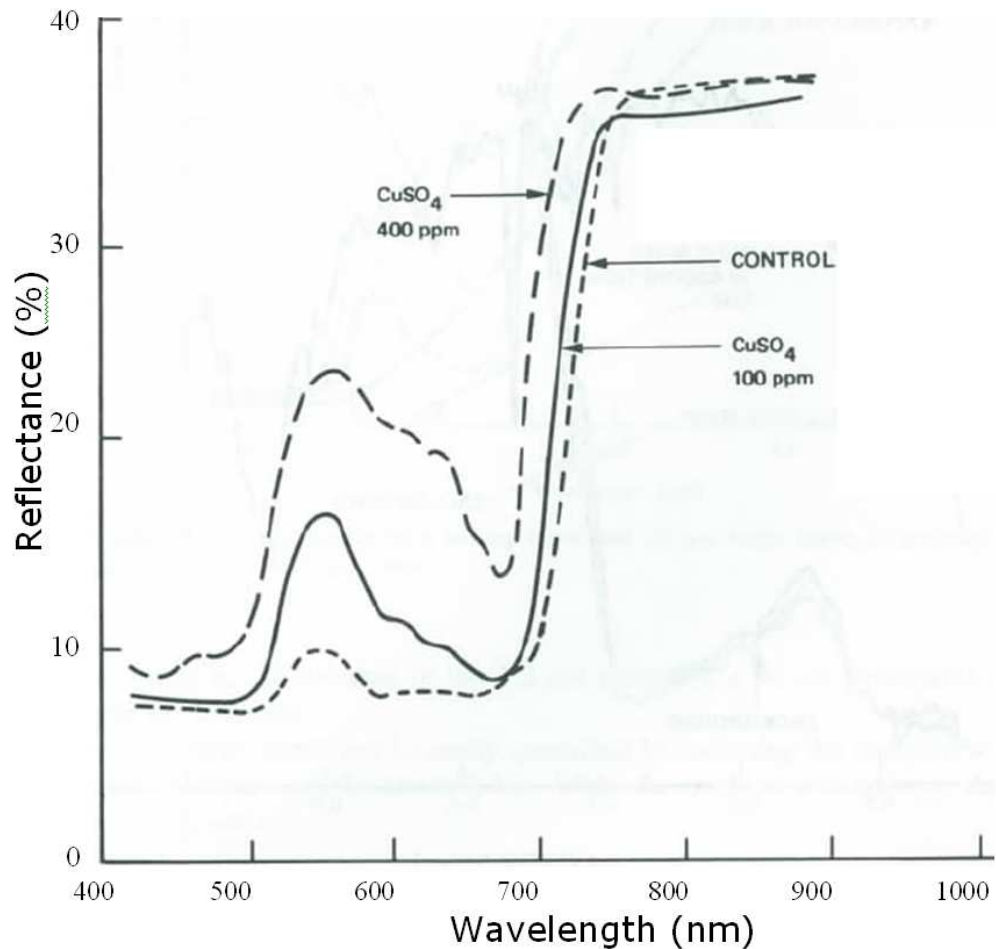
Figure 3.1: The effects of copper sulphate contamination on vegetation. Source: Chang and Collins 1983.

and hydrocarbon contamination (Bammel and Birnie 1993; Yang *et al.* 1999; Yang *et al.* 2000) (e.g., figure 3.1). Additionally, iron deficiency in a plant can be caused by the antagonistic effect of high soil concentrations of chromium (Cr), cobolt (Co), copper (Cu), manganese (Mn), nickel (Ni) and zinc (Zn) (Brooks 1972).

3.2.1　The effect of hydrocarbon contamination on vegetation

Shorter chain aqueous phase hydrocarbons (nC_5 to nC_9) have a toxic effect on the tender portions of plant shoots and roots but have little effect on the woody parts
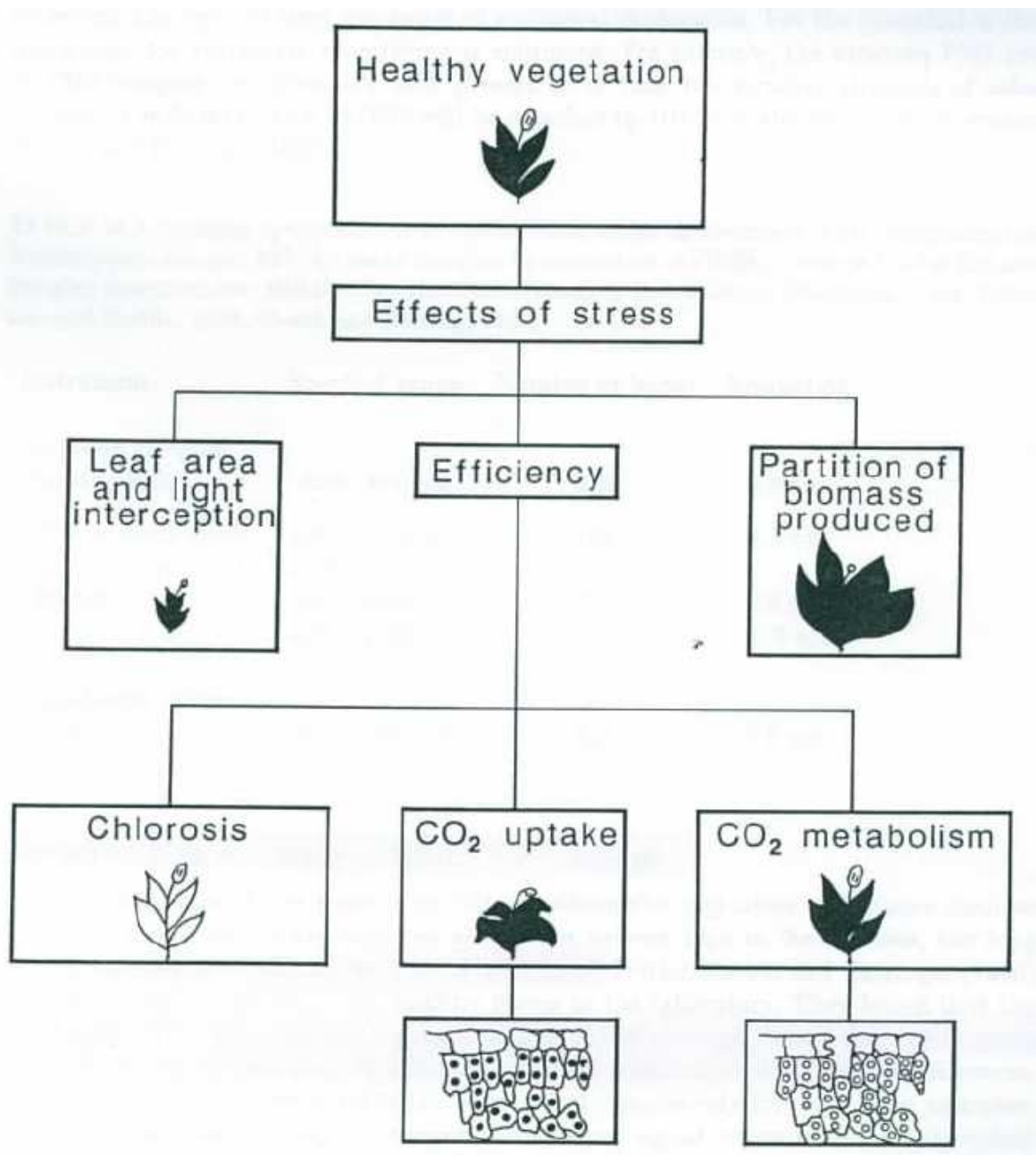
Figure 3.2: Schematic model of vegetation responces to stress. Counter-clockwise from top: Healthy vegetation; reduction in leaf and light interception; loss of chlorophyll (represented by white leaves); reduction of CO_2 uptake by close of stomata; restrictions to the uptake and metabolism of CO_2 within the cell; changes in the partition of biomass produced, leading to a reduction in the total harvestable component.
Source: Steven *et al.* 1990.

Table 3.1: Biochemical effects of excessive concentrations of heavy metals in plants. Source: Kabata-Pendias and Pendias 1984

Elements	Biochemical effect
Ag, Au, Cd, Cu, Hg, Pb, F, I, U	Changes in the permeability of cell membranes
Hg	Inhibition of protein synthesis
Ag, Hg, Pb, Cd, Tl, As(III)	Bonding to sulphydryl groups
Most heavy metals, Al, Be, Y, Zr, lanthanides	Affinity for phosphate groups, and ADP, AATP groups
Cs, Li, Rb, Se, Sr	Replacement of essential atoms
Arsenate, selenate, tellurate	Occupation of sites for essential groups, e.g. PO_4^{3-}, tungstate, bromate, fluorate
TL, Pb and Cd	Inhibition of enzymes
Cd, Pb	Decrease in respiration
Cd, Pb, Hg, Tl, Zn	Decrease in photosynthesis
Cd, Pb, Hg, Tl, As	Decrease in transpiration
Cd, Co, Cr, F, Hg, Mn, Ni, Se, Zn	Chlorosis

of shrubs (Siddiqui and Adams 2002). Remote sensing studies have mapped plants affected by hydrocarbon stress (Bammel and Birnie 1993; Jago *et al.* 1999; Smith *et al.* 2000; Li *et al.* 2005; Silvestri and Omri 2008) and linked the presence of hydrocarbons to negative physiological effects on the plants. The negative effects of gas seepage (primarily methane and ethane) on vegetation (e.g. (Steven *et al.* 2006) have been attributed to changes in the availability of soil oxygen related to soil bacteria and soil mineralogy; more generally ethane (in particular) has been described as decreasing the photosynthetic activity of plants (Noomen *et al.* 2006). Conversely in other conditions gas seepage may provide fertilisation for a crop (Yang *et al.* 1999). In such studies, (e.g., Yang *et al.* 2000; Smith *et al.* 2000; Noomen *et al.* 2003; Noomen *et al.* 2006; Steven *et al.* 2006) reflectance spectra showed differences between those areas exposed and unexposed to the gas.

3.2.2 The effect of heavy metal contamination on vegetation

High concentrations of heavy metals are toxic to plants ((Joshi and Mohanty 2004; Mishra and Gopal 2005; Ouzounidou *et al.* 2006) and may cycle via flora and fauna on a seasonal basic (Darch and Barber 1983). As with many other heavy metals, high concentrations of nickel (Ni) reduce the metabolic activity and growth of plants (Gopal *et al.* 2002). Those plants that are not killed may be impaired and outcompeted by plant types (or evolved varieties) more suited or tolerant to local conditions. Essential nutrients for plant growth are nitrogen (N), calcium (Ca), phosphorous (P), potassium (K), sulphur (S), and magnesium (Mg) but minor or trace elements are also required: iron (Fe), manganese (Mn), copper (Cu), boron (B), molybdenum (Mo) and zinc (Zn). Soil nitrogen is of particular importance because of its relationship with photosynthesis (Taiz and Zeiger 1998). Other minor elements also occur in plants; these are not essential for growth and include sodium (Na), chlorine (Cl), aluminium (Al), silicon (Si), selenium (Se) and cobalt (Co) (Spedding 1971). Many of these elements can have an adverse effect on vegetation (table 3.1). The difference between a classification of an element as a nutrient or contaminant may be dependent on environmental concen-

tration, though an element can simultaneously have a beneficial and malign effect on different plant processes or have modified effects when present in combination with other elements.

For many years, remote sensing used this principle to identify mineral deposits (e.g., Collins *et al.* 1983), from contamination to mining (e.g., Farrand and Harsanyi 1997, Ferrier 1999, Kemper and Sommer 2003), geobotanical anomolies (e.g. (Darch and Barber 1983) and floodplain deposits of heavy metals (e.g., zinc and cadmium, Kooistra *et al.* 2001; Kooistra *et al.* 2003) and has been broadly expanded to identify heavy metal stress on grassland (e.g., Zagajewski 2001). A specific example of vegetation stress is the effect of lead (Pb), cadmium (Cd), nickel (Ni) and titanium (Ti) on *Helianthus annuus* (sunflowers). The inhibition of transpiration in this species was attributed to reduced stomatal functioning (Bazzaz *et al.* 1974; Bazzaz *et al.* 2006) and the effect on photosynthesis of a reduction in chlorophyll content (e.g., Bazzaz and Govindjee 1974). Bazzaz *et al.* (1974) demonstrated that rates of photosynthesis and transpiration were halved (in *Helianthus sp.*) if the root system was exposed to high concentrations of heavy metals (higher than 193ppm of Pb, 96ppm of Cd, 79ppm of Ni or 63ppm of Tl) (Lagerwerff and Specht 1970; Rolfe 1973).

3.2.3   The effect of other contamination on vegetation

Other contaminants can have a variety of effects on vegetation. For example Richter *et al.* (2008) found that mine tailings, a primary source of acid mine drainage (AMD), were detectable at the Kam Kotia mine (Ontario, Canada) using remote sensing and spectral mixture analysis due to the negative effect the AMD had on vegetation. Other contaminants can react to cause deficiencies in oxygen or essential minerals and therefore cause vegetation stress by a more indirect pathway. Beans (*Phaseolus sp.*) exposed to magnesium (Mg) deficiency suffer interveinal chlorosis (followed by necrosis) on their leaves (Marschner and Cakmak 1989; Chaerle *et al.* 2007). Similarly, iron deficiency (Mariotti *et al.* 1996) and excessive soil water salinity (Farifteha *et al.* 2007; Farifteha *et al.* 2007; Naumann *et al.* 2008) or water status (e.g., Suárez *et al.* 2008) can have

a severely detrimental effect on plant growth.

3.2.4   The effect of biotic stress on vegetation

Many other experiments have artificially treated vegetation with agents likely to cause stress. For example, Carter *et al.* (1996) treated *Pinus sp.* (pine trees) with a herbicide (diuron, DCMU) and reported that a spectral response around 694 nm was more sensitive than previously used thermal data for the detection of stress effects. They attributed this sensitivity to the narrowing of the absorption response by chlorophyll in the 690 to 700 nm range (as per Gates *et al.* 1965; Gates 1980). Further investigations have observed the effects of common environmental variables capable of inducing stress, such as water availability, humidity and heat. Dobrowski *et al.* (2005) used heat and water restriction to investigate *Vitis sp.* canopies (grapevine), and concluded that these stress agents affected the plant's photosynthetic status. Similarly, a range of infections (fungal and invertebrate) (e.g., Sterckx *et al.* 2003) have a variety of effects on specific vegetation types but may be summarised as having a negative effect on growth and metabolic / photosynthetic efficiency. Studies of these effects have used a range of instruments and platforms, from the field systems (e.g., ASD FieldSpec Pro), to airborne systems (e.g., AVIRIS, AISA Eagle) and to satellite systems (e.g., IRS-P3-MOS-B). In most cases the success is not only related to the vegetation type and the contaminant but also the spectral (and to some extent spatial) resolution of the sensor system. Quite simply, the finer the resolution, the richer the range of spectral tools available.

3.2.5   Proximity of roots to soil contaminants

A plant's uptake of nutrients from the soil is controlled by its root system and the supply of water. Therefore, the primary mechanism by which soil contamination impacts vegetation is by transfer through their roots. A determining factor as to whether a plant suffers the effects of a soil contaminant is the proximity of the plants roots to

the contaminant. The rate at which a plant absorbs an element from the soil (table 3.2) (as indicated by the root transfer coefficient) may be species-specific, dependent on soil organic matter or soil pH (Kloke *et al.* 1984). In general the longer the root system the less transfer of elements to the upper part of the plant (Brooks 1972). The difference between shallow and deep-rooted species may be due to the greater difficulty of translocation of ions through the root system (Brooks 1972) where ions tend to accumulate in aerial parts situated on the same side of the plant as to where they are located in the root-zone (Brooks 1972). Indications of soil contamination are therefore dependent on the type of root system and the relative position of soil contamination (figure 3.3).

Different vegetation types, and specific species, have different root depths. Therefore, one plant may be affected while another, growing immediately next to the first may be unaffected. Figure 3.3 demonstrates the limitations of basing an assessment of contamination on a single piece of evidence. One effect of aluminium (Al) toxicity is the inhibition of root growth (Ryan *et al.* 1993) but tolerant varieties of wheat (*Triticum sp.*) have mechanisms to exclude Al from the root meristems (Samuels *et al.* 1997).

Table 3.2: Root transfer coefficients of heavy metals in the soil-plant system.
Root transfer coefficients refer to the concentration of metal in areal portion of the plant relative to the total concentration in the soil. High values indicated rapid transfer rates.
Source: Kloke *et al.* 1984

Elements	Root transfer coefficient
Cd, Ti & Zn	1-10
Hg, Ni, Pb & Se	0.1-1
As, Be, Co, Cr, Cu, Pb & Sn	0.01-0.1
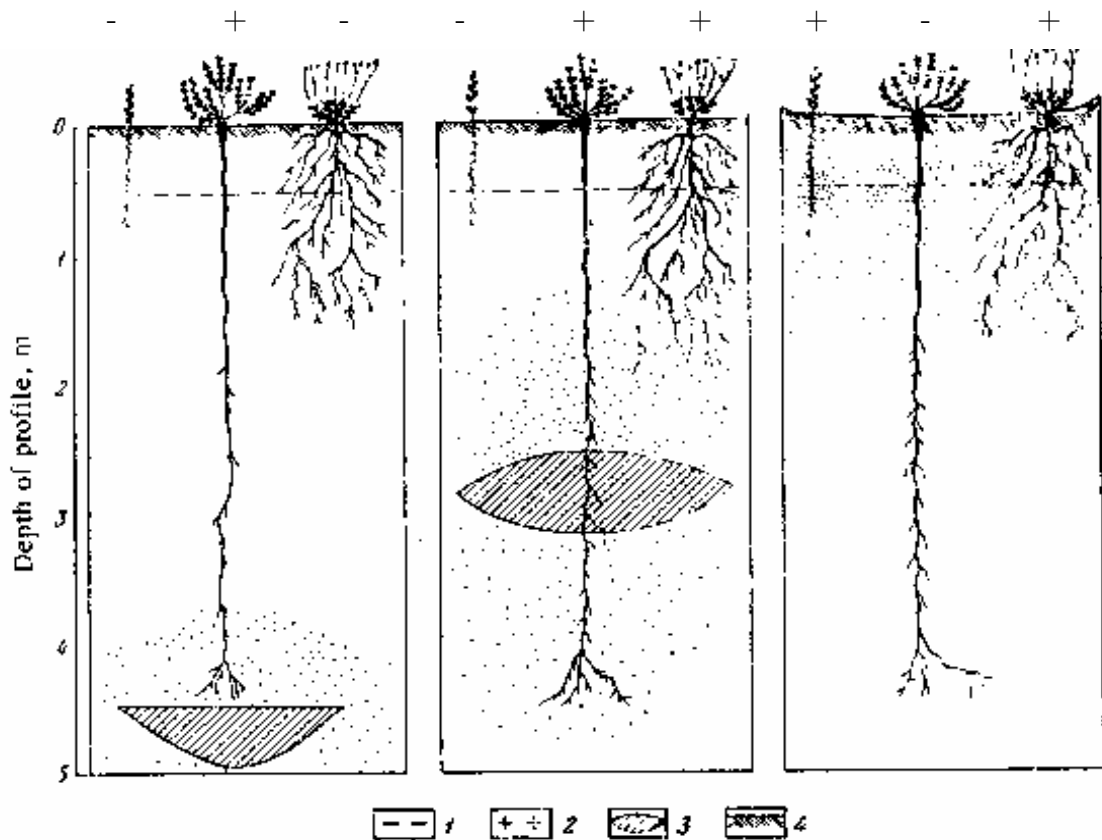
1. Background concentration of contaminant in plant.

2. High contaminant concentration in plant.

3. Horizons enriched by contaminant.

4. Soil.

5. (dots) Secondary enrichment by contaminant.

Figure 3.3: Plant indicators as a function of the root system

Adapted from Brooks (1972) and Malyuga (1964).

3.3 Temporal considerations

A soil contaminant may affect vegetation temporal characteristics in two ways. One is the seasonality of plant maturation and senescence and the other is a change to
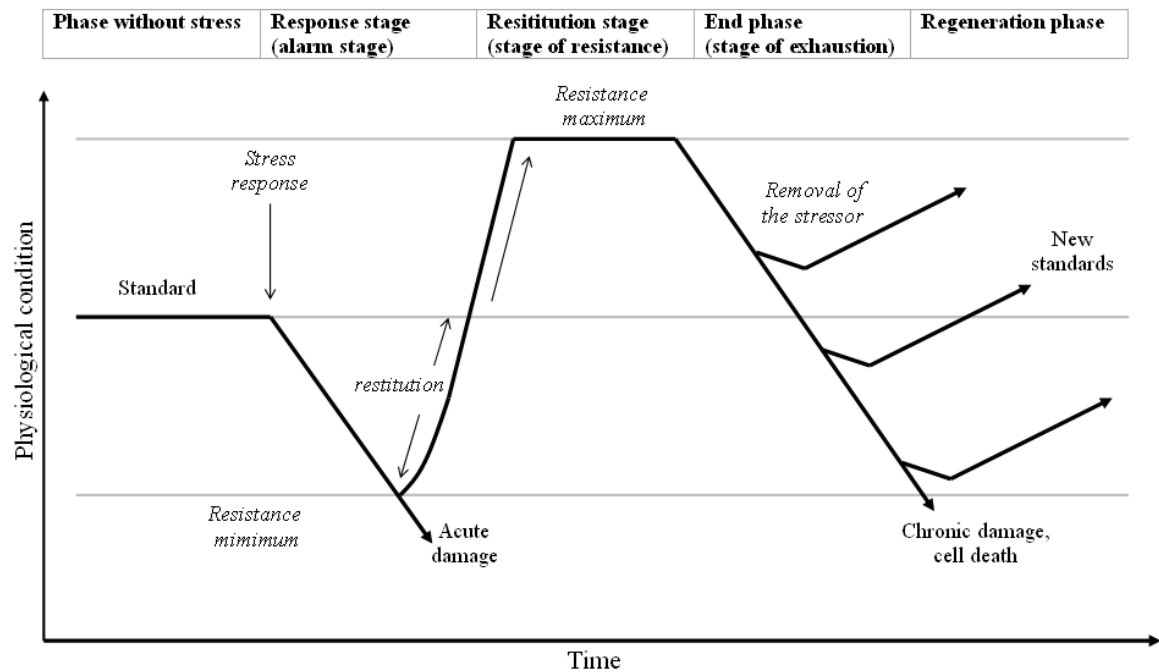
Figure 3.4: General concept of the phase sequences and responses in plants by stress exposure. Source: Lichtenthaler 1996.

the vegetation profile. The vegetation profile is the combination of species types, biomass, height, health and structure within an area of ground. The contribution of time to a vegetation profile may be considered using Lichtenthaler's (1996) four stages of vegetation stress related to the severity and duration of exposure (figure 3.4). These are the response stage (the beginning of the stress), the restitution stage (continuing stress), the end phase (long-term stress) and the regeneration phase. The difference between these stages is a reasonable expectation, especially if long-term contamination stress and the immediate effects of a contamination are compared. A long-term exposure to ground contamination can cause a change in species dominance and an evolution of species tolerance to a contaminant.

Some vegetation species can evolve a tolerance in less than ten years (Wu *et al.* 1975) and studies have found that tolerant and non-tolerant varieties of *Festuca rubra* showed little or no spectral difference as a response to nickel contamination (Hardy *et al.* 2001). Examples of the effects of very long term contamination stress maybe the emergence

of indicator species (Milton and Mouat 1989). Indicator species are divided into two classes according to their distribution; universal indicator species and local indicator species (Brooks 1972). Universal indicator species will only grow under certain soil conditions. For example, *Viola calaminaria* (calamine violet) will grow with high concentrations of zinc and *Becium homblei* (copper flower) with high concentrations of copper (Peterson 1993). Local indicators are species that have adapted to tolerating the ground in which they grow but are able to grow elsewhere providing that there is not major competition from other species (Brooks 1972). Both universal and local indicators can have a primary and secondary component. Primary indicators have a direct response to the element or compound while secondary indicators are influenced by indirect factors such as a change in pH or water availability.

> *"Plants growing at a physiological standard condition will respond to and cope with stress. After removal of the stressor(s), new standards of physiology can be reached depending on time of stressor removal as well as the duration and intensity of the stress."*

Lichtenthaler 1996, p.8

The interaction of species with time can act over different periods of time. Specialised seleniferous, nickeliferous and uraniferous flora, for example, have developed over geological time, whereas recent pollutant emissions have given rise to apparent metal-tolerant vegetation (Peterson 1971; Peterson 1979; Peterson 1983). With recently evolved metal-tolerant varieties a gradation between low and high degrees of tolerance can be measured (Peterson 1983). In the shorter term, microbial activity in the soil due to hydrocarbon degradation can result in competition for soil nitrogen and an abundance of *Legminosae* (legumes), e.g., *Trifolum sp.* (Gudin and Syratt 1975). Their increase may be attributed to the competitive advantage offered by the symbiotic nitrogen fixing relationship with *Rhizobium sp.* and the presence of growth regulators in common hydrocarbon contaminants (Gudin 1973).

3.4   Grass and grassland

Grassland is a combination of vegetation, debris and soil of which grass forms a fundamental component. Within a scene these separate elements are integrated into a single remotely sensed signal. However, more generally the distribution of grassland is dependent on climate, geology, topography, ground water, salinity (of ground water and atmosphere) and human influence. Most British grassland is a biotic plagioclimax, i.e., composed of 'vegetation stabilised by pasturing' (Tansley 1939) and varying degrees of contemporary land management, i.e., mowing and the application of fertilisers, pesticides and herbicides. The agricultural distinction between sown and semi-natural grassland (Davies 1960) relates to the degree by which the land is actively managed and greatly affects the structure and species richness. A sown grassland, regularly mown and with a high application of chemicals (e.g. a bowling green) will typically have low species richness (few species) and a short clipped erect structure. In contrast, an area of semi-natural grassland is characterised by its large number of species where grasses may represent only 10 - 20 per cent of that number (Spedding 1971), and will typically have a tall, seasonally changeable structure. This study focuses on semi-natural areas of grassland that have a low level of land management and are typically mown only once or twice a year which acts to minimise the presence of pioneer shrubs.

3.4.1   The structure of grasses

Grass (*Poacea*, formally *Gramineae*) is a family of low growing monocotyledonous plants that are widespread in the British Isles and are able to adapt to a variety of harsh environments. Grass has a structure of roots, stems, leaves, flowers and seed heads (figure 3.5). The stem (culm) is formed by cylinders of unequal length jointed by nodes; where the hollow portions between nodes are called inter-nodes. Leaves are generally long and narrow with parallel veins and arranged in two rows alternating on opposite sides of the stem and originating from the nodes. The flat portion of the leaf is termed the blade while the cylindrical basal section is termed the sheath. At the

junction between sheath and blade is a thin whitish membranous outgrowth known as the ligule. More comprehensive descriptions of the structure and variety of the grasses in the British Isles are available in Hubbard (1984).
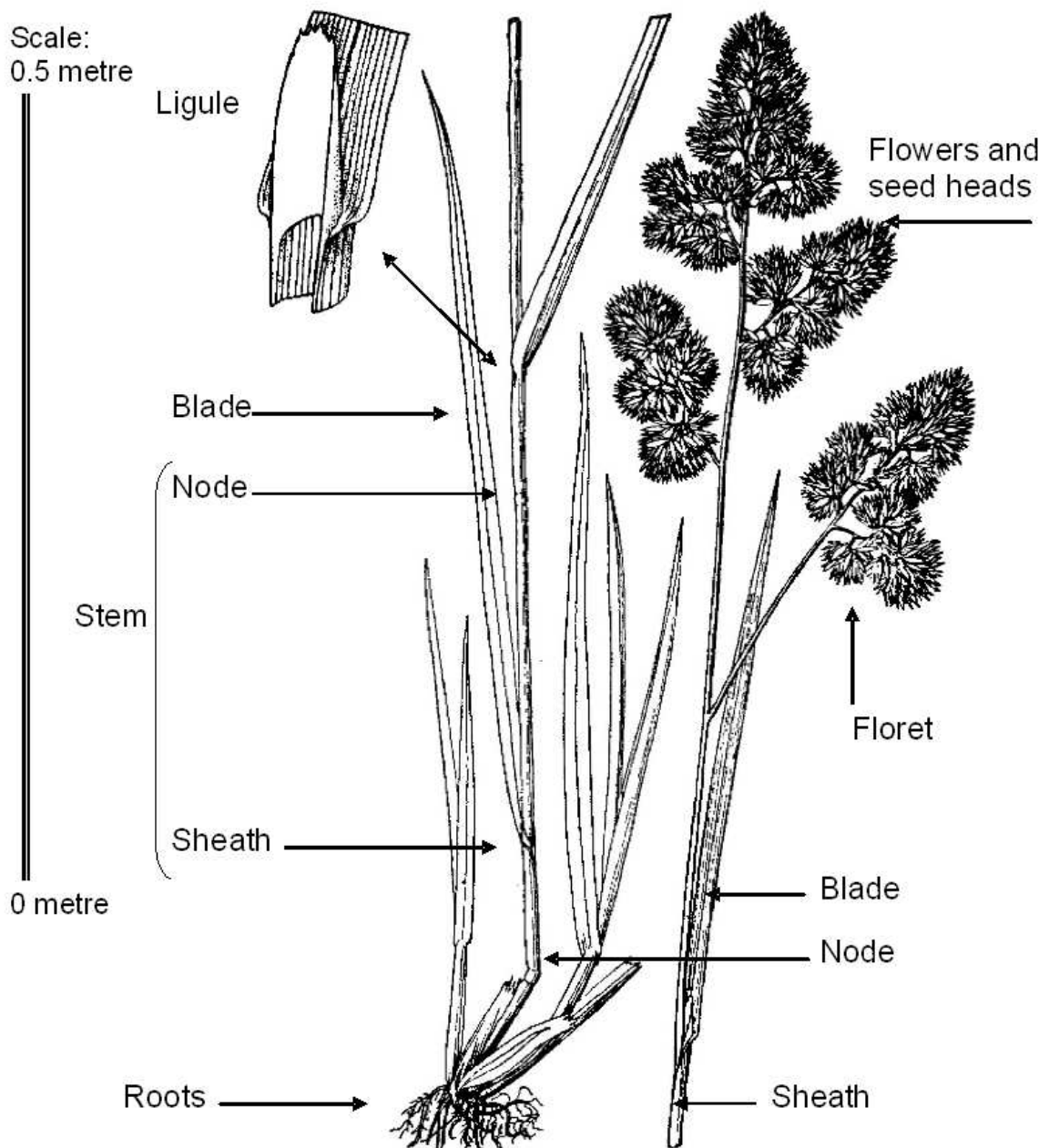
Figure 3.5: The structure of grass (*Dactylis glomerata*). Adapted from Hubbard 1984

3.4.2   The structure of a grass canopy

"Canopy structure and composition are defined by the leaf area, number of layers, and leaf angle distributions within the canopy and the distribution of different canopy components, specifically the stems, green foliage, and litter and finally the soil and understory vegetation if the vegetation has multiple layers."

Ustin *et al.* 1999, p.199

A grass canopy structure includes the leaf density, the relative positions and angles of leaves and the presence of stem and head assemblages. Many aspects of the canopy are described by indices. Four examples of indices are the leaf area index, extinction coefficient, leaf angular distribution and leaf overlap index. The leaf area index (LAI) is the ratio of leaf area (one side only) to ground area (e.g., Curran 1980). The extinction coefficient (K) is the ratio of leaf area when it is projected onto the ground, to the total leaf area (Pearson and Ison 1987), though this is strictly only true for black leaves (pers. com. M. Steven). The leaf angle distribution (LAD) describes the relative inclination of the leaf (Kimes *et al.* 1987) and the leaf overlap index (LOI) describes the amount of duplicated coverage (Ferns *et al.* 1984). Erect canopies with vertical leaves (e.g., grasses) in which K may be about 0.3, require a substantially higher LAI for complete interception of radiation ('canopy closure') than do prostrate canopies, e.g. legumes, where K may be 0.7 - 0.9 (Pearson and Ison 1987). Grasses may intercept virtually all (95 percent) radiation at LAIs of 6 - 9 whereas temperate legumes will do so at LAIs of 2.5 - 4 (Pearson and Ison 1987). Where less radiation is intercepted, growth will be reduced (Warren-Wilson 1971). The contribution of litter, understory and soil will be discussed in section 3.8.2.

3.4.3   The structure of grassland

Where grassland is not subject to intensive management it contains a wide variety of species, including grasses, flowering plants and legumes (Hubbard 1984). Semi-natural grassland is a plant community in which the dominant species are perennial grasses, where there are few or no shrubs and no trees (Moore 1964). Legumes (Leguminosae) are a major constituent of natural grassland and for both grasses and legumes most of the biomass seasonally dies back (Spedding 1971). Grassland species may be described as annuals, biennials or perennials. Annual varieties have a one-year growth cycle, biennial varieties have a two-year growth cycle with seeding and flowering in successive years. Perennial varieties last for longer and tend to have tufted tussock to prostrate, creeping or straggling forms (Barnard 1964), spreading either over the surface of the soil by creeping stems termed stolons (e.g., *Agrostis stolonifera*) or through the soil by rhizomes (e.g., *Poa pratensis*).

Daily flowering periods may be regular among individual plants but may be influenced by weather with florets remaining closed on dull or wet days (Hubbard 1984). Most of the grasses of the British Isles flower during May, June and July with the greatest number in bloom towards the end of June and early in July. Flowering may last for 4 - 12 days (mostly 7 - 8) and most grasses flower only once a day. This single period may be either in the morning (4:00-9:00 hrs.), midday or afternoon and evening (15:00-19:00 hrs.) (Hubbard 1984). Therefore, the time of day at which a survey is conducted can affect the range and type of grassland species in flower.

3.5   The remote sensing of grass and grassland

Remote sensing has been used to estimate primary productivity (e.g., Pearson and Miller 1972, Tucker and Sellers 1986), biomass (e.g., Todd *et al.* 1998, Tucker 2006), forage quality (e.g., Marten *et al.* 1989) and for the indication of environmental conditions (e.g., Jago *et al.* 1999). Remote sensing surveys have ranged from the scale of

a leaf (e.g., Schutt *et al.* 1984) to that of a continent (e.g., Tucker and Sellers 1986). They have explored change in reflectance over time (e.g., Kanemasu 1974), variations with wavelength (e.g., Rabinowitch 1951) and the effects of both viewing and illumination geometry (e.g., Guyot *et al.* 1992). In this review I have restricted discussion to techniques that use visible / near infrared (NIR) wavelengths, indices that use the red-edge spectral region and factors that influence the red-edge.

3.6   State variables

State variables are the smallest set of variables that are needed to fully describe the physical state of the system under consideration (Verstraete and Pinty 1996). For remote sensing in optical and NIR wavelengths, state variables relate to the variables that absorb, emit, refract or reflect radiation and are associated with the scene (e.g., atmosphere and background) and a target of interest (Curran *et al.* 1998). Two types of state variable characterise a system: those that define constituent properties and those that define configurational properties (Huggett 1993). Constituent properties are specific components that influence reflectance, e.g., concentration of photosynthetic leaf chemicals. While configurational properties are those that influence the quantity of constituent, properties such as the amount of a constituent property observed in a FOV e.g., leaf area per ground area.

Remotely sensed data attributed to a target can only provide indirect estimates of state variables (figure 3.6). State variables cannot directly provide information concerning factors that do not themselves alter the spectral response of a target. Also they can not distinguish between the similar (or equifinal) effects of multiple state variables because most soil contamination does not directly influence radiation in the visible or NIR wavelengths. To maintain a conceptual understanding of how soil contamination is being identified, any technique used to estimate levels of soil contamination should identify, those state variables affected by the contamination.
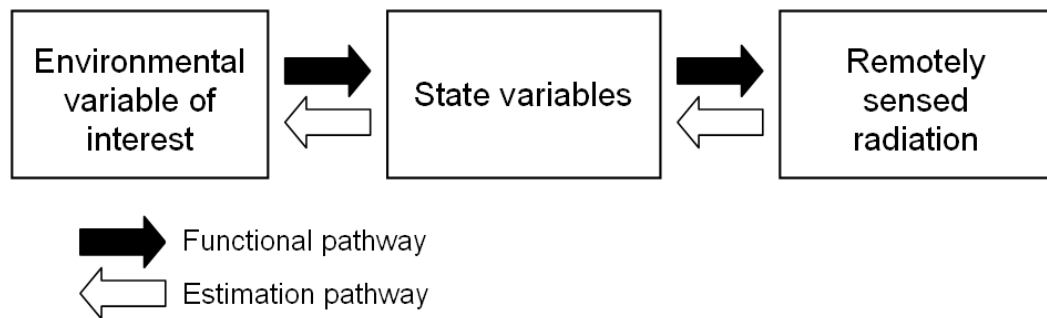
Figure 3.6: The indirect nature of the relationship between remotely sensed radiation and the environmental variable of interest. Source: Curran *et al.* 1998

3.7   The grassland red-edge at the leaf scale

The red-edge is the spectral boundary between red ($\sim$690 nm) and NIR ($>$700 nm) wavelengths. In terrestrial vegetation this spectral region marks the transition between the light harvesting processes of photosynthesis and the cellular scattering promoted by vegetation structure. The contrast between high absorption in the red wavelengths and high scattering in NIR wavelengths has proven the basis for many spectral indices designed to identify vegetation (vegetation indices), its amount and its health. However, to evaluate the effect of soil contamination on vegetation we must first identify those influences on vegetation state variables in the absence of soil contamination.

At the leaf scale, the influence of independent variables can be controlled but when measurements are conducted at the canopy scale the accuracy of the variable estimated may be decreased. At the canopy scale, variables that describe the uniformity and structure of the canopy become important as they are likely to exceed the variation found in a single leaf. At the canopy scale, a remote sensing system integrates a signal over a field-of-view. The signal is therefore less influenced by extreme components but can also be regarded as less sensitive to them. This means that important data can be missed because it is diluted among 'normal' levels. Such data are only resolved if the spatial scale of measurments are sufficient to capture specific spatial differences

in the scene. Therefore, the approach that produces the most accurate prediction of chlorophyll a amount will depend on the scale of observation and the characteristics of the target (table 3.3). Measurement of chlorophyll can be by concentration (per unit mass, i.e., mg g^{-1}) or content (per unit area i.e., per leaf or per ground area; mg m^{-2}); both have been derived from physical and chemical extraction procedures with transmission spectrometry (Yoder and Daley 1990) or for whole leaves by use of reflectance spectrometry (Rollin and Milton 1991).

Table 3.3: The measurement of chlorophyll amount for different grass conditions

Scale and conditions	Chlorophyll concentration (mass per mass)	Chlorophyll content (mass per leaf)	Chlorophyll content (mass per ground area)
Leaf e.g., a blade of grass	✓✓	✓	✓
Spatially homogeneous Canopy e.g., a bowling green	✓✓	✓	✓✓
Spatially heterogeneous Canopy e.g., semi-natural grassland	ς	ς	✓✓

ς an inaccurate representation;

✓ an accurate representation;

✓✓ a very accurate representation.

Many variables relevant to the study of the red-edge (specifically configurational properties) may be held constant at the leaf scale. This can be achieved by careful sample selection, the elimination of atmospheric and background effects and the careful positioning of the sample against a background of minimal reflectance. The leaf is the most significant plant structure in terms of its effect on light. It has evolved to:

1. harvest energy (photosynthesis) from the visible wavelengths of light (photosynthetically active radiation, PAR);

2. allow the transfer of carbon dioxide (for photosynthesis) and oxygen (for respiration);

3. allow the controlled movement of liquids, via a vascular network and transpiration of gasses via stomata;

4. and finally, provide protection from environmental extremes.

The structural arrangement of a leaf is a careful balance that allows all of the its functions to be best achieved, but this balance can be upset by the stress from growing in contaminated conditions. Reflected radiation from grass is influenced by biochemical compounds such as those that enable the plant to harvest visible wavelength energy (photosynthesis) and scattering effects as a result of the leaf structure (e.g., Gates 1970). The main observed influence for changes in the red-edge is a change in the amount of photosynthetically active pigments, specifically chlorophyll (e.g., Clevers and Büker 1991; Guyot *et al.* 1992), although other factors related to leaf structure and physiology (e.g., Gausmann 1974) have an effect.

3.7.1 Photochemically active pigments

PAR (400-700 nm) is absorbed by photo-reactive pigments for photosynthesis, protection from radiation saturation or to provide display to aid pollination, seed dispersal or provide environmental protection. The pigments of higher plants consist of chlorophylls a and b and carotenoids. They are contained in intra-cell structures called chloroplasts. Also within the chloroplast are the components of the electron carrier system and enzymes (which catalyse the conversion of CO_2 and water to carbohydrate). The electron carrier system transfers energy within the photosystem and requires more energy than liquid-water absorption which acts by changing a molecule's state (Gates 1970). All chlorophylls, caratenoids (except violaxanthin; Lichtenthaler

1987) and electron carriers are bound to membranes called thylakoids while the CO_2 fixation enzymes are distributed thoughout the rest of the inner volume of the chloroplast (the stroma) (Markwell *et al.* 1979). Observations of the spectrum for the white sections of variegated leaves in comparison to green sections (e.g., Billings and Morris 1951) demonstrate that NIR wavelengths are not influenced by chlorophylls and carotenoids and that the influence on the shoulder of the red-edge is therefore determined by characteristics associated with the leaf structure and physiology.

3.7.1.1   Chlorophyll

Two main forms of chlorophyll are present in green plants; these are chlorophyll *a* ($C_{55}H_{72}MgN_4O_5$) and chlorophyll *b* ($C_{55}H_{70}MgN_4O_6$). Chlorophylls contain a stable ring-shaped molecule (porphyrin ring) around which electrons migrate. The gain of electrons and loss of electrons energised by solar radiation feed the photosystems by which plants harvest sunlight (Berg 1998). Chlorophyll *a* absorbs radiation between 420435 nm (blue light) and 660680 nm (red light) although the exact shape of the absorption spectrum depends on the polarity of light in the environment in which the chlorophyll is placed (Halliwell 1984) and the wavelength studied (Coulson 1966). Experiments with polarised light in the laboratory have indicated that chlorophyll has a polarising effect but that this is too slight to be used outside of the laboratory environment (Halliwell 1984).

3.7.1.2   The influence of the chlorophyll *a/b* ratio on the red-edge

The ratio of chlorophyll *a* to chlorophyll *b* occurs in an approximate ratio of 3:1 but tending to a 2:1 ratio for plants growing in bright illumination conditions (Anderson 1986; Thomas 2004). Different parts of a single plant can show adaptations to local light conditions (Terashima 1989). Cells in an upper leaf surface can have characteristics of leaves grown in full sunlight and cells in the same plant positioned in the lower leaf surface have characteristics of leaves found in the shade (Terashima 1989). Gen-

erally shade leaves are thinner, have more total chlorophyll as well as a higher ratio of chlorophyll a to chlorophyll b (Taiz and Zeiger 1998).

3.7.1.3   The influence of accessory and photo-reactive pigments on the red-edge

Carotenoids are accessory pigments, they can absorb solar energy but cannot pass the accumulated solar energy directly to the photosynthetic pathway but instead transfer the energy to chlorophyll a by the process of 'inductive resonance (Hall and Rao 1994). Carotenoids are usually red, orange or yellow pigments and include the compound carotene. Primary carotenoids are active in green photosynthetically active plant tissue while secondary carotenoids are found in fruits and flowers (Lichtenthaler 1987). Primary carotenoids may be divided into oxygen-free carotenoids (α carotene & β carotene) and xanthophylls. Within the chloroplasts of higher plants, β carotene and its derivatives (e.g., xanthophylls; zeoxanthin, violaxanthin and antheraxanthin) serve as accessory pigments or protect chlorophyll from photoxidation (Lichtenthaler 1987).

3.7.1.4   The influence of fluorescence on the red-edge

Fluorescence is the re-emission of previously absorbed energy, normally at a higher wavelength. Fluoresced energy will be less than that initially absorbed and so the fluorescence spectrum is shifted to longer wavelengths (Stokes shift). Steady state natural fluorescent bands act as de-excitation pathways for photochemical (and non-photochemical) quenching (Dobrowski *et al.* 2005) as a response to excess light. Dobrowski *et al.* (2005) further explain that there are two main controls on the relaxation pathways. One control determines the levels of quenching by photochemistry and is dependent on the redox state of the primary stable electron acceptor of PSII (plasto-quinone). The other control influences the non-photochemical quenching process. This is the light-induced protective processes that result in the de-excitation of the chloro-

phyll singlet to the ground state with the production of heat (Johnson *et al.* 1994; Pospisil 1997; Müller *et al.* 2001). Chlorophyll content in leaves has been determined from the ratio of fluorescence at wavelengths of 685 nm and 735 nm (Lichtenthaler 1987; Lichtenthaler and Buschmann 1987; Guyot and Major 1988). In green leaves approximately 90% of emitted chlorophyll fluorescence at 685 nm is reabsorbed by leaf chlorophyll (Gitelson *et al.* 1998). Therefore, some researchers (e.g., Gitelson *et al.* 1999) use longer wavebands (735 nm and 700 nm) to determine chlorophyll concentration from these fluorescence emissions.

3.7.2   Plant physiology

A leaf cross section shows distinct layers. These are the cuticle, epidermis, palisade layer and the spongy mesophyll (figure 3.7). They are composed of several tissue types: parenchyma, chlorenchyma and sclerenchyma. Parenchyma is living tissue composed of thin-walled cells and permeated by a system of intercellular spaces containing air; chlorenchyma is parenchyma containing chloroplasts (Abercrombie 1992). Sclerenchyma has thicker walled cells usually deposited with lignin and provides a plant with mechanical support (Abercrombie 1992). The distribution of these leaf components is species-dependent (figure 3.8). For example the distinction between the palisade layer and spongy mesophyll for monocotyledonous leaves is less distinct than for dicotyledonous leaves (Hopkins 1999). Grass typically has veins surrounded by parenchyma; around small veins this becomes tightly packed and is called a bundle sheath (Fahn 1990). This configuration of cells is characteristic of grass with 'Krantz' anatomy, an adaptation for high irradiance that uses a C4 photosynthetic pathway (e.g., Fitter and Hay 1981). Haberlandt (1914) used the word Krantz to refer to the wreath of radially-arranged mesophyll cells that surrounded the bundle sheath although the term is now applied to the entire suite of distinctive structural characteristics (Krantz anatomy) (Brown 1975). Although some C3 leaves have Krantz anatomy, it is of particular importance for the operation of C4 biochemistry and physiology (Dengler and Nelson 1999). Among the species associated with Krantz anatomy are two monocotyle-
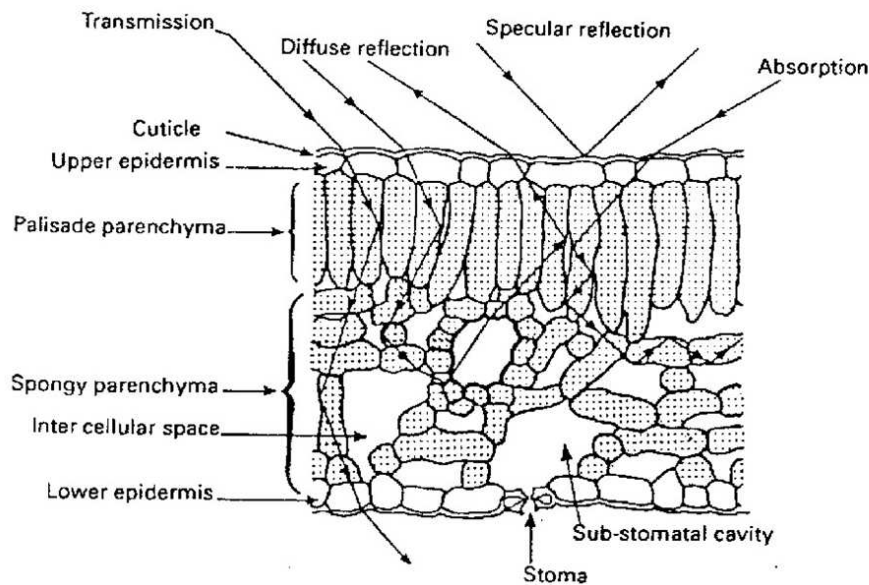
Figure 3.7: Schematic cross-section of a leaf and interaction of incoming radiation with leaf tissues. Source: Guyot 1990; Lichtenthaler and Pfister 1978

donous families; *Poaceae* (a grass) and *Cyperaceae* (a sedge). The C4 grasses have a high tolerance to drought conditions and dominate the North American temperate tallgrass prairies and South American tropical savannas (Knappe and Medina 1999). C3 grasses are favoured by higher nitrogen availability (Wedin and Tilman 1993) but can be out-competed by C4 grasses in conditions where there is a high frequency of fire (Blair 1997). Up to 75% of leaf organic nitrogen is in the chloroplasts (Evans and Seemann 1989). This influences the rate of photosynthesis (Sharkey 1985) due to a positive correlation between the assimilation rate of CO_2 and nitrogen content (Field and Mooney 1986; Evans 1989). This relationship was extended by Garnier *et al.* (1999) to the leaf thickness of 14 species of *Poaceae* (grasses) where a thicker leaf contained more organic nitrogen and had a high rate of photosynthesis.

3.7.2.1   Cuticle and epidermis

The cuticle and epidermal cells provide physical protection to internal leaf tissue. Also attributed to the cuticle are non-Lambertian (unevenly distributed) scattering and the

Figure 3.8: Cross-sections of grass leaves. Source: Fahn 1990
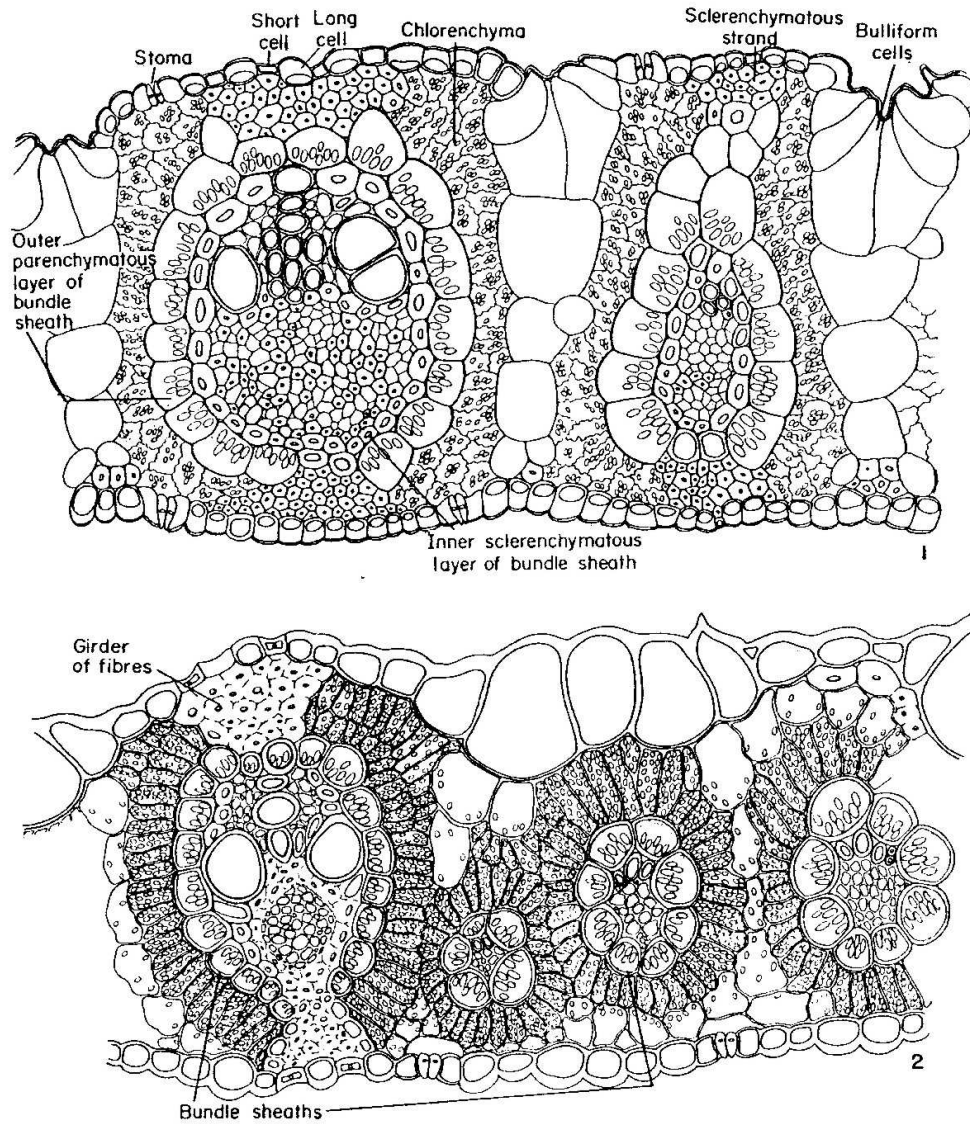
1. *Desmotachya bipinnata* in which the bundles sheath consists of two layers, the outer parenchymatous and the inner sclerenchymatous. X 260.

2. *Hyparrhenia hirta* in which the bundle sheath consists of a single layer of chloroplast- containing cells. X 260.

attenuation of illumination levels that could saturate the photo-systems (e.g., Breece and Holmes 1971). Non-Lambertian characteristics are due to epicuticular waxes and leaf surface roughness. Schutt *et al.* (1984) found that when the cuticle of *Triticum aertivum* wheat leaves was removed, or when the surface was polished, reflectance was reduced. Where surface undulations are large (relative to the incident wavelength) they affect the magnitude and angular dependence of the surface reflectance (Breece and Holmes 1971) and where scattering is specular (directionally distributed), effects are greatest at large angles of incidence but have little effect at near-normal angles (Sinclair *et al.* 1973). Observations of the reflectance of adaxial versus adaxial surfaces of dorsiventral leaves (Gausman *et al.* 1977) and experiments with polarised light (e.g., Vanderbilt *et al.* 1985) have supported this. Light from many sources has no clear dominance in magnitude or direction in its electromagnetic field but when light is channelled or restricted polarisation may result. Epidermal cells are transparent but modify the passage of light by forming cellular lenses (Vogelmann *et al.* 1989). The cellular lenses focus light towards chloroplasts so increasing the PAR received above ambient levels (Vogelmann *et al.* 1996). The polarisation characteristics depend on the geometric arrangement of leaves and stalks in the canopy and the distinctive wavelength-dependency of vegetation reflectance (Talmage and Curran 1986). The effect of wavelength on polarisation properties of grass was studied by Coulson (1966). He found that radiation reflected in the chlorophyll absorption wavelengths (490 nm and 640 nm) was highly polarised with lower polarisation being recorded from radiation reflected from the mesophyll layer in a NIR wavelength (1000 nm). Talmage and Curran (1986) and Egan (1968) found that damage to the leaf structure of a plant by pollution, disease, lack of water or other stress reduced polarisation. This may have been due to changes in the alignment of chloroplasts or changes in the general cellular structure of the leaves.

3.7.2.2   Palisade layer

The palisade layer is composed of pillar like cells set at right angles to the epidermis. Intra-cellular migration of chloroplasts within the chlorenchyma provides a mechanism

to avoid light saturation but requires that they are distributed heterogeneously within the cell. This means that light may pass through the cell without passing through a chloroplast and has been termed the 'sieve effect' (Terashima and Saeki 1983; Vogelmann *et al.* 1989). The sieve effect may have relevance to the REP in terms of the optical thickness of a canopy and the transmitted radiation that reaches a vegetation under-storey.

3.7.2.3   Spongy mesophyll

The spongy mesophyll is characterised by a large surface area provided by irregularly shaped cells separated by interconnected air spaces (e.g., Gates 1980). Loss of unused PAR is minimised by diffuse scattering within the leaf (figure 3.7) and is achieved by a combination of reflection, refraction and scattering (Goel 1988). This can extend the path length of PAR four times the thickness of the leaf (Richter and Fukshansky 1996) and aid gas exchange and transpiration. The redirection of light back towards chloroplasts is enhanced by the orientation of microfibrils within cell walls of the mesophyll and palisade layers (Sinclair *et al.* 1973). Redirection of PAR is maximised when reflection is at non-critical (Grant 1987) or large angles of incidence (Sinclair *et al.* 1973). These factors increase the probability that PAR will be harvested by one of the photosystems in the chloroplasts and promotes 'anomalous dispersion' in the wavelength vicinity of absorption bands (Latimer 1958).

High reflection at critical angles within the leaf structure was described and located at interfaces between intra-cellular spaces and the cell wall by Willstätter and Stoll (1928). The boundary between the cell wall (hydrated cellulose of refractive index 1.47) and air cavities (refractive index 1.0) gives rise to Fresnel reflection forming a boundary of 'refractive discontinuity' (Gausmann 1977). The role of such interfaces in diffuse scattering has been shown in experiments where void spaces within the leaf were filled with water (Knipling 1969; Knipling 1970) or vacuums infiltrated with oil (Wooley 1971). Other work has been conducted using the Kubela-Munk scattering coefficient to model the effect (e.g., Myers and Allen 1968; Gausmann *et al.* 1970).

This approach was able to simulate laboratory observations with Fresnel reflections from 35 air interfaces, at normal incidence, along the mean optical path through the leaf (Myers and Allen 1968) and with even fewer interfaces when oblique reflections were included (Gausmann 1974). Similar agreements between predicted and measured results have been reported from tracing the unique path of each ray of light (ray tracing) and the principle of refractive discontinuities (e.g., Allen *et al.* 1973; Kumar and Silva 1973. The contribution of scattering (Rayleigh and Mie) has been attributed a minor importance because cell dimensions within a leaf are generally too large, relative to visible and NIR wavelengths. A minor contribution may be made by intra-cellular structures, for example chloroplast and grana dimensions (grana $\sim$ 500 nm length and 5 nm diameter (Gates *et al.* 1965) or mitochondria and ribosomes).

3.7.3   Leaf water

The value of radiation as a resource for a plant depends critically on its supply of water (Begon *et al.* 1996) but water is also the means by which a plant transfers nutrients from its roots to other assemblages and maintains its structural resilience due to cell turgidity and hydrostatic pressure. Water is transpired through opening and closure of stomata in a leaf but the same apertures are the means by which a plant acquires CO_2 for photosynthesis (Begon *et al.* 1996). If the stomata are open water is lost but CO_2 and O_2 can be exchanged. The diffusion pathways for water vapour from the wet cell surfaces of the mesophyll to the outside atmosphere are controlled by structural features such as sunken stomata and the restriction of stomata to specialised areas on the lower surface; this slows down water loss (Begon *et al.* 1996). Stomatal closure can respond to day-to-day or minute-to-minute changes while a waxy cuticle and hairs on the leaf surface reflect a proportion of non-PAR radiation and so keep the leaf temperature down and reduce water loss (Begon *et al.* 1996). Plants use these measures to maintain their water content between narrow limits.

There are water absorption features at wavelengths of approximately 720 nm and 960 nm but studies into the influence of within-leaf water on the red-edge have shown

the influence to be restricted to extreme conditions (Filella and Peñuelas 1994). Simulations indicate that these limits on the influence of water may also be true for grass (Llewellyn and Curran 1999) and that influence at extreme hydric conditions may be due to physiological or canopy structural changes rather than biochemical change. Leaf moisture was shown to affect the red-edge for the leaves of *Zea mays* (corn) (Hoffer and Johannsen 1969, figure 3.9) and *Picea rubens* (red spruce) and *Tsuga canadensis* (eastern hemlock) Rock *et al.* (1994) though the later study also identified changes in cell density.

3.7.4   Taxonomy and phenology

Both species type and the stage in a species' seasonal cycle can influence reflectance (e.g., Boochs *et al.* 1990). Taxonomy is the theory and practice of classification and can be applied to grass at the genus and species level. Phenology is the study of the periodicity phenomena in plants, such as timing of flowering or senescence. The timing of flowering can indicate environmental conditions while the presence of flowers in a canopy can shift the red-edge to shorter wavelengths (Milton and Rollin 1990). Of the phenological changes, senescence has attracted particular study. Senescence is a deterioration of cells and tissues akin to ageing (Abercrombie 1992). The steps and timing of chlorophyll degradation in a senescing leaf are unknown and not always correlated with other aspects of a leaf's functioning (Woolhouse 1967) and some plants die without any chlorophyll loss at all (Thomas and Stoddart 1975). Senescence processes are encountered in all plants and at all stages of the life cycle (Woolhouse 1978). In addition to a redistribution of chlorophyll (Boyer *et al.* 1988) there are also physical changes which may influence reflectance. Such effects are: the number of cell layers (Gausmann *et al.* 1970), the size of the cells, their heterogeneity (Gausmann 1974; Grant 1987) and their orientation (Sinclair *et al.* 1973; Gausmann 1974; Grant 1987). Unlike senescence, abscission refers to the shedding of plant structures, characterised by the degradation of cell walls at the point of weakening (Sexton and Woolhouse 1984). Plants in open meadows characteristically shed their leaves in rapid succession
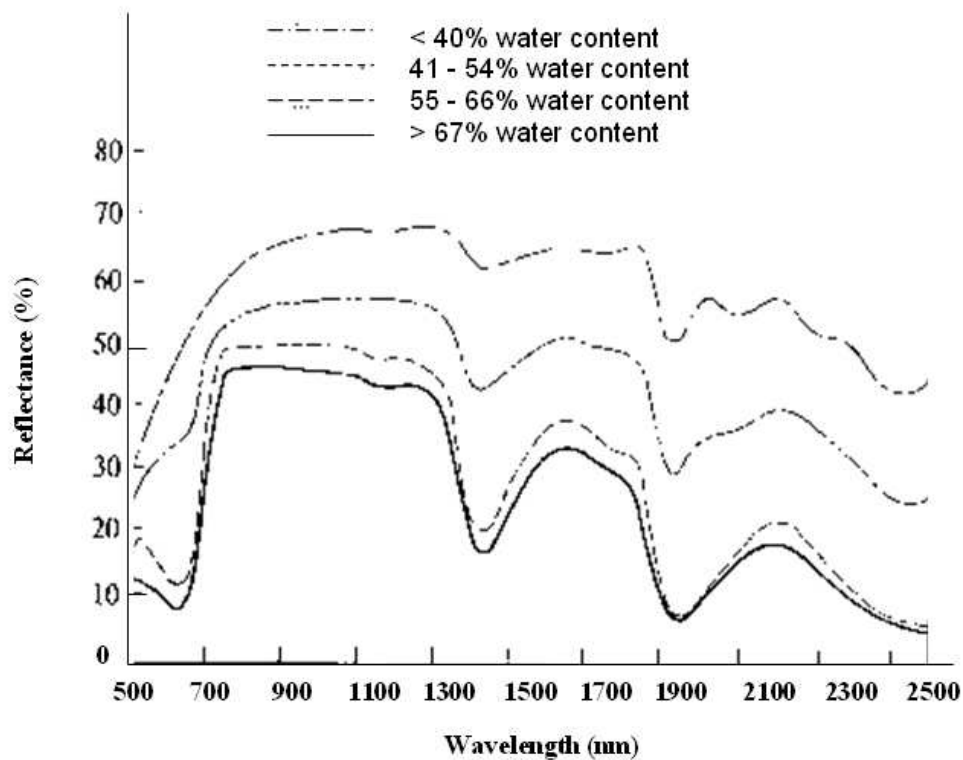
Figure 3.9: Effect of water content on reflectance of corn leaves. Source: Hoffer and Johannsen 1969.

as new ones are developed above in order to compete with neighbouring plants for light, this is a process of sequential senescence (Woolhouse 1967; Woolhouse 1974). In a more general comparison between immature and mature cotton leaves, Gausmann *et al.* (1970) noted that immature leaves had compact mesophylls and small cells while the mature leaves had a loose cellular structure in the mesophyll and a larger cell size. The mature leaves had lower transmittance and higher reflectance levels in the NIR. This was attributed to an increase in the number of surfaces of 'refractive disconti-nuity' due to the increase in intercellular air space voids. Additionally, some leaves show strong longitudinal gradients of chlorophyll. Wagner *et al.* (2003) found that the chlorophyll concentration in barley leaves increased within the first 5-8 cm from the leaf base and then did not significantly change for the remaining part of the leaf.

This relationship, demonstrated by leaf maturity, also applies to plant type. Leaves

Table 3.4: Wavelength-dependent variabilitiy in optical properties. Source: Asner 1998

Component	Visible wavelengths	NIR wavelengths	SWIR wavelengths
Green vegetation	Low	High	-
Woody material	-	High	Low
Standing leaf	Low	Low	High

from dicotyledonous species reflect more radiation than leaves from monocotyledonous species (Hoffer and Johannsen 1969; Sinclair *et al.* 1971. However because monocotyledonous species have a more homogeneous distribution of chloroplasts throughout the leaf mesophyll than dicotyledonous species, the NIR radiation from abaxial and adaxial surfaces are more alike (Terashima and Saeki 1983).

3.8 The grassland red-edge at the canopy scale

At the canopy scale many variables that are controlled in the laboratory exert an influence on the red-edge (e.g., Clevers and Büker 1991; Guyot *et al.* 1992). Asner (1998) found that the different components of a grassland canopy had different wavelength dependent effects on the measured reflectance, these are summarised in table 3.4. The red-edge can be influenced by leaf area (Guyot *et al.* 1992; Danson and Plummer 1995), the structure and architecture of the canopy (Blackburn and Milton 1995; Hobson and Barnsley 1996), background (Jago and Curran 1996), atmosphere (Chavez 1988) and the scene that surrounds an instruments field-of-view (FOV). Depending on the environment studied, the magnitude of these influences can obscure many of the relationships identified at the leaf scale (Llewellyn and Curran 1999). However, the relatively simple canopy structure of grass, compared to larger vegetation types, should make the evaluation of major leaf scale variables, such as chlorophyll content easier .

3.8.1 Scene variables

For the purposes of this discussion, the scene is the reflectance integrated within a field-of-view (FOV), the geometry by which the FOV is illuminated and viewed, and the varying spatial and temporal contexts within which the FOV is placed (Strahler *et al.* 1986). These factors can be contamination-dependent or independent and include the atmosphere between the source of radiant illumination and between the FOV and the sensor. Many scene variables are independent of the effects of soil contamination.

One set of independent influences on the red-edge is the observation and illumination geometry (e.g., Guyot *et al.* 1992; Kim and Reid 2007. Unless they are measured or modelled the influence of state variables on the red-edge may be unpredictable (Shoshany 1991) with potential effects such as those found with leaf stacking (e.g. Schutt *et al.* 1984). These problems can be minimised with reference to the relationship identified in equation 2.4 (page 22) where space, time, wavelength and viewing geometry were discussed. Conducting measurements using nadir views and at solar noon add control to the remote sensing survey, but these solutions are not always possible. The inversion of bidirectional reflectance distribution function (BRDF) models is a solution that allows data from sensors with multi-look angles and variable acquisition times to be used to estimate vegetation variables (Sridhar *et al.* 2008).

In the case of airborne, and particularly spaceborne, systems the signal being attributed to a ground property is subject to atmospheric modification. The atmosphere has a non-linear influence on reflectance caused by absorption and scattering. Absorption rates are dependent on atmospheric composition and altitude while scattering is wavelength dependent (Rayleigh scattering) or related to airborne particulates (Mie scattering and non-selective scattering). The correction of these potential errors may be specific to the sensor, applications and environments. Techniques for atmospheric correction include the histogram minimisation method (Chavez 1975) and a variety of atmospheric correction models, e.g., LOWTRAN (Kneizy *et al.* 1988), MODTRAN (Berk *et al.* 1989).

3.8.2   Background

The background is the scene element against which the grass is observed. At canopy scales a FOV is typically composed from the area-weighted interaction of reflectance from the bare soil, the layer of litter and the under-storey that becomes convoluted with the leaf spectra (Dawson *et al.* 1997). Of these, standing litter can significantly influence the reflectance of grassland canopies (Asner 1998). The red-edge has been reported to be insensitive to variations in background (Collins *et al.* 1980) and the contributions of non-vegetative reflectance components may be limited by the use of first derivative spectra (Boochs *et al.* 1990). Modification of the litter, under-storey or non-grass species cover may be more rapid than for a dominant grass canopy especially if an under-storey is more adaptive or responsive to a contaminated environment.

> *"The calculation of derivative spectra eliminates additive constants (e.g., illumination changes) and reduces linear functions (e.g., uniform increase in background reflectance with wavelength) to constants. This has led researchers to conclude that the red-edge is essentially invariant with illumination or the amount of background within the field-of-view of the spectrometer."*

<div align="right">Curran et al. 1990, p.34</div>

An assumption that the background is spectrally flat can be maintained in the laboratory and simple light and dark backgrounds have been found to give very little influence on the position of the red-edge (Vogelmann *et al.* 1993). Some mineral soils give a uniform increase in background reflectance with wavelength (Demetriades-Shah *et al.* 1990; Ustin and Curtiss 1988; Ustin *et al.* 1989) and can be related to a constant. Nevertheless, where an under-storey is present it may invalidate any estimates of over-storey biophysical properties (Boschetti *et al.* 2003). Therefore, where the background reflectance varies non-linearly with wavelength (such as with an under-storey), then both components must be evaluated separately.

3.8.3   Spatial variation

The evaluation of the spatial variability of soil contamination is related to both the intrinsic scale of variation in the scene and the scale at which measurements are recorded. Even when a location is level and contains a single vegetation type, such as grass, the location may contain major elements that determine the spatial variability. Spatial variability may be due to ground contamination, localised soil characteristics or the age, health or natural species distribution of vegetation present. Tussocks and clumps of a dominant vegetation species or patches of restricted growth may provide contiguous elements. Other elements may be due to underlying ground reflectance, detectable through gaps in a canopy and shadow (Sailsbury *et al.* 1987; Dawson *et al.* 1997).

Soil contamination can be from a discrete point or diffuse source. It may have a heterogeneous distribution with different contaminants deposited by a variety of processes each in a random manner (Hackenbush 2008) or be directly associated with past structures or storage areas or geological or hydrological features. Spatial variation of vegetation properties (state variables) has been evaluated using spatial statistics (Garrigues *et al.* 2006). If the data conforms to basic assumptions (e.g., stationarity) then the variogram may be used to identify scales of spatial dependency (Isaaks and Srivastava 1989). These spatial statistics can also be used to optimise sampling strategies, aid interpolation techniques or produce an input variable for classification. A geostatistical term used to describe the size, geometry and orientation of the space on which an observation is defined is support. In remote sensing, the size of the 'support' is equivalent to the spatial resolution (Atkinson and Curran 1995). Spatial resolution is a significant factor with the next generation of spaceborne sensor systems (e.g., Sentinal 2). At coarser spatial resolutions more variation is integrated and the definition of fine spectral resolution features, such as the REP, is reduced. In addition, at progressively finer resolutions (spectral, spatial or radiometric) the signal-to-noise ratio decreases.

3.8.4   Land management variables

The scene can be greatly influenced by the management strategy applied to the soil and vegetation present. Chemical treatments (fertilisers and herbicides), planting regimes and mechanical treatments (e.g., mowing) affect the vegetation and its resilience to stress. Traditional wisdom has found that species rich grassland sites are more stable than those that are species poor (Schläpfer and Schmid 1999). This relates to the hypothesis that a large number of species provide more adaptability and allow the growth of unique local environments (Martinez and Levinton 1996). However, Kennedy *et al.* (2003) found that grassland sites with a low species-richness were statistically more resilient (to drought) than sites with a high species-richness and that once the drought had passed were quicker to recover. In this environment (the South African Savanna) the dominant vegetation may simply be the most drought-resistant.

3.9   Derivative reflectance spectrum

Although the first derivative is the most commonly published (e.g., Estep and Carter 2005), further derivatives (e.g., second derivative, Demetriades-Shah *et al.* 1990) have been used to minimise noise or background effects. Horler *et al.*'s (1983a) observations of the first derivative spectrum highlighted the subtle structure of the red-edge not evident from a standard reflectance spectrum. This feature was a multiple peak (usually described as a double-peak in the 690-710 nm spectral range); there has been much discussion among the remote sensing community as to its cause. Popular techniques for smoothing and obtaining derivative data (e.g., Savitsky and Golay 1964) and the availability of contiguous narrow band data sets have allowed the debate to thrive (e.g., Tsai and Philpot 1998). The double-peak has specific relevance to the observation of stressed vegetation (Jago and Curran 1996; Smith *et al.* 2004) with the longer wavelength peak being less evident (or absent) where vegetation are stressed. Speculation that this feature was associated with fluorescence have been present since the 1980's (e.g., Lichtenthaler *et al.* 1990). However, difficulties in measuring it have

been complicated by the presence of any illumination; a favoured solution has been the use of Fraunhofer line-depth techniques (Plascyk 1975; Li *et al.* 2005)). However, work by Zarco-Tejada and co-workers (Zarco-Tejada *et al.* 2000; Zarco-Tejada *et al.* 2003) attributed the peaks entirely to chlorophyll fluorescence. Further work with radiometers with a sub-nanometre resolution have added weight to this conclusion (Meroni and Colombo 2006). The double-peaks are therefore commonly attributed to the steady-state natural fluorescent emission bands centred at 690 and 730 nm (Zarco-Tejada *et al.* 2003). However, some observed relationships are either not explained or there are alternative mechanisms by which they may occur (S. Ustin, pers. comm., 2008).

The cause of *double peak* commonly observed in the derivative spectra of vegetation has been a source of long discussion in the research community. In many cases derivative spectra actually include multiple peaks; the lesser of these have been attributed to noise and removed by smoothing. Some authors focus on a single feature and refer to the *double peak* in reference to a main peak, at approximately 720 nm, and a subsidiary peak, at shorter wavelengths, as the second peak (e.g., Zarco-Tejada *et al.* 2003). Other authors use a system where the peak at the shortest wavelength is referred to as the first peak; subsequent features at progressively longer wavelengths are then known as a second or third peak (e.g., Jago 1998). In this brief discussion the derivative features are referred to as short and long wavelength features and are accompanied by a wavelength value where possible (table 3.5).

Table 3.5: First derivative spectral features of the red-edge

Reference	Flora	Smoothing window size	Polynomial	Short wave-length (nm)	Middle wave-length (nm)	Long wave-length (nm)
Gitelson *et al.* 1996	Horse chestnut (*Aesculus hypocastanum .L*) & Norway maple (*Acer platanoides. L*)	?	?	685-706	710	725+740
Jago 1998	Grass (various)	?	?	699-705	718-725	
Smith 2002	Grass (various), winter wheat (*Hordeum vulgare*) & field beans (*Vicia faba*)	5 band weighted mean moving average (5nm)		702	718-725	760
Lamb *et al.* 2002	80% Rye grass (*Lolium*& 15% clover (*Trifolium sub-terranean*)			705-709 (703-704.2)		724-740 (726-730)
Zarco-Tejada *et al.* 2003	*Acer negundo*		2nd order	690	720	
le Maire *et al.* 2004	Various broad leafed vegetation #	8nm	4th order	770	720	
Smith *et al.* 2004	Grass (various), winter wheat (*Hordeum vulgare*) & field beans (*Vicia faba*)	5 band weighted mean moving average (5nm)		702	718-725	760
Cho and Skidmore 2006				690	720	
This study	Grass (various)	5 band average (5nm)	2nd order	695-712	719-722	721-735

Traditionally, the shorter wavelength peak has been attributed to chlorophyll concentration and the longer wavelength peak (or peaks)to scattering effects. As chlorophyll content includes some aspects of a structural measure, i.e. biomass or leaf area, it is also more associated with the longer wavelength peak than chlorophyll concentration. Zarco-Tejada *et al.* (2003) attributed the double peak affect to being due solely to steady-state chlorophyll fluorescence (CF) effects. Yet other studies (e.g., Lamb *et al.* 2002 and le Maire *et al.* 2004) have observed the *double peak* with respect to LAI and chlorophyll concentration respectively. However, these studies used daylight or white light and thus did not restrict the possibility of fluorescence.

3.10 Vegetation indices

Vegetation indices (VIs) summarise spectral data to a single value related to vegetation biophysical parameters, such as biomass, leaf area and vigour. They can aid vegetation research in two ways (i) quantitatively by monitoring specific variables associated with growth and production and (ii) qualitatively as a mapping tool (Campbell 1996). The selection of the most appropriate vegetation index (VI) for each application depends on the environment in which measurements are conducted and the sensor used to collect the data. Environmental considerations include the influence of non-green vegetated components on reflected radiation, within a sensor's field-of-view, and the scattering and absorption of the radiation as it passes between the target and the sensor. Vegetation indices (VIs) are designed to enhance the sensitivity of a sensor to vegetation variables while restricting the influence of the soil background, atmospheric attenuation and solar angle (Steven *et al.* 1990). Running *et al.* (1994) expanded on this specification to produce five criteria. These are:

1. The index should maximise sensitivity to plant biophysical parameters, preferably with a linear response in order that sensitivity be available for a wide range of vegetation conditions, and to facilitate the calibration of the index.

2. The index should normalise or model external effects such as Sun angle, viewing angle and atmosphere.

3. The index should normalise internal effects such as canopy background variations, topography and differences in senesced or woody vegetation (non-photosynthetic components of a canopy).

4. The index should be a global product, allowing precise and consistent spatial and temporal comparisons of vegetation conditions.

5. The index should be coupled to some specific, measurable biophysical parameter such as the fraction of photosynthetically active radiation (FPAR) as part of the validation effort and quality control.

Spectrometric techniques are not easily applied to data collected by field, airborne or spaceborne sensors due to constraints imposed both by the SNR and the greater variability of the measuring environment compared with that of the controlled environment within a dedicated laboratory instrument. However, data from spectral bands can be transformed to VIs by the exploitation of the general influence of green terrestrial vegetation on reflected radiation. There are many VIs, most of which utilise the vegetation red-edge. Any classification of VIs into different classes is restricted because some VIs will inevitably straddle different classes. Nevertheless, in this discussion VIs will be considered both in terms of the data that they use (broad or narrow-spectral bandwidths) and the manner in which they are calculated. The initial descriptions of VIs are in terms of broadband data. This will introduce the principles that most VIs use and will be developed with reference to narrow-band (around 6 nm or less) VIs. There are three ways in which VIs can be calculated: arithmetically, orthogonally and positionally (specifically to calculate the red-edge position). Arithmetic VIs use standard arithmetic operators (i.e., subtraction, addition, division and multiplication), orthogonal VIs use measurements and transformations of spectral features (e.g., soil line) while positional VIs estimate of the wavelength position of a spectral feature in a vegetation spectrum. The REP identifies an inflexion point, a peak or a modelled point between peaks.

3.10.1 Vegetation indices in feature space

Arithmetic VI are calculated from a combination of spectral bands in such a way that accentuates those characteristics that distinguish vegetation by its interaction with reflected radiation. This combination of data may be considered within a region defined by the linear combination of two or more continuous variables, e.g., spectral bands associated with red and NIR wavelengths. Arithmetic VIs can be marked in the feature space with lines of equal vegetation (isovegetation lines) (e.g., Mather 1999). Difference based VIs, e.g., difference vegetation index (DVI, Lillesand and Kiefer 1994) plotted in the feature space produce parallel isovegetation lines while ratio based VIs, e.g., simple ratio vegetation index (RVI, Jordan 1969) produce converging isovegetation lines (figure 3.11). These simple VIs show two representations of radiation reflected from vegetation, though both are without a scale maximum. The normalised difference vegetation index (Kriegler *et al.* 1969) combines both difference and ratio-based operators and standardises the variation as a value between one and minus one.

3.10.1.1 Countering the effect of soil

Underlying surfaces (e.g., the soil) may influence a VI where vegetation is optically thin or has an incomplete canopy cover. Examination of image data plotted from Landsat MSS bands (3 & 4, red & NIR) distinguished vegetation from soil and attributed a relative movement from this soil feature, labelled a soil brightness line, through the growing season (Kauth and Thomas 1976) (figure 3.10). A transform (Tasselled-cap transform) is performed to shift the axis by which the data is evaluated such that it is solely attributed to the influence of soil brightness. The soil line is a two-dimensional representation of Kauth and Thomas's soil brightness line estimated by using linear regression (Richardson and Wiegand 1977). The soil line may be used with orthogonal measurements to identify the influence of the soil on vegetation data and thereby is used in VIs to reduce the influence of soil on the estimate of vegetation properties (figure 3.11). The perpendicular vegetation index (PVI, Richardson and Wiegand 1977) uses the orthogonal (Euclidean) distance from each data point to the soil line as

a VI; PVI therefore assumes isovegetation lines to be parallel. Kauth and Thomas 1976 devised a series of indices to describe attributes of the feature space, e.g., the green vegetation index. These were developed by Crist (1985) using later Landsat sensor data.

To reduce the influence of soil on other VIs, arithmetic calculations have been supplemented with variables associated to the soil line. The weighted difference vegetation index (WDVI, Clevers 1988) is a difference-based VI modified by the gradient of the soil line; it is therefore functionally equivalent to PVI but has an unrestricted range Ray and Dadhwal 2001. The soil adjusted vegetation index (SAVI, Huete 1988) is a ratio-based VI that is modified by a constant derived from the soil line. If plotted in feature space where NIR and red are positive and compared with those of RVI and NDVI the isovegetatation lines of SAVI appear parallel. This is because SAVI isovegetation lines converge at a point where both NIR and red values are negative (Ray and Dadhwal 2001). The inclusion of a normalised constant (L) minimises the effects of soil brightness variation. L equals 0 for very high vegetation optical thickness and L equals 1 for very low vegetation optical thickness; for most applications an L value of 0.5 is suggested (Huete and Liu 1994). Although less susceptible to the effects of soil variation, ratio-based indices are more sensitive to atmospheric variation than difference-based indices (Gibson and Power 2000). This is also the case with orthogonal indices that are designed to reduce the influence of soil on vegetated spectra; PVI and WDVI have been identified as being especially sensitive to atmospheric variation (Qi *et al.* 1995).

3.10.1.2   Countering the effects of atmosphere

Between the target and the sensor, the atmosphere can attenuate the passage of reflected radiation. Some VI, counter the influence of the atmosphere, e.g., atmospherically resistant VI (ARVI), soil and atmospherically resistant VI (SARVI), enhanced VI (EVI) by the inclusion of additional spectral data. Data in the blue wavelengths of the spectrum are typically included in such VI but this necessitates a decrease in
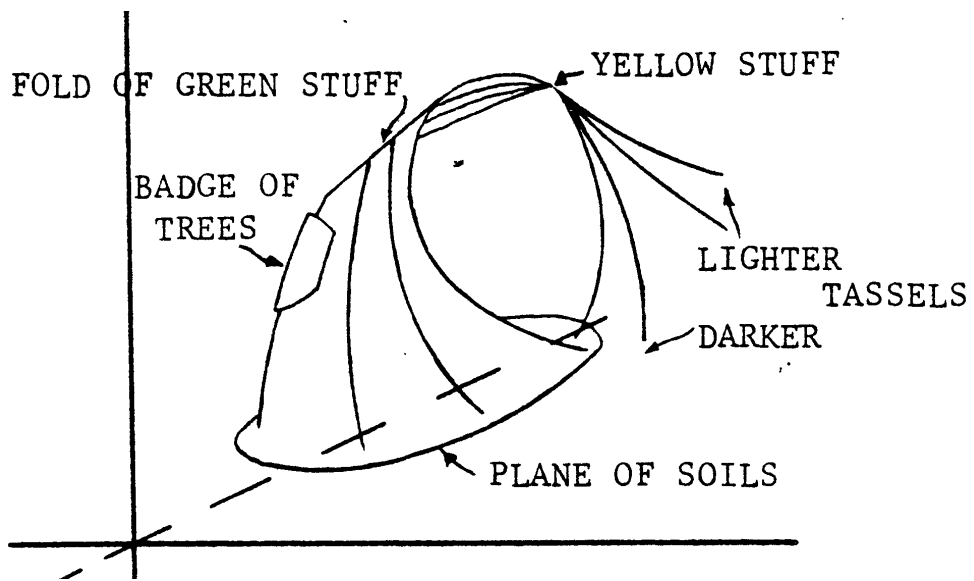
Figure 3.10: Tasselled cap transformation. Source: Kauth and Thomas 1976.
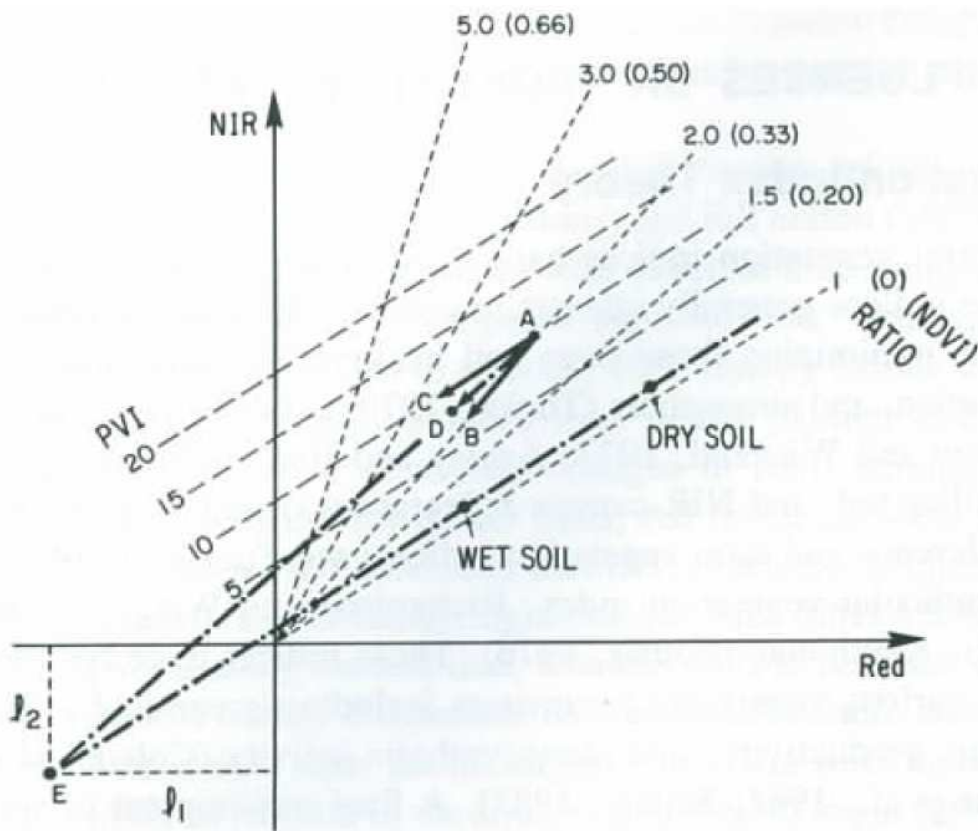
Figure 3.11: The use of a soil line. Source: Richardson and Wiegand 1977.

sensitivity to vegetation related state variables.

3.10.1.3　Reference data sets and measurements

Although the transformation of data to VI allows some comparison between data sets the variation incurred by the environment and the sensor do not allow a true comparison. Within a feature space, patterns have been identified and observed to vary with time (e.g., Kauth and Thomas 1976) and though evident in VI, they are more reliably compared with other data if transformed to absolute terms (e.g., reflectance). Correction for these factors requires known reference standards. By the same principle, estimates of green vegetation biophysical variables can be enhanced by the use of pre-separated or reference library data sets (e.g., Chappelle *et al.* 1992).

3.11　Classifying vegetation indices

Vegetation indices (VI) can be calculated from broad and fine spectral resolution data and collected from laboratory, field, airborne or spaceborne instruments. VIs are designed to enhance the sensitivity of an instrument to vegetation variables while restricting the influence of the soil background, atmospheric attenuation and solar angle (Steven *et al.* 1990). Vegetation indices can aid vegetation research (i) quantitatively by monitoring specific variables associated with growth and production and (ii) qualitatively as a mapping tool Campbell (1996). They can be categorised into three types:

1. Ratio based, e.g., ratio vegetation index (simple band ratio), normalised difference vegetation index (Tucker 1977), the pigment specific simple ratio and pigment specific normalised difference indices (Blackburn 1998b);

2. 'Orthogonal' or feature-space based, e.g., perpendicular vegetation index (Richardson and Wiegand 1977), green vegetation index (Kauth and Thomas 1976) and soil adjusted vegetation index (Huete 1988) and

    3. Red-edge position (e.g., Collins (1978).

Both ratio and 'orthogonal' based indices can be derived from fine (around 6 nm or less) or broad band data. Broad band vegetation indices can provide estimates of general vegetation characteristics (e.g., Tucker 1977) while fine band indices may be used to estimate specific pigment concentrations (e.g., Chappelle *et al.* 1992; Blackburn 1998b). The red-edge position estimates the wavelength position of a spectral feature or virtual feature on the spectral red-edge, (e.g., Guyot and Baret 1988). For red-edge wavelengths this requires a bandwidth (sufficient to resolve the feature) and a continuous spectrum, but where unavailable features may be interpolated using modelled relationships.

Differences in radiation at selected wavelength bands can be used to distinguish between different surfaces. Ratioing between two or more wavelength regions provides an index to extenuate the differences. Orthogonal based indices take into account the background spectra (e.g., from soil). For example, the perpendicular vegetation index (PVI) is so called because of its relationship to the soil line in the feature space. PVI has been used for the study of grassland leaf area index (LAI) (Wardley and Curran 1984) but is sensitive to changes in viewing geometry (Wardley and Curran 1983).

le Maire *et al.* (2004) and le Maire *et al.* (2008) sumarised most of the chlorophyll spectral indices published before 2002. Since then the rate of newly published indices for specific applications or sensors has been maintained. Consequently only those indices that specifically relate to chlorophyll extraction using the red-edge have been added to the summary table (table 3.6).

Table 3.6: Summary of a selection of vegetation indices

Band difference or ratio based indices	Abbreviation	Summary	Reference
Ratio vegetation index (simple band ratio)	VI	$NIR - R$	
Normalised difference vegetation index	NDVI	$(NIR - R)/(NIR + R)$	Tucker 1977
Structure insensitive pigment index	SISI	$(R_{800} - R_{445})/(R_{800} - R_{680})$	Peñuelas *et al.* 1995
Normalised total pigment to chlorophyll *a* ratio index	NPCI	$(R_{680} - R_{430})(R_{680} + R_{430})$	Peñuelas *et al.* 1993
MERIS global vegetation index	MGVI	$g_0(pR_{681}, pR_{865})$	Gobron *et al.* 1999
Ratio analysis of reflectance spectra for chlorophyll *a*	RARS$_a$	$(R_{675}/R_{700})/(r_{675}/r_{700})$	Chappelle *et al.* 1992
Ratio analysis of reflectance spectra for chlorophyll *b*	RARS$_b$	$(R_{675}/R_{650} \times R_{700})/(r_{650} \times r_{700}/r_{675})$	Chappelle *et al.* 1992
Ratio analysis of reflectance spectra for carotenoids	RARS$_{car}$	$(R_{760}/R_{500})/(r_{760}/r_{500})$	Chappelle *et al.* 1992
Pigment specific simple ratio for chlorophyll *a*	PSSR$_a$	R_{800}/R_{680}	Blackburn 1998b

Summary of vegetation indices continued from previous page

Band differ-ence or ratio based indices	Abbrev-iation	Summary	Reference
Pigment specific simple ratio for chlorophyll b	PSSR$_b$	R_{800}/R_{635}	Blackburn 1998b
Pigment specific simple ratio for carotenoids	PSSR$_{car}$	R_{800}/R_{470}	Blackburn 1998b
Pigment specific normalised difference for chlorophyll a	PSND$_a$	$(R_{800} - R_{675})/(R_{800} + R_{675})$	Blackburn 1998b
Pigment specific normalised difference for chlorophyll b	PSND$_b$	$(R_{800} - R_{650})/(R_{800} + R_{650})$	Blackburn 1998b
Pigment specific normalised difference for carotenoids	PSND$_{car}$	$(R_{800} - R_{500})/(R_{800} + R_{500})$	Blackburn 1998b
Chlorophyll fluoresence		F_{685}/F_{700}	Gitelson *et al.* 1999
Perpendicular vegetation index	PVI	$\sqrt{(R_s - R_v)^2 + (NIR_s - NIR_v)^2}$	Richardson and Wiegand 1977
Soil adjusted vegetation index	SAVI	$(\frac{NIR-R}{NIR+R+L})1 + L$	Huete 1988

Positional indices

Summary of vegetation indices continued from previous page

Band differ-ence or ratio based indices	Abbrev-iation	Summary	Reference
Red-edge posi-tion	REP/MIP of red-edge	Various (see section 3.11.2)	Various (see section 3.11.2)
Index of red-edge shift	IRES	$\left(\frac{R_{758.25}-R_{739}}{\lambda_{758.25}-\lambda_{739}}\right) - \left(\frac{R_{739}-R_{719.75}}{\lambda_{739}-\lambda_{719.75}}\right)$	Yang *et al.* 1999

where:

R_x = reflectance at a wavelength x (nm).

r_x = reflectance of a reference spectrum at a wavelength x (nm).

F_x = fluorescence at a wavelength x (nm).

R_v = vegetation reflectance; 600 to 700 nm.

NIR_v = vegetation reflectance; 800 to 1100 nm.

R_s = soil reflectance; 600 to 700 nm.

NIR_s = soil reflectance; 800 to 1100 nm.

g_0 = polynomial coefficient.

p = bidirectional reflectance rectified against reflectance at 442 nm.

L = empirically-derived constant set to minimise the vegetation index sensitivity to soil background.

Reflectance = reflected radiation (chapter 2.1).

3.11.1 Narrow-band vegetation indices

If narrow-band data are also configured in a continuous band sequence then many of the analysis techniques commonly used with laboratory spectrometry may be used. The calculation of first derivative reflected radiation spectra may be used directly for the calculation of an arithmetic VI (e.g., Carter 1998) or as the basis for the identification

of positional VIs. Positional VIs either require continuous narrow-band data or use models to estimate the spectral feature from broadband measurements at selected wavelength positions.

If a sensor's bandwidth is sufficient to resolve the spectral absorption effects of a single biochemical then the quantity of that biochemical may be estimated by contrasting the band that resolves the spectral absorption with one that does not (e.g., Chappelle *et al.* 1992; Blackburn 1998a). There are a huge variety of narrow-band arithmetic VI but none are modified to correct for the presence of soil or for atmospheric attenuation. Broadband VI are used by the substitution of equivalent narrow-bands positioned at wavelengths within the spectral width of the broader-band and many of the broader-band indices performed with a higher accuracy when narrower bandwidths were used (Elvidge and Chen 1995). Of the VI tested by Elvidge and Chen (1995) SAVI was the best at the very narrowest bandwidth.

One function of VIs is facilitation of batch processing by the transformation of a spectrum of data to a summary value; this is a requirement of predominantly broadband applications. Many narrow-band data are collected in the field. Such data are spectrally degraded and used to calibrate airborne or spaceborne sensors or are explored individually where specific spectral components can be extracted and evaluated for site-specific applications.

3.11.2   The identification of the red-edge position

The red-edge position (REP) can be defined as (a) the maximum inflection point (MIP) of reflectance spectra with the red-edge wavelength range (Collins 1978), (b) a dominant derivative spectra peak or (c) a Lagrangian second order polynomial model applied to first derivative spectra (Dawson and Curran 1998). These techniques allow a quantitative comparison of any shift in wavelength and therefore (in controlled conditions) can allow an evaluation of change in state variables.

3.11.2.1   The identification of the REP from the reflectance spectrum

Clevers (1994) discusses three techniques for the identification of the REP from the reflectance spectrum. These are the interpolation of a continuous polynomial function (Clevers and Büker 1991), the inverted Gaussian technique (Bonham-Carter 1988; Miller *et al.* 1991) and linear interpolation (Guyot *et al.* 1992; Danson and Plummer 1995). The first of these is required as preparation for other analysis techniques and can be applied to first derivative spectrum by the use of high-order curve fitting techniques (Savitsky and Golay 1964; Horler *et al.* 1983b; Demetriades-Shah *et al.* 1990; Railyan and Korobov 1993; Chen and Elvidge 1993).

The second method uses an inverted Gaussian model (Bonham-Carter 1988; Miller *et al.* 1990) fitted to the red-edge by means of a least squares procedure (Lucas *et al.* 1995) and the third uses a linear interpolation that assumes the red-edge slope to be a straight line from which a simple linear equation can be derived as an estimate of the REP (Guyot *et al.* 1992; Danson and Plummer 1995).

3.11.2.2   The identification of the REP from the first derivative of the reflectance spectrum

The first derivative of the reflectance spectrum (figure 3.12) can be represented by the slope between two known points on the reflectance spectrum and has been used to produce indices related to the red-edge (Boochs *et al.* 1990; Filella and Peñuelas 1994; Vogelmann *et al.* 1993). For accurate, high precision spectral data, such as from a laboratory or field spectrometers, analysis of the first derivative spectrum can enhance the detail in the red-edge (Ferns *et al.* 1984; Steven *et al.* 1990) by suppressing non-vegetative reflectance components (Boochs *et al.* 1990). This procedure has allowed the identification of multiple peaks (Dockray 1981; Horler *et al.* 1983b; Boochs *et al.* 1990; Railyan and Korobov 1993; Jago and Curran 1996) (e.g., figure 3.12) and allowed some distinction between vegetation groups; for example cereals showed a particularly strong separation between the two first derivative features (Horler *et al.* 1983a). The

position of these first derivative features has been primarily attributed to the influence of chlorophyll concentration and the leaf area index (LAI) (Boochs *et al.* 1990). Dominance between different first derivative red-edge features can change and therefore alter the REP. A shift in dominance between different first derivative red-edge features is due to differences in leaf and canopy variables (Horler *et al.* 1983b; Schutt *et al.* 1984) and the contribution of the background (Curran *et al.* 1990; Jago and Curran 1996).

A complex ground cover reduces the magnitude of the lower wavelength of the first derivative features but maintains its wavelength position (Horler *et al.* 1983b). A quantitative comparison of first derivative peak to the maximum inflection point of the red-edge (MIP) has been achieved in leaf stacking experiments. The dominant peak differed by between 1 and 4 nm for single or stacked leaves respectively, as evaluated against an inverted Gaussian model (Miller *et al.* 1990). This is a crude measure of the detail lost by integration to a single REP value and highlights the fact that the wavelength differences can be small.

3.11.2.3   The identification of the REP from a Lagrangian interpolation technique

Unlike other methods that identify the REP the three point Lagrangian interpolation technique does not assume a priori knowledge of the spectrum and (using simulated, noise-free reflectance data) gives a comparable performance to linear and inverted Gaussian techniques (Dawson and Curran 1998). A disadvantage of this method is that it relies on only three measurements and so is extremely susceptible to noise, especially if the measurements are derived from bandwidths that are relatively wide (greater than 10 nm).
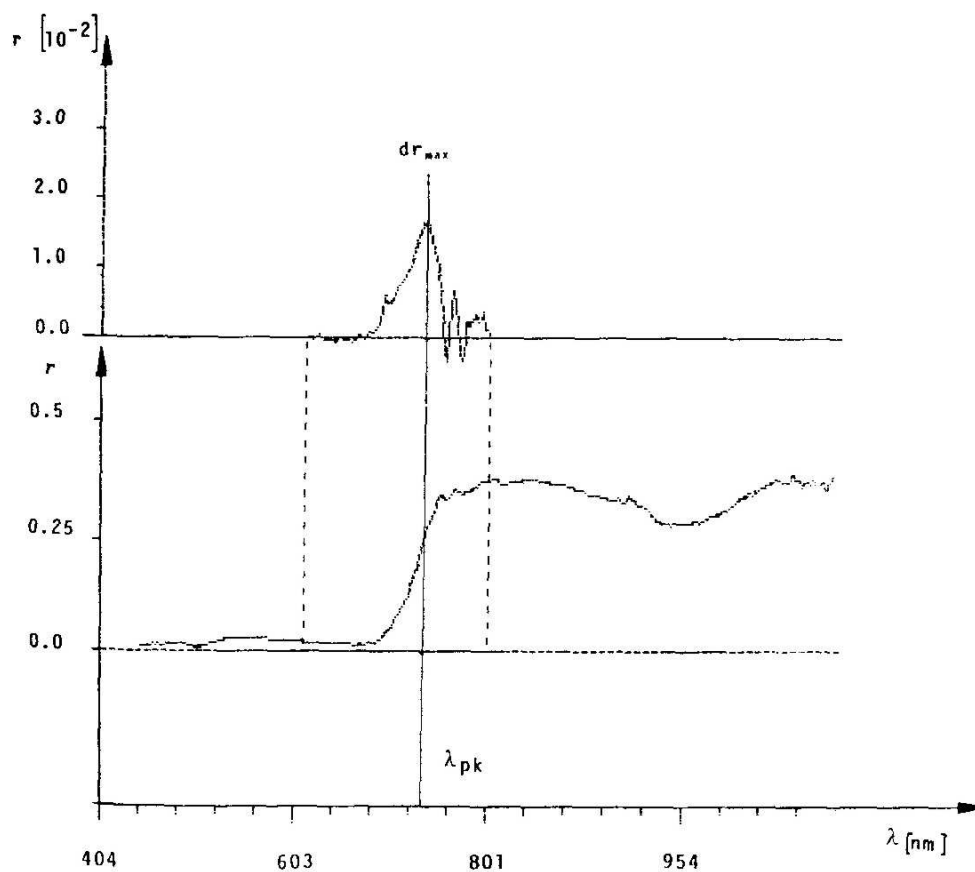
Figure 3.12: A reflectance spectrum and its first derivative, for *Triticum aertivum* (wheat) Source: (Boochs *et al.* 1990)

Table 3.7: A summary of the advantages and attributes of published techniques for the determination of the red-edge position

Technique	Application to reflectance or derivative reflectance spectra	Opportunity to resolve details in the derivative spectra	Complexity	Suitability for discontinuous spectra
Inverted Gaussian	Reflectance	No	Low	No
Linear interpolation	Reflectance	No	High	Yes
First derivative spectra	Derivative	Yes *	Low	No
High-order curve fitting techniques	Derivative	No	High	Yes
Lagrangian	Derivative	No	Low	Yes
Gaussian	Derivative	No	Low	Yes

Adapted from Dawson and Curran 1998.

* Only suitable with high spectral resolution instruments, such as Airborne Visible / InfraRed Imaging Spectrometer or AISA Eagle.

3.11.3 Continuum removal

Continuum removal is a method that allows for the comparison of absorption features by the standardisation of the reflectance spectra across the spectral range of the feature. Its use with techniques such as comparing absorption-band-depth (e.g Kokaly and

Clark 1999; Curran *et al.* 2001; Mutanga *et al.* 2004; Mutanga *et al.* 2005) on spectra from grasses grown under different treatments, yielded better results than those with absolute reflectance (Mutanga and Skidmore 2003).

(1) Some comprehensive comparisons of VI have been made (e.g. le Maire *et al.* 2004) the performance of which are traditionally tested with regression-based statistics, such as coefficient of determination and root mean square error (Ji and Peters 2007).

(2) Other VI contrast the red-edge with longer wavelengths, e.g. $\mathrm{ND}_{chl} = \frac{\rho_{925} - \rho_{710}}{\rho_{925} + \rho_{710}}$ (le Maire *et al.* 2008). This matches an increasing trend to use SWIR wavelengths (le Maire *et al.* 2008; Delalieux *et al.* 2008; Inoue *et al.* 2008).

(3) Some studies go to great lengths to eliminate spatial variability (in their evaluation of VIs) in the canopy environment (e.g. Pinty *et al.* 2009).

3.12 The red-edge position

Photo-reactive pigments can influence the REP if the influence of their absorption extends into the wavelength region of the red-edge. For some red pigments (e.g., amaranthin) this can be for concentrations as low as $0.01\mathrm{mg.g}^{-1}$ (Curran *et al.* 1991). In comparison to chlorophyll, carotenoids have both a higher rates of accumulation and are less preferentially degraded (Buschmann *et al.* 1989) therefore under stressed conditions the relative amount of accessory pigments may increase in proportion to that of chlorophyll. The relationship between carotenoid content and the REP can be stronger than that for chlorophyll content (e.g., r = 0.88 compared with r = 0.86 for chlorophyll *a* and r = 0.81 for chlorophyll b; Blackburn 1998a). This may suggest a high degree of correlation between carotenoids and chlorophyll and between carotenoids and the canopy structure (Blackburn 1998a) thus highlighting the important contribution of canopy structure.

Cutler and Curran (1996) suggest that spatial resolution may be related negatively to

Table 3.8: Examples of maximum measured shifts in the red-edge position collected from laboratory, field and airborne studies Source: Cutler and Curran 1996.

Author	Measurment conditions	Size of support (interval between measurements)(distance over measurments were conducted)	Maximum measured shift in the REP (nm)
Horler *et al.* 1983b	Laboratory	Around a few cm	26
Vogelmann *et al.* 1993	Laboratory	Around a few cm	35
Curran *et al.* 1995	Field	Around 1 m	19
Jago *et al.* 1999	Field	Around 1 m	8
Rock *et al.* 1988	Airborne	Around a few m	5
Clevers and Büker 1991	Airborne	Around a few m	5
Cutler and Curran 1996	Airborne	Around a few m	7.4

the observable shift in REP such that even sensors with a moderate to coarse spatial resolution may not be able to resolve the REP shift (table 3.8). They further recognised that this is related to the intrinsic scale of variation inherent in the scene and the sampling properties of the sensor. Table 3.8 showed the a range of REP shifts reported in the literature. However specific comparison is impossible due to differences in the vegetation, setting, instruments used to collect the data and methods by which the REP are calculated.

Differences in the upper limit of the REP for a species may be manifest due to maximum levels of absorption imposed by the saturation of photo-receptive sites (Gates 1980; Buschmann and Nagel 1993). Horler *et al.* (1983a) divided species into three groups based on quantitative analysis; these were trees (dicotyledonous), temperate cereals

and maize. Maize differs from other cereals in having distinct bundle sheaths that tend towards Krantz anatomy.

A common definition of REP is as the inflection point of the red-edge, REIP. However, when the red-edge inflection point is compared with derivative spectra, e.g. with an inverted Gaussian model (Lamb *et al.* 2002), the inflection point lies between the short and long wavelength peaks. Clevers *et al.* (2001) and Cho and Skidmore (2006) report this as a failing of the derivative spectrum. Their methods of deriving the REP extrapolate is to approximated inflexion point between the peaks and so removes some of the information present within the derivative spectrum. To gain the maximum information from the red-edge the derivative spectra should be considered as a whole and not focused on one of a number of features.

A switch in the position of the maximum of first derivative vegetation spectra (referred to in some literature as a peak jump) was observed in this study and has been observed in numerous other studies (e.g. Horler *et al.* 1983a; Banninger 1990; Boochs *et al.* 1990; Filella and Peñuelas 1994; Miller *et al.* 1990; Lamb *et al.* 2002; Zarco-Tejada *et al.* 2003; Smith *et al.* 2004; le Maire *et al.* 2004). Horler *et al.* (1983a), found that the magnitude of the longer wavelength peak increased when maize leaves were stacked. This had little effect on the magnitude of the shorter wavelength peak. Conversely, Miller *et al.* (1990), found that differences in the derivative spectrum from measurements along the leaves of Bur Oak (*Quercus macrocarpa*) were mainly in the short wavelength peak. Lamb *et al.* (2002) attributed these to variation in chlorophyll concentration along a leaf. In their own studies, Lamb *et al.* (2002) found rye grass leaves (*Lolium sp.*) with different levels of chlorophyll concentration were associated with different peaks. Leaves with low levels of chlorophyll concentration (or chlorotic) had a pronounced short wavelength peak. Leaves with high levels of chlorophyll concentration had a pronounced long wavelength peak. le Maire *et al.* (2004) identified a switch in the peak from 705 to 714 nm and attributed it to a specific chlorophyll content threshold, 45 μg / square cm. They found that the decrease of the short wavelength peak to a threshold where the longer wavelength appeared and then increased explained the switching.

3.12.1   Chlorophyll concentration and content

Laboratory studies have shown a strong correlation between the REP and both chlorophyll concentration (e.g., Filella and Peñuelas 1994) and chlorophyll content (e.g., Gates *et al.* 1965; Buschmann and Nagel 1993. This relationship is described by increases in chlorophyll concentration accompanied by broadening of the chlorophyll absorption feature (Dockray 1981; Horler *et al.* 1983a; Sailsbury *et al.* 1987; Rock *et al.* 1988; Ustin and Curtiss 1988; Curran *et al.* 1995) which shifts the REP to longer wavelengths. This process has been described in spectroscopy terms by the Beer-Lambert Law (Wiffen 1972; Banwell 1983) and in foliar biochemistry terms by differing bandwidths (and positions of maxima) for multiple forms of chlorophyll *a* (French *et al.* 1972). In the Beer-Lambert explanation the width of the absorption feature is a function of concentration where a decrease in chlorophyll concentration would cause a narrowing of the absorption feature while maintaining the same wavelength maximum. In the second explanation the process is a change in the species of chlorophyll *a* as a response to changing environmental conditions. In either case, or as a combination of both, the result of contamination dis-stress (negative effect) is a shift of the REP to shorter wavelengths (Horler *et al.* 1983a) and eu-strees (positive effect) may cause a shift to longer wavelengths (Yang *et al.* 1999). This relationship between the REP and chlorophyll concentration is maintained only if the photoreceptive sites within the chloroplast are not saturated (Gates 1980; Buschmann and Nagel 1993). Munden *et al.* (1994) found that the linear relationship for wheat was maintained until a chlorophyll concentration of 0.5 mg.g^{-1}. This agrees with asymptotic relationships in leaf studies (Monje and Bugbee 1992) while the linear relationship reported in canopy studies (e.g., Curran *et al.* 1990; Curran *et al.* 1991; Curran 1994 suggests that under normal conditions the chlorophyll concentration of the canopy does not exceed the absorption maxima (Munden *et al.* 1994).

Most studies have evaluated the REP shift against total chlorophyll (e.g., Banninger 1991) possibly because the influence of the chlorophyll *a/b* ratio on the REP is difficult to observe (Chang and Collins 1983; Horler *et al.* 1983a; Horler *et al.* 1983b). However,
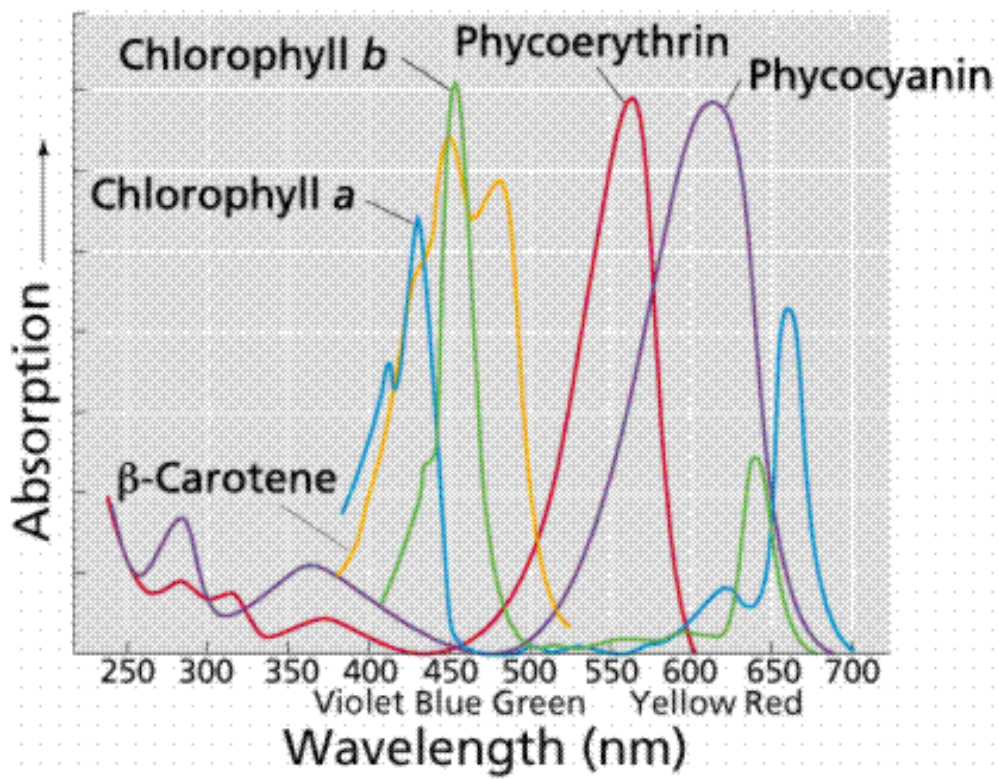
Figure 3.13: Absorption spectra for chlorophyll *a* & *b* and accessary pigments. Source: Farabee 2007

the size and direction of a REP shift is not always consistent with a reduction in total chlorophyll (Banninger 1991). A decrease in the amount of chlorophyll *a* can be concealed by an increase in the amount of chlorophyll *b*. Chlorophyll *a* should have a greater influence on the red-edge than chlorophyll *b* because its absorption maxima are approximately 20 nm wavelength higher than that of chlorophyll *b* (Curran *et al.* 1990) (figure 3.13). This should make the REP more sensitive to changes in chlorophyll *a* but red-edge can also be influenced by other pigments.

Airborne studies observing conifer forest (Curran *et al.* 1995; Curran *et al.* 1997) and grassland (Pinar 1994; Pinar and Curran 1996; Jago and Curran 1997) have shown that a relationship between the red-edge (REP) and chlorophyll is maintained at the canopy scale (chlorophyll content, r=0.93, n=83; Pinar and Curran 1996). REP is better
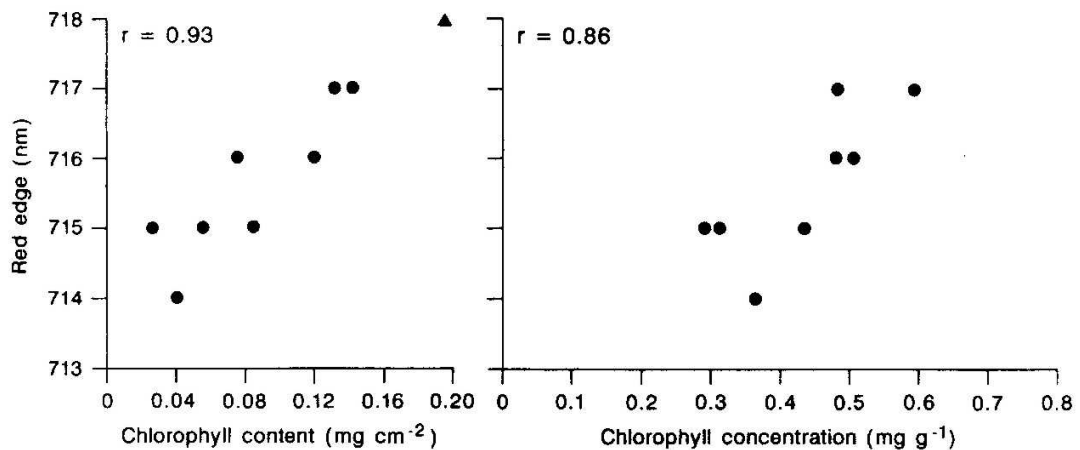
Figure 3.14: Chlorophyll content and concentration and the red-edge position. Source: Pinar and Curran 1996

correlated with chlorophyll content than chlorophyll concentration (Matson *et al.* 1994; Pinar and Curran 1996) (figure 3.14) but chlorophyll concentration may be estimated from calculations using chlorophyll content measurements in conjunction with values for total biomass (Pinar and Curran 1996). The difference between chlorophyll content and concentration is greatest where the canopy is not optically thick and /or where the biomass is spatially invariant (Pinar and Curran 1996). Leaf stacking experiments have shown that the net result of an increase in the number of leaf layers, and therefore the optical thickness, is a shift of the REP to longer wavelengths (e.g., Miller *et al.* 1991; Vogelmann *et al.* 1993) although the relative contribution of different state variables is not identified.

3.12.1.1   The influence of fluorescence of the red-edge

The influence of the fluorescence maximum (at 685 nm) on the nearby chlorophyll absorption peak, in a vegetation spectrum (Nobel 1983; Lichtenthaler *et al.* 1986; Rinderle and Lichtenthaler 1989), may enhance a REP shift to shorter wavelengths when the chlorophyll concentration is very low (Lichtenthaler and Buschmann 1987;

Lichtenthaler 1989). Technical developments may make laser induced fluorescence more viable. It has already been used to investigate nickel (Ni) contamination in plants (e.g Mishra and Gopal 2005).

3.12.2   The influence of leaf area and canopy structure and architecture on the red-edge

Danson and Plummer (1995) found that in addition to chlorophyll content, REP for *Pincea sitchensis* (Sitka spruce) was influenced by LAI (figure 3.15) while modelling (e.g., Clevers and Büker 1991; Guyot *et al.* 1992; Hobson and Barnsley 1996; Llewellyn and Curran 1999) has shown that REP is also influenced by LAD. This may be demonstrated by the specular nature of a 'smooth' planophile canopy compared with a 'rough' erectophile canopy (Cutler and Curran 1995). A shift in the REP can be described solely by changes in the canopy structure. Logically, factors like solar tracking, the process by which plants continuously adjust their leaf orientation such that they are perpendicular to the Sun's rays (Vogelmann and Björn 1986), must also influence the inclination of leaves and photosynthetic efficiency. A shift of REP to longer wavelengths in wheat (Schutt *et al.* 1984) was explained by changes in the exposure of leaf surfaces by leaf movement and considered differences between the abaxial / adaxial leaf surfaces, such as cell density, structure, colour and relief (Wooley 1971). Differences between leaf surfaces may be reduced by leaf damage but shift the REP to shorter wavelengths for both surfaces (Hoque and Hutzler 1992).

3.12.3   Background

Abrupt changes in the REP have been recorded where the background is organic and for low canopy covers of *Pinus elliottii* (slash pine) (Curran *et al.* 1990). The contribution of the background has also been demonstrated for deciduous canopies where changes in the red-edge wavelength region were associated with a transfer of dominant
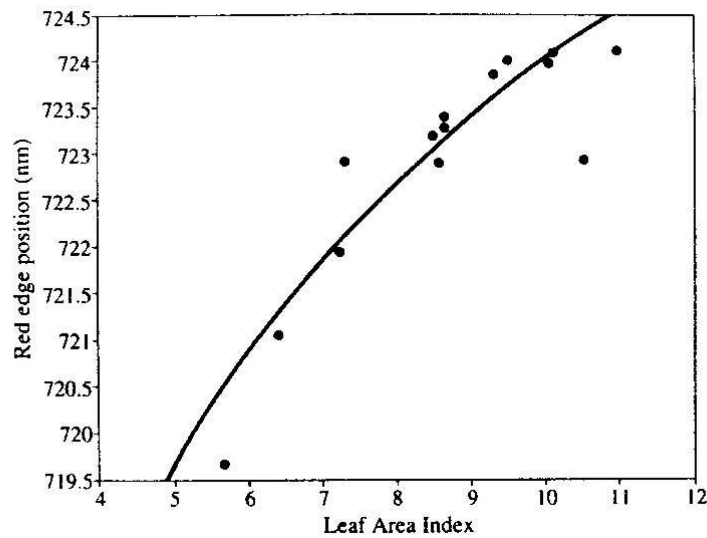
Figure 3.15: Leaf area index and the red-edge position, for grassland (with a power function fitted). Source: Danson and Plummer 1995

scene elements from bark and litter to a photosynthetically active canopy, throughout the growing season (Blackburn and Milton 1995). Spectral mixture modelling has been applied to forest canopies (Curran *et al.* 1990) and grassland (Jago and Curran 1996) and shown that combinations of live and dead vegetation and different canopy covers can influence the REP. Curran *et al.* (1990) found that REP recorded over a canopy of live pine needles was influenced by the lower REP contribution of a vegetated understorey and litter layer of dead pine needles. Variability in REP is dominated by the amount of canopy within an instrument's FOV, not the amount of chlorophyll. In the first derivative reflectance spectra (Curran *et al.* 1990) noted that a progression from a longer wavelength REP feature was associated with an increase in the influence of the background. Jago and Curran (1996) applied a similar investigation to grassland and demonstrated a double-peaked first derivative maxima. They modelled a simple combination of grassland canopy over a soil-dominated background based on a linear mixture of spectra representative of the two extremes and modelled a shift in dominance of the REP feature.

3.12.3.1   Soil and the red-edge position

At canopy scales a FOV is typically composed from the area-weighted interaction of reflectance from the bare soil, layer of litter and understorey that becomes convoluted with the leaf spectra (Dawson *et al.* 1997). The REP has been reported to be insensitive to variations in background (Collins *et al.* 1983) and the contributions of non-vegetative reflectance components may be suppressed by calculating the first derivative (Boochs *et al.* 1990).

> *"'The calculation of derivative spectra eliminates additive constants (e.g. illumination changes) and reduces linear functions (e.g. uniform increase in background reflectance with wavelength) to constants. This has led researchers to conclude that the red-edge is essentially invariant with illumination or the amount of background within the field-of-view of the spectrometer'."*

Curran *et al.* 1990, p.34.

3.12.3.2   Background vegetation and the red-edge position

Vegetation affects reflected radiation within a FOV via the influence of the vegetation canopy, litter and under-storey layers and the soil on reflected radiation (Dawson *et al.* 1997). Abrupt changes in the REP have been recorded for low canopy covers of *Pinus elliottii* (slash pine) with an organic background (Curran *et al.* 1990). The contribution of the background has also been demonstrated for deciduous canopies where changes in the red-edge wavelength region were attributed to a change of dominant scene elements from bark and litter to a photosynthetically active canopy, throughout the growing season (Blackburn and Milton 1995). Spectral mixture modelling has been applied to forest canopies (Curran *et al.* 1990) and grassland (Jago and Curran 1996) and shown that combinations of live and dead vegetation and different canopy covers can influence

the REP. Curran *et al.* (1990) found that REP recorded over a canopy of live pine needles was influenced by the lower REP contribution of a vegetated under-storey and litter layer of dead pine needles.

In the first derivative reflectance spectra Curran *et al.* (1990) noted that a progression from a longer wavelength REP feature to a shorter wavelength feature was associated with an increase in the influence of the background. A similar investigation on grassland (Jago and Curran 1996) demonstrated a double-peaked first derivative maxima. Jago and Curran (1996) modelled a simple combination of a grass canopy over a soil-dominated background based on a linear mixture of spectra representative of the two extremes and modelled a shift in dominance of the REP feature. The REP shifted to longer wavelengths as the proportion of the grass canopy was increased. In these cases it should be noted that although changes in the magnitude of the features were gradual, such that as one reduced the other increased, the switch from one REP to another was a result of the method of deriving the REP (i.e., calculate the maximum of the first derivative reflectance). A first derivative reflectance spectrum gives the most detail concerning changes in the red-edge and the REP the only method so far of summarising these changes. However, the maximum first derivative REP is a simplification of information within the red-edge wavelength region and whilst retaining more information than other methods of REP calculation distorts the underlying data.

Experiments on corn showed that nutrient deficiency also caused a decrease in chlorophyll concentration (Al-Abbas *et al.* 1974). This reduced chlorophyll absorption shifted the REP to a shorter wavelength position (blue shift). Similarly the controlled exposure by acid mist caused moisture stress in coniferous trees (Westman and Price 1988). The moisture stress was as a result of modified stomatal behaviour and this caused damage to cell and chloroplast membranes (Guderian *et al.* 1985) and resulted in a shift in the REP (Westman and Price 1988).

3.12.4   Direct, indirect and transmitted illumination

Direct illumination may be considered as an additive constant for the determination of the REP. It has travelled directly from the radiation source to the target without reflection, refraction or scattering. Indirect illumination is illumination that has been interacted with the atmosphere, objects or surfaces before illuminating the FOV. Transmitted illumination has passed through a media (other than the atmosphere) before illuminating the FOV or within the FOV. If the surrounding scene contains vegetation modified by the effects of contamination then the transmitted illumination may have its wavelength composition modified. Some wavelengths may be enhanced, from ambient reflectance or scattering, and others may be deficient where absorption has occurred. In this way a scene can be influenced by shadow, reflection and scattering from within and outside the FOV.

3.12.4.1   The application of techniques for the identification of the REP to sensor systems

Few airborne systems (e.g., AVIRIS and AISA Eagle) have sufficient spectral resolution to calculate a first derivative reflectance spectrum. Most airborne and spaceborne systems (e.g. CASI; Compact Airborne Spectrographic Imager, ROSIS; Reflective Optic System Imaging Spectroradiometer and MERIS respectively) require an interpolation model and three or four (depending on the technique used) accurate, well-positioned, narrow bandwidth (about 6 nm or less) measurements. Such an approach integrates the subtle multi-peak features resolvable in the first derivative spectrum, but gives a useful approximation of the REP. A high spectral resolution imager may be more informative than an imaging spectrometer (Miller *et al.* 1990) where narrow spectral resolution is available for a fragmented or limited wavelength region in key positions. In such cases a high spectral resolution imager can focus resources to a small number of narrow bandwidth measurements optimised to the resolution of a feature, such as the red-edge.

Spatial resolution is a significant factor with the next generation of spaceborne sensor systems (e.g., Medium Resolution Imaging Spectrometer). At coarser spatial resolutions more variation is integrated and the definition of fine spectral resolution features, such as the REP, is reduced. In addition, at progressively finer resolutions (spectral, spatial or radiometric) the signal to noise ratio decreases. Cutler and Curran (1996) suggest that spatial resolution may be related negatively to the observable shift in REP such that even sensors with a moderate to coarse spatial resolution may not be able to resolve the REP shift (table 3.8). They further recognised that this is related to the intrinsic scale of variation inherent in the scene and the sampling properties of the sensor.

3.13   Modelling

Inter-relationships within the soil contamination / REP relationship can be explored in a modelled environment. Components in this relationship need to be identified and measured to determine which are dominant (major state variables) (figure 3.6). To understand the dynamics of the red-edge the system needs to be simplified, controlled and systematically manipulated. Modelling provides the most effective way to achieve this because it is the only technique that allows individual variables to be controlled with a certainty that other variables are not also affected. The problem is highlighted by wavelengths selected by multiple linear regression using biochemical assay data; these are often not consistent with absorption features of the biochemicals within the leaves (Dawson *et al.* 1998). Models can be formulated to inform at almost all scales and can account for atmospheric effects, leaf and canopy scale variables, vegetation under-storey and soil contributions and spatial patterns in the scene (table 3.9).

At ground level modelling vegetation spectra requires: a leaf optical properties model, a soil optical properties model and a plant canopy reflectance model (Jacquemond 1993). Other components such as the atmosphere and spatial distribution are associated but separate aspects of the problem. Many grass canopies can be assumed to

be homogeneous and for these the radiative equation can be solved to obtain canopy reflectance (Goel 1988) and are the basics for many leaf models.

Table 3.9: Variables that influence the red-edge

Major state variables	Estimated by laboratory or field measurement	Controllable at		Can be modelled?
		Leaf scale	**Canopy scale**	
Chlorophyll content	✓	✓	Σ	✓ (1 & 2)
Leaf physiology #	Σ	Σ	Σ	✓
Leaf size / Leaf area index (LAI)	?	✓	Σ	✓ (2)
Leaf angle distribution (LAD)	?	✓	Σ	✓ (2)
Leaf stack / Leaf overlap index (LOI)	?	✓	Σ	υ
Leaf density	✓	✓	Σ	✓
Soil reflectance	✓	✓	Σ	✓ (2 & 4)
Under-canopy vegetation	✓	✓	Σ	(4)
Atmosphere	✓	✓	ς	✓ (3)
Indirect illumination from surrounding objects	υ	✓	Σ	✓ (2υ)

Major non-state variables

Illumination geometry	✓	✓	✓	✓ (2)
Viewing geometry	✓	✓	✓	✓ (2)

Minor variables

Accessory pigment content & photo-reactive display chemicals	✓	✓	Σ	✓

... continued from previous page

Major state variables	Estimated by laboratory or field measurement	Controllable at		Can be modelled?
		Leaf scale	Canopy scale	
Fluorescence	✓	✓	Σ	υ
Photo-saturation level of photo-synthetic chemicals	υ	✓	Σ	υ
Water content (major if saturated or drought stressed)	✓	✓	Σ	✓
Intra-canopy variations	?	N/A	Σ	υ

Key for table 3.9

Σ	Partially controlled by site or sample selection
υ	Possible / probable
?	A satisfactory measurement technique is yet to be identified
#	Includes: cell density, cell diameter & inter-cellular air spaces
N/A	Not applicable
✓	Yes
ς	No
(1)	Leaf models e.g., LIBERTY (Leaf Incorporating Biochemistry Exhibiting Reflectance and Transmittance Yields) Dawson *et al.* 1998
(2)	Canopy models e.g., SAIL (Scattering from Arbitrarily Inclined Leaves) Verhoef 1984; Verhoef 1985
(3)	Atmospheric models
(4)	Spectral mixture model

3.13.1 Leaf scale models

Radiative transfer models are derived from the radiative transfer equation and can be probabilistic or deterministic (Ganapol *et al.* 1998). The probabilistic approach utilises the more complicated but realistic ray tracing methods (Govaerts *et al.* 1996) to map the multiple photon paths in a simulated environment. One disadvantage is that ray tracing tends to be computationally intensive and difficult to numerically implement. The deterministic approach uses solutions of the radiative transfer equation to describe the absorption and scattering characteristics of the leaf. A popular solution for the radiative transfer equation is based on KM theory (Kubelka and Munk 1931); it makes several assumptions concerning the scattering characteristics of the medium and the passage of light within it such as that light travels either towards or away from the surface and interacts with a parallel plane geometry. The KM solution was interpreted by (Suits 1972) and further developed, by the inclusion of the Plate model, to account for the specifications of the law of photon deflection (Allen *et al.* 1970). The plate model assumes the leaf to be composed of one or a series of transparent surfaces (Jacquemond and Baret 1990) and models that use this approach are PROSPECT (Jacquemond and Baret 1990) and LIBERTY (Dawson *et al.* 1998).

Other solutions to the radiative transfer equation have been used (e.g., Siewert *et al.* 1980; Ishimaru 1978). Siewert *et al.* (1980) used the 'FN method' and it has been adopted by Ganapol *et al.* (1998) for their leaf model; LEAFMOD (Leaf Experimental Absorptivity Feasibility MODel). LEAFMOD has only been verified for dicotyledonous species in one dimension although its creators claim that it will be easier to relax the general assumptions made for radiative transfer solutions, i.e., isotropic scattering and the presence of homogeneous medium. Ishimaru (1978) used two steps the first to calculate the phase function from the properties of the vegetation canopy and the second to solve the radiative transfer equation for a given phase function and boundary condition.

Of the well known radiative transfer models PROSPECT was designed to model the effects of chlorophyll and water content in a basic leaf structure. Its updated form

(PROSPECT-redux) incorporates the biochemicals of cellulose, lignin and protein Jacquemond *et al.* (1996) giving PROSPECT similar input variables to LIBERTY. LIBERTY was developed specifically to model pine foliage but is flexible enough to model other vegetation canopies such as grassland (Dawson. personal communication 1999). Both models are able to predict vegetation spectra and have been used to derive the REP but presently have insufficient spectral resolution (3 nm and 5 nm respectively) to fully explore the first derivative details of the red-edge.

Once calibrated, a model can inform the user of reflectance processes by use of model inversion. This is an alternative to semi-empirical approaches such as spectral mixture analysis, where end members contribute to the whole scene's response. To constrain the inversion process a knowledge of key variables is required (Jacquemond 1993; Dawson *et al.* 1997) but these can be provided from published data, simple laboratory tests and laboratory spectroscopy measurements. The inversion process can be applied to single or combined models and can provide an impressive analysis tool for the understanding of the driving factors in the movement of the REP.

3.13.2   Incorporating the canopy scale

A summary and discussion of canopy models and their development can be found in the review by Goel (1988). Canopy models represent the structure and architecture of the canopy by descriptive variables such as LAI and LAD. Combined models such as LCM2 (Ganapol *et al.* 1999) combine leaf and canopy radiative transfer models. In the case of LCM2, LEAFMOD was combined with CANMOD (Ganapol and Myneni 1992) which was developed from a canopy model called THREEVER (Myneni and Ross 1991) but combinations with other canopy models may be possible depending on similarities between the input and output variables. Another example is FLIGHT (Forest LIGHT; North 1996). It is a hybrid geometric optical / radiative transfer model that utilises ray tracing and has been successfully used in conjunction with LIBERTY to investigate conifer forests canopies (Dawson 1997).

SAIL (Verhoef 1984; Verhoef 1985) is a deterministic radiative transfer model that represents the canopy structure and characterises radiation as a downward flux of direct radiation and an upward and downward flux of diffuse radiation but includes components to account for the leaf area index and the average inclination angle (Verhoef 1984). PROSPECT and SAIL have been combined (e.g., Jacquemond 1993; Hobson and Barnsley 1996). Hobson and Barnsley (1996) explored the complex interrelationship that exists in the physiology of forest vegetation, the extent to which leaf biochemical properties can be retrieved from remotely sensed data and confirmed that knowledge of various parameters that describe canopy structure was required. In addition they demonstrated that the adding of multiple leaf layers in a canopy can lead to significant errors in the estimation of leaf chlorophyll content. This highlighted the problem of equifinality where a high chlorophyll content may be due to high levels of chlorophyll concentration in the leaves or many leaves stacked together, each individual leaf with a lower chlorophyll concentration. The same result, high chlorophyll content, may be due to either eventuality.

3.14   Discussion

The direct remote sensing of contamination on the soil is limited because most contaminants do not have a distinct spectral signature or are obscured by soil and vegetation. Therefore, for remote sensing to be effective, especially in visible and NIR wavelengths, it must rely on the vegetation being affected by soil contaminants and any affect being of a magnitude and nature to be different from other vegetation in uncontaminated conditions. Figure 3.16 is a development of figures and information reported earlier in the chapter and shows the components that need to be addressed to successfully detect contaminants in a grassland soil. To facilitate the investigation of these stages four hypotheses were introduced in chapter 1.1.

1. (H_1) *differences in the relative concentration of contaminants in a grassland soil can be detected using the position and shape of the red-edge of reflected radiation,*

2. (H_1) *stress effects in vegetation (attributed to the effects of soil contaminants) can be measured in the vegetation that grows in that soil,*

3. (H_1) *stress effects in vegetation (attributed to the effects of soil contaminants) are greater than those found by natural variation,*

4. (H_1) *stress effects in vegetation (attributed to the effects of soil contaminants) can be detected using the position and shape of the red-edge of reflected radiation,*

Examples and evidence from previous work have guided the investigation of these hypotheses, as presented in the following chapters. This review has, (i) identified clear evidence of the effect of soil contaminants on vegetation, including grassland vegetation, (ii) considered the existing body of research that has explored and identified stress effects in vegetation, including grassland vegetation and (iii) summarised some of the research that has been directed into the extraction of vegatation properties, specifically chlorophyll content and LAI, from remotely sensed grassland data. Stress effects generally relate to measurements of vegetation state variables outside of their normal range. The attribution of these effects to the actions of soil contamination relies on extra information. Some of this information may relate generally to the vegetation type while other information will be site specific. In the course of these investigations, areas where details were thin or absent were explored. Certainly, there is much scope for further research in the study of grassland, the red-edge and how contaminants in the soil influence them. From this initial assessment it will be clear that a description of the natural variation of grassland vegetation has not been included. This is because the range of grassland types includes many diverse land covers in most cases not even sharing common species. Published literature showed grassland to be a diversely described land cover with spatial variation related to the local conditions and the scale of measurement. The assessment of grassland, when considered within the specifics of remote sensing examples is predominantly based on line scanned data from aircraft or satellites. With new developments and the availability of finer resolution data this was one obvious area where additional work is required. Figure 3.16 is a summary of the areas to be considered. Of the boxes in 3.16 a, only the 'non-state

variables affected by plant stress' were not considered. The possibilities for modelling these relationships and processes (figure 3.16 b) will be considered in this discussion.

3.14.1 The remote sensing of soil contamination

The remote sensing of soil cointamination has drawn heavily on the research and practices of geological prospecting. Developments in our understanding were conducted by Horler *et al.* (1980), Horler *et al.* (1983a) and Horler *et al.* (1983b) and are particularly noteworthy as they identified the first derivative spectra in the red-edge wavelength region as being of particular interest. Specific works in the remote sensing of soil contaminants in the grassland environment have been conducted more recently by Jago (1998) and Smith *et al.* (2000) and related investigations into disturbed ground added by White *et al.* (2008). While these bodies of work showed that soil contaminants can be remotely sensed they did not show that the techniques were applicable for the range of grassland environments which may require their use. However, to do so requires a improved understanding of what grassland is in terms of how it enables the detection of soil contamination.

3.14.2 The effects of soil contamination on vegetation

A soil contaminant was regarded as something in the soil, other than that found there naturally. A wide range of contaminants (natural and artificial) have the potential to cause detrimental effects to the growth of vegetation and promoted specific biophysical effects (figure 3.17). However, in some cases a substance may have a beneficial effect at low concentrations but a detrimental effect at higher concentrations. In other instances a contaminant could interact with another or have an indirect effect. Examples covered two areas, a reaction with soil chemicals that deplete the availability of an element essential for growth or vigour, and the provision of conditions favoured by an invasive vegetation species while having no direct limit to the grown of the indigenous species. Additionally, it was shown that because a contaminant may be located at a specific

(a) Soil contamination and REP

(b) Modelled interactions

Figure 3.16: The relationship between soil contamination and red-edge position
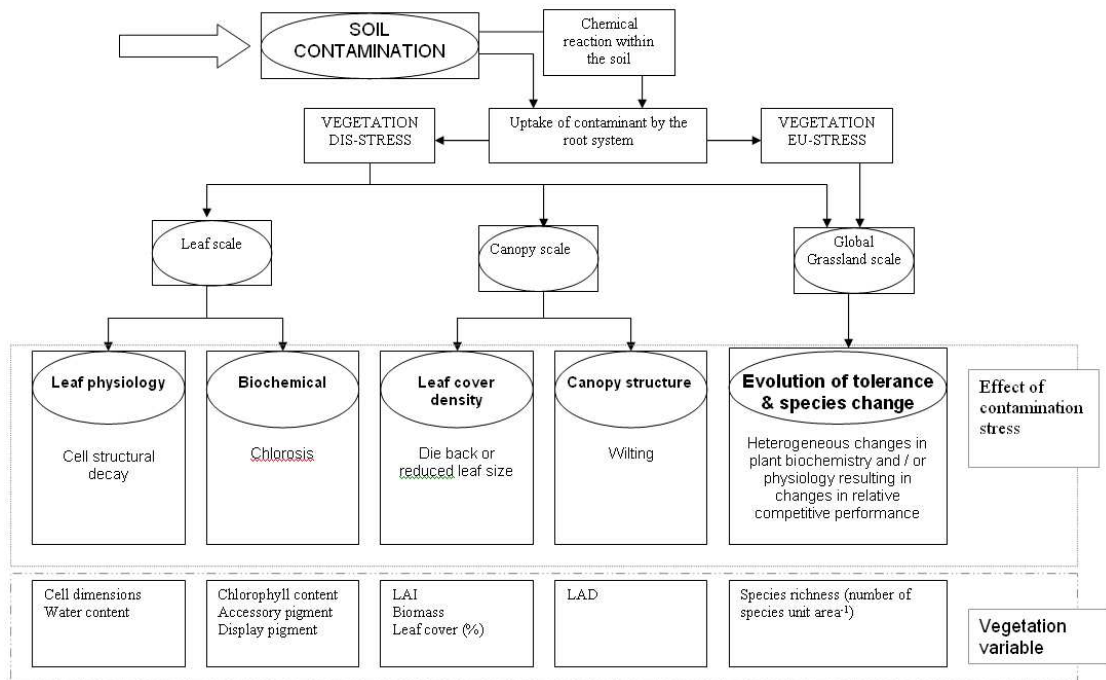
Figure 3.17: The effect of soil contamination on vegetation

depth or location it may allow one set of species to be unaffected by a contaminant while another suffers marked effects (Brooks 1972). Finally, the effects of time were shown to be fundamental to any consideration of soil contamination (Lichtenthaler 1996) with longer recovery or exposure periods giving rise to the evolution of tolerance or the invasion of a more robust set of species (e.g., Baker 1987; Pearson and Ison 1987; Antonovics *et al.* 1971). Although some studies of prairie grassland and agricultural crops had been conducted, the specific long term effects of soil contaminants on semi-natural grassland vegetation as found in England have not been identified. Nevertheless, using other vegetation types as a guide, grassland vegetation exposed to soil contamination was anticipated as suffering restricted growth, chlorosis and changes in species profile.

3.14.3 Remote sensing grassland vegetation state variables

A major area in the development of remote sensing has been for the measurement of vegetation variables, this has led to the production of spectral vegetation indices. Spectral vegetation indices have been produced for many vegetation types in many environments and for many applications. When not limited by sensor restrictions many narrow band vegetation indices have proven to be very specific in their functional capabilities.

A spectral wavelength region particularly sensitive to differences in vegetation is the red-edge. Spectral vegetation indices that used the red-edge to predict chlorophyll content and leaf area index were established in the late 1980's and early 1990's but were limited by the poor understanding of the feature on which they were based (the red-edge). Since then VI have developed and made use of a greater number of wavebands and narrower wavebands. However, substructures (*a double or multiple peak*) in the first derivative reflectance spectra were variously attributed to the influences of chlorophyll, LAI, or fluorescence. Exploration of these features has correlated them with chlorophyll and LAI and more significantly for this study, used them to detect vegation stress effects related to soil contamination (e.g. Horler *et al.* 1983b; Jago 1998; Smith 2002). Adding to this body of work are dedicated studies into grassland vegetation Pinar and Curran (1996) and the first derivative of red-edge reflectance spectrum Miller *et al.* 1990; Zarco-Tejada *et al.* 2000; Cho 2004. The changes in the fine detail in the red-edge region are yet to be modelled or explored with airborne data, and may provide the answer to what defines the REP. Nevertheless, there is still much to understand concerning the dynamics of these first derivative features in a grassland environment, especially with regard to spectral mixing within a sensor's FOV and the spatial distribution (between different FOVs) within an area of interst. Although, grassland has been described as 'a relatively homogeneous environment at coarser scales' (Goel 1988) ecological surveys identify considerable heterogeneity at scales less than a metre (Curran and Williamson 1986).

The stucture of the red-edge was first resolved by the use of laboratory instruments.

Over the years this spectral capability was been extended to field instuments, then airborne instuments and now to spaceborne instruments. With multispectral instruments the subtle fine structure of the red-edge has been treated as a mere curiosity. As spectraradiometers improved, research into the red-edge gained interest. A collection of calculation methods have been developed to determine the REP. As a background independent spectral vegetation index the REP has advantages over other indices, but it requires a combination of spectral bands unavailable to some sensor systems, suffers from complexities of computing and can be susceptible to signal noise (depending on the method used). Therefore, in comparison to the other indices developed for airborne and saellite multispectral data, it had been little used. However, with the greater availability of fine spectral resolution spectroradiometers and hyperspectral sensor systems the use of the red-edge wavelength has received an increasing amount of attention. Within the last ten years there has been a growth of interest in the first derivative of the red-edge reflectance spectrum. Other techniques, such as continuum removal will undoubtedly have applications where they are prominant. Nevertheless, for the remote sensing of soil contamination, the use of REPs and ratios of narrow wavelength first derivative spectral bands has considerable unrealised potential.

The development of new sensors and spectral vegetation indices to evaluate data from them highlights a general deficiency in the reporting of results. While research groups diligently record metadata, many published remote sensing accounts fail to report the scale at which measurements are recorded, the instruments used, the contaminant, the concentration, the vegetation and the data processing methods used. For a comprehensive comparison of research methods and results these omissions place limitations on any overall assessments of patterns made. Some published work is deficient in one or more of these areas or simply uses relative measures for its evaluation. However, some of the most important considerations are not (or cannot) be measured in any but controlled laboratory and field studies.

3.14.4   Modelling interactions with vegetation state variables

The prediction of relative soil contamination may be conducted using a model (figure 3.16 b). However, for remotely sensed data that relate to soil contamination to be separated from the total spectral signal other factors need to be accounted for. These may be conducted by the use of models. Within this chapter some of the options for the modelling of the atmosphere and changes in illumination angle were described. The remotely sensed signal associated with uncontaminated soil may be modelled with a radiative transfer model that accounts for both leaf and canopy effects with regard to the specific characteristics of the vegetation to be modelled. Once these factors are removed a regression derived prediction of soil contamination may be used directly or via the vegetation state variables. If the methodology for the evaluation of variation within a FOV was available then a regression derived prediction of soil contamination may be better allied using an estimated state variable, such as chlorophyll content.

3.15   Conclusion

High concentrations of oil have been detected directly from remotely sensed data, especially in SWIR wavelengths. However, the stronger techniques, potentially more adaptable to different environments, have been directed towards the use of the spectral red-edge to detect vegetation stress by the effects of soil contamination. Work by Jago 1998; Smith 2002; Cho 2004 and White *et al.* (2008) showed that the red-edge wavelength region of the reflectance spectrum still holds information within it and that some of this information can be attributed to the effects of vegetation stress resulting from exposure to contamination in the soil. The extension of existing work to account for different grassland environments is essential if these techniques can be developed for the practical detection and mapping of soil contamination. Any final technique would have to be robust and cope with the range of grassland vegetation structures present on many contaminated sites.

The remote sensing of soil contamination is based on an indirect relationship between a, normally hidden, contaminant in the soil and reflected radiation. Therefore, other potential causes of stress may result in the same measured response. These cannot be resolved using remotely sensed data unless they, and their effects, can be identified separately . The basic mechanism used for the detection of contamination in grassland soil starts with the transfer of nutrients and contaminants from the soil into a plant's roots. This causes a range of biophysical effects that mark the stressed vegetation from non-stressed vegation. Finally, the stressed vegetation are detected by their differences from the non-stressed vegetation by those vegetation state variables that mark that difference, chlorophyll and leaf area. The strong relationship between REP and chlorophyll in grassland vegetation Pinar and Curran (1996) made them particularly good candidates for use in the detection of stressed grassland.

Jago (1998) used chlorophyll content as a linking state variable in the relationship between soil contamination and the red-edge and found that chlorophyll content was strongly correlated with the REP. She also crudely demonstrated the influence of a vegetated background on the red-edge. This research continues on from Jago's (1998) work and will extend it to another site to test the repeatability of her work and will fill gaps in our understanding of what shifts the REP and identify those factors that define the REP. Other work has identified the value of canopy variables but has not fully considered the combination of different grassland canopy characteristics mixed within the same FOV. Background components can be mixed within an instruments FOV; these influence the REP and may be influenced independently by soil contamination. This has not been explored but must be understood if different grassland environments are to be mapped with the same techniques. The modelled environment allows the control and capability to systematically influence an environment. Simple radiative transfer models have been developed for a range of vegetations and vegetated land covers. However, a suitable model to account for the tight cell structure found in monocotyledonous plants, such as grass, is absent. Nevertheless, the leaf model, LIBERTY, can model different cellular parameters and will be developed to simulate grassland vegetation. This will allow some of the causes of features in the red-edge

to be identified and allow clearer understanding of how vegetation stress effects are detected in remotely sensed data.

It is clear that remote sensing can be used for the detection of contamination. Biological restrictions may weaken the use of the red-ege but do not prevent it from being effective if the range of variation can be evaluated. The development of a flexible technique for the detection (and mapping of soil contamination) requires testing over different grassland areas and a better understanding of the semi-natural grassland present on many contaminated sites. The following chapters will address this need.

Chapter 4

Field data methods

4.1 Introduction

To explore relationships between soil contamination, vegetation variables and reflected radiation, each needed to be measured. Measurements were made at six grids and seven transects on a grassland site with different levels of soil contamination and three transects and three grids from grassland sites with no history or indication of soil contamination. This work continued reasearch initiated by Jago in 1998 at a soil-contaminated site with a similar history to the one in this study. Descriptions of the field sites will be followed by a general description of the instruments and methods used to collect data for this research.

4.1.1 Background

Jago (1998) explored the effects of hydrocarbon contamination on grassland on the Isle of Grain (Kent) owned by British Gas. She measured chlorophyll, lignin, cellulose and nitrogen concentrations and concluded that chlorophyll concentration was the most strongly correlated with the levels of contamination and spectral vegetation indices

calculated from the reflected radiation. The Isle of Grain site was not available for further measurements but a replacement site was selected after extensive discussion with the major oil companies. Use of this second soil-contaminated site provided an opportunity to investigate not only if the red-edge / chlorophyll concentration relationship relationship but if the relationships reported by Jago were site-specific or were more generally applicable to soil-contaminated grassland.

4.1.2   Sites

Within this study, four grassland sites were investigated; three had no history of soil contamination and the fourth had clear evidence of different levels of soil contamination as provided by a 'consultant' report (ERM 2000). The three 'uncontaminated' grassland sites had differant land management regimes but all fell into the National Vegetation Classification (NVC) as 'managed grassland' (MG1). The first uncontaminated grassland was on Thorney Island (Chichester Harbour). This site lay at the southern end of the main runway of a semi-used second world war airfield (figure 4.1 a). The area was regularly mown and was visited on three occasions at different stages of growth. These were for a North - South transect (transect 10), three quadrat measurements (grids 8, 9 & 10) and a set of goniometer measurements. The second area was to the North East of Southampton Common and was managed for the mantainance of a conservation habit (woodland rides). This area was intensively sampled in a single quadrat, grid 7 (figure 4.1 b). The third uncontaminated area comprised of two fields on a farm to the North East of Maiden Castle, Dorset. Both fields were used for sheep grazing, one had recently been grazed and the other had recovered.

The soil-contaminated site used in this study was within an perimeter of an oil refinery. Although now grassland, it had been used for oil storage, chemical works, workshops and the dumping of acid tar (figures 4.2 & 4.3). Due to commercial confidentiality the exact location is withheld, although it was on a floodplain in the South of England. The site's owners commissioned environmental consultants to identify principal sources and locations of soil contamination. Six boreholes (drilled by the consultants) lay within

the main study areas. These results and those from trenches were available at a spatial resolution that was too coarse for this investigation but were used to plan the more comprehensive soil survey used in this work. The stratigraphy of the soil was fill/made ground (up to 2 m) over marine alluvium comprising clays and silty clays. The area's principal cover was rough semi-grassland vegetation (within the NVC-MG1) similar to that described as being present on the Isle of Grain (Jago 1998). Seven transects and six grids were sampled from this site (transects 1 to 7 & grids 1-6).

4.2   Methods

Data were collected to investigate the relationships between (i) soil contamination and reflectance (including vegetation indices), (ii) vegetation indices and vegetation state variables and (iii) soil contamination and vegetation state variables. To ensure that the range of values measured was as large as possible, *a priori* information from the site owner was used to define areas likely to be representative of high and low levels of soil-contamination. Reflected radiation and vegetation and soil variables were measured (or interpolated) for common locations in three grids. Additional measurements of reflected radiation were collected along four transects (with a measurement interval of half a metre) and at fifty individually surveyed locations. Sampling grids were used to estimate local spatial variability within the contaminated site. Within each grid 400 m^2 quadrats were randomly located and grids and quadrat locations surveyed to a common coordinate system. Additionally, spatial variability along transects were measured for specific spectral vegetation indices. Spectroradiometer measurements and some vegetation measurements were collected *in situ* while other measurements were made in laboratories at the University of Southampton (in the Departments of Geography and Chemistry) or at the University of Nijmegen (in the Department of Chemometrics).
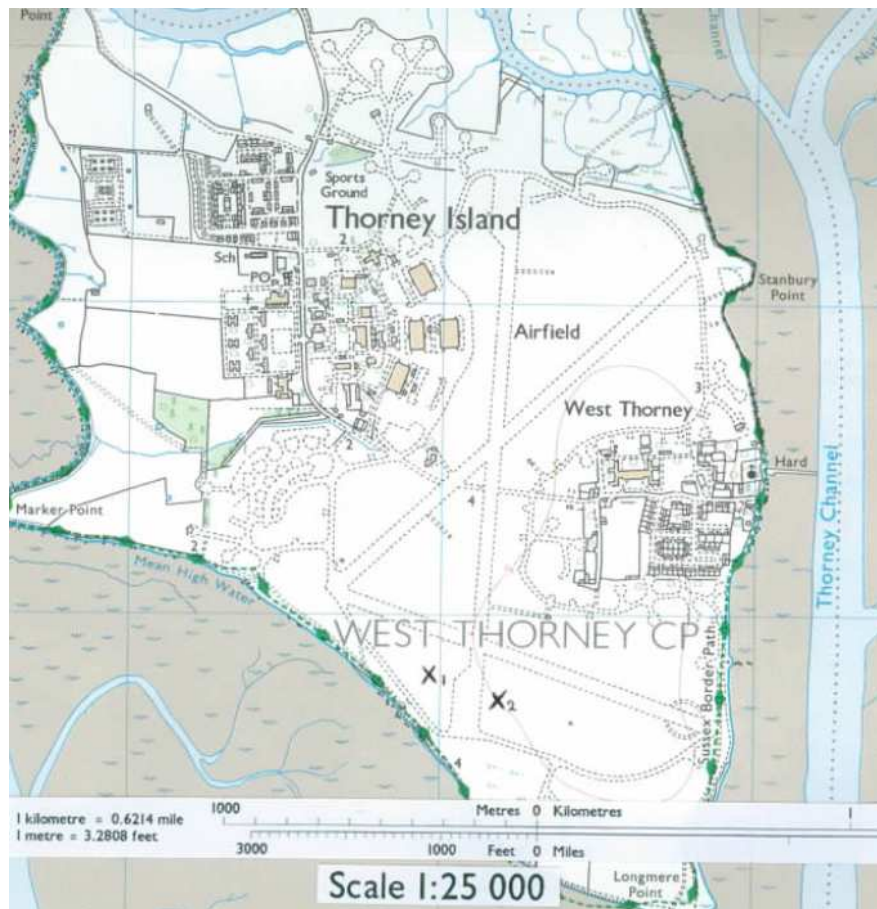
(a) Thorney Island (Chichester Harbour)
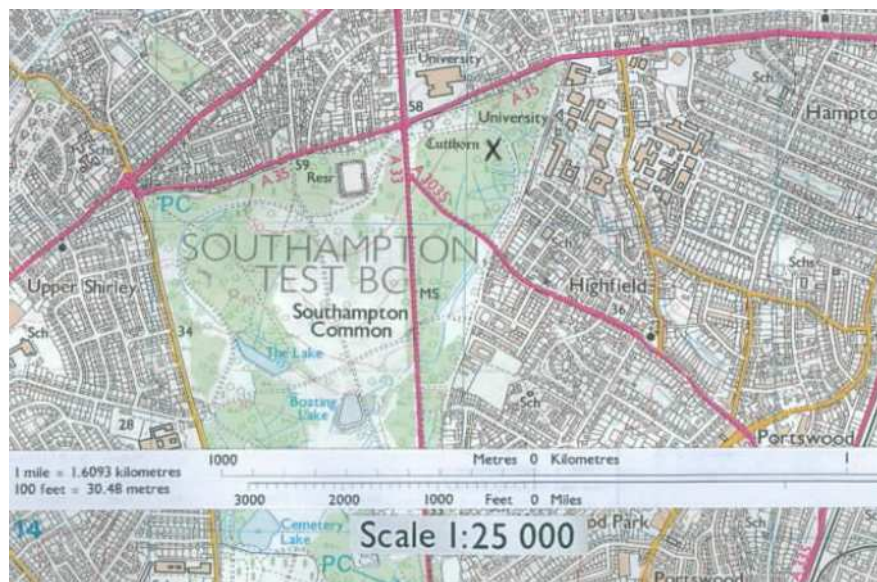
(b) Southampton Common

Figure 4.1: Plan of uncontaminated grassland sites.

On the Thorney Island site, X_1 marks the location of grids 8, 9 & 10 (OS grid ref. 475967 101825) and X_2 the centre of transect 10 (OS grid ref.476190 101737). On the Southampton Common site, X marks the location of grid 7 (OS grid ref. 442118 115216).

(a) West area (WP6)   (b) East area (EC9)
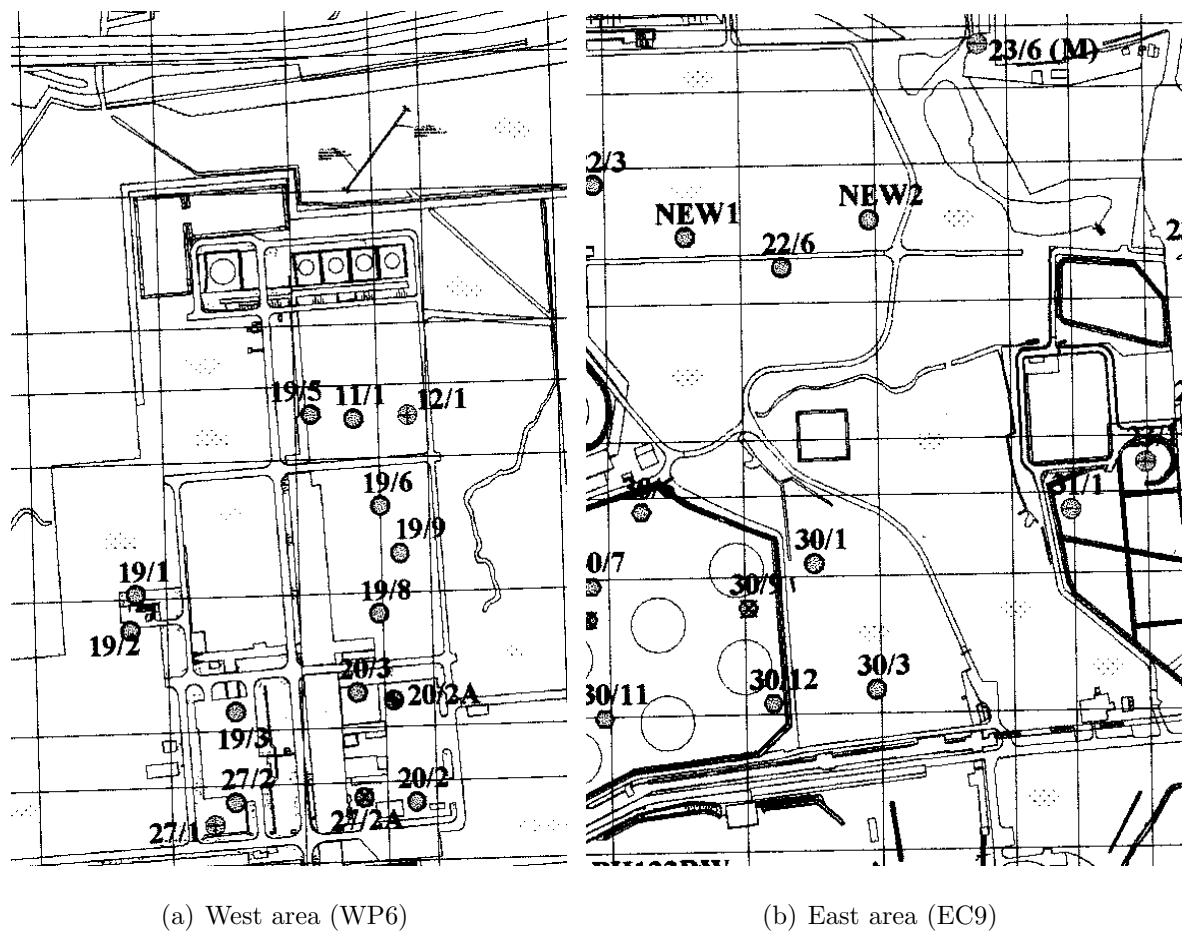
Figure 4.2: Plan of grassland site with different levels of soil contamination.
Labelled circles indicate bore holes from which the soil measurements were made by the
environmental consultants employed by the site owners (ERM 1998).

(a) East area (EC9)

(b) East area (EC9)

Figure 4.3: Grassland with different levels of soil contamination

4.2.1   Sampling

"Samples are not always representative …. Descriptive and inferential statistics will be of little or no use if they are summaries of non-representative samples."

Matthews 1981, p.62

The accuracy (or representativeness) of a variable interpolated or extrapolated from fine scale measurements depends on (i) the variation within the area over which the fine scale measurements were made and (ii) on the variation within the total area over which the variable is to be estimated. Terms that describe spatial distribution of variables, such as homogeneous and heterogeneous, depend on the scale at which measurements are conducted. Many grass canopies can be described as homogeneous (Goel 1988) over areas of tens of m^2, especially when compared to vegetated land covers such as forest. Nevertheless, within an area of less than a few m^2, grassland is heterogeneous. A support is the size, geometry and orientation of the space over which a measurement is made (Atkinson 1993); it therefore has a component related to the scale at which the measurement was made. For field-based remote sensing the support comprises of (i) the field-of-view (FOV), (ii) the weighting of the signal within a FOV and (iii) the optical and viewing geometry. In some cases variables were measured on different supports. A regional variable is an estimate of a variable at a scale larger than that over which the variable was actually measured (local or fine scale). The accuracy of the estimate of a regional variable is dependent on the variation in that variable, therefore an accurate estimate of a regional variable is only obtained if local measurements of the variable are sufficient to account for any variation. Such local measurements are arranged according to a sampling strategy, optimal sampling therefore provided data from which an accurate regional variable can be calculated. For chlorophyll concentration, unrepresentative estimates arise because a sample may contain either species other than grass, assemblages other than leaves or too many
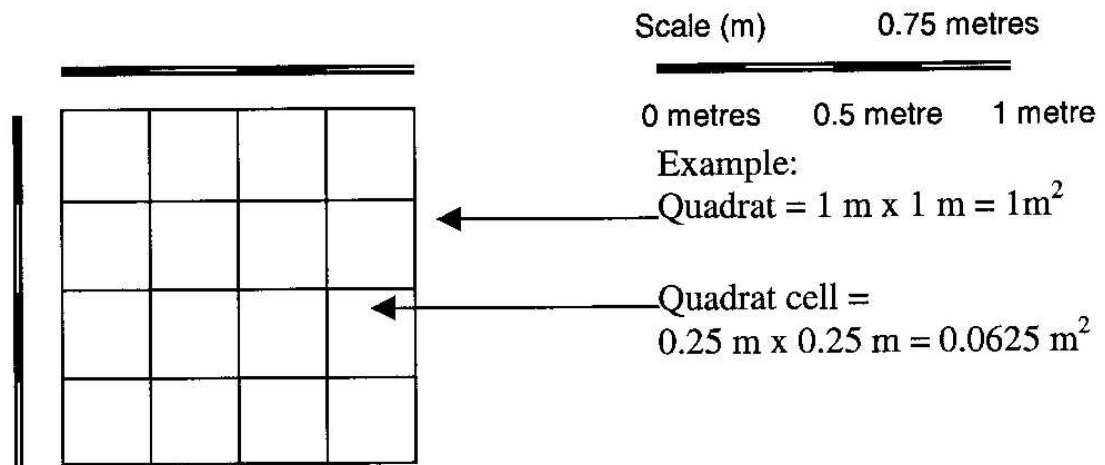
Figure 4.4: 25 square cm Quadrat (0.0625m^2)

leaves to measure without further sub-sampling. Vegetation sampling considerations included the selection of (i) positions on a leaf, (ii) leaves from a plant, (iii) plants from a quadrat cell, (iv) quadrat cells from a quadrat (figure 4.4) and (v) quadrats positioned within a field site.

4.2.1.1 Sampling strategy

A sampling strategy combines a sampling frame, a sampling scheme and a sampling density. The sampling frame comprises the area in which sampling is conducted. For this study the sampling strategy included grids and transects positioned by *a priori* information. The sampling scheme was the arrangement by which spatial data were collected (e.g. random, systematic, stratified, hybrid: figure 4.5) and aimed to capture the amount of variability necessary to fulfil the specific sampling objectives. The sampling density of each grid or transect described the number of measurements or samples collected per unit area. Of the possible sampling strategies, a systematic sampling strategy is the most efficient for the calculation of spatial patterns of variation. However, such a strategy may be inaccurate if there are (i) scale related patterns e.g., periodicity, (ii) *a priori* information that can stratify the sample area or (iii) if the sample spacing or sample grid were determined by constraints such as, spatial
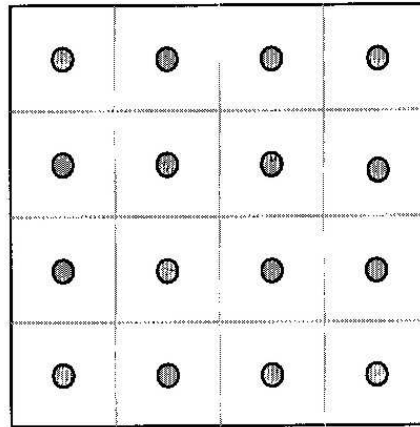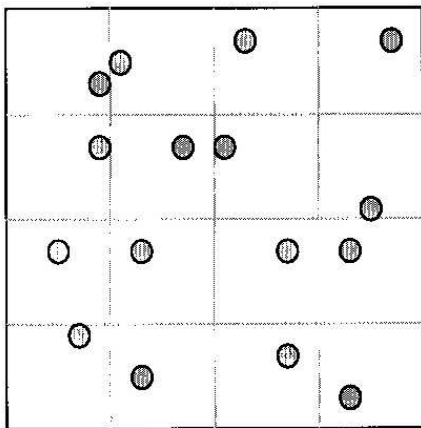
Figure 4.5: Sampling schemes

resolution of airborne data or localised physical restrictions at the place of sampling. Systematic and random sampling schemes were compared by Abt *et al.* (1999) at an extensively sampled *'superfund'* site in Missouri (USA) where the soil was contaminated with dioxin. The data were used to (i) predict linear combinations of data (explicitly) from coincident locations and (ii) estimate covariance parameters (implicitly) from displaced locations. Abt *et al.* (1999) found that linear predictors with coefficients derived from a model (fitted to the logarithms of the data) gave accurate predictions of soil-contamination and that replicate sample pairs ensured an accurate estimate for measurement error variance.

4.2.1.2   Sampling objectives

The purpose of sampling in this study was to gain representative estimates of vegetation variables (e.g. chlorophyll concentration, biomass), reflected radiation (for areas defined by the FOV of a field radiometer) and levels of soil contamination (e.g. concentration of lead or copper) from the same location. Additionally, the measurements of vegetation variables also needed to be collected at the same time as the reflectance measurements, or a close as possible. Sub-sampling was used for measurements where the support was smaller than a FOV. In this survey the sampling strategies used were determined by two objectives; these are outlined in table 4.1.

4.2.1.3   The optimal sampling strategy (Number of samples and sample size)

Time and equipment availability placed a practical limitation on the number of measurements made while the degree of spatial variation in the site was initially unknown. Techniques for the determination of the samples required to characterise an area are available using data acquired in a pilot study (Rao and Ulaby 1977) but require the pilot to be of a similar size and extent as the main study. This study fulfiled that requirement but suffered from additional requirements of the data set, such as local

Table 4.1: Sampling objectives

Sampling objective	Section in which considered
1. To provide an accurate estimate of vegetation, reflected radiation and soil variables and the spatial variation of those variables.	Sampling at the canopy scale (section 4.2.1.5). Determining the optimal sampling strategy (section 4.2.1.3), Sampling at the sub-leaf scale (4.2.1.6) Sampling at the leaf scale (section 4.2.1.7)
2. To provide an accurate estimate of the spatial variation of vegetation, soil and reflected radiation variables	Determining the optimal sampling strategy (section 4.2.1.3)
3. To provide coincident vegetation variables and reflected radiation variables.	Sampling at the canopy scale (section 4.2.1.5). Determining the optimal sampling strategy (4.2.1.3)

comparison between data and the training of a model.

Therefore a compromise between gathering spatial information and characterising the site with coincident measurements of different variables was made. The compromise had three components designed to address the sampling objectives. These were:

1. Firstly to collect a transect of reflected radiation measurements using a GER 1500 in single beam mode for each of the study locations (figure 4.2) each with an interval of half a metre. These measurements provided pilot data about (a) the differences in reflected radiation for different areas and (b) spatial variation of VIs within these areas.

2. From these data, three grids each with a measurement interval of two metres and external dimensions of twenty metres by eighteen metres were constructed (figure 4.6). Within each grid there were 110 possible measurement locations. 50 locations were selected at random. At all 50 locations reflected radiation

was recorded using a GER 1500 in dual beam mode, at 40 of these locations two vegetation samples (one for SPAD 502 measurements and the other to assay and biomass measurements), Sunfleck Ceptometer measurement and a digital photograph were taken.

3. At approximately the same location as the previous three grids, an additional three grids with a measurement interval of five metres and external dimensions of twenty metres by twenty metres were constructed (figure 4.7). Within these five by five grids soil was sampled systematically at 25 locations.

From these data a measure of spatial variation was calculated for the red-edge position (first derivative maximum and linear interpolated REP) and soil related variables. All grids were located by surveying with a Spectra Precision Instruments Total Station and co-located on a National Grid coordinate system (figures 4.6 and 4.7) such that different data sets could be matched for statistical comparison. Twenty-five measurements from between ten and twenty blades of grass contribute to a single estimate of chlorophyll concentration. These measurements were combined with others to provide a regional estimate of chlorophyll concentration within the 200 cm^2 area a field spectrometer would view (FOV). This investigation into the influence of state variables on the REP and the mapping of relative levels of soil-contamination from remotely sensed data used a systematic random sampling strategy, transects for the soil-contaminated grassland and quadrats for the uncontaminated grassland. These strategies aimed to provide (i) data representative of the areas from which they have been sampled for the estimation of the local mean and (ii) data representative of the regional mean and variance. Replicate samples were used to estimate the measurement error variance. Optimisation of a sampling strategy was achieved by identifing specific sampling objectives and settling on a compromise between them for the greatest net gain. A combination of different sampling schemes was adopted to accurately estimate regional variables while also co-locating measurements. This enabled the statistical comparisons of local and regional scales. Some schemes captured spatial variation while others maximised the number of measurements. The spatial distribution of variables measured from reflected radiation, vegetation samples and soil samples were modelled to allow

(a) Grid 1

(b) Grid 2

(c) Grid 3

(d) Legend
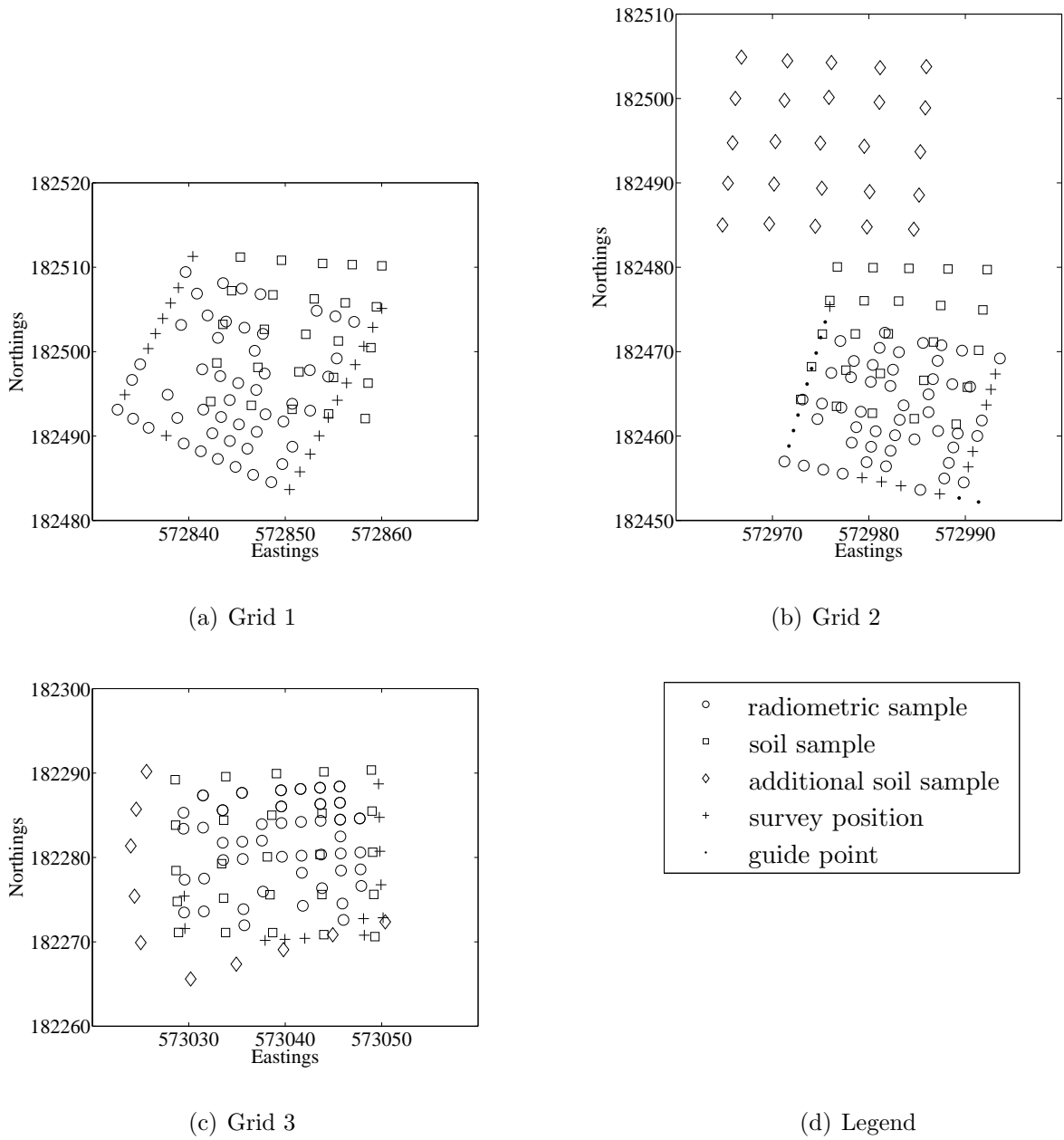
Figure 4.6: Vegetation and radiometric sampling positions per grid on the soil-contaminated grassland
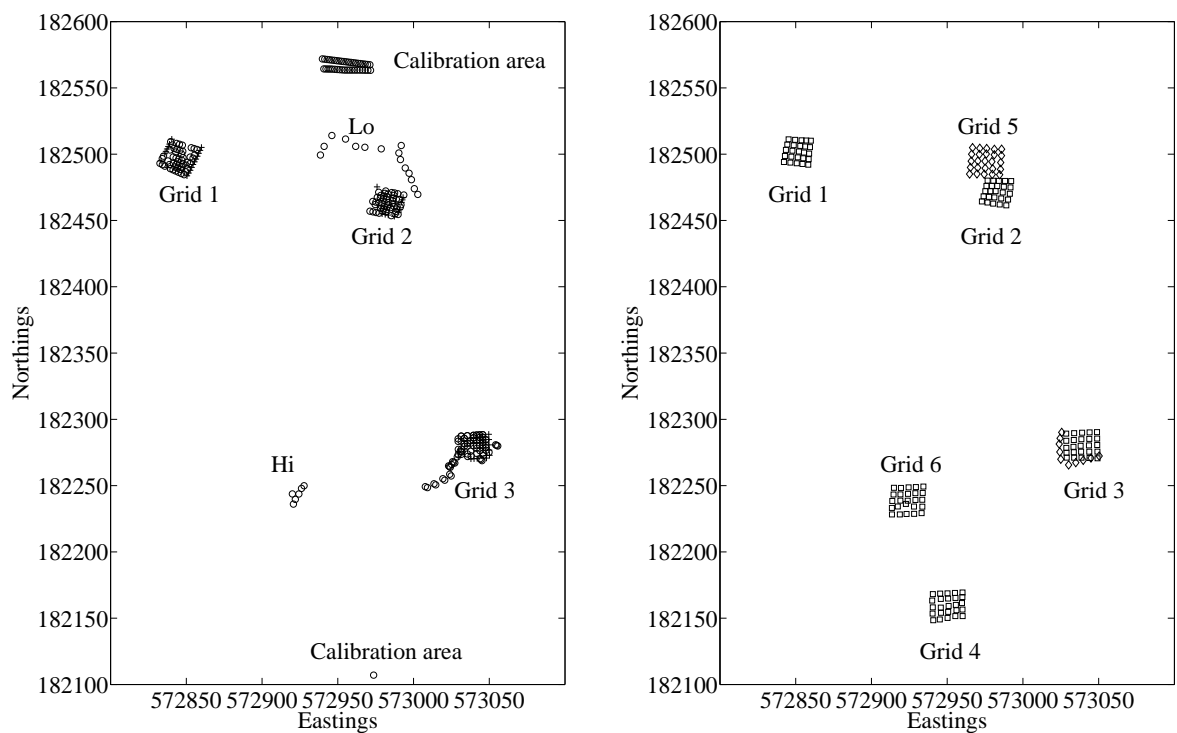
(a) Relative positions of radiometric measurments

(b) Relative positions of soil samples

Figure 4.7: Relative positions of radiometric measurements and vegetation and soil samples on the soil-contaminated grassland

the interpolation of variables where co-location of different variables was not achieved.

4.2.1.4   Data matching

Practical constraints prevented the measurement of all variables at the same time and at exactly the same location. This was because of (i) limitation in available time during individual field work campaigns, (ii) safety restrictions that prohibited the placement of markers in the subsoil and (iii) movement of industrial vehicles that removed location markers from the soil surface. Twenty two soil samples were within 10 cm of vegetation and reflectance measurements, these allowed a direct comparison between variables. Additionally, all measurements were surveyed and plotted on a common co-ordinate grid. This allowed the interpolation of reflected radiation (and vegetation variables) for soil locations, and soil variables for reflected radiation (and vegetation variables) (figures 4.7). Interpolations of soil data used spatial data (semivariances) calculated from soil variables from the twenty five measurements at each grid location. Interpolations of vegetation indices used spatial data (semivariances) calculated from the nearest transect of reflected radiation measurements (assuming no directional bias).

4.2.1.5   Soil sampling

Soil samples from the site of contaminated grassland were sampled to a depth of between 0 and 10 cm (due to site restrictions). 161 soil samples were measured for pH and assayed for heavy metals (Ni, Cd, Cu, Zn, Se, Pb) and long-chain hydrocarbons (C7-16). A stratified sampling strategy ensured that at least 30 samples were collected from grassland with high levels of soil-contamination and 30 from grassland indicated to have low levels of soil contamination. Indications of 'high', 'intermediate' and 'low' levels of soil contamination are derived from existing soil survey data, site history and soil analysis. These were translated into identified ground locations using a preliminary assessment of compact airborne spectrographic imager (CASI) data. An excess of $10,000 \ \mu g$ of hydrocarbon per gram of soil was considered to indicate high levels of

soil contamination, whereas areas with under 1,000 μg of hydrocarbon per gram of soil were low. Intermediate levels of soil contamination were those areas between high and low.

4.2.1.6   Sampling at the sub-leaf and leaf scale

Vegetation analysis included a measure of leaf thickness and two sub-leaf measurements; (i) cell dimensions by the use of a microtome and microscope and (ii) chlorophyll concentration data estimated by wet-assay of 2 cm leaf sections. From each 400 cm^2 quadrat, vegetation was sampled from two 100 cm^2 quadrat cells (figure 4.5). Samples of plant assemblages were separated into *Poaceae* and non-*Poaceae*. Leaf samples measured using a SPAD 502 were returned to the sample from where they came (once all 25 measurements had been made). Leaf samples to be used for the wet-assay of chlorophyll concentration were removed from the stem and homogenised. Accuracy of the chlorophyll concentration estimate was increased by extraction of four replicate samples from each homogenised sample.

4.2.1.7   Sampling at the canopy-scale

The percentage ground cover of broad floral species types (*Poaceae* and non-*Poaceae*) were estimated in each quadrat and the vegetation mass determined by biomass samples and measurements of LAI. An additional fine scale (less than 1 m×1 m) investigation into grassland canopy variation in biomass and SPAD 502 values were assessed for 400 cm^2 and 1 m^2 quadrats from uncontaminated grassland (Southampton Common and Thorney Island). From 1 m^2 quadrats either 100 % or 25 % (25 of 100 cells) vegetation cover were sampled and from 400 cm^2 quadrats 50 % (2 of 4 cells) vegetation cover were sampled.

4.2.1.8   Storage and handling of samples

Where measurement of samples in the field was not possible they were collected and transported to the place of analysis. Samples for SPAD 502 measurement were placed into sealable plastic bags stored in a cool box and measured within four hours. Cell dimension samples were transplanted, transported to the University of Southampton and prepared as thin section slides at the earliest opportunity. For laboratory analysis, vegetation samples were placed into sealable plastic bags stored in a cool box for the journey to the University of Southampton, and stored in a freezer at -18°C until the time of analysis.

4.2.1.9   Sampling error

There are two types of error: (i) sampling error and (ii) non-sampling error (Matthews 1981). Sampling error occurs when the sampling strategy used does not provide data representative of the population from which it was sampled. This may be because it does not adequately account for variation in the area of measurement. It may also be due to an inadequate sample size or sampling scheme for accurate estimation of population of variables. An example of such a case is the use of a single measurement to estimate the regional mean of the variable measured for a larger heterogeneous area. Non-sampling errors may be attributed to (i) instrument errors, (ii) inconsistencies in the methodology and from (iii) errors in data processing. Errors are accumulated throughout the process of collecting, measuring and processing data. These accumulated errors were investigated and were considered, to evaluate the validity of conclusions drawn from the results. Some inconsistencies in conditions and methodology have been assessed by the repetition of measurements. Fifty repeat field radiometry measurements were recorded for the site of contaminated grassland during each of the main periods of data collection and twenty five SPAD 502 measurements per quadrat location. Two wet-assays of chlorophyll concentration were conducted on each sample used to calculate the transformation equation between SPAD 502 values and chlorophyll concentration and sixteen repeat wet-assays of chlorophyll concentration

were conducted on the same vegetation sample to assess consistency in chlorophyll extraction methodology. Non-sampling error may have been incurred due to changes in vegetation variables during transportation and frozen storage of vegetation samples. It was not possible to quantitatively evaluate this.

4.2.2   Soil variables

The soil samples were composed of a matrix of clay and silt within which there were coarser sediments, roots and contaminants. Potential contaminants as identified from the initial survey in the soil-contaminated field site were heavy metals (e.g., cadmium, copper, nickel, zinc and lead) and non-aqueous phase hydrocarbons liquids (NAPL) and solids (e.g., acid tar). 116 samples that were collected from the site of soil contamination were analysed. Identification and quantification of the content of each contaminant within the soil samples were conduced at the University of Nijmegen and the University of Southampton. At the University of Nijmegen (Department of Chemometrics), heavy metals were derived by induced couple plasma (ICP). Hydrocarbons were extracted at the University of Southampton, Department of Geography and Department of Chemistry by soxhlet extraction in dichloromethane.

4.2.2.1   Determination of metal concentration

Total metal concentrations were determined at the University of Nijmegen (Department of Chemometrics), laboratory for analytical chemistry. Approximately 20 g of soil were dried at 105°C for 24 hours. Samples were ground with a mortar and particles larger than 2 mm were removed by sieving. Dried soil samples (1 g) were treated with a HNO_3/H_2O_2 solution in Teflon-lined bombs using the microwave digestion method (Janssen *et al.* 1997; Bettinelli *et al.* 2000; Durand *et al.* 2004). After mineralisation, total cadmium (Cd), copper (Cu), nickel (Ni), zinc (Zn) and lead (Pb) concentrations were measured using inducted coupled plasma atomic emission spectrometry (ICP-AES).

Figure 4.8: Soxhlet reflux extraction

4.2.2.2   Determination of solvent extractable matter

Solvent extractable matter is a gravimetric measure of the total dissolvable hydrocarbon from a soil sample (the protocol for this method is in Appendix B). Dichloromethane (DCM) was a solvent for many hydrocarbon contaminants found in soil samples (Guerin 1999). Using soxhlet extraction with 250 ml of DCM (figure 4.8) hydrocarbon contaminants were collected over 16 hours with a reflux approximately every 10 minutes. DCM and contaminants were then separated by evaporation out of a pre-weighed 150 ml flask using a Buchi rotary evaporator (figure 4.9). The accumulation of 'total solvent extracted matter' (minus DCM) in the 150ml flask was weighed and determined by difference. This was termed total extracted hydrocarbon (TEH) but is referred to as solvent extracted hydrocarbon (SEH) in some literature.

4.2.2.3   Gas layer chromatography

Samples of hydrocarbon contaminants (in solution with DCM) were analysed by gas layer chromatography. By this method the hydrocarbon contaminants were carried by

Figure 4.9: Buchi rotary evaporator

nitrogen through a gas chromotography column packed with an inert material. This caused the hydrocarbons to travel at different rates and therefore became separated. An analyser module (flame ionisation) at the end of the column is then used to identify each component as it reaches the end of the column.

4.2.2.4   Loss-of-ignition of soil

Loss-of-ignition (LOI) is a measure of the soil mass combusted during four hours within a furnace at 550°C is (the protocol for this method is in Appendix B). LOI includes combusted hydrocarbon and organic material, such as roots.

4.2.2.5   Water content

Dry soil mass subtracted from the original soil mass gave a measure of the water content. Water was removed from the soil sample by heating the sample in an oven until there was no change in mass. The temperature was restricted to 85°C to minimise the degradation of biochemical and physiological structures within the soil.

4.2.2.6   Acidity / alcalinity (pH value)

Acidity can influence growth of vegetation and the distribution of vegetation communities (Hubbard 1984). pH is the logarithm of the concentration of hydrogen ions and is a general scale of acidity / alkalinity where pH 1 is strongly acid, pH 14 is strongly alkali and pH 7 is neutral. The pH was measured using a Hanna Instruments pHep (HI98127) Digital pH meter calibrated with Watman pH buffer solutions. The protocol for this method is in Appendix B.

4.2.3   Field and laboratory measurements of reflected radiation

Reflectance data were collected in the laboratory using a Perkin Elmer Lambda 19 (section 4.2.3.1) and in the field using GER 1500s (section 4.2.3.2) and a prototype goniometer (section 4.2.3.4). These data allowed the evaluation of reflected radiation at different scales and under a variety of conditions (table 4.2).

Table 4.2: Grassland datasets

Date	Location	Number of samples	Instrument	Spectra	Chlorophyll	Contam - ination
18.05.99	Thorney Island	43	Perkin Elmer lambda 19 (laboratory)	175-3200 nm (1 nm res.) (4.2.3.1)	yes, SPAD	no
18.05.99	Thorney Island	79	GER3700	300-2500 nm (1.5 nm res.) (4.2.3.3)	yes	no
27.04.00	Soil-contaminated grassland (transects)	approx. 750	GER 1500 (single beam mode)	300-1100 nm (1.5 nm res.) (4.2.3.2)	no	yes
12-13.06.00	Soil-contaminated grassland (grids)	133	GER 1500 (dual beam mode)	300-1100 nm (1.5 nm res.) (4.2.3.2)	yes, SPAD	yes
03.06.00	Soil-contaminated grassland	50	GER 1500 (dual beam mode)	300-1100 nm (1.5 nm res.) (4.2.3.2)	yes, SPAD	yes
03.06.00	Calibration areas on or near soil contaminated grassland	4 positions (between 20 and 50 / position)	GER 1500 (single beam and dual beam mode)	300-1100 nm (1.5 nm res.) (4.2.3.2)	no	no

4.2.3.1   Perkin Elmer Lambda 19

The Perkin Elmer Lambda 19 is a computer driven, dual-beam, double monochromator (UV and VIS / NIR) ratio recording, laboratory spectrometer with a spectral range of 175 to 3200 nm (Anon. 1991). Holographic gratings were used in each monochromator and a filter wheel (synchronised automatically with the monochromator) fed radiation to (i) a photomultiplier for the UV / VIS wavelength range, and (ii) a lead sulphide (PbS) detector for NIR wavelengths. Filter changes were at 562.4 nm, 690.4 nm, 810.4 nm and the detectors changed at between 819.2 and 920.4 nm (Anon. 1991). Mirrors reflected radiation into a chopper assembly that rotated to alternately bring a mirrored segment, a window segment and a dark segment into the radiation beam. The mirror segment directed radiation reflected from the sample. The window segment directed radiation from a reference (a 60 mm gold-laminated VIS/NIR integrating sphere). The dark segment blocked the radiation beam and created a dark signal (residual detector signal with no input) for internal calibration. A tungsten-halogen lamp (for measurements at VIS and NIR wavelengths) and a deuterium lamp (for autocalibration) provided illumination. Spectral resolution (spectral bandpass) was dependent on the nominal wavelength bandwidth for each wavelength. The Lambda 19 provided a nominal slit width of 0.1 nm for VIS and 0.2 for NIR. For a nominal wavelength bandwidth of 1 nm the spectral resolution was 0.99 nm at 400 nm, 0.93 nm at 600 nm, 0.91 nm at 656.1 nm and 0.86 nm at 800 nm (Anon. 1991). During the detector initialisation process the spectral resolution was calibrated automatically against the bandwidth of the deuterium emission at 656.1 nm. The instrument accuracy for the UV/VIS range was ± 0.15 nm and in the NIR range ± 0.6 nm (Anon. 1991). Repeatability of results was less than 0.02 nm in the UV / VIS range and less than 0.08 nm in the NIR range, as determined by the standard deviation of ten measurements (Anon. 1991). The instrument allows the measurement of radiance (Wm^{-1} steradian^{-1}) transformed to biconical reflectance (case 5, as per Schaepman-Strub *et al.* 2006) using a dual measurement from an integration sphere.

4.2.3.2   GER 1500

The GER 1500 is a field spectroradiometer with a spectral range of 300 nm to 1100 nm
(MacArthur 2007). It has a sampling interval of 1.5 nm, a spectral bandwidth of
3 nm, 16-bit encoding and an integration time (typically) of one second. The fore
optics provided a cone of acceptance FOV of 3° with a nadir surface footprint of ap-
proximately 18 cm radius from a height of 1.2 metres. Reference measurements used
Spectralon panels of known (near Lambertian) reflective properties. The GER 1500's
were operated in both single-beam mode and in dual-beam mode. Single-beam mode
used a single spectroradiometer with alternate measurements of target and reference
surfaces. Dual-beam mode used two spectroradiometers to record near-simultaneous
measurements of the target and reference (figure 4.10). Inter-calibration of the two
instruments was achieved by the use of two Spectralon panels and inter-calibration
software provided by NERC EPFS. Dual-beam mode required a frequent repeat of the
inter-calibration process but proved to be operationally quicker than single-beam mode
(MacArthur 2007). This reduced the time difference between the measurement of tar-
get and reference and this minimised the effect of any variation in atmospheric and
solar conditions between these measurements. The GER 1500 spectroradiometers were
loaned by the Natural Environment Research Council Equipment Pool for Field Spec-
trometry (NERC EPFS) and were synchronised with uniform illumination conditions.
For the soil-contaminated grassland the loans of the GER 1500 spectroradiometers
were arranged with a high likelihood that the Natural Environment Research Council
Airborne Remote Sensing Facility (NERC ARSF) would collect data. The instrument
allows the measurement of radiance (Wm^{-1} steradian^{-1}) transformed to hemispherical-
conical reflectance (case 8, as per Schaepman-Strub *et al.* 2006) using the spectralon
panels with their spectra recorded by NERC EPSF.

4.2.3.3   GER 3700

The GER 3700 has a spectral range of 350nm to 2500nm (Rollin and Anderson 2001;
Fogwill 2005). It has a sampling interval of 1.5 between 350nm and 1050nm, 6.2nm

Figure 4.10: Intercalibration of GER 1500 in dual beam mode

between 1050nm and 1900nm and 9.5nm between 1900nm and 2500nm. The instrument has a spectral bandwidth of 3nm over the 300 to 1050nm region, 11nm over the 1050 to 1900nm region and 16nm over the 1900 to 2500nm region. The 3° optics matched the GER1500 and also provided a nadir surface footprint of approximately 18cm radius from a height of 1.2 metres. A Spectralon panel was used as a reference. The GER3700 was also loaned by the NERC Environment Research Council Equipment Pool for Field Spectroscopy (NERC EPFS) and was synchronised with uniform illumination conditions. The instrument allows the measurement of radiance (Wm^{-1} steradian^{-1}) transformed to hemispherical-conical reflectance (case 8, as per Schaepman-Strub *et al.* 2006) using the spectralon panels with their spectra recorded by NERC EPSF.

4.2.3.4   Goniometer

The goniometer was used as part of additional research on Thorney Island. It was a prototype developed at the University of Southampton that used an Ocean Optics

USB2000 (VIS-NIR) Fibre Optics Spectrometer mounted on a large despoked bicycle wheel. The instrument uses a 2048 element silicon array and provided a spectral range of 350nm to 1000nm with a 1.5nm spectral full-width-half-maximum (FWHM) bandwidth. The instrument was operated under uniform illumination conditions with end optics to give a 30cm FOV. The manufacturers claim a signal-to-noise ratio of 250:1 at full signal and an integration time of between 3 millisecond and 65 seconds (Ocean Optics 2009). When used the integration time approximated 1 second. The instrument allows the measurement of radiance (Wm^{-1} steradian^{-1}) transformed to a series hemispherical-conical reflectances (case 8, as per Schaepman-Strub *et al.* 2006) using the spectralon panels with their spectra recorded by NERC EPSF.

4.2.3.5 Data pre-processing

The digital numbers (recorded by the remote sensing instruments) were transformed to absolute reflectance. This was achieved with software provided by Perkin Elmer (PECSS Anon. 1991) and NERC EPFS (REFG1500.EXE, REFGDFOV.EXE and DFOVCAL.EXE Kerr 1998). The intercalibration of GER 1500's in dual-beam mode was achieved with additional NERC EPFS software.

PECSS is a suite of operating and analysis software (version 4.01) created by Perkin-Elmer for the Lambda 16 and 19 instruments (1991). It was used to transform data collected from Perkin-Elmer laboratory spectrometers from absorbance into reflectance. REFG1500.EXE is an MS-DOS programme that transformed data collected from a single instrument in single-beam mode into absolute reflectance. It divided the reflected radiation from a target by the reflected radiation from a Spectralon panel multiplied by the absolute reflectance of the Spectrolon panel. REFGDFOV.EXE is an MS-DOS program that transformed the data from a pair of instruments in dual-beam mode into absolute reflectance using an inter-calibration file. DFOVCAL.EXE is an MS-DOS program that calculated the inter-calibration file. It used the near-simultaneous measurements of Spectralon by instruments used in dual-beam mode. Additional data for these software were the solar zenith angle correction factor and the known Spectralon

T reflectance values (Anon. 2009b). Sun angle factor was obtained from EPFS data related to the sun angle which in turn was derived from the site location and time of measurement (Sundesign 2002).

4.2.3.6 Data analysis techniques

Vegetation indices were calculated from collected spectra using custom written Matlab software (VIgo.m). VIgo calculated fine-band and broad-band vegetation indices from reflectance spectra (Appendix C). Broad-band vegetation indices were applied to simulated CASI (vegetation bandwidths), SeaWifS and MERIS spectral configurations.

4.2.4 Leaf Area Index

Leaf area index (LAI) was measured because of its commonly cited role as a major state variable. It was calculated from reflected radiation above and below the canopy using measurements from a Delta-T Devices Sunfleck Ceptometer SF80 (figure 4.11). The Delta-T Devices Sunfleck Ceptometer SF80 was a long light-sensitive probe with 80 photodiode sensors along its length (Anon. 2001). The PAR range is from 0 to 2000 (mol m^{-2}s^{-1}) with a resolution of 1 mol m^{-2}s^{-1} (Anon. 2001). In its 'PAR mode' the ceptometer measured solar irradiance from a single photodiode at its tip in units of PAR quantum flux (mol m^{-2}s^{-1}). In its 'sunfleck mode' the Ceptometer measured radiation over the whole probe length. The sunfleck fraction was displayed as the percentage of the probe length exposed to bright sunflecks (Anon. 2001). Data were stored as three values depending on the selected mode of operation: (i) time, (ii) PAR and (iii) quantum flux or sunfleck percentage.

Figure 4.11: Delta-T Sunflect Ceptometer (Anon. 2001)

4.2.5 Chlorophyll concentration and content

Chlorophyll (concentration and content) are commonly cited major state variables (e.g., Pinar and Curran 1996) susceptible to the effects of soil contamination (e.g., Jago 1998). It therefore provided a conceptually link between soil contamination and reflected radiation. Chlorophyll concentration may be directly derived by wet chemistry ($mg.m^{-2}$) but is less useful for the comparison of remotely sensed data where data relate to an area rather than a mass. Jago (1998) derived her relationships solely with with chlorophyll concentration. In this study chlorophyll content were derived by the use of biomass ($g.m^{-2}$) to relate the chlorophyll to an area. The high proportion of soft photosynthetically active tissue in the grassland (by observation) minimised errors incurred by the presence of branches and trunks in other vegetated environments. In the field, chlorophyll concentration was estimated from measurements using a Minolta SPAD 502. The SPAD 502 was loaned by Horticultural Research International and was calibrated using the solvent extraction of chlorophyll followed by transmission spectrophotometry using a WPA S106. An additional calculation was made to adjust chlorophyll content by the percentage of cover indicated by digital images at each

location. The measurement of biomass and percentage cover are described as other vegetation variables.

4.2.5.1   SPAD 502

The Minolta SPAD (Soil-Plant Analysis Development) chlorophyll meter 502 was developed to estimate chlorophyll concentration in plants by the measurement of 'leaf greenness', which is positively correlated with leaf chlorophyll (Markwell *et al.* 1995). The SPAD 502 offered a quick, non-destructive method for the estimation of chlorophyll concentration. This hand held equipment (figure 4.12) utilised two light-emitting diodes (at 650 and 940 nm) and a photodiode detector to sequentially measure transmission of radiation through the leaves. On each leaf, two readings were made at approximately one-third and two-thirds of the distance from the leaf tip to the base. Readings at the basal end of the leaf were avoided. Additionally the meter was shaded to keep direct sunlight from influencing the measured value (Pettygrove 1985). Sub-leaf sampling considered variations within a leaf, e.g., due to vascular structure (figure 6.5) and attempted to maintain a consistency in measurement position. Outlier (extreme) values may be caused by positioning of the meter's head over the leaf edge or midrib, on insect damage, or on other discoloured areas of the leaf. Although the most common error was to position the instrument over the midrib the error caused by taking such readings was not large (Pettygrove 1985). The leaf sections were measured for wet assay to calculate a transformation for SPAD 502 values to chlorophyll concentration. These were selected for consistency as indicated by five SPAD 502 measurements within a 0.5 range (of SPAD 502 values). SPAD 502 values were compared with vegetation indices collected from a Perkin Elmer Lambda 19 and GER 1500.

4.2.5.2   Solvents used for wet-assay of chlorophyll concentration

Chlorophylls, carotenoids and all prenyl pigments, are fat-soluble compounds and, if liberated from the cellular structures, can therefore be extracted from water-containing

Table 4.3: Acetone concentrations and wavelength combinations used for the solvent extraction of chlorophyll

Researcher	Solvent and concentration	Wavelength	Wavelength
Lichtenthaler and Wellburn (1983)	100 % acetone	662 nm	645 nm
Lichtenthaler (1987)	100 % acetone	662 nm	645 nm
Jeffrey (1963)	90 % acetone	645 nm	630 nm
Anon. (1966)	90 % acetone	645 nm	630 nm
Jeffrey and Humphrey (1975)	90 % acetone	645 nm	630 nm
Jago (1998)	90 % acetone	664 nm	647 nm
Lichtenthaler and Wellburn (1983)	80 % acetone	663 nm	647 nm
Lichtenthaler (1987)	80 % acetone	663 nm	647 nm
Gitelson and Merzlyak (1994)	80 % acetone	663 nm	647 nm
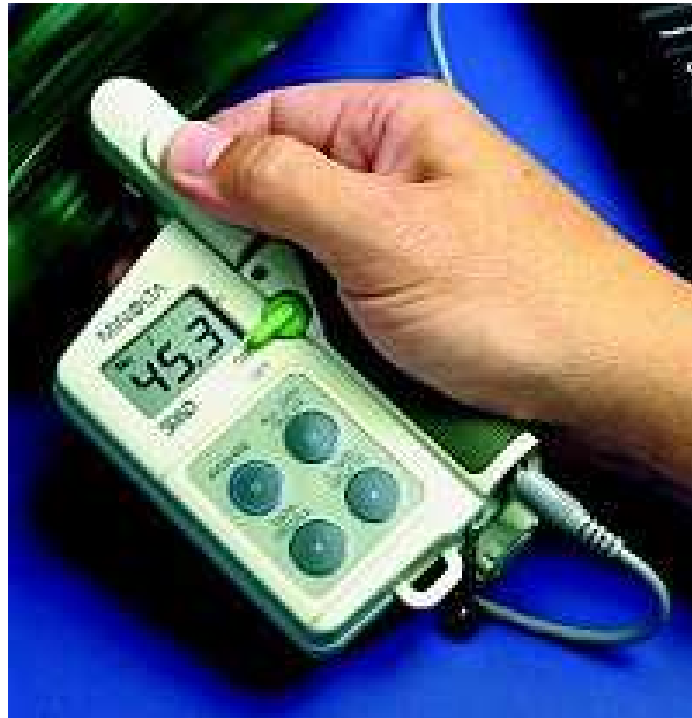
Figure 4.12: Minolta SPAD 502

living plant tissue using organic solvents tissue (Lichtenthaler 1987). The range of organic solvents and concentrations that have, in the past, been used for the wet-assay of chlorophyll concentration include: acetone (100 % v/v), acetone (90 % v/v), acetone (80 % v/v), diethyll ether (100 %), ethanol (95 % v/v), methanol (100 %) and methanol (90 % v/v). The choice of solvent was a balance between gains in extraction efficiency against shifts in absorption features and secondary reactions (Lichtenthaler 1987). For example there is a reported shift of the absorption maxima to longer wavelengths from acetone (100 %) to acetone (80 % v/v) (Lichtenthaler 1987) (table 4.2). The most widely used 'standard' method to extract photopigments uses 80 % aqueous acetone (Arnon 1949). However, this does not fully extract the less polar pigments, chlorophyll a and the polyene β-carotene (Lichtenthaler 1987). An additional step of extraction with 100 % acetone is needed to guarantee 'complete extraction' (Lichtenthaler 1987). Lichtenthaler (1987) states that aqueous solutions of organic solvents are suitable for extraction only when their water content does not exceed 5 or 10 %. A single extraction using 90 % acetone (v/v) has been adopted by some researchers as a practical com-

promise (e.g., Jeffrey 1963; Jeffrey and Humphrey 1975; Jago 1998) that originated with Mackinney (1941). However, when concentrations are greater than 90 %, acetone evaporates readily and under these conditions can give spuriously high readings (Yoder and Daley 1990). Differences between solvent extraction methods mean that results are only comparable when comparing identical methodologies or once data are transformed into a measure of concentration.

4.2.5.3   Pheophytinization

Chlorophylls *a* and *b* are easily transformed by weak acids to their magnesium-free derivatives (the pheophytins *a* and *b*). Chlorophyll *a* is more sensitive to pheophytinization than chlorophyll *b* and is accelerated with increasing temperature (Lichtenthaler 1987). To minimise these effects the homogenisation process was kept as short as possible (between one and five minutes with the mechanical homogeniser and less than one minute with liquid nitrogen) and was performed with solvents that had been stored in a jacket of cold running water (i.e., at 3 to 5°C), as per Lichtenthaler's recommendations (1987).

4.2.5.4   Selected technique and laboratory procedure

For the analysis of uncontaminated grassland the method used by Jago (1998) (90 % acetone) was repeated. However, the 90 % acetone method provided less consistent the results than the 'standard' method using 80 % acetone. Therefore, for the calibration of SPAD 502 values to chlorophyll concentration the 'standard' method using 80 % acetone (Arnon 1949) was used (the protocol for this method is in Appendix A). For both methods frozen vegetation samples were thawed for 1 hour on absorbent paper under ambient room conditions. One centimetre sections of leaf were crushed and ground, with a mechanically homogeniser or in the presence of liquid nitrogen, and then mixed with a pre-prepared acetone solution. 12 ml of the solvent were placed in a centrifuge for ten minutes at 3600 rpm. Absorbance (A) was recorded for each sam-

ple using a WPA S106 spectrophotometer. The measurement of selected wavelength regions was repeated five times and from this the average was calculated. For the 'non-contaminated' grassland the selected wavelengths were: 662 nm, 663 nm, 664 nm, 645 nm, 646 nm and 647 nm. For the calibration of the SPAD 502 to results from the standard method selected wavelengths were: 663 nm and 647 nm.

The work of Lichtenthaler (1987) provided the following relationships (equations 4.1, 4.2 and 4.3) for 80 % aceteone v/v: $A\lambda$ = absorbance at wavelength λ

$$Chlorophyll\ a = 0.01225 \times A663.2 - 0.00279 \times A646.8 \qquad (4.1)$$

$$Chlorophyll\ b = 0.02150 \times A646.8 - 0.00510 \times A663.2 \qquad (4.2)$$

$$Chlorophyll\ a\ +\ b = 0.71500 \times A663.2 - 0.01871 \times A646.8 \qquad (4.3)$$

Jago's work (1998) provided the following relationships (equations 4.4 and 4.5) for 90 % acetone v/v:

$$Chlorophyll\ a = 0.0127xA664 - 0.00269xA647 \qquad (4.4)$$

$$Chlorophyll\ b = 0.0227xA467 - 0.00468xA664 \qquad (4.5)$$

From these equations chlorophyll concentration may be derived (equation 4.6):

$$Chlorophyll\ concentration\ (mgg^{-1}) = \frac{chlorophyll\ (gl^{-1})\ *\ volume\ (l)\ *\ 1000}{Vegetation\ sample\ weight\ (g)}$$
$$(4.6)$$

4.2.5.5   S106 spectrophotometer

The WPA Ltd. S106 spectrophotometer had a spectral range of 330 to 900 nm. The illumination source was a pre-focused tungsten filament applied through a holographic diffusion grating and detected using a silicon photocell. The bandwidth was 5 nm and

the setting accuracy was 2 nm. Samples were measured from cuvettes. Glass cuvettes were used because the standard plastic cuvettes were destroyed by the solvent. To maintain accuracy consecutive measurements were made of the sample and a distilled water reference via a roller switch and before work commenced the instrument was sent to its manufacturer for servicing and recalibration.

4.2.6   Other vegetation variables

While LAI and chlorophyll concentration are commonly cited as the major state variables ((chapter 3) other vegetation variables may also influence reflected radiation. In this section the methodology for the collection of data for biomass, species richness and cell dimensions are described. Measurements have been conducted in the laboratory and in the field and have provided data for empirical analysis and as inputs for modelling.

4.2.6.1   Biomass

Vegetation was cut at approximately 3 mm from the soil surface. Wet biomass is the harvested mass of vegetation and dry biomass is the mass of vegetation once water has been removed. Water was removed from the sample by heating it in an oven until there was no change in mass. The temperature was restricted to 85°C to minimise the degradation of biochemical and physiological structures within the grass. Dry biomass subtracted from the wet biomass gave a measure of the water content. Thorney Island (Chichester Harbour) quadrat samples were weighed within 12 hours while samples from the site of soil contaminated grassland were stored, later thawed for one hour at ambient room conditions and their biomass (wet and dry) measured.

4.2.6.2 Percentage cover

Digital images were subjectively classified into different percentage ground cover components: *Poaceae* (grasses), *Trifolium* (clovers), other *Leguminosae* and low growing vegetation, tall growing vegetation (other than *Poaceae*) and a non-vegetated component (soil, stones and tar). The digital images were recorded at nadir viewing angle approximately 1.25 metres from the sample of *in-situ* grassland with a digital camera. All *in-situ* grassland samples were marked for scale by a 400 cm² (20 cm×20 cm) quadrat (with four 10 cm×10 cm cells) and a 225 cm² (15 cm×15 cm) labelled white tile.

4.2.6.3 Species richness

There are two measures of an environment's biological diversity, one is species richness, (recorded as number of species per unit area) the other is species abundance (also described as evenness or equitability) (Magurran 1988). Of these, only species richness was measured in this study. Species richness was determined by a vegetation survey using quadrats and a cumulative record of species within them. (Gilbertson and Kent 1985) recommended a suitable quadrat size for the grassland vegetation cover survey as between 1 m² and 16 m² (1 m×1 m and 4 m×4 m) depending on the nature of the grassland. To standardise against the most diverse environment (indicated as grassland with high levels of soil contamination) this study used use 1 m² (1 m×1 m) quadrats. A base number of 50 quadrats per study area (Magurran 1988) and a stratified random sampling scheme was used for each grid to characterise grassland with different levels of soil contamination. Grass species were identified by the use of field guides (e.g., Hubbard (1984), Perring (1985) and Rose (1981)) and the help of an experienced botanist (J. Shultz).

4.2.6.4   Cell dimensions

Cell dimensions were recorded from thin cross-sections of grass leaves. These were prepared using a microtome. Leaf samples were mounted in paraffin wax and clamped in the microtome. Parallel thin sections were sliced from the block face using an angle of approach of 10°-20° and an angle of tilt to about 10°. Thin cross-sections were stained (e.g., using Methyl Blue and Saphranin) and mounted between cover slides for examination under the microscope. The measurement of cell dimensions was achieved by use of a graticule, a calibrated ruler set within the eyepiece of the microscope.

4.3   Conclusion

Data from these methods were used to investigate the relationships between soil contamination, reflected radiation in the red-edge wavelength region and vegetation variables. Averages and measures of variation of vegetation variables collected from Southampton Common and Thorney Island (Chichester Harbour) were used to validate and drive a radiative transfer model (described in a later chapter). Data from the contaminated site was used to draw comparative relationships within variable groups (i.e. vegetation and soil), between variables and to drive the radiative transfer model to ensure that it was capable of operating within the range of variables observed in collected field and laboratory data. The following chapter describe and discuss the results obtained by the use of these instruments and methods.

Chapter 5

Field data results: the relationships between soil contamination and the reflected radiation of grassland

5.1 Introduction

In this chapter the detection of contamination by the use of remotely sensed passive optical data has been used, specifically in the spectral red-edge region. The first necessity was to match reflectance measurements with soil contamination. To determine the relationship between soil contamination and reflected radiation the areas where different levels of soil contamination are present need to be identified. Grassland areas with different levels of soil contamination (high, intermediate and low) were identified from borehole and pit data described in a report commissioned by the site owners (ERM 1998; ERM 2000). From these data a preliminary field survey (transects 1 - 9) was used to locate six 20 metre x 20 metres areas for further analysis (grids 1-6). In five of these areas (grids 1, 2, 3, 4 & 5) the levels of nickel (Ni), copper (Cu), cadmium (Cd), zinc (Zn), lead (Pb), selenium (Se) and total extractable hydrocarbon (TEH) present in the soil were determined by soil sampling and testing. In the sixth, only

total extractable hydrocarbon (TEH) was determined. Field spectra were measured approximately one month before the soil samples were taken. Soil and reflectance data were processed and a selection of spectral vegetation indices calculated from the latter.

Data from the grassland site with different levels of soil contamination were used to characterise each site and to allow a spectral comparison of soil contaminant concentrations with reflectance spectra. In total, there were 36 locations where matched soil and reflectance data were used to investigate the correlation between spectra (and VI) and soil variables.

These data were measured to test the hypothesis that:

1. (H_1): *differences in the relative concentration of contaminants in a grassland soil can be detected using the position and shape of the red-edge of reflected radiation,*

This hypothesis did not dismiss the logically indirect relationship between soil contamination and reflected radiation, but was directed at the more practical justification of remote sensing in this application. Those vegetation state variables that facilitated the remote sensing of soil contamination will be investigated in the next chapter (chapter 6).

Soil and reflectance results (see table 5.1) were evaluated as:

1. variations in heavy metal and hydrocarbon concentrations (section 5.2),

2. variations in reflected radiation spectra (section 5.3) and

3. variations in vegetation indices, calculated from the spectra (section 5.5)

Data were measured from grassland locations with different levels of soil contamination (table 5.1). These were compared in terms of their mean, variance and distribution. Additionally, data from sample grids were tested for statistical difference. In the process of this evaluation, the relationship between soil variables and reflectence spectra,

including their first derivative, were considered. Finally, these relationships were further investigated by the use of vegetation indices. These were tested for statistical differences between data from sample grids and their correlation with different levels of soil contamination (section 5.5.3). The results from these investigations were used to test the above hypothesis.

5.2   Soil variables

Heavy metal concentrations were measured at five grids (grids 1-5). Other soil variables (indicating hydrocarbon concentrations in the soil) were measured from the same five grids plus one additional grid (six grids). The number of samples per grid is reported in table 5.1. Each soil variable will be described in relation to data collected from grid 3 (the grid with the highest visual indication of contamination). General soil information was evaluated from all grids and reflectance data from all transects. However, only grids 1, 2 & 3 had both datasets collected. Therefore, in this chapter most of the analysis is concentrated on these three grids. Although levels of hydrocarbon were very high, and in some areas were very acidic, the overall metal concentration levels in the soil were low compared with 'action levels' of the Interdepartmental Committee for the Redevelopment of Contaminated Land (ICRCL). Of the three main study grids, grid 3 was termed as being highly contaminated, grid 2 as having low levels of soil contamination and grid 1 as having intermediate levels of soil contamination.

Using the Kolmogarov-Smirnov normality test, the soil data were not normally distributed and simple normalisation techniques did not transform them to normal. Therefore, a Kruskal-Wallis one-way analysis of variance on ranks was used to analyse differences between the three grids (grids 1, 2 & 3), where both soil and reflectance measurements were made and were determined to be different (P<0.001). Dunn's method of pairwise multiple comparison showed that the three grids were all different for loss-of-ignition (LOI) and that the total extractable hydrocarbon (TEH, wet and dry) identified in grid 3 differed from grids 1 and 2 (P<0.05 in both cases). The

(a) Obvious surface contamination   (b) Grid 3

Figure 5.1: Obvious surface contamination at the grassland site with different levels of soil contamination

maximum, minimum, median, mean, and quartile ranges were used to analyse the distribution of data in all grids. These are illustrated in box plots, figures 5.3 and 5.4.

5.2.1   Metal concentrations

Metal concentrations will be described individually, but are presented for comparison in Figure 5.3. These relate to the top 20cm of the soil. Those patches where soil contamination was particularly evident (figure 5.1 a) were not sampled because of their absence of vegetation; however, some other areas with some evidence of surface contamination and thin vegetation were (figure 5.1 b). The soil type was similar across the site with a combination of alluvial deposits and dredged material. Isolated areas of concrete, brick and metal were found in grids 1 and 6, but were scattered among the vegetation and soil across the site.

5.2.1.1   Nickel

The overall nickel concentration had a bimodal frequency distribution; nevertheless the average (median and mean) nickel concentration was highest in grid 4 (125 mg.Kg^{-1}),

Table 5.1: Number and type of measurements at the grassland with different levels of soil contamination

Sampling type	Soil	Reflectance
Transect 1 (shb)		54
Transect 2 (shc)		61
Transect 3 (shr)		22
Transect 4 (shl)		111
Transect 5 (shn)		219
Transect 6 (shi)		121
Transect 7 (shh)		100
Transect 6 (shw)		103
Transect 8 (Hi)		15
Transect 9 (Lo)		15
Calibration area (C1)		86
Calibration area (C2)		50
Grid 1 (NI)	25	54
Grid 2 (NL)	25	50
Grid 3 (HSE)	35	49
Grid 4	25	
Grid 5	25	
Grid 6	25	

lower in grid 3 (99.3 mg.Kg^{-1}) and lowest in grids 2 and 5 (70 mg.Kg^{-1}) (figure 5.3). The Kruskal-Wallis test showed a significant difference between the nickel concentrations measured in samples collected from different grid areas (table 5.2). Dunn's pairwise multiple comparison identified soil in grid 2 as different from soil in grids 1 and 3 (P<0.05).

5.2.1.2 Copper

Except for those data collected in grid 3, overall copper concentration data formed an approximately normal distribution. The average (median and mean) copper concentration was highest in grid 1 (160 mg.Kg^{-1}). However, the highest individual sample concentration was in grid 3 (almost 300 mg.Kg^{-1}). Grid 3 also contained the lowest average copper concentrations (60 mg.Kg^{-1}) and therefore the highest range (figure 5.3). The Kruskal-Wallis test did not show a significant difference between the copper concentrations measured in samples collected from different grid areas (table 5.2).

5.2.1.3 Cadmium

Average (median and mean) cadmium concentrations were highest in grid 1 (2.5 mg.Kg^{-1}) and lowest in grid 4 (0.6 mg.Kg^{-1}) (figure 5.3). The overall distribution was normal except for isolated concentrations of up to 6.2 mg.Kg^{-1} from grids 3 and 4. The Kruskal-Wallis test showed a significant difference between the cadmium concentrations measured in samples collected from different grid areas (table 5.2). Dunn's pairwise multiple comparison identified soil in grid 1 as different from soil in grids 2 and 3 with respect to cadmium (P<0.05).

5.2.1.4 Zinc

The overall distribution of zinc concentrations was skewed to higher values. Average (median and mean) zinc concentrations were highest in grids 1 and 4 (380 mg.Kg^{-1})

(figure 5.3). Grid 4 also had some extremely high individual sample zinc concentrations (in excess of 900 mg.Kg^{-1}). The lowest zinc concentrations were in grids 2, 3 and 5 and were of a similar level to each other (300 mg.Kg^{-1}). The Kruskal-Wallis test showed a significant difference between the zinc concentrations measured in samples collected from different grid areas (table 5.2). Dunn's pairwise multiple comparison identified soil from all the grids (1, 2 and 3) to be different with respect to zinc (P<0.05).

5.2.1.5   Lead

Average (median and mean) lead concentrations were highest in grid 1 (310 mg.Kg^{-1}) but were also high in grid 3 (250 mg.Kg^{-1}) (figure 5.3). However, the highest individual lead concentrations, in excess of 550 mg.Kg^{-1}, were in grid 4. The Kruskal-Wallis test showed a significant difference between the lead concentrations measured in samples collected from different grid areas (table 5.2). Dunn's pairwise multiple comparison identified soil from all the grids (1, 2 and 3) to be different with respect to lead (P<0.05).

5.2.1.6   Selenium

Average (median and mean) selenium concentrations were highest in grids 2, 4 and 5 (between 1 & 2 mg.Kg^{-1}) but selenium concentration were generally low (figure 5.3). The Kruskal-Wallis test showed a significant difference between the selenium concentrations measured in samples collected from different grid areas (table 5.2). Dunn's pairwise multiple comparison identified soil in grid 2 to be different from soil in grids 1 and 3, with respect to selenium (P<0.05).

Table 5.2: Pairwise comparison proceedure (Kruskal-Wallis test) used to determine similarities between sites (n=6). The H value denotes the association. The P value describes the probability of the result occuring by chance. The lower the P value the less likely the result occured by chance. Total Extractable Hydrocarbon (TEH) was calculated from wet and dry soil while loss-of-Ignition (LOI) was related to dried samples.

Soil variable	H_5	P value
Ni	55.2	<0.001
Cd	35.0	<0.001
Cu	57.7	<0.001
Zn	54.5	<0.001
Pb	54.3	<0.001
Se	24.2	<0.001
TEH (wet)	61.6	<0.001
TEH (dry)	61.2	<0.001
LOI	40.5	<0.001
Soil water content	10.3	<0.006
pH	6.7	<0.035
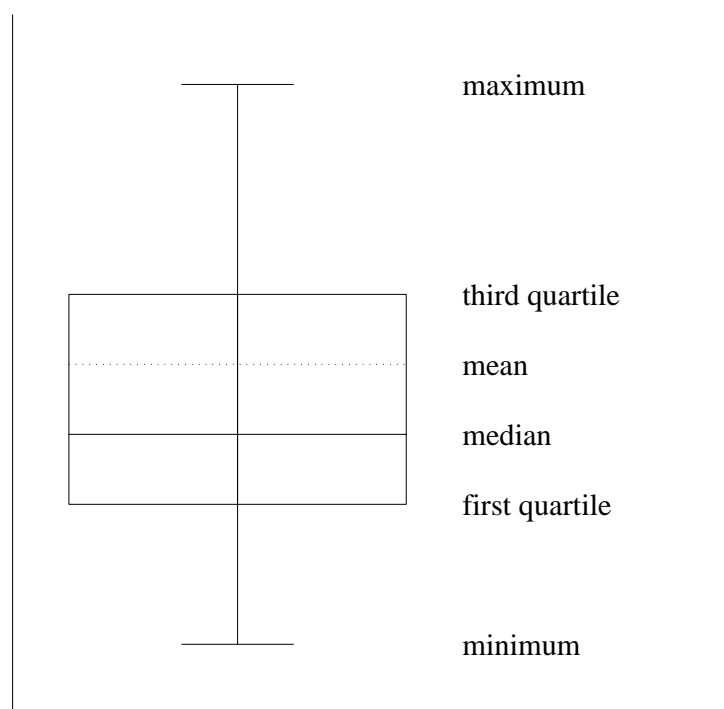
Figure 5.2: Box plot key
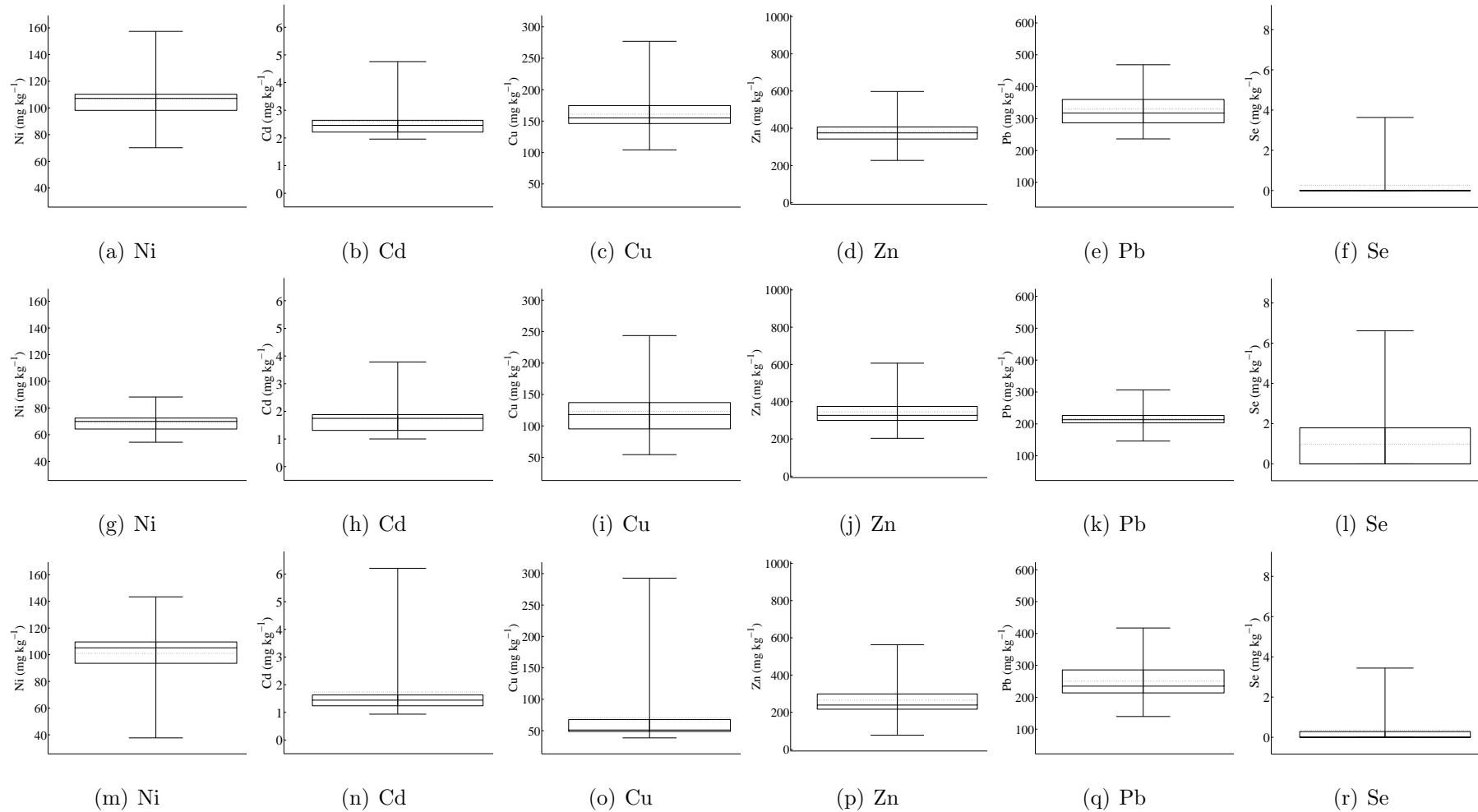
Figure 5.3: Heavy metal concentrations from soil samples. Top row (*a-f*), grid 1; middle row (*g-l*), grid 2 & bottom row (*p-r*), grid 3. Grids 1 had higher levels of heavy metal contamination than other grids but all were low in respect to ICRCL action levels. For the box plot key see figure 6.2

5.2.2 Hydrocarbon related contamination

Total extractable hydrocarbon (TEH) is the mass removed from a soil sample by virtue of reflux with a solvent. Loss-of-ignition (LOI) is the mass removed by pyrolysis. Grid 3 had the highest average (mean and median) TEH from both wet and dry soil. Some of these measurements were by far the highest recorded from any of the grids on contaminated grassland; they exceeded 600 mg of hydrocarbon per gram of soil (figure 5.4). The Kruskal-Wallis test showed a significant difference between the the levels of TEH measured in samples collected from different grid areas (table 5.2). Dunn's pairwise multiple comparison identified the levels of TEH in soil from grid 3 to be different from levels from grids 1 and 2 (P<0.05).

The highest average (mean and median) loss-of-ignition (LOI) was in grids 3 and 6 (figure 5.4). Grid 6 contained the highest average values, while grid 3 included some samples that were almost all organic matter. The Kruskal-Wallis test showed a significant difference between the the levels of TEH measured in samples collected from different grids (table 5.2). Dunn's pairwise multiple comparison identified the levels of LOI from grids 1, 2 and 3 to be significantly different from each other (P<0.05).
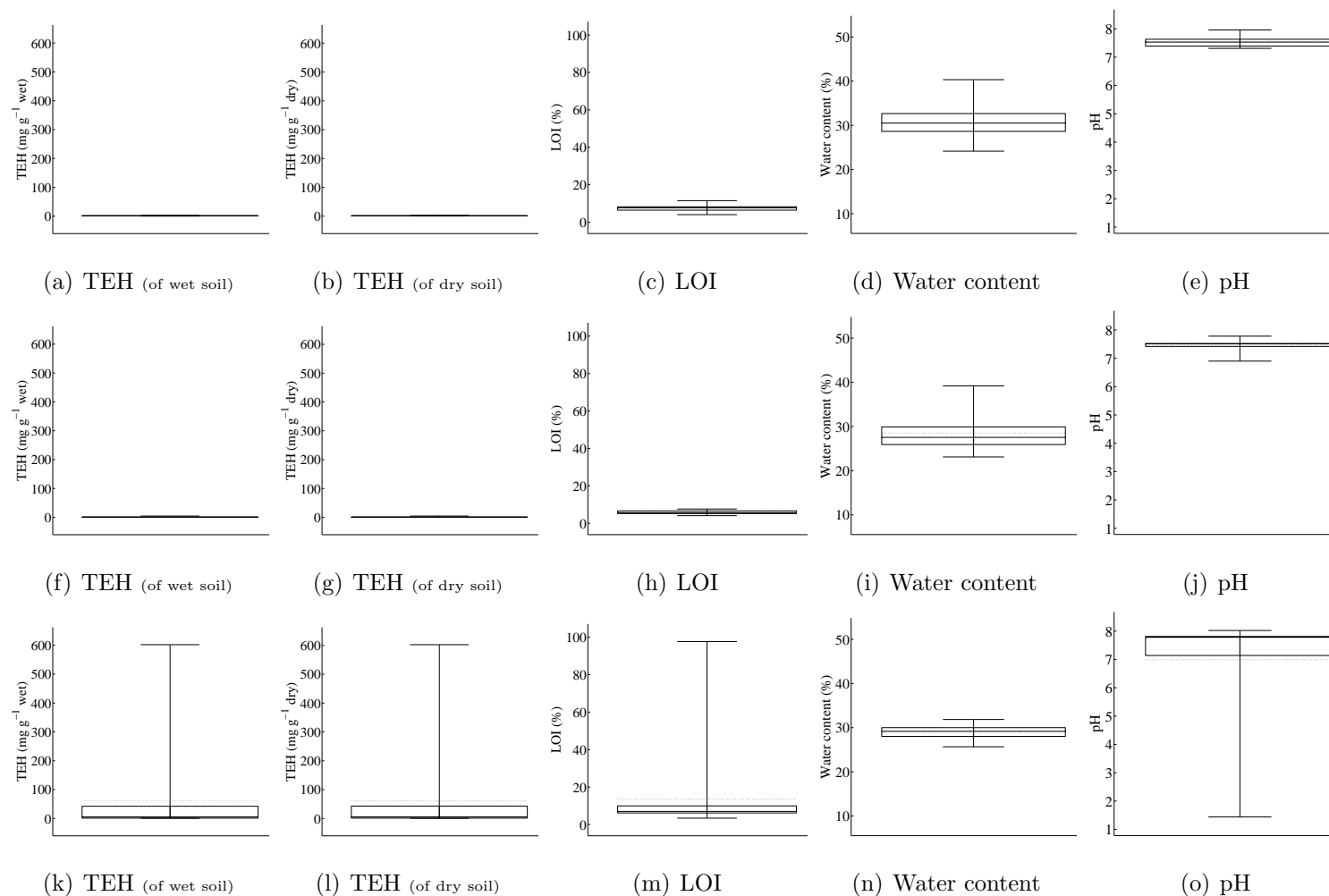
Figure 5.4: Total extractable hydrocarbon (TEH), loss-of-ignition (LOI), soil moisture and pH measurements from soil samples. Top row (*a-e*), grid 1; middle row (*f-j*), grid 2 & bottom row (*k-o*), grid 3. For the box plot key see figure 6.2.

5.2.2.1   Soil water and acidity

Soil water content was measured due to its potential to influence, or be influenced by the presence of hydrocarbon in the soil and it effect on vegetation (chapter 6). The measured values were normally distributed with grids 1, 2 and 5 having slightly lower water content than the average (mean and median) (figure 5.4). Although generally dry, some samples from grids 2 and 5, as well as a few samples from grid 6 were very wet. The Kruskal-Wallis test showed a significant difference between the the soil water content in samples collected from grids from the the grassland with differents levels of soil contamination (table 5.2). Dunn's pairwise multiple comparison identified soil in grid 1 to be different from soil in grid 3 (P<0.05). Acidity / alkalinity, as measured by pH, showed lightly alkali soil conditions over most of the contaminated grassland (figure 5.4). The exceptions were a few samples from grid 3, which were extremely acidic (pH 1.5).

5.2.3   Relationships between contaminants

The combined data set was used to identify co-relationships between soil variables. Spearman's rank correlation was used because the data failed the Kolmogorov-Smirnov normality test and were not transformable to a normal distribution. The Spearman's rank correlation is a non-parametric version of the Pearson product-moment coefficient where the datasets are ranked prior to calculating the coefficient. The correlation coefficient (r) varies between +1 and -1. A correlation of -1 indicates a perfect negative relationship between the two variables. A correlation of +1 indicates a perfect positive relationship between the two variables. A correlation of 0 indicated no relationship between the two variables.

TEH was related positively to LOI and soil water content (figure 5.5). Although LOI also included organic root matter, the majority was hydrocarbon, as verified by observation during preparation. LOI was correlated more strongly with TEH, calculated from wet rather than dry soil mass (figure 5.6). TEH and LOI were very high (e.g. in

grid 3), where acid tar was present. Nickel and lead concentration had a positive correlation with TEH. Copper, zinc, cadmium and lead concentration were correlated to each other. However, while copper and zinc were present in all grids, it was correlated negatively with TEH.
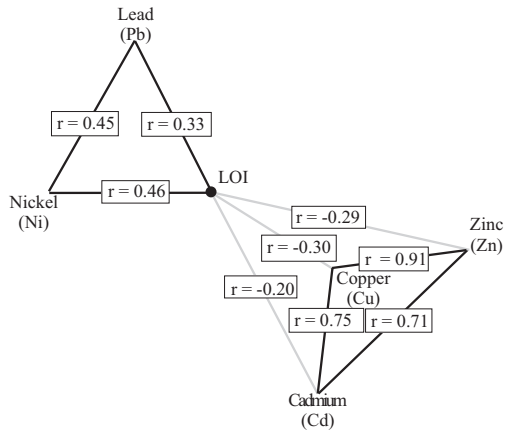
(a) Soil variable relationships with loss-of-ignition data (P<0.0001 except Cd when P<0.07)
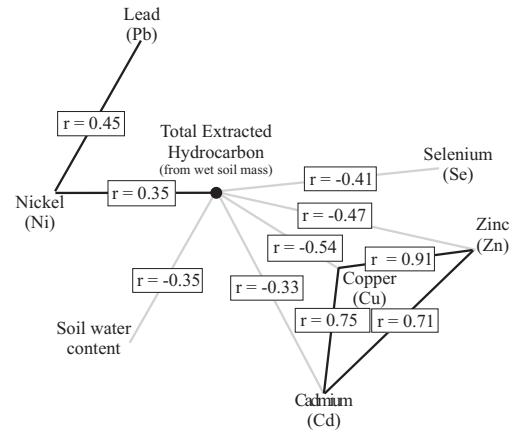
(b) Soil variable relationships with total extractable hydrocarbon data (calculated from wet soil mass)(P<0.0001 except Cd when P<0.002)
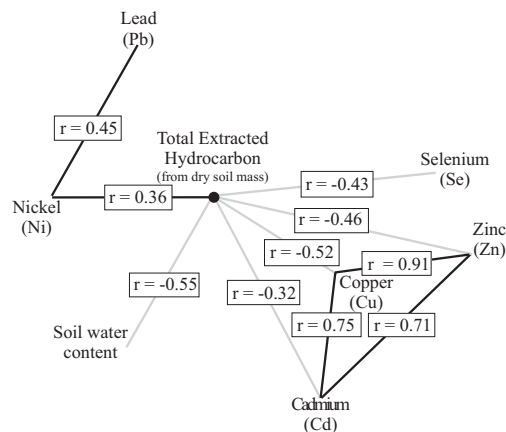
(c) Soil variable relationships with total extractable hydrocarbon data (calculated from dry soil mass)(P<0.0001)

Figure 5.5: Interrelationships between soil variables measured from grassland with different levels of contamination (grids 1-5). All shown relationships were significant.
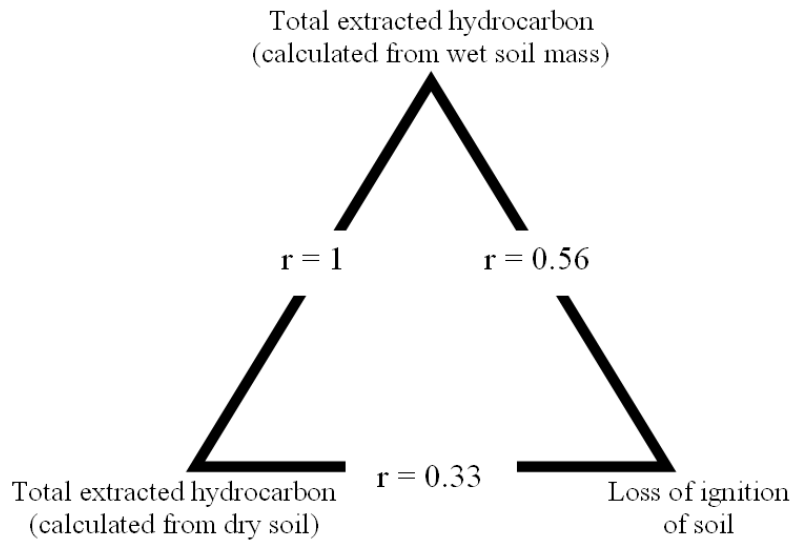
(a) Loss of ignition and total extractable hydrocarbon (P<0.01)

Figure 5.6: Interrelationships between soil variables measured from grassland with different levels of contamination (grids 1-6). All shown relationships were significant.

5.3   Spectral reflectance

Spectral measurements were obtained from three grassland sites (two uncontaminated) and used three instruments (including two GER1500s in dual beam mode) (see chapter 4). A Perkin Elmer Lambda 19 was used in a controlled laboratory environment while the data collected using the GER3700 and the GER1500 were from field conditions (table 5.3). Additionally, reflectance spectra were collected from different locations, on different dates and at different times of the day. Meteorological conditions were generally consistent but the very act of measurement inevitably introduced error. These factors were investigated before spectral variation was related to soil properties Derivative spectra were smoothed to reduce noise whilst preserving the signal. The determination of the most effective size of smoothing window will be considered later in this chapter (section 5.3.2).

Table 5.3: Soil variables and spectral data recorded from grassland sites (and the date on which it was collected)

Reference	Location	GER1500	GER3700	Lambda 19	soil variables
Transect 10	Thorney Island		18.05.99	18.05.99	
Transects 1-9	Contam. site	27.04.00			
Grids 1-3	Contam. site	12-13.05.00			13.11.00
Grid 4	Contam. site	13.05.00			13.11.00
Grids 5-6	Contam. site				13.11.00

5.3.1   Spatially independent variation

Goniometer measurements of uncontaminated grassland (Thorney Island) demonstrated that bidirectional effects were one source of variation in grassland reflectance (figure 5.7). These data indicated that at the solar zenith angles (34°, 37° and 62°) at which reflectance data were collected, reflectance was constant for the spectral bands around the red-edge. For the same data, the first derivative maximum REP and NDVI showed minor variation (less than 0.7nm & 0.5, respectively). Mean reflectance spectra for the three solar zenith angles showed less than a 0.4% difference (between 400 & 1000nm) between the different angles (figure 5.8). The standard deviation of reflectance spectra was highest for the lowest solar zenith angle; but was less than 3.4% of the reflectance signal. These comparisons were conducted using intercalibration spectra measured from two near-Lambertian Spectralon panels (Anon. 2009b). These spectra indicated that, within red-edge wavelengths, there was mininal difference. Those variations that were present (figure 5.8 c) may be attributed to changes in atmospheric conditions or solar zenith angle. However, the main field measurements were conducted using two GER1500s operated in dual beam mode in order to minimise these factors. Spectral variation as a function of measurement methodology was investigated by fifty repeat nadir measurements of a single grassland target (figure 5.9). These data indicated a slight difference; at 700nm the standard deviation was 7.3% of mean reflectance while at 750nm it was 4.2%. These variations were coincident with the time of gusts of wind on the grassland canopy.

5.3.2   Smoothing spectral data

The most appropriate level of smoothing was investigated for the evaluation of first derivative spectra (figure 5.10). Only the SavitzkyGolay smoothing filter was used (Savitsky and Golay 1964). For this study a moving average (non-weighted mean) was used with a second order polynomial to fit the resultant data. The balance between the removal of noise and the retention of a useful level of spectral detail was made with
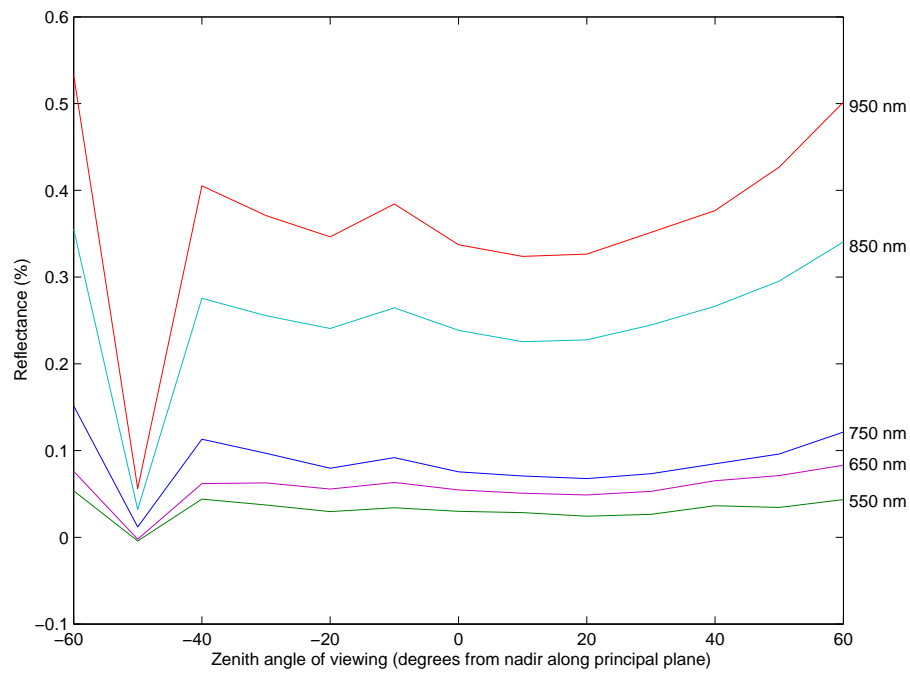
(a) Multiple wavelengths
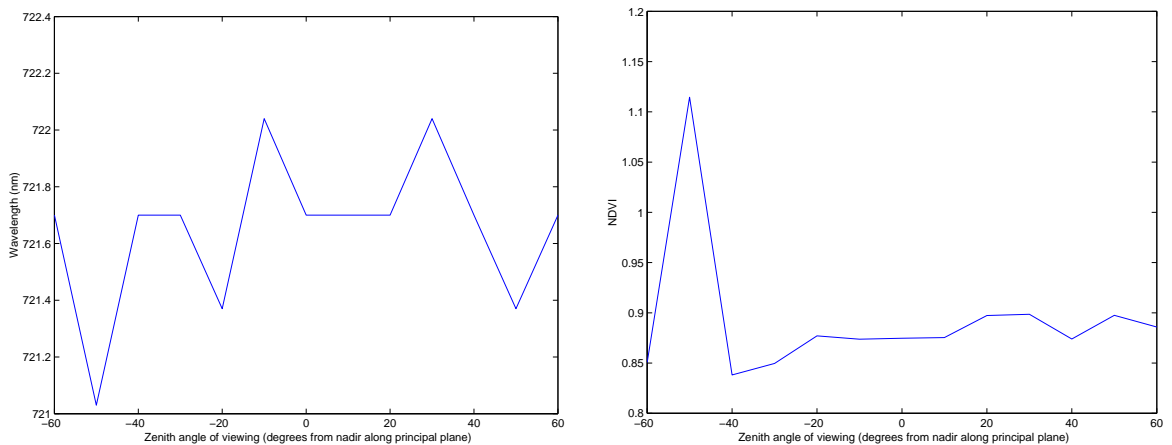
(b) First derivative maximum red-edge position

(c) Normalised difference vegetation index

Figure 5.7: Bidirectional variation in five wavebands, the first derivative maximum REP and NDVI of grassland. In all cases measurements were conducted for solar nadir conditions (+ and - 40 minutes) and within two weeks of mid-summer (04.07.02, Thorney Island) to limit the effects of different solar azimuth angles (solar zenith angle was 16°). The features at -50 degrees are related to shadow cast by the measurement arm of the instrument.
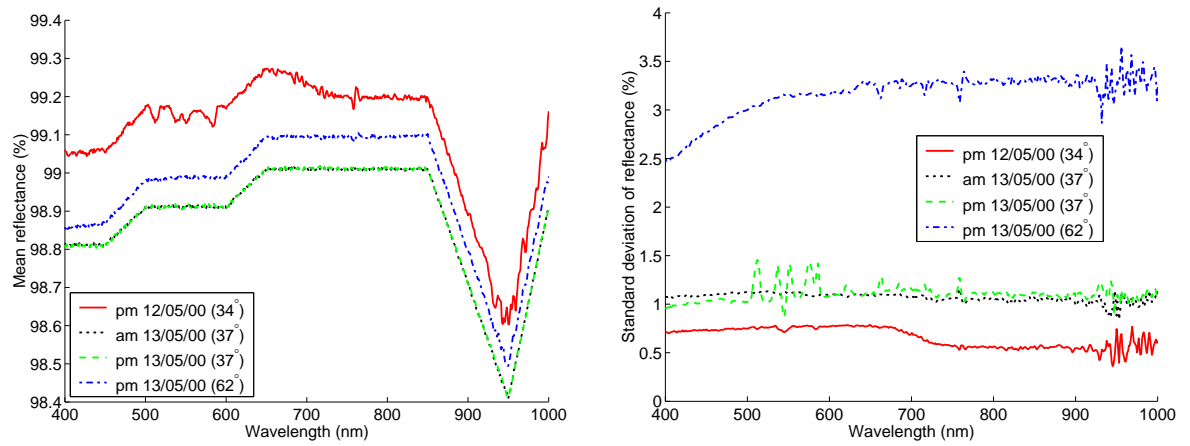
(a) Mean reflectance spectra for four time periods (3 solar zenith angles)

(b) Standard deviation of reflectance spectra for four time periods (3 solar zenith angles)
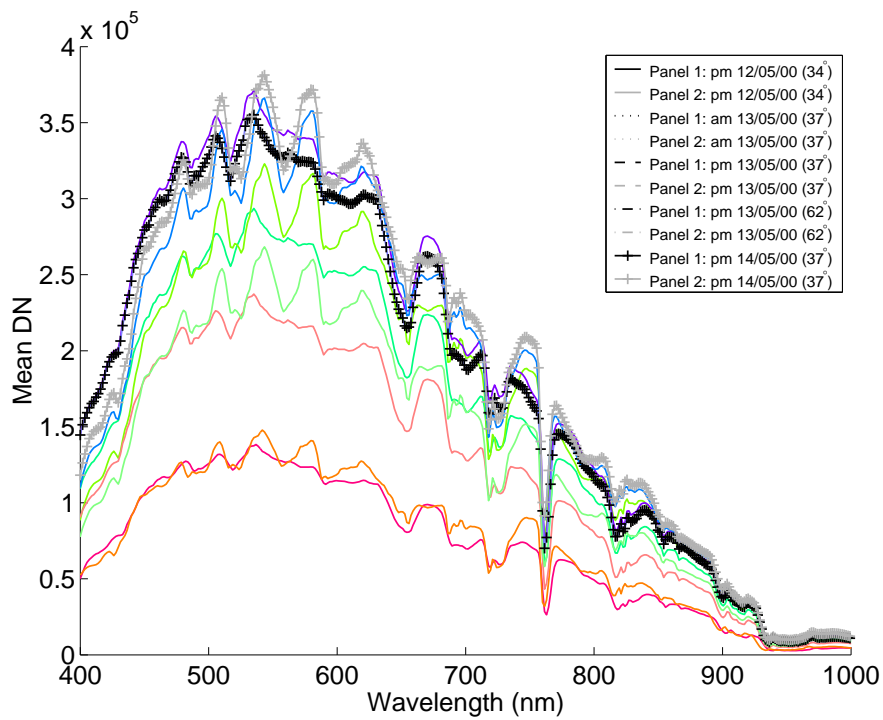
(c) Spectralon panel spectra

Figure 5.8: Spectralon reflectance spectra from two panels and four time periods (3 solar zenith angles)
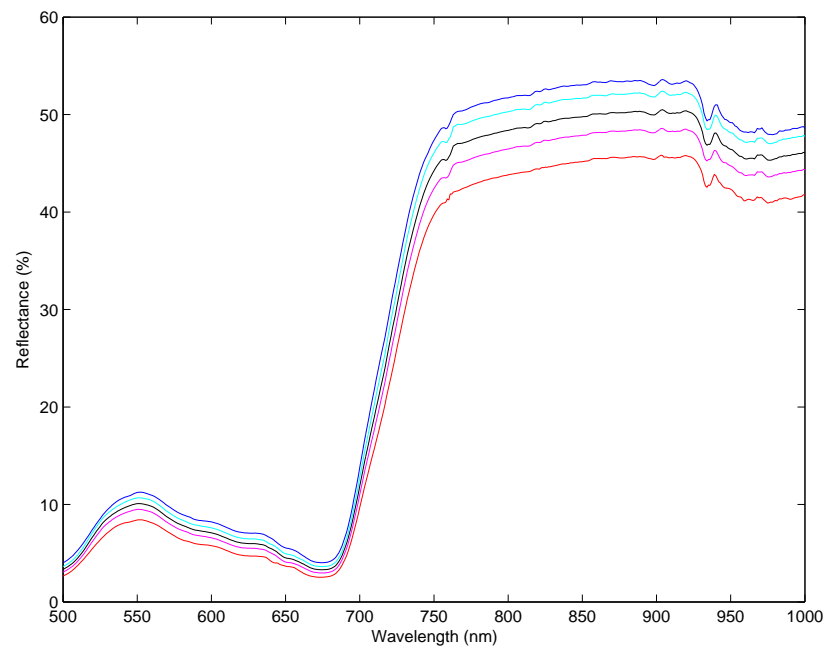
Figure 5.9: Variation in 50 spectra of the same target. Mean average (black), Maximum (blue), minimum (red), avearge plus one standard deviation (cyan) and average minus one standard deviation (magenta).

a window size of 7 with a second order polynomial. This allowed typical first derivative spectra for areas with different levels of soil contamination to be identified from the relative dominance of peaks in the first derivative spectra (figure 5.10).

5.4   Spatially dependent spectral variation on grassland

Reflectance spectra collected from contaminated grassland were different to those collected from uncontaminated grassland (figure 5.11). The wavelength region where such differences were most evident was the red-edge. Compared with grassland with low levels of soil contamination (grid 2 & transect 2), spectra from grassland with high levels of soil contamination (grid 3 & transect 6) generally had a higher reflectance in visible wavelengths and lower reflectance in NIR wavelengths. However, compared with other spectra from intermediate locations (grid 1) this general trend did not provide a clear means of identification. The variance of reflectance showed a clearer pattern. Spectra measured from grassland with higher levels of soil contamination had a greater variance than other areas.

Generally, spectra collected from locations where there were high levels of soil contamination (e.g., grid 3) had a high reflectance in wavelengths between 650 and 700 nm and a lower reflectance in wavelengths between 720 and 770 nm. In the first derivative spectra, there were three first derivative peaks in the red-edge. These were positioned at approximately 700, 720 and 730 nm. Derivative spectra for grassland with high levels of soil contamination had a more pronounced short wavelength peak (700nm). Conversely, derivative spectra for grassland with low levels of soil contamination (or no soil contamination) had a pronounced long wavelength peak (730nm). Each peak retained its relative position with the other peaks, although the exact wavelength of each peak varied by up to 5nm. In cases where only one or two first derivative peaks were present, there was a strong indication that a dominant peak (usually the longer wavelength peak) had obscured those at short wavelengths. The remnants of these
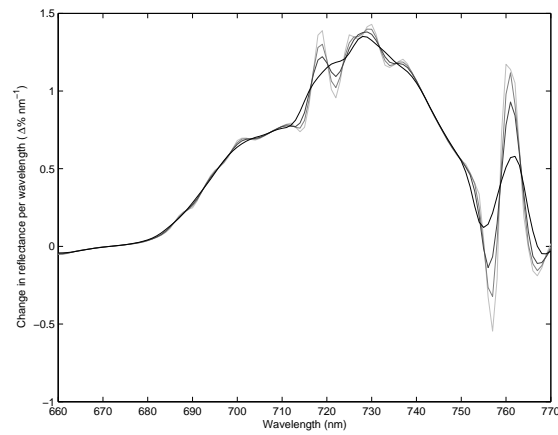
(a) The effect of four levels of smoothing (3, 5, 7, 11) on data from grid 1 (NL18)
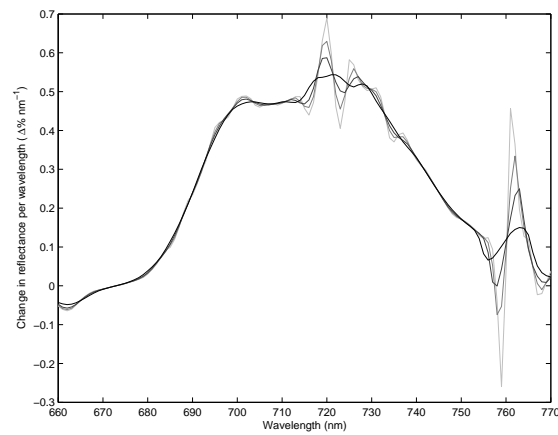
(b) The effect of four levels of smoothing (3, 5, 7, 11) on data from grid 2 (NI34)
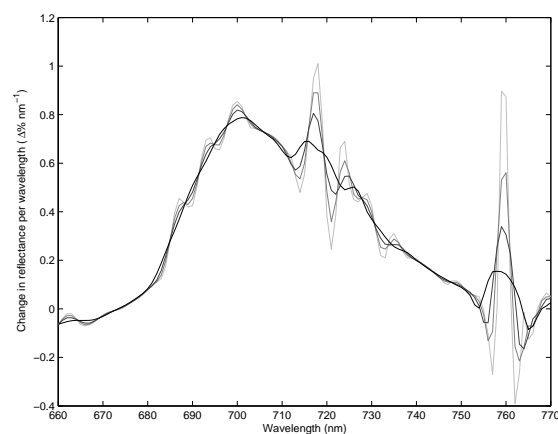
(c) The effect of four levels of smoothing (3, 5, 7, 11) on data from grid 3 (HSE37)

Figure 5.10: Differences in spectra from grids 1, 2 and 3. The darkest tone indicates a smoothing window of 11 while the lightest tone indicates a smoothing window of 3.

(a) Mean grassland reflectance   (b) Variance of grassland reflectance
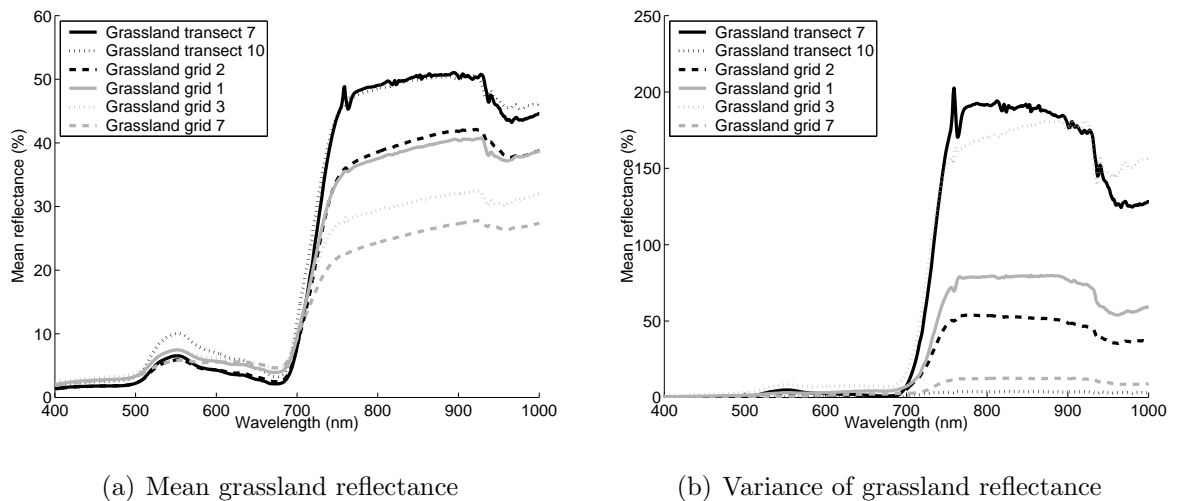
Figure 5.11: Mean and variance of grassland reflectance spectra (%). Transect 7 & grid 3 were collected from areas with high levels of soil contamination; grids 1 & 2 were collected from areas with low or intermediate levels of soil contamination and transect 10 & grid 7 were collected from areas with no soil contamination. n=100.

were evident as a shoulder on the short wavelength limb.

5.4.1   Spectra from grassland with different levels of soil contamination

The previously identified features in the first derivative spectra were used to characterise grassland with different levels of soil contamination. The maximum first derivative of the spectral red-edge was calculated for 250 spectra from areas with high levels and low levels of soil contamination (500 in total)(figure 5.12). From these data three aspects were identified:

- the peaks were divided into three groups with no maxima occurring between the first two groups,

- the longer wavelength peak was more associated with those areas of low levels of soil contamination and

- some spectra from areas of high soil contaminatation had peaks at longer wavelengths.

Spectra from nine transects were collected across different areas of the contaminated grassland. The sampling interval for these measurements was 0.5 of a metre. From these data the maximum first derivative grassland red-edge was calculated (figures 5.13, 5.14, 5.15 & 5.16). Those transects from areas with low levels of soil contamination had consistently long wavelength peak positions in the first derivative reflectance. Those transects areas with high levels of soil contamination had short wavelength positions, but also exhibited frequent switching between long and short wavlengths.
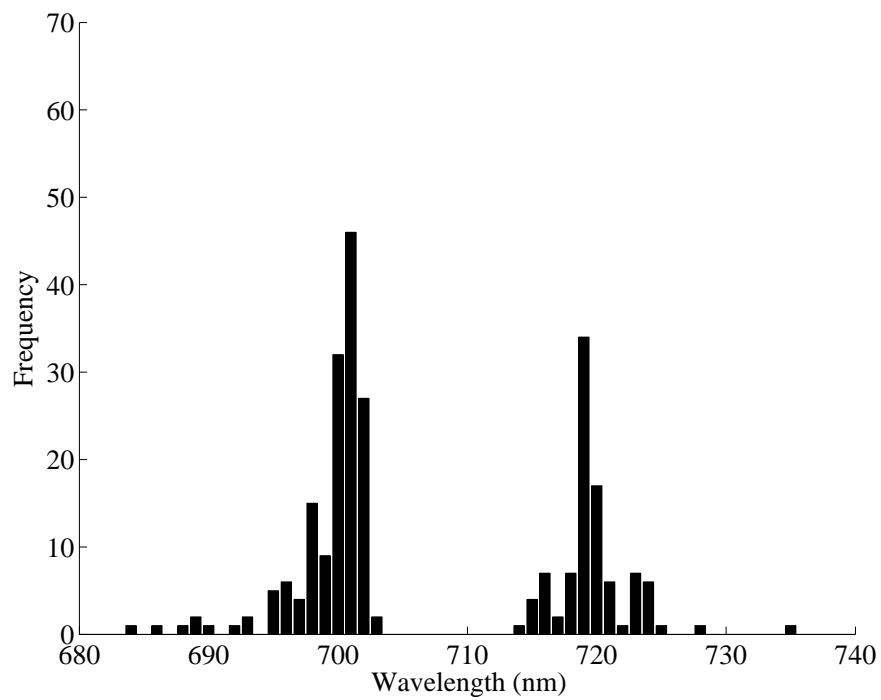
(a) Grassland with high levels of soil contamination
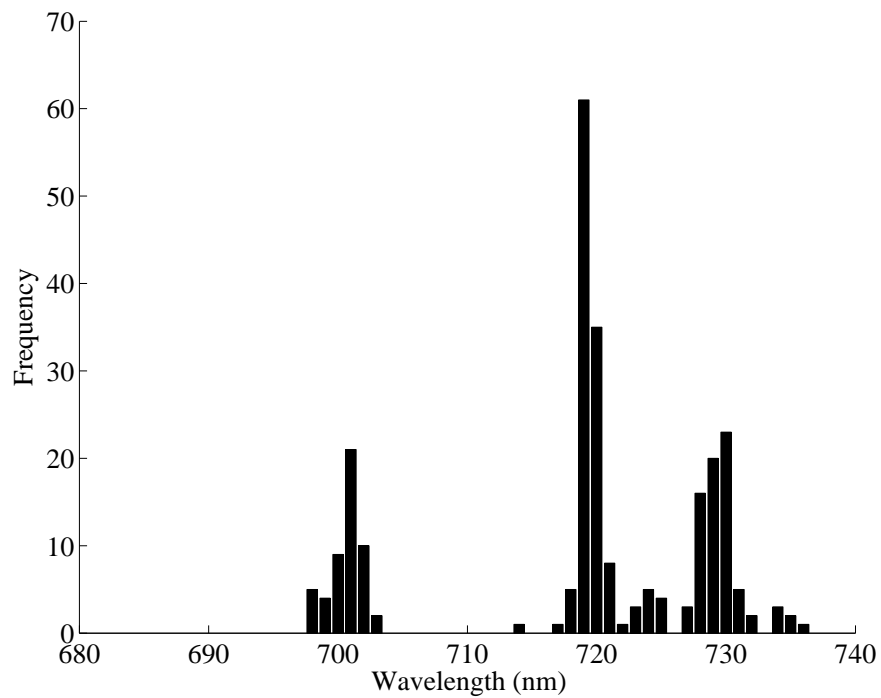
(b) Grassland with low levels of soil contamination

Figure 5.12: REP (first derivative maximum) for areas of grassland with high and low levels of soil contamination (high contamination conditions were collected from grids 3 and 4 and transects 5 & 6). For each group n=250.
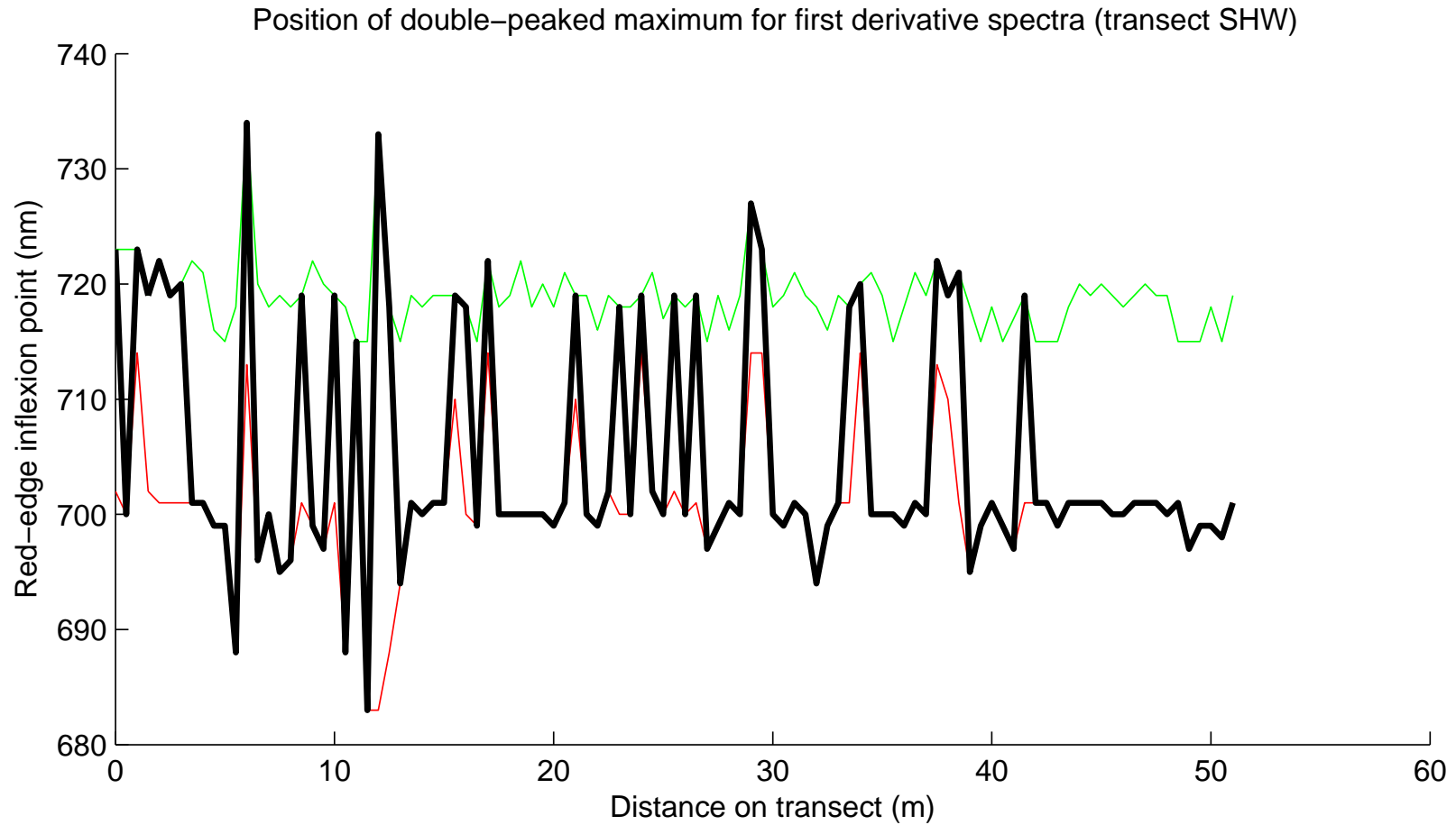
Figure 5.13: Transect of first derivative maxima from a transects on grassland with high levels of soil contamination (transect 6), n=103 (sampling interval was 0.5m). Maximum in wavelength region 670 to 714 (red), maximum in wavelength region 715 to 750nm (green) and maximum in 670 to 750 (black).
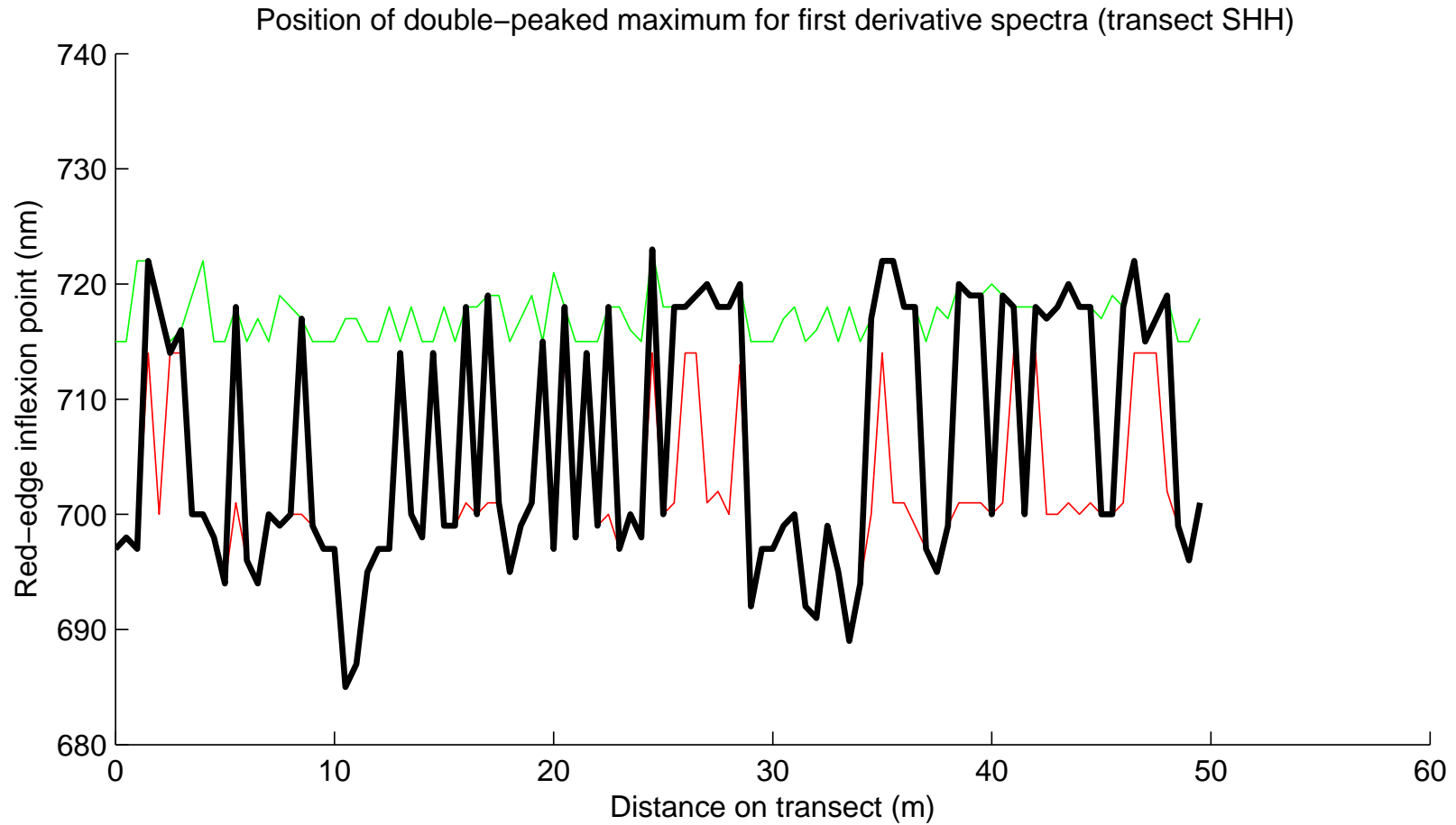
Figure 5.14: Transect of first derivative maxima from a transects on grassland with high levels of soil contamination (transect 5), n=100 (sampling interval was 0.5m). Maximum in wavelength region 670 to 714 (red), maximum in wavelength region 715 to 750nm (green) and maximum in 670 to 750 (black).
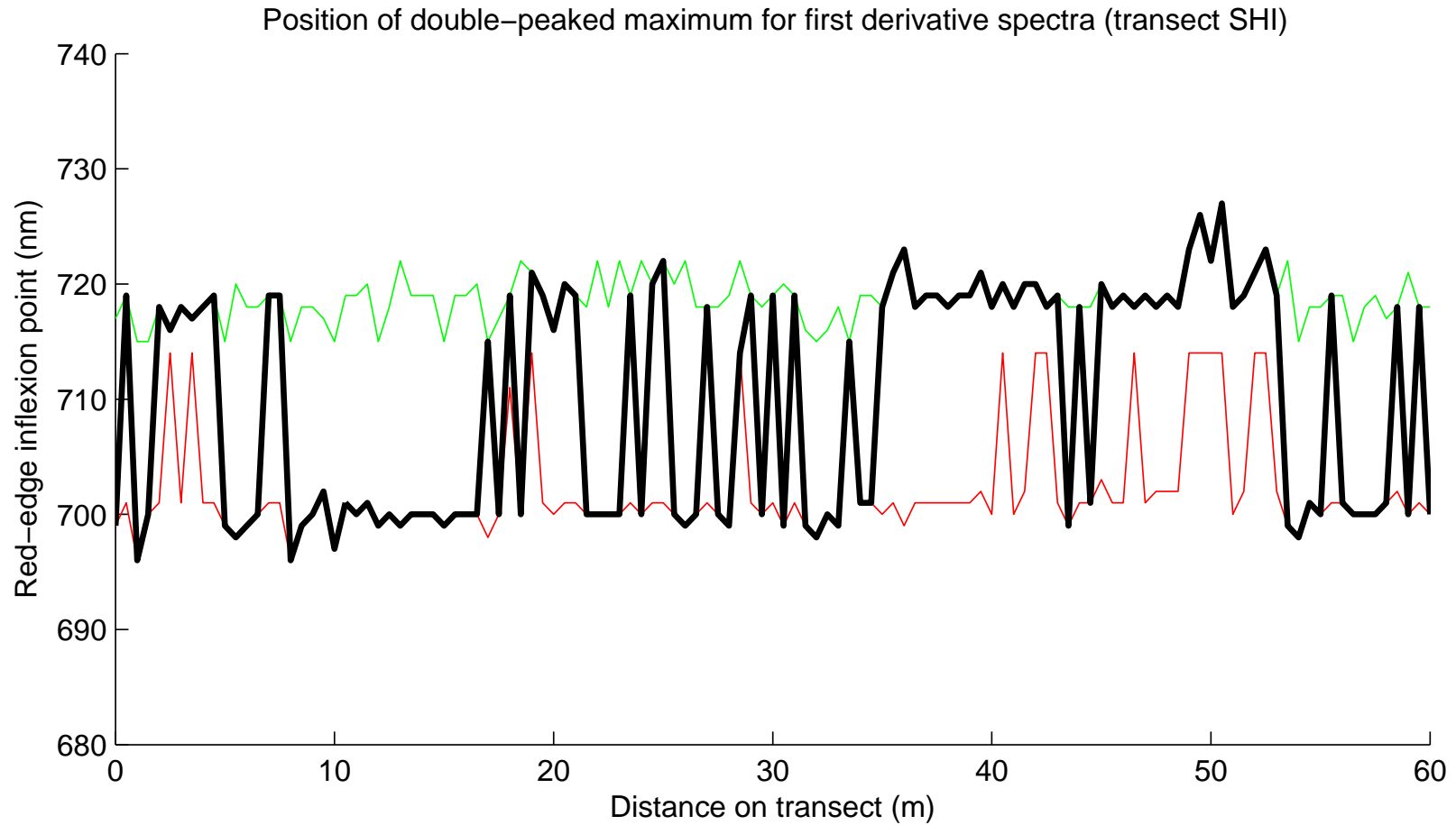
Figure 5.15: Transect of first derivative maxima from a transects on grassland with intermediate levels of soil contamination (transect 4), n=121 (sampling interval was 0.5m). Maximum in wavelength region 670 to 714 (red), maximum in wavelength region 715 to 750nm (green) and maximum in 670 to 750 (black).
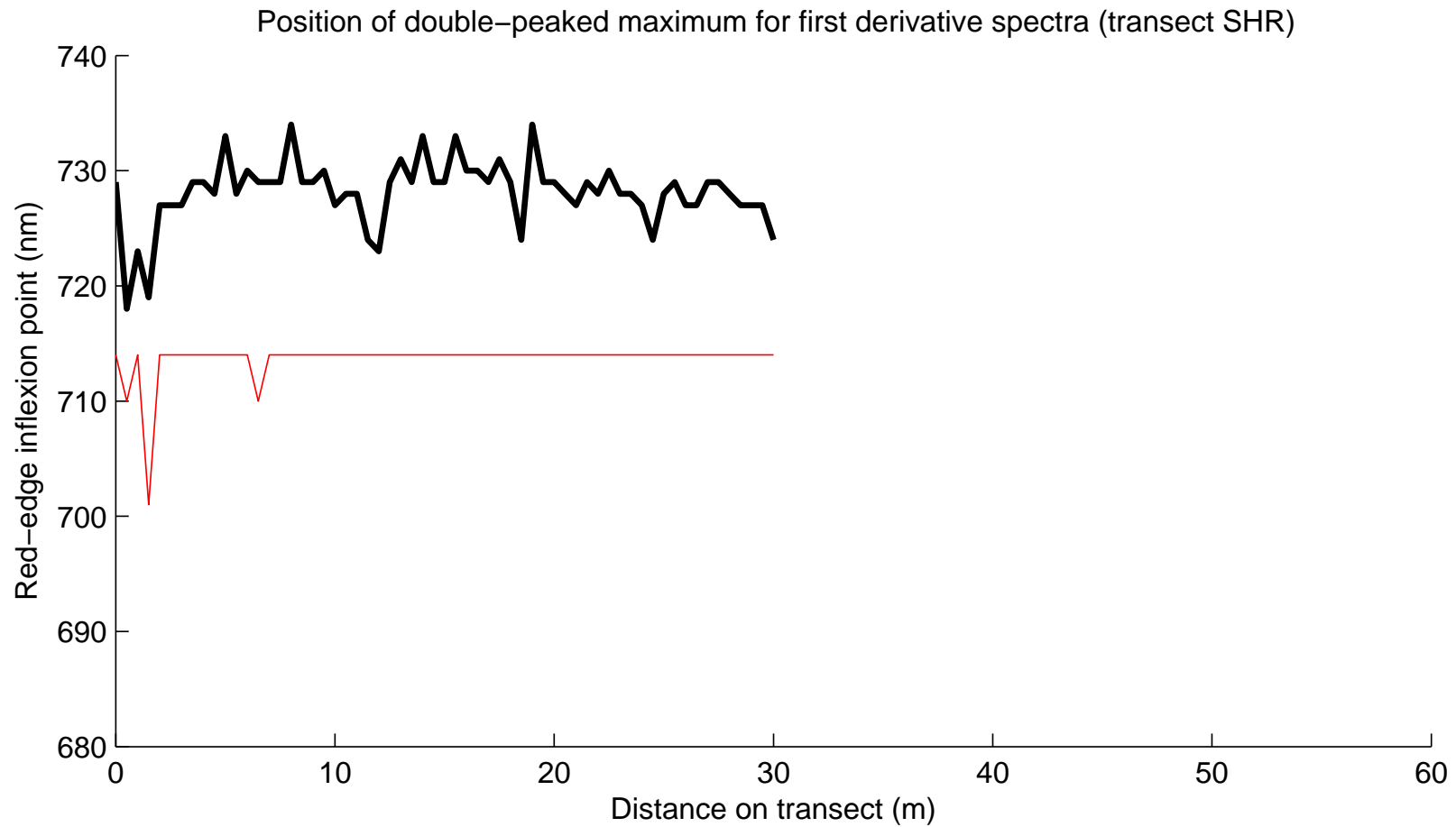
Figure 5.16: Transect of first derivative maxima from a transects on grassland with low levels of soil contamination (transect 1), n=61 (sampling interval was 0.5m). Maximum in wavelength region 670 to 714 (red), maximum in wavelength region 715 to 750nm (green) and maximum in 670 to 750 (black).

5.4.2   Comparison of the first derivative spectral shape with levels of total extractable hydrocarbon in the soil

Reflectance spectra for 36 locations were matched by soil samples. Unfortunately, only four of these were located in the area with low levels of soil contamination, consequently a comparison categorised per grid was not possible. However, the grassland reflectance spectra were found to have three basic profiles in their first derivative spectra (figure 5.17). These profiles were distinguished by: (i) a pronounced peak at short wavelengths (700-710nm), (ii) a dominant peak at long wavelengths (greater than 725nm) or (iii) an intermediate peak between the other two. Although in some cases the shortest wavelength peak was obscured by a longer wavelength one all spectra we able to be separated in these three groups. Each group was compared and related to the levels of soil contamination found at each location (figure 5.18 and table 5.5).

(a) Reflectance spectra

(b) First derivative spectra
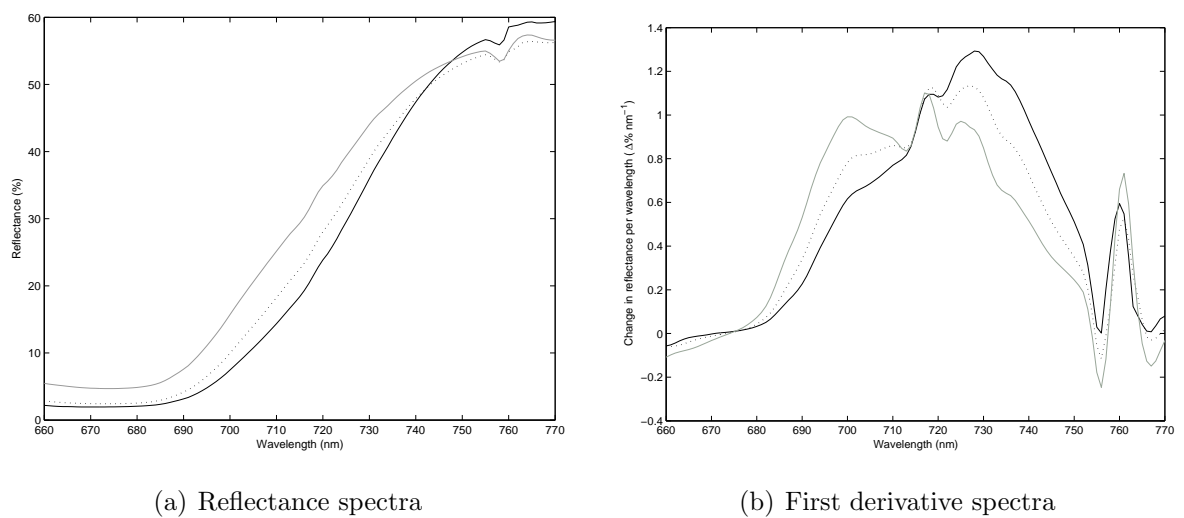
Figure 5.17: Three basic forms in the first derivative spectra for the grassland red-edge. The grey line denotes a convex red-edge and a short wavelength first derivative peak. The black line denotes a concave red-edge and a long wavelength first derivative peak. The dotted line denotes an intermediate situation.
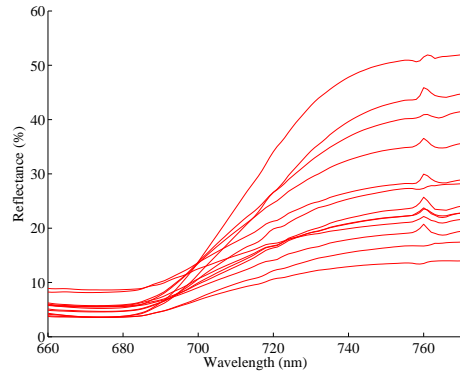
(a) Reflectance red-edge with a short wavelength peak
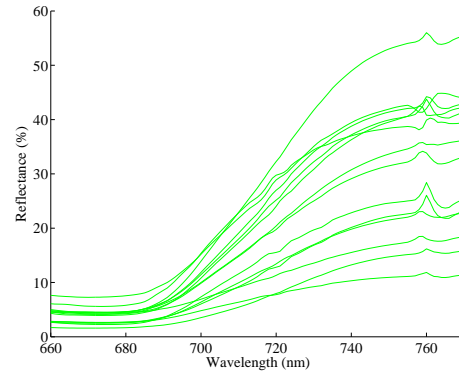
(b) Reflectance red-edge with an intermediate wavelength peak
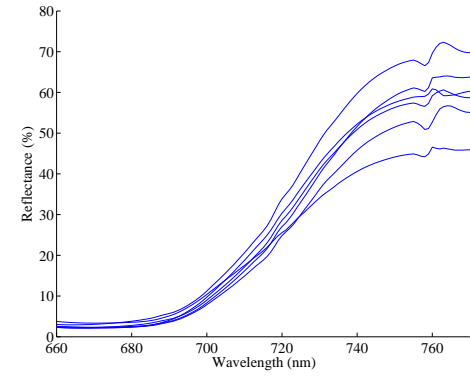
(c) Reflectance red-edge with a long wavelength peak
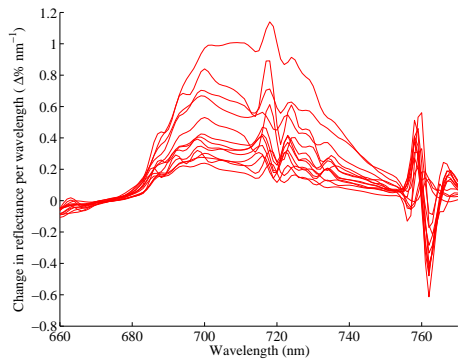
(d) First derivative reflectance red-edge with a short wavelength peak
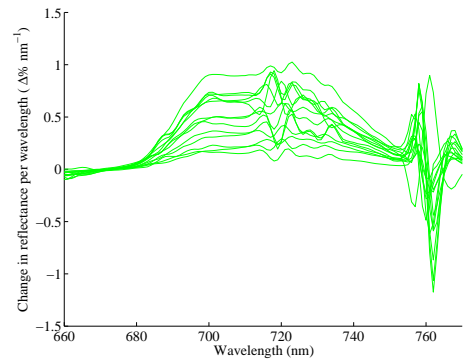
(e) First derivative reflectance red-edge with an intermediate wavelength peak
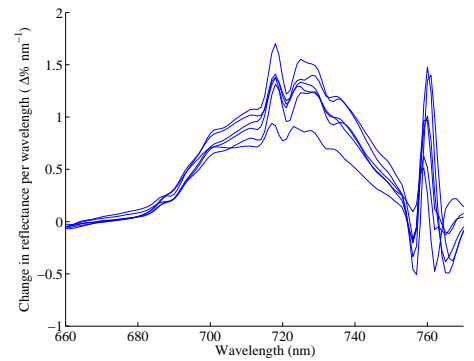
(f) First derivative reflectance red-edge with a long wavelength peak

Figure 5.18: Wavelength sections of the grassland red-edge (soil contaminated grassland, grids 1, 2 & 3), n=36.

5.5 Spectral vegetation indices

Spectral vegetation indices (VIs) were calculated from reflected radiation spectra. Selected VIs were plotted as histograms within which the main three study grids (1, 2 and 3) were identifed; grid 1 was separated into a and b to indicate that the data were collected on two consecutive days. Some soil data failed the Kolmogorov-Smirnov normality test and were not able to be transformed to a normal distribution. Therefore, Spearman's rank correlation was used to determine any association between vegetation indices and soil variables. However, a subset of 36 coincident soil and reflectance measurements were used to predict relative levels of soil contamination for TEH, the main contaminant. To validate the predictive equations there were two options, (i) recalculating with a dataset of 20 and using the remaining 16 to check the equation or (ii) jack-knifing (leave-one-out method). Neither were conducted at this stage but scatter plots and correlation coefficients indicated the strength of associations and confidence in the predictive capability for the identification of soil contamination from vegetation indicies.

5.5.1 Red-edge positions

These spectral vegetation indices were used to calculate a wavelength position for use as an indicator value. A more comprehensive description of the different methods of determining REP is presented in chapter 3. One of the most successful tools for the detection of soil contamination was the REP, yet different methods for its calculation yielded different results figure 5.19). The choice of method could result in a REP difference of over fifty nm (e.g. for a chlorophyll content of $100.\text{mg m}^{-2}$). Nevertheless the trend between different linearly interpolated REPs was consistent.

The spectra from the area of highest soil contamination (grid 3) were most clearly identifed with the linear extrapolation methods, the two inverted Gaussian methods and the Lagrangian method (figure 5.20). The three existing linear interpolation methods

Table 5.4: Total extractable hydrocarbon in dried soil (mg.g^{-2}) related to specific sections of the spectral red-edge, derived from paired data from the same location.

	Short wavelength section of the red-edge	**Intermediate wavelength section of the red-edge**	**Long wavelength section of the red-edge**
Average (mean)	61.92	26.32	33.20
Standard deviation	42.41	32.75	71.82
Minimum	16.29	0.7	0.76
First quartile (min)	16.72	1.32	0.96
Second quartile (median)	41.18	1.81	0.98
Third quartile	81.69	52.86	1.62
Fourth quartile (maximum)	269.23	82.86	161.66
Count	16	15	5

Table 5.5: Total extractable hydrocarbon in dried soil (mg.g^{-2}) related to specific sections of the spectral red-edge, derived from paired data from the same location.

	Short wavelength section of the red-edge	**Intermediate wavelength section of the red-edge**	**Long wavelength section of the red-edge**
Average (mean)	61.92	26.32	33.20
Standard deviation	42.41	32.75	71.82
Minimum	16.29	0.7	0.76
First quartile (min)	16.72	1.32	0.96
Second quartile (median)	41.18	1.81	0.98
Third quartile	81.69	52.86	1.62
Fourth quartile (maximum)	269.23	82.86	161.66
Count	16	15	5

were supplemented by an 'optimised' minimum/maximum method (described below). Only the inverted Gaussian method 1 separated grid 3 from grid 1 and only for the shortest wavelengths of the grid 3 data.

5.5.1.1   'Optimised' linear interpolation method for calculating REP

One reason for the diverse array of VI to variation in the spectral red-edge relating to differences in the vegetation viewed. A strong relationship between one VI and a vegetation type is often not maintained for other sites or vegetation types. The typical response is for new or modified VI to be produced. This is probably why three methods of using linear interpolation to determine the REP have been produced. To address this situation, the 'optimised' linear interpolation method was developed (see equation 5.1). The intention was to provide a flexible vegetation index capable of adapting to the different sites and vegetation types for which it may be used. The linear interpolation method used the half reflectance as measured between two wavebands and relies on the assumption that there is a linear relationship between reflectance and wavelength between 700 and 740nm. Instead of using a specific wavelength band it uses the minimum reflectance in the red wavelengths and the maximum in the NIR. Therefore, for some vegetation it tends towards Guyot and Baret's selection (1988), in others Danson and Plummer's (1995) and for other Clevers *et al.* (2002) and also allows for other possibilities with a set wavelength ranges (650-700nm and 740-780nm) are also possible. In equation 5.1 R_{700} is the reflectance at 700nm, R_{740} is the reflectance at 740nm and R_{REP} is the reflectance of half difference between the minimum and maximum reflectance between 650 and 780nm ($R_{650-780}$).

$$REP = 700 + 40 * \left(\frac{R_{REP} + R_{700}}{R_{740} + R_{700}} \right) \tag{5.1}$$

where:

$$R_{REP} = \frac{(MAXR_{650-780}) - (MINR_{650-780})}{2} \tag{5.2}$$
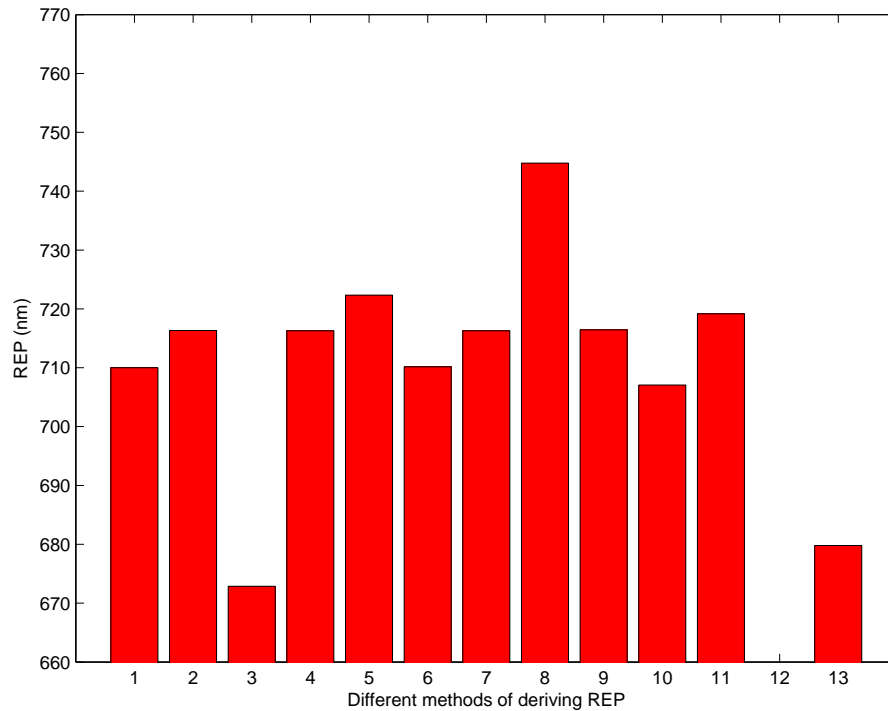
Figure 5.19: REP derived by different methods for two spectra (Grid 3, HSE12).

1. first derivative maximum (Savitsky and Golay 1964), 2. linear extrapolation (Cho and Skidmore 2006), 3. Lagrangian interpolation (Dawson and Curran 1998), 4. Linear interpolation (Guyot and Baret 1988), 5. Linear interpolation (Danson and Plummer 1995), 6. Linear interpolation (Clevers *et al.* 2002), 7. Inverted Guassian, method 1 (Miller *et al.* 1990), 8. Inverted Guassian, method 2 (Miller *et al.* 1990), 9. Clevers' linear interpolation applied to a CASI bandset, 10. Clevers' linear interpolation applied to a MERIS bandset, 11. Lagrangian applied to a CASI bandset, 12. Lagrangian applied to a SeaWIFS bandset, 13. Lagrangian applied to a MERIS bandset.

(a) First derivative maximum REP (Savitsky & Golay 1964)

(b) Linear extrapolation REP (Cho & Skidmore 2006)

(c) Lagrangian interpolated REP (Dawson & Curran 1998)

(d) Linearly interpolated REP (Guyot & Baret 1988)

(e) Linearly interpolated REP (Danson & Plummer 1995)

(f) Linearly interpolated REP (Clevers *et al.* 2002)

(g) Inverted Gaussian REP (method 1) (Miller *et al.* 1990)

(h) Inverted Gaussian REP (method 2) (Miller *et al.* 1990)

(i) Linearly interpolated REP ('optimised' linear interpolated REP)

Figure 5.20: Red-edge positions calculated for grids in grassland with different levels of contamination. White: Grid 1a, intermediate levels of soil contamination; Yellow: Grid 1b, intermediate levels of soil contamination; Blue: Grid 2, low levels of s oil contamination; Red: Grid 3, high levels of soil contamination. (Savitsky and Golay 1964; Cho and Skidmore 2006; Dawson and Curran 1998; Guyot and Baret 1988; Danson and Plummer 1995; Clevers *et al.* 2002; Miller *et al.* 1990)

5.5.2   Ratio-based vegetation indices

A selection of narrow band spectral vegetation indices were equally effective at identifying the area of lowest soil contamination (grid 2) (D_{754}/D_{704}, D_{715}/D_{705}, R_{740}/R_{720}, D_{740}/D_{720}, D_{702}/D_{725}), R_{700}/R_{670} & MTCI. Of the other spectral vegetation indices, figure 5.21 showed that the derivative indices were generally more effective at separating the area of highest contamination than those that used the reflectance spectrum. The most effective VI used D_{730}/D_{706}, though even this confused the area with intermediate levels of soil contaminations. No ratio based index performed as well as the best of the REP methods. Those that were most successful at discriminating between the three grids (R_{740}/R_{720}, R_{700}/R_{670}, NIR/$R_{705:715}$ and IRES) were little better than NDVI.

(a) D_{754}/D_{704} (Datt 1999)

(b) D_{754}/D_{704} (Datt 1999)

(c) $(D_{688}*D_{710})/(D_{697}*D_{697})$ (Zarco-Tejada *et al.* 2003)

(d) MIP: D_{703}/D_{max} (Carter 1994)

(e) D_{715}/D_{705} (Vogelmann *et al.* 1993)

(f) D_{705}/D_{722} (Zarco-Tejada *et al.* 2003)

(g) D_{730}/D_{706} (Zarco-Tejada *et al.* 2003)

(h) D_{740}/D_{740} (Vogelmann *et al.* 1993)

(i) D_{702}/D_{725} (Smith *et al.* 2004)
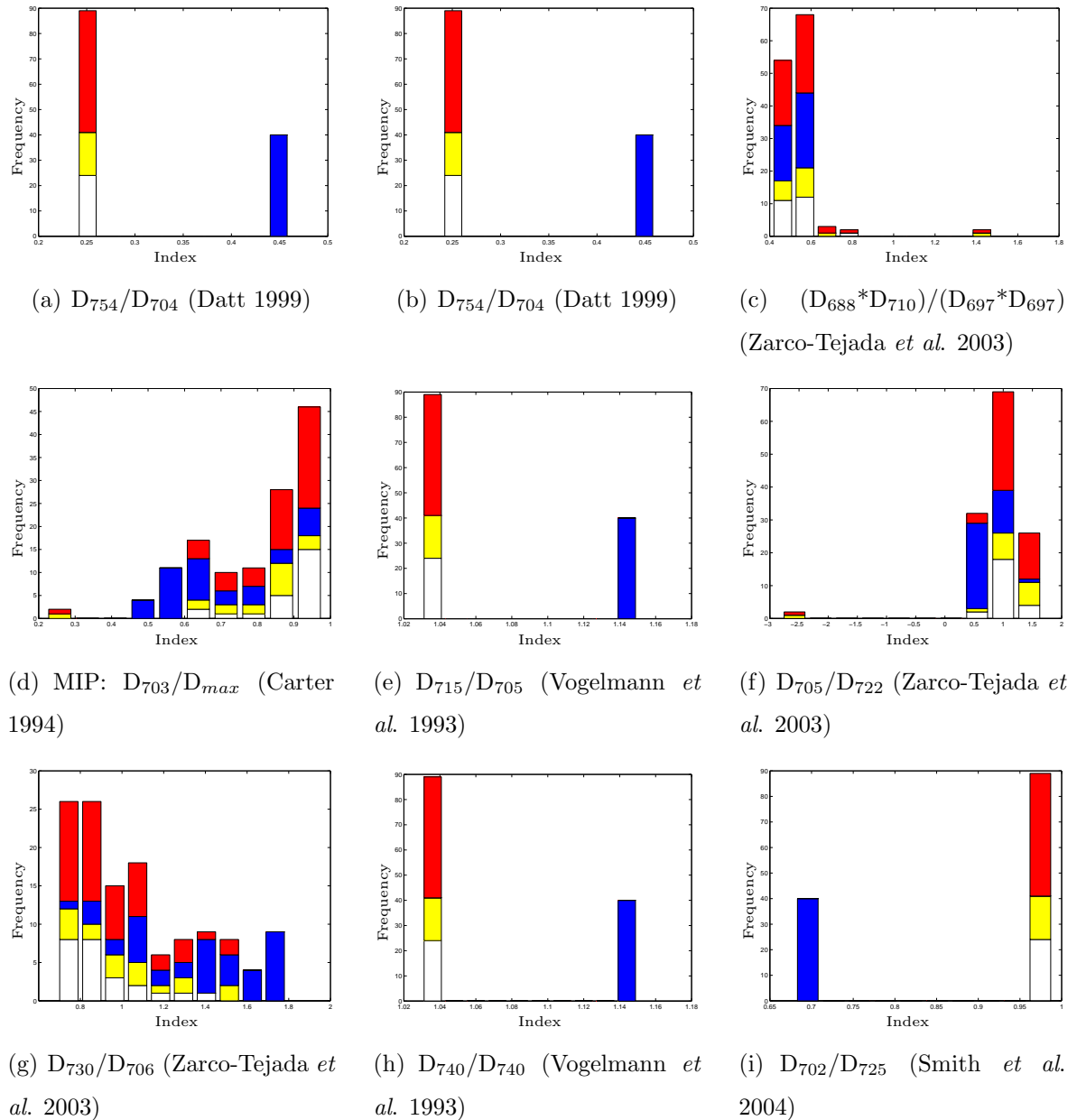
Figure 5.21: Ratio based vegetation indices calculated for grids in grassland with different levels of contamination. Vegetation indices where one spectral derivative band was divided by another. White: Grid 1a, intermediate levels of soil contamination; Yellow: Grid 1b, intermediate levels of soil contamination; Blue: Grid 2, low levels of s oil contamination; Red: Grid 3, high levels of soil contamination. (Datt 1999; Zarco-Tejada *et al.* 2003; Carter 1994; Vogelmann *et al.* 1993; Smith *et al.* 2004)
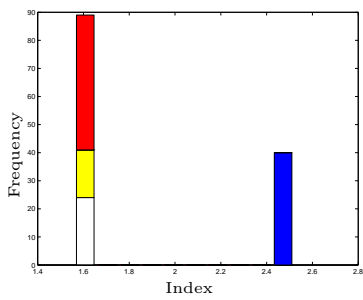
(a) MTCI: $R_{750:757.5}$-$R_{704:713}$ / $R_{704:713}$-$R_{677.5:685}$ (Dash and Curran 2004)
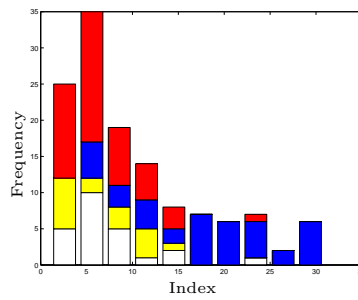
(b) NIR/$R_{705:715}$ (Gitelson *et al.* 1996)
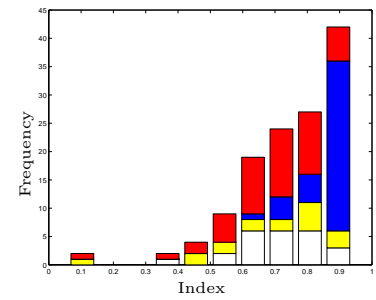
(c) NDVI: $(R_{775:784}$-$R_{675:665})/(R_{675:665}$+$R_{775:784})$
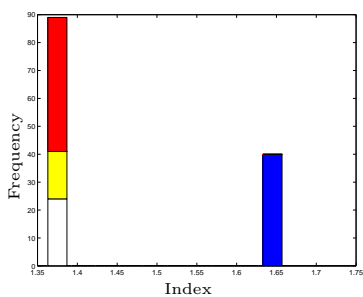
(d) R_{740}/R_{720} (Vogelmann *et al.* 1993)
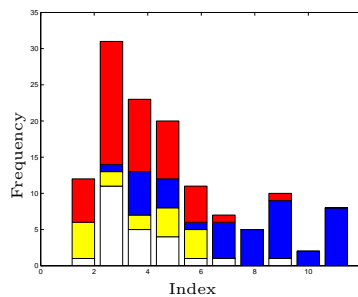
(e) R_{750}/R_{695} (Gitelson and Merzlyak 1996)
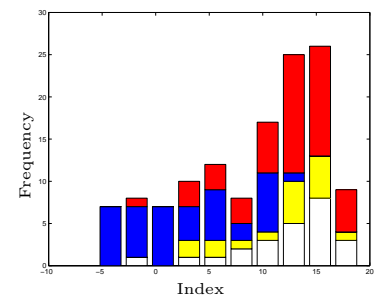
(f) IRES: $((R_{758}$-$R_{739})/(19))$-$((R_{739}$-$R_{720})/(19))$(Yang *et al.* 1999)
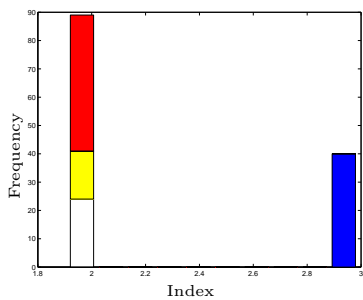
(g) R_{700}/R_{670} (McMurtrey *et al.* 1994)
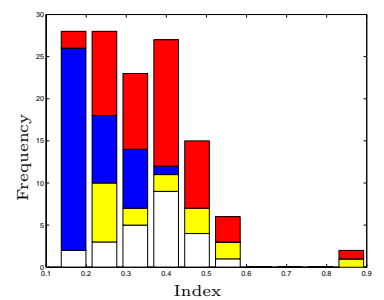
(h) R_{701}/R_{820} (Carter 1998)

Figure 5.22: Selected spectral vegetation indices calculated from grassland with different levels of contamination. White: Grid 1a, intermediate levels of soil contamination; Yellow: Grid 1b, intermediate levels of soil contamination; Blue: Grid 2, low levels of s oil contamination; Red: Grid 3, high levels of soil contamination. (Dash and Curran 2004; Gitelson *et al.* 1996; Vogelmann *et al.* 1993; Gitelson and Merzlyak 1997; Yang *et al.* 1999; McMurtrey *et al.* 1994; Carter 1998)

5.5.3   The relationship between soil contamination and vegetation indices

In addition to the general comparisons reported previously, VI were calculated for the 36 areas where specific soil contaminant concentration levels were known. Most spectral vegetation indices were negatively related to TEH (and LOI). The REPs generally had a stronger correlation with TEH than the ratio based spectral vegetation indices. Nevertheless the strongest predictive relationship, provided with the 'optimised' linear interpolation method for the calculation of the REP (R^2=0.28, P<0.01, n=36) was close to that from the strongest ratio based index, D_{730}:D_{706} (R^2=0.27, P<0.01, n=36). The correlation between spectral vegetation indices and soil variables (figures 5.23 & 5.24) showed selenium as having the strongest correlation and the previously associated soil variable as sharing common relationships with the spectral vegetation indices. Those indices with the strongest relationships (table 5.6) were dominated by REPs and were strongly correlated with TEH from dry soil samples. Predictive relationships (figure 5.25) indicated that these soil variables were able to be predicted by the use of spectral vegetation indices.

5.6   Discussion

Areas with different relative levels of soil contamination were initially identified from the findings of a consultancy report commissioned by the site owners and a series of field surveys and soil measurements. Subsequent surveys provided a finer resolution of data and absolute values that were coincident with reflectance measurements. Field observations additionally indicated that contaminated areas of grassland had a patchy land cover; the most extremely contaminated areas (several metres across) were black, had a pH of 1.5 and were unvegetated (this group were not sampled). Grid 3 was identified as having high levels of hydrocarbon in the soil as indicated by measurements of total extractable hydrocarbon and LOI. Grid 6 also had high levels of contamination in the soil but was not used other than to characterise an area through which transect
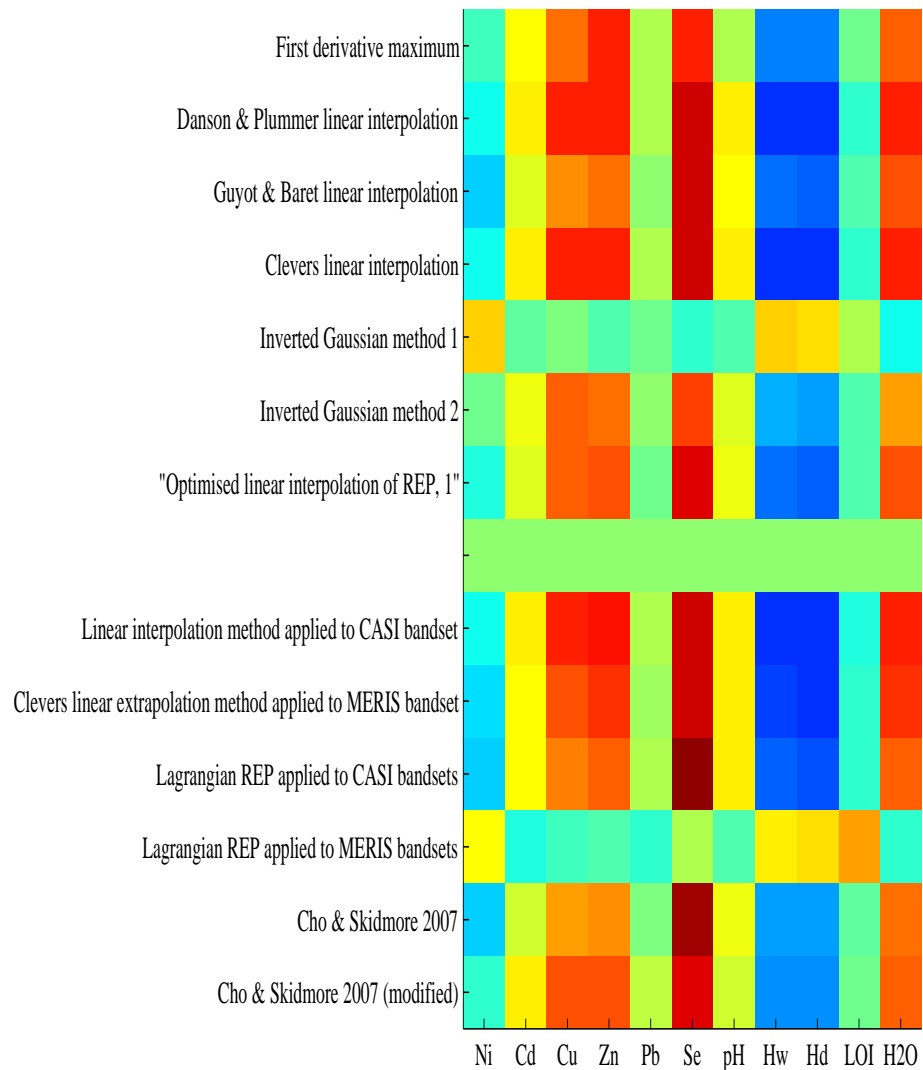
(a) Positional vegetation indices
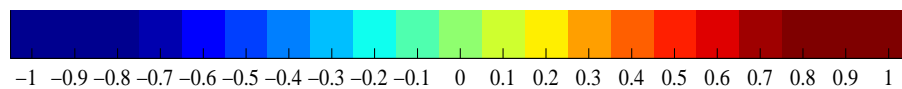
(b) Correlation coefficient (r)

Figure 5.23: Correlation matrix of relationships between soil variables and red-edge position (REP). The correlation coefficient is a number that varies between -1 and +1. A correlation of -1 indicates there is a perfect negative relationship between the two variables. A correlation of +1 indicates there is a perfect positive relationship between the two variables. A correlation of 0 indicated no relationship between the two variables.
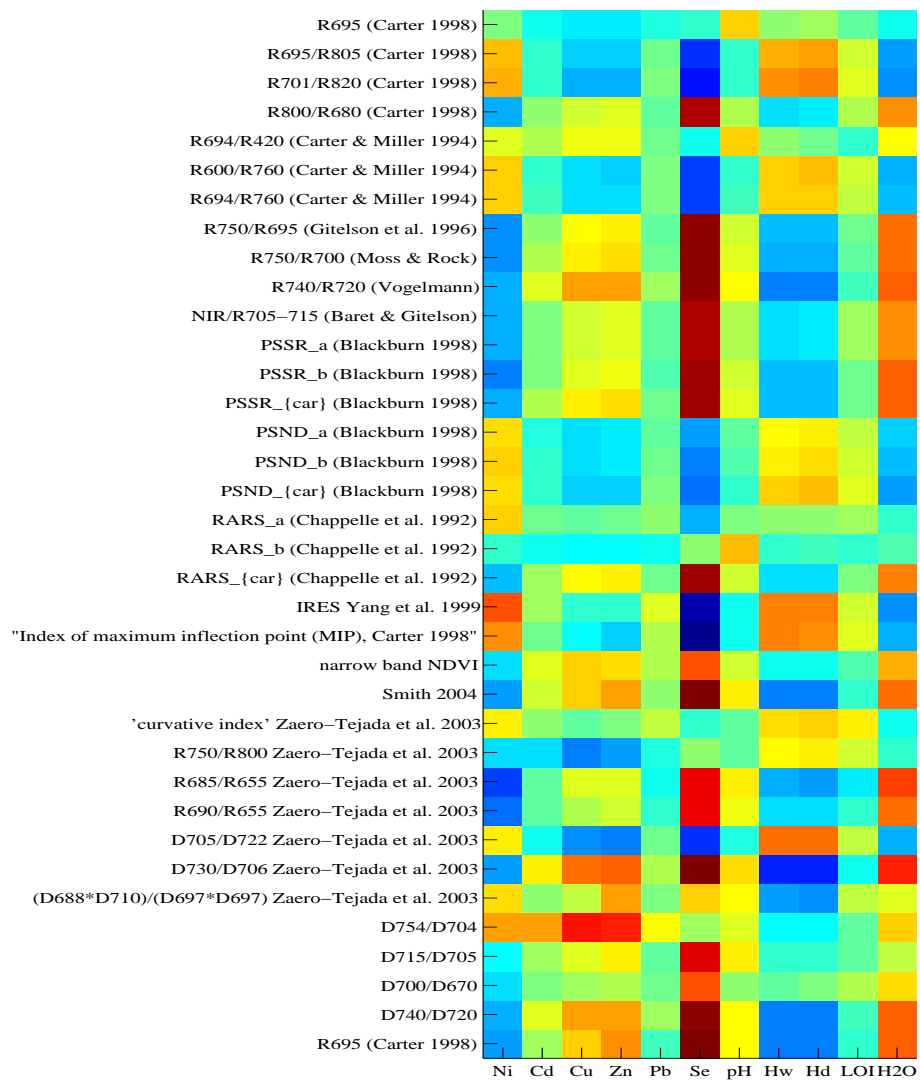
(a) Ratio based & normalised vegetation indices
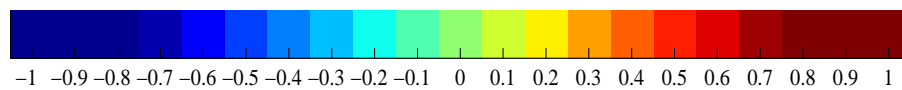
(b) Correlation coefficient (r)

Figure 5.24: Correlation matrix of relationships between soil variables and ratio based and normalised vegetation indices. The correlation coefficient r is a number that varies between -1 and +1. A correlation of -1 indicates there is a perfect negative relationship between the two variables. A correlation of +1 indicates there is a perfect positive relationship between the two variables. A correlation of 0 indicated no relationship between the two variables.

Table 5.6: Pairwise regression of total extractable hydrocarbon (mg.g^{-1} from selected spectral vegation indices (n=36). The higher the R^2 the closer the coefficient of determination. The P value describes the probability of the result occuring by chance. The lower the P value the less likely the result occured by chance.

Index	Author	r value	R^2 value	P value
REP (Optimised linear interpolation method)	This thesis	-0.53	0.28	0.0077
REP (Linear interpolation method)	Danson and Plummer 1995	-0.52	0.27	0.0099
REP (Linear interpolation method)	Clevers *et al.* 2001	-0.52	0.27	0.0308
REP (Inverted Gaussian method 2)	Miller *et al.* 1990	-0.47	0.22	0.0213
REP (Linear extrapolation method)	Cho 2004	-0.46	0.21	0.0245
D730/D706	Zarco-Tejada *et al.* 2003	-0.52	0.27	0.0097
D705/D722	Zarco-Tejada *et al.* 2003	0.45	0.20	0.0282
R740/R720	Vogelmann *et al.* 1993	-0.45	0.19	0.0339
R701/R820	Carter 1998	-0.40	0.16	0.0524
D725/D702	Smith *et al.* 2004	-0.35	0.12	0.0960
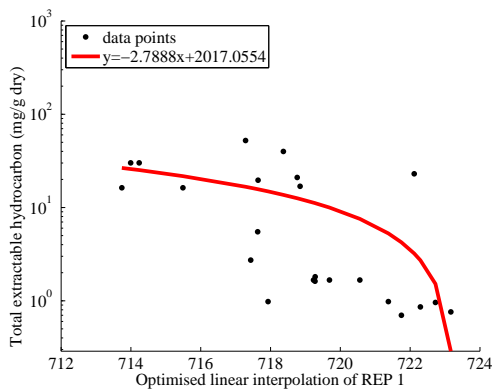
(a) REP ('Opimised' linear interpolation method)
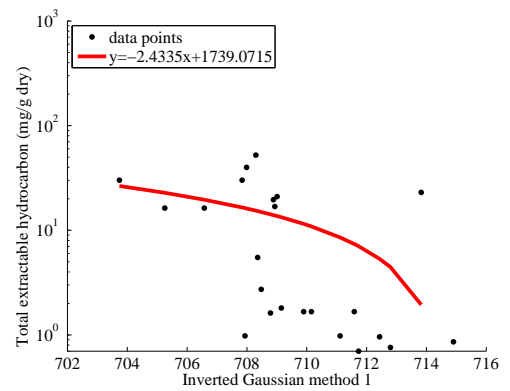
(b) REP (Inverted Guassian method 2) (Miller *et al.* 1990)
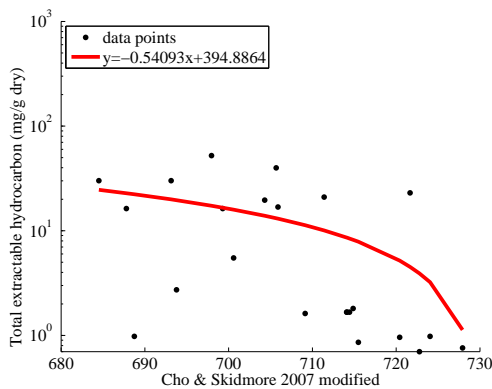
(c) REP (Linear extrapolation method, (Cho 2004)
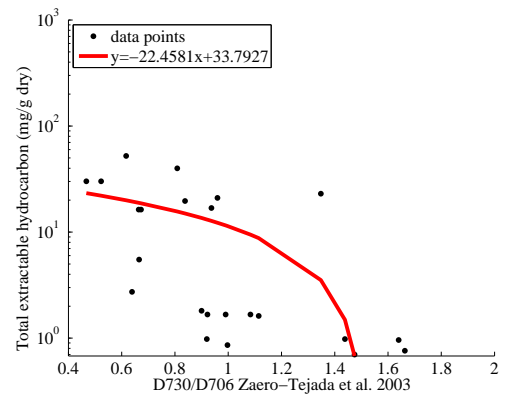
(d) D_{730}/D_{706} (Zarco-Tejada *et al.* 2003)
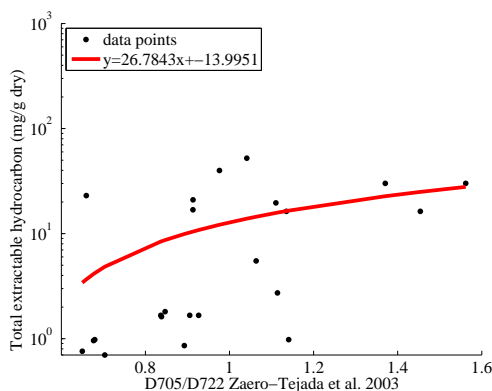
(e) D_{705}/D_{722} (Zarco-Tejada *et al.* 2003)
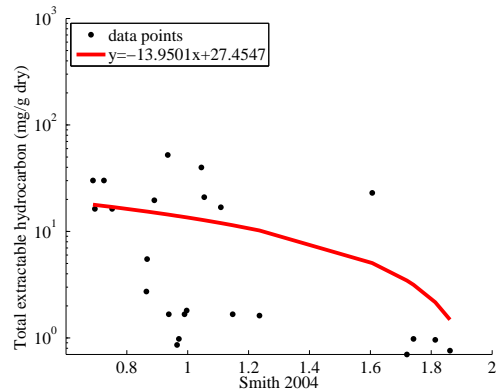
(f) D_{702}/D_{725} (Smith *et al.* 2004)

Figure 5.25: Regression lines and scatter plots for total extractable hydrocarbon (mg.g^{-1}) from spectral vegetation indices (n=36). (Miller *et al.* 1990; Cho 2004; Zarco-Tejada *et al.* 2003; Smith *et al.* 2004)

measurements were made. The average of both soil and reflectance measurements per grid provided a summary description and allowed the comparison of more general characteristics. For example, grid 2 had relatively low levels of soil contamination and had higher spectral vegetation index values. In this case, this difference was almost certainly related to grassland management factors and is therefore discussed in the next chapter.

The hypothesis posed at the start of this chapter stated that:

1. (H_1): *differences in the relative concentration of contaminants in a grassland soil can be detected using the position and shape of the red-edge of reflected radiation,*

The results reported in this chapter show that there was a weak association between soil contamination and VIs (e.g. R^2=0.28, P<0.01, n=36) but also that variation was an important indicator of high levels of soil contamination. Many VIs use the red-edge and a close analysis of the red-edge found a match between soil contamination and short, middle and long wavelength features in the first derivative red-edge. Following these general comments this discussion will consider the results in the following order:

1. the distribution of soil contamination (section 5.6.1),

2. the use of spectral features in the derivative spectra (section 5.6.2) and

3. the use of spectral vegetation indices (section 5.6.3)

5.6.1   The distribution of soil contamination

Within the soil contaminated site, there was the potential of past leakage from storage tanks and pipes as well as areas where hydrocarbon (acid tar) had been dumped by shallow burial. From visual observations, most of the LOI was due to hydrocarbon (ie., not roots or floral detritus). Nevertheless, LOI proved to be only weakly correlated with TEH. The presence of TEH was correlated with that of nickel and lead.

This may be due to their presence (Ni & Pb) in crude oil and as a common catalyst in the refining process (Shell 1953). Similarly, the negative association between TEH and copper, cadmium and zinc may be attributed to a wide spatial deposition of these metals, perhaps as atmospheric particulates. In this scenario the areas of high hydrocarbon concentration may also be related to low soil porosity. Therefore, atmospheric contaminants may be more easily washed out of these areas. Certainly the negative relationships between the soil concentrations of copper, cadmium and zinc with TEH and LOI indicated that different processes led to the accumulation / removal of these contaminants.

5.6.2 Reflectance spectra

Spectra were collected from 36 locations where specific levels of soil contamination had been measured and from 131 locations where relative levels of soil contamination were inferred by location (supported by 101 soil measurements). Conversely, those spectra from locations with the highest levels of soil contamination were characterised by a pronounced peak in the shorter wavelength region of the first derivative red-edge. Those spectra from locations with the lowest levels of soil contamination were characterised by a pronounced peak in the longer wavelength region of the red-edge. From these observations, the first derivative red-edge was classified into three forms. When these forms were investigated in conjuction with the 36 spectra for which soil contamination concentration were known, they matched the areas and had different levels of average TEH concentration. The longer wavelength form only had five examples and four of these came from an area with low levels of soil contamination (grid 2). The shorter wavelength form had 16 examples all of which came from an area with high levels of soil contamination (grid 3). The last (intermediate/middle) form had 15 examples, half of which came from an area of high and half from areas of low soil contamination. This separation was further supported by different levels of TEH. Coincident TEH measurements with the spectra in the short wavelength group had average TEH concentration of 61.7mg.g^{-1}, the middle wavelength region had average concentration of 26.3mg.g^{-1}

and the long wavelength group had average concentration of 33.2mg.g^{-1}. The association of the short wavelength form with high levels of soil contamination seems clear but relatively high concentration associated with the longer form are conceptually less obvious; this made the establishment of a robust statistical relationship elusive. The likely reason for the association of high levels of hydrocarbon in the soil with the long wavelength form will be discussed in the next chapter.

Continuum removal and derivative analysis served similar functions, e.g., to minimise general trends and thereby allow the observation in finer detail in the spectrum. Certainly, details observed in the first derivative spectrum related to subtle features in the change of gradient in the red-edge slope and included multiple changes in the gradient along the red-edge. Some of the observed features were related to the effects of stress. This election of specific wavebands limited any evaluation of the features to previous evaluations that had identified the best wavelength band for that application. The 'Optimised' approach identified a feature (e.g., maximum reflectance) and then extracted the reflectance and wavelength position of that feature instead of relying on a preset waveband.

5.6.2.1   Specific observations concerning the first derivative spectra

The magnitude and relative dominance of peaks in first derivative spectra were dependent on the convexity of the reflectance spectrum; this determined the relative gradient at the short or long wavelengths of red-edge. If the slope was convex, the magnitudes of features in the whole first derivative red-edge were enhanced. If the slope was concave, only the longer wavelength features in the first derivative red-edge were enhanced (figure 5.26). The specific association of the first derivative red-edge in terms of convexity implies the action of broad band absorption rather than the actions of a single narrow wavelength feature (e.g. a fluoresence feature). When spectra with the same reflectance at the lower end of the red-edge were compared (figure 5.27), those spectra with a concave red-edge (in the reflectance spectrum) influenced all the first derivative red-edge wavelengths beyond 690 nm, while those spectra with a convex red-edge in-

(a) Reflectance spectra   (b) First derivative spectra
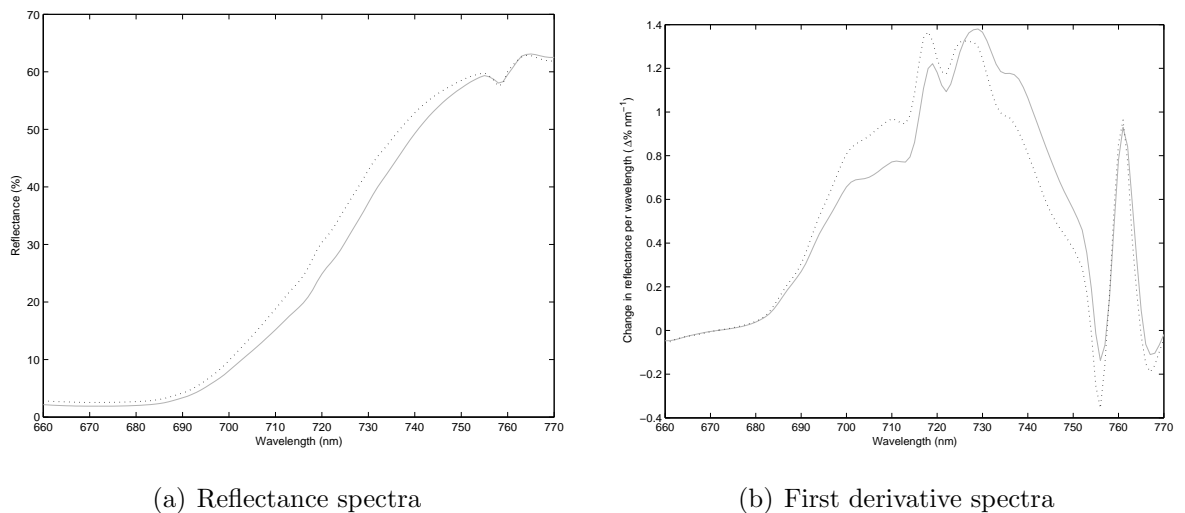
Figure 5.26: The affect of convexity of the red-edge on the first derivative

fluenced only the wavelengths beyond 700 nm. Similar expressions of this effect occur up to 715 nm and would determine the appearance of a short wavelength feature and therefore the relative dominance of the longer wavelength first derivative wavelength features. These observations are investigated in a modelled environment in chapter 7.

5.6.2.2   The double-peak in the first derivative grassland spectra

Double peak / multi-peaks observed in first derivative spectra (subsection 5.17) were similar to those described for grassland by Jago (1998) and Smith (2002) and for other vegetated environments (table 5.5). Grassland data collected by Jago (1998) included measurements that showed the presence of a short wavelength feature between 699 and 705 nm, as well as a longer wavelength feature between 716 and 723 nm. Spectra collected by (Smith 2002) from three grassland sites through which gas had percolated, showed the presence of a short wavelength feature at between 698 and 708 nm, and as a longer wavelength feature between 728 and 736 nm. In many of the spectra (reflectance spectra and the first derivative) measured in this study (and those observed by Smith (2002) an additional feature between 758 and 765 nm was present. Traditionally, this has been associated with instrument characteristics, but there is some doubt about the validity of this assumption (Anderson, Choi & Reidmann, pers. comm. 2001). Instead
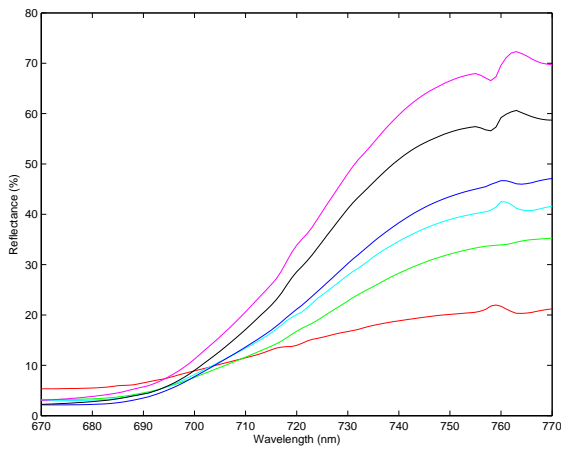
(a) Reflectance spectra
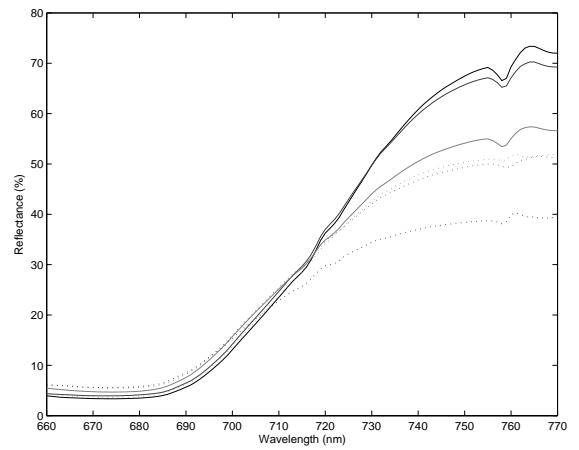
(b) Reflectance spectra
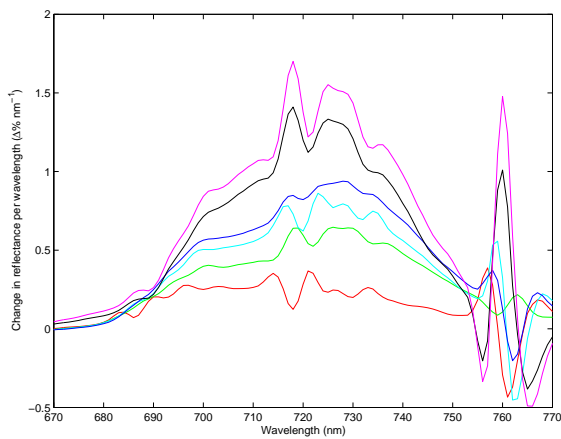
(c) First derivative spectra
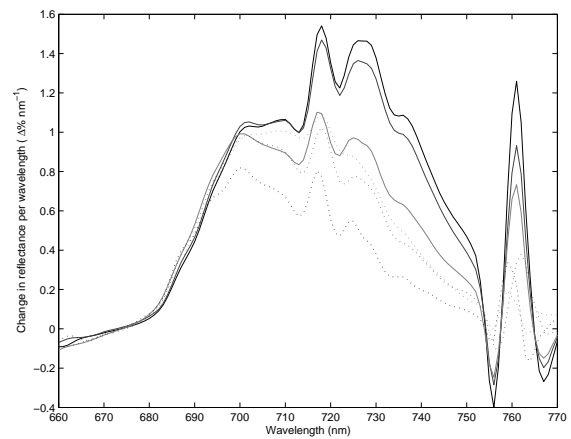
(d) First derivative spectra

Figure 5.27: Differences in the first derivative red-edge spectra determined by spectra with the same wavelength at shorter end of the red-edge.

it may be an expression of passive fluorescence only resolvable using instruments with a band width of 2nm or narrower. The cause and interpretation of these features were discussed in section 3.7.1.4 and related the to switch between short and long wavelength first derivative peaks to changes in chlorophyll (le Maire *et al.* 2004), LAI (Lamb *et al.* 2002) and passive fluoescence (Zarco-Tejada *et al.* 2003). Although passive fluorescence provides some of the explanation for the longer wavelength feature in the red-edge, it is not the whole story (S. Ustin, pers. comm.,2008). The influence of chlorophyll concentration and LAI are considered in the next chapter.

5.6.3   Vegetation indices

The strongest correlations between VI and TEH reported in section 5.5.3 were negative (as strong as r=0.53, P<0.01, n=36). High levels of total extractable hydrocarbons in the soil were correlated with low VI values. The REPs were particularly well correlated with TEH, with the 'optimised' linear interpolation method the strongest. The association of low spectral vegetation index values (including REPs) with the areas where soil contaminant concentrations were highest (and the vegetation was most stressed) made logical sense and showed that remote sensing was a viable tool for the detection of soil contamination. Spectral vegetation indices were also particularly effective at distinguishing the spectral data collected from grid 2 from other areas (grid 1 & 3). This may be of considerable use in other applications, but only served to make the task of picking out spectra collected from grid 3 more difficult. Nevertheless, as part of a staged hierarchical classification process it could aid the overall assessment by allowing the early exclusion of uncontaminated areas. However, for the separation of grids 1 and 3 it should be considered that some of the spectra collected in grid 3 also had high values and in some cases the lowest VI values included spectra from grid 1; this complicated the use of VI for the separation of these two areas.

The use of an assumed linear relationship between reflectance and wavelength in the central wavelengths of the red-edge served the analysis of multi-spectral remote sensing data sets well and is fundamental to the method by which the linear interpolated REP

works. The linear interpolated method for determining REP is one of the most effective techniques for the detection of soil contamination. However, the convexity of the red-edge observed in field spectra showed this assumption to be incorrect. Therefore (logically), the use of derivative ratios should have been a more effective method of identifying stress related effects, e.g. from the ratio of the short and long wavelength derivative features (Smith *et al.* 2004; Williams *et al.* 2008). However, when this approach was 'optimised' it did not perform any better than the indices from which it was derived; this maybe because they had already identified the optimal wavelength. Unfortunately, the correlation between these indices and TEH (hydrocarbons in the soil) were not significant.

5.6.3.1   The use of specific vegetation indices

Some similarly calculated VI had different values. There was a noticable difference between REP calculated from the three linear interpolation methods. The REP calculated using Danson and Plummer's method (Danson and Plummer 1995) was almost 10 nm shorter that that calculated by the other two methods. The only difference between these methods was the specific bands selected to mark the reflectance range of the red-edge. To ensure that the most effective bands were used, an 'optimised method' was tested and performed slightly better than the existing methods archiving the strongest correlation (r=0.53, R^2=0,27, P<0.01, n=36). However, for grassland the automatically selected bands were almost identical to either those identified by Guyot and Baret's linear interpolation method (uncontaminated grassland) or Danson and Plummer (soil contaminated grassland). Those methods that used a modelled line or curve or matched two gradients achieved the separation of spectra from grid 3 from other spectra with the greatest success. The best of these was the inverted Gaussian method 2, which in previous studies has performed poorly in comparison with the other methods. The relatively poor performance by the linear interpolation methods may be explained by the previously discussed convexity in the red-edge slope. Similarly, the maximum first derivative REP's poor performance was due to the presence of long wavelength features in association with high levels of contamination. The most

successful ratio-based vegetation index was a derivative based ratio, D_{730}/D_{706} Zarco-Tejada *et al.* 2003, its strength correlation with TEH matched many of the REPs (r=-0.52, R^2=0.27, P<0.01). Why this VI performed better than other similar VIs must relate to the specific wavelength bands selected. The difference between it and (Smith *et al.* 2004) was particularly striking because the band combinations were so close yet D_{725}/D_{702} was not significantly correlated with TEH (r=-0.35, p<0.1).

5.7 Conclusion

Differences in the relative level of soil contamination were identified using the red-edge of reflected radiation. The soil in grid 3 (and grid 6) had significantly higher levels of hydrocarbon contamination than that from other grids. Soil sampled from grid 3 (and 6) was statistically different from soil sampled from other other grid areas; the main difference was in the presence of hydrocarbon in the soil. Heavy metal concentrations were also statistically different, but despite the levels of hydrocarbon did not exceed published action levels. These areas of high contamination were measured over the general area and evaluated by virtue of paired measurements (of soil and reflectance). Spectral vegetation indices (VIs) from these locations were assessed in terms of the area of contamination and individually by correlation and regression. Some spectral vegetation indices indicated a statistically significant correlation with levels of hydrocarbon in soil. Of these, methods of calculating the red-edge position were generally the most successful though some ratio based were nearly as effective. The strongest correlation and predictive relationship was provided by an 'optimised method for the calculation of the REP, using a linear interpolation. However, general results supported those found by Jago (1998) and Smith (2002). Passive optical remote sensing is capable of detecting the presence of contamination due to hydrocarbons in grassland soil. However, additional information was also present in the variation of spectra (specifically the first derivative maximum). Transects across soil contaminated areas showed a clear switching between REPs and was tracked to differences in the first derivative red-edge. Areas with higher levels of soil contamination had greater

variation and this may be particularly usable with airborne or satellite data sets that can collect a swath of pixels along a flightline, thereby covering a relatively large spatial area compared with field surveys. Although differences in VI were identified, it was the variation within them that was the best identifier of areas of soil contamination and their relative level of contamination. Nevertheless, conceptually, the association between soil variables and reflected radiation is indirect. On many occasions while collecting field data it was clear that other processes associated with the vegetation growing in the contaminated soil were relevant to the understanding of the result presented in this chapter. The clearest example was the high VI and prominence of a long first derivative red-edge feature present in some spectra collected near a contaminated location. The reason for these unresolved anomalies will be explored in the next chapter, where vegetation cover is considered.

Chapter 6

Field data results: the relationships between soil contamination, vegetation and the reflected radiation of grassland

6.1 Introduction

Grassland vegetation provided a means to gain information on the nature of the soil in which it grew. Levels of soil contaminant may be indicated in patterns of vegetative growth. It was established in the previous chapter that relative levels of soil contamination could be detected by the classification of spectra, VI and by variation. However, it was also evident that other processes associated with vegetation cover influenced reflectance as measured over a sensor's field-of-view (FOV). The role of vegetation in this scenario was as a link between the soil contamination and reflectance. In this chapter grassland vegetation is investigated in its role as providing state variables that have been influenced by the effects of soil contamination *and* that directly influence the absorption or scattering of radiation or both. Other vegetation variables determine

the degree by which these effects are observed. For example, absorption in the red-edge wavelength region is influenced by biochemicals (and water) and scattering by cellular structures in the leaves; both are attenuated by the mass or area of vegetation as may be reported using measures of biomass and leaf area index (LAI). However, they are also influenced by the relative angle at which they interact with radiation; this is partially reported using measures of leaf angular distribution (LAD).

In this study, spectral measurements at each grid location on the contaminated grassland site (chapter 5), were accompanied by measurements of vegetation variables. Vegetation and reflectance samples were collected from coincident points while soil samples were collected within the same defined area. The 36 soil samples that were in the same location to the vegetation and reflectance measurement locations were used to form a paired dataset for correlation and regression. Other soil samples were used to characterise the area in terms of a relative level of soil contamination (low, intermediate and high, as per chapter 5). Vegetation in contaminated areas was used to explore the influence of soil contamination. Vegetation in uncontaminated areas (Southampton Common, Thorney Island and an agricultural area in Dorset) was used to establish typical grassland conditions.

Field measured vegetation variables were, SPAD 502 measurements, biomass (wet and dry), leaf area index (LAI) and percentage grass cover. These were accompanied by a vegetation species survey and measurements of leaf thickness and leaf cellular dimensions. Leaf thickness was determined using calipers and leaf cellular dimensions via thin-section microscopy. Laboratory analysis was also used to calibrate a SPAD 502 with specific chlorophyll concentrations for grass. The SPAD 502 was then used as the primary means of collecting estimates of chlorophyll concentration (see chapter 4). The full range of field data collected from the uncontaminated grassland sites supported that collected from contaminated grassland sites (chapter 5) and are presented in table 5.3. Results from these data were used to test the hypotheses that:

- (H_1): *stress effects in vegetation (attributed to the effects of soil contaminants) can be measured in the vegetation that grows in that soil,*

- (H_1): *stress effects in vegetation (attributed to the effects of soil contaminants) are greater than those found by natural variation,*

- (H_1): *stress effects in vegetation (attributed to the effects of soil contaminants) can be detected using the position and shape of the red-edge of reflected radiation,*

1. The first hypothesis will be tested by the statistical comparison of levels of each contaminant in the soil and vegetation variables (section 6.3).

2. The second hypothesis will be tested by the comparison of vegetation data from contaminated and uncontaminated grasslands . An assessment of the variation in vegetation variables in grassland vegetation without any history or evidence of soil contamination will be made from at least three different areas. The summary statistics from this dataset will then be compared with those calculated from the grassland site with soil contamination. A comparison of averages, variance and pairwise analyisis will determine if the grassland with contaminated soil is different from that without any contaminants in the soil (section 6.2).

3. The third hypothesis will be tested by the comparison of vegetation indices with vegetation variables ((section 6.5).

The data to support these investigations were collected from four sites using grids and transects to collect samples and conduct field measurements. Additional measurements and the analysis of samples was conducted in laboratories in the University of Southampton (England) and the University of Nijmegen (the Netherlands).

6.2 Variations in vegetation variables

Four grassland areas were studied, three with no indications or history of contamination and one on an oil-refinery undergoing decommissioning. The 'uncontaminated'

grassland sites were: Thorney Island (grids 8, 9 and 10 and transect 10), Southampton Common (grid 7) and a site in Dorset (transects 11 and 12). The distribution of vegetation data collected is reported in table 6.1.

6.2.1   Thorney Island

Two vegetation datasets were collected from Thorney Island (chapter 4). The first was referenced 'transect 10' centred on a position marked X_2 on Figure 4.1 (chapter 4), OS grid reference 476190 101737. Transect 10 was a North South transet with a sampling interval of 0.5 metres. GER3700 and LAI measurements were conducted on site under bright clear conditions (18.05.99). Samples were collected from the study site and transported to a laboratory at the University of Southampton for biomass measurement and the wet chemical extraction of chlorophyll concentration (Appendix A). Chlorophyll content was derived from chlorophyll concentration and biomass measurements. A second set of measurements were collected from Thorney Island (23:02.01) under clear but windy conditions. Measurements were conducted using three quadrats, referenced as grids 8, 9 and 10 and set about a position marked X_1 on Figure 4.1, OS grid reference 475967 101825. From each grid / quadrat, 25 sets of 25 SPAD 502 measurements and 25 vegetation samples were collected for the measurement of biomass at the University of Southampton. SPAD 502 mesurements were transformed to estimates of chlorophyll concentration, chlorophyll content was derived from these and biomass.

6.2.2   Southampton Common

The grassland on Southampton Common was sampled using a quadrat set at a position marked X_1 on Figure 4.1, OS grid ref. 442118 115216. This was sampled on the 21.02.01 when conditions were cool and overcast, it was referenced as grid 7. The one m^2 quadrat was intensively sampled (all 100 cells). SPAD 502 measurements were transformed to estimates of chlorophyll concentration, chlorophyll content was derived from these and biomass. In addition to these measurements, 100 leaf thickness measurements

were made. These included the whole length and different growth stages. Four grass samples were retained and encapsulated for thin section microtombing and analysis under a microscope, from these 612 cell dimensions were made.

6.2.3 Dorset farm

The grassland on a farm in Dorset was sampled as part of an European Space Agency MERIS Terrestrial Chlorophyll Index validation exercise exercise on 04.08.06. Conditions were hot and clear. Sampling comprised a of a transect of LAI and SPAD 502 measurements. The two grassland transects from which data are reported were referenced as transect 8 and 9. SPAD 502 measurements were transformed to chlorophyll content using LAI.

6.2.4 Grassland with contaminated soil

The grassland with different levels of soil contamination was sampled for vegetation on the 13.11.00. Vegetation sampling was conducted on three grids (referenced grid 1, 2 and 3) in conjunction with reflectance measurements. Details of the sampling scheme are described in section 4.2.1.3. During the course of sampling, 3175 SPAD 502 measurements were recorded, 127 were assesed for % grass cover and samples were retained for later biomass measurements, 31 LAI measurements were conducted with a Delta T-Ceptometer and 3 vegetation surveys were conducted by a botanist (section 4.2.1.3). This was one of six visits to the site. Other visits collected extra spectral data, surveyed structures and extracted soil samples, these lasted a year (between 12.05.00 and 01.05.01.

Different SPAD 502 instruments were used in the field and different spectrometers were used in the laboratory to derive a transformation model for SPAD values to chlorophyll concentration. Measurements at Thorney Island, Southampton Common and the site with different levels of soil comtamination used a SPAD 502 owned by HRI. This

was calibrated using a WPA S106 and 80% acetone as a solvent. This proceedure derived chlorophyll concentration from a known leaf mass and used biomass measured over a known field area to derive chlorophyll content. Measurements in Dorset used a SPAD 502 owned by the School of Geography, University of Southampton. This was calibrated using a U-2000 Hitachi spectrometer and 100 % DMF as a solvent. This proceedure derived chlorophyll concentration from a known leaf area and used LAI to derive chlorophyll content.

The implication of using different SPAD-502s, extraction solvents and spectrometers is that a direct comparison between different sites may only be regarded as approximate. Calibrations for SPAD-502s are instrument-specific, extraction efficiency depends on the solvent and different spectrometers will provide data with different levels of precision. Differences between laboratory spectrometers may relate to accuracy (precision and bias) in measuring at specific wavelengths. Both spectrometers that were used to determine the transform equation for the determinationion of chlorophyll amount from SPAD-502 measurements, had been calibrated within the four months before measurements. Nevertheless, because all the data from the site with contaminated soil were collected using the same combination of instruments and solvents they are comparable. The data from other sites are used to provide a wider context.

Using the Kolmogarov-Smirnov normality test, some data were not normally distributed and simple normalisation techniques did not transform the data to a normal distribution. Therefore, a Kruskal-Wallis one way analysis of variance on ranks was used to show differences between the various sites and locations where data were measured. For those comparisons where all the data passed the Kolmogarov-Smirnov normality test a one way analysis of variance was conducted and supplemented by the Holm-Sidak method for pairwise comparison.

Table 6.1: Grassland sites used and measured vegetation variables (* SPAD 502 calibration measurements)

Reference	Location	Field spectral measurements	leaf thickness	leaf cell dimensions	SPAD 502	Chlorophyll concentration (as determined by extraction using wet chemistry)	biomass	LAI	% grass cover	species group	date
Transect 10	Thorney Island	GER3700				78	78	51			18.05.99
Grids 8-10	Thorney Island				1875		625				23.02.01
Grid 7	Southampton Common		100	612	2500	106*	100				21.02.01
Transects 11,12	Dorset				160	50*		50			04.08.06
Grids 1-3	Contam. site	GER1500			3175		127	31	127	3	12-13.05.00

6.2.5　Variation in vegetation variables in uncontaminated grasslands

Vegetation data were used to determine the level of variation for each variable within and between areas of uncontaminated grassland. These data were to provide a comparison against which measurements from grassland with different levels of soil contamination could be evaluated. Specific consideration was given to the level of variation that may be present. The comparison was restricted to biomass, LAI and chlorophyll concentration. Chlorophyll content was not used as it introduced a cross correlation with biomass from which it was partially derived.

6.2.5.1　Local variation

Local variation (between 10 cm^2 cells in a 1 m^2 quadrat, grid 7) of data from Southampton Common (figure 6.1) showed variation in biomass and the mean chlorophyll concentration across the 1m^2 area. Additionally, variation in chlorophyll concentration within each 10 cm^2 cell was indicated by a standard deviation of chlorophyll concentration. The average chlorophyll concentration for this area was 1.952 mg.g^{-1} with a standard deviation of 0.292 mg.g^{-1}. However, differences in chlorophyll concentration within a single cell were as high as 2 mg.g^{-1}. The maximum biomass difference between the 100 cells in the same area (1 m^2) was 871 g.m^{-2} compared with an average of 566 g.m^{-2} and a standard deviation of 183 g.m^{-2} (figure 6.1). At a slightly coarser scale, three quadrats (grids 8,9 and 10), each within 3 metres of the other showed a significant difference (Kruskal-Wallis test) between the chlorophyll concentrations measured at three loactions (N=3, H$_{(2)}$=36.6, P<0.001). Dunn's pairwise multiple comparison identified all to be different (P<0.05). The combined average biomass for the three qudrats was 1266 g.m^{-2} and their individual averages, 1272.3, 1212.4 and 1315.5 g.m^{-2}. This was matched with average chlorophyll concentrations of 2.9 mg.g^{-1} and individual concentrations of 2.9, 3.0 and 3.0 mg.g^{-1}, respectively.

(a) Biomass (n=1, per cell)

(b) Mean chlorophyll concentration (n=25, per cell)

(c) Standard deviation of chlorophyll concentration (n=25, per cell)

(d) Scale for biomass (g.m^{-2})

(e) Scale for mean of chlorophyll concentration (mg.g^{-1})

(f) Scale for standard deviation of chlorophyll concentration (mg.g^{-1})
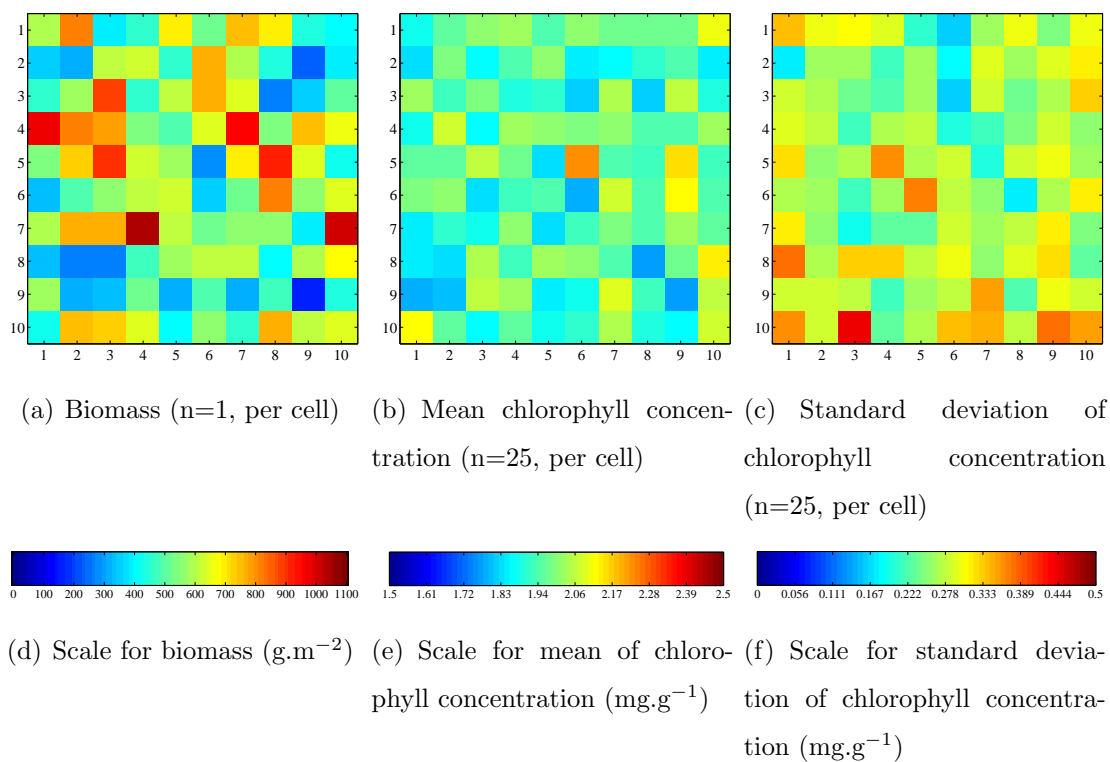
Figure 6.1: Biomass and chlorophyll concentration measurements from a one square metre (100 cells) on Southampton Common.

6.2.5.2 Variation between sites

The three quadrats, grids 8, 9 and 10, measured at the Thorney Island site (23:02.01) had higher biomass and higher chlorophyll concentration than the quadrat on Southampton Common (21.02.01). Both appeared to be representative of far wider areas within their specific site. The Thorney Island site (18.05.99) had an average biomass of 386 g.m^{-2}. The average LAI from this site (transect 10) was 2.3. This compared with 2.9 and 4.2 for the two sites in Dorset (transects 11 and 12). The data passed the Kolmogarov-Smirnov normality test and the Kruskal-Wallis test indicated that the LAI of these two agricultural grassland sites on the same farm (transects 11 and 12) was significant difference (N=2, $H_{(1)}$=26.3, P<0.001). Variations in biomass and LAI between all sites were observationally associated with vegetation height and density. A one-way analysis of variance showed a significant difference between chlorophyll concentrations at these sites (P=0.025) and chlorophyll concentrations between all the sites and locations (Kruskal-Wallis test) were significantly different (N=7, $H_{(6)}$=37.5, P<0.001). However, with the larger data set Dunn's pairwise multiple comparison identified some comparisons as not significantly different, these were Thorney Island quadrats 1 and 3 and Thorney Island quadrat 2 and the data from Southampton Common. The sites in Dorset were not compared with those on Thorney Island or Southampton Common because of the differences in instrumentation and methodology. Nevertheless, summary statistics for all the sites are shown as box plots (figures 6.3 & 6.4). It is noted that variation may also be dependent on differences in the date and time of the day in which data were collected and anteceedent conditions. However, the main data from the soil contaminated site were collected together. Other data serve, mainly, as measures of wider variation in grassland.
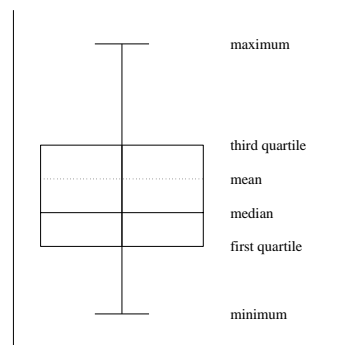
Figure 6.2: Box plot key
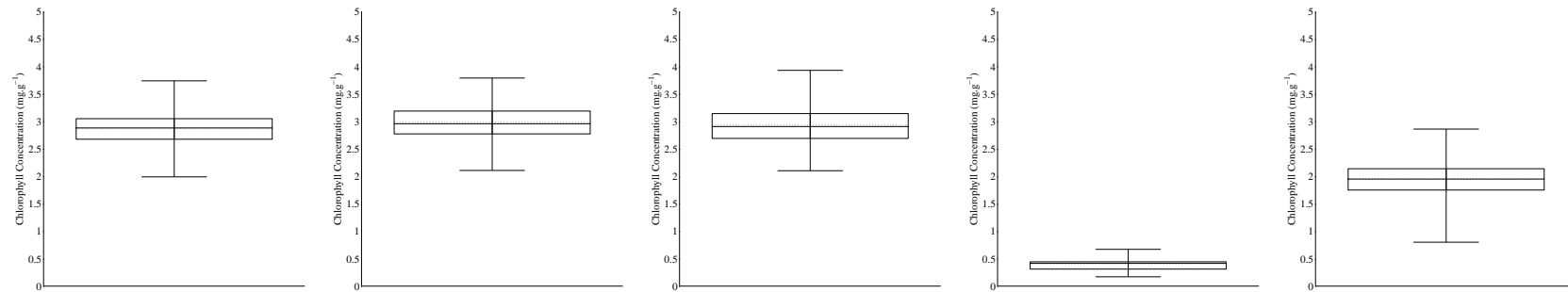
(a) Chlorophyll concentration, Thorney Island, grid 8, n=625

(b) Chlorophyll concentration, Thorney Island, grid 9, n=625

(c) Chlorophyll concentration, Thorney Island, grid 10, n=625

(d) Chlorophyll concentration, Thorney Island, transect 10, n=25

(e) Chlorophyll concentration, Southampton Common, grid 7, n=2500
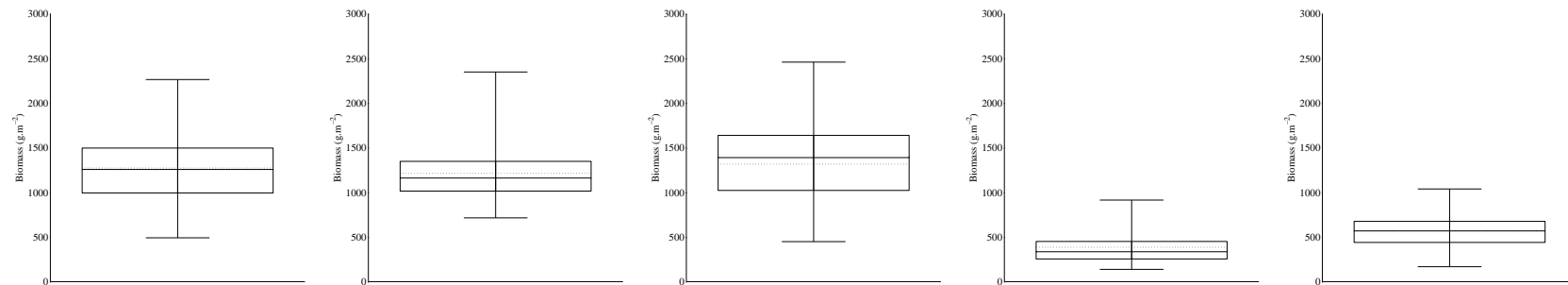
(f) Biomass, Thorney Island, grid 8, n=25

(g) Biomass, Thorney Island, grid 9,n=25

(h) Biomass, Thorney Island, grid 10,n=25

(i) Biomass, Thorney Island, transect 10, n=25

(j) Biomass, Southampton Common, grid 7, n=25

Figure 6.3: Chlorophyll concentrations from uncontaminated grassland. For box plot key see figure 6.2.

(a) LAI, Thorney Island, (b) LAI, Dorset, transect (c) LAI, Dorset, transect 12,
transect 10, n=25   11, n=25   n=25
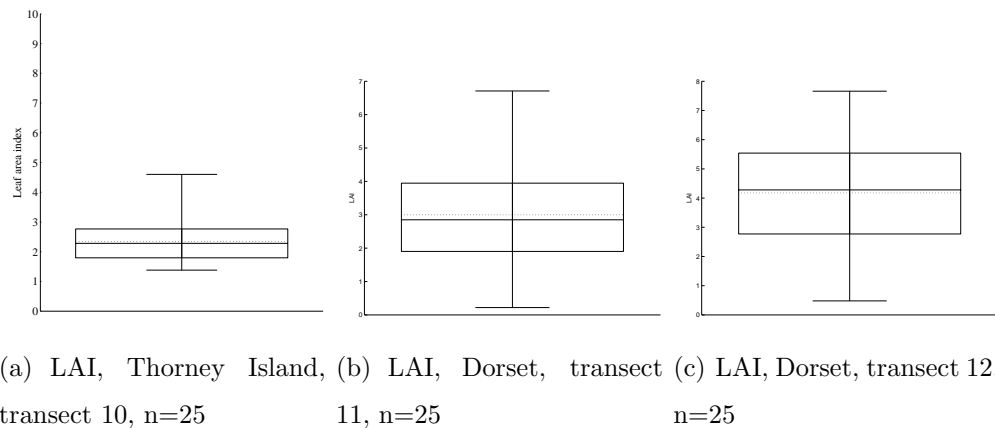
Figure 6.4: LAI from uncontaminated grassland. For box plot key see figure 6.2.

6.2.5.3 Additional measurements

Additional measurements of cell dimensions and leaf thickness were conducted on grass-
land vegetation from Southampton Common. These were primarily collected to guide
the modelling described in chapters 7 and 8. Cell dimensions (n=600) were measured
for seven grass species: *Festuca pratenisis, Lolium perenne, Anthoxanthum odoratum,
Poa annua, Dactylis glomerata, Agrostis stolonifera* and *Poa angustifolia* (figure 6.5).
These had an average cell size of 15.7 μm and a standard deviation of 6.3 μm. Leaf
thicknesses (n=100) were measured for the same range of *Poaceae* species. These had
an average leaf thickness of 0.14mm and a standard deviation of 0.03 mm (non-*Poaceae*
species averages thicknesses between 0.1 and 0.5mm) In summary, grass leaves were
therefore considered to be thin relative to the leaves of other species.

6.2.5.4 Correlation between vegetation variables

The relationship between vegetation variables was also investigated (figure 6.7). For
the Thorney Island site (transect 10) the biomass compared against LAI showed the
two to be related and the vegetation to be dense with a high biomass and relatively
low LAI. This may have been due to the regular mowing required in the proximity of
the runway. On this site both chlorophyll concentration and biomass were statistically
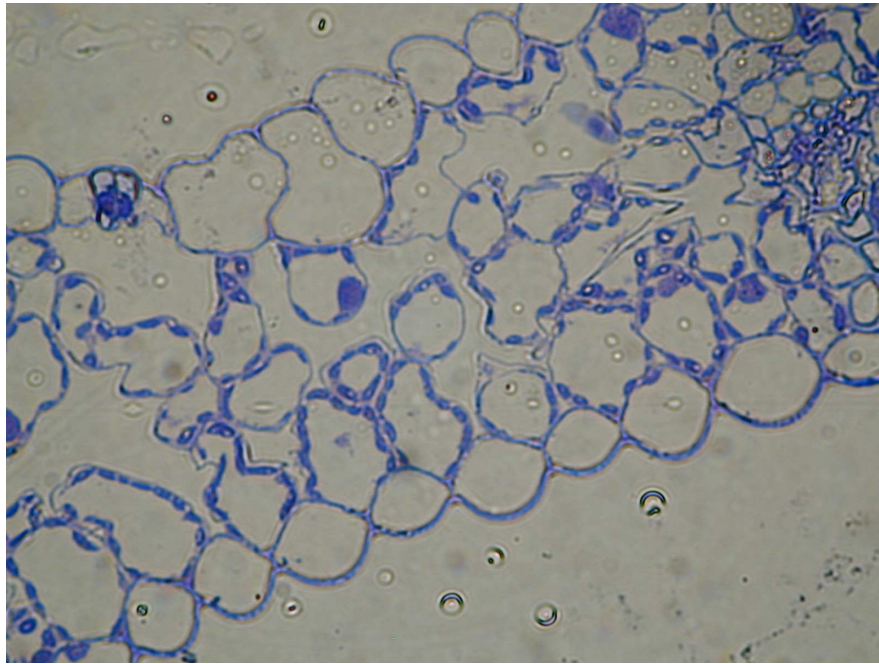
Figure 6.5: Thin section of a grass leaf (*Agrostis stolonifera*). Cell size is approximately 15.7μm diameter.

(a) Leaf thickness

(b) Cell size
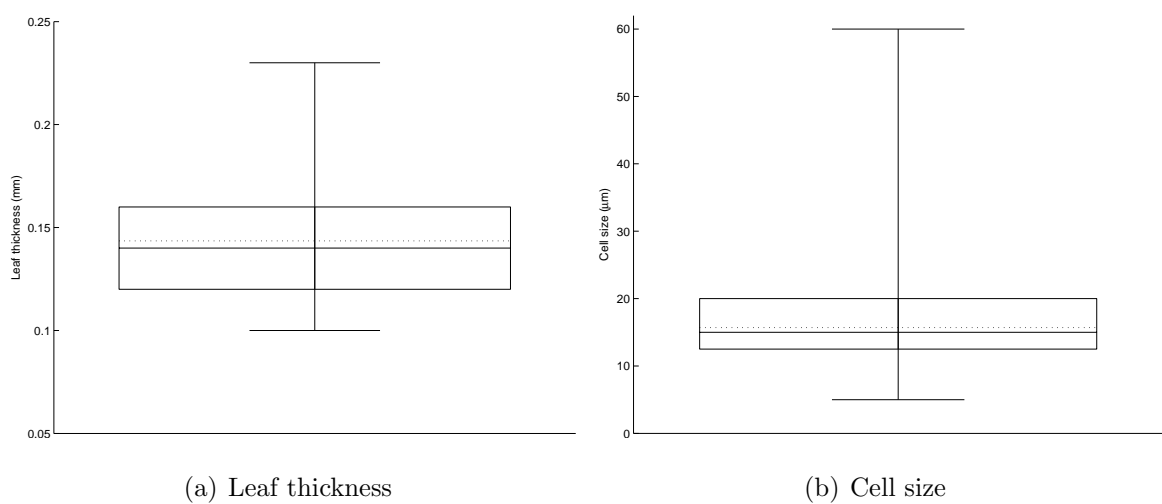
Figure 6.6: Grass leaf and leaf cell dimensions
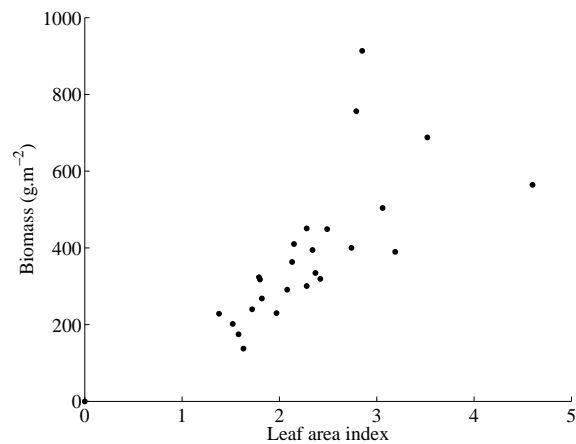
Figure 6.7: Scatter plot of Biomass against LAI, Thorney Island, transect 10, n=25

correlated with LAI. These data have been used as a comparison with grassland on a soil contaminated site later in this chapter.

6.2.6   Variation in vegetation variables in grasslands with different levels of soil contamination

Differences in species type and the management methods were identified as occuring within the grassland area identified as having different levels of soil contamination (grids 1, 2 and 3). Representative quadrats from the three grids are shown in figure 6.8. Generally grid 1 vegetation was tall and dense, grid 2 vegetation as short with a high proportion of clover (*Trifolium repens*) and grid 3 vegetation as tall and diverse with bare patches. A survey of vegetation species in each grid in figure 6.2 identified grid 3 to have the highest diversity of species and grid 2 the least. Of the species types, many in grid 3 were ruderal and associated with rough ground. Among the grids (1, 2 & 3) grid 1 had the most consistent grass cover and the highest chlorophyll concentration and content (figure 6.9), grid 2 had the lowest LAI and grid 3 had the highest proportion of bare ground. The following statistical summary of these data will report on the biomass, LAI and chlorophyll concentration of each grid. A statistical anaylsis of these data continues with biomass, LAI and then chlorophyll concentration and content.

(a) Grid 1   (b) Grid 1

(c) Grid 2   (d) Grid 2

(e) Grid 3   (f) Grid 3

Figure 6.8: Digital photographs of contaminated grassland (nadir viewing).
Dimensions of the white tile are 15 cm × 15 cm.

Table 6.2: Floral species richness identified in grassland where the soil was contaminated with heavy metals and hydrocarbons ($\times$ indicates species presence)

Floral species	Grid 1	Grid 2	Grid 3
Achillea millefolium		$\times$	$\times$
Agrostis canina			$\times$
Agrostis stolenifera	$\times$	$\times$	
Antriscus sylvestis		$\times$	
Arrhima elatius		$\times$	
Brassicacae sp.	$\times$		$\times$
Bromus mollis		$\times$	$\times$
Bromus sterilis	$\times$	$\times$	$\times$
Carex sp.			$\times$
Cerastium glomeratum	$\times$		$\times$
Cirsium arense	$\times$	$\times$	$\times$
Cirsium vulgoire	$\times$		
Convolvolus sp.			$\times$
Dactylis glomerata			$\times$
Daucus curota		$\times$	$\times$
Galium aparine	$\times$		$\times$
Geranium sp.	$\times$	$\times$	$\times$
Lamium purpurcum	$\times$		
Lotus corniculatus			$\times$
Matricia moritima			$\times$
P. lanceolatei			$\times$
Planlago lancedata		$\times$	
Plvagunilis arundinacea			$\times$
Poa compressa			$\times$

Continued on next page

Floral species richness continued from previous page

Floral species	Grid 1	Grid 2	Grid 3
Ranunculus bulbosus	×		
Ranunculus repens			×
Ranunculus sardous	×		
Rusus sp.			×
Sagina procumibens	×		
Sclerochloa dura			×
Serecio vemalis		×	×
Trifolium dusium			×
Trifolium repens	×		
Vicia augustifolia	×	×	×
Vicic hirsuta		×	

6.2.6.1   Biomass

The highest average dry and wet biomass (median and mean) was in grid 1, while the average biomass of grids 2 and 3 were similar (figure 6.9). All biomass values were slightly skewed to lower values. The data passed the Kolmogarov-Smirnov normality test and the Kruskal-Wallis test showed a significant difference (N=3, $H_{(2)}$=18.7, P<0.001) between biomass measured at the three grids locations. Dunn's pairwise multiple comparison identified grid 2 to be different from grids 1 and 3 (P<0.05). Additionally it showed that there was no significant difference between grids 1 and 3 (P<0.05). When compared with data from Thorney Island (grids 8, 9 and 10) the Kruskal-Wallis and Dunn's pairwise multiple comparison showed a significant difference between grids 1, 2 and 3 and the three locations on Thorney Island (N=6, $H_{(5)}$=134.9, P<0.001).

(a) Grid 1   (b) Grid 2   (c) Grid 3

(d) Grid 1   (e) Grid 2   (f) Grid 3

(g) Grid 1   (h) Grid 2   (i) Grid 3
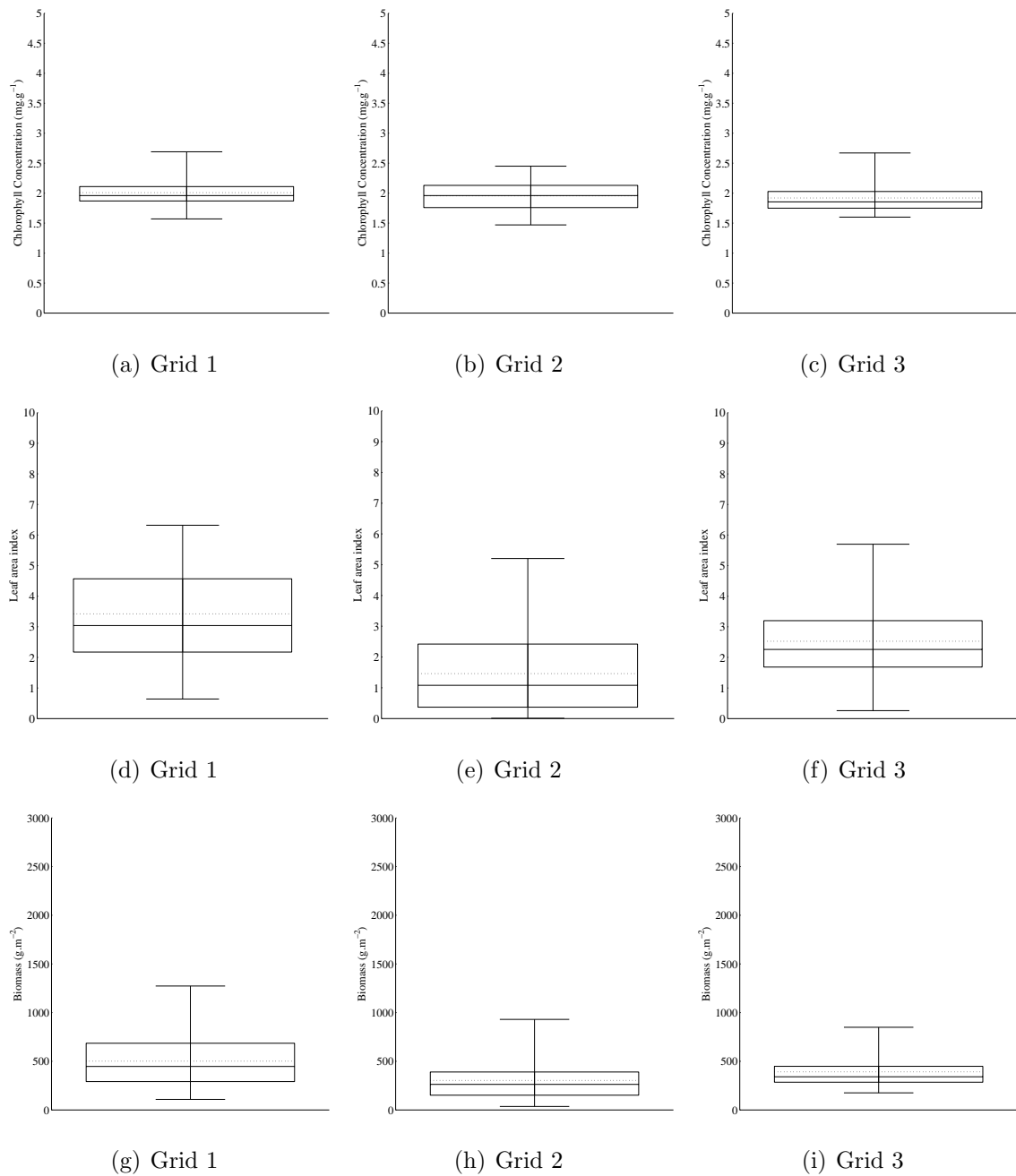
Figure 6.9: Chlorophyll concentration, LAI and wet biomass of *Poaceae* species, in grassland with different levels of soil contamination. For box plot key see figure 6.2.

6.2.6.2 Leaf area index (LAI)

LAI was lower in grid 2 than grid 1 whereas the LAI in grid 3 was larger than grid 2 and lower than grid 1. All LAI values were slightly skewed to lower LAI. (figure 6.9). The Kruskal-Wallis test showed a significant difference between the LAI (N=3, $H_{(2)}$=32.5, P<0.001) of the three grids. Dunn's pairwise multiple comparison identified that this difference was between all of them (P<0.05). When compared with the two sites in Dorset the Kruskal-Wallis test showed a significant difference (N=5, $H_{(4)}$=81.0, P<0.001). Further analysis with Dunn's pairwise multiple comparison identified all the grids to be statistically different from the one of the Dorset sites and only grid 2 as being different from the other (P<0.05).

6.2.6.3 Percentage grass cover

The median percentage cover of grass for all the grids was approximately 80%. Data from grids 1 and 2 had higher medians than this value while the median attributed to grid 3 data was lower. The highest percentage grass cover was in grid 1. Grids 2 and 3 also had areas of high percentage grass cover but other areas where grass cover was very low.

6.2.6.4 Chlorophyll concentration

The transformation equation (SPAD 502 to chlorophyll concentration) was derived from co-measurements by SPAD 502 and wet assay for chlorophyll concentrations of vegetation samples (figure 6.10). It had a correlation coefficient of 0.5, 0.3 and 0.5, for chlorophyll a, b and $a+b$ respectively (P<0.001). Common with most vegetation studies chlorophyll concentrations were highest for upper canopy leaves and near the leaf tip of individual leaves (Boochs *et al.* 1990). A detailed analysis of the distribution of chlorophyll in the leaf and canopy was beyond the scope of this research but did present a practical consideration when collecting field data.

Average chlorophyll concentrations (a and b) were highest in grid 1 and lowest in grid 3 and a dramatic negative skew was present in data from grid 2 (figure 6.9). The average chlorophyll a, b and $a+b$ concentrations (median and mean) were similar in both grid 1 and grid 2, and lowest in grid 3 (figure 6.9). The Kruskal-Wallis test showed that there was not a significant difference between the chlorophyll concentration (N=3, $H_{(2)}$=3.5, P<0.001) of the three grids (1, 2 & 3) on the site with different levels of soil contamination. However, when compared with the 'uncontaminated' grassland sites the Kruskal-Wallis test showed a significant difference with data from Thorney Island (N=6, $H_{(5)}$=419.7, P<0.001), Southampton Common (N=4, $H_{(3)}$=179.9, P<0.001) and Dorset (N=5, $H_{(4)}$=247.5, P<0.001). Dunn's pairwise multiple comparison showed that all data from the grids (1, 2 & 3) differed from that from the area against which they were compared (P<0.05).

6.2.6.5   Chlorophyll content

Chlorophyll content was derived from biomass and chlorophyll concentration, The highest average (median and mean) chlorophyll a contents were in grid 1 and the averages (and ranges) for grids 2 and 3 were similar. The lowest average (median & mean) chlorophyll b content were in grid 2, and the averages for grids 1 and 3 were similar. Grid 3 had the lowest average (median and mean) chlorophyll $a+b$ content and the narrowest first to third quartile range.

As the transformation equation was calibrated specifically for grass the chlorophyll content was also adjusted to account for the percentage grass cover at the location. For this modification the highest average (mean and median) of chlorophyll a, b and $a+b$ content in grass were grid 1. As with the unadjusted chlorophyll concentration and content data, grids 2 and 3 had similar averages and indicated areas not covered by grass. Additionally, grid 3 had a narrower range of chlorophyll content in grass than did grids 1 or 2. For all chlorophyll measures, values were skewed negatively. Grid 2 included spurious negative values, but in all cases these only extended to low value outliers.
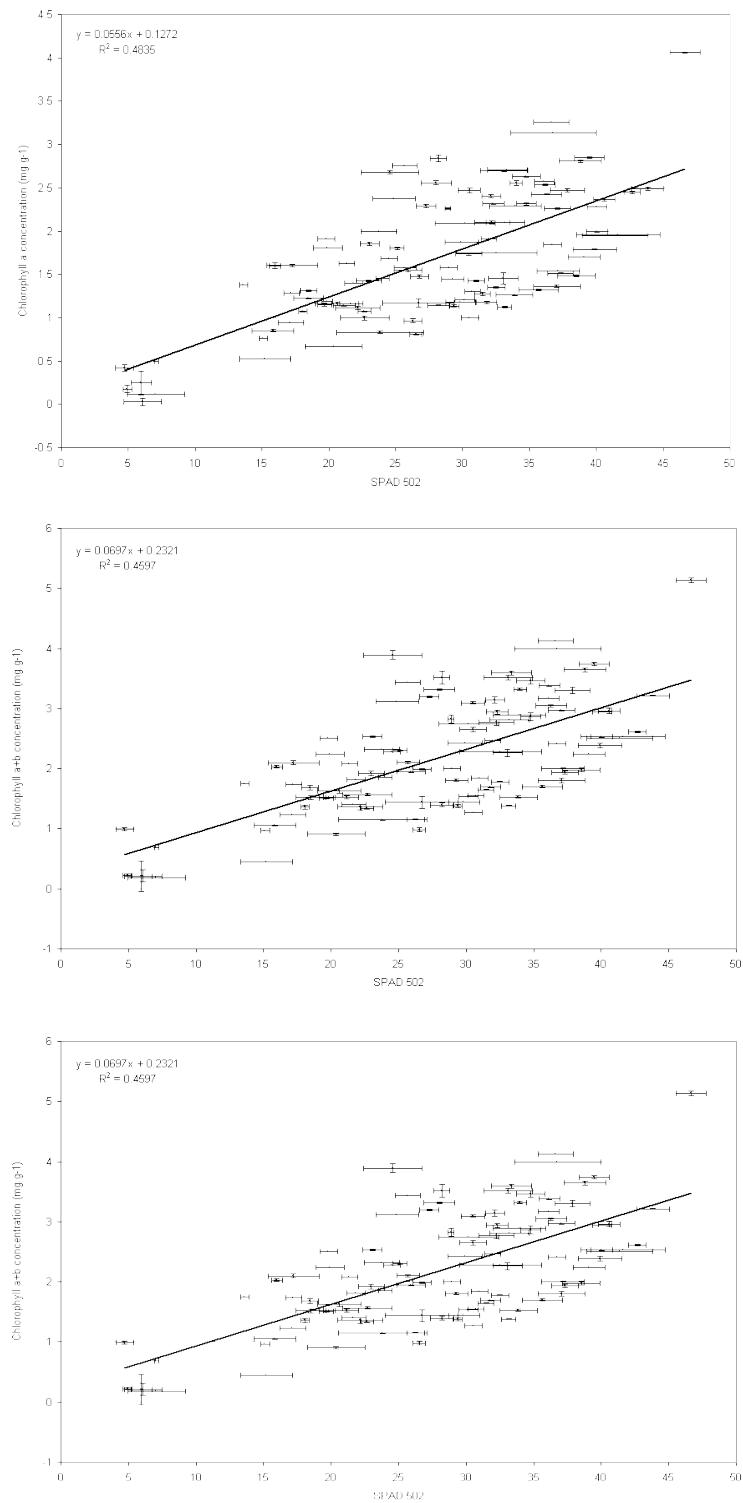
Figure 6.10: Transformation equation for SPAD 502 values to chlorophyll *a*, *b* & *a+b* concentrations (mg g^{-1}) for contaminated soil sites (R^2 were 0.48, 0.29 & 0.46 respectively, P<0.01, n=106)

6.2.7   Interrelationships between vegetation variables

Figure 6.11 shows the interrelationship between chlorophyll concentration, content and content adjusted for percentage grass cover. The weakest association was between concentration and content adjusted for percentage grass cover. The relationship between chlorophyll content and biomass was greatly influenced by the use of the biomass data to transform chlorophyll concentration data to content. The further adjustment for percentage grass cover reduced the strength of this correlation. Chlorophyll concentration had a significant positive correlation with biomass, LAI and percentage grass cover (at a 0.01 confidence level). LAI was significantly related to wet and dry biomass at a confidence level of 0.01.

The correlation between biomass and LAI was compared with that measured from the uncontaminated site on Thorney Island (transect 10). For the three contaminated grassland grids where vegetation measurements were conducted (grids 1, 2 and 3) the correlation between LAI and biomass was similarly tested. Where regression lines were fitted (to predict biomass) the statistically significant relationship identified on Thorney Island was not present at any of the locations on the contaminated site. Additionally, LAI and biomass were more strongly related in grid 3 than at any of the other site on the grassland with soil contamination (figure 6.13).

(a) Chlorophyll *a*

(b) Chlorophyll *b*
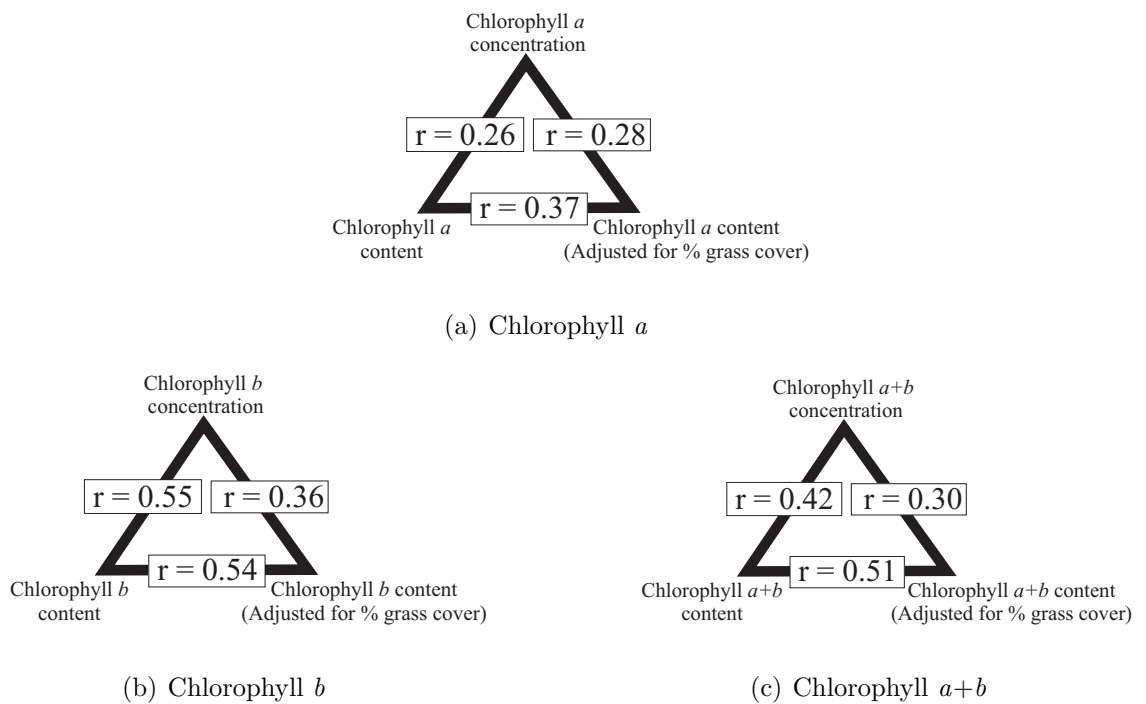
(c) Chlorophyll *a+b*

Figure 6.11: Interrelationship between chlorophyll concentration, content and content-adjusted for % grass cover (P<0.01)
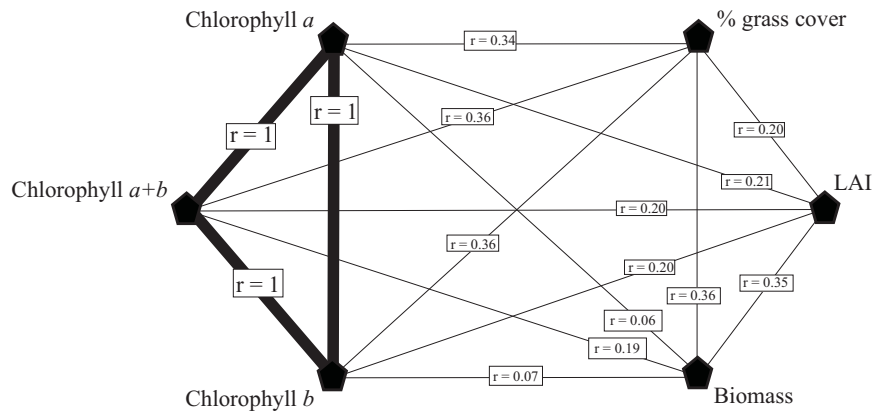
(a) Chlorophll concentration
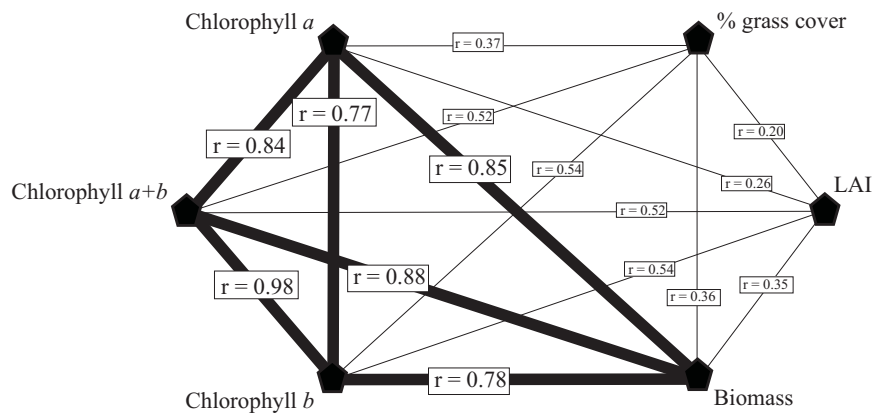
(b) Chlorophyll content
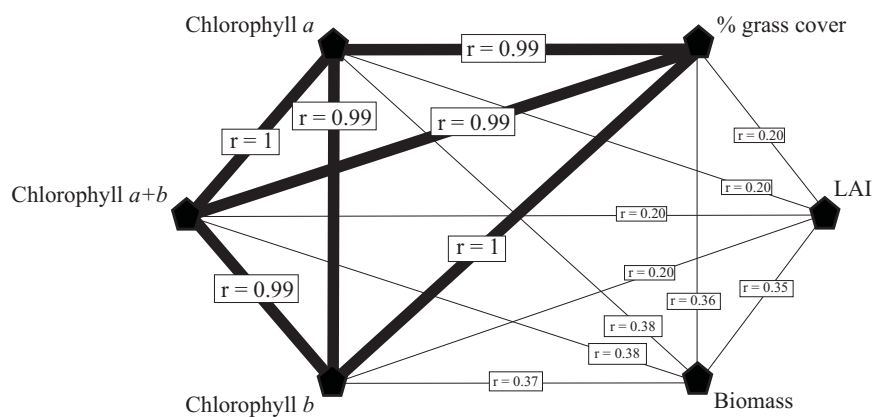
(c) Chlorophyll content (adjusted for % grass cover)

Figure 6.12: Interrelationship between vegetation variables measured from grassland with different levels of contamination (P<0.01). Thicker lines represent a strong correlation (r<0.75)
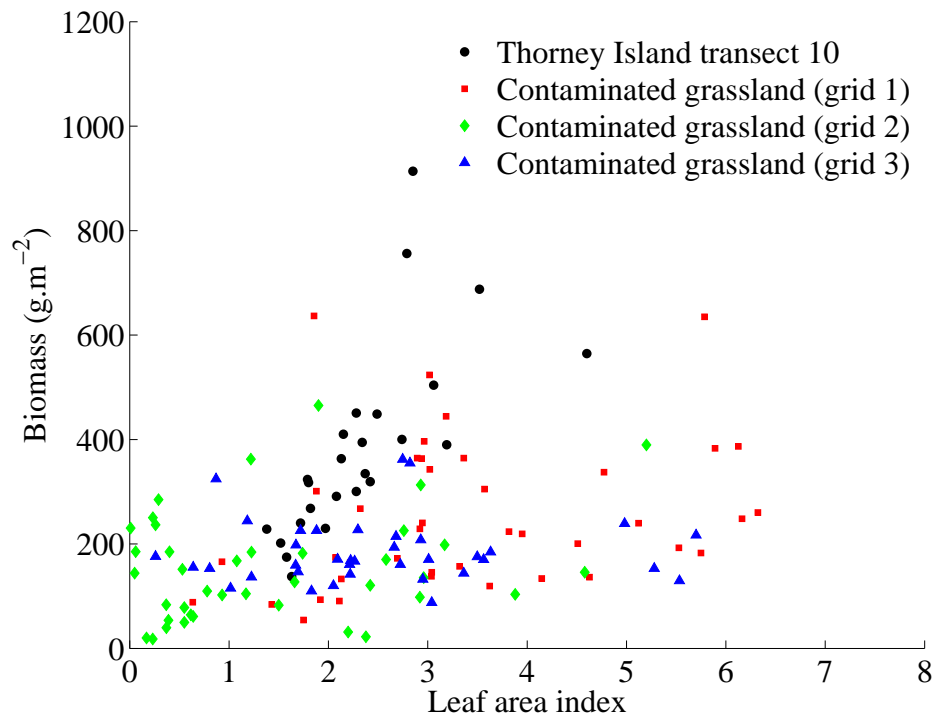
Figure 6.13: Scatter plot of Biomass against LAI, for three locations on a grassland with different levels of soil contamination (grids 1, 2 and 3 (n=43, 40 & 41 respectively) from the grassland site with different levels of soil contamination and transect 10, from the uncontaminated grassland at Thorney Island (n=25).

6.2.8 Difference between uncontaminated grassland and grassland with different levels of soil contamination

A comparison of the boxplots for each site shows that there is a considerable range in biomass and LAI between different grasslands. The more relevant comparison is between chlorophyll concentrations. Table 6.3 shows that though there are some site defined diferences the variation is fairly limited. The magnitude of contamination effects caused measurable differences between sites with different levels of soil contamination. However, the range of variation attributed to different levels of soil contamination exceeds that found on a single uncontaminated grassland site but fell within the range presented by different sites.

Table 6.3: Comparison of chlorophyll content $(mg.g^{-1})$ from uncontaminated grassland and grassland with different levels of soil contamination

Location	Mean average	Standard deviation	Sample size	Date
Uncontaminated site (transect 10)	0.41	0.12	25	18.05.99
Uncontaminated site (grid 7)	1.94	0.28	2500	21.02.01
Uncontaminated site (grid 8)	2.88	0.29	25	23.02.01
Uncontaminated site (grid 9)	2.98	0.33	25	23.02.01
Uncontaminated site (grid 10)	2.98	0.23	25	23.02.01
Site with low levels of soil contamination (grid 1)	2.01	0.23	43	13.05.00
Site with intermediate levels of soil contamination (grid 2)	1.96	0.24	39	12.05.00
Site with high levels of soil contamination (grid 3)	1.91	0.24	45	13.05.00

6.3 The relationship between soil variables and state variables

There was a reasonable negative relationship between TEH (wet and dry) and chlorophyll concentration (r=-0.43, P<0.01, n=36). Additionally, copper, zinc and cadmium, copper, and lead had a reasonable positive relationship with chlorophyll concentration (r=0.47, 0.45, 0.32, P<0.01, n=36). Lead, nickel and selenium had a positive correlation with LAI (r=0.43, 0.27, 0.17, only Pb P<0.01, n=36). These the strength of these realtionship is presented in figure 6.14. Scatter plots (figure 6.15) showed the associations between soil,and chlorophyll concentration, LAI and biomass. Therefore, it is evident from these data that the chlorophyll concentrations within grassland vegetation were adversely affected by the presence of hydrocarbon contamination in the soil. At both stages of the transformation of chlorophyll concentration (i) chlorophyll concentration to content and (ii) chlorophyll content to content of grass, the correlation with TEH increased.

6.4 Vegetation spectra from a soil contaminated grassland

In the previous chapter the first derivative red-edge was classified into three forms; a short wavelength form, and middle wavelength form and a longer wavelength form. The same classification was used to separate spectra and compare then to different chlorophyll concentrations. From this comparison the short wavelength group had the lowest concentrations, then the intermediate and the long wavelength group had the highest concentrations (figure 6.16 and table 6.4).

The LAI and biomass values showed different trends. LAI was highest for the intermediate group while biomass followed the same pattern as chlorophyll with the lowest biomass matching the short wavelength form and the highest matching the long wave-
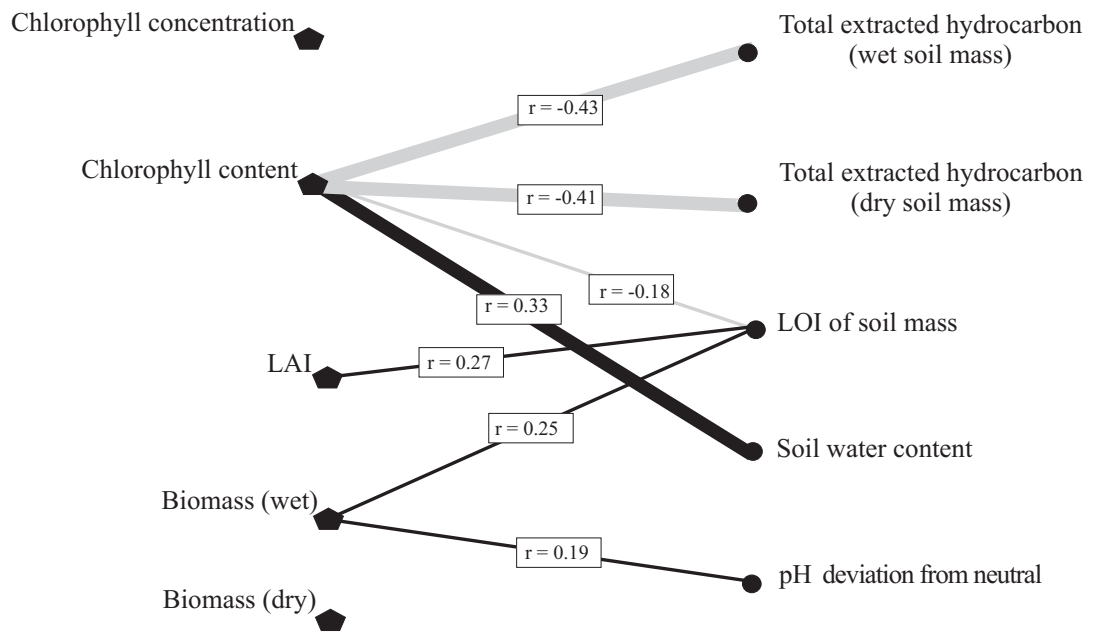
(a) The relationship between vegetation variables and soil-contamination variables
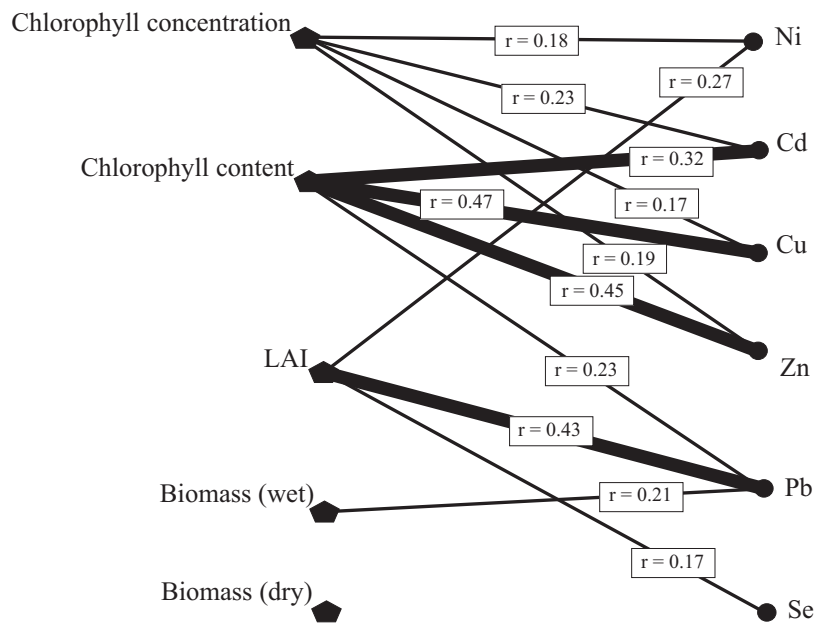
(b) The relationship between vegetation variables and soil-metal concentration variables

Figure 6.14: Relationships between narrow band vegetation indices and soil variables (P<0.01).
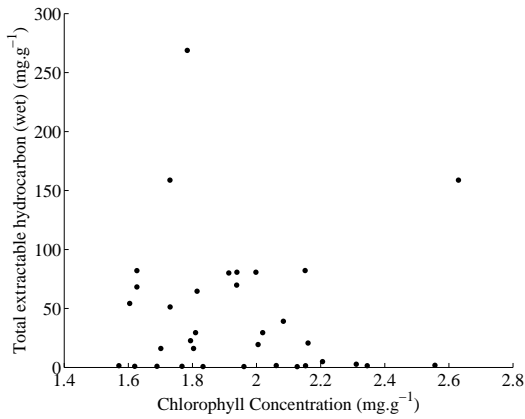
(a) The relationship between vegetation variables and soil-contamination variables
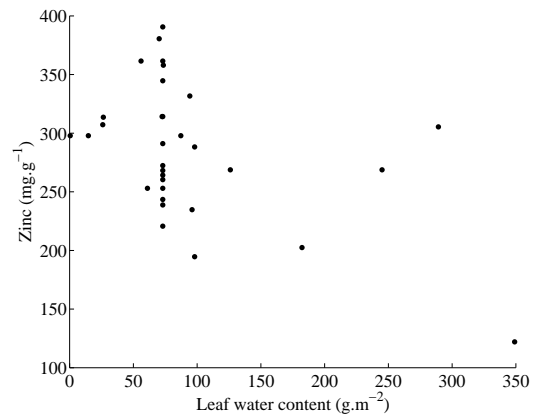
(b) The relationship between vegetation variables and soil-contamination variables
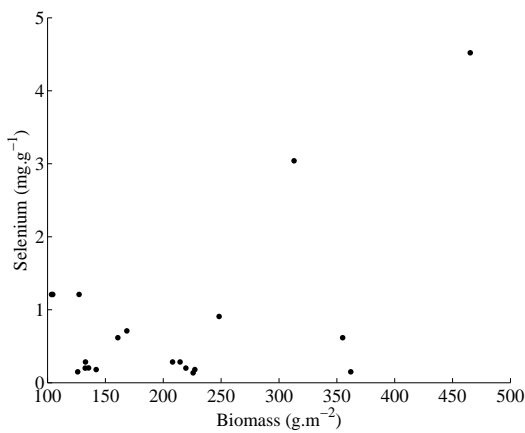
(c) The relationship between vegetation variables and soil-metal concentration variables
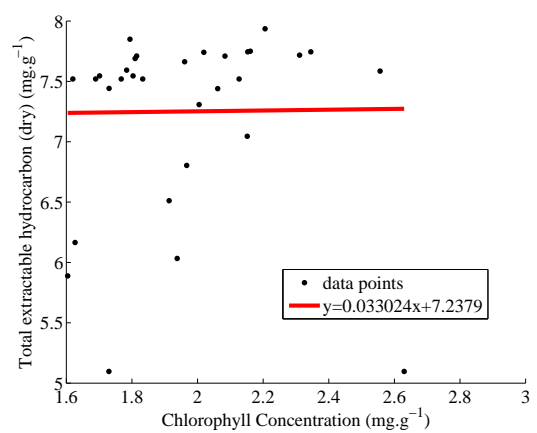
(d) The relationship between TEH $(mg.g^{-1})$ and Chlorophyll a+b concentration $(mg.g^{-1})$

Figure 6.15: Scatter plots of the relationship between soil variables and vegetation state variables (specifically Chlorophyll concentration, LAI and biomass) and for total extractable hydrocarbon $(mg.g^{-1})$ from Chlorophyll a+b concentration $(mg.g^{-1})$

length form (tables 6.5 & 6.6).
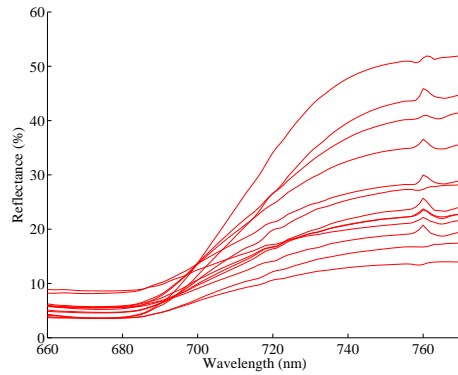
(a) Reflectance red-edge with a short wavelength peak
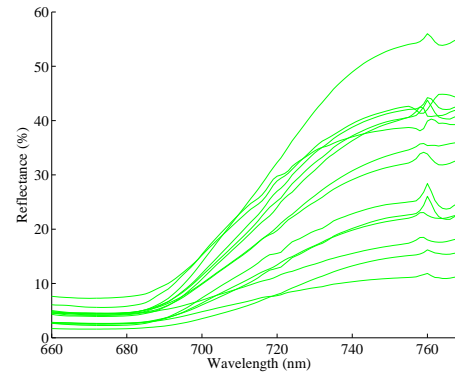
(b) Reflectance red-edge with an intermediate wavelength peak
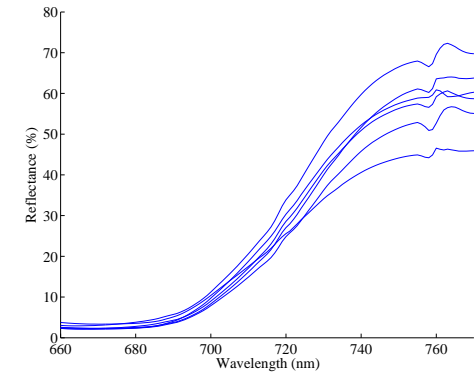
(c) Reflectance red-edge with a long wavelength peak
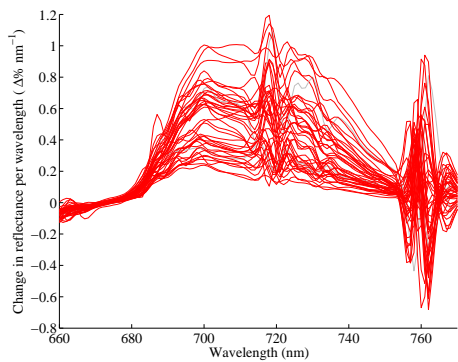
(d) First derivative reflectance red-edge with a short wavelength peak
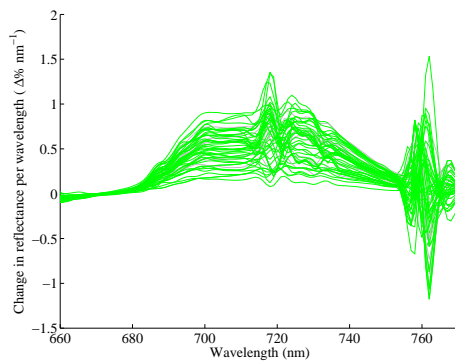
(e) First derivative reflectance red-edge with an intermediate wavelength peak
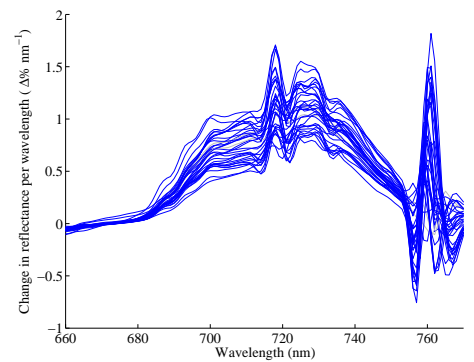
(f) First derivative reflectance red-edge with a long wavelength peak

Figure 6.16: Wavelength sections of the grassland red-edge (soil contaminated grassland data, grids 1, 2 & 3), n=92.

6.5 The relationship between reflectance and state variables

The first component of the indirect relationship between soil contamination and reflectance has been explored in the previous section, that soil can influence vegetation state variables. The second component of the indirect relationship between soil contamination and reflectance will be explored in this section; it will be determined if vegetation state variables influence reflected radiation. Within this section the spectra will be considered as reflectance spectra in their own right, with specific regard to the first derivative of those reflectance spectra and from the vegetation indices VIs) calculated from them. Relationships between the VIs and vegetation variables (specifically chlorophyll concentration, LAI and biomass) have been investigated with particular regard to those VI that calculate a REP.

6.5.1 Vegetation spectra

Spectra were collected from various location where specific levels of soil contamination had been measured and from locations where relative levels of soil contamination were inferred by location. Those spectra from locations where the highest levels of soil contamination had been found were characterised by a pronounced peak in the shorter wavelength region of the red-edge. Those spectra from locations where the lowest levels of soil contamination had been found were characterised by a pronounced peak in the longer wavelength region of the red-edge.

6.5.2 Spectral vegetation indices

Most VI had a positive relationship with chlorophyll concentration but failed the Kolmogorov-Smirnov normality test. Spearman's rank correlation showed significant relationships between the 'optimised' linear interpolated REP and chlorophyll a concen-

Table 6.4: Chlorophyll concentration (mg.g^{-1}) related to specific sections of the spectral red-edge where the main derivative peak appears, derived from paired data from the same location. The short wavelength section of the red-edge approximates the wavelength range: 690 to 710nm, the intermediate section, 710 to 720nm and the long wavelength section, 720 to 740nm.

	Short wavelength section of the red-edge	Intermediate wavelength section of the red-edge	Long wavelength section of the red-edge
Average (mean)	1.90	1.97	2.03
Standard deviation	0.28	0.22	0.26
Minimum	1.15	1.47	1.66
First quartile	1.73	1.84	1.85
Second quartile (median)	1.88	1.94	2.00
Third quartile	2.07	2.03	2.17
Fourth quartile (maximum)	2.67	2.69	2.63
Count	28	37	26

Table 6.5: LAI related to specific sections of the spectral red-edge where the main derivative peak appears, derived from paired data from the same location. The short wavelength section of the red-edge approximates the wavelength range: 690 to 710nm, the intermediate section, 710 to 720nm and the long wavelength section, 720 to 740nm.

	Short wavelength section of the red-edge	Intermediate wavelength section of the red-edge	Long wavelength section of the red-edge
Average (mean)	1.8	3.0	2.3
Standard deviation	1.5	1.5	1.8
Minimum	0.1	0.1	0.1
First quartile	0.6	2.1	1.7
Second quartile (median)	1.5	2.9	2.2
Third quartile	2.5	3.4	3.1
Fourth quartile (maximum)	5.28	6.3	6.3
Count	23	37	27

Table 6.6: Biomass (g.m^{-2}) related to specific sections of the spectral red-edge where the main derivative peak appears, derived from paired data from the same location. The short wavelength section of the red-edge approximates the wavelength range: 690 to 710nm, the intermediate section, 710 to 720nm and the long wavelength section, 720 to 740nm.

	Short wavelength section of the red-edge	Intermediate wavelength section of the red-edge	Long wavelength section of the red-edge
Average (mean)	271.6	428.1	513.1
Standard deviation	169.3	214.2	310.6
Minimum	1.0	99.5	63.0
First quartile	127.0	276.5	313.3
Second quartile (median)	283.3	348.5	451.0
Third quartile	374.77	602.0	647.9
Fourth quartile (maximum)	710.9	889.0	1273.3
Count	28	37	26

tration (r=0.26), chlorophyll b and a+b concentration (r=0.27) and biomass (r=0.35). Chlorophyll concentration relationships were significant to P<0.01 and biomass to P<0.001, n=131). LAI passed the Kolmogorov-Smirnov normality test but had a non-significant positive relationship. Other REPs and many VIs were similarly correlated (figures 6.17). The general trend was that grassland in areas of high levels of contamination resulted in lower vegetation index values than those gained from grassland in areas with low levels of contamination.

6.6   Discussion

Within this chapter vegetation state variables were measured and evaluated in respect of the effect that soil contamination had on vegetation and the the influence that vegetation had on reflected radiation. Account was given to data variation and the statistical correlation between the data groups, (i) soil and vegetation and (ii) vegetation and VIs. These results were used to test the hypotheses posed at the start of this chapter. These stated that:

- (H_1): *stress effects in vegetation (attributed to the effects of soil contaminants) can be measured in the vegetation that grows in that soil,*

- (H_1): *stress effects in vegetation (attributed to the effects of soil contaminants) are greater than those found by natural variation,*

- (H_1): *stress effects in vegetation (attributed to the effects of soil contaminants) can be detected using the position and shape of the red-edge of reflected radiation,*

6.6.1   The distribution of vegetation state variables

Common features in grassland spectra were absorption by chlorophyll (species of chlorophyll *a* and *b*), carotenoids (e.g. xanthophylls) and display pigments (e.g. aramanthin).

(a) Coeficient corre-

lation

Figure 6.17: Strength of relationships between vegetation variables and vegetation indices
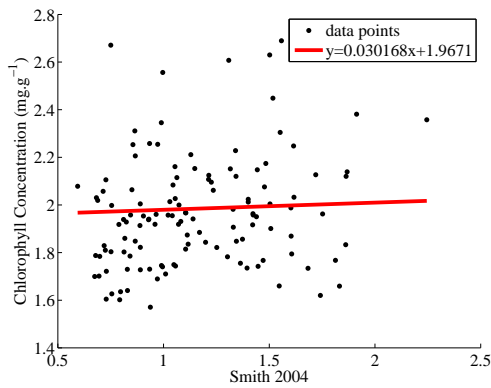
(a) Derivative ratio (Smith *et al.* 2004)
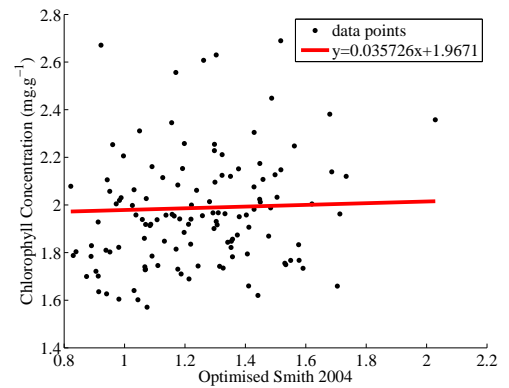
(b) Optimised version of Smith's derivative ratio
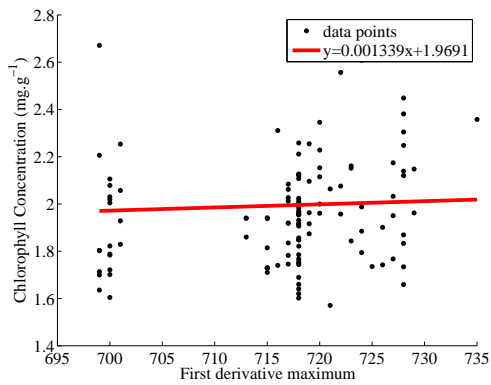
(c) First derivative maximum REP
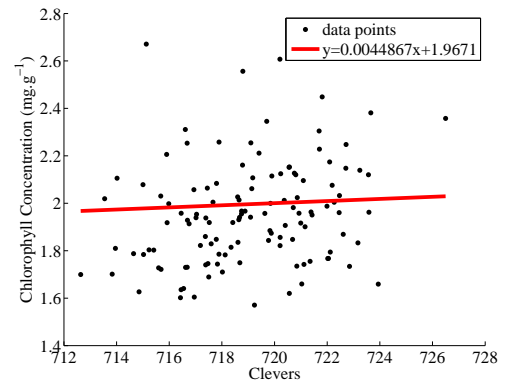
(d) Linear interpolated REP (Clevers *et al.* 2000)
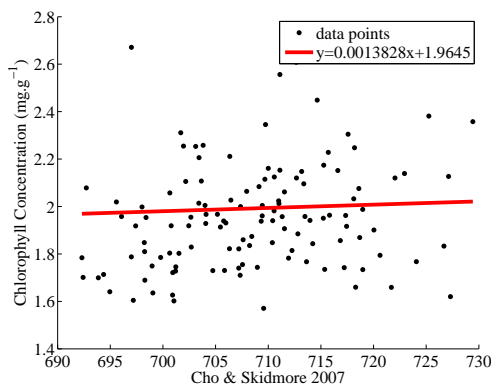
(e) Linear extrapolated REP (Cho 2004)

Figure 6.18: Regression lines and scatter plots for Chlorophyll a+b concentration (mg.g^{-1}) from spectral vegetation indices. (Smith *et al.* 2004; Clevers *et al.* 2000; Cho 2004)

These operate on a cellular level and are scaled up to the leaf and canopy scale by leaf thickness, leaf area and the general mass of photosynthetically active biomass. There are differences between cell type and the photosynthetic efficiency of different vegetation but these are integrated within the field measurement.

6.6.1.1   Variation in uncontaminated grassland

Although average biomass and LAI were similar within each site they were different between sites. The total range of averages of biomass was between 386.0 and 1315.5 g.m^{-2} and for average LAI between 2.5 and 4.2. This was almost certainly related to differences in the management regime (e.g. grazing & mowing) or the tming of data collection. Differences in the sample size limited the comparison of variation between sites but levels were similar. For transect 10 (Thorney Island) biomass and LAI were closely correlated but this location was recently mowed so limiting biomass and standardising LAI. Chlorophyll concentrations within each site were very consistent but average concentrations between sites ranged between 0.4 and 2.98 mg.g^{-1}.

The measurements of chlorophyll concentration were derived from samples with leaves wide enough for measurement and green enough to obtain a measurement. Conversely the biomass measurements included all vegetation regardless of its photosynthetic potential. Although a high percentage of *Poa* species matched the environment modelled by LIBSAIL the presence of tall, complex canopy (rather than a closely mown canopy) allowed for a more comprehensive density of vegetation to form in the overstorey, ie. that component of the canopy from which chlorophyll content and LAI were measured. The presence of high levels of chlorophyll content minimises the effect of errors in the measurement of chlorophyll content. In the field SPAD values were measured and converted to chlorophyll concentration via an equation. The accuracy of the equation was least at low levels of chlorophyll concentration because at these levels the extraction process was less effective.

6.6.1.2   Variation in contaminated grassland

Average biomass of the three grids (1, 2, & 3) were 501.7, 302.6 and 391.5g.,4^{-2}, respectively; and average LAIs were 3.4, 1.5 and 2.5. These were within the range found in uncontaminated grassland. Unlike the uncontaminated grassland, biomass was not correlated with LAI but the weakest association was found in data from grid 3. The low biomass and LAI recorded from grid 2 were related to recent mowing but this had little influence on chlorophyll concentration. Average chlorophyll concentration from the contaminated grassland grids (1, 2 & 3) were 2.0, 2.0 and 1.9 mg.g^{-1} (standard deviation of grids 1, 2 & 3, 0.24 mg.g^{-1}, a minimum of 1.47 and a maximum of 2.69 mg.g^{-1}. These compared with Jago's (1998) slightly lower values of 1.12 mg.g^{-1} from the Isle of Grain (standard deviation, 0.47 mg.g^{-1}, a minimum of 0.25 and a maximum of 2.61 mg.g^{-1}) and were comparable to those measured from uncontaminated grassland. However, LAI measurement did not include the canopy's lowest vegetation layer and biomass left approximately 3 mm of greenery after sampling. Additionally, most chlorophyll concentration estimates were derived from SPAD 502 measurements from the middle of leaf blades sampled from the more accessible portion of the canopy. This was required for the effective use of the transformation equation from SPAD 502 value to chlorophyll concentration as it was specifically derived for grass species but could not take into account the non-grass biomass which was greater for the most highly contaminated sites. Despite not being reflected in the chlorophyll concentration, biomass or LAI data the greatest variation was observed in the most contaminated site. This presented the possibility that the most reactive component of the grassland canopy was not measured during the vegetation survey. However, indications are that it was recorded within the FOV of a field spectroradiometer.

6.6.1.3   Correlated variables

The presence of selenium with high chlorophyll contents may be explained by its effects as a growth promoter in vegetation (Brooks 1972). However as cadmium, copper and lead were present where chlorophyll content was high, the presence or absence of cad-

mium, copper and lead also presents three possibilities: (i) they promote the growth of *Poa* species, (ii) they reduce plant competition by having a detrimental effect on non-*Poa* species or (iii) reduce predation. The positive relationship between nickel, cadmium, copper, zinc and lead with SPAD 502 values may have had a similar enhancement effect on growth because metal concentrations are low and therefore may still provide enhanced growth effects. The positive relationship between cadmium, copper and lead and chlorophyll content may indicate that at the concentrations measured these metals enhance grass growth.

However, selenium did not have a strong positive correlation with SPAD 502 or chlorophyll content. This relationship could have been weakened if the beneficial influence of selenium was exceeded by a detrimental influence of cadmium, copper and lead. The negative relationship between chlorophyll content and TEH was an indication of the effects of environmental stress. It contrasted the positive relationship of cadmium, copper and lead with chlorophyll content and the positive relationship of nickel and selinium with LAI.

6.6.2   Reflectance spectra

The FOV of a field spectroradiometer integrates reflected radiation from the whole canopy (under-storey and over-storey) and was therefore a more comprehensive set of measurements than those measured during the vegetation survey. Nevertheless, the three wavelength forms of the first derivative red-edge (identified in section 5.4.2) were explored in respect to chlorophyll concentration (section 6.4). This showed that the shortest wavelength group had a lower average chlorophyll concentration (1.90 mg.g^{-1}) than the long wavelength group (2.038 mg.g^{-1}) with the intermediate between (1.97 mg.g^{-1}). This separation on the basis of the spectral form of the first derivative red-edge matched with that based on location.

A secondary influence on the measuring of reflectance was the wind. For most occasions when data were collected (including for grids 1, 2 & 3) conditions were calm.

However, the effect of the wind was to alter the angle at which the approximately metre long leaves were presented to the solar radiation and the instrument head. Results confirmed that these changes in the relative leaf angle had an effect on the reflectance spectra. The altered signal could cause a difference in the reflectance of up to 20% of the signal with the lowest signal when the wind was blowing and the highest between gusts.

6.6.3   Spectral vegetation indices

The correlation between VI and chlorophyll concentration were poor compared with that found by Jago's study (1998). She found a (r=0.8, p<0.095) correlation between the REP (first derivative maximum) and chlorophyll concentration at the Isle of Grain but a weaker correlation with soil contamination. However, all correlations were weaker that those obtained with TEH in chapter 5. The 'Optimised linear interpolated REP's relationship with TEH was r=0.53 (P<0.01, n=36). This compared with r=0.26 (P<0.01, n=131) with chlorophyll concentration. The same trend was found with many of the ratio based VIs (e.g., R_{695}/R_{805}, R_{701}/R_{820}, R_{694}/R_{760})) These also had a stronger relationship with TEH than with chlorophyll concentration. In this study some of the most effective VIs used narrow wavelength bands. Their success over broadband VI may be because they included narrow waveband effects that would be integrated within a broad band signal. Nevertheless, the conceptual problem that the correlation between VI was stronger between VI and TEH than VI and chlorophyll concentration remained. The weaker co-relations between VI and chlorophyll concentrations in this study may be due to the complex nature of how hydrocarbons in the soil influence vegetation; i.e. both a stressing (dis-stress) effect and a fertilisation effect. In addition to this field observations suggested the presence of an under-storey vegetation canopy. If this canopy was not fully included in the samples of the vegetation canopy it may account for some of the discrepancy. The influence of a simulated vegetation under-storey on reflectance spectra will be investigated in chapter 7.

6.7   Conclusion

Spectral vegetation indices should logically have a stronger correlation with vegetation state variables than soil properties with no direct influence on visible or NIR reflectance. The fact that the statistically significant relationship between spectral vegetation indices and a soil contaminant was stronger than that with the measured vegetation state variable indicated that some factor within the vegetation was not being fully considered. The controlled environment provided by LIBSAIL allowed potential stress effects to be investigated in the context of a grassland with different levels of soil contamination and the underlying diversity of the environment to be explored. Conceptually, the association between soil variables and radiation was indirect. The REPs that were statistically correlated with the presence soil contaminants had to have done so by interacting with vegetation state variables. There were two possibilities to explain this result:

1. a synergy between state variables such that the combined influence was greater than that of any individual measured state variable, or

2. other state variables that were not measured were being influenced by soil contamination and it is these that influenced the reflected radiation measured with the field spectroradiometer's FOV.

From the digital images and biomass data, variation was identified both vertically in the canopy and laterally in the FOV. This variation was greatest in areas of highest soil contamination. The mismatch would occur, if soil contamination's main influence was *not* on the dominant/obvious vegetation but on (i) the spatial distribution of the vegetation or (ii) its under-storey, then reflected radiation may be influenced by different vegetation variables than those measured in a traditional field vegetation survey. However, the means by which these possibilities can be explored in a field environment were limited due to restrictions in the number and accuracy of simultaneous field measurements, i.e. possible in an available time period and the practical difficulties

of sampling vegetation in its totality to the bare soil level. Fortunately, modelling has developed to the extent that complex combinations of vegetation variables can be manipulated and their influence on reflected radiation assessed. This approach is investigated in the next chapter.

Chapter 7

Modelling the grassland red-edge using LIBSAIL

7.1 Introduction

The range of variables that can be explored simultaneously by modelling exceeds the range possible in a field or laboratory study. This is because the acquisition of simultaneous measurements has logistical limitations of time, scale and practicality, especially when some of the measurements are destructive. For this chapter, the radiative transfer model, LIBSAIL, was used as a tool to explore the red-edge.

The choice of model for this investigation was based on (i) the nature of the vegetation substrate, (ii) field data availability and (iii) practical constraints in terms of computational complexity. LIBSAIL combines the leaf model, LIBERTY, and the canopy model, SAIL. Although LIBERTY was initially designed for modelling Slash Pine, it was particularly suitable for modelling grassland because its input variables describe cell sizes and air voids. This was relevant because of the difference between cell density of monocotyledons (such as *Poa* species) and dicotyledonous species (most other terrestrial vegetation). Suitable canopy inputs were absent in LIBERTY but were introduced

into LIBSAIL via SAIL. However, for these investigations, the effects of viewing and illumination geometry, leaf angle, the hot spot and soil have not been evaluated.

This chapter starts with a description of the LIBSAIL radiative transfer model, how it is composed and the input data it requires. The chapter continues with a comparison between LIBSAIL output and field spectra. This comparison established LIBSAIL as an appropriate model environment with which to explore the grassland red-edge. Further investigations explored the causes of the spectral differences in the red-edge identified in chapter 5, specifically the implications and effects of a second canopy component. This second component may approximate the presence of an under-storey or lateral variation within a sensor's field-of-view (FOV) and is further explored in chapter 8. Its evaluation presented implications for the field study of grassland since it identified general deficiencies in the field methodology for most ground truthing surveys of grassland areas.

7.1.1   LIBSAIL

LIBSAIL is a radiative transfer model that uses a set of input scalar values to weight the combination of five absorption spectra to produce coefficient of absorption applied against a scattering coefficient to provide a top of the canopy vegetation reflectance spectrum. The three absorption spectra that influenced the spectral red-edge were chlorophyll, albino and water; all were original components of LIBERTY. The other input vectors affected longer wavelengths than the red-edge region, and leaf water (in this modelled environment) had only a slight influence at the longest red-edge wavelengths (figures 7.1). An 'infinite reflectance' spectrum, measured using the Perkins Elmer Lambda 19 laboratory spectrometer, from a 5mm thick stack of green grass leaves held in the instrument's viewing aperture. It was used to derive a pigment spectrum for grass. This was achieved with the assistance of Dawson using the Inverted LIBERTY model. The input scalar values that drive LIBSAIL serve to act in association with the 'coefficient of absorption'. Therefore, within LIBSAIL, most absorption is wavelength dependent and all scattering is wavelength independent.

(a) Chlorophyll

(b) Albino

(c) Leaf water

(d) Lignin and cellulose

(e) Protein
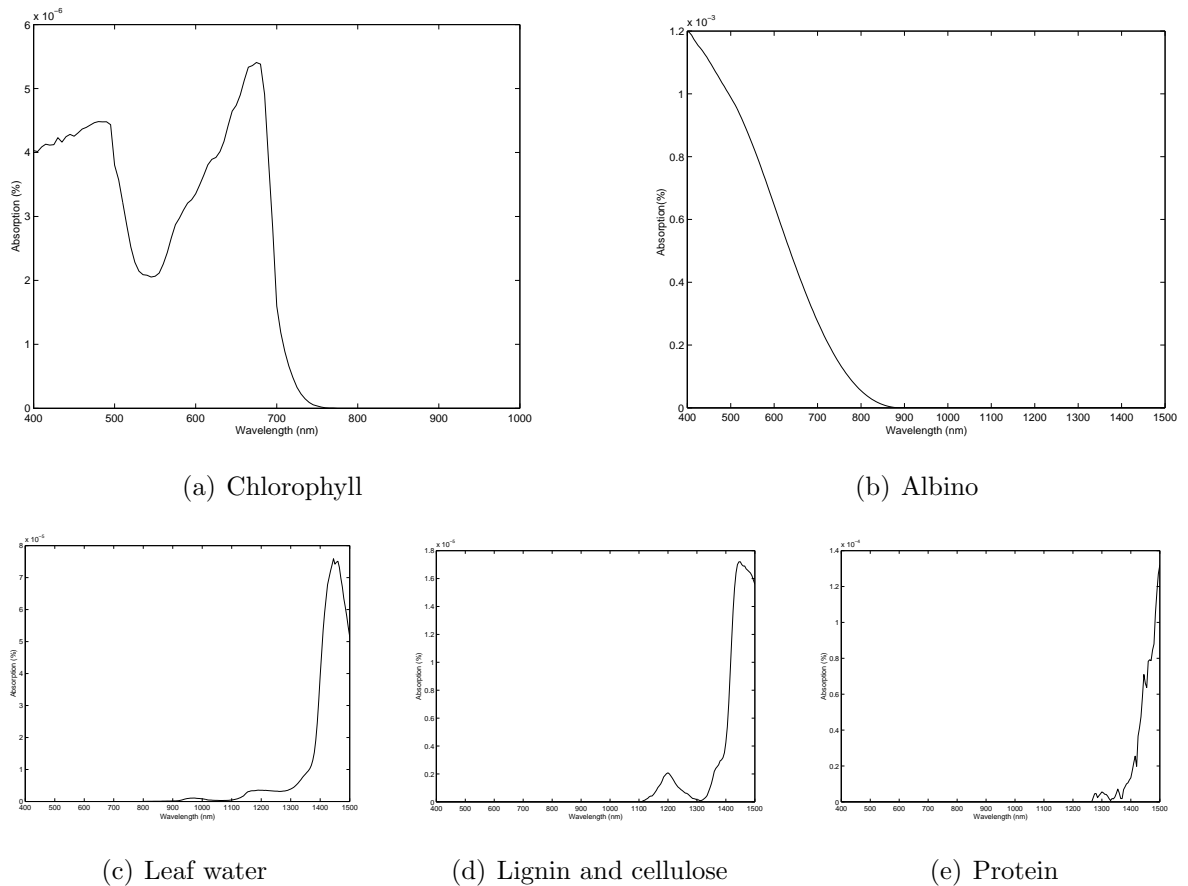
Figure 7.1: Spectra derived from input vectors used for LIBSAIL (100% concentration)

Within this chapter, LIBERTY will be assessed on its capability to model grass leaves and LIBSAIL (LIBERTY+SAIL) will be assessed on its capability to model grassland vegetation. LIBSAIL will then be used to simulate and investigate the effect of differences in vegetation variables on grassland spectra. However, before LIBSAIL could be used with any confidence it needed to be compared and validated for grassland vegetation. The validation process was conducted in three stages. First the leaf model (LIBERTY) was tested, then the combined leaf and canopy model (LIBSAIL) was tested with grassland data from sites with no history of soil contamination and finally LIBSAIL was tested with grassland data from sites with different levels of soil contamination. This last stage will be investigated in chapter 8.

7.1.2 The transcription of LIBERTY from C to Matlab

LIBERTY was transcribed from C into Matlab (Anon. 2009a) and the outputs were compared and found to be identical (figure 7.2). In the course of this action several sections of obsolete or unused code were removed. Most removed sections had been used for the automatic display of spectra in C but others calculated unused variables; these had simply not been removed when replaced by more efficient sections of code (T. Dawson, pers. comm. 2000).

(a) Reflectance spectra   (b) Comparison
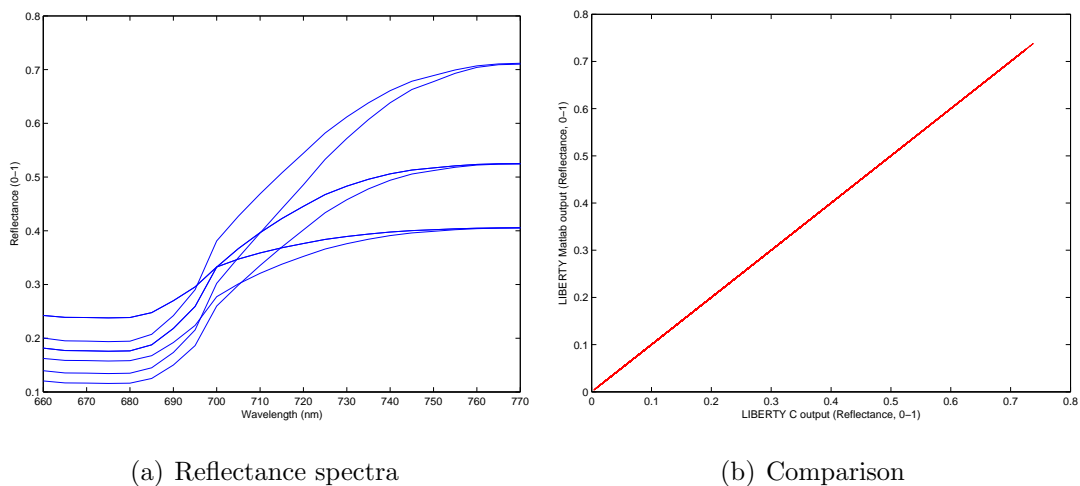
Figure 7.2: A comparison of C and Matlab simulated LIBERTY spectra. a) six sample spectra simulated using LIBERTY in C and b) shows a comparison of outputs from the C and Matlab versions of LIBERTY (using the pre-corrected calc file, Appendix E)

7.1.3 Validating the use of LIBERTY for grass leaves

Twenty five leaf samples were used to validate the use of the LIBERTY radiative transfer model. Each leaf was measured using a Perkins Elmer Lambda 19 laboratory spectrometer before having its chlorophyll extracted using a wet chemistry method (see chapter 4). The measured chlorophyll content and leaf water measurements were used as input variables for LIBERTY and the outputs were compared with measurements from the Perkins Elmer Lambda 19. Some variables (baseline, albino and the air-

void ratio) could not be measured. These variables were manipulated to provide the closest spectral match and the modal values noted. Other variables (lignin, cellulose and nitrogen) did not have an influence in the spectral red-edge wavelength region and were left at default values. Those independent variables used to constrain the simulations were chlorophyll content, leaf water content, leaf thickness and cell size. The simulated output (from LIBERTY) closely matched ($< 1\%$ reflectance difference in the wavelength range between 650 and 800nm) that spectra measured using the Lambda 19 and the few outliers were attributed to incomplete chlorophyll extraction.

7.1.4 Developing LIBSAIL

The Matlab version of LIBERTY was combined with a Matlab version of SAIL (rewritten by F.Baret, 1996). However, an error was identified by Philip Lewis (pers. comm. 2006) concerning Dawson's positioning of a bracket in his interpretation of the Benford equation (Benford 1946). In the course of correcting this, the iterative component of LIBERTY was replaced with the Newton-Raphson methodology (technique of successive approximations of real zeros) to achieve the same effect (Bostock and Chandler 1981). The effect of the error was found to be the greatest for conditions of low chlorophyll and high LAI; these are typical conditions for grassland vegetation. The erroneous code was corrected. The wide range of input variables available in LIBSAIL allowed the main influences on the red-edge to be explored. A flow diagram of LIBSAIL (figure 7.3) identifies the functional stages of the model. These will be further described in the next section.

7.2 Components of LIBSAIL

LIBERTY, SAIL and therefore LIBSAIL were composed from a series of functions that described average transmittance and scattering phase functions. These functions determine the total absorption potential of the vegetation, the scattering induced by
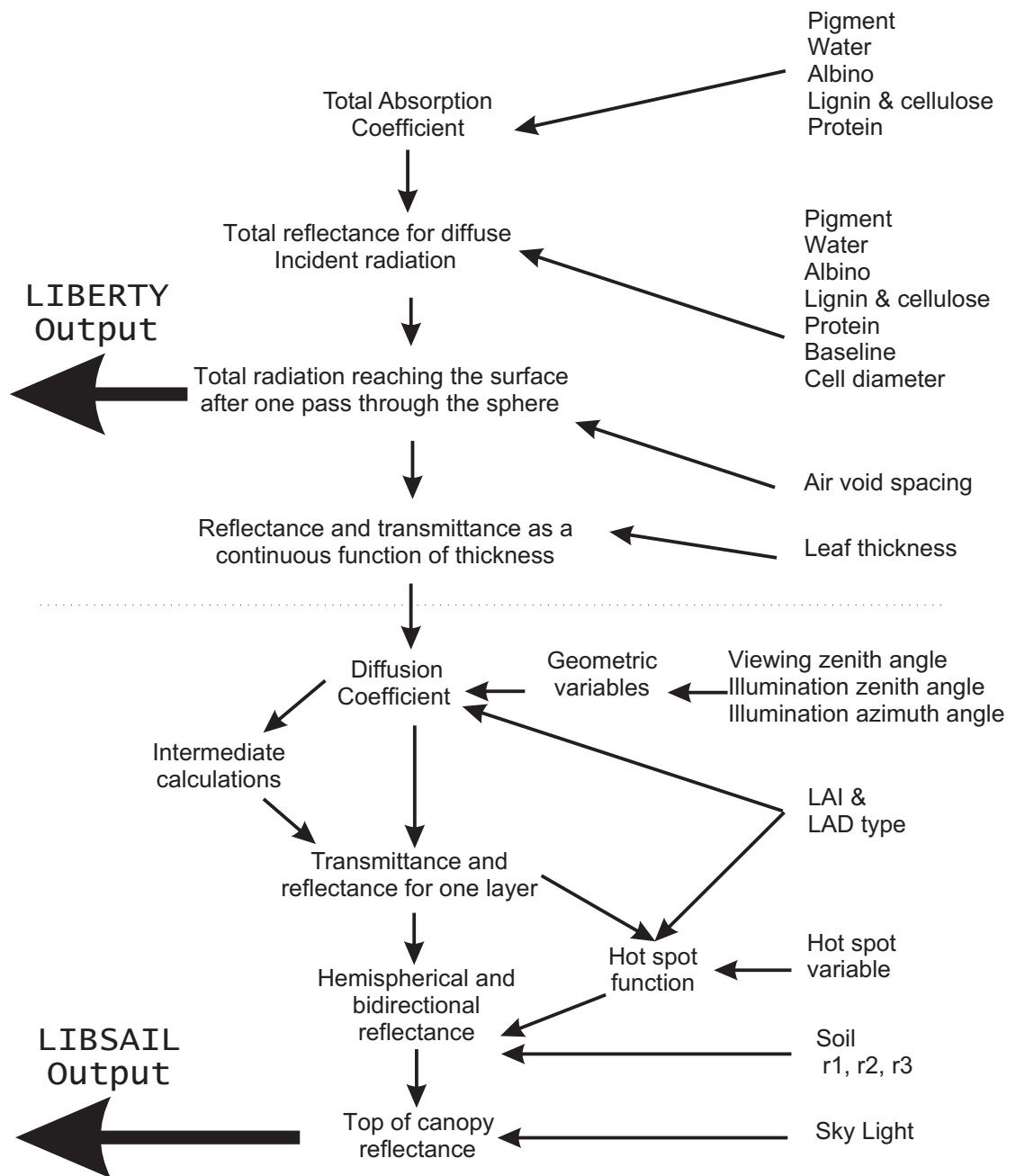
Figure 7.3: Flow diagram of the functional stages and data use within the LIBSAIL model

canopy geometry and structure as well as the diffuse and direct components of the incident radiation. In LIBERTY, the results from these calculations were used to establish the radiation reaching the surface for one pass through a sphere, ie. a leaf cell, and as a function of leaf thickness (defined by the number of layers of spheres).

The leaf scale reflectance (and transmittance) output from LIBERTY fed into SAIL and delivered a top of canopy reflectance value. Fluxes within the leaf were represented by simple two-dimensional radiation fluxes while fluxes within the canopy were represented by transmittance and bidirectional reflectance per layer (figure 7.4).

Both LIBERTY and SAIL used Allen *et al.*'s Plate model (1970) to describe a single cellular layer. The layers or plates were infinitely extended and scattering was assumed to conform to Lambert's cosine law. More fundamentally, the wavelength-dependent interactions of radiation with a medium or boundary between media were ultimately described by the Maxwell and wave equations. However, neither equation can be solved directly because the various vegetation elements are oriented and distributed in a complex manner (Goel 1988). Leaf internal cells were assumed to be spherical and surface scatter radiation was assumed to conform to Lambert's cosine law. For LIBERTY, Dawson used Melamed's theory (1963) of light interaction (with suspended powders) to model reflectance and transmittance given leaf thickness. This was achieved by the adaptation of Benford's (1946) theory to consider a diffusing medium. SAIL was derived from Suits's model (1972). In SAIL, the azimuth angles of leaf orientation were assumed to be random and the inclination was discretized into thirteen angle classes. In these investigations the leaf inclination angles were maintained as close to vertical (10-20°).

The reflectance coefficient of the surface was defined as the ratio of the reflectance of the surface to that of a Lambertian surface under the same conditions of illumination and measurement. Leaf reflectance was a function of optical absorption (in leaf cells) and internal and external scattering. Canopy reflectance was defined from general expressions for extinction and scattering coefficients. In both models, fluxes were represented in terms of upward and downward vectors. In both LIBERTY and the version

of SAIL used in this study, adjacent horizontal fluxes were assumed to be irrelevant or not included. Here follows a step-by-step overview of the stages by which data were processed within the combined model.

7.2.1 Light interaction with a single cell

Diffuse incident radiation was separated into externally incident radiation (m_e) and internally incident radiation (m_i). These were calculated from the reflectance coefficient as determined by the Fresnel equations assuming all surfaces approximated Lambertian conditions. The average value of m_e for light moving from a medium of low refractive index to one of higher refractive index was described by equation 7.1. The average value of m_i for light moving from a medium of high refractive index to one of lower refractive index is described by equation 7.2, where θ is the direction of incident radiation and θ_c is the critical angle where light becomes external to the cell sphere.

$$m_e = \int_0^{\pi/2} m(\theta) \, \sin\theta \, cos\theta \, d\theta \tag{7.1}$$

$$m_i = (1 - sin^2\theta_c) + 2 \int_0^{\theta_c} m(\theta) \, \sin\theta \, cos\theta \, d\theta \tag{7.2}$$

7.2.2 Total absorption coefficient

The total absorption coefficient, k, is assumed to be the sum of weighted infinite absorptions for the five environmental variables (figure 7.1: chlorophyll (chl), water ($H2O$), albino (alb), lignin and cellulose (lgc) and protein (pro), and a baseline absorption ($base$) that is assumed to be constant for all wavelengths (equation 7.3).

$$k = chl + H2O + alb + lgc + pro + base \tag{7.3}$$
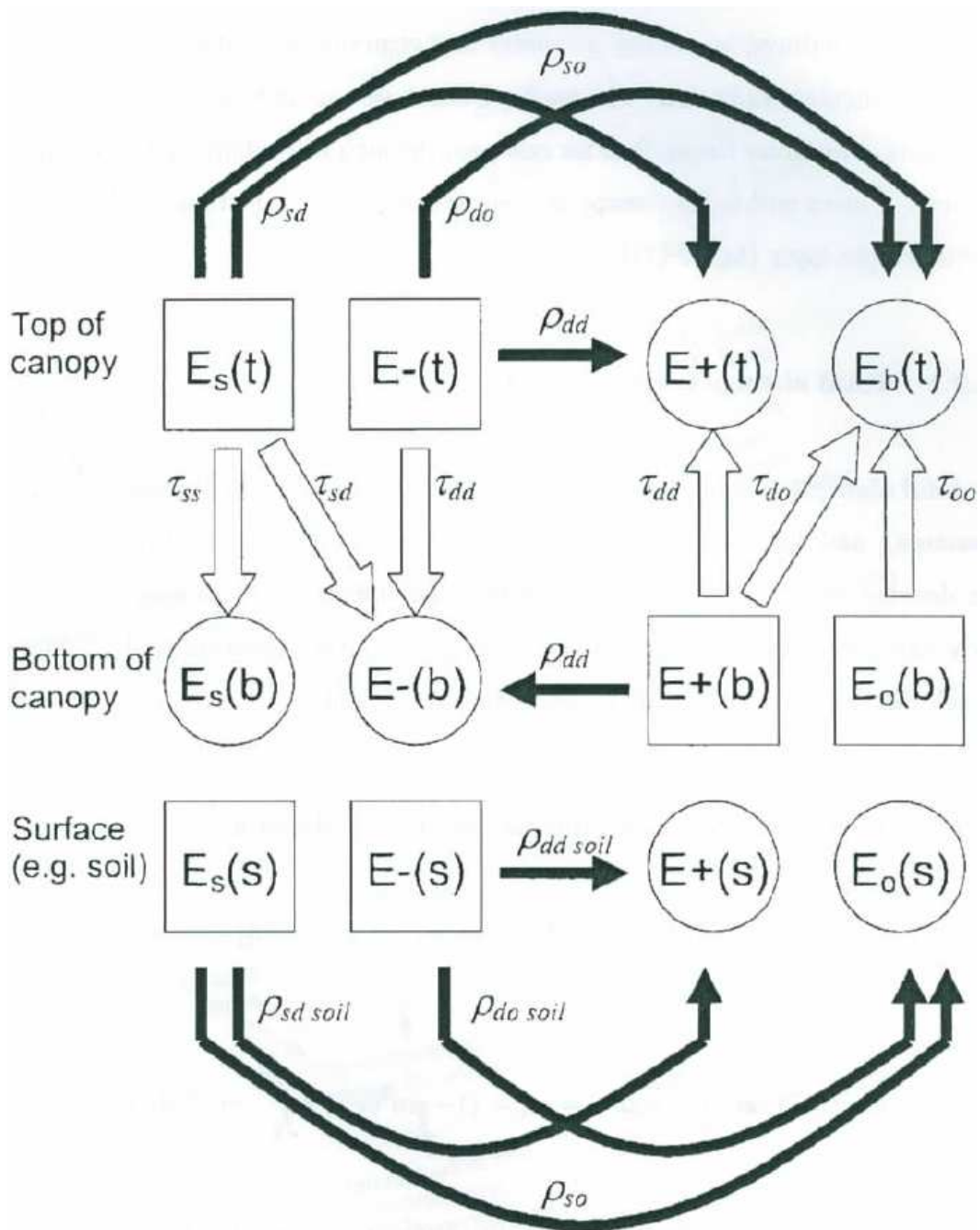
Figure 7.4: Transmittance and bidirectional reflectance (per layer). Adapted from (Verhoef 1984)

The total radiation reaching the surface after one pass through the sphere (M) was calculated according to equation 7.4, where d was the cell diameter, thus kd was the total absorption per cell.

$$M = \frac{2(1 - (kd + 1)e^{-kd})}{(kd)^2} \qquad (7.4)$$

7.2.3 Reflectance and transmittance as continuous functions of thickness

Dawson (1997) assumed that the surface had uniform scattering properties. Therefore, the total radiation after infinite interreflections (m_i) could be used to calculate the total transmitted component τ (equation 7.5). This accounted for the conditions for a single cell where the diffuse incident radiation (m_e) was evaluated for angles (of alpha) between 0 and $\pi/2$.

$$\tau = \frac{(1 - m_i)M}{(1 - m_i M)} \qquad (7.5)$$

7.2.4 Light emerging from a layer of cells

Additional assumptions were made to calculate the radiation that emerged from a layer of cells. One of these was that the structure was composed of horizontal layers. Within each layer a set of parameters, each a function of the air gap, described the movement of radiation. Probability of the total fraction of light was considered for light moving upward, adjacent or downward (x_u, x_w or x_v respectively). Dawson then discounted x_w and where kd was greater than 1 he assumed x_u to equal x_v. These assumptions facilitated the calculation of the probability coefficient, x, for the total fraction of light radiation emerging from the interior of a cell towards a layer above that is one cell diameter closer to the surface (equation 7.6).

$$x = \frac{x_u}{1 - (1 - 2x_u)\tau} \tag{7.6}$$

7.2.5 Light interaction with infinite layers of cells

By considering an infinite number of interreflections, Dawson derived a quadratic equation for the sum of all the radiative components that contributed to the total radiation emerging from the leaf R_∞. This enabled the calculation of an approximation of the root for R_∞ using the Newton-Raphson iterative technique (Bostock and Chandler 1981).

$$R_\infty = 2xm_e + \frac{x(1 - 2xm_e)\tau(1 - m_eR)}{(1 - m_eR) - (1 - x)(1 - m_e)\tau R} \tag{7.7}$$

Dawson *et al.* (1998) modified Melamed's theory for light interaction with suspended powders (Melamed 1963) using a procedure for a diffusing medium demonstrated by Benford (1946). This allowed the determination of reflectance, R, and transmittance, T, as continuous functions of thickness. The determination of R assumed that there was no underlying leaf material whose backscatter would contribute to the reflected radiation. The equation (equation 7.7) has been modified by the movement of a bracket (pers. comm. P. Lewis 2006).

7.2.6 Light interaction with a single layer of cells

To develop the model further Dawson considered light interaction within a single layer of cells. From equation 7.7 the reflectance for one layer of cells, R_1, (where there is no underlying leaf material to contribute backscatter) is defined as equation 7.8. Dawson then determines the transmittance for a single layer of cells (T_1) as equation 7.9.

$$R_1 = 2xm_e + x(1 - 2xm_e)\tau \tag{7.8}$$

$$T_1 = \sqrt{\frac{(R_\infty - R_1)(1 - R_\infty R_1)}{R_\infty}} \qquad (7.9)$$

7.2.7 Light interaction of a leaf of finite thickness

Benford calculated the total transmittance, T and reflectance R through a leaf of thickness $t = i + f$ (where i was the number of layers that constitute the thickness and f was the fractional part of the thickness). In LIBERTY, the values for transmittance through, and reflectance from a single unit layer are used to calculate transmittance and reflectance for a thickness of $1 + f$, such that

$$T_{1+f} = \frac{T_1^{1+f}[(1+T_1)^2 - R_1^2]^{1-f}}{[(1+T_1)^{2(1-f)} - R_1^2][1 + \frac{64}{3}f(f-0.5)(f-1)c]} \qquad (7.10)$$

$$R_{1+f} = \frac{1 + R_1^2 - T_1^2 - \sqrt{(1 + R_1^2 - T_1^2)^2 - 4R_1^2(1 - T_{1+f}^2)}}{2R_1} \qquad (7.11)$$

where c is a correction factor empirically derived by Benford and set to 0.001 in LIBERTY. Transmittance and reflection for the rest of the leaf is iterated for each of the $i - 1$ layers.

$$T_{i-1} = \sum_{a=1}^{i-1} \frac{T_a T_{1+f}}{1 - R_a T_{1+f}} \qquad (7.12)$$

$$R_{i-1} = \sum_{a=1}^{i-1} R_a + \frac{T_a^2 R_{1+f}}{1 - R_a R_{1+f}} \qquad (7.13)$$

Where $T_1 = 1$ and $R_1 = 0$ these values of transmittance and reflectance for the portions of leaf of thickness 1-f and i-1 are then used to calculate the transmittance and reflectance for a whole leaf.

$$T = \frac{T_{i-1}T_{1+f}}{1 - R_{1+f}R_{i-1}} \qquad (7.14)$$

$$R = R_{i-1} + \frac{T_{i-1}^2 R_{1+f}}{1 - R_{1+f}R_{i-1}} \qquad (7.15)$$

When $i = 0$, Dawson simplified Benford's solution by setting T_{i-1} to 1 and R_{i-1} to 0.

7.2.8 Light interaction with a canopy of leaves

SAIL is based on Suits's (1972) model. The Suits' model of light interaction in a canopy comprises four simultaneous linear differential equations (Duntley 1942) which describe irradiance with its associated extinction and scattering coefficients (Suits 1972).

$$\frac{dE_s}{dz} = kE_s \qquad (7.16)$$

$$\frac{dE_v}{dz} = -sE_s + aE_d - \sigma E_u \qquad (7.17)$$

$$\frac{dE_u}{dz} = s'E_s + \sigma E_v - aE_u \qquad (7.18)$$

$$\frac{dE_o}{dz} = wE_s + vE_v + uE_u - KE_o \qquad (7.19)$$

Where z represents the relative vertical thickness and E the flux vector,

- E_s = direct solar irradiance,

- E_v = diffuse downward irradiance (as assumed isotropic),

- E_u = diffuse upward irradiance (as assumed isotropic) and

- E_o = radiance in the observer's direction (L_o), multiplied by π. SAIL is built from these as described in the follows sections.

7.2.9 Total diffusion coefficient

Suits' model contains nine diffusion coefficients. Six are extinction coefficients (a, σ, k, K, s and s') and two scattering coefficients or phase function parameters (u and v). These coefficients are calculated using the reflectance and transmittance from a leaf from equations 7.14 and 7.15, respectively.

k is the extinction coefficient for direct incident radiance and K the extinction coefficient for specular radiance in the viewing direction. u is the scattering coefficient for upward diffuse flux (E_u) and v is the scattering coefficent for downward diffuse flux (E_v).

$$a = L' \left[\left(1 - \frac{R+T}{2} \right) + \left(\frac{R-T}{2} \right) \cos^2 \theta_L \right] \tag{7.20}$$

$$\sigma = L' - a(\theta_L) \tag{7.21}$$

$$k = \frac{2}{\pi} L' \left[\left(\beta_s - \frac{\pi}{2} \right) \cos \theta_L + \sin \beta_s \tan \theta_s \sin \theta_L \right] \tag{7.22}$$

$$K = \frac{2}{\pi} L' \left[\left(\beta_o - \frac{\pi}{2} \right) \cos \theta_L + \sin \beta_o \tan \theta_o \sin \theta_L \right] \tag{7.23}$$

$$s = \left(\frac{R+T}{2} \right) k(\theta_L) - \left(\frac{R-T}{2} \right) L' \cos^2 \theta_L \tag{7.24}$$

$$s' = \left(\frac{R+T}{2}\right) k(\theta_L) + \left(\frac{R-T}{2}\right) L' \, \cos^2 \theta_L \tag{7.25}$$

and the phase function parameters:

$$u = \left(\frac{R+T}{2}\right) K(\theta_L) - \left(\frac{R-T}{2}\right) L' \, \cos^2 \theta_L \tag{7.26}$$

$$v = \left(\frac{R+T}{2}\right) K(\theta_L) + \left(\frac{R-T}{2}\right) L' \, \cos^2 \theta_L \tag{7.27}$$

where L' = leaf area density, θ_s = solar zenith angle, θ_L = leaf inclination angle discreted into 13 classes. The total value for these coefficients over the 13 classes is calculated in SAIL as $\alpha = \sum_{j=1}^{13} \alpha(\theta_{Lj}, L'_j)$ where α is the expression for m_e and θ_{Lj} and L_j for the jth LAI and LAD, respectively.

Verhoef (1984) showed that a linear transform of the Suits's equations yields the intermediate constants given in the next section.

7.2.10   Intermediate calculations

$$m = \sqrt{a^2 - \sigma^2} \tag{7.28}$$

$$h_1 = \frac{a+m}{\sigma} \tag{7.29}$$

$$h_2 = \frac{a-m}{\sigma} = \frac{1}{h_1} \tag{7.30}$$

$$C_s = \frac{s'(k-a) - s\sigma}{k^2 - m^2} \tag{7.31}$$

$$C_o = \frac{v(K-a) - u\sigma}{K^2 - m^2} \tag{7.32}$$

$$D_s = \frac{-s(k+a) - s'\sigma}{K^2 - m^2} \tag{7.33}$$

$$D_o = \frac{-u(K+a) - v\sigma}{K^2 - m^2} \tag{7.34}$$

$$H_s = \frac{uC_s + vD_s}{K+k} \tag{7.35}$$

$$H_o = \frac{sC_o + s'D_o}{K+k} \tag{7.36}$$

7.2.11 Transmittance and bidirectional reflectance (per layer)

These intermediate constants are then used to derive transmittance τ and reflectance coefficients within the canopy as shown in equations 7.37 to 7.45. The subscripts refer to the source and destination of the flux where s refers to secular solar fluxes, d refers to diffuse fluxes and o refers to fluxes in the observer's direction.

$$\tau_{ss} = e^{-k} \tag{7.37}$$

$$\tau_{oo} = e^{-K} \tag{7.38}$$

$$\rho_{dd} = \frac{e^m - e^{-m}}{h_1 e^m - h_2 e^{-m}} \tag{7.39}$$

$$\tau_{dd} = \frac{h_1 - h_2}{h_1 e^m - h_2 e^{-m}} \tag{7.40}$$

$$\rho_{sd} = C_s(1 - \tau_{ss}\tau_{dd}) - D_s\rho_{dd} \tag{7.41}$$

$$\tau_{sd} = D_s(1 - \tau_{ss}\tau_{dd}) - C_s\tau_{ss}\rho_{dd} \tag{7.42}$$

$$\rho_{do} = C_o(1 - \tau_{oo}\tau_{dd}) - D_o\rho_{dd} \tag{7.43}$$

$$\tau_{do} = D_o(1 - \tau_{oo}\tau_{dd}) - C_o\tau_{oo}\rho_{dd} \tag{7.44}$$

$$\rho_{so} = H_o(1 - \tau_{ss}\tau_{oo}) - C_o\tau_{sd}\tau_{oo} - D_o\rho_{sd} \tag{7.45}$$

The light arriving at the observer is the sum of the path radiance and light reflected from and transmitted through the canopy to the observer. Verhoef (1984) expresses irradiance at the surface as equation 7.53, where the path radiance terms, L_{pa} and L_{pb}, are the atmospheric path radiance and background albedo contributions to path radiance, respectively, and the irradiance from an object comprises (where (r_{do}) is the object's directional reflectance for hemispherical incidence and was assumed to be equal (r_{sd}):

$$r_{do} = \frac{\rho_{do} + \tau_{dd}(\rho_{dd}\tau_{do} + r_{do}\tau_{oo})}{1 - r_{dd}\rho_{dd}} \tag{7.46}$$

The object's bidirectional reflectance factor (r_{so}) was calculated from the transmittance and reflectance cooefficients and fluxes and the the object's total transmittance ($T = \tau_{oo}$).

$$r_{so} = \rho_{so} + \tau_{ss}r_{so}\tau_{oo}(\tau_{ss}r_{sd} + \tau_{sd}r_{dd})\tau_{do} + \frac{+(\tau_{sd}\tau_{ss}r_{sd}\rho_{dd})r_{do}\tau_{oo}}{1 - r_{dd}\rho_{dd}} \tag{7.47}$$

Where (E_{upw}) is the upwelling radiation:

$$E_{upw} = \frac{(E_s^o cos\theta_s)(\tau_{ss}r_{sd} + \tau_{sd}r_{dd})}{1 - r_{dd}\rho_{dd}} \tag{7.48}$$

the atmospheric path radiance (L_{pa})

$$\pi L_{pa} = (E_s^o cos\theta_s)\rho_{so} \tag{7.49}$$

the background contribution to path radiance (L_{pb})

$$\pi L_{pb} = E_{upw}\tau_{do} \tag{7.50}$$

solar irradiance at ground level (E_{sun}),

$$E_{sun} = (E_s^o cos\tau_{ss}) \tag{7.51}$$

sky irradiance at ground level (E_{sky}),

$$E_{sky} = \frac{(E_s^o cos\theta_s)(\tau_{sd} + \tau_{ss}r_{sd}\rho_{dd})}{1 - r_{dd}\rho_{dd}} \tag{7.52}$$

solar irradiance on a plane perpendicular to the sunrays (E_s^o), solar zenith angle (θ_s)

$$\pi L_o(t) = \pi L_{pa} + \pi L_{pb} + E_{sun}r_{so}T + E_{sky}r_{do}T \tag{7.53}$$

7.3   Validation of LIBSAIL for grassland

The spectral data from transect 10 (Thorney Island, 18.05.99) were used, in conjunction with a measurement of the leaf water (moisture content) and average measurements of grass leaf thickness and cell sizes as inputs to LIBERTY. Measured chlorophyll content, LAI and leaf water content values were used as inputs to constrain LIBERTY and LIBSAIL. Other variables were input as constants, determined from the mean of laboratory measurements or the modal values derived from the closest match input variables from previous simulations. Leaf thickness and cell size input values (1.8 and 15.7μm respectively) fell at (or slightly below) the lower range of LIBERTY's accepted input values and represented grass rather than other grassland vegetation. The number and range of inputs increased with the linking of LIBERTY and SAIL. The validation process similarly had to include more variables to model the increased complexity and test the suitability of LIBERTY for the simulation of grass leaves and LIBSAIL for the simulation of a grassland canopy.

7.3.1   Modelling grassland with LIBSAIL

Validation of LIBSAIL as a tool for the simulation of grassland reflectance required the comparison of field measured reflectance and vegetation input values. The same 25 leaf samples used to validate LIBERTY were also used to validate LIBSAIL. The transfer from the leaf scale to a grassland canopy introduced additional input variables, e.g. LAI and LAD. Vegetation and reflectance measurements were from coincident locations. In this instance, the spectral measurements were collected in the field (Thorney Island, transect 10) using a GER3700 at the same location and within one hour of sampling. Spectral comparisons showed a close match with a slight tendency to underestimate red-edge reflectance (figures 7.5 and 7.6) but had the closest match when chlorophyll content and LAI were high. 24% of simulations had a very close match; these accounted for locations with a chlorophyll content of greater than 250 mg.m^{-2} and a LAI greater than 3.2. 16% had a fairly close match, these accounted for locations

with a chlorophyll content of between 150 and 250 mg.m^{-2} and a LAI between 2.5 and 3.2. 48% had an approximate match, these accounted for locations with a chlorophyll content of between 100 and 150 mg.m^{-2} and a LAI between 1.9 and 2.4. 12% had a poor match, these accounted for locations with a chlorophyll content of less than 90 mg.m^{-2} and a LAI of less than 1.9. It was noted that the chlorophyll content range where LIBSAIL performed least well (less than 100 mg.m^{-2}) was uncommon for the study site with different levels of soil contamination (12 out of 114). When comparing spectral vegetation indices, LIBSAIL underestimated the REP (figure 7.7). REP were not normally distributed (as per the Kolmogarov-Smirnov normality test) and were not transformed to a normal distribution (biomodal). Therefore, a Spearmans Rank correlation between LIBSAIL modelled REP and REP calculated from field data was tested and found to be statistically significant (Clevers *et al.* 2001, r=0.54, P<0.001, n=25). Based on these results, LIBSAIL was adopted for the simulation of grassland spectra.

7.4 A brief critique of LIBSAIL

LIBSAIL is a combination of two radiative transfer models specifically selected to simulate *Poa* species. While LIBERTY allowed the inclusion of variables to represent the cell structure of *Poa* species, SAIL enabled the investigation of the effects of LAI. Various assumptions, were embedded in the theories from which LIBSAIL was constructed. Some were general to the use of turbid medium, radiative transfer models while others related to the specific solutions used to solve the radiative transfer equations. Some calculations were duplicated in LIBERTY and SAIL but addressed in different ways. This is not a problem in itself; however, because the solutions derived in each model required specific assumptions the final output is a generalisation that discounts much of the variation present in a field environment. In addition to these assumptions, the accuracy of LIBSAIL was limited by the manner by which data were input. For example, the 5nm resolution of absorption spectra limited the output resolution to 5nm. Additionally, because some of the input variables (especially the arbitrarily scaled vari-

(a) Reflectance spectra

(b) Reflectance spectra

(c) First derivative spectra

(d) First derivative spectra
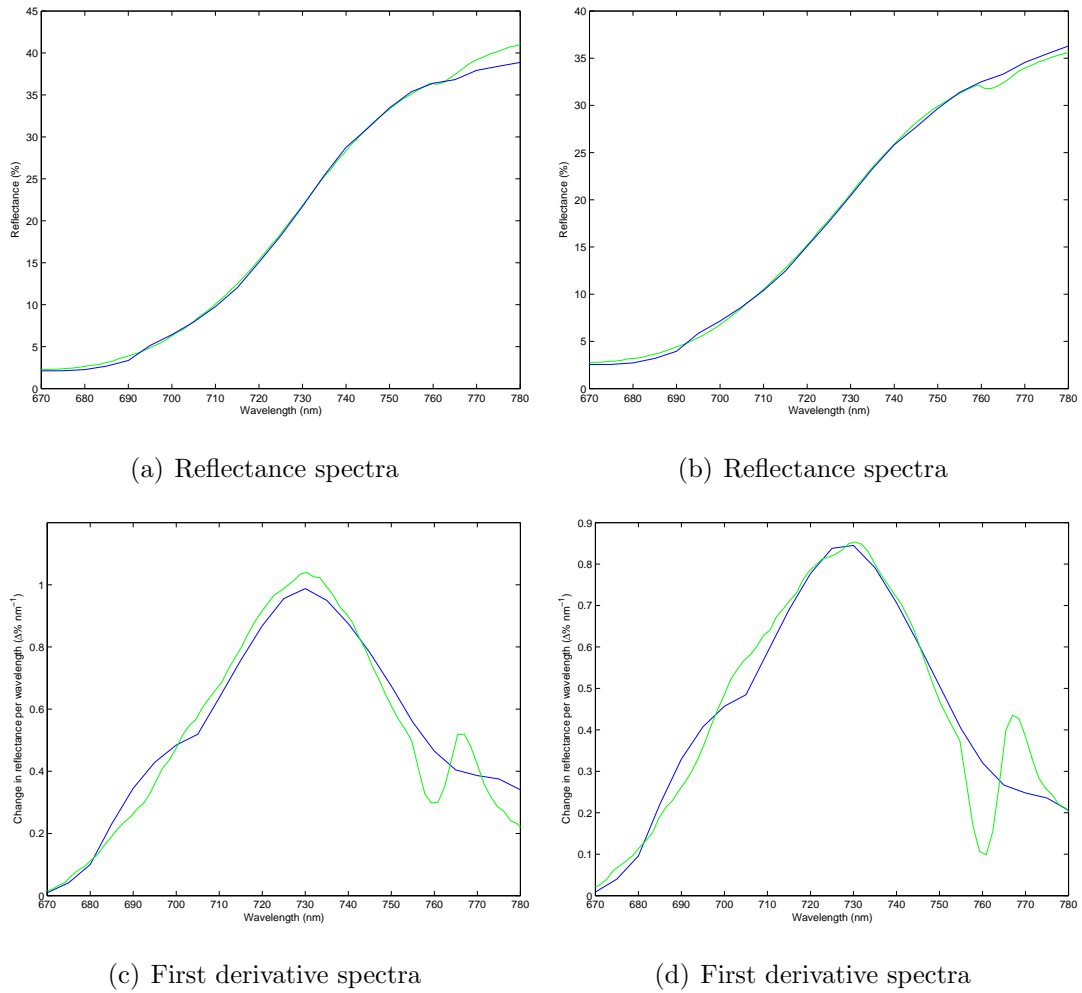
Figure 7.5: A comparison of LIBSAIL simulated grassland spectra compared with spectra collected from Thorney Island (transect 10) using a GER3700 (green). Spectra a and c (blue) were modelled with 330 mg.m^{-2} chlorophyll content, 3.5 LAI and 673 mg.m^{-2} leaf water content. Spectra b and d (blue) were modelled with 237 mg.m^{-2} chlorophyll content, 3.2 LAI and 378 mg.m^{-2} leaf water content.

(a) Reflectance spectra

(b) Reflectance spectra

(c) First derivative spectra

(d) First derivative spectra
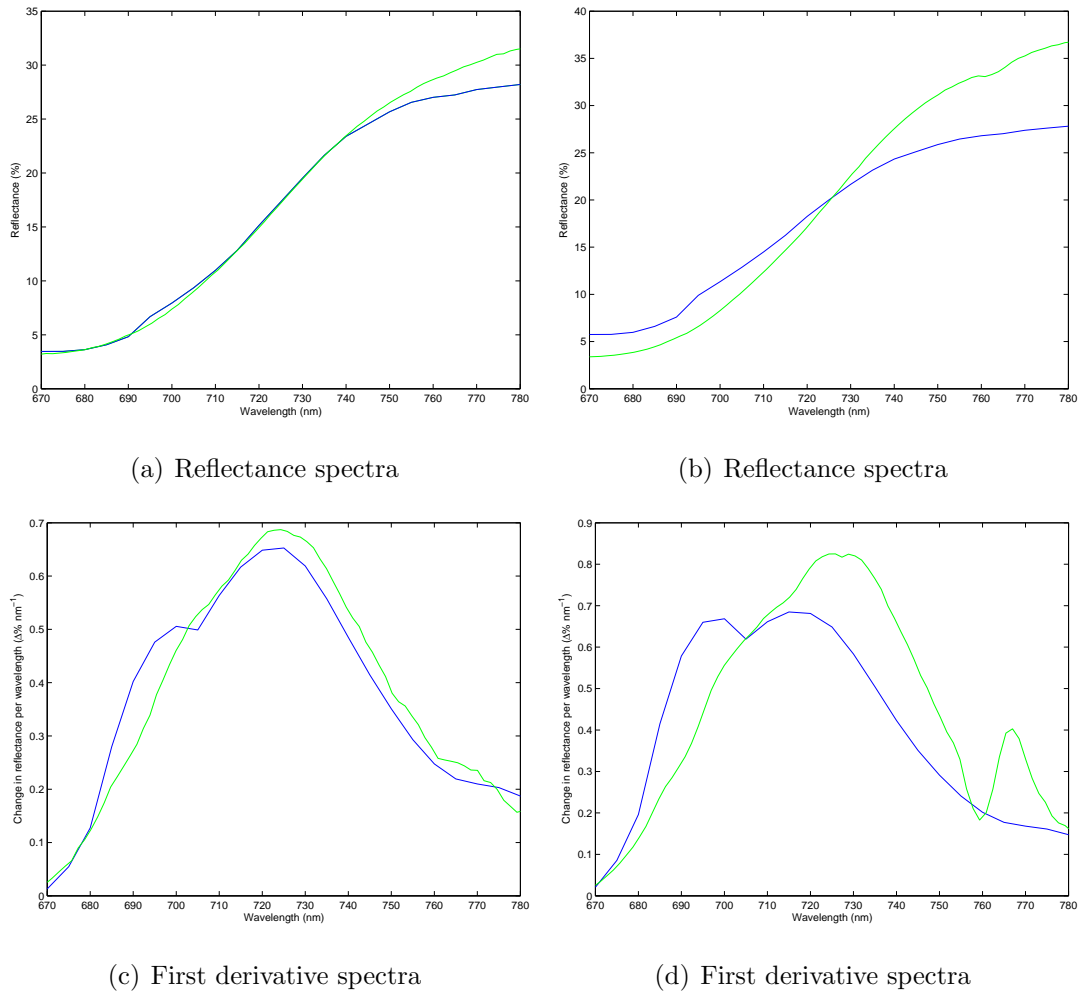
Figure 7.6: A comparison of LIBSAIL simulated grassland spectra compared with spectra collected from Thorney Island (transect 10) using a GER3700 (green). Spectra a and c (blue) were modelled with 133 mg.m^{-2} chlorophyll content, 2.4 LAI and 310 mg.m^{-2} leaf water content. Spectra b and d (blue) were modelled with 81 mg.m^{-2} chlorophyll content, 1.8 LAI and 315 mg.m^{-2} leaf water content.
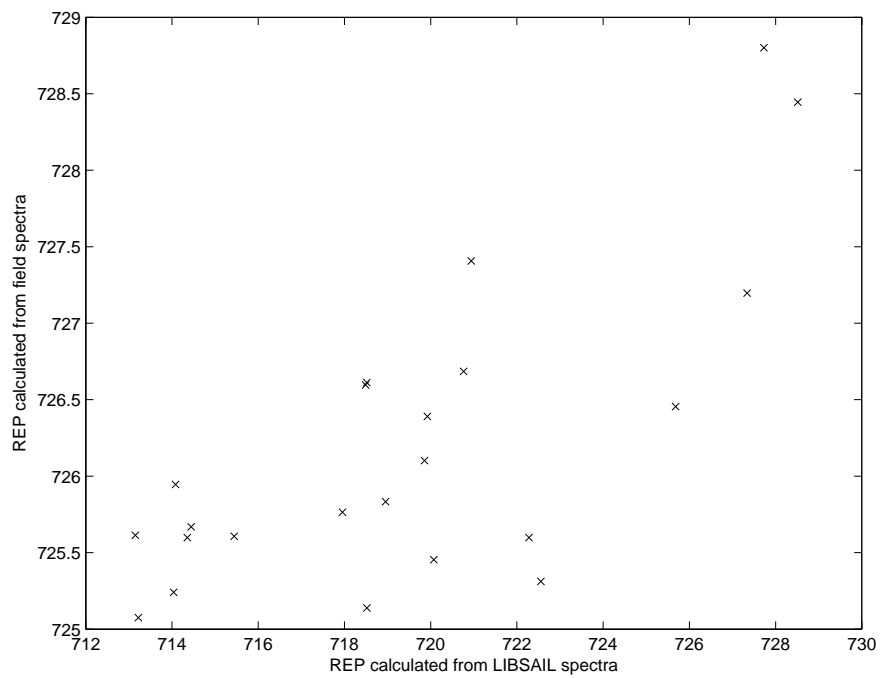
(a) Linear interpolation method (Clevers *et al.* 2001)
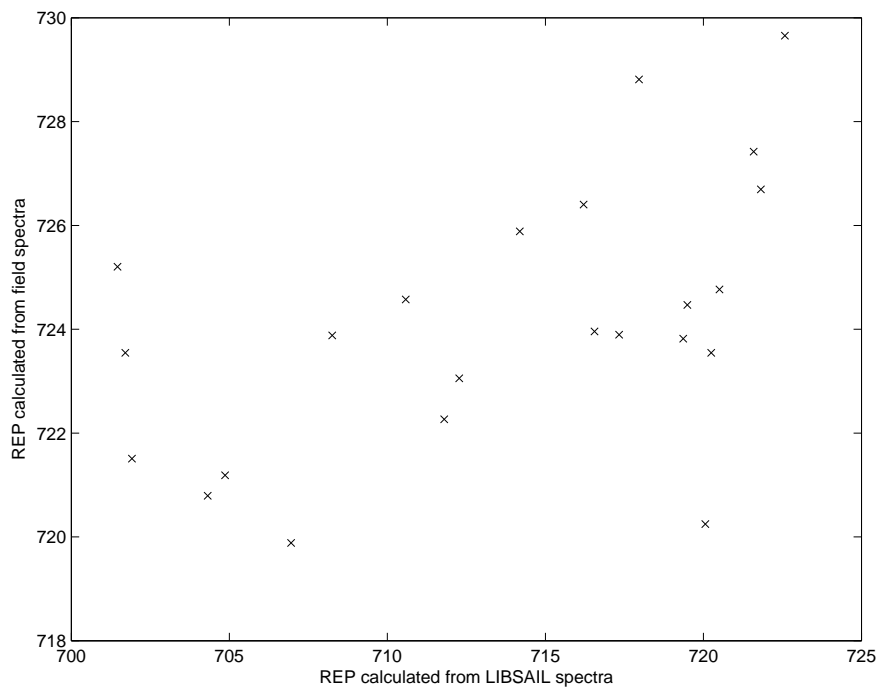
(b) Linear extrapolation method (Cho & Skidmore 2007)

Figure 7.7: A comparison of REP calculated from LIBSAIL simulated spectra and and field spectra from Thorney Island (transect 10) colleced using a GER3700, n=25. (Clevers *et al.* 2001; r=0.54, P<0.001. Cho 2004; r=0.25, P<0.001).

ables) were difficult to measure they had to be estimated from modal values derived from 'best fit' matches from previous simulations. By necessity most of the scalar and all vector inputs were averages or selected extremes. LIBSAIL also has some deficiencies. It did not account for the effects of polarisation, frequency shifting interactions or emission processes within the canopy (e.g., fluorescence). While most of these effects may not have had a significant contribution to the modelling of the red-edge their absence weakened the model. The contribution of fluorescence may have been included in the absorption spectral inputs but there was no specific component to account for this process. The accuracy level of a model output is no higher that that of the model input parameters (Verhoef 1985) therefore, for LIBSAIL the full variation present in a field canopy was never fully represented. Nevertheless, the full representation of the main input variables (as indicated by published literature and field results) allowed LIBSAIL to be a functioning tool for the exploration of a simulated grassland environment.

7.5   Discussion

The exact combination of variables that most accurately represented the true field conditions were not resolvable. This was because only some of the values could be (and were) determined from field measurements, others could not be measured or had arbitary or relative input values. The use of input values to model uniform condition at the leaf scale fell within narrow margins of measured variance across a leaf. However, when the leaf meaurements were extrapolated to describe the whole canopy the margin for error greatly increased. Grassland has widely been described and measured as species-diverse, even the use of accurate mean inputs values to model a spectrum would not capture the variation within the canopy as measured in the field. The presence of non-*Poa* species in the FOV meant that the input values were unlikely to be representative of the grassland canopy and would not include any of the variation inherent in real grassland conditions.

7.5.1   Under-estimation of spectral vegetation indices

Spectral vegetation indices calculated from LIBSAIL-simulated data were lower that those calculated from field spectra. Chlorophyll content was measured from the un-contaminated grassland (with no history of soil contamination), where the validation excercise was conducted, by the use of chlorophyll extraction by wet chemistry using acetone. This process is prone to a slight under-extraction of chlorophyll. Therefore, the input values were likely to be under-representations of those present in the field. The LIBSAIL spectra simulated from these data will, therefore, have been modelled for conditions with a lower level of chlorophyll content than in the field. As the spectral vegetation indices are strongly correlated with chlorophyll content, low chlorophyll resulted in lower values for the indices.

7.6   Conclusion

The LIBSAIL model combined LIBERTY, a leaf scale radiative transfer model and SAIL, a canopy scale radiative transfer model, for the simulation of grassland conditions. LIBERTY was modified for the simulation of grass spectra and a validation with laboratory derived spectra produced close spectral matches between them. LIBERTY was coupled with SAIL and validated for grassland conditions where there was no evidence of soil contamination. A close match was found between field and LIBSAIL-simulated grassland spectra and the correlation between REP (Clevers *et al.* 2001) calculated from paired data was statistically significant (r=0.54, P<0.001, n=25). LIBSAIL was, therefore, found to be suitable for the modelling of a grassland environment where chlorophyll concentrations were greater than 100 mg.m^{-2} and a LAI of greater than 2. This accounted for most of the studied grassland. The general match of spectra and spectral vegetation indices showed LIBSAIL to be capable of simulating grassland spectra. The next stage was to apply this model to a grassland environment with different levels of soil contamination.

Chapter 8

Investigating the modelled red-edge using LIBSAIL

8.1   Introduction

The range of variables that can be explored simultaneously by modelling exceeds those that may be measured in a field or laboratory study. This is because the acquisition of simultaneous measurements has logistical limitations of time, scale and practicality, especially when some of the measurements are destructive. In the previous chapter (chapter 7), LIBSAIL was validated for the modelling of grassland vegetation that had no history of soil contamination. Within this chapter LIBSAIL will be used as a tool to explore the red-edge in a soil contaminated grassland environment. In particular, it will be used to explore canopy interactions within a stressed multi-storeyed grassland canopy. Results in chapters 5 and 6 identified a weak correlation between chlorophyll and reflectance. However, this correlation was weaker than that found between soil hydrocarbon levels and reflectance. It was evident that before remote sensing techniques could reliably be used to detect and map soil contamination some of the vegetation interactions that determined the measured spectral signal needed to be better understood. Therefore, an investigation into the grassland canopy that allowed a degree

of control impossible in field condition was conducted. Measured vegetation variables were used to constrain LIBSAIL. Where field spectra were poorly matched with LIBSAIL simulated spectra a second canopy components (an under-storey) were simulated and linearly mixed. These results were also assessed in respect to testing the hypothesis that:

1. (H_1): *stress effects in vegetation (attributed to the effects of soil contaminants) can be detected using the position and shape of the red-edge of reflected radiation*

8.2 Modelling soil contaminated grassland with LIBSAIL

LIBSAIL-modelled spectra were compared with those measured from grassland with different levels of soil contamination. Chlorophyll content (via SPAD values), LAI, leaf water content and reflectance were measured from coincident field locations while cell size and leaf thickness were input as mean values for grass. These variables were used to constrain LIBSAIL. The closest matches ($< 1\%$ reflectance difference in the wavelength range between 650 and 800nm) were found with data collected and simulated from areas with high and low levels of soil contamination (figure 8.1). Other paired comparisons between collected and LIBSAIL modelled were less impressive. Field collected and simulated data were also compared using the most successful REPs identified in the results reported in chapter 6 and selected narrow-band, ratio-based vegetation indices. These comparisons are also reported in this section.

8.2.1 Unconstrained input variables

The 114 data sets used to simulate field spectra using LIBSAIL included key input variables to constrain the simulation but did not inculde all the input variables. Those varables not included were systematically tested across their potential range. The
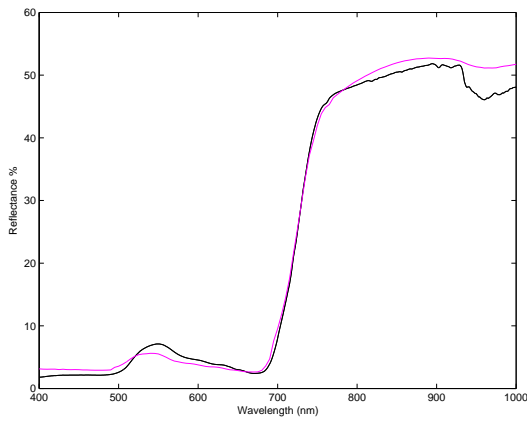
(a) Reflectance spectrum (grid 1; NI11))
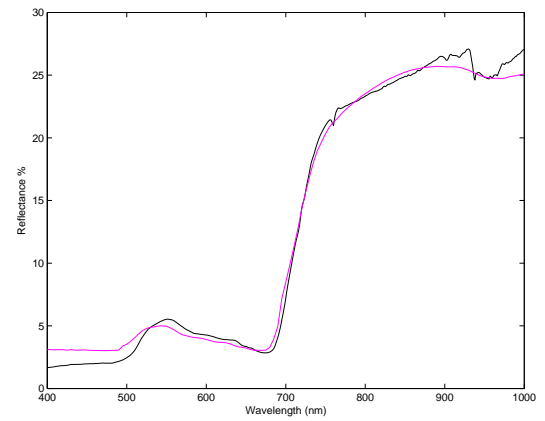
(b) Reflectance spectrum (grid 3; HSE12))
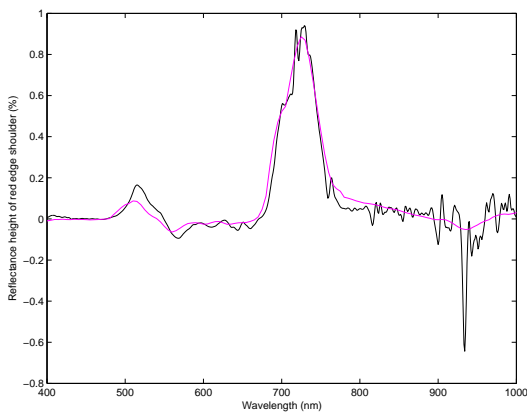
(c) First derivative reflectance spectrum (grid 1; NI11)
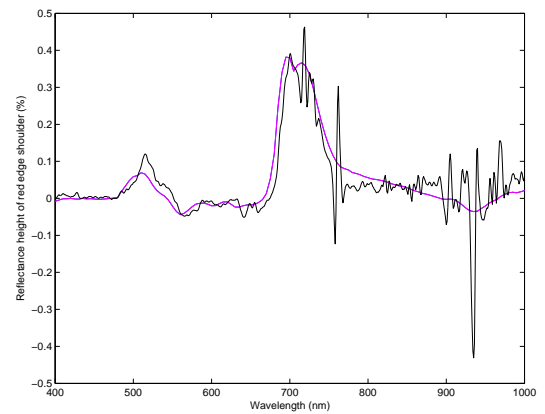
(d) First derivative reflectance spectrum (grid 3; HSE12)

Figure 8.1: Comparison of LIBSAIL modelled spectra with a field measured spectra. Field spectra are denoted in black, LIBSAIL simulated spectra in red and blue.

Table 8.1: Vegetation variables derived from modal, maximum and minimum values during the validation process of LIBSAIL for grassland (* indicates the modal value)

LAD	air void ratio	baseline	Albino
10*	0.004	0.0004*	0
20	0.006	0.001	0.5*
30	0.008	0.0016	1
40	0.010*	0.0022	2
50	0.012	0.0028	3
60	0.014	0.0034	4
70		0.004	
80			

modal values of those input values that were defined to acquire a 'best fit' are presented in table 8.1, modal values are marked with a star. These variables indicated an erectophile canopy with low baseline absorption, little secondary absorption and large voids within the leaf structure; they are consistent with grassland canopy as reported in the literature (chapter 3). However, some other spectra were poorly simulated. In 57 LIBSAIL simulations (50%) a concave red-edge relectance curve was modelled. This differed from the linear or convex red-edge reflectance observed in the associated field spectrum. In some of these a 'cross-over' mismatch between modelled and field spectra prevented a close match while in 8 LIBSAIL simulations (9%) the closest matched spectrum was only derived with a LAD that indicated a canopy contrary to the erectophile canopy associated with grasses.

8.2.2   First derivative of the reflectance spectra

The first derivative of spectra produced by LIBSAIL simulated the short and long
wavelength features observed in the first derivative of grassland reflectance spectra.
However the middle peak (observed in field spectra) was absent or merged with the
longer wavelength peak (figure 8.2). Despite this, the three different spectral profiles
(or patterns) in first derivative spectra, identified in chapter 5, were simulated using
LIBSAIL. In figure 8.2 data from grid 3 represented the lower wavelength spectral
profile and data from grid 1 represented the longer wavelength spectral profile.

8.2.3   Convexity of the red-edge edge

Approximately half (58 of 114) of the LIBSAIL modelled spectra were more concave
in red-edge wavelengths than field spectra. The effect of greater convexity on the first
derivative spectrum was to displace the spectral profile to longer wavelengths (fig-
ures 8.3 & 8.4). The most concave LIBSAIL modelled spectra had high chlorophyll
contents though the relationship between magnitude of convexity and chlorophyll con-
tent was not statistically significant.

8.2.4   The red-edge position

Compared with field data, spectral vegetation indices calculated from LIBSAIL spectra
tended to have higher values and had a wider range of values (for REP 30 nm versus
10 nm). Additionally, the first derivative maximum REP calculated from LIBSAIL
spectra did not simulate the two distinct clusters of first derivative wavelength posi-
tion found in field data. This may have been due to an over-estimation of chlorophyll
content, the poor relationship between chlorophyll content and LAI in the field data
and the variety of non-*Poa* species among grassland vegetation. Table 8.2 shows scat-
terplots for a linear interpolated REP (Clevers *et al.* 2001) and a linear extrapolation
method (Cho 2004). LIBSAIL REPs were correlated with field measured REPs but
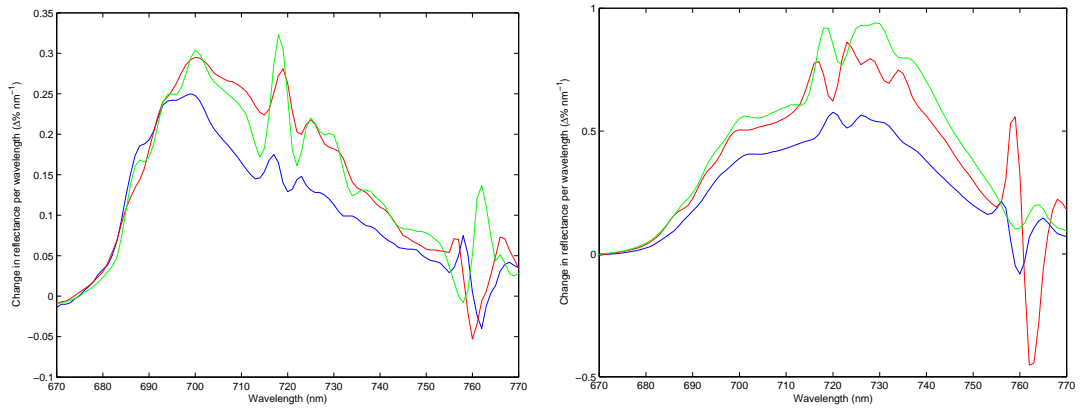
(a) Field data of from grid 3 (HSE2, HSE5 & HSE15)

(b) Field spectra from grid 1 (NI11, NI20 & NI40)
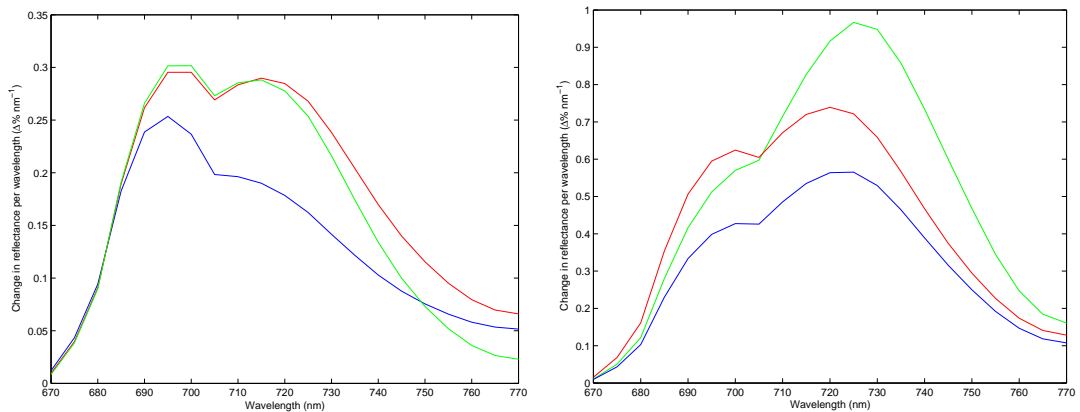
(c) LIBSAIL simulations using grid 3 data (HSE2, HSE5 & HSE15)

(d) LIBSAIL simulations using grid 1 data (NI11, NI20 & NI40)

Figure 8.2: First derivative of reflectance spectra comparing LIBSAIL data with field data. HSE2 and NI11 are in green, HSE5 and NI40 are in red and HSE15 and NI20 are in blue.

(a) Reflectance spectrum

(b) Reflectance spectrum

(c) First derivative spectra

(d) First derivative spectra
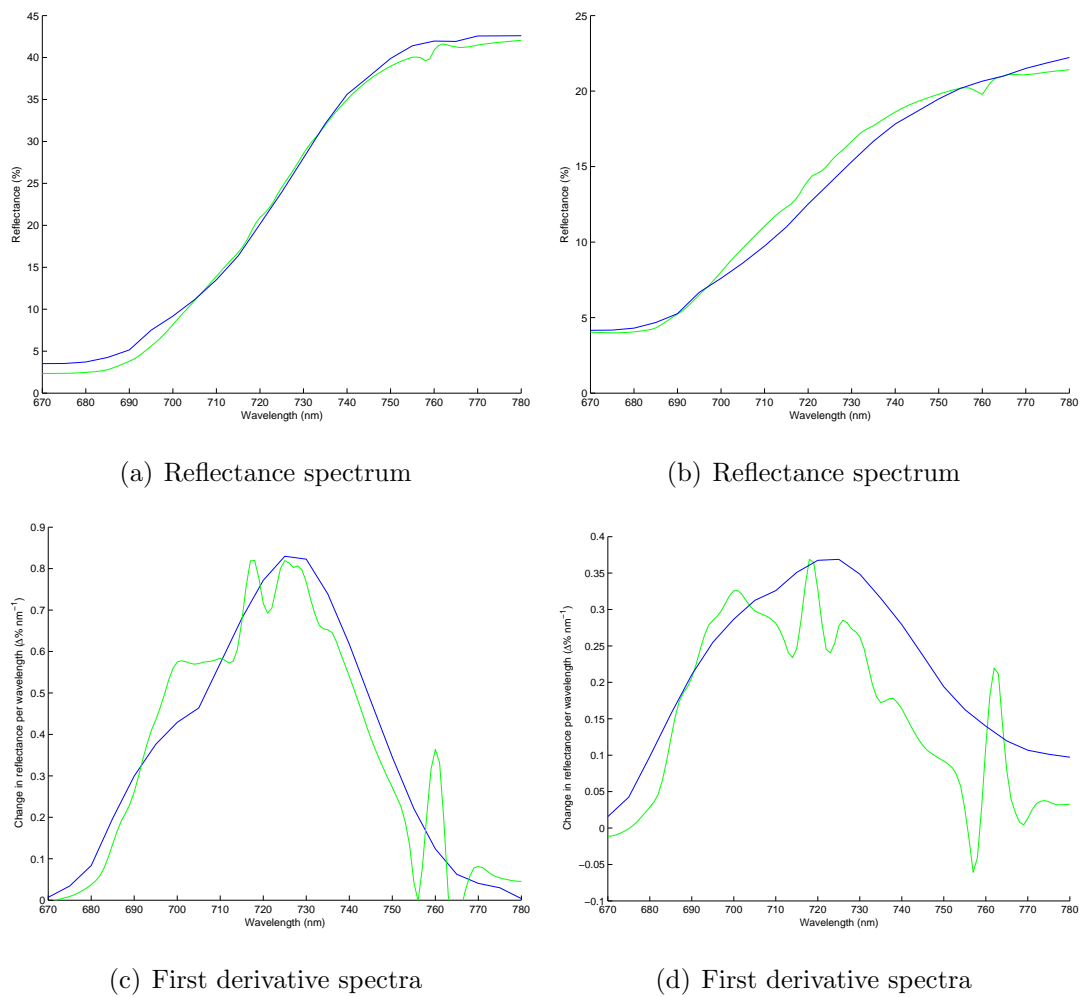
Figure 8.3: Differences in red-edge convexity on first derivative spectra (comparing LIBSAIL (blue) and field spectra (green))

(a) Reflectance spectrum

(b) Reflectance spectrum

(c) First derivative spectra

(d) First derivative spectra
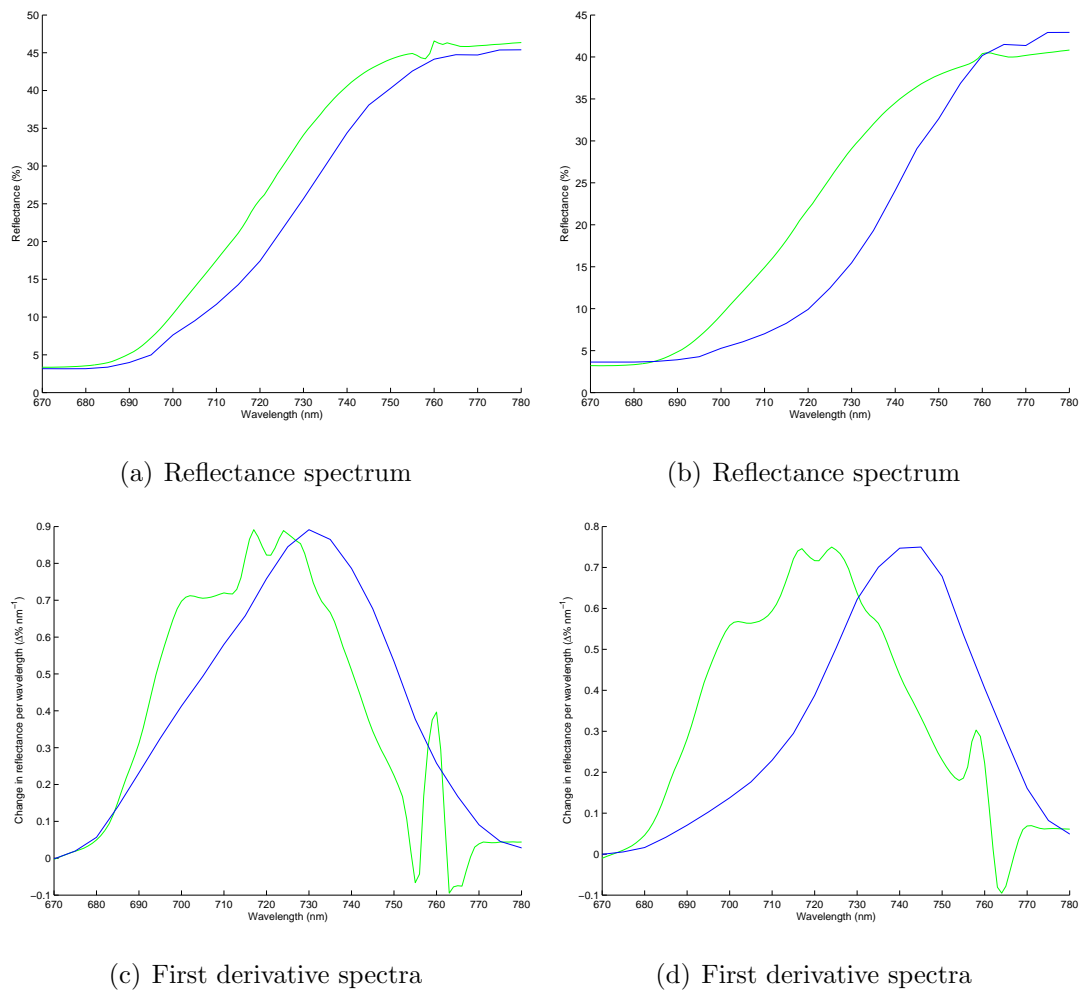
Figure 8.4: Differences in red-edge convexity on first derivative spectra (comparing LIBSAIL (blue) and field spectra (green))

Table 8.2: A validation of REPs calculated from LIBSAIL simulated data for a grassland with different levels of soil contamination (grids 1, 2 & 3). Pearson's product moment correlations and regression models, n=114.

Index	Author	r value	R^2 value	P value<
REP (Optimised linear interpolation method)	This thesis	0.42	0.18	0.001
REP (Linear interpolation method)	Danson and Plummer 1995	0.44	0.20	0.001
REP (Linear interpolation method)	Clevers *et al.* 2001	0.44	0.20	0.001
REP (Linear interpolation method)	Guyot and Baret 1988	0.44	0.20	0.001
REP (Linear extrapolation method)	Cho 2004	0.29	0.09	0.01
REP (IG method 1)	Miller *et al.* 1990	NS	NS	NS
REP (IG method 2)	Miller *et al.* 1990	0.22	0.22	0.05
REP (first drivative maximum)	Savitsky and Golay 1964	0.44	-	0.0001

the relationship was weaker than for uncontaminated grassland (chapter 7). From the paired data (field reflectance and vegetation) those areas where a percentage of *Poa* species of 90% or greater were selected. However, when the vegetation data were used to run LIBSAIL the correlations were no better than than the full data set.
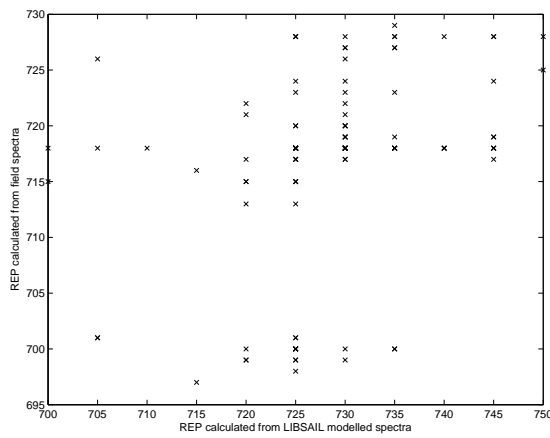
(a) First derivative maximum (Savitsky-Golay 1964)
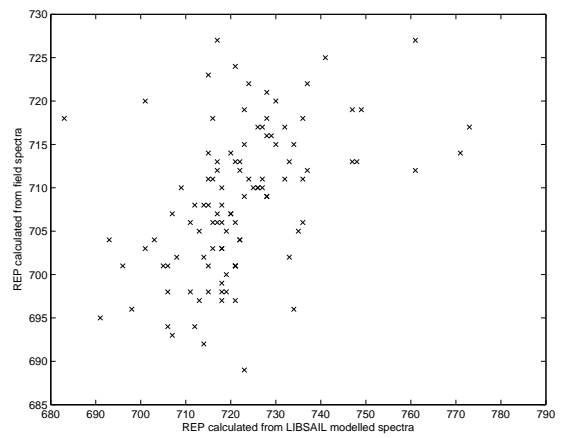
(b) Linear extrapolation method (Cho & Skidmore 2006)
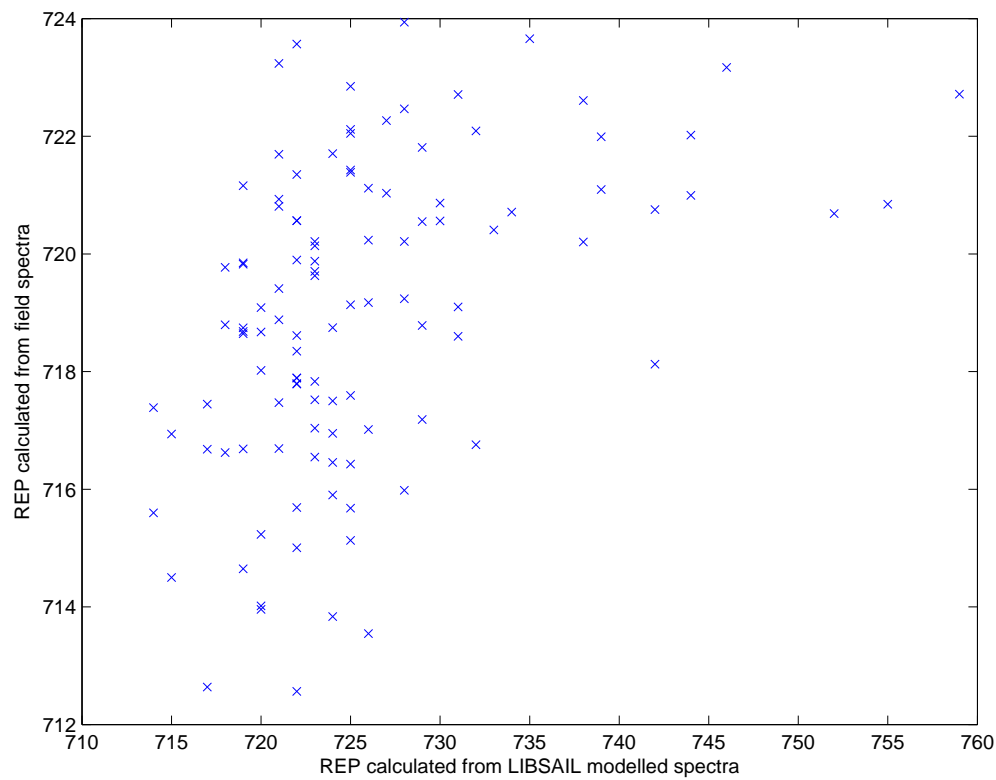
(c) Linear interpolation method (Clevers *et al.* 2002)

Figure 8.5: Comparison of REP calculated from LIBSAIL modelled and field meausred spectra

8.3   Sensitivity of LIBSAIL

This investigation identified those variables that influenced the red-edge and determined (and defined) the wavelength of specific features in the first derivative of the red edge. For each section of the analysis, the effects on the first derivative red-edge were considered by spectral comparison and by their effect on two methods of calculating the REP (the first derivative maximum and Clevers' interpretation of the linear interpolation method). Within LIBSAIL, influences on the red-edge were caused by wavelength-dependent absorption against a background of wavelength independent absorption and scattering. The magnitude of absorption and scattering was also affected. Chlorophyll, albino, water and baseline were used to derive the 'total absorption coefficient' by their multiplication with cell size. The smaller the cell size the less absorption was applied to the simulated spectrum. Similarly, the air-void ratio was the primary variable that determined scattering, the smaller the air-void the more scattering. Both absorption and scattering were influenced by leaf thickness, leaf area (LAI) and the leaf angle distribution (LAD). As these variables were not wavelength-dependent they all influence the NIR and therefore the reflectance of the NIR shoulder, though not the wavelength at which it occurred.

To explore the influence of different input values, systematic changes were applied to one variable at a time. Other variables were kept constant as per the mean or modal average derived from measurements or previous simulations (figure 8.1) or default values were used (table 8.3). Those variables where field measurements had been collected, were tested between minimum, mean and the interquartile range. The range was drawn from field and laboratory measurements of contaminated and uncontaminated grasslands (tables 8.4 & 8.5). However, because cell size and leaf thickness were tested at the low end of the input range, these variables were explored to the maximum measurements found from a range of vegetation. The effects of unmeasured variables were explored by running LIBSAIL with a range of values for these variables. These values were set at regular intervals between maximum and minimum values identified by those simulations in previous investigations that resulted in the closest match between

LIBSAIL-simulated and field-measured spectra. When not being investigated, these variables were set to their modal value. In addition to spectral comparisons, LIBSAIL and field spectra were compared using spectral vegetation indices. Of those tested for grassland in chapters 5 & 6 the REP was particularly effective. Throughout this chapter the main REPs used were derived using a linear interpolation method (Clevers *et al.* 2002) and the maximum first derivative of reflectance (Savitsky and Golay 1964). For the evaluation of REP, chlorophyll content was used as a standard x-axis variable.

8.3.1 The effect of absorption on the red-edge

Logically, those variables that influenced the red-edge must be those that had an influence in the wavelength range of the red-edge. In LIBSAIL the only input spectra (vectors) that directly influenced the red-edge wavelength range were chlorophyll content, albino, water and baseline. Of these, baseline was not wavelength dependent, water only had an minor effect on the red-edge shoulder if chlorophyll was low and albino high. In the absence of chlorophyll or albino there was no red-edge.

8.3.1.1 Chlorophyll content

The extinction gradient for chlorophyll was steeper than that for albino. Therefore small differences in chlorophyll content had a greater effect on the red-edge than differences in albino. Higher levels of chlorophyll content caused a deepening and widening of the chlorophyll absorption, extending its influence to longer wavelengths (figure 8.6). Under conditions of very high chlorophyll content this extension caused a subtle change in the gradient of the red-edge. The effect of higher levels of chlorophyll content on the first derivative spectrum was to reduce the level of reflectance of a feature approximately centred at 690nm, and to increase the prominance of a second peak at 720nm. At higher levels of chlorophyll content this longer wavelength peak was shifted to longer wavelengths.

Table 8.3: Input values for LIBSAIL. Values in italics were derived from average field and laboratory measurments for contaminated grassland. Input values derived from average field and laboratory measurements for contaminated grassland (NU = no/relative units)

Input variable	Value	Units
Chlorophyll content	937	mg m^{-2}
Water content	80	g m^{-2}
Leaf area index	2.5	
Cell size	15.7	m^{-6}
Leaf thickness	1.8	NU
Leaf angular distribution	10	
Albino	0.5	NU
Baseline	0.0004	NU
Air void value	0.01	NU
		NU
Lignin & cellulose	40	g.m^{-2}
Nitrogen	1	g.m^{-2}
Hotspot parameter	0.001	NU
Viewing zenith angle	0	
Solar zenith angle	0	
Solar azimith angle	0	
Difuse skylight franction	0.1	
Bidirectional reflectance distribution parameters (3)	0.2	
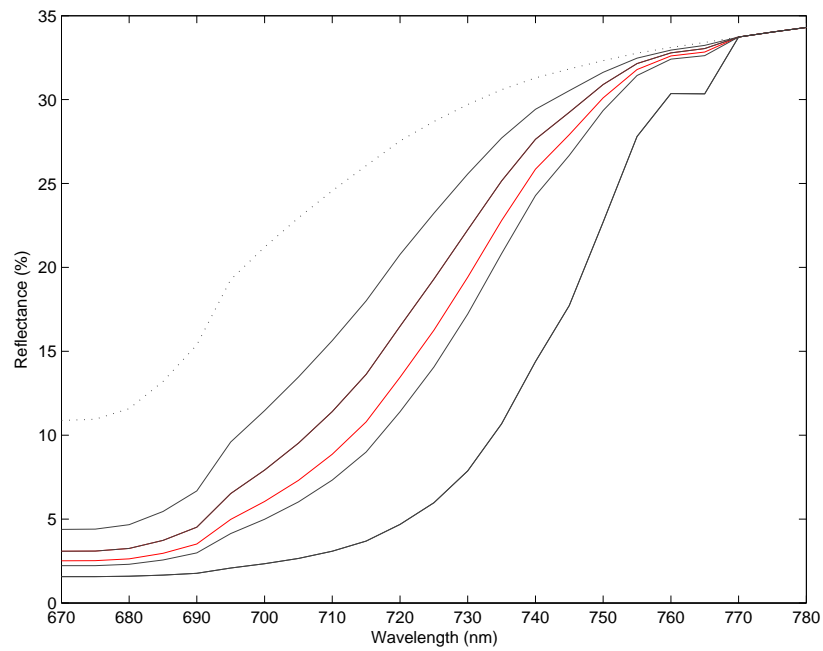
(a) Reflectance spectra
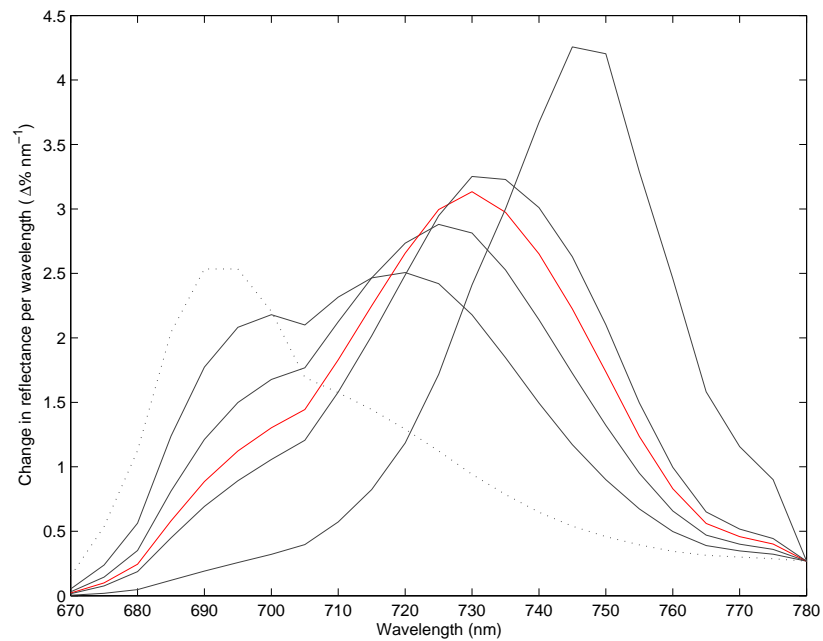
(b) First derivative reflectance spectra

Figure 8.6: The influence of chlorophyll content on the red-edge. Red spectra denote a modelled spectrum using the average chlorophyll content, dotted spectra denote a modelled spectrum using the minimum and other spectra indicate the quartile range (1, 2, 3 & 4).

Table 8.4: Vegetation variables derived from contaminated grassland.

	Chlorophyll content	LAI	Leaf water content
Units	mg.m−2		g m^{-2}
Average (mean)	937.20	2.5	79.88
Standard deviation	477.45	1.3	59.00
Minimum	65.62	0.3	0.50
First quartile	477.50	1.7	49.75
Second quartile (median)	681.25	2.2	73.04
Third quartile	984.96	3.0	73.04
Fourth quartile (maximum)	2854.17	5.7	349.04
Population (count)	126	31	123

At levels of chlorophyll content greater than 50 mg.m^{-2} the reflectance spectrum approximated a concave-convex form with a point of inflexion marking the transition. The higher the chlorophyll content the more concave the red-edge reflectance became and the longer the wavelength of the peak in the first derivative reflectance spectrum. Within the LIBSAIL simulated environment, changes in chlorophyll content consistent with those found in grassland spectra yielded a range of differences in the wavelength of the first derivative maximum of 15nm. However, this also included the influence of other absorption spectra such as the albino variable.

8.3.1.2   Albino

The extinction gradient for albino was gradual compared with that for chlorophyll (figure 254, 254). Therefore, small differences in albino had a smaller effect on the red-edge than differences in chlorophyll content. However, the influence of albino absorption extended to longer wavelength than that for chlorophyll. The most evident effect of

Table 8.5: Vegetation variables derived from an average field and laboratory measurments from uncontaminated grassland

	Chlorophyll content	LAI	Leaf water content
Units	mg.m−2		
Average (mean)	251.1	2.5	127.0
Standard deviation	224.5	1.6	138.9
Minimum	21.5	0.2	0.5
First quartile	92.7	1.6	55.0
Second quartile (median)	164.1	2.3	73.0
Third quartile	343.7	3.1	124.1
Fourth quartile (maximum)	1427.1	8.6	890.1
Population (count)	252	143	149

albino on reflectance spectra was to smooth the red-edge shoulder (figure 8.7). Opposite to the effects of chlorophyll, the higher the albino the less concave the red-edge. In addition, because the effects of albino were gradual and extended to wavelengths beyond those of the red-edge its influence on the first derivative red-edge affected the whole red-edge wavelength region evenly.

When modelled in conjunction with higher levels of chlorophyll (i.e. greater than 100 mg.m^{-2}) the effect of albino on the reflectance spectrum was to cause the gradient of the red-edge to decrease only at longer wavelengths. This boundary between the two absorption influences caused an additional manifestion in the first derivative spectrum as an additional peak. This effect was most evident when albino levels were low and chlorophyll content were high. In the absence of albino absorption the shorter wavelength in the first derivative was more pronounced.

REP was positively related to levels of albino (figure 8.8). However, because REP was also positively related to chlorophyll content, and because chlorophyll had a shorter maximum wavelength extent, low levels of chlorophyll content allowed the minor variable to become dominant. Higher levels of chlorophyll content were related to longer REPs. Figure 8.8 shows the steady positive relationship at high levels of chlorophyll content.
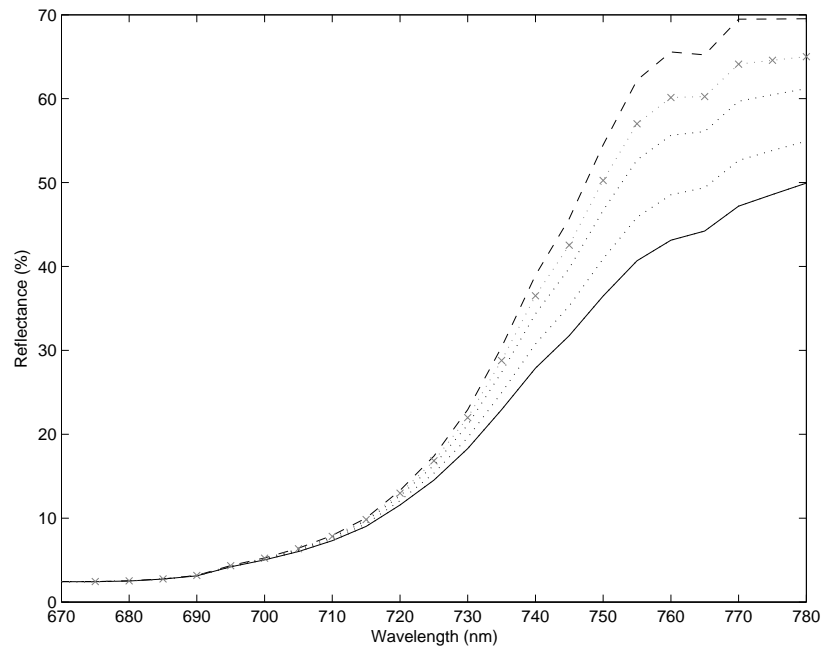
(a) Reflectance spectra
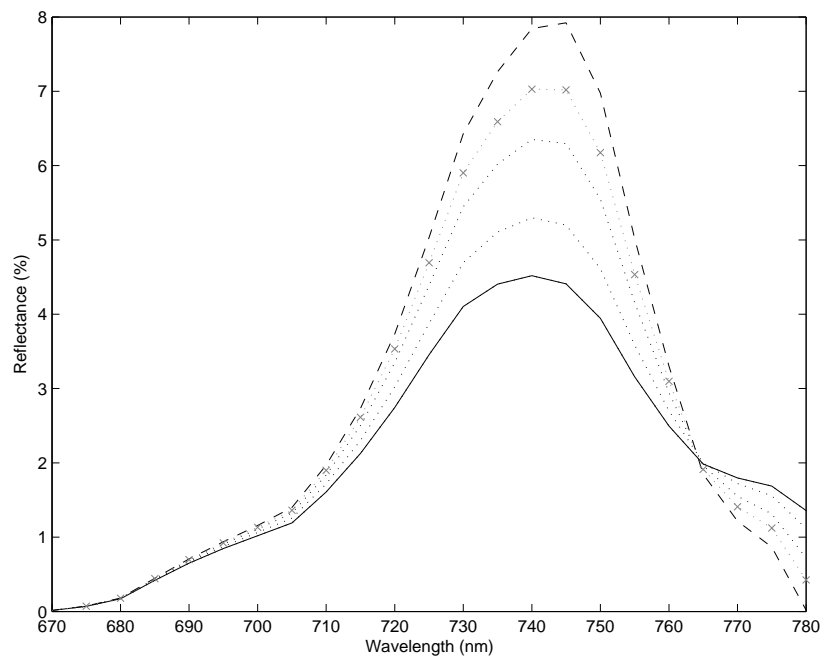
(b) First derivative reflectance spectra

Figure 8.7: The influence of the albino on the spectral red-edge. The dashed line denotes a modelled spectrum using the minimum albino (0), the solid line denotes a modelled spectrum using the maximum albino (4) and the line marked with a series of x's denotes a modelled spectrum using the modal albino (0.5).

8.3.1.3 Water

The absorption range of leaf water was higher than that for chlorophyll but intersected that of albino. Therefore, the only influence that water had on the modelled red-edge was in conjunction with the albino variable. In these cases the maximum reflectance of the red-edge shoulder was reduced when the influence of water was large. Water influenced the magnitude of the maximum peak in the first derivative but did not affect the wavelength position of the maximum peak. However, because the magnitude of the red-edge shoulder was affected by water content, it also affected the half height red-edge reflectance and therefore the wavelength of the half height reflectance (i.e. the linearly interpolated red-edge). Nevertheless, this influence was small: the maximum range of albino and water content effects constituted less than 1 nm change in the linearly interpolated REP.

8.3.1.4 Baseline

The baseline determined the background, non-wavelength dependent absorption. It therefore influenced the maximum reflectance of the red-edge shoulder and wavelength dependent absorption. A low baseline resulted in a high reflectance red-edge shoulder while a high baseline resulted in a low reflectance red-edge shoulder (see figure 8.9). However, because the baseline was a component of the total absorption coefficient, it also had a direct effect on the short wavelength end of the red-edge. The effect of a high baseline was to make other sources of absorption less distinct. Therefore, absorption (by chlorophyll, albino or water) had a greater influence on the red-edge when the baseline was small. The effect of a large baseline was to 'dilute' the influence of any specific source of wavelength dependent absorption. Though subtle in the reflectance spectra the effect of the different chlorophyll contents is evident in the first derivative. The affect of the baseline absorption on the spectra was that when the baseline was low (0.0004) the features has a greater magnitude than when the baseline was high (0.001). These factors also influenced the REP. REPs were at longer wavelengths when the baseline was small. The effect of differences in REP was the most evident for the linear

(a) First derivative maximum REP (0-300 mg.m^{-2})

(b) Linear interpolated REP (0-2000 mg.m^{-2})
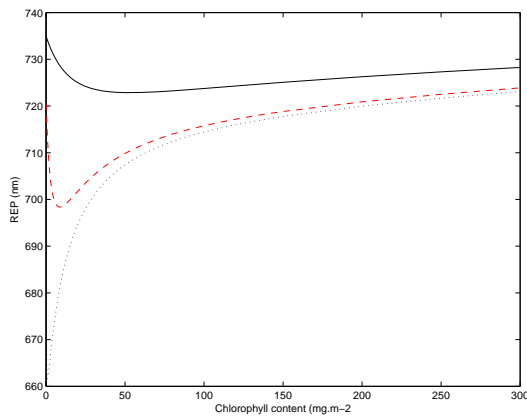
(c) First derivative maximum REP (0-300 mg.m^{-2})
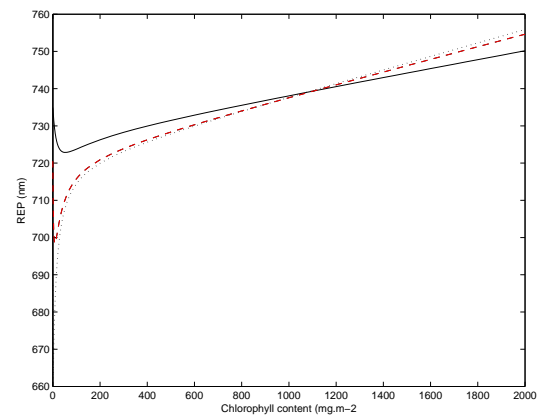
(d) Linear interpolated REP (0-2000 mg.m^{-2})

Figure 8.8: The influence of the albino and chlorophyll content on the REP. The dotted line denotes a modelled spectrum using the minimum albino (0), the solid line denotes a modelled spectrum using the maximum albino (4) and the dashed line denotes a modelled spectrum using the the modal albino (0.5).

interpolated REP and least for the Inverted Gaussian, method 1 (figure 8.10). This was because a difference in the NIR reflectance of the red-edge shoulder, even without a change in the reflectance of the short wavelength end of the red-edge, or the gradient of the red-edge, affected the position of half reflectance and therefore also its wavelength (linear interpolation method).
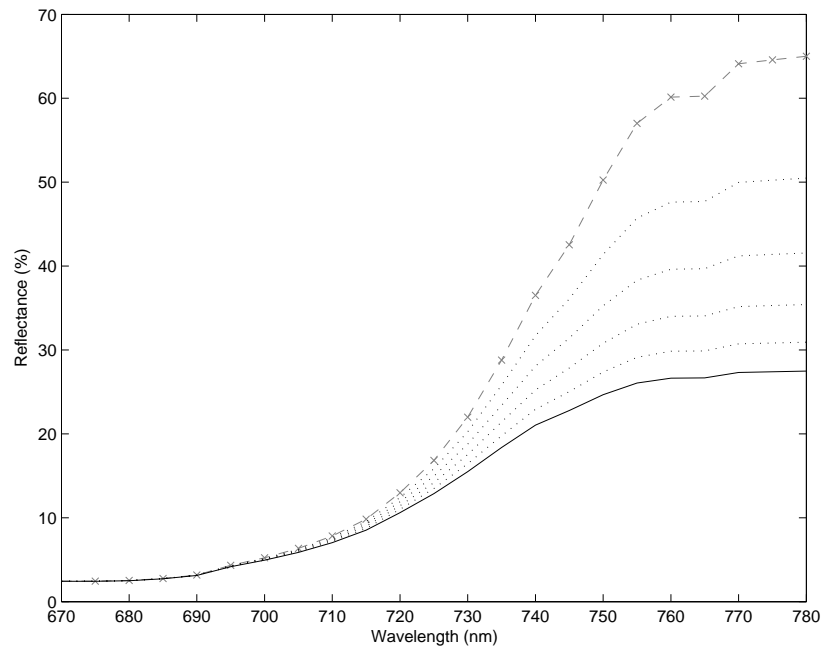
(a) Reflectance spectra
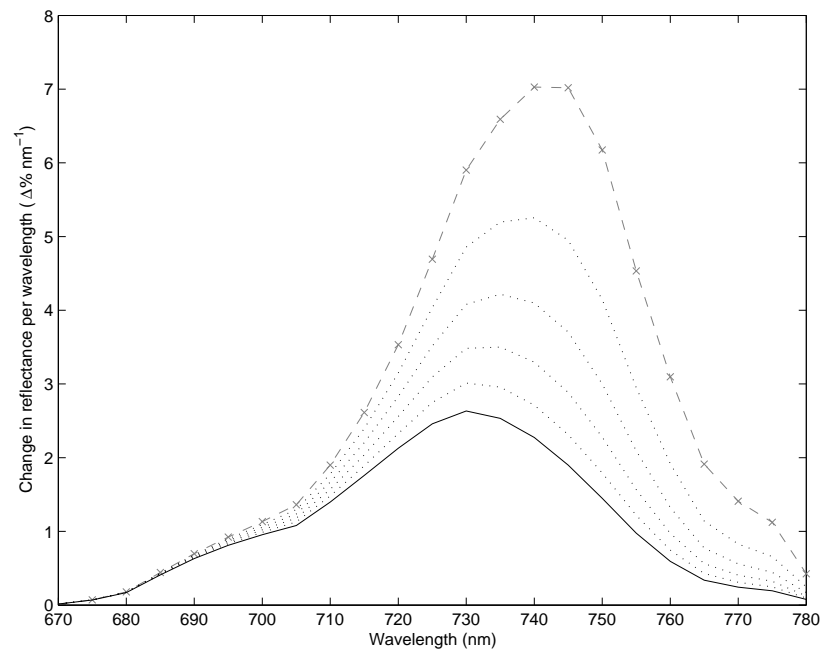
(b) First derivative reflectance spectra

Figure 8.9: The influence of the baseline on the red-edge spectra. The dashed line denotes the minimum baseline (0.0004), the solid line denote the maximum baseline (0.0012) and the line marked with a series of x's denotes the modal baseline (0.001).

8.3.2 The effect of scattering variables on the red-edge

The air void variable was used in conjunction with the total absorption coefficient to determine the total reflected radiation. It directly affected the proportion of radiation that was scattered as it passes through the leaf. The reflectance range was greatest when the air void ratio was large and least when it was small (figure 8.11). The influence of the air void ratio was explored for the range of values that provided the closest match to field spectra in previous simulations (the validation of LIBSAIL for grassland and the matching of spectra collected from a grassland with contaminated soil). Though a determining factor, the air-void ratio had little influence without those variables that determined the magnitude of its effect.

8.3.3 The effect of quantitative variables on the red-edge

Leaf area index (LAI) and leaf thickness influenced the magnitude of the effects of other LIBSAIL variables. Neither were specifically related to absorption or scattering. Their influence on the red-edge was dependent on the relative magnitude of the variables that they were affecting regardless of whether it related to absorption or scattering. Other input variables acted on specific effects to promote or restrict their influence while not themselves causing the effect.

8.3.3.1 Cell size

In LIBSAIL, cell size was the variable by which the absorption components were multiplied to derive the total absorption coefficient. Its contribution to scattering was via its effect on absorption; the smaller the cell size the less absorption affected the modelled spectrum. The reflectance range was greatest when the cell size was small and least when the cell size was large (figure 8.12).
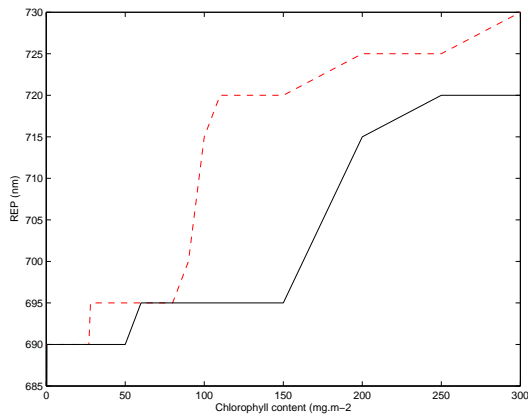
(a) First derivative maximum REP (0-300 mg.m^{-2})
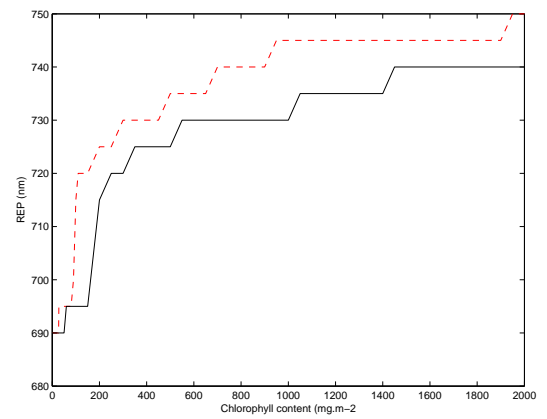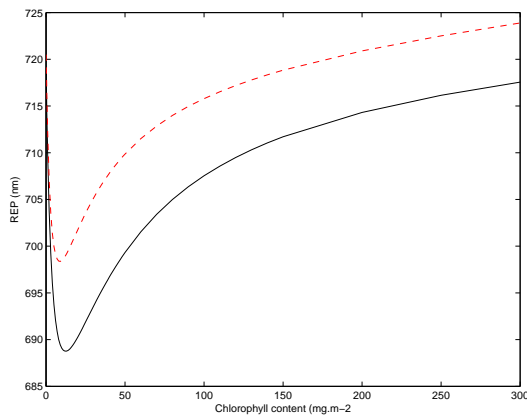
(b) First derivative maximum REP (0-2000 mg.m^{-2})

(c) Clevers' linear interpolated REP (0-300 mg.m^{-2})
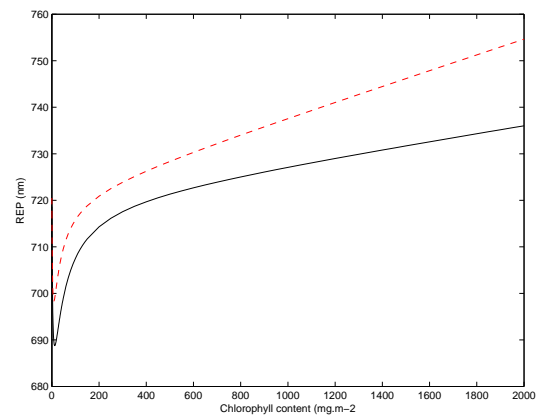
(d) Clevers' linear interpolated REP (0-2000 mg.m^{-2})

Figure 8.10: The influence of the baseline and chlorophyll content on the REP. The dotted line denotes a modelled spectrum using the minimum baseline (0.0004), the solid line denotes a modelled spectrum using the maximum baseline (0.0012) and the dashed line denotes a modelled spectrum using the modal baseline (0.001).
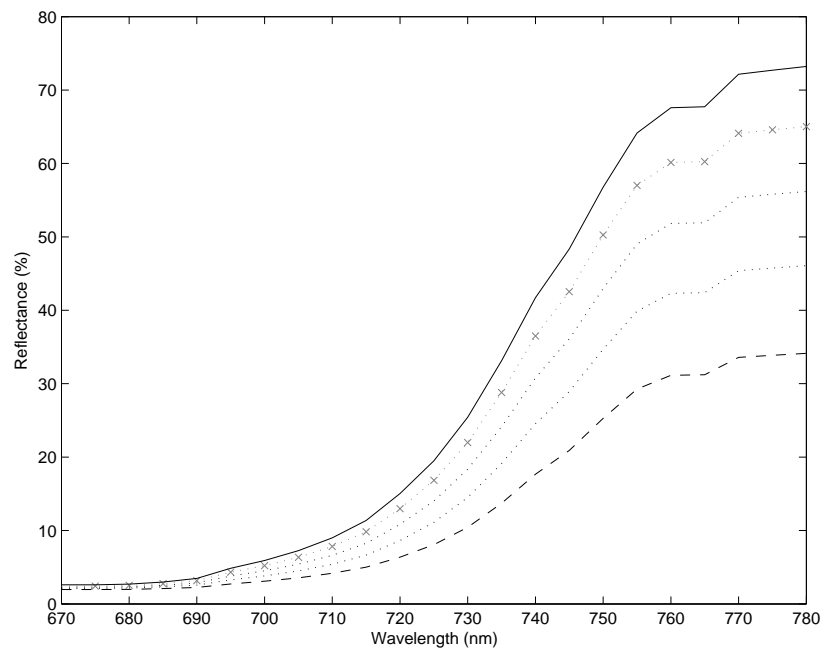
(a) Reflectance spectra
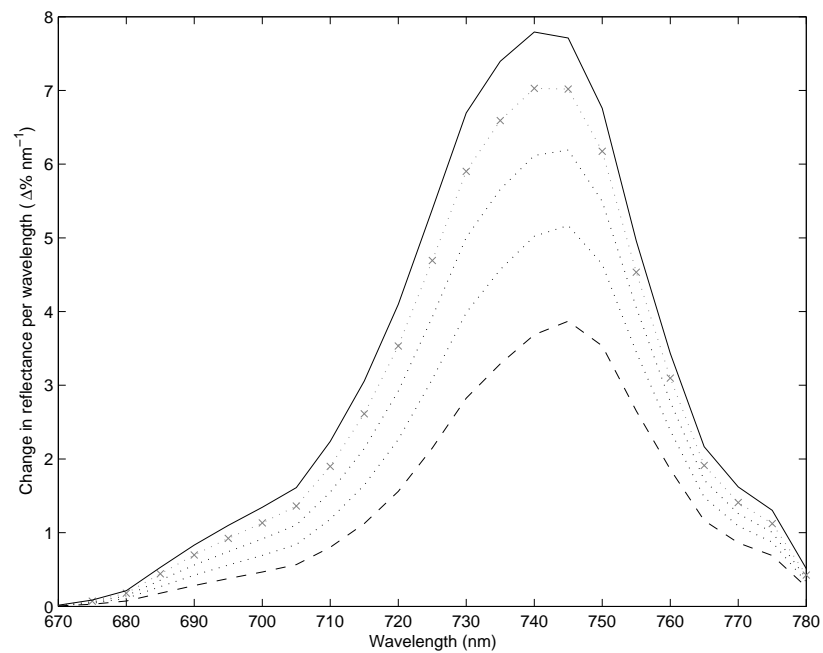
(b) First derivative reflectance spectra

Figure 8.11: The influence of the air void ratio on the red-edge spectra. The dashed line denotes a modelled spectrum using the minimum air void ratio (0.004), the solid line denotes a modelled spectrum using the maximum air void ratio (0.012) and the line marked with a series of x's denotes a modelled spectrum using the modal air void ratio (0.01).
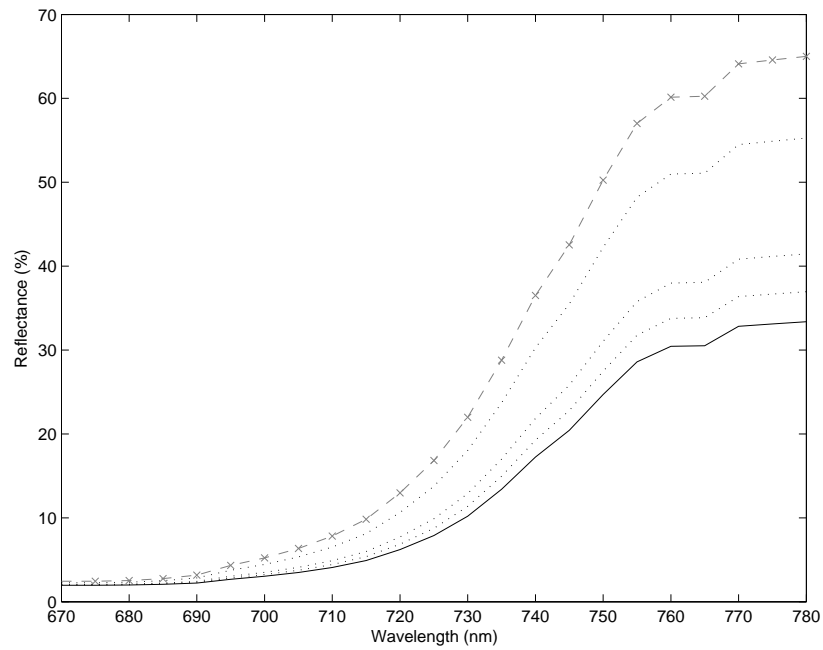
(a) Reflectance spectra
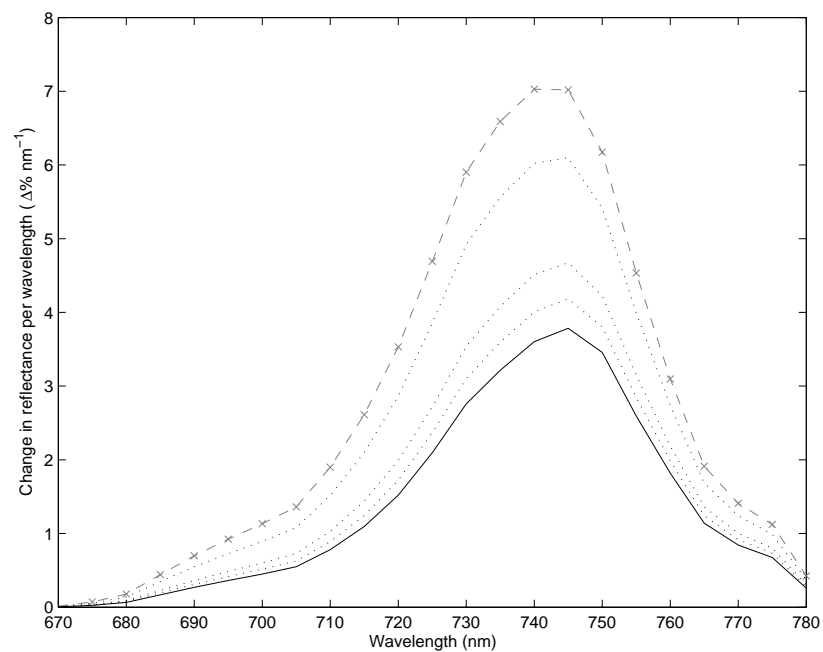
(b) First derivative reflectance spectra

Figure 8.12: The influence of the cell size on the red-edge spectra. the dashed line denotes a modelled spectrum using the minimum cell size (1), the solid line denotes a modelled spectrum using the maximum cell size (10) and the line marked with a series of x's denotes a modelled spectrum using the mean cell size (1.8).

8.3.3.2   Leaf thickness

Within LIBSAIL, the leaf thickness variable determined the number of scattering layers
present. Its effects were greatest at a leaf thickness of 2.5 such that leaf thickness values
near 2.5 caused higher scattering than those higher or lower than 2.5. This was likely
to be an anomaly with LIBERTY rather than a physical phenomena. This point
matches the intersection of reflectance and transmittance (Dawson 1997, page 69) and
represents a shift in dominance of the two processes. However, the level of scattering
influenced the maximum NIR reflectance and therefore the reflectance of the red-edge
shoulder (figure 8.13). It therefore could influence some REP methods and ratio based
vegetation indices.

8.3.3.3   Leaf area index

Absorption and scattering were determined by specific variables in the leaf model (LIB-
ERTY). Leaf area index (LAI) did not directly affect absorption or scattering but
magnified these processes. One result from influencing the magnitude of both absorp-
tion and scattering was that changes in LAI could promote a gradient change in the
red-edge. This did not determine the wavelength position of any peaks, features or
the red-edge shoulder but influenced how easily they were resolved in the spectrum.
Figure 8.14 show that for a chlorophyll content of 60 mg m^{-2} a high LAI resulted
in (i) high absorption and (ii) a high red-edge shoulder reflectance (indicating high
levels of scattering). Conversely a low LAI resulted in (i) lower absorption and (ii) a
lower red-edge shoulder reflectance. REP was influenced by LAI such that a high LAI
resulted in a REP at longer wavelengths (figure 8.15). However, the effects of LAI on
REP (for all calculation methods in this research) were minor compared with that of
chlorophyll content, cell size, air void or baseline.
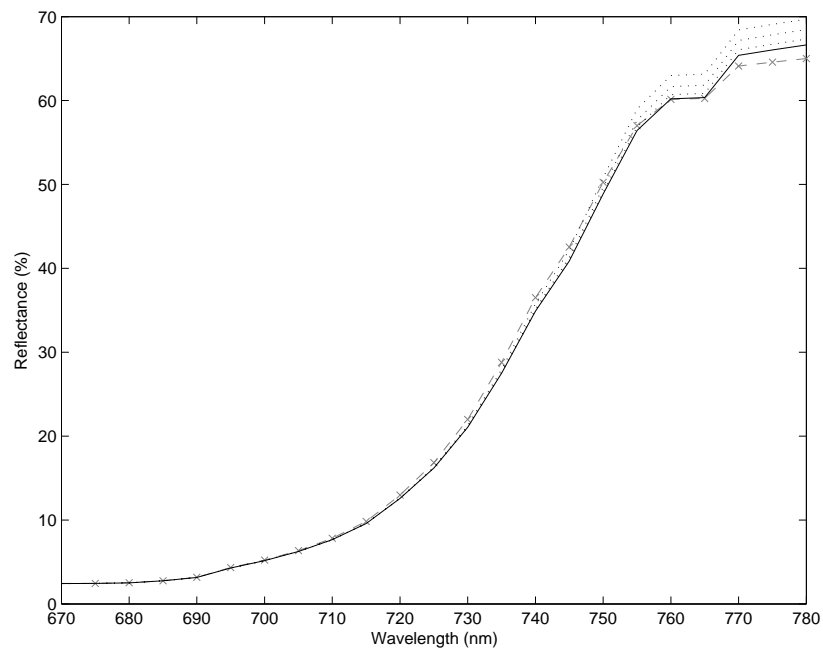
(a) Reflectance spectra
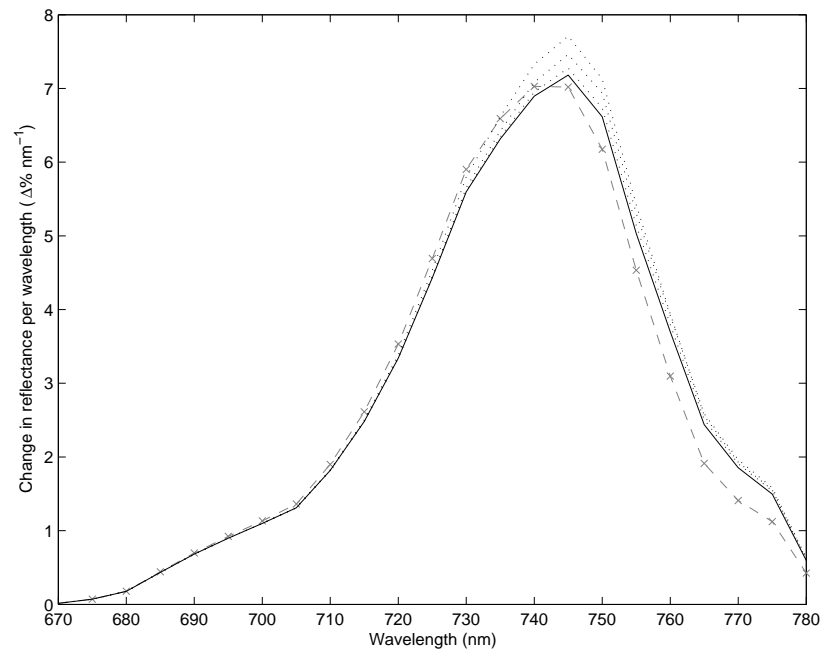
(b) First derivative reflectance spectra

Figure 8.13: The influence of the leaf thickness on the red-edge spectra. the dashed
line denotes a modelled spectrum using the minimum leaf thickness (1), the solid
line denotes a modelled spectrum using the maximum leaf thickness (4) and the line
marked with a series of x's denotes a modelled spectrum using the mean leaf thickness
(1.8).
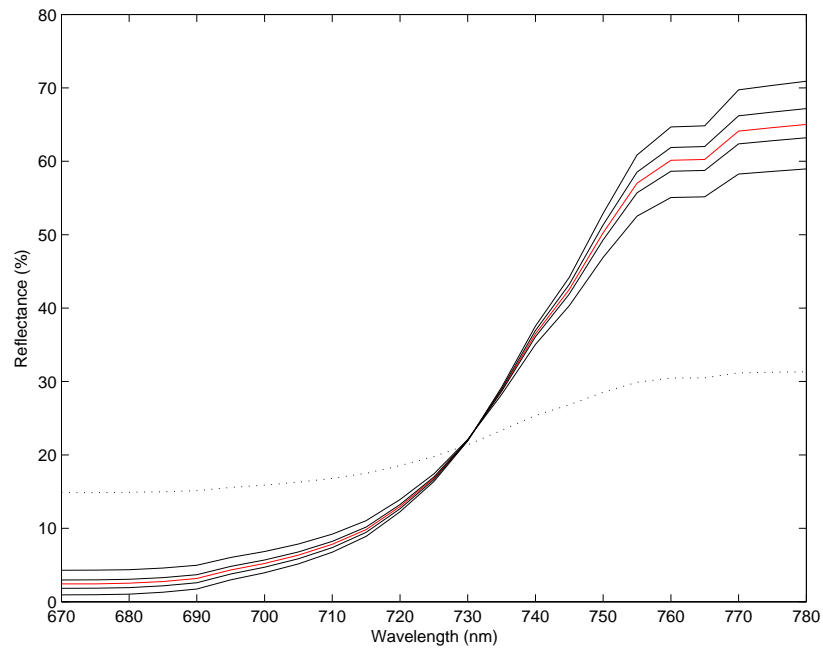
(a) Reflectance spectra
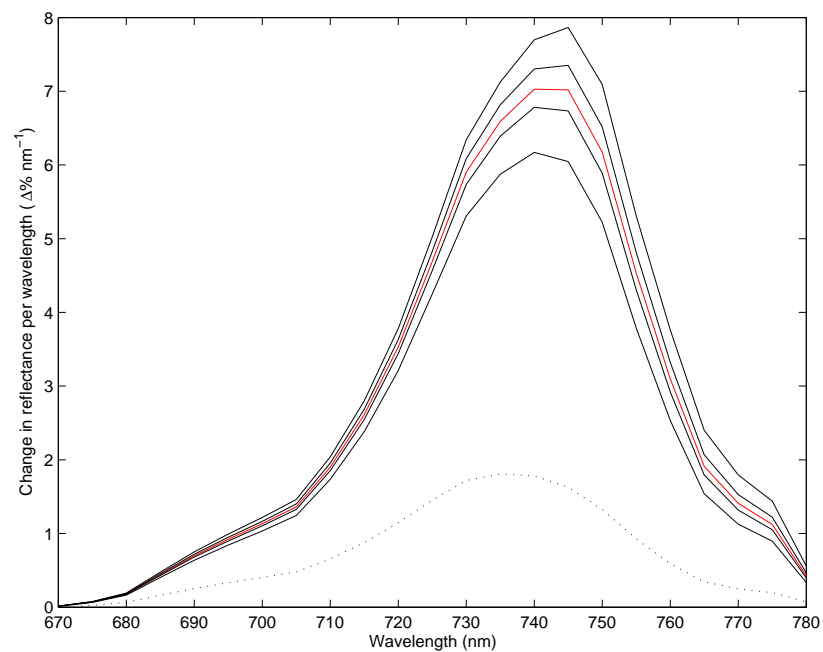
(b) First derivative reflectance spectra

Figure 8.14: The influence of LAI on the red-edge spectra. The red spectra denotes a modelled spectrum using the average LAI (2.5), the dotted spectra denotes a modelled spectrum using the minimum LAI (0.3) and the other spectra indicate the quartile range (1, 2, 3 & 4).
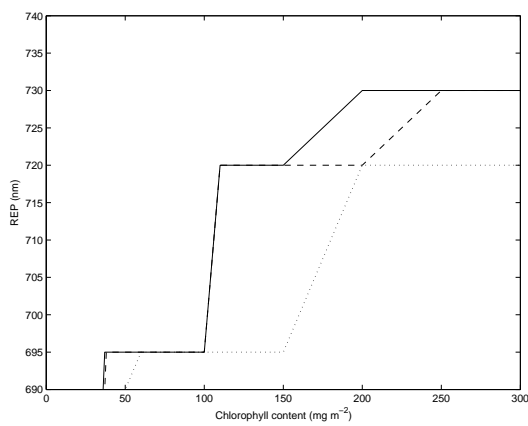
(a) First derivative maximum REP (0-300 mg.m^{-2})
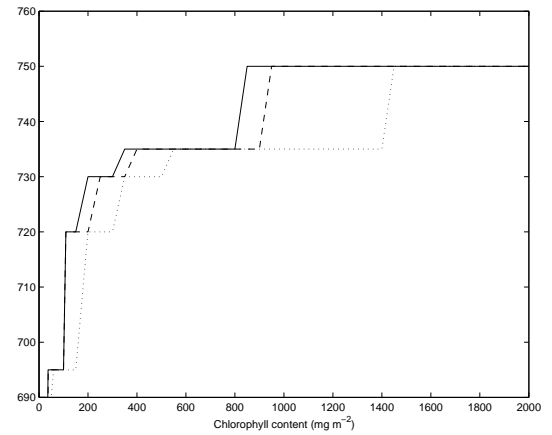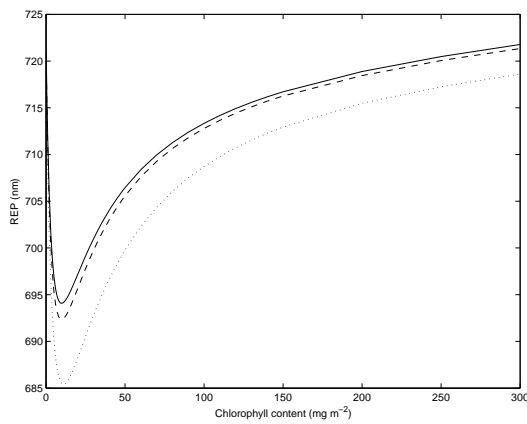
(b) First derivative maximum REP (0-2000 mg.m^{-2})

(c) Clevers' linear interpolated REP (0-300 mg.m^{-2})
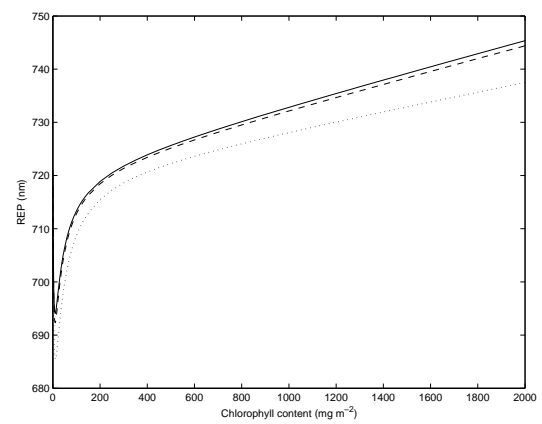
(d) Clevers' linear interpolated REP (0-2000 mg.m^{-2})

Figure 8.15: The influence of the LAI and chlorophyll content on the REP. The dotted line denotes a modelled spectrum using the minimum LAI (0.3), the solid line denotes a modelled spectrum using the maximum LAI (5.7) and the dashed line denotes a modelled spectrum using the mean LAI (2.5).

8.3.3.4   Leaf angular distribution

The leaf angular distribution described the degree from nadir of the leaf mass. To
simplify this investigation, the solar and view zenith angles were kept as zero. Never-
theless, the capability to investigate low illumination and oblique viewing were present.
The erectophile upright form of grasses was supported by a modal LAD value of 10 but
other LAD values were explored (figure 8.16). LAD influenced the REP in a similar
manner as LAI (figure 8.17)

8.3.4   Maximum red-edge reflectance range

Absorption in the red-edge wavelengths was due to chlorophyll content and albino and
was potentially attenuated by LAI. These variables determine the minimum reflectance
at the short wavelength end of the red-edge. Maximum reflectance at the long wave-
length end of the red-edge was determined by the wavelength independent variables
also attenuated by LAI and LAD. However, certain combinations of variables caused
the red-edge reflectance to be maximised (figure 8.18). Under these conditions features
in first derivative spectra were enhanced and variations in sources of absorption were
most pronounced. Figure 8.18 shows that if most input variables are configured for
maximum scattering the NIR reflectance at the red-edge shoulder can be modelled as
a reflectance of almost 80%. At this magnitude even minor absorption features in the
red-edge may become resolved. Similarly, exploitation of scattering allowed a modelled
difference in the REP of 5nm regardless of levels of chlorophyll content (figure 8.19).

8.3.5   Equifinality

With a large number of input variables and the fundamental influences of those vari-
ables limited to aspects of absorption and scattering it is inevitable that some common
effects will ocurr due to different causes. This was why measurements of the main veg-
etation input variables were conducted. The unconstrained (or partially constrained)
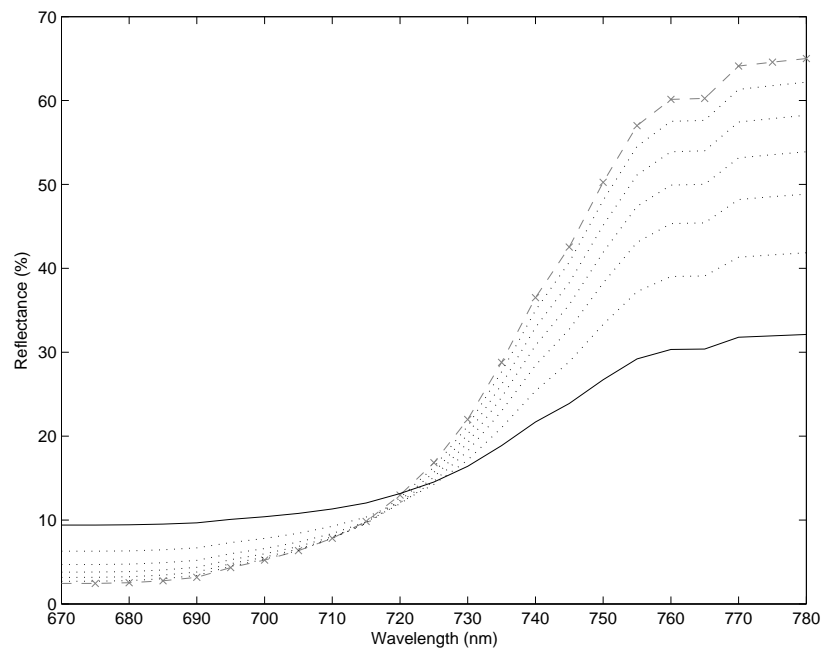
(a) Reflectance spectra
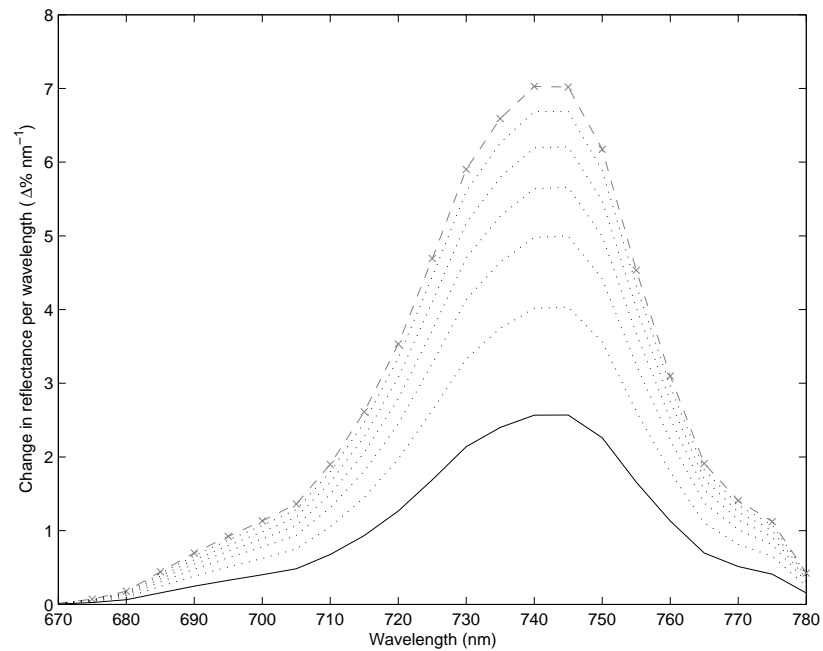
(b) First derivative reflectance spectra
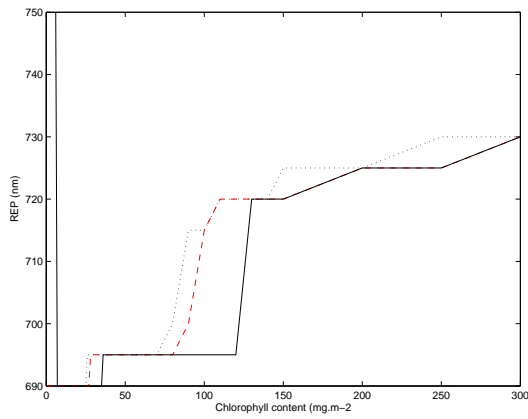
Figure 8.16: The influence of LAD on the red-edge spectra. The dashed line denotes a modelled spectrum using the minimum LAD (10), the solid line denotes a modelled spectrum using the maximum LAD (70) and the line marked with a series of x's denotes a modelled spectrum using the modal LAD (10).
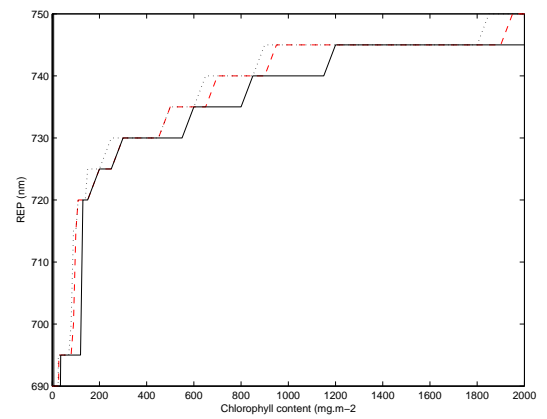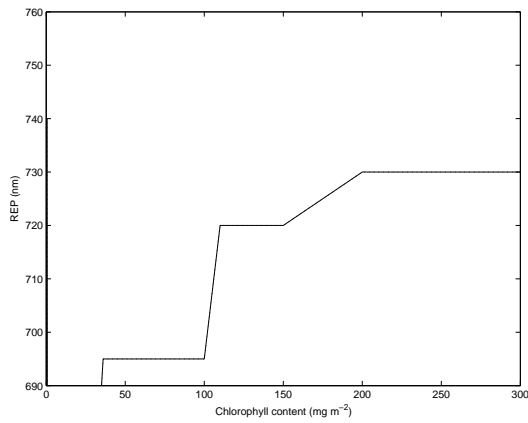
(a) First derivative maximum REP (0-300 mg.m^{-2})
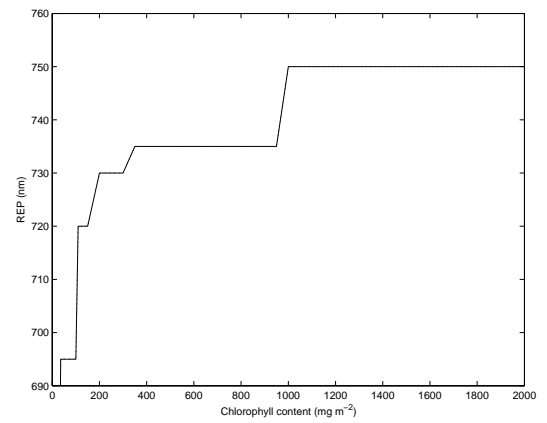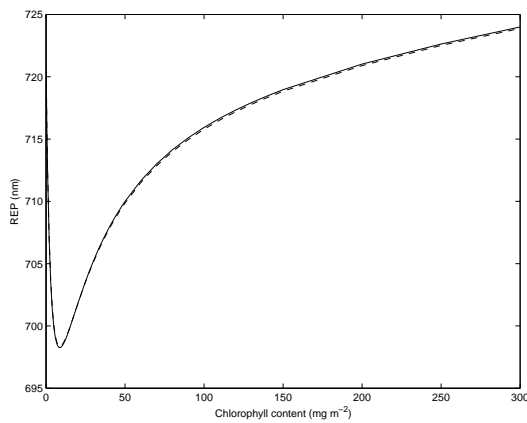
(b) First derivative maximum REP (0-2000 mg.m^{-2})

(c) Clevers' linear interpolated REP (0-300 mg.m^{-2})
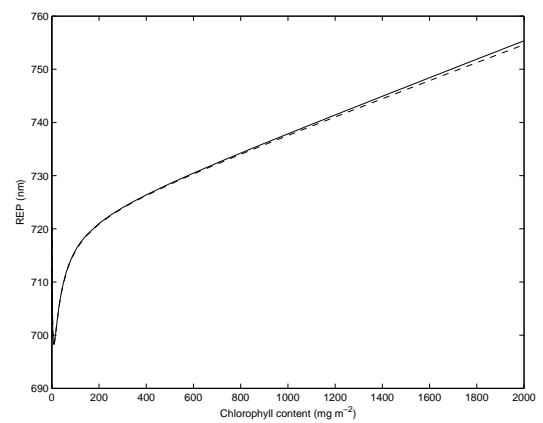
(d) Clevers' linear interpolated REP (0-2000 mg.m^{-2})

Figure 8.17: The influence of the LAD and chlorophyll content on the REP. The dashed line denotes a modelled spectrum using the the minimum and modal LAD (10), the solid line denotes a modelled spectrum using the the maximum LAD (70).
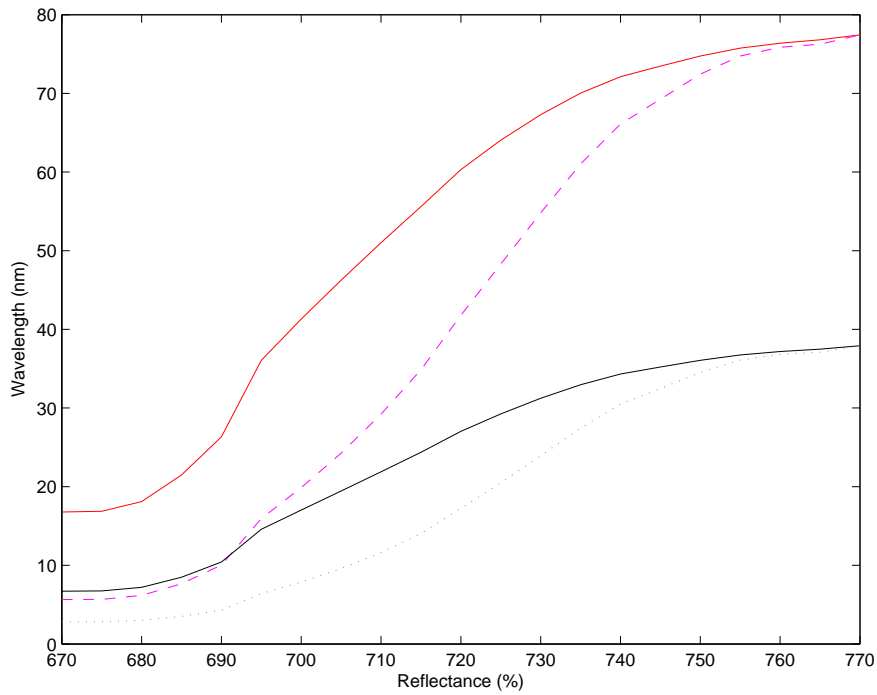
(a) Reflectance spectrum
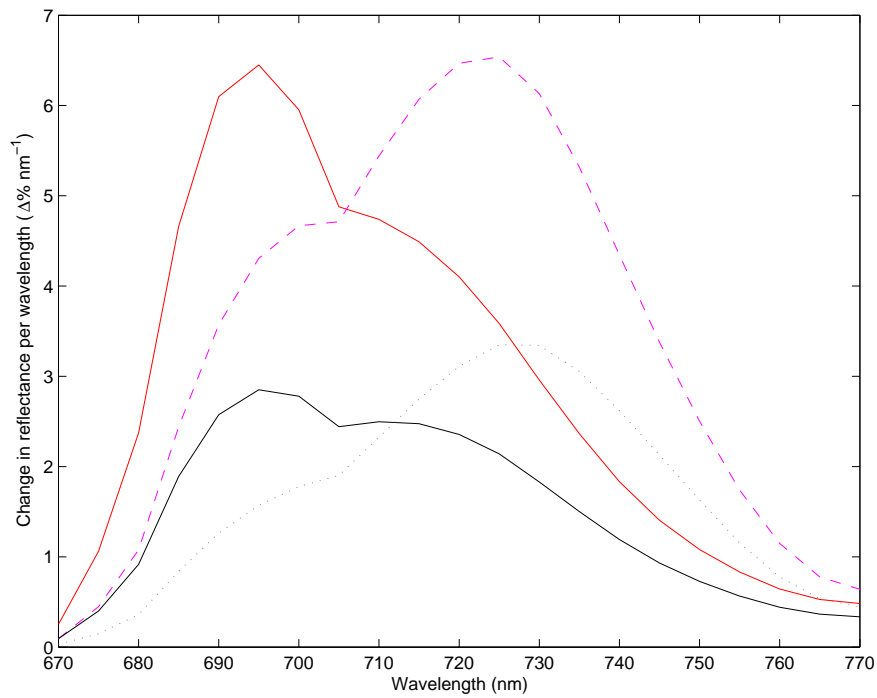
(b) First derivative of reflectance spectrum

Figure 8.18: LIBSAIL modelled spectra with two chlorophyll contents (red and black are 10 mg m^{-}2 and dotted and dashed are 200 mg m^{-}2). The black and dotted lines are mean variables that define standard levels of scattering and red and dashed lines are variables that promote high levels of scattering.
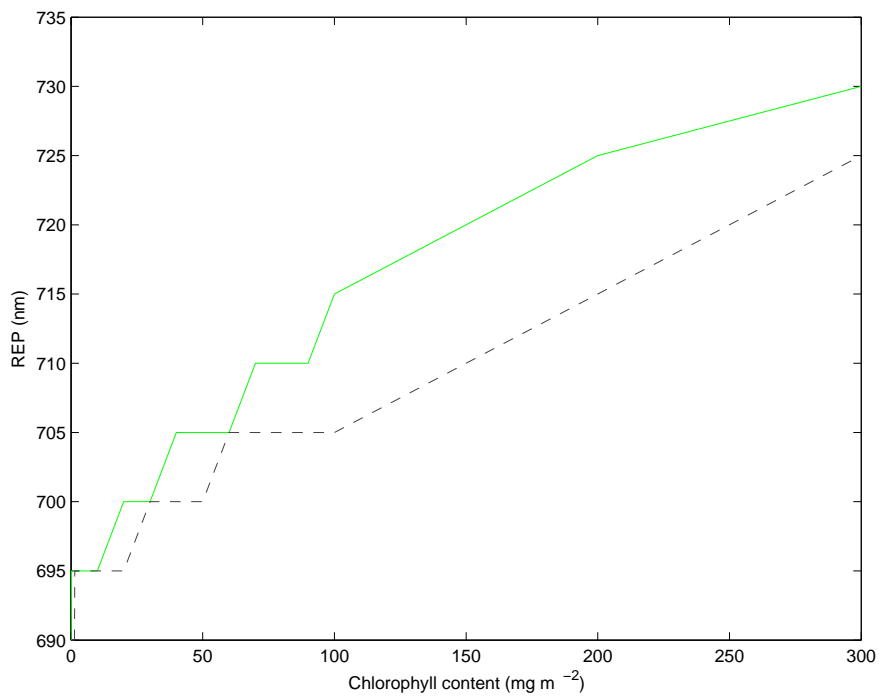
(a) First derivative maximum REP
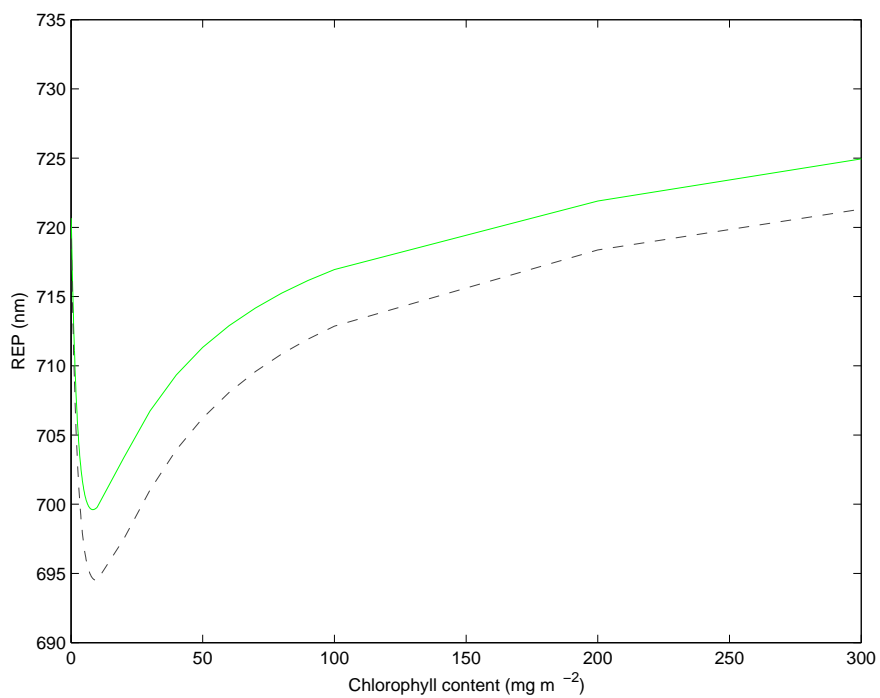
(b) Linear interpolated REP

Figure 8.19: LIBSAIL modelled REP spectra with standard mean variables (black line) and those that promote maximum scattering (dashed line).

input of variables that were not guided by field and laboratory measurements were potentially able to produced equifinal results. An example is cell size and air-void variables. Cell size was defined by an average determined by field and laboratory measurements; the air-void was not but was indicated by published literature to be small for grass. A large cell size limits a high reflectance due to its enhancement of absorption effects. Conversely, a high air-void ratio promotes a high reflectance due to scattering. These variables can act independently to cause the same result or together (figure 8.20. For a chlorophyll content of 100 mg m^{-2}, the linearly interpolated REP for a combination of variables of cell size 20, air-void of 0.001 and a baseline of 0.001 had the same REP (697.6 nm) as that calculated from a combination of variables of cell size 100, air-void of 0.01 and a baseline of 0.0004. For spectra modelled with an air-void value of 0.001 the linearly interpolated REP was within 2 nm as that for 100 mg m^{-2} or within 0.5 nm for 300 mg m^{-2} if either the cell size was 20 or the baseline was 0.001. For spectra modelled with a cell size of 100 the linearly interpolated REP was within 1.5 nm for 100 mg m^{-2} or within 2 nm for 300 mg m^{-2} if either the air-void was 0.01 or the baseline was 0.0004.

8.4 Investigating the modelled red-edge with two canopies

In those cases where field spectra were a poor match to their associated field spectra the mismatches had two main forms; the LIBSAIL spectra were either too concave or the gradient of the LIBSAIL-modelled spectra were different from that of the field spectra (a 'cross-over'). Both these errors were explored with the use of a second canopy component; in field conditions this approximated the presence of an understorey. Following from these, a comparative investigation into the spectral mixing of high and low chlorophyll canopies will be presented. The section will end with a consideration of the influence of the pigment absorption spectrum and the effect of it modification.
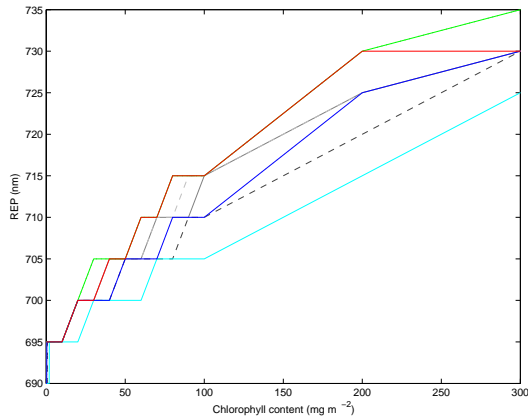
(a) First derivative maximum REP
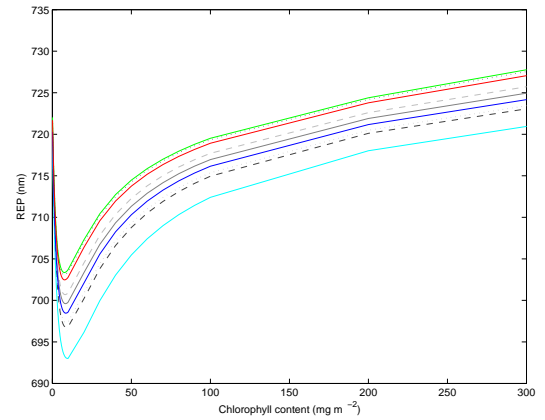
(b) Linear interpolated REP (Clevers *et al.* 2002)
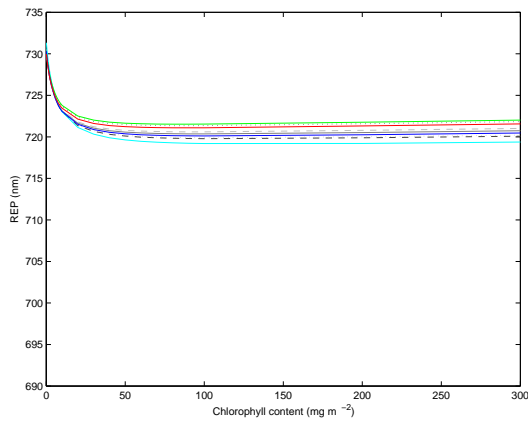
(c) Inverted Gaussian REP (method 1) (Miller *et al.* 1990)
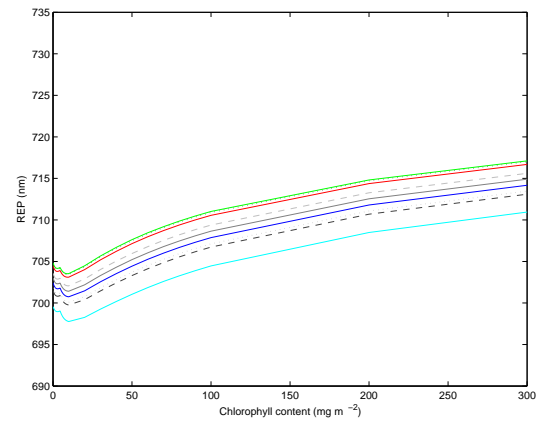
(d) Inverted Gaussian REP (method 2) (Miller *et al.* 1990)

Figure 8.20: LIBSAIL modelled REP with different levels of chlorophyll content and the combined effect of different levels of cell size and air-void spacing. The red dotted line denotes a modelled spectrum using the the input minimum cell size (1), the red solid line denotes a modelled spectrum using the the input maximum cell size (10) and the red dashed line denotes a modelled spectrum using the the measured mean cell size (1.8). The blue dotted line denotes a modelled spectrum using the the input minimum air-void spacing (0.004), the blue solid line denotes a modelled spectrum using the the input maximum air-void spacing (0.012) and the blue dashed line denotes a modelled spectrum using the the modal air-void spacing (0.01) from previous 'best fit' simulations.

8.4.1   Matching field spectra by the inclusion of a vegetated

under-storey

The contribution of an under-storey to the whole canopy spectrum was investigated
using 57 of the 114 LIBSAIL-modelled spectra described in section 8.2. When com-
pared against their associated field spectrum these spectra had a concave red-edge
and/or a mismatch of red-edge slope gradients (a 'cross over'). These spectra were
treated as over-storey canopies against which under-storey canopies were individually
modelled. In these simulations the second LIBSAIL-modelled canopy, the under-storey,
contributed between 5 and 20% of the whole canopy signal, where the over-storey con-
tributed the remaining share and the under-storey share was kept to a minimum. The
under-storey was simulated by systematically modelling a 'best fit' match for the whole
canopy (including the over-storey) using a range of LIBSAIL input values determined
by the input maximum and input minimum of field measurements and previous simu-
lations (figure 8.21). In almost all cases a close match to field spectra was obtained. In
these investigations the influence of an under-storey was found to be greatest when an
over-storey had different absorption characteristic to those of the over-storey and when
it had a high potential for NIR scattering. Linear mixing of these spectra showed that
as the proportion of the spectrum representing low levels of chlorophyll content was
increased the red-edge became more convex as the red-edge slope was shifted to shorter
wavelengths. This countered the one of the main discrepancies identified in section 8.2,
i.e. convexity. The 'cross-over' mismatch effect was explained and countered by the
influence of LAI and LAD as these affected levels of absorption and scattering. Both
the convexity and the cross-over effects were countered by the contribution of a second
canopy component (an under-storey).
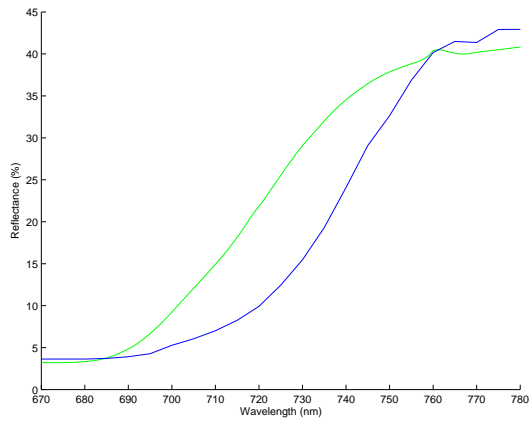
(a) Reflectance spectrum
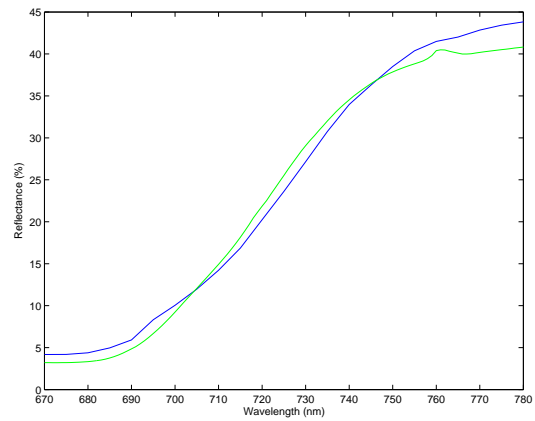
(b) Reflectance spectrum
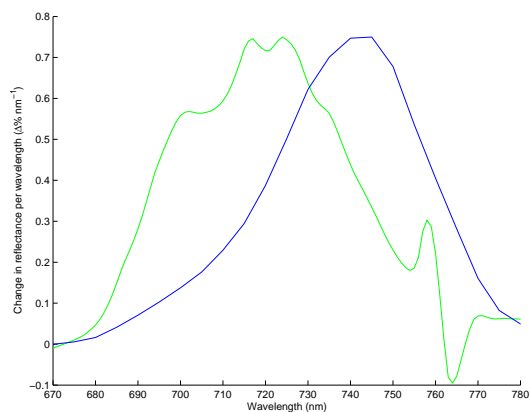
(c) First derivative spectra
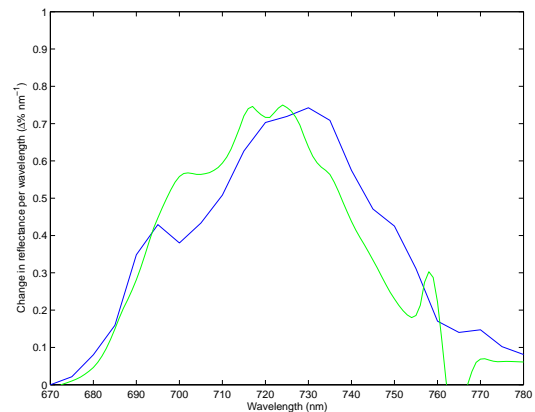
(d) First derivative spectra

Figure 8.21: Resolution of the convexity mismatch. The spectrum to the left was modelled with a single canopy (figure 8.4). The spectrum to the right was modelled to include the influence of a 5% vegetated under-storey.

8.4.2   Vegetated under-storeys with different chlorophyll contents

The effects of two canopies were further explored with two scenarios, each using two canopy components (an over-storey and an under-storey). Low chlorophyll conditions were deliberately selected to enhance effects at the shorter wavelengths of the red-edge. Although such conditions were evident in the grassland with different levels of soil contamination they were not represented in the measured field data (see chapter 6). Each canopy was modelled using LIBSAIL constrained by input variables within the range of those found in the grassland environment. The under-storey canopies were simulated from field measurements derived from uncontaminated grasslands but the over-storey (same in both scenarios) represented a location on the grassland with intermediate levels of soil contamination (grid 2, NI011) with an open canopy, a chlorophyll content of 60 mg m^{-2} and a LAI of 2.1. Between each over-storey - under-storey combination mixed spectra were calculated at 5% mixture intervals between the over-storey and under-storey. The REP for each of the three unmixed spectra and the wavelength difference between them are represented in table 8.6, each REP difference was calculated with respect to a 100% over-storey canopy. The spectra and three mixtures (25%, 50% & 75%) are shown in figures 8.22 & 8.23. A spectral mixture of 95% over-storey and 5% under-storey with a low level of chlorophyll content had a 2.7 nm difference in REP (Clever's linear interpolation method, Clevers *et al.* 2001). A spectral mixture of 95% over-storey and 5% under-storey with a high level of chlorophyll content had a 0.6 nm difference in REP. A spectral mixture of 80% over-storey and 20% under-storey with a low level of chlorophyll content had a 9.1 nm difference in REP. A spectral mixture of 80% overstorey and 20% under-storey with a high level of chlorophyll content had a 2.2 nm difference in REP. Compared with othe REP calculation methods the greatest REP difference was found for the Guyot and Baret's method (Guyot and Baret 1988) though all maintained the same trend.

To further investigate these results the influence of a vegetated under-storey was tested. The same over-storey as used in the previous scenarios (with a chlorophyll content of

Table 8.6: REP for modelled spectra with 21.5, 60 and 220 mg m^{-2} chlorophyll content and the REP difference between different spectra.

Method of deriving REP	21.5 mg m^{-2}	60 mg m^{-2}	220 mg m^{-2}
First derivative maximum (Savitsky and Golay 1964)	695 nm	705	725
Linear Interpolation (Clevers *et al.* 2001)	688.0 nm	712.9 nm	721.1 nm
Linear Interpolation (Danson and Plummer 1995)	688.1 nm	712.9 nm	721.1 nm
Linear Interpolation (Guyot and Baret 1988)	612.2 nm	668.8 nm	688.8 nm
Inverted Gaussian 1 (Miller *et al.* 1990)	718.3 nm	720.5 nm	717.5 nm
Inverted Gaussian 2 (Miller *et al.* 1990)	691.1 nm	706.0 nm	709.5 nm
Method of deriving REP	**21:60 mg m^{-2}**	**60:220 mg m^{-2}**	**21:220 mg m^{-2}**
First derivative maximum SavitskyG64	5 nm	5 nm	5 nm
Linear Interpolation (Clevers *et al.* 2001)	9.05 nm	2.15 nm	14.82 nm
Linear Interpolation (Danson and Plummer 1995)	9.02 nm	2.14 nm	14.76 nm
Linear Interpolation (Guyot and Baret 1988)	20.57 nm	5.22 nm	34.22 nm
Inverted Gaussian 1 (Miller *et al.* 1990)	0.81 nm	0.50 nm	0.06 nm
Inverted Gaussian 2 (Miller *et al.* 1990)	4.58 nm	0.89 nm	6.46 nm
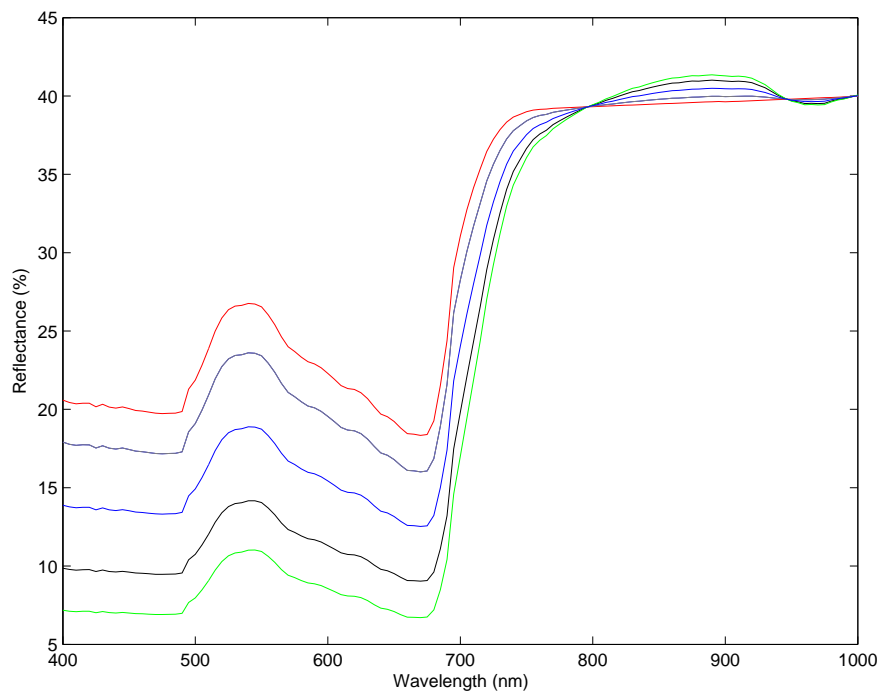
(a) Reflectance spectrum (low levels of chlorphyll)
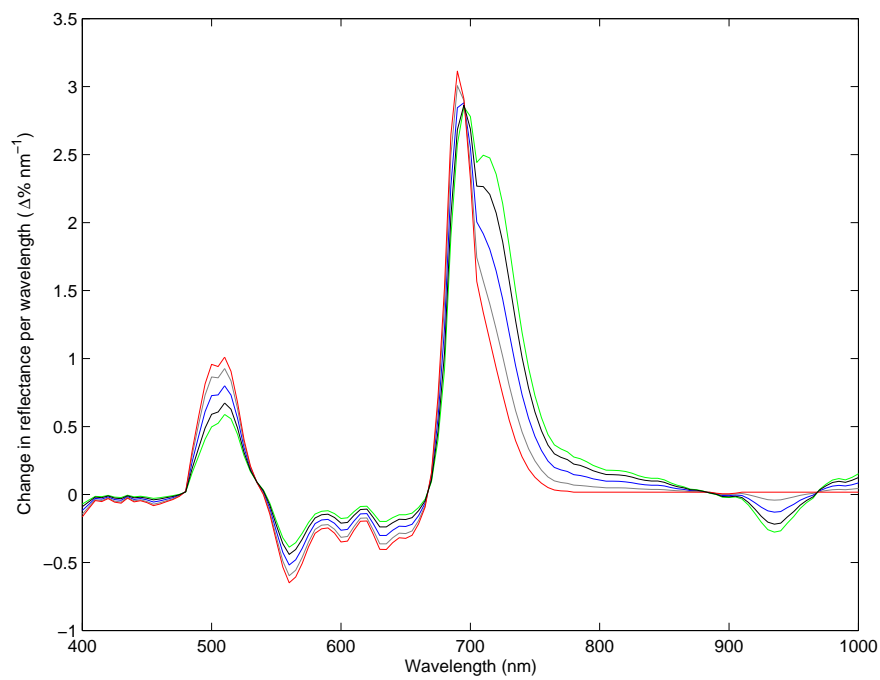
(b) First derivative reflectance spectrum (low levels of chlorphyll)

Figure 8.22: Transition between canopy components with different levels of chlorophyll content.

Where the green spectrum indicates a grass spectrum with a chlorophyll content of 60 mg.m^{-2}). The red spectra show an under-storey with a chlorophyll content of 21.5 mg.m^{-2}. Blue spectra marked a 50% mixture between the red and green and black a 25% or 75% mixture.
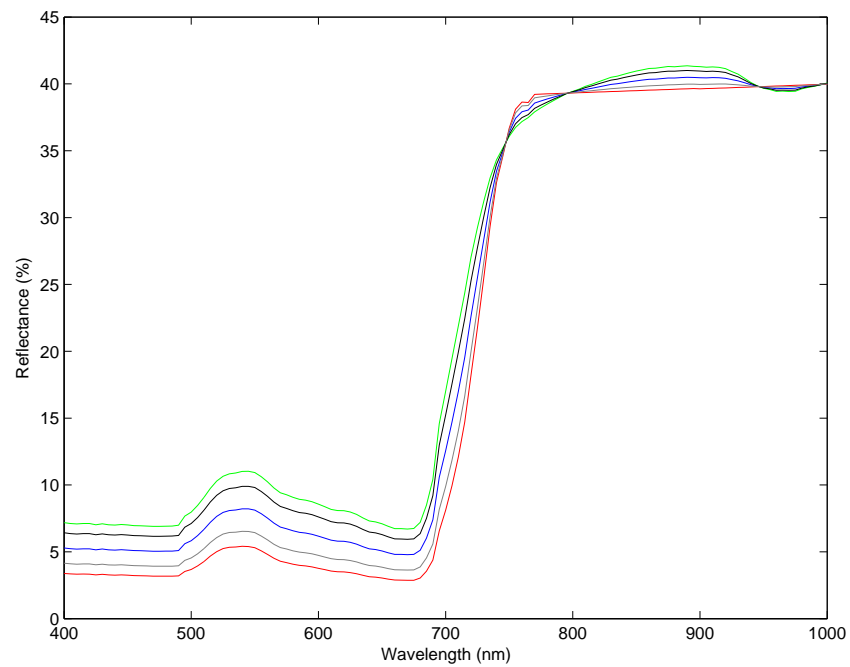
(a) Reflectance spectrum (high levels of chlorphyll)
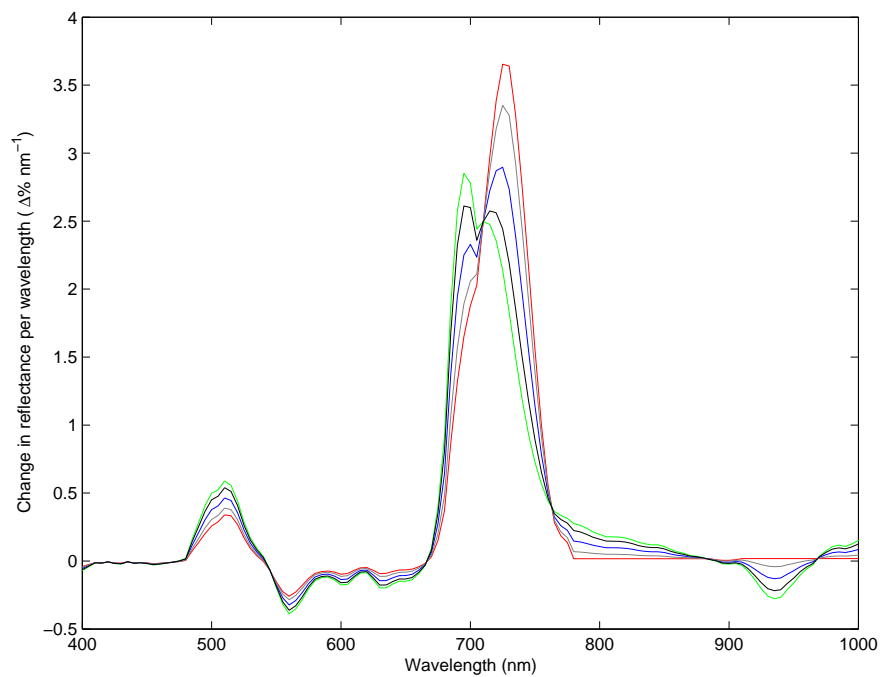
(b) First derivative reflectance spectrum (high levels of chlorphyll)

Figure 8.23: Transition between canopy components with different levels of chlorphyll content.

Where the green spectrum indicates a grass spectrum with a chlorophyll content of 60 mg.m^{-2}). The red spectra show an under-storey with a chlorophyll content of 220 mg.m^{-2}. Blue spectra marked a 50% mixture between the red and green and black a 25% or 75% mixture.

60 mg.m^{-2}, LAI 2.1) was mixed with an under-storey with input variables selected to promote high scattering in NIR wavelengths. This under-storey was modelled with four chlorophll contents, 10, 50, 100 and 200 mg.m^{-2} and four LAIs, 0.1, 1,2 and 4 (figure 8.24). From this investigation it was found that for an over-storey with a higher chlorophyll content than the under-storey, the difference in REP was 4.8 and 14.8 nm for 95% and 80% respectively. For an over-storey with a lower chlorophyll content than the under-storey, the difference in REP was 32.6 and 30.8 nm for 95% and 80% respectively. For the influence of an under-storey to he high, it was reasoned that the over-storey must be as open as possible (have a high ratio of gaps to canopy cover) to allow the influence of the under-storey to be expressed. Figure 8.24 shows the effect of different levels of LAI on the potential influence of an under-storey on the whole canopy reflectance spectrum. If the under-storey had a lower level of chlorophyll content (<60 mg m^{-2}) its influence was only evident when its % contribution was very high ($<80\%$). However, if the under-storey had a higher level of chlorophyll content (>100 mg m^{-2}) and a LAI of greater than 0.5 then its influence on the whole canopy reflectance spectrum cause cause a 1nm difference in the REP with 20% and a 2.5nm difference with 80%.

8.4.3   The influence of differences in absorption within a canopy

A grassland canopy includes a variety of floral species that are not grass. These different species, different grasses and the over-storey grasses may have different 'infinite' absorption characteristics. Certainly, the Slash Pine absorption spectrum in LIBERTY was different from the grass spectrum that replaced it for this study. The effects of the same grass spectrum displaced by 5 and 10nm to shorter wavelengths was investigated (figure 8.25). There was little noticable effect on the reflectance spectrum but when observed in the first derivative spectrum the shorter wavelengths were seen to move the short wavelength peak to shorter wavelength while having little influence on the long wavelength peak. Nevertheless, the use of a shorter wavelength aborption spectrum has little effect in the improvement of matching field spectra.

(a) LAI 0.1

(b) LAI 1

(c) LAI 2

(d) LAI 4
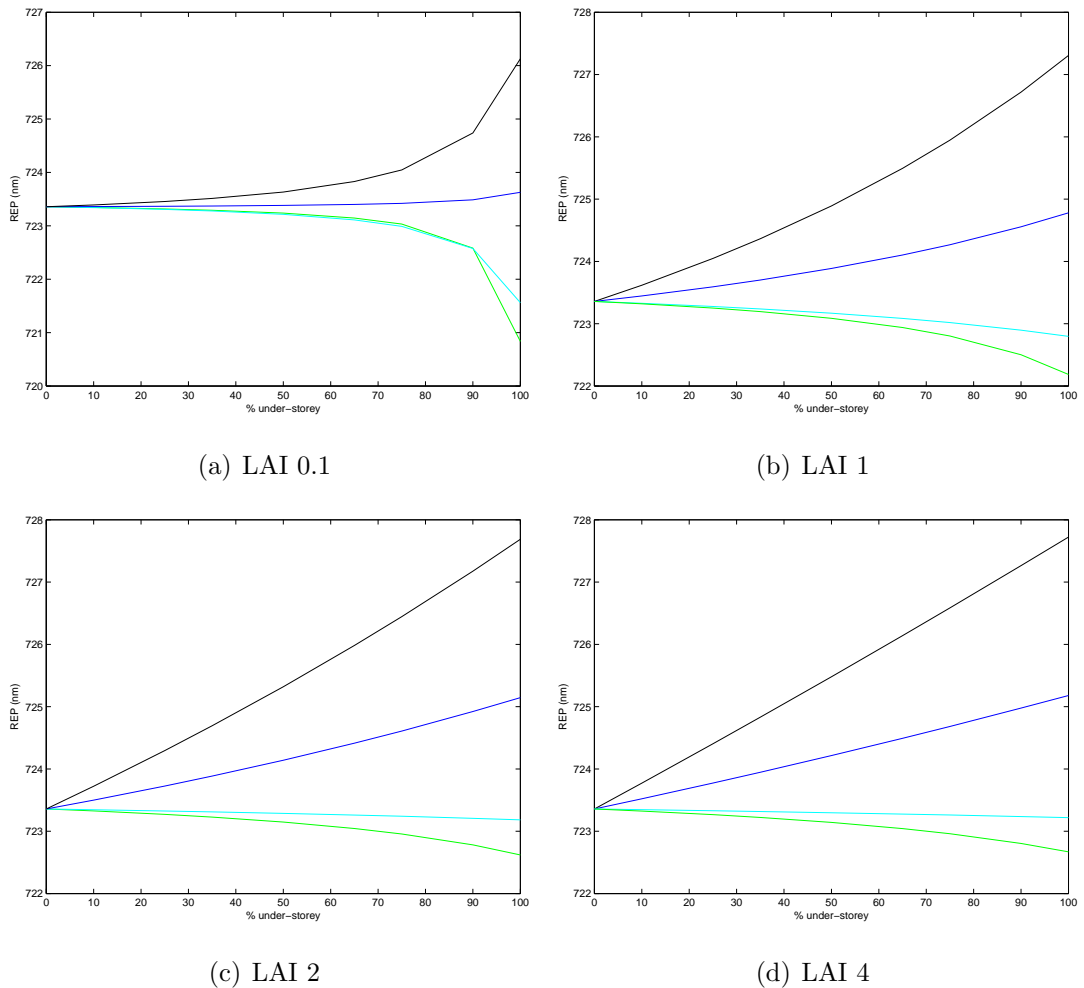
Figure 8.24: The contribution of an under-storey on the REP (Clevers *et al.* 2001). Green lines indicate a chlorophyll content of 10 mg.m^{-2}, cyan lines indicate 50 mg.m^{-2}, blue lines indicate 100 mg.m^{-2} and black lines indicate 200 mg.m^{-2}

(a) First derivative spectra   (b) First derivative spectra
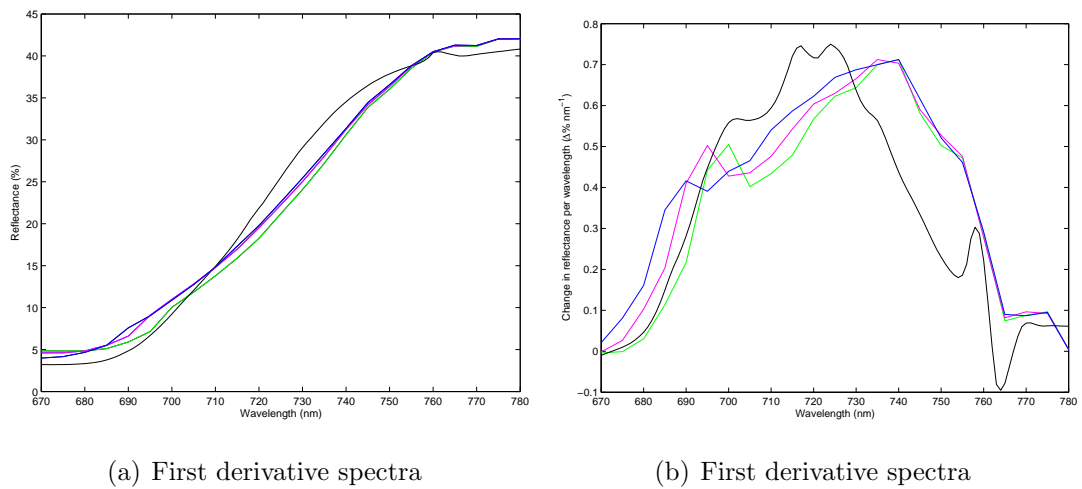
Figure 8.25: The influence of different under-storey absortpion spectra on reflectance
spectra.

The black line marks the field spectrum, green lines were derived from a LIBSAIL simulation
using a representative grass pigment as an input file, cyan lines were derived from a
simulation where the grass pigment was displaced by 5nm to shorter wavelengths and blue
lines where it was displaced by 10nm to shorter wavelengths

8.5   Discussion

LIBSAIL is a combination of two radiative transfer models specifically selected to simulate *Poa* species. While LIBERTY allowed the inclusion of variables to represent the cell structure of *Poa* species, SAIL enabled the investigation of the effects of LAI and LAD. The exact combination of variables that accurately represented grassland conditions was unknown because only some of the values could be (and were) determined from field measurements, others could not. Additionally, a single value was used to represent that variable throughout the whole canopy. This did not account for any variation within the FOV. Similarly, some variables (cell size and leaf thickness) provided a single value for the whole vegetation type, grassland. However, semi-natural grassland (especially contaminated grassland) are species-diverse environments. The presence of non-*Poa* species in the FOV meant that the spectrum contained a variety of disparate signals, some of which did not match those for which LIBSAIL had been optimised. LIBSAIL-modelled spectra matched field data most closely when the coincident data used to constrain the modelling process had high levels of chlorophyll content and high LAI. Within those bounds, LIBSAIL input variables had specific affects on the spectral red-edge (table 8.7).

Differences in the red-edge were determined by absorption (and fluorescence). The main influence on the red-edge was by chlorophyll content and the effect of differences in chlorophyll content on the REP were greatest when chlorophyll content was low (i.e. less than 150 mg m^{-2}). However, within LIBSAIL the reflectance range over which the red-edge extended was related to other variables (baseline, cell size and dimensions of air-voids within the leaf).

Furthermore, LAI and leaf thickness were related to the *magnitude* of both absorption *and* scattering effects; these effects were more directly calculated from the previously identified variables. Within this range of possible combinations of variables, there is considerable scope for equifinality; especially when chlorophyll content was low and within-the-leaf scattering was high. These are exactly the conditions found in grassland

stressed due to the actions of soil contamination.

8.5.1 Validation of LIBSAIL

LIBSAIL was capable of modelling grassland with different levels of soil contamination but in many cases this required the inclusion of a vegetated under-storey for which there were no data to constrain its modelling. When modelled with a single canopy the spectral match with field data was not as close as that found in chapter 7 for uncontaminated grassland. For the soil contaminated grassland approximately half the LIBSAIL-modelled spectra matched field spectra but two errors recurred, these were that the LIBSAIL-modelled spectra were too concave and/or had a different gradient of the red-edge slope. Inclusion of a vegetated under-storey allowed the field spectra to be matched and gave information on the conditions that may be present in the grassland under-storey but resulted in an over-estimation of spectral vegetation indices.

8.5.2 Over-estimation of spectral vegetation indices

Many of the spectral vegetation indices calculated from LIBSAIL simulated spectra were higher than those calculated from field spectra associated with the same location. This, and the concave red-edge slopes observed indicated an over-estimation of absorption variables and related to the discussion in chapter 6. If the measured chlorophyll contents were too high then the spectra modelled from their use as model inputs would be inaccurate. Such a situation would result in a red-edge spectrum with an excessively concave slope and high values for spectral vegetation indices. These were the conditions present. The main reservation concerning the accuracy of chlorophyll content measurements was that they may have been measured from a representative section of the vegetation and when then scaled up to account for the whole canopy using a measure of biomass this inaccuracy would be propagated to include non-photosynthetically active material. However, LAI was also an input to LIBSAIL and was measured from the majority of the vertical canopy profile. Therefore, it served to moderate any fail-

Table 8.7: The effect of high LIBSAIL input variables on the red-edge

Input variable	Effect on reflectance spectrum	Effect on first derivative reflectance spectrum	Evidence in field data?
Chlorophyll content	Low reflectance in red wavelengths	Determines the wavelength position of the maximum	Yes
Albino	Low reflectance in red wavelengths	Determines the wavelength position of the maximum	Partial /indications
Water	Low reflectance between 930 - 1010 nm	Deepening of a feature centered at 935nm	Yes
Cell size	Low NIR reflectance		Partial /indications
Air-void spacing	High NIR reflectance	Slight enhancement of the shortest wavelength feature	Partial /indications
Leaf thickness	Enhanced the effects of both absorption and scattering	Increased magnitude	Partial /indications
LAI	Enhanced the effects of both absorption and scattering	Increased magnitude	Yes

ings introduced by an inaccurate chlorophyll content. Additionally, high chlorophyll content levels did not explain all of the differences (e.g. a 'cross-over' mismatch) and when reduced chlorophyll levels were investigated they also did not provide a close match for some spectra.

8.5.3   Inclusion of an under-storey

The weak correlation between chlorophyll and REP (compared with that with biomass and soil hydrocarbon) in the field data indicated that either the field measured chlorophyll did not fully represent the grassland canopy or that REP did not fully represent chlorophyll in the field. REP was derived from reflectance data which itself was an integrated signal over an instrument's FOV. This contrasts with measurements of LAI which were unable to measure below a certain distance from the ground due to the dimensions of the probe or measurements of chlorophyll content (via use of a SPAD 502) which required leaves larger than the viewing aperture and deliberately concentrated on *Poa* species. Therefore, a possible discrepency was identified as being the ommitence of an important component of the canopy for the measurement of LAI and chlorophyll content. As measured chlorophyll content and LAI related specifically to the over-storey (or those leaves large enough to measure), it was likely that an additional canopy component, such as an under-storey, was an influence on the measured reflectance spectrum.

LIBSAIL allowed for the inclusion of an under-storey canopy with which a main over-storey canopy was linearly mixed. One effect of this process was to dilute the high chlorophyll levels and cause the red-edge to adopt a more convex form. However, the facility to model additional features in the first derivative spectrum identified the importance of under-story in an instrument's FOV. The influence of an under-storey was found to be significant if the over-storey had a low chlorophyll content and if its spectral form differed. However, because any match that relied on the unconstrained modelling of the under-storey and a 'best-fit' match the technique could only be used to indicate potential influences rather than statistical relationships. However, these

investigations found that the influence of an over-storey was greatest when the over-storey and under-storey had different absorption characteristic and when it had a high potential for NIR scattering. Grassland conditions allowed both to be present independently of each other. Additionally, an under-storey with low chlorophyll content could cause a particularly notable effect of the REP. A 95% over-storey with a chlorophyll content of 220mg.m^{-2} with a 5% contribution of an under-storey with a chlorophyll content of 60mg.m^{-2} resulted in a difference (against a 100% over-storey) in the REP of 2.2nm; a 80% to 20% mix of the same canopy resulted in a difference in the REP of 9.1nm (section 8.4.2). However, in similar conditions when the under-storey was configured for high scattering in the NIR the REP differences were as high as 32.6nm and 30.8nm (80% and 95% over-storey respectively. In each case because the linear interpolation and extrapolation methods were associated with the inflexion point they were more vulnerable to the effects of an under-storey (compared to the first derivative maximum) when chlorophyll content were low. Conversely, because the first derivative maximum switched from one first derivative peak to another at a threshold defined by the calculation of a maximum once at the longer peak was less vulnerable to the effects of a second canopy component, especially when if its chlorophyll content was high.

8.5.4 The importance of the pigment file

In addition, the variable that described chlorophyll content was itself derived from a vector input that described 'infinite' absorption. This vector was composed of not only chlorophyll *a* and *b* but also carotenoids, xanthophylls, display pigments and sensory pigments. It was a combination of these absorption responses that determined the wavelength position of the modelled red-edge. Additionally, as the input pigment spectrum was measured with an active, illuminated instrument it may also include a fluorescence signal. One omission in LIBSAIL was a variable and function to represent passive fluorescence, however, if it is incidentally included then quantifying its effect is almost impossible. The multiple peaks in the first derivative spectra were represented by (i) chlorophyll, (ii) by contrasting chlorophyll with albino and (iii) the presence of

two distinct canopy components. Therefore, passive fluorescence can not be regarded as the *sole* explanation for any long wavelength first derivative peak. Nevertheless, within the first derivative spectra of field data there was a constant feature at 718 nm. This was absent in LIBSAIL data and was not related to any identified characteristic of field spectra or related field data. Its cause is unknown but may relate to the effects of passive fluorescence.

The strong match between LIBSAIL-simulated spectra and those collected from an uncontaminated grassland compared to some areas of the grassland with contaminated soil was tracked to the comparison between the pigment file (input vector) with the spectral features of the red-edge. For the uncontaminated grassland the pigment file was at a slightly shorter wavelength while for the contaminated grassland it was at slightly longer wavelengths. Indications were that although both sites contained a similar range of grass species the additional species present in the contaminated canopy influenced the measured reflectance.

8.6   Conclusion

The modelling in this study served to explain a mismatch between the field results and the logical interaction of radiation and the grassland environment. The modelled grassland environment allowed a range of investigations to be conducted that would have been impossible in the field. To determine how and why spectral vegetation indices were more strongly correlated with the presence of soil contamination than vegetation state variables require the contaminated grassland to be understood. LIBSAIL was validated as capable for the accurate modelling of uncontaminated grassland. However, to fully account for the variation present in the grassland with soil contamination LIBSAIL had to also model the effects of a vegetated under-storey. This has allowed one of the hypotheses posed throughout this work to be tested. The proposal was that,

1. (H$_1$): *stress effects in vegetation (attributed to the effects of soil contaminants)*

can be detected using the position and shape of the red-edge of reflected radiation,

This work has supported this hypothesis by the identification of low levels of chlorophyll content. Chlorophyll was identified because in many grassland sites biomass and LAI are influenced by management activity. Therefore, chlorophyll content was the most releable target variable. Previous research (e.g., (Horler *et al.* 1980; Jago 1998)) has identified chlorophyll as vulnerable to the effects of soil contamination but because of differences in root depth the most obvious or dominant variation may not be affected by the presence of a contaminant in the soil. However, if within the vegetation canopy there is vegetation suffering stress effects then it may be identified in a vegetation spectrum despite the presence of longer wavelength features. Grassland spectra modelled by LIBSAIL showed that a small (5%) contribution of an under-storey with low chlorophyll content and high within-the-leaf scattering could cause a shift in the REP from that of the over-storey by upto 30nm. Even in conditions representative of the grassland with soil contamination a shift in the REP (from that of the over-storey) of over 9nm was identified. Therefore, even when an over-storey canopy shows no sign or effect of soil contamination an impacted under-storey can still allow the potential presence of contamination to be detected. However, within a grassland environment there is spatial variation of vegetation spectra. This variation extends both vertically within a canopy and laterally within a sensor's FOV and between different FOVs. If data from complex vegetation canopies are to be fully utilised in application such as the detection of soil contaminants the variation within then needs to be characterised and understood. Failure to do so will lose the important detail in the myriad of secondary vegetation interactions unrelated to the actions of any soil contaminant.

Chapter 9

Synthesis and discussion

9.1 Introduction

To fulfil the requirements of legislation, the concentration of a contaminant must be measured and compared with published levels that indicate if it is potentially hazardous and needs remediation. The identification and mapping of soil contamination to fulfil these requirements cannot be provided by remote sensing alone as these techniques cannot provide a measure of soil contaminant concentrations with the required degree of confidence or accuracy. This is because most terrestrial contamination is concealed in soil or covered by vegetation or artificial surfaces. Where vegetation is present, its interaction can, and has been, used to provide information on the soil in which it grows. These techniques are similar to those used by prospecting geologists in their search for minerals. Remote sensing can provide valuable assistance to the detection and mapping of soil contamination by dramatically improving the efficiency of the required field survey. Remote sensing can indicate the relative concentration and the extent of the effects of a contaminant. However, for situations other that those found on the contaminated grassland studied in this work, there is no guarantee that there is a measurable relationship between soil contamination and VIs. Only those remotely sensed observations accompanied by field measurements of soil contamination can be

330

attributed to a specific concentration. Nevertheless, considering the low number of soil measurements used in most soil contamination surveys (pers. com. N. Rogers, 2009) a means of ensuring that limited resources are best deployed can be valuable. The following chapter will: summarise the results presented in previous chapters, explore, develop and discuss how these build on the existing knowledge, identify further research and draw conclusions.

Previous research, conducted by Jago (1998), Hardy (2003), Smith (2002) and Kooistra (2004) showed that soil contamination could be identified using the spectral red-edge. However, although Jago's work identified potential effects of background in a grassland environment, it did not develop this line of research. Smith's work was more thorough but dealt with gas seepage as the main contaminant and used managed crops of barley, beans and radish as the studied vegetation. This was later extended to grassland (Smith *et al.* 2004) and has been developed by Williams *et al.* (2008). Kooistra's work primarily dealt with heavy metals deposited in a flood plain and Hardy examined tolerance in vegetation growing in contaminated soil (Hardy *et al.* 2001; Hardy 2003). Additionally, observations of the first derivative red-edge (Zarco-Tejada *et al.* 2003; Cho 2004) have increased our understanding of the vegetation effects that define the red-edge but have left many details that relate to a semi-natural grassland environment unexplained.

9.2   Synthesis of work

In chapter 5 the identification of soil contamination was considered in terms of a spectral response in the red-edge associated with the presence of soil contamination. In chapter 6 the role of chlorophyll and other vegetation state variables was considered in conjunction with measurements of soil and reflected radiation. These data allowed an evaluation of how soil contamination was detected, and determined the direction of investigation in the LIBSAIL modelled grassland environment (chapter 8). The importance of identifying the direct relationship between soil contaminants and vegetation,

and vegetation and the spectral red-edge, nested within the indirect relationship between soil contamination and the spectral red-edge, have been discussed at the end of these chapters and throughout this work.

The first stage in this investigation of the remote sensing of soil contamination was to establish the level of soil contamination present in the test. A second step was to identify if it had a measurable effect on vegetation. These measurements allowed the identification of soil contamination and the exploration of the red-edge. Within this body of research are three areas where observations and experiments have been developed beyond previous research. These are summarised below.

1. The relationship between soil-contamination and the red-edge (as reported in other research), including variation in the red-edge (REP and other VIs) as exemplified by 'switching' between different REPs as reported in chapter 5.

2. The multiple peak feature in the red-edge wavelength region of first derivative reflectance spectra (as reported in other research) and the range of possible causes for the effect (chapters 5 and 8).

3. The influence of an under-storey on the remotely sensed signal captured from a sample area (e.g., FOV) containing a multi-layered canopy.

These areas were explored through hypotheses based on field and laboratory observations and existing published results. The contribution of this work to these areas will be considered and evaluated in the discussion.

9.2.1   Hypothesis testing

The relationship between the data sets: soil, vegetation and VNIR spectral data, were used to test the hypotheses. The first hypothesis (posed in chapter 5) evaluated soil and spectral data and explored and supported the general capability for detection of hydrocarbon contaminants by the use of VIs. The latter three hypotheses (posed in

chapter 6) evaluated vegetation state variables in relation to other data. The investigation of these intermediate relationships explained the indirect relationship between soil contamination and the red-edge investigated by the first hypothesis. These hypotheses stated that:

1. (H_1): *differences in the relative concentration of contaminants in a grassland soil can be detected using the position and shape of the red-edge of reflected radiation,*

2. (H_1): *stress effects on vegetation (attributed to the effects of soil contaminants) can be measured in the vegetation that grows in that soil,*

3. (H_1): *stress effects on vegetation (attributed to the effects of soil contaminants) are greater than those found by natural variation,*

4. (H_1): *stress effects on vegetation (attributed to the effects of soil contaminants) can be detected using the position and shape of the red-edge of reflected radiation,*

- *differences in the relative levels of soil contamination could be identified using the spectral red-edge.*

- *the degree by which chlorophyll content or LAI are influenced by the effects of soil contamination is sufficient to be identified by differences in reflectance spectra,*

- *chlorophyll content or LAI are influenced by the effects of soil contamination* and

- *chlorophyll content or LAI influence reflected solar radiation as seen in reflectance spectra.*

Results from testing these hypotheses led to the use of a model (LIBSAIL). This model could simulate the spectral red-edge for simple grassland conditions but not for those found in a contaminated grassland. However, conditions of contaminated soil could be simulated by two spectra combined. The characterisation of the grassland study sites for the testing of hypotheses and the driving of LIBSAIL depended on field and laboratory measurements. The limitations on all measurements (and simulations) will

be evaluated below and allows a means to investigate the strength of conclusions derived from them. This will start with a consideration of the sampling scheme used, the data collected and the relationships explored to test the hypotheses.

9.2.2   Methods

From the onset, the field data collected in this research were designed to support airborne data. However, during the course of the research it was discovered that the richest areas of new research related to spectral resolutions finer than those that may be acquired from airborne systems that were current in the UK. Itres CASI-2 data were acquired (by the NERC ARSF) and REP maps were created but these duplicated the of research of Jago (1998). The data have the potential to explore the spatial variation of a REP over a contaminated grassland but that work is not included in this thesis.

The type and quality of data used in this research was determined by the manner in which they were collected. Data collected to support this research were of four broad types: (i) soil samples and measurements, (ii) vegetation samples and measurements, (iv) spectral measurements and spectral simulations using the LIBSAIL model. LIBSAIL data were trained and validated using vegetation and spectral measurements. Within the individual sets of soil, vegetation and spectral measurements, some variables were correlated. These correlations were related to common processes, e.g., atmospheric deposition (cadmium, copper and zinc) or vegetation growth (LAI and biomass) or methods of calculation, e.g., biomass and chlorophyll content. As these data sets provided the basic components from which the wider indirect relationship (between soil contamination and spectral data) and the intermediary direct relationships were formed, an examination of the strengths and weaknesses of these data sets will be considered in the following subsections.

9.2.3   Data

Data were collected using either a stratified random grid or a transect. Both were used to characterise areas identified in the initial consultant's survey (ERM 2000) but the grid was used specifically to extend a characterisation of the soil, vegetation and spectra to a defined area in preparation for further analysis using an airborne multi-spectral data set (Itres CASI-2) collected by the NERC Airborne Research and Survey Facility. Vegetation measurements and samples were supplemented with spectral measurements at the same time but soil sampling was conducted several months later. Unfortunately, markers to match the different sampling surveys had been removed. Nevertheless, because each measurement point was surveyed the relative positions were determined after the soil samples were extracted. Specific point measurement issues will be discussed in each data subsection.

9.2.3.1   Soil data

The contamination in the main study site was by long-chain aliphatic hydrocarbons in the soil, although low concentration levels of heavy metals were also present. The concentration of these contaminants was broadly indicated by a consultants report but was more precisely determined by laboratory analysis. Grids 3 and 6 and transect 7 contained the highest levels of contamination in the soil. These data were used as a baseline for the rest of the work. To test the first hypothesis, the levels of soil contamination present within 6 grids were quantified using a total of 161 soil samples. Loss-of-ignition (LOI) levels, total extracted hydrocarbon (TEH) and specific heavy metals were significantly different between the 6 grids on the contaminated grassland site (R^2=0.61, P<0.05, n=6). However, the concentration levels of heavy metals were low compared with ICRCL action levels. The highest LOI and TEH averages (mean and median) were indicative of the presence of high levels of long-chain aliphatic hydrocarbon contamination in the soil, e.g. gasoline (C_{8-11}), diesel (C_{12-15}), paraffin (C_{25}) and asphalt (C_{35}). Individual samples did not correlate with any spectral anomalies in the red-edge region. The grassland soils in most grids were alkali but acid patches

(pH 1.5) were only evident in one grid. However, these were not distributed widely enough for inclusion as anything other than observations. The distribution of metals matched known associations with hydrocarbons and by local atmospheric deposition. These measurements established the levels of contamination. Without them, the comparison would only have been a general association derived from the initial sparse measurements described within the environmental consultants report ((ERM 2000).

9.2.3.2   Vegetation data

There was less variation in chlorophyll concentration from grassland with high levels of soil contamination than that measured from grassland with low levels of soil contamination. However, this was most likely to be due to an under-representation of the range of vegetation within the more contaminated areas. Chlorophyll concentration was derived from SPAD 502 measurements and these were measured *specifically* from grass leaves because the transformation equation to derive chlorophyll concentration was vegetation-specific. An additional practicality of using a SPAD 502 was that measurements were taken from the widest, most consistent section of each grass leaf. Most suitable leaves were found in the over-storey layer of the canopy, other suitable leaves were found lower in the canopy (the under-storey) but were from mature plants more representative of a low over-storey.

Unlike biomass and LAI, the percentage cover of grass was correlated to levels of soil contamination. It was lowest where there were high levels of soil contamination and highest where there were low levels of soil contamination. Therefore, the estimate of chlorophyll concentration for areas with a high level of soil contamination was derived from a far smaller sample than for areas with a low level of soil contamination. The percentage cover of grass not only influenced the amount of grass in a FOV but also indicated differences in the canopy structure, particularly the presence of an understorey. This was because those areas with very high percentages of grass cover (greater than 80%) typically had a less defined under-storey. In other areas, because grass was commonly the most chlorophyll-rich vegetation in a FOV, this methodology prob-

ably overestimated chlorophyll concentration. This was particularly true for highly contaminated areas.

The problem was compounded when chlorophyll concentration was transformed to chlorophyll content using biomass. This related chlorophyll concentration to a m^2 area. Additionally, the transformation equation used to estimate chlorophyll concentration from SPAD 502 measurements (derived by regressing *106* observations) was significant, but weak (R^2=0.5, P<0.01, n=106). The weak strength of the regression equation was attributed to the use of an old broad waveband analogue laboratory spectrometer. Chlorophyll content was derived from SPAD 502 and biomass measurements. Any failure to collect all the biomass (including the under-storey) will have introduced inaccuracies.

The spatial variation in spectral measurements was not evident in the over-storey canopy. Sampling errors have been identified for the measurement of chlorophyll concentration and content, but this variation was also not evident in measurements of LAI or biomass. The situation was complicated because vegetation measurements sampled different sections of the vegetation canopy. The limitations of chlorophyll concentrations measurements to the over-storey have been identified in the previous paragraph, LAI sampled the canopy from its top to its lowest few centimetres, biomass sampled the canopy from the top to the lowest few millimetres but was poor at capturing non-planiphile leaves in the lowest centimetre. In contrast, spectral measurements captured the whole canopy. Therefore, any canopy component correlated to the variation observed in the spectral data would have to be in the lowest few centimetres of the canopy. Field observations introduced the potential importance of the under-storey canopy to the recorded spectral measurements within the FOV, especially as grassland was not observed at any location to have a closed canopy. The observed presence of lush green vegetation in close vertical proximity to yellowed and wilted vegetation supported the possibility that markedly different vegetation types could contribute to the remotely measured data. Simulations of grassland (using LIBSAIL) showed that spectral features in the red-edge could be determined by the under-storey when the over-storey vegetation had low chlorophyll concentration. This was a possible scenario in this

environment.

9.2.3.3   Spectral data

To support the data from the soil samples, reflectance measurements were made at 367 locations. It was not possible to precisely co-locate these with the soil samples but the 22 locations where a reflectance measurements were made within 2m of where the soil was sampled were used to determine the association between these two data sets. Spectral data were collected using two GER1500 spectroradiometers in dual beam mode. These data were analysed as reflectance spectra, first derivative reflectance spectra and as VIs. Spectral data collected from areas with different levels of soil contamination and areas with no history of soil contamination were different. Spectra collected from areas with high levels of soil contamination had a generally more convex red-edge, a more pronounced short wavelength first derivative peak (in red-edge wavelengths) but could also show signs of an area of rich growth, a concave red-edge and a more pronounced long wavelength first derivative peak (in red-edge wavelengths). However, the reverse was not found, i.e., in areas where there was no soil contamination the the red-edge was not convex and the short wavelength first derivative peak was not evident.

As the red-edge wavelength region was the primary region of interest.The sensitivity of the spectral red-edge to both absorption and scattering by cellular structure made it more difficult to separate the relative influence on the spectrum of chlorophyll content from LAI and biomass. The continuum removal technique was investigated and had the potential to normalise the general form of the red-edge and thereby remove effects which are primarily related to within-the-leaf scattering. However this would have required each spectrum to be reconfigured in relation to the maximum absorption and scattering. This would bias one component of the canopy with little or no indication of the degree of bias applied. Therefore, because the analysis of variation within the red-edge wavelengths was of particular interest, derivative analysis was used in preference. This allowed the spectral features within the red-edge to be examined while preserving the relative contribution of the vegetation component. The subtleties of the red-edge

were *most clearly observed* in the fine resolution (<5 nm) first derivative reflectance spectra as described by other works (e.g. Smith 2002 (2002), Cho 2004 (2004)). Multiple peaks were present in the first derivative field spectra. These approximated the 690 nm, 710 nm first derivative peaks observed by Jago (1998), the 702, 718, 725, 735 and 760 nm first derivative peaks observed by Smith (2002), the 700, 716, 724 nm first derivative peaks observed by Clevers *et al.* (2004) and the multiple first derivative peaks around 700, 720, 730 and 760 nm observed by Cho (2004). Generally, in the spectral data collected in this work three peaks were present, though the exact wavelengths differed by up to 10 nm. These three peaks led to the classification of three first derivative spectral profiles. The spectral profile with a obvious short wavelength peak was related to locations with high levels of hydrocarbon contamination in the soil. However, the spectral profile with a obvious long wavelength peak was related to locations with low or high levels of hydrocarbon contamination in the soil. The spectral profile with a flat or dominant middle wavelength peak was related to intermediate conditions and was poorly modelled by LIBSAIL.

9.2.4   Spectral vegetation indices

To manage the large number of VIs (including REPs), a Matlab script was written to automatically calculate VIs from spectral data. This enabled many spectra to be evaluated and associated patterns to be derived. Of those VI calculated, the most successful for the identification of soil contaminated by hydrocarbons were the REPs. Differences in convexity in the red-edge weakened the basic assumption of the linear interpolation method for the determination of the REP. Nevertheless, this method of calculating REP produced strong correlations with levels of soil contamination (particularly TEH) and the strongest correlation was achieved by an 'optimised linear interpolation' method for the determination of the REP. Instead of using set wavebands, this technique used maximum and minimum values to determine the position of half red-edge reflectance (the wavelength of this position determined the REP). It was therefore more flexible at capturing the local specific conditions while maintaining

a consistent basic methodology. Those ratio-based VIs that used red-edge wavelengths (especially in the derivative spectra) also were correlated with levels of hydrocarbon contamination in the soil (e.g., D_{725}/D_{702}, Smith 2002 and D_{730}/D_{706}, Zarco-Tejada *et al.* 2003. A similar 'optimised' approach was trialled with narrow first derivative wavebands but delivered equivalent results to the original. Other trials using maximum and minimum values (with set wavelength ranges) to provide 'reactive' / 'flexible' spectral vegetation indices gave only a marginal advantage over the fixed wavelength originals. Generally, spectral vegetation indices had a negative relationship with the presence of soil contamination. Narrow band wavebands (especially when 'optimised') were better correlated with soil contamination than broad wavebands because they allowed a clearer distinction between absorption and scattering features and were more precise in the determination of the wavelength where these effects were strongest. The search for the greatest contrast between absorption and scattering features for different applications based on different vegetation types, soil conditions and sensors may account for the many published VI and the variable results obtained when they are used by different researchers for circumstances that differ from those for which they were devised.

9.2.5 Relationships between soil hydrocarbon contamination and spectral vegetation indices

The strongest correlation with TEH (LOI and Ni) were found with REP. Of these the 'optimised' linearly interpolated REP was the strongest (R^2,0.28, P<0.01, n=36). Spectra measured from grassland with high levels of soil hydrocarbon contamination (grid 3 and transect 7) had a greater variance than other areas. Conversely, grassland with low levels of soil hydrocarbon contamination (grid 2) had the lowest variance. The use of variance proved a clearer means for identifying relative levels of contamination than specific VIs. A comparison of transects across areas with different levels of soil contamination showed a higher frequency of switching between the short wavelength REP and long wavelength REP in the first derivative maximum REP. This related to

the relative dominance of first derivative peaks between a short and long wavelength positions. Grassland with low levels of soil contamination had most of the REPs at long wavelengths. Grassland with intermediate levels of soil contamination had sections where the REP alternated between short and long wavelengths and grassland with high levels of soil contamination had a high frequency of 'switching' between long and short REP. The reasons for this effect may be attributed to the distribution of coherent patches of contamination. Use of variance would require a number of measurements for the statistics to be calculated in order to assess an area. This may be possible using airborne data if the resolution allowed sufficient pixels to characterise the spatial scale of soil contamination. In this instance, a moving variance window may allow the identification of the presence and extent of soil contamination.

9.2.6   Direct relationships between variables

The conceptual model assumes a relationship between soil contamination and vegetatio state variables, and between vegetation state variables and the red-edge but a weaker relationship between soil contamination and the red-edge. However, the statistical strength of the indirect relationship between soil contamination and the red-edge was strongest. For example, VIs had stronger relationship (negative) with TEH (REP, R^2=0.28, P,0.01, n=36) compared with chlorophyll concentration and content (R^2=0.23, P,0.01, n=136). There were several reasons why these weaknesses in the conceptual relationship could be present:

- errors in vegetation measurements,

- errors in spectral measurements,

- errors in spatial matching of vegetation and spectral measurements,

- another unmeasured factor influencing the VI other than the soil or over-storey vegetation.

The spatial variation of vegatation and spectral variables was evident but considerable effort was applied to the matching of these data with accuracies comparable to that of the FOV of the spectroradiometer (18cm diameter). Therefore, the most likely weakness was identified as relating to the measurement of vegetation state variables (as discussed in section 9.2.3.2). The way in which vegetation state variables link soil hydrocarbon and spectral measurements will be summarised and considered in the following subsections with specific regard to the weak link between vegetation measurements and VIs. This coupled relationship was fundamental to the remote sensing of soil contamination using the spectral red-edge.

9.2.6.1   Soil and vegetation state variables

Hydrocarbon contamination has a negative effect on the growth of vegetation. Within areas with high levels of contamination, the range of species was different and more diverse than that of areas with low levels of contamination. A strong negative statistical relationship was present between chlorophyll content and TEH (R^2=-0.43). However the strongest relationship was between chlorophyll concentration and copper (Cu), chlorophyll concentration and zinc (Zn) (R^2=0.47 and 0.45 respectively). These metals match the overall pattern attributed to atmospheric deposition (without the higher run-off attributed to the hydrocarbon contaminated areas) and therefore may indicate the absence of hydrocarbon contamination rather than a growth enhancing effect.

9.2.6.2   Spectra vegetation indices and vegetation state variables

Spectral vegetation indices were developed to estimate vegetation variables and strong statistical relationships are commonly reported in published literature (e.g. chlorophyll content estimates in a grassland by Pinar and Curran 1996). Within this study, the strongest relationship between chlorophyll and a VI (most REPs) was R^2=0.33. While significant, this was weaker than that found for the indirect relationship between spectral VIs and soil contamination.

The limitation of the methodology for the estimation of chlorophyll content have been discussed in a previous section. However, indications are that the over-storey that contributed most of the vegetation data only accounted for a portion of the vegetation spectral signal measured. The most comprehensive vegetation measurement was biomass because it was a sample of the whole canopy. Consequently, VIs were more strongly correlated with biomass than chlorophyll (content or concentration). It can be concluded that the most likely cause for the weaker relationship, in this study, was because measurements were regressed against vegetation variables sampled from the over-storey rather than the whole canopy. In many other studies, the grassland vegetation was managed ryegrass (*Lolium sp.*) and clover (*Trifolium sp.*) and therefore did not have the diversity present in the environment studied in this research.

It was technically and logistically difficult to measure any grassland vegetation other than the over-storey. This was partially due to limited manpower and availability of time but also the adverse condition of the site (contaminated such that protective clothing needed to be worn and the soil could only be penetrated under controlled and limited conditions). One option of experimenting in ways not possible in the field or laboratory is modelling. LIBSAIL is a combination of the radiative transfer leaf model, LIBERTY (Dawson 1999), with the radiative transfer canopy model, SAIL (Verhoef 1984), translated into Matlab. LIBERTY was selected due to its capability to model a dense cellular bundled structure as found in grasses (*Poacecea*).

An approximation of field spectra was simulated using measurements of typical values for vegetation in variables in semi-natural grassland (as sampled from Southampton Common and Thorney Island). However, the more complex canopies and less managed canopies had weak relationships when assessed against field data.
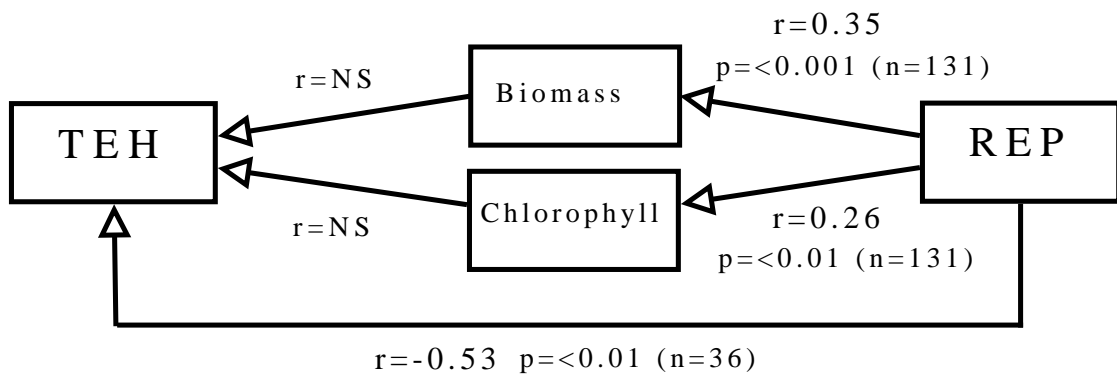
Figure 9.1: The remote sensing of hydrocarbons in soil (correlations)

9.3 Discussion

Within the scope of detecting soil contamination (and areas of soil contamination) a series of specific research issues were investigated. These developed existing published research, provided new direction for future research may be directed and indicated areas where improved field methodology and awareness would enhance the collection of data from complex vegetated environments. Each issue will be considered within this discussion, although the focus will be on the provision of an effective supplement to existing methods of assessing soil contamination. In this research, differences in the red-edge were correlated with differences in the level of hydrocarbon in grassland soil. Therefore, this wavelength region was identified as being particularly suitable for the detection of soil contamination. This study aimed to assess the success of the use of spectral data for the identification of relative levels of soil contamination.

Jago *et al.* (1999) considered the VNIR and SWIR wavelengths and found the red-edge to be a strongest wavelength region for the detection of hydrocarbon contamination in grassland soil. Similarly, Smith *et al.* (2004) and Williams *et al.* (2008) identified the same wavelength region as capable of detecting methane seepage in soil. The results from this study supported those of these previous studies and showed a spectral response correlated to the presence of hydrocarbon contamination in grassland soil.

9.3.1   Influences on the red-edge

The widening of the biochemical absorption features may be due to two processes. The first is the widening (deepening) of absorption, associated with increases in concentration as described by the Lambert-Beer law. The second process is due to the presence of different chlorophyll species (French *et al.* 1972; Barzda *et al.* 1998). The chlorophyll *a* molecule has three tautomeric isomers (chapter 3) but differences in chlorophyll species are formed from the excited energy states possible in single (monomer) or associated (dimers and trimers) chlorophyll molecules. When excited trimers triplets can extend its absorption maximums at 740 nm. Such excited molecules act as accessary pigments and are called long wavelength chlorophylls. Healthy vegetation canopies are more prone to have less stable more productive absorption effects that extend to longer wavelengths than those in diverse, harsh conditions.

9.3.2   Convexity in the spectral red-edge

The convexity of the red-edge determined the wavelength position of peaks in the first derivative spectrum. Convexity was crudely recorded by the comparison of three wavelength positions (650, 720 and 780nm) but was generally classed as concave, linear or convex. Within this research the first derivative spectrum was classified into three spectral profiles. A convex red-edge was related to a spectral profile with a prominent short wavelength peak and to high contamination conditions. A concave red-edge was related to a spectral profile with a prominent long wavelength peak and low contamination conditions. A combination of previously published research and field and LIBSAIL simulated spectra related these differences to levels of absorption. Therefore, the premise that multiple peaks were related to multiple absorption effects was considered. In field spectra there were three main peaks in first derivative spectra. However, in the single canopy version of LIBSAIL there were only two peaks. The single canopy version of LIBSAIL only had two absorption variables that related to the red-edge range of wavelengths (chlorophyll and albino). LIBSAIL was also used

to simulate an over-storey and and under-storey canopy and provided four potential absorption variables. Consequently, up to four first derivative peaks could be simulated (when using a second pigment file).

9.3.3 Spectral features in the first derivative reflectance spectrum

In this study, although the relative position of first derivative peak was consistant the exact wavelength position differed between different grasslands and different location on the same grassland. However, in general the shortest wavelength peak was prominent for low chlorophyll conditions whilst the longest wavelength peak was prominent for high chlorophyll conditions. Of the three identified peaks (short, middle and long wavelength) the shortest wavelength peak decreased in height as the amount of chlorophyll increased. This continued to a point where the short and long peaks were approximately equal. Higher amounts of chlorophyll caused an increase in the longer wavelength peak with a steady obscuring of the shorter wavelength peaks.

An important component regarding the multiple peaks in the first derivative reflectance spectrum was related to fluorescence (Zarco-Tejada *et al.* 2003). Nevertheless, this effect did not fully (or solely) account for what may be observed in field spectra. If one of the peaks was solely related to fluorescence then more consistency in the wavelength position of one of the longer wavelength peaks would have been observed. In a sequence of different chlorophyll concentrations from low to high the short wavelength peak increased and then decreased before the longer wavelength peak became dominant. The same relationship was simulated with LIBSAIL with additional canopy components and high chlorophyll causing shorter wavelength peaks to be obscured.

9.3.4   Variation within the field-of-view

Field data showed a stronger correlation between the REP and total extractable hydrocarbon than chlorophyll concentration. This mismatch was related to two issues. The first was possible over-estimation of chlorophyll concentration (and content) as considered in section 9.2.3.2. The REP was related to absorption and scattering effects within vegetation in the whole FOV while most chlorophyll concentration was measured from the canopy over-storey. Curran and Williamson (1988) identified non-uniformity of grassland vegetation within the FOV as one source of variation in absorption and scattering. Although the red-edge wavelength region is sensitive to the influences of both absorption *and* scattering (Curran 1980), only absorption was wavelength dependent in the LIBSAIL modelled environment. Scattering in LIBSAIL was wavelength-independent and served to determine the maximum reflectance of the red-edge shoulder. The shape and wavelength positions of the red-edge were defined by absorption. Variation in a canopy can been at the leaf scale any in terms of canopy layers.

Leaves grow from their bases (Schutt *et al.* 1984) and migrate the highest, most stable distribution of chlorophyll towards the leaf tip. Some of the observed variation in chlorophyll concentration measurements (via the SPAD 502) was consistent with a greater biochemical and physiological maturity towards the leaf tip compared with the leaf base (Schutt *et al.* 1984). Therefore, absorption will be highest further from the leaf base. Variation was associated with multiple absorption features and this in turn was associated with multiple canopy components. A diverse vegetation profile (laterally and vertically) yielded more variation in recorded radiation spectra than a relatively uniform vegetation profile. However, while variance in a canopy was difference between locations averages were often the same.

9.3.5   The role of a vegetated under-storey

As grassland spectra are influenced by standing litter (Asner 1998), the influence of a photosynthetically active under-storey canopy component was logically even greater. Within a simulated environment (LIBSAIL, with a simulated over-storey and an under-storey) it was found that a 10% additive mixture of a chlorophyll-rich under-storey and a 90% chlorophyll-poor over-storey was dominated by the under-storey. Therefore, a validation of spectra based solely on over-storey vegetation variable would give unrealistic and misleading results. Nadir view photographs of study quadrats (figure 6.8) and the difference in species composition within each grid in the soil contaminated grassland showed the differences in the community composition of different areas and the difference in spatial variability each community.

Modelling allowed the effects of an increase in chlorophyll to be observed and for the linear mixing of a chlorophyll-rich spectrum with a chlorophyll-poor spectrum (i.e. simulating an over-storey and an under-storey). Both conditions simulated effects observed in field spectra. with the caveat that, because some variables relevant to field conditions were not measured, typical values were used. Additionally, the limit of LIBERTY's 5 nm resolution, meant that many narrow features observed in spectra collected using the GER1500 could not be matched.

9.3.6   How does spatial variation affect the detection of soil contamination?

Although many of the vegetation variables had similar averages, their ranges of variation differed. Variation was greatest in those areas where soil contamination levels were highest as highly contaminated areas of grassland had both very high and very low vegetation variable values and a high species richness (chapter 6, table 6.2). Consequently, spectral variation was greatest in grid 3 and transect 7 (no spectral data were collected in grid 6); this corresponded to high variation in soil variables (TEH, LOI and pH) and

vegeation variables (chlorophyll concentration). The conflicting presence of enhanced growth related to areas of highly contaminated soil would have made the identification of contamination from VI alone . However, this research found that spatial variability was a stronger indicator of hydrocarbon contamination in the soil than the spectral signal. This variability was related to the dual effects of impeded growth and enhanced growth; the former related to toxic effects and later to fertilisation. The implication is that any field survey that assessed spatial variability would need to cover a wide area with a sufficient sampling interval to capture the variability in the scene. In this study, transects of field data were used to investigate the principle for an assessment of soil contamination, these data would most efficiently be collected by the use of remote sensing. For grassland a sampling interval of 0.5m was found to be effective and transects showed the first derivative maximum to exhibit a high frequenct of switching between short and long wavelength positions when covering areas with high soil contamination.

9.3.7   The influence of grassland management

The remote sensing of contamination is complex and is obscured by other factors. Grassland can undergo management treatments that affect its biomass (e.g. mowing or grazing), growth vigour (e.g. fertilisation) and stress levels (e.g. flooding or pest control). Because remote sensing of soil contamination is based on an indirect relationship, other potential stressors could cause a measured response and these needed to be identified and evaluated. A second issue for the evaluation of stress by the effects of soil contamination is the normal background variation. For any effect to be attributed to soil contamination, it must exceed any response found in uncontaminated areas. One problem here is the multitudinous array of stress effects. These can have an additional effect when considered with respect to the time since contamination occurred and the regularity of any contamination (a single or a regular event). The effects of these factors mean that evolved tolerance (e.g. Hardy et al. 2001) and the potential for changes by virtue of invasive species more suited to the new conditions need to be identified and evaluated before any realistic assessment of soil contamination can be made. It is

these effects that are likely to lead to the spatial variability observed in this research.

To utilise red-edge spectra for the detection of soil contamination the establishment of background measurements that establish both averages and the degree of variation is needed. Without these measurements the relative effects of soil contamination cannot be evaluated but the implication is that the uncontaminated areas need to have similar management regimes and similar vegetation profiles as the contaminated sites. This presents analogous restrictions as those presented by the need for stationarity in geostatistics.

9.3.8   The influence of phenology

Green leaf phenology is the temporal pattern of seasonal leaf development and senescence as determined by climate, day length, species type, age and substrate (Schaber and Badeck 2003), see also section 3.7.4. Differences within this range affect the comparison of vegetation data sets. The standard sequence of phenologic change is greening up, maturity, senescence and dormancy (Fenner 1998, Zhang *et al.* 2003). Methods of evaluation, based on this sequence, are ideally applied to a nested sequence of vegetation classes (continual, subannual, annual and supra-annual) (Newstom and Frankie 1994). Both date and time of the day can affect what is viewed in an area of grassland and therefore can influence the the spectral red-edge (e.g Miller *et al.* 1991) over large grassland areas (Butterfield and Malmström 2009).

The specific grassland structure (see section 3.4) and the diurnal variation (see subsection 3.4.3) present specific problems that would need to be investigated using a focused experimental design. Added to these variables, are those of anteceedent conditions and annual differences (differences between years). To fully consider these factors would need time (several years) and resources beyond the scope of this thesis. Throughout this thesis, dates and times have been reported to allow comparison with other data sets.

This study was focused on evaluating the spectral effects of soil contamination. Comparitive sets of measurements, between areas with different levels of soil contamination, were collected within a day of each other. There may have been some diurnal changes because field data were collected throughout the day (up to three hours either side of solar noon) but these were not evident from field observation. The comparison between this site and other sites is limited because data were collected at different dates and times of the day. Even a repeat of vegetation measurements from the grassland with different levels of soil contamination would be limited because growth differs between years.

9.3.9 The use of *a priori* information

The detection of minerals through their influence on overlying vegetation has a long history but the provision of the extra information required for an assessment of soil contamination needed a measure of the uncertainty incurred in the soil contaminated environment to be understood. This required *a priori* knowledge of a number of factors. These included general properties related to the vegetation type, e.g. average and variation in root depth, management regime, e.g. mowed, grazed or left alone; and specific information relating to the site, e.g. the approximate period and nature of any contamination. In those situations where the time period after the last contamination event may be measured in years additional consideration may need to be evaluated; foremost of these are the evolution of a tolerance to the contaminant and the presence of other stress effects. Nevertheless, the evidence that soil contamination had a negative impact (and in many cases a short term positive) effect on plant growth is strong. Many successful studies have utilised agricultural grassland with a defined and controlled *Trifolium sp. Lolium sp.* (clover / ryegrass) cover optomised for forage grazing efficiency or used specially planted monocultures. Industrial sites tend to have a more ruderal and diverse grassland vegetation mix.

Although, many vegetation indices and spectral features were correlated to soil contamination the strength of this relationship was weaker than that found by many other

studies. To fully exploit the use of remote sensing for the detection and mapping of soil contamination these vegetation-related uncertainties were investigated.

9.3.10   Improvements may be made to the collection of vegetation data in support of remote sensing

This research found that the potential influence of a vegetated under-storey on the measured spectral reflectance and highlighted the importance of characterising the whole canopy, especially in a diverse vegetated enironment. The nature of soil contamination is that it is very dependent on a range of site and time specific variables. These include the contaminant, concentration, vegetation cover, management regime, climate and time. Specific measurement conditions (e.g. time of day and season) can control some variables whilst support measurements can control others (e.g. identifying the contaminants present). However, the collection of field data from vegetation canopies to train, drive or validate models is dependent on the nature of the canopy (figure 9.2).

The combination of an incomplete over-storey canopy closure and the presence of an under-storey canopy coverage was common in a grassland environment. Observations were supported by modelling using LIBSAIL (chapter 8) and showed that total canopy reflectance integrated from two canopy components (e.g. an over-storey and a under-storey) could be influenced by one of them having a high level of chlorophyll content, even if that component contributed a minor proportion of the signal. A grassland environment was simulated with LIBSAIL where a high biomass, low chlorophyll content, erectophile over-storey was contrasted by a semi-obscured, high chlorophyll content, planophile, under-storey. In this setting the under-storey influenced the total canopy reflectance even when the under-storey contributed only 5% of the signal. Therefore, where there is an under-storey, the common practice to base field validation solely on the sampling of the over-storey is flawed. The implications of this for field validation are considerable. A solution would be to re-measure the spectrum from each location after in situ vegetation measurements have been made and the complete over-storey

biomass removed. If a reliable estimate of the contribution of the under-storey (e.g. by spectral un-mixing) can be made, the specific contribution of the over-storey may be determined and the whole vegetation canopy contribution used for validation with confidence. The following systematic method is suggested to allow for such a result (figure 9.2). Additionally, to record the spatial dimension of these data these vegetation measurements should be recorded along a transect (or densely sampled grid) with sufficient samples to provide statistical strength to any evaluation (50-100).
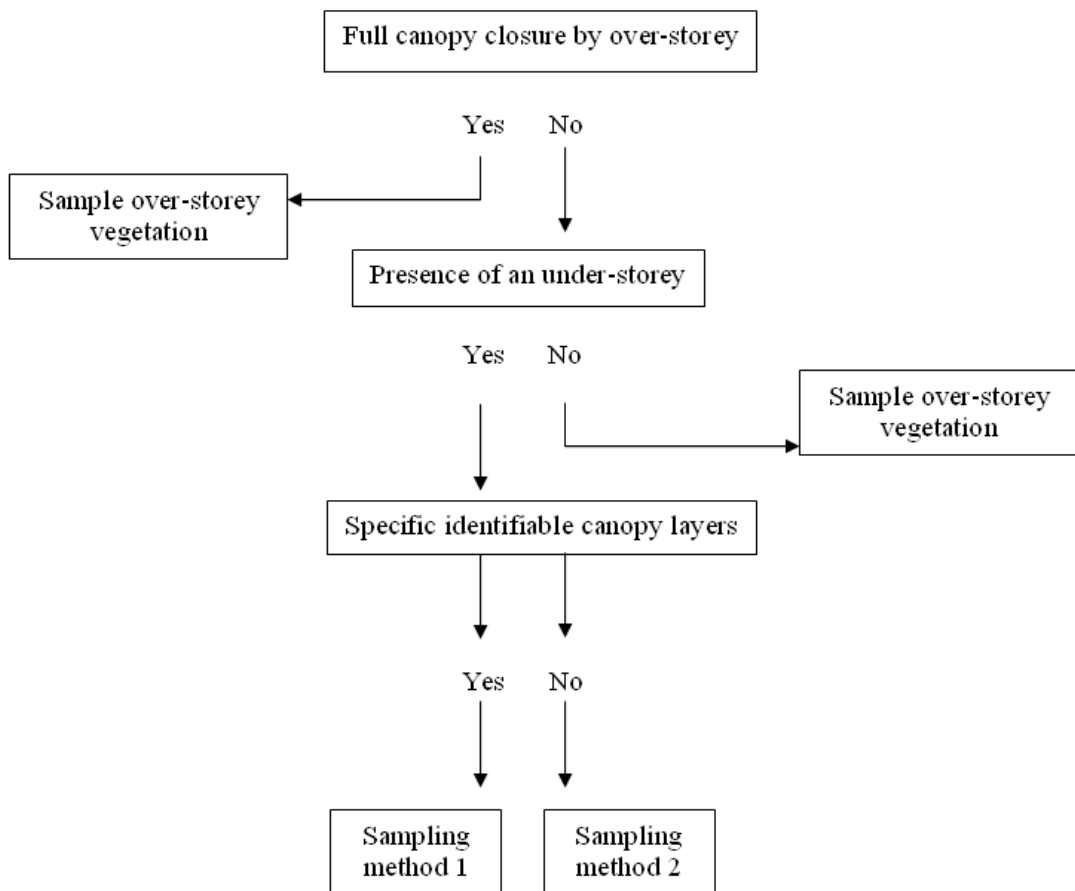
Figure 9.2: Field guide for the collection of vegetation data in support of remote sensing

Sampling method 1:

1. Measure the total canopy reflectance,

2. sample the upper canopy layer *,

3. remove the vegetation in the sampled canopy layer,

4. re-measure the reflectance in the remaining canopy,

5. sample the upper canopy layer *,

Repeat stages 4 and 5 until no vegetation remains then measure the reflectance of the bare substrate.

Sampling method 2: As sampling method 1 except the canopy is divided into sections defined by 25% of the total canopy height or 10cm if less.

* SPAD 502, biomass, LAI and any other vegetation sampling or measurement components.

9.4   Further research

Future developments of this work have two main directions. The first is in the practical application of techniques in the field environment with a specific focus on the support and validation of airborne collected data. The second concentrates on the development of the simulated environment to allow for differences in vegetation type with a single FOV and relate vegetation state variables values to the potential stress effects caused by contaminants in the soil.

9.4.1   Airborne hyperspectral survey of soil contaminated grassland

The new generation of sensors make the effective remote sensing of soil contamination practical. Hyperspectral data can be collected from an airborne platform at a

sub-metre spatial resolution and a spectral resolution of approximately 5nm. Modern hyperspectral airborne instruments are capable of collecting data with a IFOV of 0.6m (wide) but at the altitude required to collect data at this spatial resolution presents problems relating to the integration time of the instrument which results in pixels elongation in the direction of flight. It would be possible to address this limination by flying reciprocal flight lines, additional flight lines at 90° to each other and applying careful geocorrection and resampling. Collection of these data would allow the spectral and spatial analysis to be applied to a whole soil contaminaed site. Such data would allow the detection and mapping of soil contamination and allow the techniques outlined in this work to be fully assessed.

More immediately, an existing CASI-2 dataset (collected by the NERC ARSF, reference number: 00/04) can be processed and the REP and spatial variation (using its 2 metre pixels) could be used as a component for a supervised classification to map levels of soil contamination. In this instance, areas of known (measured) hydrocarbon and heavy metals in the soil could be used for training sites while three previously unused grids of measured soil data would be used to validate any classification. From the REP and classified data, the spatial scale of variation may be determined (if over 2m) using the teory of regionalised variables (geostatistics) and retained for comparison with other soil contamination surveys.

9.4.2   Inverted LIBSAIL-soil contamination model

At present even an inverted LIBSAIL model could only deliver selected vegetation state variables. However, there are several enhancements that may allow the models capabilities to be extended to indicate the potential presence of soil contamination. Each enhancement would add more data and thereby require more constraint to allow the model to be inverted.

The first enhancement would be to allow the more comprehensive modelling of the grassland environment using *a priori* data. An inverted two layer canopy model would

require data to determine the canopy mix and separate data to describe the nature of each canopy (including the inclusion of representative absorption spectra for different vegetation types) and separate input values typical of that vegetation. These may be provided by field observations or other remotely sensed data sets, e.g. from LiDAR. Typical extra input data could include % grass, % scrub, % other to provide root depth data relating to typical grassland environments and typify the expected contamination for comparison with other possible stress effects (e.g., hydric status) and likelihood of evolved tolerance.

The second enhancement would develop a set of non-site specific input variables (perhaps from a pre-prepared range of vegetation types and combinations). These sets would be used in conjunction with multiple regression relationships to relate specific stress effects (as determined by the inverted LIBSAIL model) to vegetation state variables. Specific stress effects would be matched to a vegetation component and with details on root depth could be related to depths in the soil. For example, a series of stress effects on an under-storey may be related to a different root depth to that of the over-storey and stress effects on both over-storey and under-story may indicate a range of depths. With such a model, additional stress effects would have to be discounted and considerable site specific information known and included in the model for it to operate on different sites. If then a measure of the relative levels of soil contamination and an estimate of the depth of the contamination may be automatically obtained from spectral data.

The last enhancement would be on LIBSAIL's spectral resolution. This would require the measurement of input absorption spectra at 1nm instead of the existing 5nm absorption spectra. This would allow the fine resolution features in the first derivative vegetation spectra to be more comprehensively investigated and with additional absorption effects from the canopy componets may allow an investigation into why there was no middle peak present in the LIBSAIL simulated first derivative spectrum.

9.5   Conclusion

Remote sensing is very suited to the detection, mapping or monitoring of land with contaminated soil because any contaminant has a spatial distribution. In some cases the direct measurement of a contaminant may be possible but in other situations contaminants are concealed in soil and under vegetation and therefore can not be measured directly. The role of remotely sensed visible and NIR data is to provide a guide for a subsequent field investigation into location, extent and concentration of a contaminant in soil and thereby improve the efficiency and effectiveness of such a survey. Two main types of data can be obtained for this application by remote sensing visible and near-infrared radiation. These are the spectral data from the sensor and the spatial arrangement of the data from the sampling strategy (e.g., swath along a flight line from a line scanner). This body of work used spectral data for the detection of soil contamination; it used selected vegetation indices, particulary REPs. A new 'optimised linear interpolation method' of calculating the REP was particularly effective. This REP method did not use fixed wavebands and was therefore more flexible in its application to different environments. The first derivative maximum was also found to be a useful tool because it was sensitive to subtle differences in the red-edge that could be attributed to stress effects. This work showed that remote sensing bridged the gap between time consuming, expensive and logistically difficult field measurements of soil and the wide spatial extent of most survey areas. Indeed, a standard survey proceedure for the rudimentary interpretation of airborne spectral data has recently been employed by Shell to detect and monitor leaks from oil pipelines in the Balkans (per. comm. P. Goy 2009). The areas where published research has been supported by the results in this work are:

1. associating sections of the first derivative red-edge with ground properties (specifically soil contamination), see section 5.4.2,

2. showing that despite any evolved tolerance soil contamination could still be identified solely based on its spectral signal in wavelengths defined by the spectral

red-edge, see section 5.5.3.

In this site, soil contaminated with hydrocarbons was detected by the use of spectral data. This study extended the already proven use of visible and NIR spectral data for the detection of hydrocarbon contaminants in grassland soil to a new site. Like other studies, first derivative spectra were observed to be particularly sensitive to stress effects in the vegetation. Grassland vegetation was an important factor in this study. Measureable effects in the red-edge implicitly required that grassland vegetation grew in the proximity of hydrocarbon contamination and the contaminant having some measurable effect on the vegetation. Additionally, the magnitude of the effect had to be distinguished from any background variation. The main grassland study site had a long history of contamination which allowed time for any a tolerance to the effects of the contamination to develop. The fact that soil contamination was detected using spectral data showed that tolerance to the effects of that contamination was not a major limiting factor.

Previous research has been conducted in this field but a series of new areas have been developed and investigated for this application. This research also had the following novel aspects:

1. associating the convexity of the reflectance red-edge to spectral profiles in the first derivative red-edge,

2. showing that the vegetated under-storey can be a significant contributer to the signal measured by a remote sensing instrument,

3. identifying spatial variation as a valuable factor related to the identification of different levels of soil contamination in grassland.

Field observations and simulations were used to relate a concave red-edge with a short wavelength first derivative peak and a convex red-edge with a long wavelength peak. The concave red-edge was related to conditions of high absorption and the convex

red-edge was related to low absorption. A middle wavelength first derivative peak was not modelled (in LIBSAIL) and its origins were unidentified. The height of the red-edge shoulder was unrelated to absorption effects at shorter wavelengths and was shown to be determined by within-the-leaf scattering. However, the wavelength position of the shoulder was determined by absorption effects. Compared with heavily managed grasslands, the semi-natural contaminated grasslands were laterally and vertically heterogeneous. Lateral variation across the FOV and vertical variation within the canopy produced a mixed spectral signal. Some measured field spectra could only be modelled with the inclusion of a vegetated under-storey allowed. This indicated the importance of canopy structure. Variation in over-storey vegetation variables did not share the variation observed in spectral data. This led to the conclusion that the vegetated under-storey may be more sensitive to the effects of soil contamination than the over-storey. The difficulties of measuring the under-storey must be overcome if effective ground validation and model development are to be achieved. This additional level of field measurement is particularly important in complex, diverse environments such as semi-natural grassland.

Hydrocarbon contaminants in the soil of semi-natural grassland were also detected by the use of spatial variation in the spectral data. Where an area had high levels of hydrocarbon in the soil it also had a high level of variation. The level of variation measured in the associated spectral vegetation indices was a strong indicator of contamination and the relative level of contamination. This related to the presence of both negative vegetation stress and patches of enhanced growth in these areas. Although this effect weakened the correlation between spectral VIs and soil contamination, it provides a potential new method of detecting contamination. The indication is that spatial variation of spectral indices (especially the REP) may be more useful than the spectral index value for the detection and mapping of soil contamination.

The most effective method of collecting spectral data over a wide spatial area (at an appropriate resolution for sub-metre ground evaluation) is by the use of airborne sensor platforms and hyperspectral sensors. The combination of spectral REP values and the spatial distribution of these values will detect areas of soil contamination.

An inverted radiative transfer model and regression model may be developed that relates effects on state variables to soil contamination. This tool would allow the rapid and effective survey of potentially contaminated vegetated areas to guide any field soil survey to efficiently determine the absolute concentrations of contamination in the soil. Remote sensing can and is being used for the detection of contamination but major improvements to the techniques used are possible and further developments could make remote sensing the routine scoping tool for this application.

Appendix A

Chlorophyll extraction and measurement of spectral absorption

A.1 Summary of potential risks

- Risks from liquid nitrogen are from cold burns to skin and eyes. Quantities used in this procedure should be less than those that incur a risk of asphyxiation (less than 5 litres).

- Risks from acetone (proponone) are due to inhalation and flammability.

A.2 Preparing the sample

Equipment:

- Mechanical processor or / and scissors,

- Analytical balance,

- Boiling tubes (four) or

- Mortar and pestle

Precautions:

- General care when using a mechanical processor or scissors.

Method

1. Cut or mechanically process the vegetation sample (depending on quantity).

2. Weigh 0.025 g (+/- 0.002 g) of vegetation sample and place in a glass boiling tube. For vegetation samples greater than 1 g but less than 25 g place in a mortar. The boiling tube should be mounted in a stable polystyrene boiling tube holder.

A.3   Addition of liquid nitrogen

Equipment:

- Dewar of liquid nitrogen,

- Ladle,

- Polystyrene boiling tube holder, Boiling tubes (four) and homogenising rods (four) or

- Mortar and pestle.

- Personal safety clothes (laboratory coat and safety glasses).

Precautions:

- The liquid nitrogen should be stored in a dewar.

- Liquid nitrogen must never be contained in a fully sealed container (during storage or homogenisation of samples).

- When pouring liquid nitrogen the boiling tube must be stable to prevent spillage and encapsulated to capture glass if the boiling tube shatters. This may be achieved by setting boiling tubes in polystyrene holders that angle the tube away from the pourer (to avoid the risk of being back-splashed).

- If spilt, avoid contact between liquid nitrogen and skin.

- Do not wear gloves (unless specifically designed for cryogenic use and then with extreme caution). This is to avoid a persistent direct contact with the skin.

- Direct contact with glass should not occur. Apparatus should be arranged so as to ensure that liquid nitrogen cooled apparatus dose not come into direst contact with skin (e.g., use polystyrene boiling tube holders).

- Wear laboratory coat and safety goggles.

- Work should be conducted in a quite, non-busy, unconfined area.

- If liquid nitrogen spilt vacate the area and secure it from access until the liquid nitrogen has evaporated (for less than 5 litres 20 minutes is sufficient).

Method

1. The sample and a homogenising rod / pestle are placed in the boiling tube / mortar.

2. Between 10 and 100 ml (enough to observe the presence of liquid in the vessel) of liquid nitrogen is lifted from the dewar and poured into a stable and secure boiling tube / mortar using a ladle (with non-conducting handle). A small quantity of liquid nitrogen should be poured into each tube / mortar in order to cool the tube / mortar followed by main quantity the to freeze the sample.

A.4   Homogenisation of the sample

Equipment:

- Polystyrene boiling tube holder, Boiling tubes (four) and homogenising rods (four) or Mortar and pestle,

- Solvent + 0.1 mg of $CaCO_2$ (to prevent secondary reaction) (e.g., 80% acetone v/v Lichtenthaler 1987, 90% acetone v/v, Jago 1998).

- Volumetric flask (25 ml) covered in aluminium foil,

- Plastic pipettes (four),

- Centrifuge,

- Centrifuge tubes (four),

- Glass cuvettes (four),

- Spectrophotometer (e.g., S106),

- Distilled water for washing used containers,

- Personal safety clothes (laboratory coat and safety glasses),

- Liquid nitrogen.

Precautions:

- If liquid nitrogen is spilt, avoid contact between liquid nitrogen and skin.

- Do not wear gloves.

- Direct contact with the glass should not occur.

- Wear laboratory coat and safety goggles.

- Work away from hot surfaces, fire or the risk of sparks and in a well ventilated room.

- Work should be conducted in a quite, non-busy area.

Method

1. Crush and grind the sample in the boiling tube. Do not touch the glass of the tube.

2. Add the acetone solution to the sample and homogenise until all the green pigment is visibly removed from the sample and is no longer transferred to the solvent.

3. After all liquid nitrogen has evaporated (at least 30 seconds) decant the contents of each boiling tube into a 12 ml centrifuge tubes.

4. Centrifuge for 5 minutes at 3600 rpm.

5. Pipette the supernatent into a 25 ml volumentric flask. (the volumetric flask should be covered in aluminium foil to prevent light reacting with the extracted chlorophyll within).

6. Add additional solvent to that in the volumetric flask up to 25 ml with solvent.

7. Pipette approximately 2 ml of aliquot from the volumetric flask into a glass cuvette (plastic cuvettes react with acetone).

8. Place cuvette in photospectrometer and record the absorption value for each of the selected wavelength regions (e.g., 647 nm and 664 nm for 90% acetone v/v; Jago 1998) five times and calculate the average.

Lichtenthaler's work (1987) provided the following relationships (equation A.1, A.2, A.3) for 80% aceteone v/v2

$$Chlorophyll\ a\ \ = 12.25 \times A_{663.2} - 2.79 \times A_{646.8} \qquad (A.1)$$

$$Chlorophyll\ b\ = 21.50 \times A_{646.8} - 5.10 \times A_{663.2} \tag{A.2}$$

$$Chlorophyll\ a\ +\ b\ = 715 \times A_{663.2} - 18.71 \times A_{646.8} \tag{A.3}$$

Jago's work (1998) provided the following relationships (equations A.4,A.5) for 90% acetone v/v:

$$Chlorophyll\ a\ = 0.0127 \times A_{664} - 0.00269 \times A_{647} \tag{A.4}$$

$$Chlorophyll\ b\ = 0.0227 \times A_{467} - 0.00468 \times A_{664} \tag{A.5}$$

From these equations chlorophyll concentration may be derived (equation A.6):

$$Chlorophyll concentration(mg.g^{-1})\ = \frac{chlorophyll(gl^{-1})}{Vegetation sample weight(g)}\ \ \times volume(l) \times 1000 \tag{A.6}$$

Appendix B

Solvent extraction of hydrocarbons from soil samples

B.1   Summary of chemical hazards

- Dichloromethane (DCM) can potentially cause irreversible effects, an irritant by skin contact, to the respiratory system and to the eyes.

- Potassium hydroxide (in ethanol) can cause very severe burns, is harmful if swallowed, is an irritant by skin contact, to the respiratory system and to the eyes and because the KOH is in ethanol it is flammable.

B.2   Preparing the sample

Equipment:

- Personal protective equipment (laboratory coat and safety glasses).

- flask,

- extraction thimbles,

- glass wool,

- desiccate (activated silica gel),

- 2mm sieve,

- evaporating dish,

- analytical balance and

- sodium sulphate,

Precautions:

- Wash hands after sample preparation.

Method:

1. Sieve approximately 10 grams of soil.

2. Separate the soil sample into an evaporating dish and place in the desiccater for 24 hours.

3. Weigh approximately 1 gram of sodium sulphate.

4. Sieve approximately 10 grams of soil.

5. Add exactly 1 gram of sodium sulphate to the sieved soil and mix.

6. Weigh thimble.

7. Place approximately 11 grams of mixed sample (approximately 10 grams of sieved soil and 1 g sodium sulphate) into the weighed thimble (upto approximately 50% the thimbles height).

8. Weigh thimble and soil sample.

9. Place a glass wool cap on the thimble.

10. Weigh flask (plus anti-bumping granules if used).

B.3   Solvent extraction

Equipment:

- Personal protective equipment (laboratory coat, nitrile gloves and safety glasses).

- Reflux extraction glassware,

- condenser,

- pre-weighed flask,

- appropriate Quick fit adapter sections

- measuring cylinder (250 ml)

- heating mantle.

- retort stands and dichloromethane (DCM).

Precautions:

- Wear Personal protective equipment at all times while in the laboratory.

- Work accompanied within office hours.

- Extraction must be conducted in an area with local exhaust ventilation.

- If local exhaust ventilation fails remove heat, lower sash and leave the area.

- If spillage occurs mop up with disposable tissues. Place disposable tissues in the area of local exhaust ventilation for the solvent to evaporate.

Method:

1. Measure 200 ml of DCM into the pre-weighed flask.

2. Fit the thimble (containing the sample) in the reflux glassware.

3. Assemble the glassware (see diagram 1).

4. Slowly pour 50 ml of DCM through glassware to moisten the thimble.

5. Start the water supply to the condenser.

6. Turn on the heating mantle.

7. Adjust the heat so as to allow supply signs of condensation and the required rate of reflux.

8. Continue after the first reflux cycle for 8 hours.

9. Check apparatus every two hours to ensure that at least 50 ml of DCM/DCM+extracted hydrocarbon remains in the lower flask. Add additional DCM if necessary.

10. After 8 hours turn off the source of heat.

11. Allow the flask to cool.

12. Remove the flask and transfer to the rotary evaporator.

B.4   Rotary evaporation

Equipment:

- Personal protective equipment (laboratory coat, nitrile gloves and safety glasses).

- flask with sample,

- flask,

- appropriate Quick fit adapter sections

- analytical balance,

- rotary evaporator,

- water bath,

- heating mantle and.

- retort stands.

Precautions:

- Wear Personal protective equipment at all times while in the laboratory.

- Work accompanied within office hours.

- Extraction must be conducted in an area with local exhaust ventilation.

- If local exhaust ventilation fails

- If spillage

Method:

1. Assemble the rotary evaporator glassware (see diagram 2).

2. Place the exhaust tube into an area of local exhaust ventilation.

3. Start the rotary evaporator

4. Heat the water bath.

5. Continue until distillate stops entering the collection flask.

B.5 Cleaning the reflux glassware and extraction flask

Equipment:

- Personal protective equipment (laboratory coat, nitrile gloves, laboratory protective gloves and safety glasses).

- Base bath in plastic bucket (with lid) and

- tongs,

Precautions:

- Wear Personal protective equipment at all times.

- Work accompanied within office hours.

- Base bath must be stored in an area that minimises the chance of spillage.

- Base bath must be clearly labelled both on bucket, lid and on the area where it is stored.

- If spillage occurs use absorbent buffered granules or boom to soak up spillage. Once the spill is soaked up dispose of the material in a secure plastic container by the appropriate special route for hazardous waste. Wash the area of the spill totally with water and detergent. Dispose of gloves.

Method:

1. Place glassware into base bath using tongs and leave over-night,

2. Remove glassware from base bath using tongs and place in a sink,

3. Wash glassware with tap water,

4. Wash glassware with distilled water,

5. Lightly rinse glassware with propanone (acetone).

6. Dry glassware in oven.

Appendix C

Calculation of vegetation indicies

C.1 'Vigo.m' Matlab script

The following script is reproduced as last used. As such it does not contain full comments. Instead it is provided as a guide to how large number of vegetation indices were repeatedly calculated throughout this research.

```
function [nVIgo,bVIgo,casiVIgo,SeaWIFSVIgo,merisVIgo,REPgo,nVInames,REPnames] = ...
VIgo(dataM,centreL,ref,window,basefilename,IDs)
%[nVIgo,bVIgo,casiVIgo,SeaWIFSVIgo,merisVIgo,REPgo] = ...
% VIgogo(NI(:,2:end),NI(:,1)',ref,7,basefilename,ID);
%[nVIgo,bVIgo,casiVIgo,SeaWIFSVIgo,merisVIgo,REPgo] = ...
% VIgogo(NI(:,2:end),centreL,ref,7,'ThorneyIslandGrid1');
%  ref: vector giving a reference spectrum for RARS
%  centreL: vector giving the centre wavelengths (in nm)
%  of the bands corresponding to each row.
%  basefilename: a string giving the basic filename to which the data will
%  be written - with appropriate extensions. Give a path if a specific
%  location for the file is required.
%  ID: is a cell array of IDs for each input column in dataM. Optional -
%  printed to header of output ascii files.
%  By Isabel Sargent imjs@soton.ac.uk
%  & Gary Llewellyn gml195@soton.ac.uk, 2002.
%  Modified 2007.
if (nargin<4)
    error('there must be at least four input arguments')
```

```
end
if (min(size(centreL))~=1)
    error('centreL must be a vector')
end
[numbands numobs]=size(dataM);
if size(centreL,2)>1; centreL=centreL'; end
if (numbands~=length(centreL))
    error(['number of elements in ', ...
    ' centreL must be the same as rows in dataM'])
end
nVIgo=zeros(37,numobs);
bVIgo=zeros(3,numobs);
casiVIgo=zeros(3,numobs);
SeaWIFSVIgo=zeros(3,numobs);
merisVIgo=zeros(4,numobs);
REPgo=zeros(15,numobs);
REPnames=cell([1,15]);
casiVInames=cell([1,3]);
merisVInames=cell([1,4]);
nVInames=cell([1,37]);
bVInames=cell([1,3]);
%
B=[420, 430, 445, 470, 500, 600, 635, 650, 670, 673, 675, ...
680, 694, 695, 700, 701, 703, 715, 720, 739, 740, ...
750, 758, 760, 780, 800, 805, 820, 655, 683, 685, 688, 690, ...
697, 705, 706, 710, 720, 722, 725, 730, 740];
bands = repmat(B,numbands,1);
centres = repmat(centreL,1,size(bands,2));
dists = abs(bands-centres);
[m bandlocs] = min(dists);
if (max(m)>10)
    [ma i]=max(m);
    disp(['no measurement near ', ...
    num2str(bands(1,i)),' nm']);
end
% test if same band is used for more than one position
testbandlocs=bandlocs;
for i=1:length(B)-1
    if sum(testbandlocs(i+1:end)==testbandlocs(i))
        disp('Modelled bands used more than once for narrow band vegetation indices')
        disp('Libsail has a 5 nm bandwidth output!')
    end
end
R420 = dataM(bandlocs(1),:);
R430 = dataM(bandlocs(2),:);
R445 = dataM(bandlocs(3),:);
R470 = dataM(bandlocs(4),:);
```

```
R500 = dataM(bandlocs(5),:);

R600 = dataM(bandlocs(6),:);

R635 = dataM(bandlocs(7),:);

R650 = dataM(bandlocs(8),:);

R670 = dataM(bandlocs(9),:);

R673 = dataM(bandlocs(10),:);

R675 = dataM(bandlocs(11),:);

R680 = dataM(bandlocs(12),:);

R694 = dataM(bandlocs(13),:);

R695 = dataM(bandlocs(14),:);

R700 = dataM(bandlocs(15),:);

R701 = dataM(bandlocs(16),:);

R703 = dataM(bandlocs(17),:);

R715 = dataM(bandlocs(18),:);

R720 = dataM(bandlocs(19),:);

R739 = dataM(bandlocs(20),:);

R740 = dataM(bandlocs(21),:);

R750 = dataM(bandlocs(22),:);

R758 = dataM(bandlocs(23),:);

R760 = dataM(bandlocs(24),:);

R780 = dataM(bandlocs(25),:);

R800 = dataM(bandlocs(26),:);

R805 = dataM(bandlocs(27),:);

R820 = dataM(bandlocs(28),:);

R655 = dataM(bandlocs(29),:);

R683 = dataM(bandlocs(30),:);

R685 = dataM(bandlocs(31),:);

R688 = dataM(bandlocs(32),:);

R690 = dataM(bandlocs(33),:);

R697 = dataM(bandlocs(34),:);

R705 = dataM(bandlocs(35),:);

R706 = dataM(bandlocs(36),:);

R710 = dataM(bandlocs(37),:);

R720 = dataM(bandlocs(38),:);

R722 = dataM(bandlocs(39),:);

R725 = dataM(bandlocs(40),:);

R730 = dataM(bandlocs(41),:);

R740 = dataM(bandlocs(42),:);


bands = repmat([500, 650, 670, 675, 700, 760],numbands,1);

centres = repmat(centreL,1,size(bands,2));

dists = abs(bands-centres);

[m reflocs] = min(dists);


r500 = ref(reflocs(1),:);

r650 = ref(reflocs(2),:);

r670 = ref(reflocs(3),:);
```

```
r675 = ref(reflocs(4),:);
r700 = ref(reflocs(5),:);
r760 = ref(reflocs(6),:);


%%%% %% %% %%%%   %%%%% %%%%%   %%%% %% %% %%%%%
rededge = repmat([650, 700, 740, 780], [numbands,1]);
centres = repmat(centreL,1,size(rededge,2));
dists = abs(rededge-centres);
[m rededgeloc] = min(dists);
[minval, minloc] = min(dataM(rededgeloc(1):rededgeloc(2),:),[],1);
[maxval, maxloc] = max(dataM(rededgeloc(3):rededgeloc(4),:),[],1);


%%%%%%%%%%%%%%%%%%%%%%%%%%%%%%%%%%%%%%%%%%%%%%%%%%%
% find start & end locations for the range 675 - 750 nm
sten = repmat([675 750],numbands,1);
centres = repmat(centreL,1,size(sten,2));
dists = abs(sten-centres);
[m startend] = min(dists);
%%%%%%%%%%%%%%%%%%%%%%%%%%%%%%%%%%%%%%%%%%%%%%%%%%%
% Savitzky-Golay smoothing & first derivative
fddata=savgol(dataM',window,2,1);
fddata=fddata';
[value, posfd]=max(fddata(startend(1):startend(2),:),[],1);
%%%%%%%%%%%%%%%%%%%%%%%%%%%%%%%%%%%%%%%%%%%%%%%%%%%
dba=[680, 688, 694, 697, 700, 702, 703, 704, 705, 706, 710, ...
711, 715, 720, 722, 724, 725, 730, 732, 750, 754, 760];
Dbands=repmat(dba, [numbands, 1]);
centres = repmat(centreL,1,size(Dbands,2));
dists = abs(Dbands-centres);
[m Dlocs] = min(dists);


D680 = fddata(Dlocs(find(dba==680)),:);
D688 = fddata(Dlocs(find(dba==688)),:);
D694 = fddata(Dlocs(find(dba==694)),:);
D697 = fddata(Dlocs(find(dba==697)),:);
D700 = fddata(Dlocs(find(dba==700)),:);
D702 = fddata(Dlocs(find(dba==702)),:);
D703 = fddata(Dlocs(find(dba==703)),:);
D704 = fddata(Dlocs(find(dba==704)),:);
D705 = fddata(Dlocs(find(dba==705)),:);
D706 = fddata(Dlocs(find(dba==706)),:);
D710 = fddata(Dlocs(find(dba==710)),:);
D715 = fddata(Dlocs(find(dba==715)),:);
D720 = fddata(Dlocs(find(dba==720)),:);
D722 = fddata(Dlocs(find(dba==722)),:);
D724 = fddata(Dlocs(find(dba==724)),:);
D725 = fddata(Dlocs(find(dba==725)),:);
```

```
D730 = fddata(Dlocs(find(dba==730)),:);

D732 = fddata(Dlocs(find(dba==732)),:);

D750 = fddata(Dlocs(find(dba==750)),:);

D754 = fddata(Dlocs(find(dba==754)),:);

D760 = fddata(Dlocs(find(dba==760)),:);

D700710 = fddata(Dlocs(find(dba==700)):Dlocs(find(dba==710)),:);

D711730 = fddata(Dlocs(find(dba==711)):Dlocs(find(dba==730)),:);

%%%%%%%%%%%%%%%%%%%%%%%%%%%%%%%%%%%%%%%%%%%%%%%%%%%%%%

%%%%%%%%%%%%%%%%%%%%%%%%%%%%%%%%%%%%%%%%%%%%%%%%%

% % simulate the CASI channels 4, 5, 6, 7, 8 and 10

casi = repmat([665.57, 674.54, 694.28, 703.27, 705.07, 711.06, ...

735.66, 744.67, 746.47, 753.68, 775.34, 784.37],numbands,1);

centres = repmat(centreL,1,size(casi,2));

dists = abs(casi-centres);

[m casilocs] = min(dists);

if max(m)>10

disp('poor simulation of CASI bands')

end

casi4 = mean(dataM(casilocs(1):casilocs(2),:),1);

casi4w=665.57+(674.54-665.57)/2;

casi5 = mean(dataM(casilocs(3):casilocs(4),:),1);

casi5w=694.28+(703.27-694.28)/2;

casi6 = mean(dataM(casilocs(5):casilocs(6),:),1);

casi6w=705.07+(711.06-705.07)/2;

casi7 = mean(dataM(casilocs(7):casilocs(8),:),1);

casi7w=735.66+(744.67-735.66)/2;

casi8 = mean(dataM(casilocs(9):casilocs(10),:),1);

casi8w=746.47+(753.68-746.47)/2;

casi10 = mean(dataM(casilocs(11):casilocs(12),:),1);

casi10w=775.34+(784.37-775.34)/2;

casidata=[casi4;casi5;casi6;casi7;casi8;casi10];

casiwave=[casi4w;casi5w;casi6w;casi7w;casi8w;casi10w];

disp('CASI bands simulated OK')

%%%%% %% %% %%%%   %%%%% %%%%%   %%%% %% %% %%%%%

% % simulate the SeaWIFS channels 4, 5, 6, 7 and 8

SeaWIFS = repmat([500 520 545 565 660 680 745 785 ...

845 885],numbands,1);

centres = repmat(centreL,1,size(SeaWIFS,2));

dists = abs(SeaWIFS-centres);

[m SeaWIFSlocs] = min(dists);

if max(m)>10

disp('poor simulation of SeaWIF bands')

end

SeaWIFS4 = mean(dataM(SeaWIFSlocs(1):SeaWIFSlocs(2),:),1);

SeaWIFS4w=500+(520-500)/2;

SeaWIFS5 = mean(dataM(SeaWIFSlocs(3):SeaWIFSlocs(4),:),1);

SeaWIFS5w=545+(565-545)/2;
```

```
SeaWIFS6 = mean(dataM(SeaWIFSlocs(5):SeaWIFSlocs(6),:),1);

SeaWIFS6w=660+(680-660)/2;

SeaWIFS7 = mean(dataM(SeaWIFSlocs(7):SeaWIFSlocs(8),:),1);

SeaWIFS7w=745+(785-745)/2;

SeaWIFS8 = mean(dataM(SeaWIFSlocs(9):SeaWIFSlocs(10),:),1);

SeaWIFS8w=845+(885-845)/2;

%SeaWIFSdata=[SeaWIFS4;SeaWIFS5;SeaWIFS6;SeaWIFS7;SeaWIFS8];

%SeaWIFSwave=[SeaWIFS4w;SeaWIFS5w;SeaWIFS6w;SeaWIFS7w;SeaWIFS8w];

%disp('SeaWIFS bands simulated OK')

%%%% %% %% %%%%   %%%%% %%%%%   %%%% %% %% %%%%

% % simulate the MERIS channels 8, 9, 10, 11, 12, 13.

meris = repmat([677.5 685 704 713 750 757.5 758.75 762.5 ...

772 786 855 875],numbands,1);

centres = repmat(centreL,1,size(meris,2));

dists = abs(meris-centres);

[m merislocs] = min(dists);

if max(m)>10

disp('poor simulation of MERIS bands')

end

meris8 = mean(dataM(merislocs(1):merislocs(2),:),1);

meris8w=677.5+(685-677.5)/2;

meris9 = mean(dataM(merislocs(3):merislocs(4),:),1);

meris9w=704+(713-704)/2;

meris10 = mean(dataM(merislocs(5):merislocs(6),:),1);

meris10w=750+(757.5-750)/2;

meris11 = mean(dataM(merislocs(7):merislocs(8),:),1);

meris11w=758.75+(762.5-758.75)/2;

meris12 = mean(dataM(merislocs(9):merislocs(10),:),1);

meris12w=772+(786-772)/2;

meris13 = mean(dataM(merislocs(11):merislocs(12),:),1);

meris13w=855+(875-855)/2;

merisdata=[meris8;meris9;meris10;meris11;meris12;meris13];

meriswave=[meris8w;meris9w;meris10w;meris11w;meris12w;meris13w];

disp('MERIS bands simulated OK')

%

%%%%%%%%%%%%%%%%%%%%%%%%%%%%%%%%%%%%%%%%%%%%%%%%%%%%%

%              Positional vegetation indices

%%%% %% %% %%%%   %%%%% %%%%%   %%%% %% %% %%%%

% Savitzky-Golay method REP

REPgo(1,:)=centreL(startend(1)+posfd-1)';

REPnames{1}='Savitzky-Golay';

%Danson & Plummer

%ref2 = ((R780+R673)/2)+R673;

% but surely it must be a minus!

ref2 = ((R780-R673)/2)+R673;

%Guyot & Baret

ref3 = ((R675+R700)/2);
```

```
%Clevers
ref4 = (R670+R780)/2;
%Danson & Plummer method
REPgo(2,:)=700+((ref2-R700)./(R740-R700))*(740-700);
REPnames{2}='Danson & Plummer';
%Guyot & Baret method
REPgo(3,:)=700+((ref3-R700)./(R740-R700))*(780-675);
REPnames{3}='Guyot & Baret';
%Clevers method
REPgo(4,:)=700+40*((ref4-R700)./(R740-R700));
REPnames{4}='Clevers';
% Inverted gaussian method 1
REPgo(5,:)=rsrepgausnew(dataM,centreL,1);
REPnames{5}='Inverted Gaussian method 1';
% Inverted gaussian method 2
REPgo(6,:)=rsrepgausnew(dataM,centreL,2);
REPnames{6}='Inverted Gaussian method 1';
% Optimised linear interpolation of REP
ref7 = ((minval)+(maxval))/2;
delta = centreL(rededgeloc(3)+maxloc-1)-centreL(rededgeloc(1)+minloc-1);
REPgo(7,:)=700+((ref7-R700)./(R740-R700))*40;
REPnames{7}='Optimised linear interpolation of REP 1';
REPgo(8,:)=700+((ref7-R700)./(R740-R700))*delta;
REPnames{8}='Optimised linear interpolation of REP 2';
% The REP reflectance is mid way between the min and max red-edge
% reflectance.
% This is applied to the wavelength range over which the min and max are present
% via the linear relationship between reflectance and wavelength between 700 and 740 nm.
% 740 - 700 nm is wavelength over which the linear relationship interpolates REP.
% delta = total wavelengths range over which the min and max reflectance are separated.
%%%%%%%%%%%%%%%%%%%%%%%%%%%%%%%%%%%%%%%%%%%%%%%%%%%%%%%%
% Linear interpolation method applied to CASI bandset
ref9 = ((casi10-casi4)/2)+(casi4);
REPgo(9,:)=700+((ref9-casi5)./(casi7-casi5))*(740-700);
REPnames{9}='Linear interpolation method applied to CASI bandset';
casiVIgo(2,:)=REPgo(9,:);
casiVInames{2}='Linear interpolation method applied to CASI bandset';
% Clevers linear extrapolation method applied to MERIS bandset
ref10 = ((meris12-meris8)/2)+(meris8);
REPgo(10,:)=700+((ref10-meris9)./(meris10-meris9))*(740-700);
REPnames{10}='Clevers linear extrapolation method applied to MERIS bandset';
merisVIgo(2,:)=REPgo(10,:);
merisVInames{2}='Clevers linear extrapolation method applied to MERIS bandset';
% Lagrangian REP applied to CASI, SeaWIFS & MERIS bandsets
REPgo(11,:)=lagrange(casidata,casiwave);
REPnames{11}='Lagrangian REP applied to CASI bandsets';
casiVIgo(3,:)=REPgo(11,:);
```

```
casiVInames{3}='Lagrangian REP applied to CASI bandsets';
% REPgo(12,:)=lagrange(SeaWIFSdata,SeaWIFSwave);
% REPnames{12}='Lagrangian REP applied to SeaWiFS bandsets';
% SeaWIFSVIgo(3,:)=REPgo(12,:);
% SeaWIFSVInames{3}='Lagrangian REP applied to SeaWiFS bandsets';
REPgo(13,:)=lagrange(merisdata,meriswave);
REPnames{13}='Lagrangian REP applied to MERIS bandsets';
merisVIgo(3,:)=REPgo(13,:);
merisVInames{3}='Lagrangian REP applied to MERIS bandsets';
%Cho & Skidmore 2007
[REPgo(14,:),REPgo(15,:)]=ChoSkidmoreVI(D680,D694,D724,D732,D760);
REPnames{14}='Cho & Skidmore 2007';
REPnames{15}='Cho & Skidmore 2007 modified';
%
disp('Positional vegetation indices calculated')
%%%%%%%%%%%%%%%%%%%%%%%%%%%%%%%%%%%%%%%%%%%%%%%%%%%%%
%               Narrow-band vegetation indices
%%%%%%%%%%%%%%%%%%%%%%%%%%%%%%%%%%%%%%%%%%%%%%%%%%%%%
%  1: R695 (Carter 1998)
nVIgo(1,:)=R695;
nVInames{1}='R695 (Carter 1998)';
%  2: R695/R805 (Carter 1998)
nVIgo(2,:)=R695./R805;
nVInames{2}='R695/R805 (Carter 1998)';
%  3: R701/R820 (Carter 1998)
nVIgo(3,:)=R701./R820;
nVInames{3}='R701/R820 (Carter 1998)';
%  4: R800/R680 (Carter 1998)
nVIgo(4,:)=R800./R680;
nVInames{4}='R800/R680 (Carter 1998)';
%  5: R694/R420 (Carter & Miller 1994)
nVIgo(5,:)=R694./R420;
nVInames{5}='R694/R420 (Carter & Miller 1994)';
%  6: R600/R760 (Carter & Miller 1994)
nVIgo(6,:)=R600./R760;
nVInames{6}='R600/R760 (Carter & Miller 1994)';
%  7: R694/R760 (Carter & Miller 1994)
nVIgo(7,:)=R694./R760;
nVInames{7}='R694/R760 (Carter & Miller 1994)';
%  8: R750/R695 (Gitelson et al. 1996)
nVIgo(8,:)=R750./R695;
nVInames{8}='R750/R695 (Gitelson et al. 1996)';
%  9: R750/R700 (Moss & Rock)
nVIgo(9,:)=R750./R700;
nVInames{9}='R750/R700 (Moss & Rock)';
%  10: R740/R720 (Vogelmann)
nVIgo(10,:)=R740./R720;
```

```
nVInames{10}='R740/R720 (Vogelmann)';
%  11: NIR/R705-715 (Baret & Gitelson)
BGite = repmat([705 715],numbands, 1);
cent = repmat(centreL,1,size(BGite,2));
dist = abs(BGite-cent);
[m BGiteloc] = min(dists);
if max(m)>5
disp('poor simulation of Baret & Gitelson wavelength bands')
end
BGred = mean(dataM(BGiteloc(1):BGiteloc(2),:),1);
NIR=casi10;
nVIgo(11,:)=NIR./BGred;
nVInames{11}='NIR/R705-715 (Baret & Gitelson)';
%  12: PSSR_a (Blackburn 1998)
nVIgo(12,:)=R800./R675;
nVInames{12}='PSSR_a (Blackburn 1998)';
%  13: PSSR_b (Blackburn 1998)
nVIgo(13,:)=R800./R650;
nVInames{13}='PSSR_b (Blackburn 1998)';
%  14: PSSR_{car} (Blackburn 1998)
nVIgo(14,:)=R800./R500;
nVInames{14}='PSSR_{car} (Blackburn 1998)';
%  15: PSND_a (Blackburn 1998)
nVIgo(15,:)=(R800+R675)./(R800-R675);
nVInames{15}='PSND_a (Blackburn 1998)';
%  16: PSND_b (Blackburn 1998)
nVIgo(16,:)=(R800+R650)./(R800-R650);
nVInames{16}='PSND_b (Blackburn 1998)';
%  17: PSND_{car} (Blackburn 1998)
nVIgo(17,:)=(R800+R500)./(R800-R500);
nVInames{17}='PSND_{car} (Blackburn 1998)';
%
% Load reference file for RARS
% 18: RARS_a (Chappelle et al. 1992)
nVIgo(18,:)=(R675./R700)./(r670./r700);
nVInames{18}='RARS_a (Chappelle et al. 1992)';
% 19: RARS_b (Chappelle et al. 1992)
nVIgo(19,:)=(R675./R650.*R700)./(r650.*r700./r675);
nVInames{19}='RARS_b (Chappelle et al. 1992)';
% 20: RARS_{car} (Chappelle et al. 1992)
nVIgo(20,:)=(R760./R500)./(r760./r500);
nVInames{20}='RARS_{car} (Chappelle et al. 1992)';
% 21: IRES Yang et al. 1999
nVIgo(21,:)=((R758-R739)/(758-739))-((R739-R720)-(739-720));
nVInames{21}='IRES Yang et al. 1999';
% 22: Index of maximum inflection point (MIP), Carter 1998.
nVIgo(22,:)=(D703)./(value);
```

```
nVInames{22}='Index of maximum inflection point (MIP), Carter 1998';
% 23: narrow band NDVI
mincasi4 = min(dataM(casilocs(1):casilocs(2),:),[],1);
maxcasi10 = max(dataM(casilocs(11):casilocs(12),:),[],1);
nVIgo(23,:)=(maxcasi10-mincasi4)./(maxcasi10+mincasi4);
nVInames{23}='narrow band NDVI';
% 24: MTCI
nVIgo(24,:)=(meris10-meris9)/(meris9-meris8);
nVInames{24}='MTCI';
merisVIgo(4,:)=nVIgo(24,:);
merisVInames{4}='MTCI';
% 25: Smith 2004
nVIgo(25,:)=SmithVI(D702,D725);
nVInames{25}='Smith 2004';
%%%%%%%%%%%%%%%%%%%%%%%%%%%%%%%%%%%%%%%%%%%%%%%%%%%%%%%%%%%%%%%%%%%%
% 26: 'curvative index' Zaero-Tejada et al. 2003
nVIgo(26,:)=(R675.*R690)./(R683.*R683);
nVInames{26}='''curvative index'' Zaero-Tejada et al. 2003';
% 27: Zaero-Tejada et al. 2003
nVIgo(27,:)=(R750./R800);
nVInames{27}='R750/R800 Zaero-Tejada et al. 2003';
% 28: Zaero-Tejada et al. 2003
nVIgo(28,:)=(R685./R655);
nVInames{28}='R685/R655 Zaero-Tejada et al. 2003';
% 29: Zaero-Tejada et al. 2003
nVIgo(29,:)= (R690./R655);
nVInames{29}='R690/R655 Zaero-Tejada et al. 2003';
% 30: Zaero-Tejada et al. 2003
nVIgo(30,:)= (D705./D722);
nVInames{30}='D705/D722 Zaero-Tejada et al. 2003';
% 31: Zaero-Tejada et al. 2003
nVIgo(31,:)= (D730./D706);
nVInames{31}='D730/D706 Zaero-Tejada et al. 2003';
% 32: DP22; Zaero-Tejada et al. 2003
%nVIgo(32,:)= (
% 33: DPRI; Zaero-Tejada et al. 2003
%nVIgo(33,:)=
% 34: DPI; Zaero-Tejada et al. 2003
nVIgo(32,:)= (D688.*D710)./(D697.*D697);
nVInames{32}='(D688*D710)/(D697*D697) Zaero-Tejada et al. 2003';
% 35:
nVIgo(33,:)= (D754./D704);
nVInames{33}='D754/D704';
% 36:
nVIgo(34,:)= (D715./D705);
nVInames{34}='D715/D705';
% 37:
```

```
nVIgo(35,:)= (R700./R670);
nVInames{35}='D700/D670';
% 38:
nVIgo(36,:)= (R740./R720);
nVInames{36}='D740/D720';
% 39: Optimised Smith
nVIgo(37,:)=OptimisedSmithVI(D700710,D711730);
nVInames{37}='Optimised Smith 2004';


disp('Narrow-band vegetation indices calculated')
%%%%%%%%%%%%%%%%%%%%%%%%%%%%%%%%%%%%%%%%%%%%%%%%%%%
%              Broad-band vegetation indices
%%%%%%%%%%%%%%%%%%%%%%%%%%%%%%%%%%%%%%%%%%%%%%%%%%%
% NDVI from CASI bandset
bVIgo(1,:)=(casi10-casi4)./(casi10+casi4);
bVInames{1}='NDVI from CASI bandset';
casiVIgo(1,:)=bVIgo(1,:);
casiVInames{1}='NDVI from CASI bandset';
%
% NDVI from SeaWIFS bandset
bVIgo(2,:)=(SeaWIFS8-SeaWIFS6)./(SeaWIFS8+SeaWIFS6);
bVInames{2}='NDVI from SeaWIFS bandset';
SeaWIFSVIgo(1,:)=bVIgo(2,:);
SeaWIFSVInames{1}='NDVI from SeaWIFS bandset';
%
% NDVI from MERIS bandset
bVIgo(3,:)=(meris13-meris8)./(meris13+meris8);
bVInames{3}='NDVI from MERIS bandset';
merisVIgo(1,:)=bVIgo(3,:);
merisVInames{1}='NDVI from MERIS bandset';
disp('Broad-band vegetation indices calculated')

if nargin==6
    str=[basefilename,'_nVI.asc'];
    writeVIdata(nVIgo,nVInames,IDs,str)
    str=[basefilename,'_bVI.asc'];
    writeVIdata(bVIgo,bVInames,IDs,str)
    str=[basefilename,'_REP.asc'];
    writeVIdata(REPgo,REPnames,IDs,str)
%     str=[basefilename,'_CASIVI.asc'];
%  writeVIdata(casiVIgo,casiVInames,IDs,str)
%     str=[basefilename,'_SeaWiFSVI.asc'];
%  writeVIdata(SeaWIFSVIgo,SeaWIFSVInames,IDs,str)
%     str=[basefilename,'_MERISVI.asc'];
%  writeVIdata(merisVIgo,merisVInames,IDs,str)
end
```

```
% save nVIgoNI.asc nVIgo -ascii
% save bVIgoNI.asc bVIgo -ascii
% save REPgoNI.asc REPgo -ascii
```

Appendix D

The LIBSAIL model code

D.1 'LIBSAIL.m' Matlab script

The following script is reproduced as last used. As such it does not contain full comments. Instead it is provided as a guide to how the two models, LIBERTY and SAIL were combined in this research.

```
%LIBSAIL1X
%Identifier:Poa
%chl=[1:1:10,20:10:50,100:100:600];
chl=[0.1:0.1:10,20:10:100,200:100:600];
%chl=[60];
%chl=[1:1:600];
LAI=[6.36];
%LAI=[0.06,1.14,3.16,5.17,6.36];
LADtype=20;
%Cell=[9.4,15.7,22.0];
Cell=[9.4];
%Air=0.001, 0.0054, 0.01
Air=0.01;
%Thick=1, 2.5, 4, 5.5
Thick=2.5;
base=0.0004;
Albino=0.5;
H2O=35;
Ligcel=10;
```

```
N=1;
pig=pigment(:,10);
%1=SPpigment,2=newpigment.dat,3=pigment8.dat,4=pigSOton.dat,5=pigment.dat,6=newpigment-min
sailtemp1=zeros(421,length(chl)*length(Cell)*length(LAI));
sailtemp1log=zeros(3,length(chl)*length(Cell)*length(LAI));
for a = 1:length(chl)
for b = 1:length(Cell)
for c = 1:length(LAI)
f=lidfmark(LADtype);
disp([' a = ',num2str(a),' b = ',num2str(b),' c = ',num2str(c)])
libvar1=[Cell(b),Air,Thick,base,Albino,chl(a),H2O,Ligcel,N];
libout1=LIBERTY(pig,water,albino,ligcell,protein,libvar1);
librefl1=libout1(:,3);
libtrans1=libout1(:,4);
colnum=(a-1)*(length(Cell)*length(LAI))+(b-1)*length(LAI)+c;
            sailtemp1(:,colnum)=sail(LAI(c),f,0.001,librefl1,libtrans1,0.2,0.2,0.2,0,0,0,0.1);
          sailtemp1log(:,colnum)=[chl(a);Cell(b);LAI(c)];
end
end
end

[nVIgo,bVIgo,casiVIgo,SeaWIFSVIgo,merisVIgo,REPgo]=VIgo(sailtemp1,ls,ref);
REPout=[sailtemp1log;REPgo]';
nVIout=[sailtemp1log;nVIgo]';
bVIout=[sailtemp1log;bVIgo]';

REPout=REPout';
nVIout=nVIout';
bVIout=bVIout';

fddata=savgol(sailtemp1',5,2,1);
Wavelength = libout1(:,1);
wavelength = libout1(:,1);
sailtemp1=sailtemp1*100;
hold off
p=plot(REPout(1,:),REPout(4,:),'k');
hold on
p=plot(REPout(1,:),REPout(7,:),'r');
p=plot(REPout(1,:),REPout(8,:),'b');
p=plot(REPout(1,:),REPout(9,:),'g');
%set(p,'color',[0.5,0.5,0.5])
ylim([600,800])
xlim([0,300])
xlabel('Chlorophyll content (mg cm^{-2})')
ylabel('REP (nm)')
tempGo=REPout';
save REPstandardHiNIR.asc REPout -ascii
```

Appendix E

The edited LIBERTY 'calc' function

E.1 The original 'calc.m' Matlab function

The original calc function is reproduced here for comparison to the new version (section E.2) used in the modelling in this research.

```
function [T, R, x] = calc(coeff,me,mi,xu);
%Adapted from LIBERTY Dawson et al. 1996
%G.M.Llewellyn gml195@soton.ac.uk

%M - the total radiation reaching the surface after one pass through the sphere
M=((ones(421,1)*2)./(coeff.*coeff)).*(1-(coeff+1).*exp(-coeff));

%T
T= ((1-mi).*M)./(1-(mi.*M));

%x
x=xu./(1-(1-(2*xu)).*T);

a = (me.*T)+(x.*T)-me-T-(x.*me.*T);
b = 1+(x.*me.*T)-(2*x.*x.*me.*me.*T);
c = (2*me.*x.*x.*T)-(x.*T)-(2*x.*me);
```

```
%initial estimate followed by 50 iterations
R=0.5;
for i =1:50
    R=-(a.*(R.*R)+c)./b;
end
```

E.2   The edited 'calc.m' Matlab function

```
function [T,R,x]=calc(coeff,me,mi,xu);


%M - the total radiation reaching the surface after one pass through the
%sphere
M=((ones(421,1)*2)./(coeff.*coeff)).*(1-(coeff+1).*exp(-coeff));


%T
T=((1-mi).*M)./(1-(mi.*M));


%x
x=xu./(1-(1-(2*xu)).*T);


%O and N are substitute variables
O=x.*me;N=x.*T;


%in fn(R)
%a, b and c are the coefficients of the powers of R
a=N + me.*T - O.*T - me - T;
b=1 + 2*O.*me + 3*O.*T - 2*O.*N - 2*N.*(me.^2);
c=2*O.*N - N - 2*O;


%disp([Newton-Raphson interation to find R])
count=0;
oldR=zeros(421,1);R=ones(421,1)*0.5;
while max(abs(R-oldR))>0.0001

    count=count+1;
    disp([num2str(count),': ',num2str(max(R))])

    oldR=R;
    funR = c + b.*R + a.*(R.^2);
    gradfunR = b + a.*R;
    R = R - (funR./gradfunR);
end
```

Appendix F

Modelling the optical properties of vegetation

The foundations (or baseline) for modelling of radiation reflected from a vegetation canopy are (i) knowledge of the incident radiation, (ii) the proportion (iii) transmitted,(iv) absorbed or (v) emitted by vegetation biochemicals and biological structures. The strength of the absorption is determined by the concentration of the biochemicals and secondary absorption by indirect radiation. However, for a model to accurately simulate or predict radiation absorption, and therefore derive estimates of canopy variables, it must also accurately simulate (i) absorption by vegetation biochemicals, (ii) scattering of radiation by cellular structures within the leaf and stem, (iii) scattering of radiation by leaf structures within the plant, (iv) scattering of radiation by plant structures within the scene and (v) absorption and scattering of soil structures within the scene.

The components of a remotely sensed scene were discussed in chapter 2 but the modelling of these influences requires a set of theoretical descriptions how such effects occur. These theories were embedded within each model and therefore imposed assumptions or constraints under which theoretical relationships were made. A summary and discussion of early canopy models and their development can be found in Goel's review

(1988). This review discusses the need to evaluate model performance by comparing the modelled output with measured data.

A strong correlation between modelled output and measured data indicates that the model provides *an* explanation of measured data, but not that it provides the *only* explanation. Within most models there is potential for the same result to be obtained by different interactions between variables (equifinality). At each scale of observation the number of variables and complexity required to simulate the scene changes. As scales are coursened, finely detailed differences become obscured or dominated by more pronounced (coarser) effects; therefore a model optimised for one scale of measurement may be inappropriate at another. In this research, the LIBSAIL model was created by coupling a leaf and a canopy radiative transfer model (LIBERTY and SAIL, respectively). Using LIBSAIL it was possible to simulate grassland reflectance because it included cell size and air void variables that allowed the dense bundles of the monocotyledonous grass species to be represented. At the field scale, where the field-of-view of a field radiometer may result in a 'foot-print' of approximately 100 square centimetres (depending of the optics used), these variables were believed to be influential. LIBSAIL was evaluated and used with data summarised in chapter 5 to investigate the effect of stress on grassland reflectance. Geometric complexities within the scene were not simulated because the diversity of grassland vegetation structure precluded precise geometric modelling.

F.1   Theories and solutions

A canopy may be represented as a series of geometrical structures, a homogeneous layer composed of a turbid medium or a hybrid. The former have two main components. The first uses geometric optics theory to calculate those areas that are illuminated and those that are shadowed. The second uses average transmittance theory to determine the penetration of radiation in the canopy by using a simplified form of the radiative transfer equation. Turbid medium models assume the canopy to be a parallel plane

extending infinitely in all directions and therefore allow the radiative transfer equation to be solved.

Alternatively, canopy models can be described as probabilistic or deterministic on the basis of the methodology used to formulate them. The probabilistic method utilises a Monte Carlo approach to evaluate the relative dominance of individual photon paths in a simulated environment. These methods are commonly known as ray-tracing (Govaerts *et al.* 1996); they are realistic but are computationally intensive and difficult to implement numerically (Ganapol *et al.* 1998). The deterministic approach uses solutions of the radiative transfer equation to describe absorption and scattering characteristics of the leaves; these characteristics were introduced in chapter 2. The modelling of radiation interaction with vegetation relies on the modelling of absorption, scattering and transmittance of radiation as it intercepts vegetation. Absorption has been briefly addressed, while scattering and transmittance may be described by the scattering phase function and average canopy transmittance theory. These are brought together in the radiative transfer equation to calculate changes in radiation intensity along a path where absorption and scattering are accounted for. However these models do not account for emission.

F.1.1   Scattering phase function

The scattering phase function is a representation of the law of photon deflection (e.g. Goel 1988; Ganapol *et al.* 1998). It describes the probability that radiation in a specified direction will be scattered within a solid angle in a specified direction while it passes through a medium *or across a boundary between media*. This component of the radiative transfer equation has been subject to two methods of solution. The first method derives a numerical solution by the use of iterative estimation, while the second imposes strict assumptions about the media and boundary of the vegetation canopy such that they form a turbid medium.

F.1.2   Average canopy transmittance theory

Average transmittance theory may be used to calculate the proportion of radiation that intercepts the vegetative surfaces (scattering and absorption or extinction coefficients). This is achieved by first determining the amount of direct (collimated) radiation and indirect (skylight) radiation and then calculating the proportion that was not intercepted by vegetative surfaces. Monsi and Saeki (1953) identified non-interception as:

$$P = (1 - \sigma /A)^N \qquad \qquad (\text{F.1})$$

Where the propability of non-interception $= P$, individual leaf area $= \sigma$, ground area over which the leaves are randomly distributed $= A$ and the number of leaves (σ) within area $A = N$. However for most grassland vegetation surveys σ is much smaller than A and therefore the probability becomes

$$P = exp(N\sigma/A) = exp(-F_c) \qquad \qquad (\text{F.2})$$

where F_C is the leaf area index calculated downwards from the canopy top.

In summary, average canopy transmittance theory allows calculation of: (i) radiation intercepted by the fraction of vegetation area projected in the direction of illumination (extinction coefficient), (ii) probability of a single ray and (iii) the penetration of the diffuse radiation (Norman 1975). The probability of interception determines the penetration of diffuse radiation and therefore the probability of non-interception may be determined.

F.1.3   Radiative transfer theory

The transfer of radiation between vegetation media combines the effects of scattering and transmittance with biochemical absorption. The radiative transfer equation is an

intero-differential equation developed by Chandrasekhar (1960) and Ishimaru (1978). It was initially used for astronomic and atmospheric media but was later developed (e.g., Ross 1981) for the modelling of vegetation. When equation F.4 was formally intergrated for a turbid medium it stated that upward radiation at optical path τ is a result of upward attenuated radiation at τ_0 plus that scattered into the beam along the path *tau* and τ_0.

Solving the radiative transfer equation requires (i) a solution of the scattering-phase function, (ii) average canopy transmittance and (iii) a measure of canopy architecture. The first two of these are captured in the radiative transfer equation (equation F.3) while the latter has been the subject of later developments.

The equation is built on scattering-phase function and canopy transmittance theory. The former is commonly split into the specular leaf scattering-phase function and the diffuse leaf scattering-phase function. All solutions to the radiative transfer equation use canopy transmittance theory and use one of three methods to solve the scattering-phase function. Drawn from the options presented by the scattering phase function, the three methods are: (i) a numerical solution to the radiative transfer equation using an iterated estimate of the scattering-phase function, (ii) KM theory approximation by defining and then calculating a scattering-phase function assuming a turbid medium and (iii) a discrete solution. Hybrids of these three methods model some of the greater complexities of a canopy or the generalisation of a turbid medium layer. Each will be summarised.

Consideration of the vegetation as a turbid medium allowed specification of a defined scattering-phase function and boundary condition via Stoke's equation. The solution was developed into the generalised plate model by the assumption that the scattering properties media were regular or completely random and that each medium was a homogeneous parallel plane that was infinitely extended. However, scattering properties in vegetation media are generally heterogeneous and complex and arranged in coherent structures. In the generalised plate model, leaf structure was described as parameter N; where paramamer N equated optical thickness as a number of layers and was similar

to the scattering coefficient described below in n-flux models.

$$\partial I(\tau^s)/\partial \tau = -I(\tau^s) + (\frac{1}{4\pi}) \int P^{(s;s)} I(\tau^{s'}) dw' + \epsilon^{(r;s)} \sigma \rho \qquad (F.3)$$

Where: I = Intensity, position = r, direction = s, optical distance = $\tau = \int \sigma \rho ds$, the element of the solid angle = dw', the number of particles = ρ, the scattering-phase function = $P^{(s;s')}$ and the sum of absorption and scattering across a section of a median particle = σ.

$$\mu \partial \, I(\tau \mu, \psi)/\partial \tau = I(\tau \mu, \psi) - K(\tau \mu, \psi) \qquad (F.4)$$

Where $\mu = \cos \theta$, the optical distance between thetop of a canopy and the base = τ, $d\tau = \sigma \rho$ dz scattering coefficient = s, absorption coefficient = α, the albedo for single scattering = α

$$\alpha = s/(\alpha + s), \sigma \, p = (\alpha + s) \qquad (F.5)$$

$$K = (a/4\pi) \int_0^{2\pi} d\psi' \int_{-1}^{+1} d\mu' p(\mu, \psi; \mu', \psi') \, I \, (\tau; \mu'; \psi') \qquad (F.6)$$

F.1.4   Numerical solutions

Ishimaru (1978) used two steps to numerically calculate the radiative transfer equation. The first step was to calculate the phase function from the properties of the vegetation canopy and the second, to solve the radiative transfer equation for that phase function under defined boundary conditions. Siewert *et al.* (1980) used the 'FN method' (developed from transport theory e.g., Ganapol 1995). This solution was adopted by Ganapol *et al.* (1998) for LEAFMOD (Leaf Experimental Absorptivity Feasibility MODel). LEAFMOD has only been verified for dicotyledonous species in one dimension although Ganapol *et al.* (1998) claimed that the general assumptions

(i.e., isotropic scattering and the presence of homogeneous media) were easier to relax in LEAFMOD.

F.1.5   KM theory approximation

A popular solution for the radiative transfer equation is based on KM theory (Kubelka and Munk 1931). This theory makes several assumptions concerning the scattering characteristics of the medium and the passage of light within it. One such assumption is that light travels either towards or away from the surface and interacts with a parallel plane geometry. The KM solution was interpreted by Suits (1972) and further developed, by the inclusion of the plate model, to specify the law of photon deflection (Allen *et al.* 1970). The plate model assumes the leaf to be composed of one or a series of boundaries between different media (Jacquemond and Baret 1990).

The 'N-flux' equations are simplifications of radiative transfer theory that initially used four fluxes to calculate a scattering and absorption coefficient (Fukshansky *et al.* 1991; Martinez v. Remisowsky *et al.* 1992). The four fluxes were diffuse downward (E-), diffuse upward (E+), specular downward (F-) and specular upward (F+). This was followed by two flux (Allen and Richardson 1968) and three flux (Allen *et al.* 1970) models. The two flux model only considered diffuse flux (F-=F+=0) and the three flux model (using Duntley theory, 1942) did not consider upward specular flux (F+=0). The three flux model was further developed to allow unequal absorption and scattering coefficients for diffuse fluxes (E- and E+). The Suits model (1972) used the three flux model with absorption coefficients determined by the Park-Deering model (1982) and a numerical solution (by initial guess and iteration).

Verhoef and Bunnik (1975) and Youkhana (1983) relaxed the assumption that the horizontal and vertical vegetation structure was continuous and uniform by allowing for any distribution of leaf angles; this led to the production of the SAIL model.

$$dE - /\, d(-\tau) = -(\alpha + \gamma)E_- \; + \; \gamma E_+ \; + \; S_1 F_- \; + \; S_2 F_+ \tag{F.7}$$

$$dE + /\, d(\tau) = -(\alpha + \gamma)E_+ \; + \; \gamma E_- \; + \; S_1 F_+ \; + \; S_2 F_- \tag{F.8}$$

$$dF - /\, d(-\tau) = -(k + S_1 + S_2)F_- \tag{F.9}$$

$$dF + /\, d(\tau) = -(k + S_1 + S_2)F_+ \tag{F.10}$$

F.1.6   Discrete solutions

The discrete solutions are so named because the range of possible layers and angles are segmented. The canopy depth (optical thickness or density) is divided into a finite number of layers while illumination (incident) and viewing directions are divided into solid angle sections of a hemisphere. Thus the algebraic equations could describe upward and downward fluxes (as opposed to specular or diffuse fluxes) at each level of the canopy. Intensity of scattered light incident on a layer was calculated from all the layers above and below it. The light distribution function was calculated from the leaf angle distribution (LAD) function; where the LAD function is the cumulative frequency distribution of intercepted light and the sine of the angle between the leaf and the illumination beam. Instead of treating interception of incident light as a function of LAD, LAI and S (n=LAI/S), discrete models treated it as a function of optical distance, illumination and view direction, referring to it as a cumulative light distribution function (canopy density $(J) = S\,(J)$). This was used to calculate the proportion of leaves which received radiation within each angular catagory. Examples of discrete models include: Idso and de Witt (1970, Goudriaan (1977, Cooper *et al.* (1982, Dauzat *et al.* (1984) and (Norman 1975; Norman 1979).

F.1.7   PROSPECT and LIBERTY

PROSPECT (Jacquemond and Baret 1990) and LIBERTY (Dawson *et al.* 1998) are two leaf models that use the Kubelka and Munk approximation to solve the radiative transfer equation. PROSPECT was designed to model the effects of chlorophyll and water content in a basic leaf structure. Its updated form (PROSPECT-redux) incorporated the biochemicals of cellulose, lignin and protein (Jacquemond *et al.* 1996) giving PROSPECT similar input variables to LIBERTY. LIBERTY was developed specifically to model pine foliage but is flexible enough to model other vegetation canopies such as grassland (Dawson. personal communication 1999). Both models are able to simulate vegetation spectra between 400 and 2500 nm, but presently have insufficient spectral resolution (3 nm and 5 nm respectively) to fully explore the first derivative details of the red-edge.

SAIL (Verhoef 1984; Verhoef 1985) is a deterministic radiative transfer model that uses a turbid medium to represent a homogenious canopy structure. Of the various deterministic canopy models SAIL has proved to be robust and is widely used. SAIL characterises radiation as a downward flux of direct radiation and an upward and downward flux of diffuse radiation (Verhoef 1984). SAIL also includes components to account for the leaf area index and the average inclination angle (Verhoef 1984).

F.2   Coupled leaf and canopy models

By coupling a leaf and canopy model leaf scale variables can be considered alongside canopy scale variables. This assumes that all leaf variables are estimates for the whole canopy, so the accuracy of such models increases with canopy regularity. Any leaf and canopy model may be combined if the input and output variables are compatible. The leaf model LEAFMOD was combined with the canopy model CANMOD (Ganapol and Myneni 1992) which was itself developed from a canopy model called THREEVER (Myneni and Ross 1991) to form the combined leaf and canopy model LCM2 (Ganapol

et al. 1999). LIBERTY (Dawson 1997) was coupled with FLIGHT (North 1996) to form a hybrid geometric optical / radiative transfer model to investigate conifer forests canopies (Dawson 1997). PROSPECT and SAIL have been combined (e.g., Jacquemond 1993; Hobson and Barnsley 1996; Clevers and Jongschaap 2001). Hobson and Barnsley (1996) explored the complex inter-relationship that exists in the physiology of forest vegetation, the extent to which leaf biochemical properties can be retrieved from remotely sensed data and confirmed that knowledge of various parameters describing canopy structure was required. They also demonstrated that adding multiple leaf layers in a canopy could lead to significant errors in the estimation of leaf chlorophyll content as well as highlighting the problem of equifinality.

Bibliography

Abercrombie, M, 1992. *The Penguin Dictionary of Biology.* Penguin Books Ltd.

Abt, M, W. J Welch, and J Sacks, 1999. Design and analysis for modeling and predicting spatial contamination. *Mathematical Geology* **31**, 1–22.

Al-Abbas, A. H, R Barr, J. D Hall, F. L Crane, and M. F Baumgardner, 1974. Spectra of normal and nutrient-deficient maize leaves. *Agronomy Journal* **66**, 16–20.

Allen, W. A, H. W Gausman, and A. J Richardson, 1973. Willstätter-Stoll theory of leaf reflectance evaluated by ray tracing. *Applied Optics* **12**(10), 2448–2453.

Allen, W. A and A. J Richardson, 1968. Interaction of light with a plant canopy. *Journal of the Optical Society of America* **58**(8), 1023–1028.

Allen, W. A, G. T V, and R. A J, 1970. Plant-canopy irradiance specified by the Duntley equation. *Journal of the Optical Society of America* **60**(3), 372–376.

Alloway, B. J and D. C Ayres, 1993. *Chemical principles of environmental pollution.* London: Blackie Academic and Processional.

Anderson, J. M, 1986. Photoregulation of the composition, function, and structure of thylakoid membranes. *Annual Review of Plant Physiology* **37**, 93–136.

Anon. What is spectral resolution and spectral sampling interval? http://www.asdi.com/forest-products/faq/what-is-spectral-resolution. Last accessed 19th June 2009.

Anon., 1966. The report of SCOR - UNESCO working group 17. Technical report, UNESCO.

Anon., 1991. *Lambda 19 UV/VIS and UV/VIS/NIR spectrometer instrument manual.* Ueberlingen: Perkin Elmer.

Anon., 2001. *DeltaT Sunfleck Ceptometer.* Delta T.

Anon., 2009a. Matlab - the language of technical computing. http://www.mathworks.com. Last accessed 19th December 2009.

Anon., 2009b. Spectralon reflectance standards care and handling guidelines. labsphere@labsphere.com. Last accessed 19th Decamber 2007.

Antonovics, J, A. D Bradshaw, and R. G Turner, 1971. Heavy metal tolerance in plants. *Advances in Ecological Research* **7**, 1–85.

Arnon, D, 1949. Copper enzymes in isolated chloroplasts. polyphenoloxidase in *Beta vulgaris. Plant Physiology* **24**, 1–15.

Asner, G. P, 1998. Biophysical sources of variability in canopy reflectance. *Remote Sensing of Environment* **64**, 234–253.

Atkinson, P. A and P. J Curran, 1995. Defining an optimal size of support for remote sensing investigations,. *IEEE Transactions on Geoscience and Remote Sensing* **33**, 769–776.

Atkinson, P. M, 1993. The effect of spatial resolution on the experimental variogram of airborne mss imagery. *International Journal of Remote Sensing* **14**, 1005–1011.

Baker, A. J. M, 1987. Metal tolerance. *New Phyologist* **106**, 93–111.

Bammel, B. H and R. W Birnie, 1993. Spectral response of big sagebrush to hydrocarbon-induced stress in the bighorn basin, wyoming. *Photogrammetric Engineering and Remote Sensing* **60**, 87–96.

Banninger, C, 1990. The red-edge shift as a measure of stress in coniferous forests. In *Abstracts of Beltsville Agricultural Research Center Symposium XV on Remote Sensing for Agriculture16-18 May*, Beltsville, Maryland. USDA-ARS.

Banninger, C, 1991. Phenological changes in the red edge shift of norway spruce needles and their relationship to needle chlorophyll content. In Le Roy (1991), pp. 155–158.

Banwell, C. N, 1983. *Fundamentals of molecular spectroscopy.* (third ed.). London: McGraw Hill.

Barnard, C, 1964. *Grasses and grasslands.* London: McMillan & Co, Ltd.

Barrett, E. C and L. F Curtis, 1982. *Introduction to Environmental Remote Sensing.* Chapman and Hall.

Barton II, F. E and D Burdick, 1983. Prediction of forage quality with NIR reflectance spectroscopy. In *Proceedings of the 14th International Grassland Congress*, Lexington, KY, pp. 532–534. Westview Press, Boulder, CO.

Barzda, V, R Erwin J G Peterman, van Grondelle, and H van Amerongen, 1998. The influence of aggregation on triplet formation in light-harvesting chlorophyll *a/b* pigment-protein complex ii of green plants. *Biochemistry* **37**, 546–551.

Bazzaz, F. A, R. W Carlson, and G. L Rolfe, 1974. The effects of heavy metals on plants: Part 1, inhibition of gas exchange in sunflowers by Pb, Cd, Ni and Ti. *Environmental Pollution* **7**, 241–246.

Bazzaz, F. A, G. l Rolfe, and R. W Carlson, 2006. Effect of Cd on photosynthesis and transpiration of excised leaves of corn and sunflower. *Physiologia Plantarum* **32**, 373–376.

Bazzaz, M. B and Govindjee, 1974. Effects of cadmium nitrate on spectral characteristics and light reactions of chloroplasts. *Environmental Letters* **6**(1), 1–12.

Begon, M, J. L Harper, and C. R Townsend, 1996. *Ecology. : individuals, populations and communities.* Blackwell Science.

Benford, F, 1946. Radiation in a diffuse medium. *Journal of the Optical Society of America* **36**, 524–554.

Berg, S, 1998. Photosynthesis. http://bio.winona.msus.edu/berg/308s99/Lecnote/chap13.htm. Last accessed 8th February 2000.

Berk, A, L. S Bernstein, and D. C Robertson, 1989. MODTRAN: A moderate resolution model for LOWTRAN-7, gl-tr-89-0122is. Hanscom AFB.

Bettinelli, M, G. M Beone, S Spezia, and C Baffi, 2000. Determination of heavy metals in soil and sediments by microwave-assisted digestion and inductively coupled

plasma optical emission spectrometry analysis. *Analytica Chimica Acta* **424**, 289–296.

Billings, W. D and R. J Morris, 1951. Reflection of visible and infrared radiation from leaves of different ecological groups. *American Journal of Botany* **38**(5), 327–331.

Blackburn, G. A, 1998a. Quantitying chlorophylls and carotenoids at leaf and canopy scales: An evaluation of some hyperspectral approaches. *Remote Sensing of Environment* **66**, 273–285.

Blackburn, G. A, 1998b. Spectral indices for estimating photosynthetic pigment concentrations: A test using senescent tree leaves. *International Journal of Remote Sensing* **19**, 657–675.

Blackburn, G. A and E. J Milton, 1995. Seasonal variations in the spectral reflectance of deciduous tree canopies. *International Journal of Remote Sensing* **16**, 709–720.

Blair, J. M, 1997. Fire, N availability, and plant responces in grassland: a test of the transient maxima hypothesis. *Ecology* **78**, 2359–2368.

Bonham-Carter, G. F, 1988. Numerical procedures and computer program fitting an inverted gaussian model to vegetation reflectance data. *Computers and Geosciences* **14**, 339–356.

Boochs, F, G Kupfer, K Dockter, and W Kuhbauch, 1990. Shape of the red edge as vitality indicator for plants. *International Journal of Remote Sensing* **11**, 1741–1753.

Boschetti, M, I Gallo, M Meroni, P. A Brivio, and E Binaghi, 2003. Retrieval of vegetation understorey information fusing hyperspectral and panchromatic airborne data. *3rd EARSeL workshop on Imaging Spectroscopy, Herrsching*, 483–491.

Bostock, L and F. S Chandler, 1981. *Mathamatics-the core course for A level*. London: Nelson-Thornes.

Boyer, M, J Miller, M Belanger, E Hare, and J Wu, 1988. Senescence and spectral reflectance in leaves of northern pin oak. *Remote Sensing of Environment* **25**,

71–87.

Breece, H. T and R. A Holmes, 1971. Bi-directional scattering characteristics of healthy green soybean and corn leaves *in vivo*. *Applied Optics* **10**, 119–125.

Brooks, R. R, 1972. *Geobotany and biogeochemistry in mineral exploration*. New York: Harper & Row.

Brown, W. V, 1975. Variation in anatomy, associations and origins of Kranz tissue. *American Journal of Botany* **62**, 395–402.

Buschmann, C and E Nagel, 1993. *In vivo* spectroscopy and internal optics of leaves as basis for remote sensing of vegetation. *International Journal of Remote Sensing* **14**, 711–722.

Buschmann, C, U Rinderle, and H. K Lichtenthaler, 1989. Detection of stress of coniferous forest trees with the VIRAF spectrometer. In *Quantitive Remote Sensing: An Economic Tool for the Nineties: 12th Canadian Symposium on Remote SensingInternational Geoscience and Remote Sensing Symposium '89*, Vancouver, pp. 2641–2644.

Butterfield, H. S and C. M Malmström, 2009. The effects of phenology on indirect measurements of aboveground biomass in annual grasses. *International Journal of Remote Sensing* **30**, 3133–3146.

Campbell, J. B, 1996. *Introduction to Remote Sensing* (Second ed.). The Guildford Press.

Card, D. H, D. L Peterson, P. A Matson, and J. D Aber, 1988. Prediction of leaf chemistry by the use of visible and near infrared reflectance spectroscopy. *Remote Sensing of Environment* **26**, 123–147.

Carter, G. A, 1994. Ratio of leaf reflectances in narrow wavebands as indicators of plant stress. *International Journal of Remote Sensing* **15**(3), 697–703.

Carter, G. A, 1998. Reflectance wavebands and indices for remote sensing of photosynthesis and stomatal conductance in pine canopies. *Remote Sensing of Environment* **63**, 61–72.

Carter, G. A, W. G Cibula, and R. L Miller, 1996. Narrow-band reflectance imagery compared with thermal imagery for early detection of plant stress. *Journal of Plant Physiology* **148**, 515–522.

Carter, G. A and A. K Knapp, 2001. Leaf optical properties in higher plants: linking spectral characteristics to stress and chlorophyll concentration. *American Journal of Botany* **88**, 677–684.

Chaerle, L, D Hagenbeek, X Vanrobaeys, and D Van Der Straeten, 2007. Early detection of nutrient and biotic stress in *Phaseolus vulgaris*. *International Journal of Remote Sensing* **28**(16), 3479–3492.

Chandrasekhar, S, 1960. *Radiative transfer*. Oxford: Clarendon Press.

Chang, S. H and W Collins, 1983. Conformation of the airborne biogeophysical mineral exploration technique using laboratory methods. *Economic Geology* **78**, 723–736.

Chappelle, E. W, M. S Kim, and J. E McMurtrey III, 1992. Ratio analysis of reflectance spectra (RARS): An algorithm for the remote estimation of the concentrations of chlorophyll a, chlorophyll b and caratonoids. *Remote Sensing of Environment* **39**, 239–247.

Chavez, P. s, 1975. Atmospheric, solar, and M.T.F. corrections for ERTS digital imagery. In *Proceedings of the American Society of Photogrammetry*, Volume 1, Phoenix, AZ, pp. 1–14. ISPRS.

Chavez, P. S, 1988. An improved dark-object subtraction technique for atmospheric scattering correction of multispectral data. *Remote Sensing of Environment* **24**, 459–479.

Chen, Z and C Elvidge, 1993. Description of derivative based high spectral-resolution (AVIRIS) green vegetation index. In *Proceedings of the SPIE: Imaging Spectrometry of the Terrestrial Environment*, Number 1937, pp. 43–54.

Cho, M. A, 2004. *Hyperspectral remote sensing of biochemical and biophysical parameters: the derivate red-edge "double-peak feature", a nuisance or an opportunity?* Ph. D. thesis.

Cho, M. A and A. K Skidmore, 2006. A new technique for extracting the red-edge position from hyperspectral data: the linear extrapolation method. *Remote Sensing of Environment* **101**, 181–193.

Choe, E, F. D van der Meer, F. J. A van Ruitenbeek, H. M. A van der Werff, J. B de Smeth, and K Kyoung-Woong, 2008. Mapping of heavy metal pollution in stream sediments using combined geochemistry, field spectroscopy, and hyperspectral remote sensing : a case study of the Rodalquilar mining area, SE Spain. *Remote sensing of Environment* **112**(7), 3222–3233.

Clark, D. H, 1989. *Near infrared reflectance spectroscopy (NIRS): Analysis of forage quality*, Chapter History of NIRS analysis of agricultural products, pp. 7–11. United States Department of Agriculture.

Clark, R. N, 1999. *Spectroscopy of rocks and minerals, and principles of spectroscopy* (third ed.). In Rencz (1999). Mar-58.

Clayton, D, 2000, May). A study in brown. *GEOEurope*, 45–46.

Clevers, J, L Kooistra, and E Salas, 2004. Study of heavy metal concentration in river floodplains using the re-edge position in spectroscopic data. *International Journal of Remote Sensing* **25**, 1–13.

Clevers, J. G and C Büker, 1991. Feasability of the red edge index for the detection of nitrogen deficiency. In Le Roy (1991), pp. 165–168.

Clevers, J. G. P. W, 1988. The derivation of a simplified reflectance model for the estimation of leaf area index. *Remote Sensing of Environment* **25**, 53–69.

Clevers, J. G. P. W, 1994. *Imaging Spectrometry - A tool for environmental observations. Euro Courses Remote Sensing*, Volume 4, Chapter Imaging spectrometry in agriculture-plant vitality and yield indicators, pp. 193–219. Dordrecht: Kluwer Academic Publishers.

Clevers, J. G. P. W, S. M DeJong, G. F Epema, E. A Addink, F. V van der Meer, W. H Bakker, and A. K Skidmore, 2000. MERIS and the red-edge index. In *Second EARLSeL workshop on imaging spectroscopy*.

Clevers, J. G. P. W, S. M DeJong, G. F Epema, F. V van der Meer, W. H Bakker,

A. K Skidmore, and E. A Addink, 2001. MERIS and the red-edge position. *JAG* **3**, 313–319.

Clevers, J. G. P. W, S. M DeJong, G. F Epema, F. V van der Meer, W. H Bakker, A. K Skidmore, and K. H Scholte, 2002. Derivation of the red-edge index using the MERIS standard band setting. *International Journal of Remote Sensing* **23**, 3169–3184.

Clevers, J. P. G. W and R Jongschaap, 2001. *Imaging Spectrometry: Basic Principles and Prospective Applications*, Chapter Imaging spectrometry for agricultural applications, pp. 157–199. Dordrecht: Kluwer Academic Publishers.

Clutis, E. A, 1989. Spectral reflectance properties of hydrocarbons: remote sensing implications. *Science* **245**, 165–168.

Coleman, S. W, 1989. *Near infrared reflectance spectroscopy (NIRS): Analysis of forage quality*, Volume Agric. Handbook No. 643, Chapter In vivo and in vitro measurements of forage quality, pp. 83–95. Washington, DC: ARS. USDA. Agric. Handbook No. 643.. ARS. USDA. p.

Collins, W, 1978. Remote sensing crop type and maturity. *Photogrammetric Engineering and Remote Sensing* **44**, 43–55.

Collins, W, S. H Chang, G Raines, F Canney, and F Ashley, 1983. Airborne biogeochemical mapping of hidden mineral deposits. *Economic Geology* **78**, 737–749.

Collins, W. E, S.-H Chang, J. F Kuo, and A Mancinelli, 1980. Biogeochemical laboratory studies to establishe the spectral properties of mineral-induced stress in plants. Technical Report PB 80-196769, National Technical Information Service. 69p.

Cooper, K. D, J. A Smith, and D Pitts, 1982. Reflectance of a vegetation canopy using the adding method. *Applied Optics* **21**, 411–4118.

Coulson, K. L, 1966. Effects of reflection properties of natural surfaces in aerial reconnaissance. *Applied Optics* **5**(6), 905–917.

Coulson, M. G and E. M Bridges, 1984. The remote sensing of contaminated land. *International Journal of Remote Sensing* **5**, 659–669.

Counts, G. E and H. D Radloff, 1979. The potential of infrared analysis in forage evaluation. *Journal of Animal Science* **53**(1), 261.

Crist, E. P, 1985. A TM tasseled cap equivalent transformation for reflectance factor data. *Remote Sensing of Environment* **17**, 301–306.

Curran, P. J, 1980. Multispectral remote sensing of vegetation amount. *Progress in Physical Geography* **4**, 315–341.

Curran, P. J, 1994. Imaging spectrometry. *Progress in Physical Geography* **18**, 247–266.

Curran, P. J, 2001. Imaging spectrometry for ecological applications. *JAG* **3**(4), 305–312.

Curran, P. J and J. L Dungan, 1989. Estimation of signal-to-noise: A new procedure applied to AVIRIS data. *IEEE Transactions on Geoscience and Remote Sensing* **7**, 620–628.

Curran, P. J, J. L Dungan, and H. L Gholz, 1990. Exploring the relationship between reflectance red edge and chlorophyll content in slash pine. *Tree Physiology* **7**, 33–48.

Curran, P. J, J. L Dungan, B. A Macler, and S. E Plummer, 1991. The effect of a red leaf pigment on the relationship between red edge and chlorophyll concentration. *Remote Sensing of Environment* **35**, 69–76.

Curran, P. J, J. L Dungan, B. A Macler, S. E Plummer, and D. L Peterson, 1992. Reflectance spectroscopy of fresh whole leaves for the estimation of chemical concentration. *Remote Sensing of Environment* **39**, 153–166.

Curran, P. J, J. L Dungan, and D. L Peterson, 2001. Estimating foliar biochemical concentration of leaves with reflectance spectrometry. *Remote Sensing of Environment* **76**, 349–359.

Curran, P. J and J. A Kupiec, 1995. *Advances in environmental remote sensing*, Chapter Imaging spectrometry: A new tool for ecology, pp. 71–88. Chichester: Wiley.

Curran, P. J, J. A Kupiec, and G. M Smith, 1997. Remote sensing the biochemical composition of a slash pine canopy. *IEEE Transactions on Geoscience and Remote Sensing* **35**, 415–420.

Curran, P. J, E. J Milton, P. M Atkinson, and G. M Foody, 1998. *Remote sensing: from data to understanding.* Chichester: John Wiley and Sons.

Curran, P. J and H. D Williamson, 1985. The accuracy of ground data used in remote sensing investigations. *International Journal of Remote Sensing* **6**, 1637–1651.

Curran, P. J and H. D Williamson, 1986. Sample size for ground and remote sensed data. *Remote Sensing of Environment* **20**, 31–41.

Curran, P. J and H. D Williamson, 1987. GLAI estimation using measurements of red, near infrared and middle infrared radiance. *Photogrammetric Engineering and Remote Sensing* **53**, 181–186.

Curran, P. J and H. D Williamson, 1988. Selecting a spatial resolution for estimation of per-field green leaf index. *International Journal of Remote Sensing* **9**, 1243–1250.

Curran, P. J, W. R Windham, and H. L Gholz, 1995. Exploring the relationship between reflectance red edge and chlorophyll concentration in slash pine leaves. *Tree Physiology* **15**, 203–206.

Cutler, M. E. J and P. J Curran, 1995. The effects of specular and anisotropic reflectance upon the correlation between wheat canopy reflectance and leaf chlorophyll concentration. In *Remote sensing in action : proceedings of the 21st Annual Conference of the Remote Sensing Society.*

Cutler, M. E. J and P. J Curran, 1996. An observation of shifts in the position of the red edge at different spatial resolutions. In *RSS96 Remote Sensing Science & Industry. Proceedings of the 22nd Annual Conference of the Remote Sensing Society*, Durham, pp. 290–297.

Cutler, M. E. J and P. J Curran, 2000. *Specular and anisotropic reflectance effects on the relationship between remotely sensed data and wheat canopy chlorophyll concentration*, Volume 60 of *Remote Sensing in Agriculture, Aspects of Applied*

Biology, pp. 115–122. Royal Agricultural College.

Danson, F. M and S. E Plummer, 1995. Red-edge response to forest leaf area index. *International Journal of Remote Sensing* **6**(1), 138–188.

Darch, J. P and J Barber, 1983. Multitemporal remore sesning of a geobotanical anomaly. *Economic Geology* **78**, 770–782.

Dash, J and P. J Curran, 2004. Evaluation of the MERIS terrestrial chlorophyll index. *IEEE Transactions on Geoscience and Remote Sensing*, 254–257.

Datt, B, 1999. Visible-near infrared reflectance and chlorophyll content in *eucalyptus* leaves. *International Journal of Remote Sensing* **20**(14), 2741–2759.

Dauzat, J, M Méthy, and J. l Salager, 1984. A method for stumulating radiative transfers within canopies, subsequent absorptance and directional reflectance. *Acta Ecologica Plantarum* **5**, 403–413.

Davies, W, 1960. The relative effect of frequency and time of cutting of lucerne. *Journal of the British Grassland Society* **15**, 262–269.

Dawson, T. P, 1997. *A modelling approach to the biochemical assay of vegetation canopies from remote sensing*. Ph. D. thesis, Department of Geography, University of Southampton.

Dawson, T. P, 1999. The LIBERTY model. http://www.eci.ox.ac.uk/staff/liberty.html. Last accessed 27th October 1999.

Dawson, T. P and P. J Curran, 1998. A new technique for interpolating the reflectance red edge position. *International Journal of Remote Sensing* **19**, 2133–2139.

Dawson, T. P, P. J Curran, P. J North, and S. E Plummer, 1997. *The potential for understanding the biochemical signal in the spectra of forest canopies using a coupled leaf and canopy model*, pp. 463–470. Rotterdam: A A Balkema.

Dawson, T. P, P. J Curran, and S. E Plummer, 1998. LIBERTY- modelling the effects of leaf biochemical concentration on reflectance spectra. *Remote Sensing of Environment* **65**, 50–60.

Dawson, T. P, P. J Curran, S. E Plummer, and P. J North, 1997. Determining causal effects of foliar biochemical concentrations on forest canopy reflectance using physical models and airborne spectrometry. In *Observations and Interactions 23rd Annual Conference & Exhibition of the Remote Sensing Society*, Nottingham, pp. 123–128.

de Rosny, G, R Vanderhaghen, F Baret, B Equer, and J. P Frangi, 1995. A device for *in situ* measurements of leaf chlorophyll and carotenoid concentrations. In *International Colloquium Photosynthesis and Remote Sensing*, Montpellier, France, pp. 28–31.

Delalieux, S, B Somers, W. W Verstraeten, W Keulemans, and P Coppin, 2008. Hyperspectral canopy measurements under artificial illumination. *International Journal of Remote Sensing* **29**, 6051–6058.

Demetriades-Shah, T, M. D Steven, and M. J. A Clark, 1990. High spectral resolution derivative spectra in remote sensing. *Remote Sensing of Environment* **33**, 55–64.

Dengler, N. G and T Nelson, 1999. *Leaf structure and development in plant C4 plants*, pp. 133–172. In Sage and Monson (1999).

Dobrowski, S. Z, J. C Pushnik, P. J Zarco-Tejada, and S. L Ustin, 2005. Simple reflectance indices track heat and water stress-induced changes in steady-state chlorophyll fluorescence at the canopy scale. *Remote Sensing of Environment* **97**(3), 403–414.

Dockray, M, 1981. Verification of a new method for determining chlorophyll concentrations in plants by remote sensing. Master's thesis, Imperial College of Science and Technology.

Duntley, S. Q, 1942. The mathematics of turbid media. *Journal of the Optical Society of America*.

Durand, C, V Ruban, A Ambles, and J Oudot, 2004. Characterization of the organic matter of sludge: determinatiuon of lipids, hydrocarbons and PAHs from road retention/infiltration ponds in france. *Environmental Pollution* **132**, 375–384.

Egan, W. G, 1968. Aircraft polarimetric and photometric observations. In *Proceed-*

ings of the fifth International Symposium on Remote Sensing of Environment, Michigan, pp. 671–679. Ann Arbor.

Elachi, C, 1987. *Introduction to The Physics and Techniques of Remote Sensing.* Wiley-Interscience.

Elvidge, C. D and Z Chen, 1995. Comparison of broad-band and narrow-band red and near-infrared vegetation indices. *Remote Sensing of Environment* **54**(1), 38–48.

ERM, 1998. Environmental survey of Shell Haven. Technical report, Environmental Resources Management.

ERM, 2000. Quantative risk assessment, phase II site investigation. Technical report, Environmental Resources Management.

Estep, L and G. A Carter, 2005. Derivative analysis of AVIRIS data for crop stress detection. *Photogrammetric Engineering and Remote Sensing* **71**(12), 1417–1421.

Evans, J. R, 1989. Photosynthesis and nitrogen relationships in leave of C_3 plants. *Oceanologia* **78**, 9–19.

Evans, J. R and J. R Seemann, 1989. *Photosynthesis*, Chapter The allocation of protein nitrogen in the photosynthetic apparatus: costs, consequences, and control, pp. 183–205. New York, USA: Alan R Liss.

Fahn, A, 1990. *Plant anatomy.* Pergamon Press.

Fang, Z, J Bouwkamp, and T Solomos, 1998. Chlorophyllase activities and chlorophyll degradation during leaf senescence in non-yellowing mutant and wild type of *Phaseolus vulgaris* l. *Journal of Experimental Botany* **49**, 503–510.

Farabee, M. J, 2007. Photosynthesis. http://www.emc.maricopa.edu/faculty/farabee/BIOBK/B Last accessed 4th May 2007.

Farifteha, J, F Van der Meer, C Atzberger, and E Carranza, 2007. Quantitative analysis of salt-affected soil reflectance spectra: A comparison of two adaptive methods (PLSR and ANN). *Remote Sensing of Environment* **110**(1), 59–78.

Farifteha, J, F van der Meer, and E. J. M Carranza, 2007. Similarity measures for spectral discrimination of salt-affected soils. *International Journal of Remote Sensing* **28**(23), 5273–5293.

Farrand, W. H and J. C Harsanyi, 1997. Mapping the distribution of mine tailings in the Coeur d'Alene River valley, Idaho, through the use of a constrained energy minimization technique. *Remote Sensing of Environment* **59**(1), 64–76.

Fenner, M, 1998. *The phenology of growth and reproduction in plants*, pp. 78–91. Gustav Fischer Verlag.

Ferns, D. C, S. J Zara, and J Barber, 1984. Application of high resolution spectroradiometry to vegetation. *Photogrammetric Engineering and Remote Sensing*, 1725–1435.

Ferrier, G, 1999. Application of imaging spectrometer data in identifying environmental pollution caused by mining at rodaquilar, spain. *Remote Sensing of Environment* **68**, 125–137.

Field, C. B and H. A Mooney, 1986. *On the economy of plant form and function*, Chapter The photosynthesis-nitrogen relationship in wild plants, pp. 25–55. Cambridge University Press.

Filella, I and J Peñuelas, 1994. The red edge position and shape as indicators of plant chlorophyll content, biomass and hydric status. *International Journal of Remote Sensing* **15**(7), 1459–1470.

Fitter, A. H and R. K. M Hay (Eds.), 1981. *Environmental physiology of plants*. Academic Press.

Fogwill, F, 2005. *Field guide for the GER3700* (3.0 ed.). University of Edinburgh: Natural Environment REsaerch Council Field Spectroscopy Facility.

Foster, I, 1991. *Environmental Pollution*. Oxford: Oxford University Press.

Freedman, B, 1995. *Environmental Ecology* (second ed.). New York: Academic Press.

French, C. S, J. S Brown, and M. C Lawrence, 1972. Four universal forms of chlorophyll a. *Plant Physiology* **49**, 421–429.

Fukshansky, L, N Fukshansky-Kazarinova, and A Martinez v Remisowsky, 1991. Solving the inverse problem of the multiflux radiative transfer. *Applied Optics* **30**, 3145–3153.

Ganapol, B. D, 1995. Radiative transfer in a semiinfinate medium with a specularly reflecting boundary. *Journal of Quantative Spectroscopy and Radiative Transfer* **53**, 257–267.

Ganapol, B. D, L. F Johnson, C. A Hlavka, and D. L Peterson, 1998. LEAFMOD: a new within-leaf radiative transfer model. *Remote Sensing of Environment* **63**, 182–193.

Ganapol, B. D, L. F Johnson, C. A Hlavka, D. L Peterson, and B Bond, 1999. LCM2: A coupled leaf / canopy radiative model. *Remote Sensing of Environment* **70**, 153–166.

Ganapol, B. D and R. B Myneni, 1992. The FN method for the one-angle radiative transfer equation applied to plant canopies. *Remote Sensing of Environment* **39**, 213–231.

Garnier, E, J. L Salager, G Laurent, and L Sonie, 1999. Relationship between photosynthesis, nitrogen and leaf structure in 14 grass species and their dependence on the basis of expression. *New Phytologist* **143**, 119–129.

Garrigues, S, D Allard, F Baret, and M Weiss, 2006. Influence of landscape spatial heterogeneity on the non-linear estimation of leaf area index from moderate spatial resolution remote sensing data. *Remote Sensing of Environment* **105**, 286–298.

Gates, D. M, 1970. *Physical properties of plants*, pp. 224–252. Washingdon DC: National Academy of Science.

Gates, D. M, 1980. *Biophysical Ecology*. New York: Springer-Verlag.

Gates, D. M, H. J Keegan, J. C Schleter, and V. R Weidner, 1965. Spectral properties of plants. *Applied Optics* **4**, 11–20.

Gausman, H. W, D. E Escobar, and E. B Knipling, 1977. Relation of *Peperomia obtusifolia*'s anomalous leaf reflectance to its leaf anatomy. *photogrammetric en-*

gineering and remote sensing **43**(9), 1183–1185.

Gausmann, H. W, 1974. Leaf reflectance in near infrared. *Photogrammetric Engineering and Remote Sensing* **40**, 183–191.

Gausmann, H. W, 1977. Reflectance of leaf components. *Remote Sensing of Environment* **6**, 1–9.

Gausmann, H. W, W. A Allen, R Cardenas, and A. J Richardson, 1970. Relation of light reflectance to histological and physical evaluation of cotton leaf maturity. *Applied Optics* **9**, 545–552.

Gibson, P. J and C. H Power, 2000. *Introductory remote sensing digital image processing and applications.* London: Taylor and Francis.

Gilbertson, D. D and M Kent, 1985. *Practical ecology for geography and biology:survey, mapping and data analysis.* London: Hutchinson.

Gitelson, A, C Buschmann, and H Lichtenthaler, 1999. The chlorophyll fluorescence ratio F_735 / F_700 as an accurate measure of the chlorophyll content in plants. *Remote Sensing of Environment* **69**, 296–302.

Gitelson, A and M. N Merzlyak, 1994. Spectral reflectance changes associated with autumn sensescence of *Aesculus hippocastanum L* and *Acer platanoides L* leaves. spectral features and relation to chlorophyll estimation. *Journal of Plant Physiology* **143**, 286–292.

Gitelson, A. A, C Buschmann, and H. K Lichtenthaler, 1998. Leaf chlorophyll fluorenscence corrected for reabsorption by means of absorption and reflectance measurements. *Journal of Plant Physiology* **152**, 283–296.

Gitelson, A. A and M. N Merzlyak, 1997. Remote estimation of chlorophyll content in higher plant leaves. *International Journal of Remote Sensing* **18**, 2691–2697.

Gitelson, A. A, M. N Merzlyak, and H. K Lichtenthaler, 1996. Detection of red-edge position and chlorophyll content by reflectance measurements near 700nm. *Journal of Plant Physiology* **148**, 501–508.

Glasson, J, R Therivel, and A Chadwick, 1994. *Introduction to Environmental Impact Assessment.* UCL Press.

Gobron, N, B Pinty, M Verstaete, and Y Govaerts, 1999. Medium resolution imaging spectrometry (MERIS) level 2 vegetation index algorithm theoretical basis. http://envisat.estec.esa.nl/. Last accessed 12th November 1999.

Goel, N. S, 1988. *Models of vegetation canopy reflectance and their use in estimation of biophysical parameters from reflectance data.* Remote Sensing Reviews. London: Harwood Academic Publishing.

Goetz, A. F. H, G Vane, J. E Solomon, and B. N Rock, 1985. Imaging spectrometry for earth remote sensing. *Science* **228**, 1147–1153.

Gopal, R, S Gupta, and C Chatterjee, 2002. Excess iron and excess nickel affect growth metabolism and accumulation of nutrients in radish. *Pollution Research.*

Goudriaan, J, 1977. *Crop Micrometerology: a simulation study.* Wageningen: WAU dissertation no. 683.

Govaerts, Y. M, S Jacquemond, M. M Verstraete, and S. L Ustin, 1996. Three-dimensional radiation transfer modeling in a dicotyledon leaf. *Applied Optics* **35**, 6585–6598.

Grant, L, 1987. Diffuse and specular characteristics of leaf reflectance. *Remote Sensing of Environment* **22**, 309–322.

Guderian, R, D. T Tingely, and R Rabe, 1985. *Effects of photochemical oxidants on plants*, pp. 129–346. Berlin: Springer-Verlag.

Gudin, C, 1973. Mise en Évidence dans le pétrole de régulateurs de la croissance des plates. In *International Meeting on Organic Geochemistry*, pp. 1043–1049.

Gudin, C and W. J Syratt, 1975. Biological aspects of land rehabilitation following hydrocarbon contamination. *Environmental Pollution* **8**, 107–112.

Guerin, T. F, 1999. The extraction of aged polycyclic aromatic hydrocarbon (PAH) residues from a clay soil using sonication and a soxhlet procedure: a comparative study. *Journal Environment Monitor* **1**, 63–67.

Guyot, G, 1990. *Applications of Remote Sensing in Agriculture*, Chapter Optical properties of vegetation canopies, pp. 19–43. Butterworths.

Guyot, G and F Baret, 1988. Utilisation de la haute résolution spectrale pour suivre l'état des couverts végétaux. In *Proceedings of the Fourth International Colloquium on "Physical measurements and signatures in remote sensing"*, Volume ESA SP-287, Noordwijk, pp. 279–286. ESA.

Guyot, G, F Baret, and S Jacquemond, 1992. *Imaging spectroscopy for vegetation studies*, pp. 145–165. Dordrecht: Kluwer Academic Publishers.

Guyot, G and D Major, 1988. *Applications of chlorophyll fluorescence*, Chapter Coupled fluorescence and reflectance measured to improve crop productiviry evaluation, pp. 319–324. Dordrecht: Kluwer Academic Press.

Haberlandt, G, 1914. *Phsiological Plant Anatomy*. London: Macmillan.

Hackenbush, H. Z, 2008. www.contaminatedland.co.uk. Internet. http://www.contaminatedland.co.uk/.Last accessed 20/06/2009.

Hall, D. O and K. K Rao, 1994. *Photosynthesis* (fifth ed.). Cambridge: Cambridge University Press.

Halliwell, B, 1984. *Structure, function and isolation of chloroplasts*, pp. 1–7. Oxford: Clarendon Press.

Hardy, N, 2003. *Evolution of Tolerance: its Influence on the Ability of Remote Sensing to Detect Contaminated Ground via Vegetation Stress*. Ph. D. thesis, University of Edinburgh, School of Geosciences.

Hardy, N. J, T. J Malthus, A McLeod, and S. E Plummer, 2001. An evaluation of the spectral responses of selected grasses to heavy metal stress. In *Proceedings of RSPS*.

Hobson, P and M Barnsley, 1996. Analysis of a coupled leaf (PROSPECT) and canopy (SAIL) reflectance model. In *RSS96 Remote Sensing Science & Industry. Proceedings of the 22nd Annual Conference of the Remote Sensing Society*, pp. 87–93.

Hoffer, R. M and C. J Johannsen, 1969. *Ecological potentials in spectral signature analysis*. In Johnson (1969).

Hopkins, W. G, 1999. *Introduction to plant physiology*. John Wiley.

Hoque, E and P. J. S Hutzler, 1992. Spectral blue-shift of red edge monitors damage class of beech trees. *Remote Sensing of Environment* **39**, 81–84.

Hörig, B, F Kühn, F Oschütz, and F Lehmann, 2001. Hymap hyperspectral remote sensing to detect hydrocarbons. *International Journal of Remote Sensing* **22**, 1413–1422.

Horler, D. N. H, J Barber, and A. R Barringer, 1980. Effect of heavy metals on the absorbance and reflectance spectra of plants. *International Journal of Remote Sensing* **1**, 121–136.

Horler, D. N. H, J Barber, J. P Darch, D. C Ferns, and A. R Barringer, 1983a. Approaches to detection of geochemical stress in vegetation. *International Journal of Remote Sensing* **4**, 273–288.

Horler, D. N. H, M Dockray, and J Barber, 1983b. The red edge of plant leaf reflectance. *Advanced Space Research* **3**, 273–277.

Hubbard, C. E, 1984. *Grasses.* London: Penguin Books Ltd.

Huete, A. R, 1988. A soil-adjusted vegetation index (SAVI). *Remote Sesning of Environment* **25**(3), 295–309.

Huete, A. R and H. Q Liu, 1994. An error and sensitivity analysis of the atmospheric-andsoil-correcting variants of the NDVI for the MODIS-EOS. *IEEE Transactions on Remote Sensing* **32**(4), 897–905.

Huggett, R. J, 1993. *Modelling the Human Impact on Nature: Systems Analysis of Environmental Problems.* Clarendon Press.

Idso, S. B and C. T de Witt, 1970. Light relations in plant canopies. *Applied Optics* **9**, 177–184.

Inoue, Y, J. P nuelas, A Miyata, and M Mano, 2008. Normalized difference spectral indices for estimating photosynthetic efficiency and capacity at a canopy scale derived from hyperspectral and co_2 flux measurements in rice. *Remote Sensing of Environment* **112**(1), 156–172.

Isaaks, E. H and R. M Srivastava, 1989. *An introduction to applied geostatistics.* Oxford.

Ishimaru, A, 1978. *Wave propagation and scattering in random media.* New York: Academic Press.

Jacquemond, S, 1993. Inversion of the PROSPECT + SAIL canopy reflectance model from AVIRIS equipment spectra: theoretical study. *Remote Sensing of Environment* **44**, 281–292.

Jacquemond, S and F Baret, 1990. PROSPECT: A model of leaf optical properties spectra. *Remote Sensing of Environment* **34**, 75–91.

Jacquemond, S, S. L Ustin, J Verbout, G Schmuck, G Andreoli, and B Hosgood, 1996. Estimating leaf biochemistry using the PROSPECT leaf optical properties model. *Remote Sensing of Environment* **56**, 194–202.

Jago, R. A, 1998. *Remote Sensing of Contaminated Land.* Ph. D. thesis, Department of Geography, University of Southampton.

Jago, R. A and P. J Curran, 1996. Estimating chlorophyll concentrations of a grassland canopy for chemical monitoring using remotely sensed data. In *RSS96 Remote Sensing Science & Industry. Proceedings of the 22nd Annual Conference of the Remote Sensing Society*, pp. 135–143.

Jago, R. A and P. J Curran, 1997. Estimating chlorophyll concentrations from field and airborne spectra to infer levels of land contamination. In *Observations and Interactions 23rd Annual Conference & Exhibition of the Remote Sensing Society*, Nottingham, pp. 274–279.

Jago, R. A, M. E. J Cutler, and P. J Curran, 1999. Estimating canopy chlorophyll concentration from field and airborne spectra. *Remote Sensing of Environment* **68**, 217–224.

Janssen, R. P. T, W. J. G. M Peijnenburg, L Posthuma, and M. A. G. T van den Hoop, 1997. Equilibrium partitioning of heavy metals in Dutch field soils. i. relationship between metal partition coefficients and soil characteristics. *Environmental Toxicology and Chemistry* **16**, 2470–2478.

Jeffrey, 1963. Purification and properties of chlorophyll c from *Sargassum flavicans*. *Biochemical Journal* **86**, 313–318.

Jeffrey, S. W and G. F Humphrey, 1975. New spectrophotometric equations for determining chlorophylls a, b, c_1 and c_2 in higher plants, algae and natural phytoplankton. *Biochemie und Physiologie der Pflanzen* **167**, 191–194.

Ji, L and A. J Peters, 2007. Performance evaluation of spectral vegetation indices using a statistical sensitivity function. *Remote Sensing of Environment* **106**, 59–65.

Johnson, L. F, C. A Hlavka, and D. L Peterson, 1994. Multivariate analysis of AVIRIS data for canopy biochemical estimation along the Oregon transect. *Remote Sensing of Environment* **47**, 216–230.

Johnson, P. L (Ed.), 1969. Athens,Georgia: University of Georgia Press.

Jordan, C. F, 1969. Derivation of leaf area index from quantity of light on the forest floor. *Ecology* **50**, 663–666.

Joshi, M. K and P Mohanty, 2004. *Chlorophyll* a *Fluorescence: A Signature of Photosynthesis, Advances in Photosynthesis and Respiration*, Chapter Chlorophyll a fluorescence as a probe of heavy metal ion toxicity in plants, pp. 637–661. Dordrecht: Springer.

Kabata-Pendias, A and H Pendias, 1984. *Trace elements in soil and plants*. Boca Ration: CRC Press.

Kanemasu, E. T, 1974. Seasonal canopy reflectance patterns of wheat, sorghum and soybean. *Remote Sensing of Environment* **3**, 43–47.

Kauth, R. J and G. S Thomas, 1976. The tasseled cap - a graphic description of the spectral temporal development of agricultural crops as seen by landsat. In *Proceedings of symposium on machine processing of remote sensing data, Purdue University, West Lafayette, IN*, pp. 41–51. Purdue University.

Kemper, T and S Sommer, 2003. Mapping and monitoring of residual heavy metal contamination and acidification risk after the Aznalcollar mining accident (Andalusia, Spain) using field and airborne hyperspectral data. In *3rd EARSeL Workshop on Imaging Spectroscopy*.

Kennedy, A. D, H Biggs, and N Zambatis, 2003. Relationship between grass species

richness and ecosystem stability in Kruger National Park, South Africa. *African Journal of Ecology* **41**, 131–140.

Kerr, C, 1998. *NERC EPFS software.* Southampton: NERC EPFS.

Kim, Y and J. F Reid, 2007. Bidirectional effect on a spectral image sensor for in-field crop reflectance assessment. *International Journal of Remote Sensing* **28**(21), 4913–4926.

Kimes, D. S, P. J Sellers, and D. J Diner, 1987. Extraction of spectral hemispherical reflectance (albedo) of surfaces from nadir and directional reflectance data. *International Journal of Remote Sensing* **8**, 1727–1746.

Kloke, A, D. R Sauerbeck, and H Vetter, 1984. *Changing metal cycles and human health : report of the Dahlem Workshop on Changing Metal Cycles and Human Health*, Chapter The contamination of plants and soils with heavy metals and the transport of metals in terrestrial food chains. Springer-Verlag.

Knappe, A. K and E Medina, 1999. *Success of C4 photosynthesis in the field: lessons from communities dominated by C4 plants*, pp. 251–284. In Sage and Monson (1999).

Kneizy, F. X, E. P Shettle, L. W Abreu, J. H Chetwynd, G. P Anderson, W. O Gallery, J. E Selby, Clough, and S A, 1988. *Users Guide to LOWTRAN.* Hanscom Air Force Base.

Knipling, E. B, 1969. *Leaf reflectance and image formation on colour infrared film*, pp. 17–19. In Johnson (1969).

Knipling, E. B, 1970. Physical and physiological basis for the reflectance of visible and near infrared radiation from vegetation. *Remote Sensing of Environment* **1**, 155–159.

Kokaly, R. F and R. N Clark, 1999. Spectroscopic determination of leaf biochemistry using band-depth analysis od absorption features and stepwise multiple linear regression. *Remote Sensing of Environment* **67**, 267–287.

Kooistra, L, 2004. *Incorporating spatial variability in ecological risk assessment of contaminated river floodplains.* Ph. D. thesis, Department of Environmental Stud-

ies, University of Nijmegen.

Kooistra, L, J Wanders, G. F Epema, R. S. E. W Leuvena, R Wehrens, and L. M. C Buydens, 2003. The potential of field spectroscopy for the assessment of sediment properties in river floodplains. *Analytica Chimica Acta* **484**(2), 189–200.

Kooistra, L, R Wehrens, L. M. C Buydens, R. S. E. W Leuven, and P. H Nienhuis, 2001. Possibilities of soil spectroscopy for the classification of contaminated areas in river floodplains. *Journal of Applied Earth Observation and Geoinformation (JAG)* **3**, 337–343.

Kriegler, F, W Malila, R Nalepka, and W Richardson, 1969. Preprocessing transformations and their effects on multispectral recognition. In *Proceedings of the 6th International Symposium on Remote Sensing of the Environment*, Ann Arbor, pp. 97–131. University of Michigan.

Kubelka, P and F Munk, 1931. Ein beitrag zur optik der farbanstriche. *Zeitschrift fur technische Physik* **12**, 593–601.

Kühn, F, K Oppermann, and B Hörig, 2004. Hydrocarbon index - an algorithm for hyperspectral detection of hydrocarbons. *International Journal of Remote Sensing* **25**, 2467–2473.

Kumar, R and L Silva, 1973. Light ray tracing through a feaf cross section. *Applied Optics* **12**, 2950–2954.

Lagerwerff, J. V and A. W Specht, 1970. Contamination of roadside soil and vegetation with cadmium, nickel, lead, and zinc. *Environmental Science & Technolology* **4**(7), 583–586.

Lamb, D. W, M Steyn-Ross, P Schaare, M. M Hanna, W Silvester, and A Steyn-Ross, 2002. Estimating leaf nitrogen concentration in ryegrass (*Lolium* spp.) pasture using the chlorophyll red-edge: theoretical modelling and experimental observations. *International Journal of Remote Sensing* **23**, 3619–3648.

Lane, P and M Peto, 1995. *Blackstone's guide to the Environment Act 1995*. London: Blackstone Press Limited.

Latimer, P, 1958. Apparent shifts of absorption bands of cell suspensions and selective light scattering. *Science* **127**, 29.

le Maire, G, C Francois, and E Dufrene, 2004. Towards universal broad leaf chlorophyll indices using prospect simulated database and hyperspectral reflectance measurements. *Remote Sensing of Environment* **89**, 1–28.

le Maire, G, C Francois, K Soudani, D Berveiller, J.-Y Pontailler, N Breda, H Genet, H Davi, and E Dufrene, 2008. Calibration and validation of hyperspectral indices for the estimation of broadleaved forest leaf chlorophyll content, leaf mass per area, leaf areas index and leaf canopy biomass. *Remote Sesning of Environment* **112**, 3846–3864.

Le Roy, M (Ed.), 1991. *Proceedings of the 5th International Colloquium. "Physical measurements and signatures in remote sensing."*, Volume SP-319, Courchevel, France. ESA.

Lee, T. D, M. G Tjoelker, D. S Ellsworth, and P. B Reich, 2001. Leaf gas exchange responses of 13 prairie grassland species to elevated CO2 and increased nitrogen supply. *New Phytologist* **150**, 405–418.

Levitt, J, 1980. *Responses of plant to environmental stresses*. London: Academic Press.

Li, L, S. L Ustin, and M Lay, 2005. Application of AVIRIS data in detection of oil-induced vegetation stress and cover change at Jornada, New Mexico. *Remote Sensing of Environment* **94**, 1–16.

Lichtenthaler, H, 1987. Chlorophylls and carotenoids: pigments of photosynthetic biomembranes. *Methods in Enzymology* **148**, 350–382.

Lichtenthaler, H and K Pfister, 1978. *Praktikum der Photosynthese*. Heidelberg-Wiesbaden: Quelle & Meyer Verlag.

Lichtenthaler, H. K, 1989. Possibilities for remote sensing of terrestrial vegetation by combination of reflectance and laser-induced chlorophyll fluorenscence. In *Quantitive Remote Sensing: An Economic Tool for the Nineties: 12th Canadian Symposium on Remote SensingInternational Geoscience and Remote Sensing Sympo-*

sium '89, Vancouver, pp. 1349–1354.

Lichtenthaler, H. K, 1996. Vegetation stress: an introduction to the stress concept in plants. *Journal of Plant Physiology* **8**, 4–14.

Lichtenthaler, H. K and C Buschmann, 1987, May). Reflectance and chlorophyll fluorescence signatures of leaves. In *Proceedings of IGARSS'87 Symposium*, Number 87CH2434-9, Ann Arbor, pp. 1201–1206.

Lichtenthaler, H. K, C Buschmann, U Rinderle, and G Schmuck, 1986. Application of chlorophyll fluorescence in ecophysiology. *Radiation and Environmental Biophysics* **25**, 297–308.

Lichtenthaler, H. K, R Hak, and U Rinderle, 1990. The chlorophyll florescence ratio F690/F730 in leaves of different chlorophyll content. *Photosynthetic Research* **25**, 295–298.

Lichtenthaler, H. K and A. R Wellburn, 1983. Determination of total carotenoids and chlorophyll a and b of leaf extracts in different solvents. In *603rd meeting, Liverpool*, Volume 11, Liverpool, pp. 591–592.

Lillesand, T. M and R. W Kiefer, 1994. *Remote Sensing and Image Interpretation* (3rd ed.). John Wiley & Sons.

Llewellyn, G. M and P. J Curran, 1999. Understanding the grassland red-edge using a combined leaf and canopy model. In *25th Annual Conference of The Remote sensing Society*.

Lomas-Clarke, S. T and H. D Williamson, 1998. Remote sensing of comtaminated land. In *RSS'98: Developing International Connections*, Nottingham, pp. 187–193.

Lucas, N, P. J Curran, and S Plummer, 1995. Using the red edge inflection point to drive an ecosystem simulation model for calculating the stem carbon production of an upland coniferous forest plantation. In *Remote sensing in action : proceedings of the 21st Annual Conference of the Remote Sensing Society*, pp. 1020–1027.

MacArthur, A, 2007. *Field guide for the GER1500 -Dual beam mode: -bi-conical*

and cos-conical. University of Edinburgh: Natural Environment Research Council Field Spectroscopy Facility.

Mackinney, G, 1941. Absorption of light by chlorophyll solutions. *Journal of Biological Chemistry* **140**, 315–322.

Magurran, A. E (Ed.), 1988. *Ecological diversity and its measurement.* Cambridge University Press.

Malthus, T. L and A. C Madeira, 1993. High resolution spectroradiometry: Spectral reflectance of field bean leaves infected by *Botrytis fabae. Remote Sensing of Environment* **45**, 107–116.

Malyuga, D. P, 1964. *Biogeochemical Methods of Prospecting.* New York: Consultants Bureau.

Mannion, A and S Bowlby, 1992. *Environmental Issues in the 1990s.* Wiley.

Mariotti, M, L Ercoli, and A Masoni, 1996. Spectral properties of iron-deficient corn and sunflower leaves. *Remote Sensing of Environment* **8**, 282–288.

Markwell, J, J. C Osterman, and J. L Mitchell, 1995. Calibration of the Minolta SPAD - 502 leaf chlorophyll meter. *Photosynthesis Research* **46**, 467–472.

Markwell, J. P, J. P Thornber, and R. T Boggs, 1979. Higher plant chloroplasts: Evidence that all the chlorophyll exists as chlorophyllprotein complexes. *Proceedings of the National Academy of Sciences* **76**(3), 1233–1235.

Marschner, H and I Cakmak, 1989. High light intensity enhances chlorosis and necrosis in leaves of zinc, potassium, and magnesium deficient bean (Phaseolus vulgaris) plants. *Journal of Plant Physiology* **134**, 308–315.

Marten, G. C, G. E Brink, D. R Buxton, J. L Halgerson, and J. S Hornstein2, 1984. Near infrared reflectance spectroscopy analysis of forage quality in four legume species. *Crop Science* **24**, 1179–1182.

Marten, G. C, J. L Halgerson, and J. H Cherney, 1983. Quality prediction of small grain forages by near infrared reflectance spectroscopy. *Crop Science* **23**, 94–96.

Marten, G. G, J. S Shenk, and F. E Barton II, 1989. Near infrared reflectance

spectroscopy (NRIS) analysis of forage quality. Technical Report Handbook No. 643, United States Department of Agriculture, Washington DC.

Martinez, D. E and J Levinton, 1996. Adaptation to heavy metals in the aquatic oligochaete *Limnodrilus hoffmeisteri*: evidence for control by one gene. *Evolution* **50**(3), 1339–1343.

Martinez v. Remisowsky, A, J. H McClendon, and L Fukshansky, 1992. Estimation of the optical parameters and light gradients in leaves: multi-flux versus two-flux treatment. *Photochemisty and. Photobiology* **55**, 857–865.

Mather, P. M, 1999. *Computer processing of remotely-sensed images: an introduction* (2nd ed.). New York: Wiley.

Matson, P, L Johnson, C Billow, J Miller, and R Pu, 1994. Seasonal patterns and remote spectral estimation of canopy chemistry across the Oregon transect. *Ecological Applications* **42**, 280–298.

Matthews, 1981. *Quantitative and statistical approaches to geography: a practical manual.* Pergamon.

McMurtrey, J. E, E. W Chapplle, M. S Kim, J. J Meisinger, and L. A Crop, 1994. Distinguishing nitrogen fertilization levels in filed corn (Zea mays L.) with actively induced fluorescence and passive reflectance measurements. *Remote Sensing of Environment* **47**, 36–44.

Melamed, M. T, 1963. Optical properties of powders. part i. optical absorption coefficients and the absolute value of the diffuse reflectance. *Journal of Applied Physics* **34**, 560–570.

Meroni, M and R Colombo, 2006. Leaf level detection of solar induced chlorophyll fluorescence by means of a subnanometer resolution spectroradiometer. *Remote Sensing of Environment* **103**, 438–448.

Miller, J. R, E. W Hare, and J Wu, 1990. Quantitative characterisation of the vegetative red edge reflectance. 1. an inverted-gaussian reflectance model. *International Journal of Remote Sensing* **11**, 1755–1773.

Miller, J. R, J Wu, M. G Boyer, M Belanger, and E. W Hare, 1991. Seasonal patterns in leaf reflectance red edge characteristics. *International Journal of Remote Sensing* **12**, 1509–1524.

Milton, E. J, 1987. Principles of field spectroscopy. *International Journal of Remote Sensing* **8**, 1807–1827.

Milton, E. J, A Razak, and H. V McKay, 1995. A polygon-based approach to land cover classification for grassland management. In *Remote sensing in action : proceedings of the 21st Annual Conference of the Remote Sensing Society*, pp. 285–292.

Milton, E. J and E. M Rollin, 1990. The influence of flowers upon the seasonal trend of heathland canopy reflectance. In *RSS'90*, Nottingham.

Milton, N. M, W Collins, S.-H Chang, and R. G Schmidt, 1983. Remote sensing detection of metal anomalies on Pilot Mountain, Randolph County, North Carolina. *Economic Geology* **78**, 605–617.

Milton, N. M and D. A Mouat, 1989. Remote sensing of vegetation responses to natural and cultural environmental conditions. *Photogrammetric Engineering and Remote Sensing* **55**, 1167–1173.

Minson, D. J, K. L Butler, N Grummitt, and D. P Law, 1983. Bias when predicting crude protein, dry matter digestibility and voluntary intake of tropical grasses by near infrared reflectance. *Animal Feed Science and Technology* **9**, 211–237.

Mishra, K. B and R Gopal, 2005. Study of laser induced fluorescence signatures from leaves of wheat seedlings growing under cadmium stress. *General and Applied Plant Physiology* **31**, 181–196.

Monje, O. A and B Bugbee, 1992. Inherent limitations of nondestructive chlorophyll meters : a comparison of two types of meters. *Horticultural Science* **27**(1), 69–71.

Monsi, M and T Saeki, 1953. Light factor in plant associations and its importance in dry matter production. *Japan Journal of Botany* **14**, 2252.

Moore, R. M, 1964. Ecological effects of grazing on grasslands in south-eastern australia. In *Proceedings of the IXth International Grassland Congress*.

Morris, P and R Therivel, 1995. *Methods of Environmental Impact Assessment.* London: UCL Press.

Müller, P, X.-P Li, and K. K Niyogi, 2001. Non-photochemical quenching. a response to excess light energy. *Plant Physiology* **125**, 1558–1566.

Munden, R, P. J Curran, and J. A Catt, 1994. The relationship between red edge and chlorophyll concentration in the winter wheat experiment at rothamsted. *International Journal of Remote Sensing* **15**, 706–709.

Mutanga, O and A. K Skidmore, 2003. Continuum-removed absorption features estimate tropical savanna grass quality *in situ*. In *3rd EARSeL Workshop on Imaging spectroscopy*.

Mutanga, O, A. K Skidmore, L Kumar, and J Ferwerda, 2005. Estimating tropical pasture at canopy level using band depth analysis with continuum removal in the visible domain. *International Journal of Remote Sensing* **26**, 1093–1108.

Mutanga, O, A. K Skidmore, and H. H. T Prins, 2004. Predicting in situ pasture quality in the Kruger national park, south africa, using continuum-removal absorption features. *Remote Sensing of Environment* **89**, 393–408.

Myers, V. I and W. A Allen, 1968. Electrooptical remote sensing methods as nondestructive testing and measuring techniques in agriculture. *Applied Optics* **7**(9), 1819–1838.

Myneni, R. B and J Ross, 1991. *Photo-Vegetative Interaction.* Berlin: Springer-Verlag.

Naumann, J. C, J. E Anderson, and D. R Young, 2008. Linking physiological responses, chlorophyll fluorescence and hyperspectral imagery to detect salinity stress using the physiological reflectance index in the coastal shrub, *Myrica cerifera* . *Remote Sensing of Environment* **112**(10), 3865–3875.

Newstom, L. E and G. W Frankie, 1994. A new classification for plant phenology based on flowering patterns in lowland tropical rain forest trees at La Selva, Costa Rica. *Biotropica* **26**, 141–159.

Nobel, P. S, 1983. *Biophysical plant physiology and ecology.* San Francisco: W H Freeman and Co.

Noomen, M. F, A. K Skidmore, and F. D van der Meer, 2003. Detecting the influence of gas seepage on vegetation using hyperspectral remote sensing. In *3rd EARSeL workshop on Imaging Spectroscopy, Herrsching, 13-16 May.*

Noomen, M. F, A. K Skidmore, F. D van der Meer, and H. T Prins, H, 2006. Continuum removal band depth analysis for detecting the effects of natural gas, methane and ethane on maize reflectance. *Remote Sensing of Environment* **105**, 262–270.

Norman, J. M, 1975. *Heat and transfer in the biosphere*, Chapter Radiative transfer in vegetation, pp. 187–206. Washinton DC: Scripta Book Co.

Norman, J. M, 1979. *Modification of the aerial envionment of plants*, Chapter Modeling of complete crop canopy, pp. 249–277. St. Joseph, Michigan: ASE (Monograph No.2).

Norris, K. H, 1989. *Near infrared reflectance spectroscopy (NIRS): Analysis of forage quality*, Chapter NIRS instrumentation, pp. 12–17. United States Department of Agriculture.

Norris, K. H, R. F Barnes, J. E Moore, and J. S Shenk, 1976. Predicting forage quality by infrared reflectance spectroscopy. *Journal of Animal Science* **43**, 889–897.

North, P. R. J, 1996. Three-dimensional forets light interaction model using a monte carlo method. *IEEE Transactions on Geoscience and Remote Sensing* **34**, 946–956.

Ocean Optics, 2009, June). Products: USB2000+VIS+NIR fibre optic spectrometers. http://www.oceanoptics.com/products. Last accessed 15th June 2009.

Ouzounidou, G, M Moustakas, L Symeonidis, and S Karataglis, 2006. Response of wheat seedlings to Ni stress: Effects of supplemental calcium. *Archives of Environmental Contamination and Toxicology* **50**(3), 346–352.

Palta, J. P, 1990. Stress interactions at the cellular and membrane levels. *Horticultural Science* **25**(11), 1377–1381.

Peñuelas, J, F Baret, and I Filella, 1995. Semi-empirical indicies to assess carotenoid / chlorophyll a ratio of leaf spectral reflectance. *Photosynthetica* **31**, 221–230.

Peñuelas, J, I Filella, C Biel, L Serrano, and R Savé, 1993. The reflectance at the 950970 nm region as an indicator of plant water status. *International Journal of Remote Sensing* **14**(10), 1366–5901.

Pearson, C. J and R. L Ison, 1987. *Agronomy of grassland systems*. Cambridge: Cambridge University Press.

Pearson, R. L and L. D Miller, 1972, October). Remote mapping of standing crop biomass for estimation of the productivity of the shortgrass prairie, pawnee national grasslands, colorado. In *8th International Symposium on Remote Sensing of Environment,*, Volume 2, Ann Arbor, pp. 1355–1381. ERIM International.

Perring, F, 1985. *RSNC Guide to British wild flowers*. Rushden: Country Life Books.

Peterson, P. J, 1971. Unusual accumulation of elements by plants and animals. *Scientific Progress* **59**, 505–526.

Peterson, P. J, 1979. Geochemistry and ecology. *Philisophical Transactions of the Royal Society B: Biological Sciences* **288**, 169–177.

Peterson, P. J, 1983. *Anatomy of the Dicotyledons*, Volume 2, Chapter Unusual element accumulations as a taxonomic character, pp. 167–173. Clarendon Press.

Peterson, P. J, 1993. *Plant adaptation to environmental stress*, Chapter Plant adaptation to environmental stress: metal pollutatnt tolerance, pp. 171–188. London: Chapman and Hall.

Pettygrove, 1985. *Irrigation with Reclaimed Municipal Wastewater - A Guidance Manual*. Chelsea: Lewis.

Pinar, A, 1994. *Exploring the relationship between red edge and chlorophyll content in wintwe wheat*. Ph. D. thesis, Department of Geography, University College of Swansea, University of Wales.

Pinar, A and P. J Curran, 1996. Grass chlorophyll and the reflectance red edge. *International Journal of Remote Sensing* **17**, 351–357.

Pinty, B, T Lavergne, J. L Widlowski, N Gobron, and M. M Verstraete, 2009. On the need to observe vegetation canopies in the near-infrared to estimate visible light absorption. *Remote Sensing of Environment* **113**, 10–23.

Plascyk, J. A, 1975. The MK II Fraunhofer line discriminator /FLD-II/ for airborne and orbital remote sensing of solar-stimulated luminescence. *Optical Engineering* **14**, 339–346.

Porritt, J, 1990. *Where on Earth are we going?* London: BBC books.

Pospisil, 1997. Estimating vegetation amount from visible and near infrared reflectances. *Photosythetica* **34**(3), 343–355.

Qi, J, F Cabot, M. S Moran, and G Dedieu, 1995. Biophysical parameters estimations using multidirectional spectral measurements. *Remote Sensing of Environment* **54**, 71–83.

Rabinowitch, E. I, 1951. *Photosynthesis and related processes*, Volume II, Part 1, Chapter Absorption spectra of pigments *in vitro*, pp. 603. New York: Interscience.

Railyan, V. Y and R. M Korobov, 1993. Red edge structure of canopy reflectance spectra of triticale. *Remote Sensing of Environment* **46**, 173–182.

Rao, R. G. S and F. T Ulaby, 1977. Optimal spatial sampling techniques for ground truth data in microwave remote sensing of soil moisture. *Remote Sensing of Environment* **6**(4), 289–301.

Ray, S. S and V. K Dadhwal, 2001. Estimation of crop evapotranspiration of irrigation command area using remote sensing and GIS. *Agricultural Water Management* **49**, 239–249.

Rencz, A. N (Ed.), 1999. *Remote Sensing for the Earth Sciences: Manual of Remote Sensing* (third ed.). New York: John Wiley and Sons Inc.

Richardson, A. J and C. L Wiegand, 1977. Distinguishing vegetation from soil background information. *Photogrammetric Engineering and Remote Sensing* **43**, 1541–1552.

Richter, N, K Staenz, and H Kaufmann, 2008. Spectral unmixing of airborne hyper-spectral data for baseline mapping of mine tailings areas. *International Journal of Remote Sensing* **29**(13), 3937–3956.

Richter, T and L Fukshansky, 1996. Optics of a bifacial leaf: 2 light regime as affected by leaf structure and the light source. *Photochemical and phobiological review* **63**, 517–527.

Rinderle, U and H. K Lichtenthaler, 1989. The various chlorophyll fluorenscence signatures as a basis for physiological ground truth control in remote sesing of forest decline. In *Proceedings of the 12th Canadian Symposium on Remote Sensing and IGARSS*, Vancouver, pp. 674–677. IEEE Geoscience and Remote Sensing.

Rock, B, D. L Williams, D. M Moss, G. N Lauten, and M Kim, 1994. High-spectral resolution field and laboratory optical reflectance measurements of red spruce and eastern hemlock needles and branches. *Remote Sensing of Environment* **47**, 176–189.

Rock, B. N, T Hoshizaki, and J. R Miller, 1988. Comparison of in situ and airborne spectral measurements of the blue shift associated with forest decline. *Remote Sensing of Environment* **4**, 109–127.

Rolfe, G. L, 1973. Lead uptake by selected tree seedlings. *Journal of Environmental Quality* **2**, 153–157.

Rollin, E. M and K Anderson, 2001. *Instructions for obtaining reflectance and radiance data from the GER3700, including an explanation of spectrum matching procedures* (GER37/01/Tec/02 ed.). University of Edinburgh: Natural Environment Research Council Field Spectroscopy Facility.

Rollin, E. M and E. J Milton, 1991. The UK national environment research council equipment pool for field spectroscopy (NERC-EPFS). In Le Roy (1991), pp. 837–839.

Rose, F, 1981. *The wild flower key, British Isles -N. W. Europe.* Singapore: Frederick Warne & Co.

Ross, J, 1981. *The radiation regime and architecture of plant stands.* Norwell, Mass:

Dr W. Junk Publishers.

Rubenthaler, G. L and B. L Bruinsma, 1978. Lysine estimation in cereals by near-infrared reflectance. *Crop Science* **18**, 1039–1042.

Running, S. W, C. O Justice, V Slmonson, D Hall, J Barker, Y. J Kaufmann, A. H Strahler, A. R Huete, J.-P Muller, V Vanderbilt, Z Wan, P Teillet, and D Caneggie, 1994. Terrestrial remote sensing science and algorithms planned for eos/modis. *International Journal of Remote Sensing* **15**, 3587–3620.

Ryan, P. R, J. M Ditomaso, and L. V Kochian, 1993. Aluminium toxicity in roots: An investigation of spatial sensitivity and the role of the root cap. *Journal of Experimental Botany* **44**(2), 437–446.

Sage, R. F and R. K Monson, 1999. *C4 plant biology*. London: Academic Press.

Sailsbury, J. W, N. M Milton, and P. A Walsh, 1987. Significance of non-isotropic scattering from vegetation for geobotanical remote sensing. *International Journal of Remote Sensing* **8**, 997–1009.

Samuels, T. D, K Kucukakyuz, and M Rincon-Zachary, 1997. Al partitioning patterns and root growth as related to Al sensitivity and Al tolerance in wheat. *Plant Physiology* **113**, 527–534.

Savitsky, A and M. J. E Golay, 1964. Smoothing and differentiation of data by simplified least squares procedure. *Analytical Chemistry* **36**, 1627–.

Schaber, J and F. W Badeck, 2003. Phsiology-based phenology models foe forest tree species in Germany. *International Journal of Biometerology* **47**, 193–201.

Schaepman, M. E, 1998. *Calibration of a Field Spectroradiometer - Calibration and Characterization of a Non-Imaging Field Spectroradiometer Supporting Imaging Spectrometer Validation and Hyperspectral Sensor Modelling*. Remote Sensing Laboratories, Department of Geography, University of Zurich.

Schaepman-Strub, G, M. E Schaepman, T. H Painter, S Dangel, and J. V Martonchik, 2006. Reflectance quantities in optical remote sensingdefinitions and case studies. *Remote Sensing of Environment* **103**, 27–42.

Schläpfer, F and B Schmid, 1999. Ecosystem effects of biodiversity: a classification of hypotheses and exploration of empirical results. *Ecological Applications* **9**(3), 893–912.

Schutt, J. B, R. R Rowland, and W. H Heartly, 1984. A laboratory investigation of a physical mechanism for the extended infrared absorption ('red shift') in wheat. *International Journal of Remote Sensing* **5**, 95–102.

Sexton, R and H. W Woolhouse, 1984. Senescence and abscission. *Advanced Plant Physiology*.

Sharkey, T. D, 1985. Photosynthesis in intact leaves of C3 plants: Physics, physiology and rate limitations. *The Botanical Review* **51**(1), 53–105.

Sharp, N, 2010, January). Fwhm explained. http://www.noao.edu/image_gallery/text/fwhm.ht Last accessed 3rd January 2010.

Shenk, J. S, I Landa, M. R Hoover, and M. O Westerhaus, 1981. Description and evaluation of near, infrared reflectance spectro-computer for forage and grain analysis. *Crop Science* **21**, 355–358.

Shenk, J. S, M. O Westerhaus, and M. R Hoover, 1979. Analysis of forages by infrared reflectance. *Journal of Dairy Science* **62**, 807–812.

Shoshany, M, 1991. The equifinality of bidirectional reflectance distribution functions of various microstructures. *International Journal of Remote Sensing* **12**, 2267–2281.

Siddiqui, S and W. A Adams, 2002. The fate of diesel hydrocarbons in soils and their effect on the germination of perennial ryegrass. *Environmental Toxicology* **17**, 49–62.

Siewert, C. E, J. R Maiorino, and M. N Ozisik, 1980. The use of the FN method for radiative transfer problems with reflective boundary conditions. *Journal of Quantitative Spectroscopy & Radiative Transfer* **23**, 565–573.

Silvestri, S and M Omri, 2008. A method for the remote sensing identification of un-controlled landfills: formulation and validation. *International Journal of Remote Sensing* **29**, 975–989.

Sinclair, T. R, R. M Hoffer, and M. M Schreiber, 1971. Reflectance and internal structure of leaves from several crops during a growing season. *Agronomy Journal* **63**, 864–868.

Sinclair, T. R, M. M Screiber, and R. M Hoffer, 1973. Diffuse reflectance hypothesis for the pathway of solar radiation through leaves. *Agronomy Journal* **63**, 276–283.

Smith, K, 2002, May). *Remote sensing of leaf responses to leaking underground natural gas.* Ph. D. thesis, University of Nottingham.

Smith, K, M. D Steven, and J. J Colls, 2004. Use of hyperspectral derivative ratios in the red-edge region to identify plant stress. *Remote Sensing of Environment* **92**, 207–217.

Smith, K. L, M. D Steven, and J. A Colls, 2000. *Remote Sensing of Vegetation stress due to leaking underground gas pipes.*, Volume 60 of *Remote Sensing in Agriculture, Aspects of Applied Biology*, pp. 209–212. Royal Agricultural College.

Spedding, C. R. W, 1971. *Grassland Ecology.* Oxford: Clarendon Press.

Sridhar, V. N, A Mahtab, and R. R Navalgund, 2008. Estimation and validation of lai using physical and semi-empirical BRDF models. *International Journal of Remote Sensing* **29**(4), 1366–5901.

Sterckx, S, P Coppin, S Debacker, W Debruyn, P Kempeneers, K Meuleman, K Nackaerts, I Reusen, and P Scheunders, 2003. Information extraction techniques for monitoring stress symptoms in orchards. In *Proceedings of the 3rd EARSEL workshop on Imaging Spectroscopy*, Oberpfaffenhofen, Germany.

Stermer, R. A, Y Pomeranz, and R. J McGinty, 1977. Infrared reflectance spectroscopy for estimation of moisture of whole grain. *Cereal Chemistry* **54**, 345 – 351.

Steven, M. D, T. J Malthus, T. H Demetriades-Shah, F. M Danson, and J. A Clark, 1990. *Applications of Remote Sensing in Agriculture*, Chapter High-spectral resolution indices for crop stress, pp. 209–227. London: Butterworths.

Steven, M. D, K. L Smith, M. D Beardsley, and J. J Colls, 2006. Oxygen and

methane depletion in soil affected by leakage of natural gas. *European Journal of Soil Science* **57**, 800–807.

Strahler, A. H, C. E Woodcock, and J. A Smith, 1986. On the nature of model in remote sensing. *Remote Sensing of Environment* **20**, 121–139.

Strub, G, P Keller, M Knubuhler, D Schlapfer, M Schaepman, and K. I Itten, 1998. Extraction and validation of biophysical variables of grassland communities using field spectroradiometric measurements. In M Schaepman, D Schlapfer, and K Itten (Eds.), *1st EARSeL workshop on imaging spectroscopy*, pp. 299–306.

Suárez, L, P Zarco-Tejada, G Sepulcre-Cantó, O Pérez-Priego, J. R Miller, J. J.-M noz, and J Sobrino, 2008. Assessing canopy PRI for water stress detection with diurnal airborne imagery. *Remote Sensing of Environment* **112**(2), 560–575.

Suits, G. H, 1972. The calculation of the directional reflectance of a vegetative canopy. *Remote Sensing of Environment* **2**, 117–125.

Sundesign, 2002. Sun angle calculator. http://www.susdesign.com/sunangle/. Last accessed 22nd June 2002.

Taiz, L and E Zeiger, 1998. *Plant Physiology* (second ed.). Sunderland, Massachusetts: Sinauer Associates inc.

Talmage, D. A and P. J Curran, 1986. Remote sensing using partially polarized light. *International Journal of Remote Sensing* **7**, 47–64.

Tansley, A. G, 1939. *The British Isles and their vegetation.* Cambridge University Press.

Terashima, I, 1989. Productive structure of a leaf. *Plant biology* **8**, 207–226.

Terashima, I and T Saeki, 1983. Light environment within leaf. i. optical properties of paradermal sections of camellia leaves with special reference to differences in the optical properties of pallisade and spongy tissues. *Plant Cell Physiology* **24**, 1493–1501.

Thomas, H, 2004. Sid: a mendelian locus controlling thylakoid membrane disassembly in senescing leaves of *Festuca pratensis. TAG Theoretical and Applied Genetics* **73**, 1432–2242.

Thomas, H and J. L Stoddart, 1975. Separation of chlorophyll degradation from other senescence processes in leaves of a mutant genotype of meadow fescue (*Festuca pratensis* l.). *Plant Physiology* **56**, 438–441.

Todd, S. W, R. M Hoffer, and D. G Milchunas, 1998. Biomass estimation on grazed and ungrazed rangelands using spectral indicies. *International Journal of Remote Sensing* **19**, 427–438.

Tsai, F and W Philpot, 1998. Derivative analysis of hyperspectral data. *Remote Sensing of Environment* **66**, 41–51.

Tucker, 2006. A critical review of remote sensing and other methods for non-destructive estimation of standing crop biomass. *Grass and Forage Science* **35**, 177–182.

Tucker, C. J, 1977. Asymptotic nature of grass canopy reflectance. *Applied Optics* **16**, 1151–1157.

Tucker, C. J and P. J Sellers, 1986. Satellite remote sensing of primary production. *International Journal of Remote Sensing* **7**, 1395–1416.

Ustin, S. L and B Curtiss, 1988. Use of high spectral resolution sensors (PIDAS and AVIRIS) to detect air pollution injury in conifer forests. In Fenstermaker (Ed.), *Symposium on the Rem. Sens. of Acidic Deposition*, St. Louis, MO., pp. 72–85. American Society of Photogrametry and Remote Sensing.

Ustin, S. L, B Curtiss, S. N Martens, and V. C Vanderbilt, 1989. *Transactions: Effects of Air Pollution on Western Forests*, Chapter Early Detection of Air Pollution Injury to Coniferous Forests Using Remote Sensing, pp. 351–378. Anaheim, CA.: Air and Waste Management Association.

Ustin, S. L, M. O Smith, S Jacquemond, M Verstraete, and Y Govaerts, 1999. *Geobotany: vegetation mapping for Earth sciences* (third ed.), Chapter Remote sensing for the earth sciences: Manual of remote sensing, pp. 189–248. Volume 3 of Rencz (1999).

Vanderbilt, V. C, L Grant, L. L Biehl, and B. F Robinson, 1985. Specular, diffuse, and polarized light scattered by two wheat canopies. *Applied Optics* **24**(15),

2408–2418.

Vane, G and A. F. H Goetz, 1993. Terrestrial imaging spectrometry: current status, future trends. *Remote Sensing of Environment* **44**, 117–126.

Verhoef, W, 1984. Light scattering by leaf layers with application to canopy reflectance modeling: The sail model. *Remote Sensing of Environment* **6**, 125–141.

Verhoef, W, 1985. Earth observation modelling based on layer scattering matrices. *Remote Sensing of Environment* **17**, 165–178.

Verhoef, W and N. J. J Bunnik, 1975. *A model study on the relations between crop characteristics and canopy spectral reflectance*. 3 Kanaalweg Delft, The Netherlands: NIWARS publications.

Verstraete, M. M and B Pinty, 1996. Designing optimal spectral indices for remote sensing applications. *IEEE Transactions on Geoscience and Remote Sensing* **34**, 1254–1265.

Vogelmann, J. E, B. N Rock, and D. M Moss, 1993. Red edge spectral measurements from sugar maple leaves. *International Journal of Remote Sensing* **14**, 1563–1575.

Vogelmann, T, J Bornman, and S Josserand, 1989. Photosynthetic light gradients and spectral regime within leaves of Medicago sativa. *Philosophical Transactions of the Royal Society of London* **323**, 411–421.

Vogelmann, T. C and L. O Björn, 1986. Plants as light traps. *Physiological Plant* **68**, 704–708.

Vogelmann, T. C, J. F Bornman, and D. J Yates, 1996. Focusing of light by leaf epidermal cells. *Physiologia Plantarum* **98**(1), 43–56.

Wagner, H, M Gilbert, and C Wilhelm, 2003. Longitudinal leaf gradients of uv-absorbing screening pigments in barley (*Hordeum vulgare*). *Physiologia Plantarum* **117**, 383–391.

Wardley, N. W and P. J Curran, 1983. *Green leaf area index estimation from remotely sensed airborne MSS data*, pp. 1–12. Reading: Remote Sensing Society.

Wardley, N. W and P. J Curran, 1984. The estimation of green-leaf-area index from remotely sensed airborne multispectral data. *International Journal of Remote Sensing* **5**, 671–679.

Warren, M. H, 1997. The environment act 1995 and the contaminated land provisions. Technical Report 7, Surrey.

Warren-Wilson, M, 1971. *Maximum yield potential*, pp. 34–56. Berne: International Potash Institute.

Watson, C. A, D Carville, E Dikeman, G Daigger, and G. D Booth, 1976. Evaluation of two infrared instruments for determining protein content of hard red winter wheat. *Cereal Chemistry* **53**, 214–221.

Wedin, D. A and D Tilman, 1993. Competition amoung grasses along a nitrogen gradient: initial conditions and mechanisms of competition. *Ecology of Monocotyledons* **63**, 199–229.

Westman, W. E and C. V Price, 1988. Spectral changes in conifers subjected to air pollution and water stress: experimental studies. *IEEE Transactions on Geoscience and Remote Sensing* **26**, 11–21.

White, D. C, M Williams, and S. L Barr, 2008. Detecting sub-surface soil disturbance using hyperspectral first derivative band ratios of associated vegetation stress. In *The International Archive of the Photogrammetry. Remote Sensing and Spatial Information Sciences*, Volume XXXVII, Beijing.

Wiffen, D. H, 1972. *Spectroscopy* (second ed.). London: Longman.

Willard, H. H, L. L Merritt, and J. A Deans, 1974. *Instrumental methods of analysis*. New York: D Van Nostrand Company.

Williams, M, D. C White, and S. L Barr, 2008. The potential for robust operational vegetation stress detection from airborne visible-nir hyperspectral imaging under heterogeneous measuremnt conditions. In *Proceedings of RSPSoc 2008*.

Williams, P. C, 1975. Application of near infrared reflectance spectroscopy to analysis of cereal grains and oil seeds. *Cereal Chemistry* **52**(4), 561–576.

Willstätter, R and A Stoll, 1928. *Investigations on Chlorophyll. Methods and Results*, Volume XII. Lancaster, Pennsylvania: Science Press Printing Company.

Winch, J. E and H Major, 1981. Predicting nitrogen and digestibility of forages using near infrared reflectance photometry. *Canadian Journal of Plant Science* **61**(1), 45–51.

Wood, C, 1995. *Environmental Impact Assessment: a comparative review*. Longman, Harlow.

Wooley, J. T, 1971. Reflectance and transmittance of light by leaves. *Plant Physiology* **47**, 656–662.

Woolhouse, H. W, 1967. The nature of senescence in plants. *Symposia of the Society for Experimental Biology* **21**, 179–213.

Woolhouse, H. W, 1974. Longevity and senescence in plants. *Scientific Progress* **61**, 123–147.

Woolhouse, H. W, 1978. Senescence processes in the life cycle of flowering plants. *BioScience* **28**(1), 25–31.

Workman (Jr), J and A. W Springsteen, 1998. *Applied Spectroscopy: a compact reference for practitioners*. London: Academic Press.

Wu, L, A. D Bradshaw, and D. A Thurman, 1975. The potential for evolution of heavy metal tolerance in plants iii. the rapid evolution of copper tolerance in agrostis stolonifera. *Heredity* **34**, 165–187.

Yang, H, F van der Meer, J Zhang, and S. B Kroonenberg, 2000. Direct detection of onshore hydrocarbon microseepages by remote senseing techniques. *Remote Sensing Reviews* **18**, 1–18.

Yang, H, J Zhang, F Van der Meer, and S. B Kroonenberg, 1999. Spectral characteristics of wheat associated with hydrocarbon microseapages. *International Journal of Remote Sensing* **20**, 807–813.

Yoder, B. J and L. S Daley, 1990. Development of a visible spectroscopic method for determining chlorophyll *a* and *b in vivo* in leaf samples. *Spectroscopy* **15**, 44–50.

Youkhana, S. K, 1983. *Canopy modeling studies*. Colorado State University.

Zagajewski, B, 2001, June 2000). *A Decade of Trans-European Remote Sensing Co-operation. Proceedings of the 20th Earsel Symposium*, Chapter Assessment of a possibility of the lead detection in grasses using spectrometer SPZ-5, pp. 353–367. Dresden, Germany: Taylor and Francis.

Zarco-Tejada, P. J, J. R Miller, D Haboudane, N Tremblay, and S Apostol, 2003. Detection of chlorophyll fluorescence in vegetation from airborne hyperspectral casi imagery in the *red-edge* spectral region. *IEEE Transactions on Geoscience and Remote Sensing* **41**, 598–600.

Zarco-Tejada, P. J, J. R Miller, G. H Mohammed, T. L Noland, and P. H Sampson, 2000. Chlorophyll fluorescence effects on vegetation apparent reflectance: Ii. laboratory and airborne canopy-level measurements with hyperspectral data. *Remote Sensing of Environment* **74**, 596–608.

Zarco-Tejada, P. J, J. C Pushnik, S Dobrowski, and S. L Ustin, 2003. Steady-state chlorophyll a fluorenscence detection from canopy derivative reflectance and double-peak red-edge effects. *Remote Sesning of Environment* **84**, 283–294.

Zhang, X, M. A Friedl, C. B Schaaf, A. H Strahler, J. C. F Hodges, F Gao, B. C Reed, and A Huete, 2003. Monitoring vegetation phenology using MODIS. *Remote Sensing of Environment* **84**, 471–475.